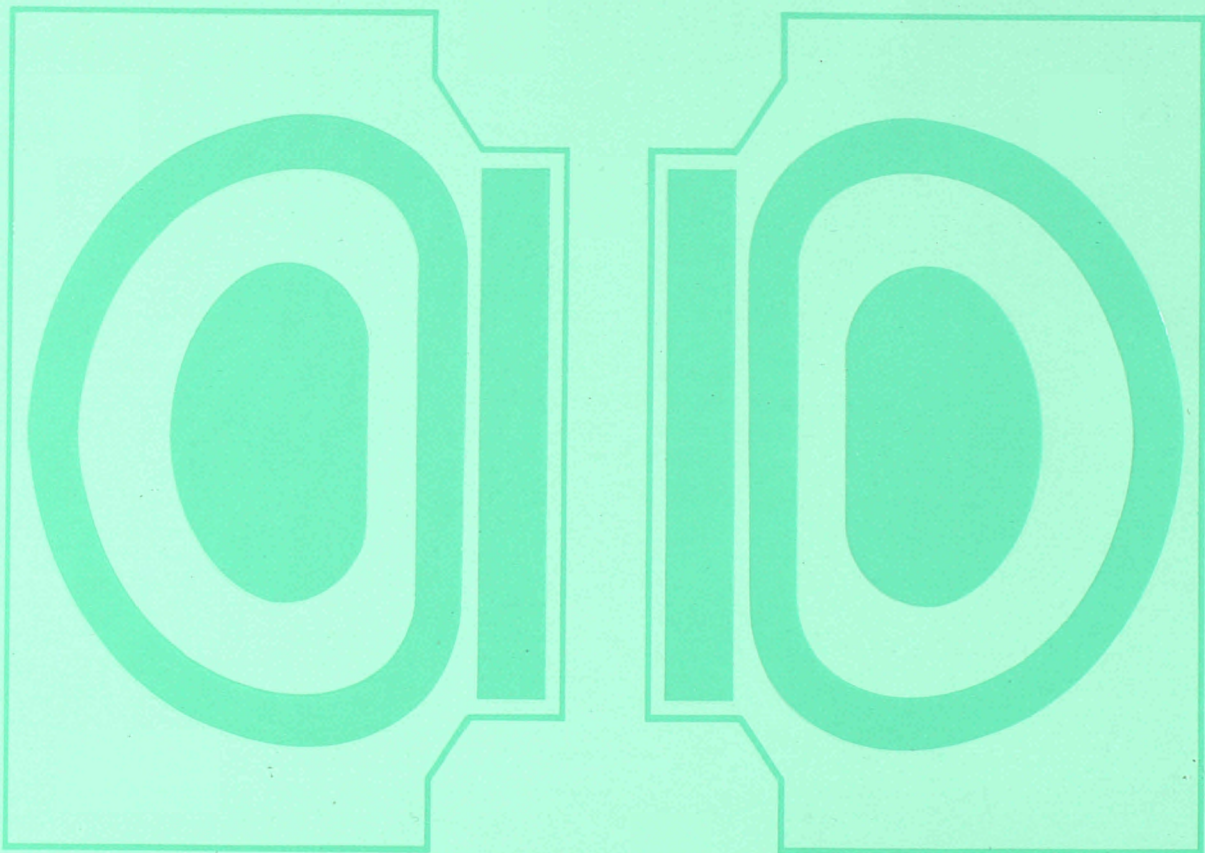


**JET
JOINT
UNDERTAKING**

**PROGRESS
REPORT
1995**



EUR 16873-EN-C

EUR-JET-PR13

JET
JOINT
UNDERTAKING

PROGRESS
REPORT
1995

APRIL 1996

*This document is intended for information only
and should not be used as a technical reference.*

EUR16873-EN-C (EUR-JET-PR13) April 1996.
Editorial work on this report was carried out by B.E.Keen.
The preparation for publication was undertaken by
JET Publications Group, JET Joint Undertaking, Abingdon, UK.

© Copyright ECSC/EEC/EURATOM, Luxembourg 1996

Enquiries about copyright and reproduction should be addressed to:
The Publications Officer, JET Joint Undertaking, Abingdon, Oxon. OX14 3EA, UK.

Legal Notice

Neither the commission of the European Communities nor any person acting on behalf of the Commission is responsible for the the use which might be made of the following information.
Catalogue number : CD-NB-16873-EN-C for the Report EUR 16873-EN-C

Printed in England

Contents

Introduction, Background and Summary	1
Technical Achievements during 1995	11
- First Wall Systems	11
- Power Supplies and Magnet Systems	19
- Neutral Beam Heating	28
- RF Heating Systems	40
- Operations Systems	58
- Vacuum Systems	66
- Waste Management	69
- Control and Data Acquisition System	71
- Data Management	76
- Diagnostic Systems	78
- Summary of Operations	109
- Summary of Technical Achievements	111
Scientific Achievements during 1995	115
- High Performance	116
- Divertor Assessment and Divertor Physics	125
- Tokamak Concept Improvements	144
- Transport and Fluctuations	159
- MHD and Beta Limits	169
- Physics Issues related to the Next Step	173
- Data Analysis and Modelling	177
- Summary of Scientific Progress and Perspective	187
Developments and Future Plans	193
- Advanced Divertor Studies	195
- Tritium Handling	196
- Plans for D-T Operation	199
- Studies for Machine Performance Enhancement	201
- Future Plans	210
Appendices	215
I JET Task Agreements 1995	215
II List of Articles, Reports and Conference Papers published in 1995	218

Foreword



This is the thirteenth JET Progress Report, which provides an overview summary and puts into context scientific and technical advances made on JET during 1995. This Report presents a more detailed account of JET's progress than that contained in the JET Annual Report. It is aimed not only at specialists and experts engaged in nuclear fusion and plasma physics, but also at a more general scientific community. To meet these aims, the Report contains a brief summary of the background of the Project, and describes the basic objectives of JET and the principal design aspects of the machine. In addition, the Project Team structure is included, as it is within this structure that activities and responsibilities for machine operation and improvements are carried out and the scientific programme is executed.

At the start of 1995, JET was in the middle of the Pumped Divertor Characterisation Phase. This phase had begun in February 1994 and ended in June 1995. The objective of this phase was to establish reliable methods of plasma purity control and plasma exhaust in operational conditions relevant for the Next Step tokamak. For this purpose, a pumped divertor which allowed the test of various configurations had been installed. The geometry of the divertor is an important aspect in achieving these objectives, and tests on the first divertor configuration (Mark I) were carried out during this period. The Mark I pumped divertor was most effective and allowed a broad-based and highly ITER-relevant research programme to be pursued. The 1995 campaign addressed the central

problems of the ITER divertor: efficient dissipation of the exhausted power; control of particle fluxes; and effective impurity screening. The excellent power handling capability of the divertor target was essential to these studies and justified the care taken in its design. At the start of the year, Carbon Fibre Composite (CFC) tiles were used in the vessel as the power handling material.

The use of the divertor cryopump has had particular advantages in both vessel conditioning and plasma performance. It has allowed good density control and facilitated the production of long, clean, stationary ELMy H-mode plasmas with electron density, effective ionic charge, radiated power loss and stored plasma energy remaining constant for up to 20s (about 40 energy confinement times). The cryopump, with argon frosting, has also pumped helium in L- and H-mode plasmas. There was no evidence for the accumulation of helium in the central plasma.

ELMy H-mode plasmas with steady conditions for many energy confinement times are considered the most credible mode of operation for ITER and these were studied at high power up to the full 6MA current capability of JET. ELMy H-modes with combined heating powers up to 32MW and detached divertor plasmas and radiative power exhaust (the operating regime foreseen for ITER) have been found to reduce the power loading to the targets, but at the expense of main plasma confinement and purity.

At 6MA current (a world record in a divertor plasma), H-modes were obtained with up to 18MW of neutral

beam injection heating. At low current, quasi-steady state stable operation has also been produced with high normalised plasma pressure, H-mode confinement and significant bootstrap current fraction (the so-called advanced tokamak mode of operation). Confinement studies in ELMy H-modes (including similarity experiments with ITER) have shown the need to provide more accurate data on the H-mode threshold power and on transport scaling close to the threshold and at high β .

Improved plasma shaping has allowed long ELM-free H-modes (up to 1.2s) to be produced with plasma currents up to 4.5MA. A neutron yield of 4.7×10^{16} neutrons per second in deuterium (a new JET record) and fusion triple product ($nT\tau_e$) $> 8 \times 10^{20} \text{m}^3 \text{keVs}^{-1}$, (which is within 10% of the previous best), were achieved at 3.8MA current and 3.4T toroidal field and with 18MW of neutral beam injection. In addition, the plasma energy reached 13.5MJ (the highest energy recorded in a JET plasma).

Whereas hot ion H-modes at low plasma current and low toroidal field reached a normalised beta (β_N) of about 2.5, high performance hot ion H-modes were limited to β_N of about 1.8, well below the Troyon limit ($\beta_N = 2.8$) by a variety of magnetohydrodynamic (MHD) instabilities. The termination of the high performance phase was delayed by reducing the NB heating power in order to maintain MHD stability. In this way, the neutron rate and the stored plasma energy remained high and steady for up to 1s.

Other experiments of significance to ITER included studies when the JET toroidal field ripple was varied. This indicated that magnetic ripple in the ITER relevant range of 0.1% to 2% at the plasma edge should not affect energetic particle confinement in ITER. In addition, Alfvén Eigenmodes have been externally excited using the saddle coils and non-linear beat waves. Most relevant for ITER is the identification of the kinetic Alfvén Eigenmode with very weak damping.

The campaign with CFC tiles was successfully completed in mid-March and was followed by a shutdown in which the CFC tiles were replaced by beryllium, which is a target material favoured by ITER. A wide range of experiments were performed to assess the performance of beryllium as a divertor target tile material and to compare it with CFC. JET is the only machine in the world, which is capable of undertaking such a comparison. The main outcome was that, under

normal operating condition, the CFC and beryllium targets result in very similar plasma behaviour and have comparable power handling characteristics. Experiments were also performed to test whether the beryllium targets would 'self-protect', by evaporating beryllium, leading to high radiation from the plasma and reduced heat fluxes, when subjected to significantly higher heat loads than normal. Significant surface melting but only moderate 'self-protection' was observed at equivalent ITER power loads.

The neutral beam injectors operated reliably and routinely delivered close to their maximum power throughout the campaign. These reached power levels of up to 20.4MW, and at these levels, the Octant No.4 injector contributed a world record 12.6MW for a single injection port. The ion cyclotron resonance frequency (ICRF) generators coupled up to 15MW power to the plasma, and high density, high power plasmas ($> 10 \text{MW}$) showed a soft transition to the H-mode, with small ELMs and high confinement. Lower hybrid (LH) frequency heating achieved a record power of 7.3MW to the plasma. This was used to fully drive a plasma current of 3MA, to produce reversed magnetic shear configurations, to control sawteeth and to soften the termination of hot-ion ELM-free H-modes.

Following completion of the experimental campaign in June 1995, a shutdown started for the installation of the 'more-closed' Mark IIA divertor and modification of the ICRF antennae. The shutdown is scheduled for completion in March 1996. At the start of the shutdown, a detailed inspection showed that in-vessel components were in good condition with no significant damage except for the deliberately induced beryllium target plate melting.

The first stage of in-vessel work in the shutdown to replace the Mark I divertor was the strip out of components. This was completed ahead of schedule. The next stage involved the installation of the modules of the Mark II divertor support structure. This structure, about 6 metres in diameter and with a weight of 7 tonnes, was assembled to an accuracy of within 0.1mm. This was a remarkable engineering achievement within the confined space of the JET vacuum vessel.

Since the Mark II divertor will become radioactive during its use with tritium plasmas, it has incorporated an important and novel feature in its design: it has been engineered to allow replacement of the divertor target structure by full remote handling techniques. To validate

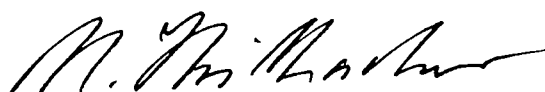
the capability of the remote handling approach, part of the Mark II divertor target plates will be installed by remote handling in early 1996. Successful trials have been carried out on a mock-up arrangement and results have provided a high degree of confidence that target plate exchange with an active machine can be achieved in a reasonable time-scale. It will be the first time that such a complex remote handling operation has been performed on an active machine, providing most valuable engineering experience for the finalisation of ITER design.

For late 1996/ early 1997, planning is underway for a limited period of D-T operation (DTE-1, producing up to 2×10^{20} neutrons), which will demonstrate long pulse fusion power production (fusion amplification factor, $Q > 1$ with more than 10MW of fusion power for a few energy replacement times). These experiments will also make important contributions to D-T physics (including H-mode threshold, ELM and confinement behaviour in D-T, and some D-T specific radio frequency heating studies) which JET alone can provide in an ITER relevant divertor configuration. DTE-1 should allow the original four areas of JET work to be completed and would provide timely input to the ITER EDA. It would also address the important technology issues of reactor relevant tritium processing and remote handling. In particular, it would demonstrate the ability

of the Active Gas Handling System (AGHS) to process tritium while supporting a reacting tokamak plasma. The commissioning of the AGHS subsystems continued successfully during 1995.

The proposal for extension of the JET Programme to the end of 1999, supported by the JET Council, is awaiting formal approval by the Council of Ministers. The programme would include studies aimed at providing data in support of the ITER divertor, while satisfying the requirements of high performance D-T operations. The subsequent programme would progress to divertor/plasma optimisation studies before a more extensive period of D-T operation (DTE-2) in 1999. In DTE-2, D-T plasmas would be studied with substantial alpha-particle heating, capitalising on the performance improvements achieved in preceding experimental campaigns. DTE-2 experiments could produce up to 5×10^{21} neutrons, but efforts would be made to reduce activation while still satisfying JET's role in supporting ITER and the World Fusion Programme.

JET is still making substantial advances in its scientific and technology programme. With the continued dedication of the staff, I am confident that the Project will meet the challenges ahead and will continue to provide crucial information to ensure that fusion will be an important source of energy for future generations.



Dr M Keilhacker
Director
April 1996

Introduction, Background and Summary

Introduction

JET Progress Reports are aimed both at specialists in plasma physics and nuclear fusion research and at the more general scientific community. This contrasts with the JET Annual Reports, which provide overview descriptions of the scientific, technical and administrative status of the JET programme, and is directed at the average member of the public.

To meet these general aims, the Progress Report contains a brief summary of the background to the Project, describes the basic objectives of JET and sets out the principal design aspects of the machine. In addition, the Project Team structure is detailed, since it is within this framework that machine activities and responsibilities are organized and the scientific programme is executed.

The main part of the 1995 Report provides overview summaries of scientific and technical advances made during the year, supplemented by detailed cross-references to the more important JET scientific and technical articles produced during the year. The final part of the Report briefly sets out developments underway to further improve JET's performance and plans for future experiments through to its foreseen completion.

Background

Objectives of JET

The Joint European Torus (JET) is the largest single project of the nuclear fusion research programme of the European Atomic Energy Community (EURATOM). The project was designed with the essential objectives of obtaining and studying plasma in conditions and with dimensions approaching those needed in a fusion reactor. These studies are aimed at defining the parameters, the size and working conditions of a tokamak reactor. The

realisation of this objective involves four main areas of work:

- (i) the scaling of plasma behaviour as parameters approach the reactor range;
- (ii) the plasma-wall interaction in these conditions;
- (iii) the study of plasma heating; and
- (iv) the study of alpha-particle production, confinement and consequent plasma heating.

Two of the key technological issues in the subsequent development of a fusion reactor are faced for the first time in JET. These are the use of tritium and the application of remote maintenance and repair techniques. The physics basis of the post-JET programme will be greatly strengthened if other fusion experiments currently in progress are successful. The way should then be clear to concentrate on the engineering and technical problems involved in progressing from an advanced experimental device like JET to a prototype power reactor.

Basic JET Design

To meet these overall aims, the basic JET apparatus was designed as a large tokamak device with overall dimensions of about 15m in diameter and 12m in height. A diagram of the apparatus is shown in Fig.1 and its principal parameters are given in Table I. At the heart of the machine, there is a toroidal vacuum vessel of major radius 2.96m having a D-shaped cross-section 2.5m wide by 4.2m high. During operation of the machine, a small quantity of gas (hydrogen, deuterium or tritium) is introduced into the vacuum chamber and is heated by passing a large current through the gas. Originally, the machine was designed to carry 4.8MA, but has been modified to achieve 7MA. This current is produced by transformer action using the massive eight-limbed

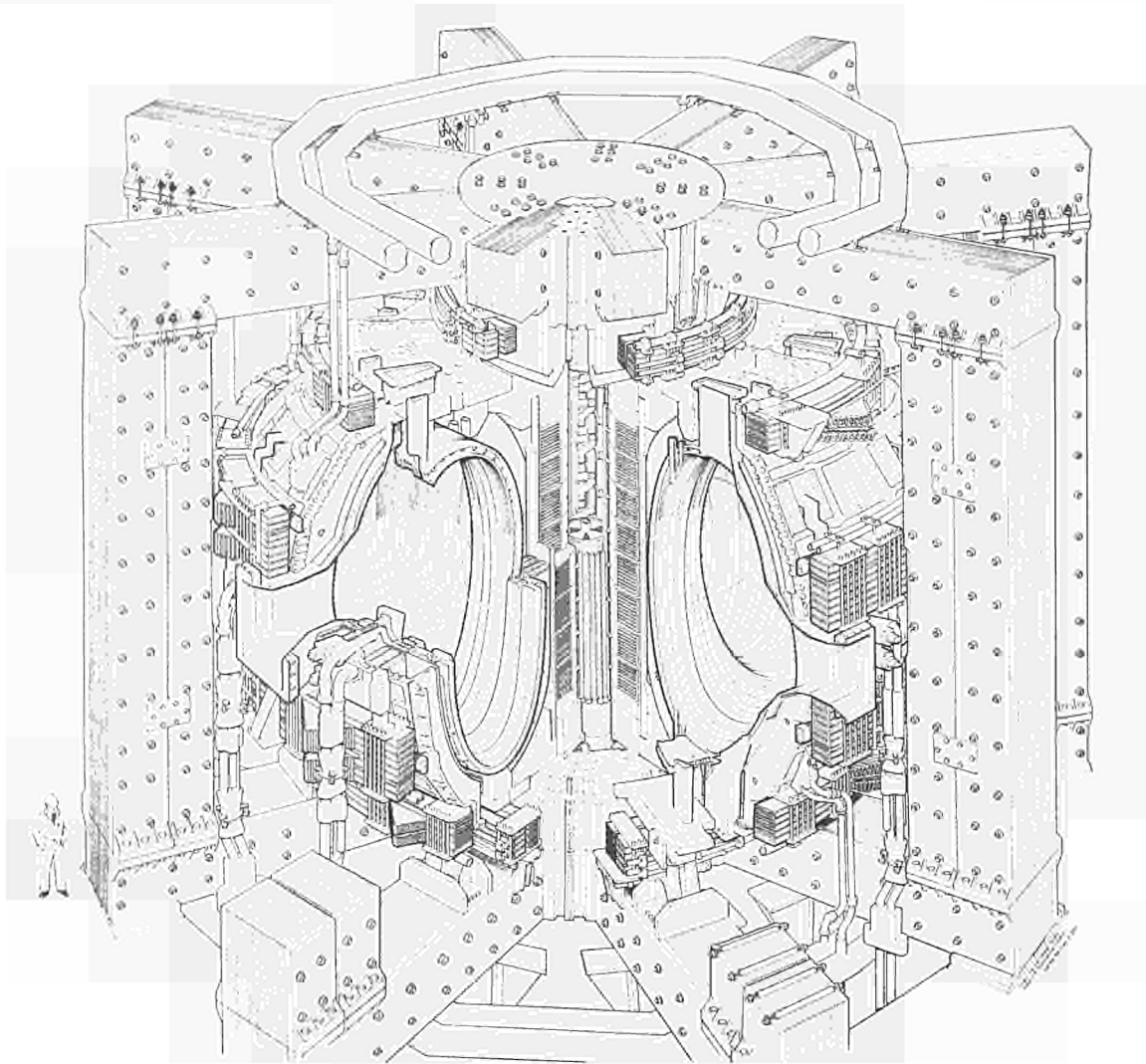


Fig.1: Diagram of the JET Tokamak.

Table I
Principal Parameters

Parameter	Value
Plasma minor radius (horizontal), a	1.25m
Plasma minor radius (vertical), b	2.10m
Plasma major radius, R_0	2.96m
Plasma aspect ratio, R_0/a	2.37
Plasma elongation ratio, $\epsilon=b/a$	1.68
Flat top pulse length	60s
Toroidal magnetic field (plasma centre)	3.45T
Plasma current, D-shaped plasma	7.0MA
Volts-seconds available	54Vs
Toroidal field peak power	380MW
Poloidal field peak power	300MW
Additional heating power (into torus)	~50MW
Weight of vacuum vessel	108t
Weight of toroidal field coils	364t
Weight of iron core	2800t

magnetic circuit, which dominates the apparatus (see Fig.1). A set of coils around the centre limb of the magnetic circuit forms the primary winding of the transformer with the plasma acting as the single turn secondary. Additional heating of the plasma is provided by the propagation and absorption of high power radio frequency waves in the plasma and by the injection of beams of energetic neutral atoms into the torus.

The plasma is confined away from the walls of the vacuum vessel by a complex system of magnetic fields, in which the main component, the toroidal field, is provided by 32 D-shaped coils surrounding the vacuum vessel. This field, coupled with that produced by the current flowing through the plasma, forms the basic magnetic field for the tokamak confinement system, which provides a full design field at the plasma centre of 3.45T. The poloidal coils, positioned around the outside of the vacuum vessel, shape and position the plasma in operation.

In addition, some scientific and technical duties are carried out within the Directorate and in Supporting Units.

The main duties of the Administration Department have been described in previous JET Annual Reports. This Report concentrates on progress made in the scientific and technical areas during 1995. To aid this description, the functions of these Departments are described below.

Torus and Measurements Department

The Torus and Measurements Department has overall responsibility for the performance capacity of the machine: this includes enhancements directly related to this (excluding heating) and the long term planning associated with integration of these elements to achieve ultimate performance. The Department is also responsible for: fusion technology requirements for the active phase including tritium handling and processing; for construction and operation of necessary measurement diagnostic systems and the interpretation of experiment data; and for data systems comprising data control, acquisition and management. The main functions of the Department are:

- to design, procure and implement enhancements to the JET device;
- to provide and maintain clean conditions inside the vessel which lead to high quality plasma discharges;
- to conceive and define a set of coherent measurements;
- to be responsible for construction of necessary diagnostics;
- to be responsible for diagnostics operation, quality of measurements and definition of plasma parameters;
- to organise and implement data acquisition and computing;
- to design and develop remote handling methods and tools to cope with JET requirements;
- to design and construct facilities for handling tritium and for waste management.

The Department consists of five Divisions and three Groups (Machine Assembly, Diagnostic Engineering and Data Management):

(a) *First Wall Division*, which is responsible for the vital area of plasma wall interactions. Its main tasks include the provision and maintenance inside the vacuum vessel of conditions leading to high quality plasma discharges. The Division develops, designs, procures and installs the first wall systems and its components

such as limiters, wall protections and internal pumping devices. The area of responsibility encompasses the mechanical integrity of the vacuum vessel as a whole and the development and implementation of mechanical and Remote Handling techniques;

(b) *Fusion Technology Division*, is responsible for all nuclear engineering aspects of this Project including tritium and gas handling, vacuum systems, waste management and regulatory approvals;

(c) *Control and Data Acquisition System Division (CODAS)*, which is responsible for the implementation, upgrading and operation of computer-based control and data acquisition systems for JET;

(d) *Experimental Division 1 (ED1)*, which is responsible for specification, procurement and operation of about half the JET diagnostic systems. ED1 undertakes electrical measurements, electron temperature measurements, surface and limiter physics and neutron diagnostics;

(e) *Experimental Division 2 (ED2)*, which is responsible for specification, procurement and operation of the other half of the JET diagnostic systems. ED2 undertakes all spectroscopic diagnostics, bolometry, interferometry, the soft X-ray and neutral particle analysis.

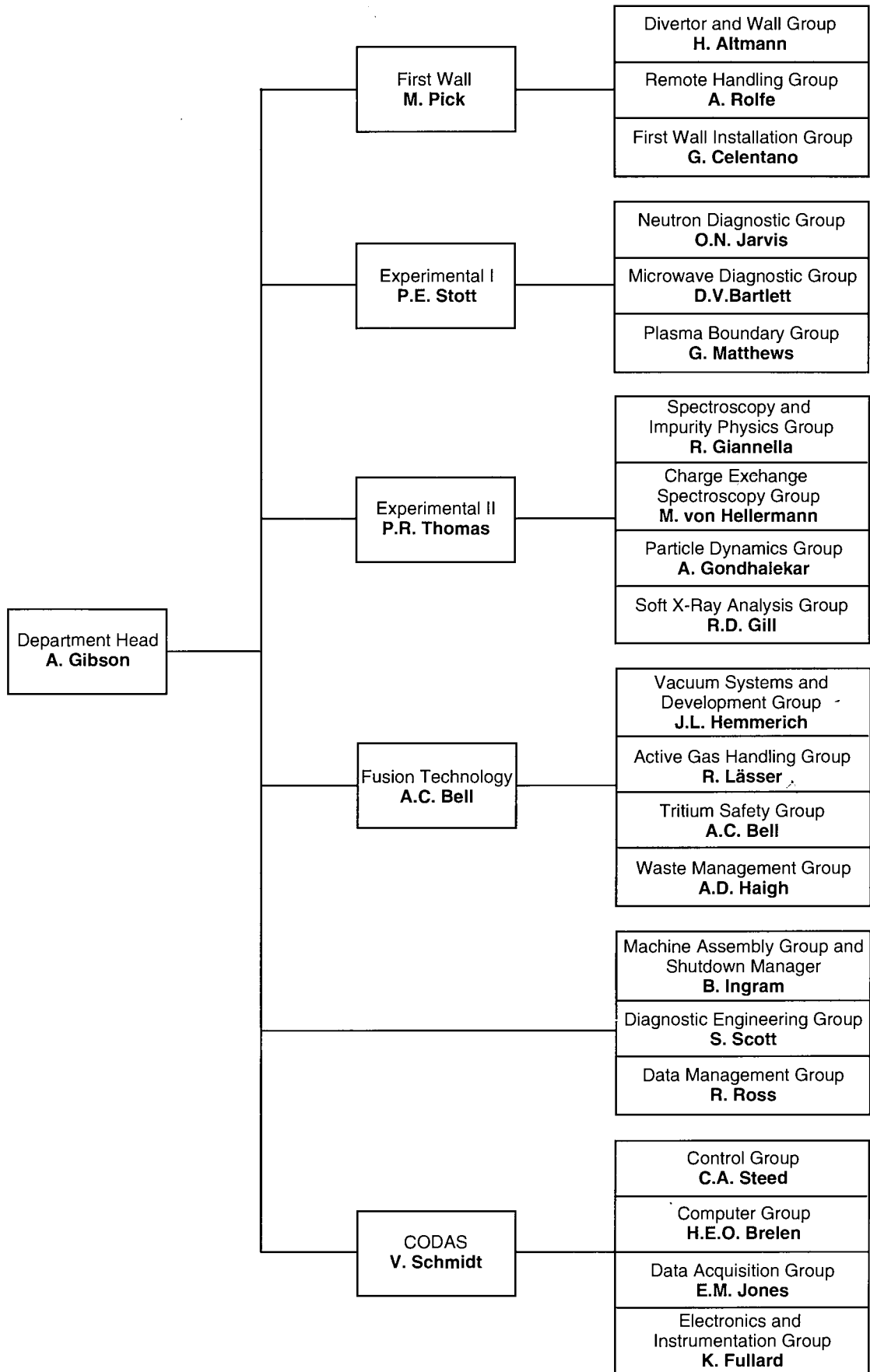
The structure of the Torus and Measurements Department to Group Leader level is shown in Fig. 2 and the list of staff within the Department is shown in Fig. 3.

Heating and Operations Department

The overall responsibility of the Heating and Operations Department is for the efficient and effective day-to-day operation of the machine. In addition, the Department has responsibility for plasma heating and auxiliary equipment and related physics; the design and operation of power supplies as well as contributing to the execution and evaluation of JET's experimental programme. The main functions of the Department are:

- preparing and co-ordinating operation of the machine across Departments and Divisions;
- heating and current drive and analysis of its effects in the plasma;
- plasma fuelling, including pellet injection;
- designing and employing power supplies for ensuring efficient operation and control of the machine.

The Department consist of two Groups (Machine Operations and Machine Services) and four Divisions:



JG96.94/2

Fig.2: Torus and Measurements Department, Group Structure
(December 1995)

TORUS AND MEASUREMENTS DEPARTMENT

Head of Department: A. Gibson

C. Earl	J. Lundquist	P. Sagar	R. Smith
C. Hancock	J. Reid	Miss. D. Samuel	A. Tiscornia
B. Ingram	Mrs. J. Roberts	S. Scott	C. Wilson
Mrs. P. Longworth	R. T. Ross		

FUSION TECHNOLOGY DIVISION

Head: A.C. Bell

S. Bryan	A. Haigh	R. Lässer	R. Pearce
P. Brennan	J. L. Hemmerich	J. Lupo	Mrs J. Pointer
C. J. Caldwell-Nichols	D. Holland	J. Mart	K. D. Walker
C. Callaghan	H. Jensen	A. Miller	R. Warren
Mrs. J. Campbell	Mrs. M. E. Jones	G. Newbert	T. Winkel
N. Green	J. F. Jaeger	J. Orchard	

FIRST WALL DIVISION

Head: M.A. Pick

H. Altmann	E. Deksnis	G. Israel	B. Macklin
P. Brown	C. Froger	M.A.Irving	A. Nowak
T.V. Businaro	L. Galbiati	L.P.D.F. Jones	J. Palmer
R.A. Cusack	F. Hurd	J.F. Junger	A. Peacock
G. Celentano	Mrs. I. Hyde	A.B. Loving	T. Raimondi
Mrs. D. Cranmer			

CONTROL AND DATA ACQUISITION SYSTEMS DIVISION

Head: V. Schmidt

M. B. Baronian	P. J. Card	E. M. Jones	C. A. Steed
Mrs. A. M. Bellido	J. J. Davis	F. J. Junique	C. Terella
H. E. O. Brelen	S. Dmitrenko	N. G. Kidd	G. Wolfers
W. J. Brewerton	S. E. Dorling	J. G. Krom	I. D. Young
T. Budd	K. Fullard	C. Perry	

EXPERIMENTAL DIVISION I

Head: P. E. Stott

S. Ali-Arshad	C. Gowers	F. B. Marcus	P. Roberts
D. Bartlett	P. J. Harbour	G. Matthews	G. Sadler
H. Bindslev	J. Hoekzema	G. Neill	A. Stevens
B. W. Brown	M. Hone	P. Nielsen	D. Summers
S. Clement	I. Hurdle	H. Oosterbeek	P. Tegg
J. P. Coad	O. N. Jarvis	Mrs N. Povey	P. van Belle
J. Ehrenberg	M. Loughlin	R. Prentice	J. Vince
J. Fessey			

EXPERIMENTAL DIVISION II

Head: P. R. Thomas

B. Alper	R. Giannella	R. König	M. Stamp
P. Beaumont	R. Gill	P. Morgan	S. A. Staunton-Lambert
Mrs. K. Bell	A. Gondhalekar	C. Nicholson	W. Studholme
G. Braithwaite	L. D. Horton	R. Reichle	M. von Hellermann
P. Breger	A. Howman	R. Robins	B. Viaccoz
A. Edwards	H. Jäckel	P. Smeulders	R. Webb

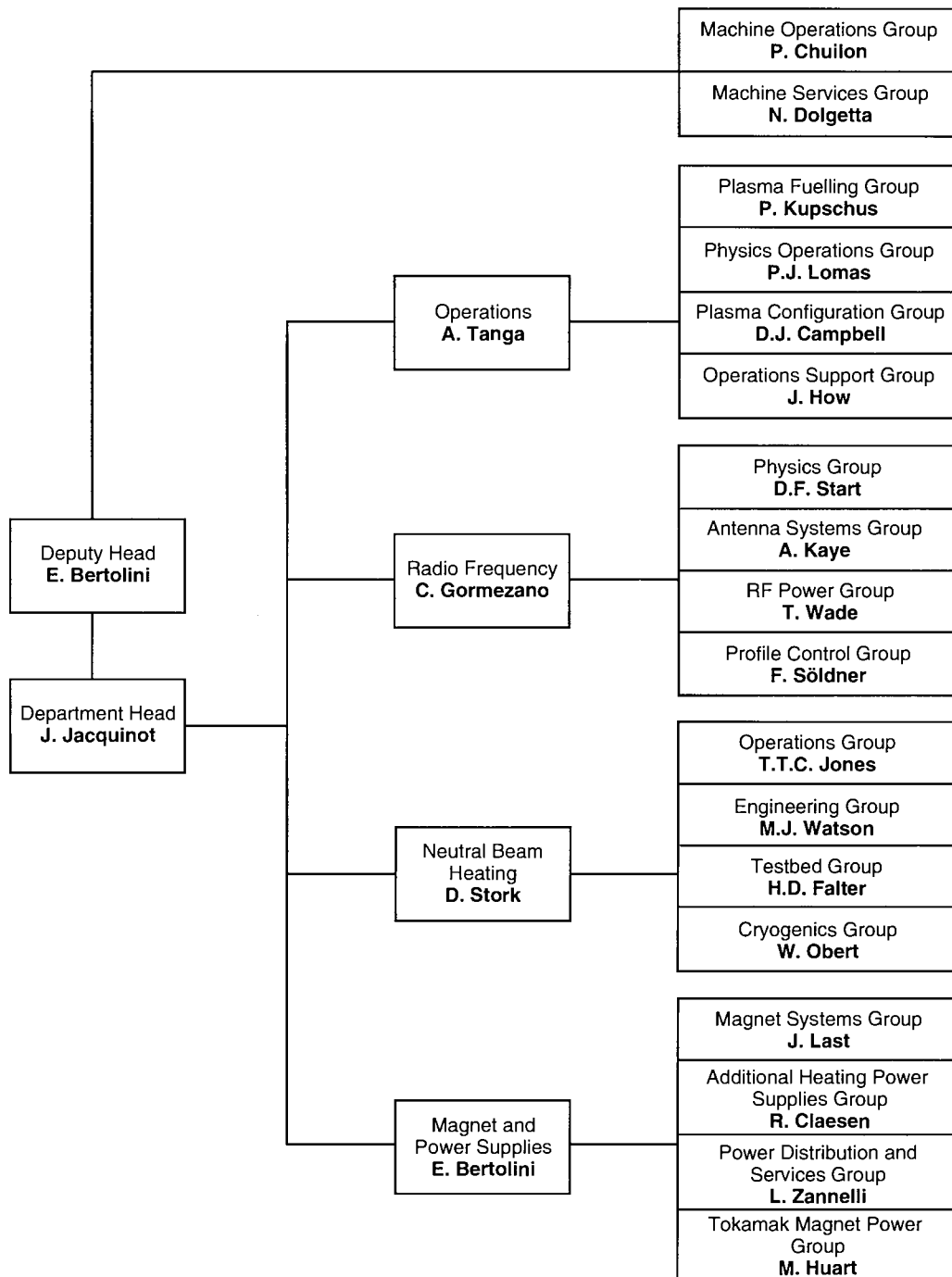
*Fig.3: Project Team Staff in the Torus and Measurements Department
(December 1995)*

JG96.94/3

(a) *Operations Division* plays a major role in the efficient planning and execution of JET's experimental programme and in the integration of existing or imminent systems into an effective experimental programme. In addition, it is responsible for effective methods of fuelling the plasma including the development of methods based on solid high speed hydrogen pellets; development of new plasma wall conditioning techniques; plasma control systems; development of

disruption control methods; training of operations staff; and monitoring of machine operations;

(b) *Neutral Beam Heating Division*, which is responsible for construction, installation, commissioning and operation of the neutral injection system, including development towards full power operation. The Division is also responsible for all cryo-systems and also participates in studies of physics of neutral beam heating;



JG96.94/4

Fig.4: Heating and Operations Department, Group Structure (December 1995)



HEATING AND OPERATIONS DEPARTMENT

Head of Department: J. Jacquinot
Deputy Head of Department: E. Bertolini

V. Bhatnagar	T. Dale	R. Meadows	W. Smith
C. Birks	R. Greenfield	C. Rayner	K. Taylor
M. Bolton	M. Hughes	B. Regan	J. Watt
P. Chuilon	M. Macrae	Miss. V. Shaw	B Workman
N. Dolgetta	S. McLaughlin		

MAGNET AND POWER SUPPLIES DIVISION

Head: E. Bertolini

A. Barnard	J. Goff	J. McKivett	P. Presle
T. Bonicelli	D. Graham	V. Marchese	S. Shaw
D. Chiron	M. Huart	G. Marcon	A. Tesini
R. Claesen	F. Jensen	Mrs. H. Marriott	J. van Veen
E. Daly	J. Jeskins	G. Murphy	C. R. Wilson
P. Doyle	J. R. Last	P. Noll	L. Zannelli
C. Folco	H. McBryan	R. Ostrom	

OPERATIONS DIVISION

Head: A. Tanga

D. J. Campbell	P. Kupschus	S. Puppin	R. Sartori
S. Cooper	M. Lennholm	L. Rossi	B. Schunke
M. Gadeberg	P. J. Lomas	G. Saibene	A. C. C. Sips
J. How	T. Martin	A. Santagiustina	M. Tabellini
M. Johnson			

NEUTRAL BEAM HEATING DIVISION

Head: D. Stork

A. Bickley	D. Ewers	F. Long	A. J. Parfitt
A. Browne	H. Falter	D. Martin	R. Parkinson
C. D. Challis	D. Godden	C. Mayaux	D. Raisbeck
J. F. Davies	L. Hackett	Mrs. D. Noyes	L. Svensson
A. Dines	Mrs. S. Humphreys	W. Obert	J. Waterhouse
H. P. L. de Esch	T. T. C. Jones	S. Papastergiou	M. J. Watson

RADIO FREQUENCY HEATING DIVISION

Head: C. Gormezano

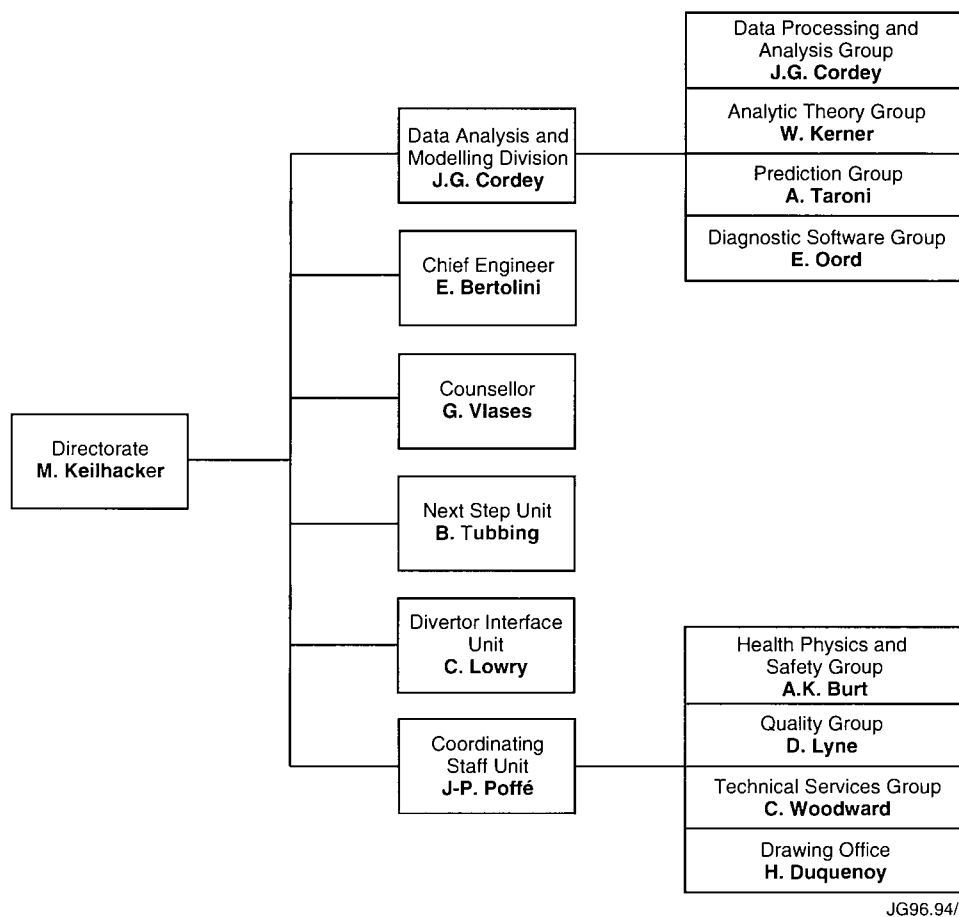
S. C. Booth	D. T. Edwards	A. Kaye	F. Söldner
M. Brandon	A. Franklin	J. Plancoulaine	D. F. Start
G. Cottrell	P. Finberg	F. Rimini	C. Steele
P. Crawley	M. Gammelmin	P. Schild	M. Timms
Mrs. R. Deitrich	M. Graham	M. Schmid	T. Wade
T. Dobbing	R. Horn	A. Sibley	

Fig.5: Project Team Staff in the Heating and Operations Department (December 1995)

JG96.94/5

(c) *Radio Frequency Heating Division*, which is responsible for the design, construction, commissioning and operating RF heating and current drive systems during the different stages of its development to full power. The Division is also responsible for the TAE excitation system and also participates in studies of the physics of RF heating;

(d) *Magnet and Power Supplies Division* is responsible for the design, construction, installation, operation and maintenance of the electromagnetic system and plasma control. The area of responsibility encompasses the toroidal, poloidal and divertor magnets, mechanical structure; and all power supply equipment needed for magnets, plasma control, additional heating and auxiliaries.



JG96.94/6

Fig.6: Directorate and Support Units, Group Structure
(December 1995)

The structure of the Heating and Operations Department to Group Leader level is shown in Fig. 4 and the list of staff in the Department is shown in Fig. 5.

In addition, both Departments are involved in:

- execution of the experimental programme;
- interpretation of results;
- making proposals for future experiments.

Directorate

Within the Directorate, there are three technical units, one Division and a Chief Engineer, reporting directly to the Director. The main responsibilities are as follows:

(a) *The Co-ordinating Staff Unit* is responsible for the availability of a comprehensive health physics and safety project organisation; and for the provision of centralised engineering support services. It comprises four Groups:

- Health Physics and Safety Group;
- Quality Group;
- Technical Services Group;
- Drawing Office.

(b) *The Data Analysis and Modelling Division* is responsible for the provision of software for the acquisition and processing of the data from JET diagnostics; for confirming the internal consistency of the processed data and assembling it into public databases; and the development and testing of theoretical models against JET data. In addition, the Division is responsible for prediction by computer simulation of JET performance, interpretation of JET data and the application of analytic plasma theory to gain an understanding of JET physics.

It comprises four groups:

- Analytic Theory Group;
- Simulation Group;
- Data Processing and Analysis Group;
- Diagnostic Software Group.

(c) *The Next Step Unit* is responsible for co-ordinating contributions from JET to the European effort in support of the ITER-EDA. This responsibility includes drawing up proposals, initiating relevant work programmes on JET and taking part in their execution and evaluation.

DIRECTORATE AND SUPPORT UNITS*Director: Dr M. Keilhacker*Mrs. C. Johnson
C. Lowry
J. McMahonT. O'Hanlon
Mrs. P. Reeve
Ms. R. ThormahlenB. Tubbing
G. VlasesD.J. Ward
M. L. Watkins**COORDINATING STAFF UNIT***Head: J-P. Poffé*Ms. L. Ashby
M. Axton
P. Barker
A.K. Burt
D. Campling
N. DaviesH. Duquenoy
A. Gibson
J. A. Green
H. D. Jones
R. Litchfield
Miss. K. LukerP. Macheta
C. Manning
M. Page
H. Panissie
B. Patel
Mrs. J. ReidK. Sandland
P. Schofield
M. Scotcher
C. Woodward**DATA ANALYSIS AND MODELLING DIVISION***Head: J. G. Cordey*B. Balet
K. Blackler
J. Christiansen
L. G. Eriksson
J. JeralW. Kerner
D. O'Brien
E. Oord
M. Ottaviani
R. SimoniniK. Slavin
E. Springmann
Mrs. P. Stubberfield
A. TaroniK. Thomsen
J. Wesson
D. Wilson
W. Zwingmann**NEXT STEP UNIT***Head: B. Tubbing***DIVERTOR INTERFACE UNIT***Head: C. Lowry**Fig.7: Project Team Staff in Directorate and Support Units (December 1995)*

JG96.947

(d) *The Divertor Interface Unit* is responsible for assessing the impact of developments in the experimental programme and operation on the design requirements for JET divertors. This includes a high level of participation in the JET experimental programme on divertor physics, themomechanical analysis of plasma induced loads on the divertor, and the definition of advanced divertor concepts.

In addition, there is a *Chief Engineer*, who reports to the Director, and is responsible for ensuring the overall coherence of technical aspects of JET operations.

The structure of the Directorate to Group Leader level is shown in Fig.6 and the list of staff in these areas is shown in Fig.7.

Report Summary

The first section of this Report provides a brief introduction and background information relevant to the Report. The

second and third sections set out an overview of progress on JET during 1995 and with a survey of scientific and technical achievements during 1995 sets these advances in their general context. This summary is specifically cross-referenced to reports and articles prepared and presented by JET staff during 1995.

The fourth section is devoted to future plans and certain developments which might enable enhancements of the machine to further improve its overall performance. Some attention has been devoted to methods of surmounting certain limitations and these are detailed in this section.

In addition, Appendix I contains a list of work topics which have been carried out under Task Agreements with various Association Laboratories. A full list is included in Appendix II of all Articles, Reports and Conference papers published by JET authors in 1995. Copies of particular papers can be obtained from JET Publications Office.

Technical Achievements during 1995

Introduction

JET started 1995 in the middle of the Pumped Divertor Characterisation Phase. This phase had begun in February 1994 and ended in June 1995. During this period, the Mark I pumped divertor was very effective and allowed a broad-based and highly ITER-relevant research programme to be pursued. The 1995 experimental campaign addressed the central problems of the ITER divertor: efficient dissipation of the exhausted power, control of particle fluxes and effective impurity screening. It started the year with using carbon fibre composite (CFC) tiles in the vessel as the power handling material.

The campaign with CFC tiles was successfully completed in mid-March and was followed by a shutdown of 22 working days in which the CFC tiles were removed and replaced by beryllium. In addition, a prototype separator for the ion cyclotron resonance frequency (ICRF) antenna was installed and eighteen French Horn cooling pipes were strengthened and replaced. The efficiency of the in-vessel work was improved with the effective use of the in-vessel training facility and the use of an observation platform, adjacent to the torus access cabin, to allow Responsible Officers to control the in-vessel work via closed circuit video cameras.

Following this shutdown, experiments were performed to assess the performance of beryllium as a divertor target tile material and to compare it with the CFC tiles. In response to the ITER Joint Central Team, beryllium melting was induced at ITER-relevant heat fluxes to see whether a protective radiative shield was established.

In June 1995, a shutdown started for the installation of the Mark IIA divertor and the modification of the ICRF antennae. The shutdown is scheduled to finish in March 1996. At the start of the shutdown, a detailed inspection

showed that in-vessel components were in good condition with no significant damage except for the deliberately induced beryllium target plate melting. The first phase of in-vessel work in the shutdown was the strip out of components. This work, which included the removal of the ICRF antennae for modification, was completed ahead of schedule.

The installation of the Mark II support structure constituted a major development in JET. This support structure is designed to allow JET to investigate a wide variety of divertor geometries by the installation of different tile carriers. These carriers can include the necessary diagnostics and can be attached to the support structure easily, quickly and with high precision. The diagnostics are simply plugged into the support structure. The whole procedure is designed to be possible by remote handling.

This phase of in-vessel work involved installation of the modules of the Mark II divertor support structure, which is about 6 metres in diameter and has a weight of 7 tonnes. This was assembled on time and to an accuracy of within 0.1mm. The ICRF antennae, modified to improve the coupling of ICRF power to the JET plasma, were then reinstalled. At the end of the year, work to install other in-vessel components was continuing.

Preparations are also continuing for the next period of D-T operation (DTE-1), which is scheduled for the end of 1996. Work is also continuing on the procurement of the ITER specific Mark II Gas-box divertor target assembly, which is due to be installed by remote handling in 1997.

The Remote Tile Exchange, during which the Mark IIA tile carriers will be exchanged for the Mark II Gas-box tile carriers, will be the first fully remote task undertaken on JET and the most significant fully remote han-

dling task undertaken on any fusion device in the world. Accordingly, extensive preparations are being made for the proving of equipment function, performance and reliability together with the derivation and development of task procedures and operator training.

The following sections detail the main technical achievements made during 1995.

First Wall Systems

Introduction

The main activities associated with First Wall systems during 1995 were related to: the procurement and preparations for and implementation of the shutdown to install the Mark II Support Structure and Mark IIA Divertor Tile Carriers; preparations for the fully remote replacement of Mark IIA Divertor Tile Carriers with the Mark II Gas-Box tile carriers immediately after the Deuterium-Tritium Experiment (DTE1); and, in addition, completion of the Mark II Gas-Box Divertor design. In addition to preparations for and execution of the major planned Mark II Installation Shutdown which started in June 1995, two additional vessel interventions were also carried out.

The installation of the Mark II support structure constitutes a major development in JET. This support structure is designed to allow JET to investigate a wide variety of divertor geometries by the installation of different tile carriers. These carriers can include the necessary diagnostics and can be attached to the support structure easily, quickly and with a high precision. The diagnostics are simply plugged into the support structure. The whole procedure is designed to be possible by remote handling.

The Remote Tile Exchange, during which the Mark IIA tile carriers will be exchanged for the Mark II Gas-box tile carriers, will be the first fully remote task undertaken on JET and the most significant fully remote handling task undertaken on any fusion device in the world. Accordingly, extensive preparations are being made for the proving of equipment function, performance and reliability together with the derivation and development of task procedures and operator training.

Interventions in the Vessel during 1995

Two short in-vessel interventions, one of which had been previously scheduled, were carried out during 1995, followed by the main shutdown to install the Mark II divertor structure.

Intervention to Repair GDC Electrodes

The unscheduled shutdown took place in February 1995 and was due to problems arising from the bending of Glow Discharge Cleaning (GDC) electrodes. This was a short four day shutdown performed in full pressurised suits and based on three shifts per day. The in-vessel radiation level at the beginning of the intervention was $130 \pm 7 \mu\text{Sv}/\text{hour}$.

The repair procedure for the GDC electrodes consisted of removing the spiral coil of the GDC electrode and reconnecting the current feed to the electrode back plate. The intervention was used to carry out some additional work including: removal from the divertor of the tip of the plasma boundary probe which had broken during a disruption; cleaning of three beryllium evaporator heads at Octants Nos. 1, 5 and 7; surveys and inspections of numerous in-vessel components; and some minor repairs to damaged diagnostics.

Intervention for Tile Exchange

The scheduled intervention took place in March 1995. The purpose of this shutdown was primarily to exchange the carbon fibre reinforced carbon (CFC) divertor tiles to beryllium tiles. An additional task was to install an antenna separator between a pair of RF antennas at Octants No. 6/7. The shutdown started on the 17 March and ended on the 12 April. It was based on three shifts per day for six days per week with work proceeding in full pressurised suits. The radiation level at the start of the shutdown was $165 \mu\text{Sv}/\text{hour}$. The installation work was performed as planned and with no unexpected problems.

Detailed in-vessel inspections revealed only relatively minor problems:

- Some ICRH antennae upper protection rails had bent towards the plasma by about 17mm;
- Ceramic discs and ceramic spacers on 18 positions out of 96 on the so-called French Horns had cracked or were missing. There was also some deposition of beryllium metal onto these ceramics. A temporary repair was carried out by removing the affected supports and refurbishing them in the J1A Beryllium Handling area;
- Several diagnostic activities were carried out during this shutdown:
 - K α 1 Lost Alpha-particle system was installed in Octant No.7 MHP;
 - RF antenna separator/rail current shunt installed;
 - Inner Wall Guard Limiter current shunts installed;

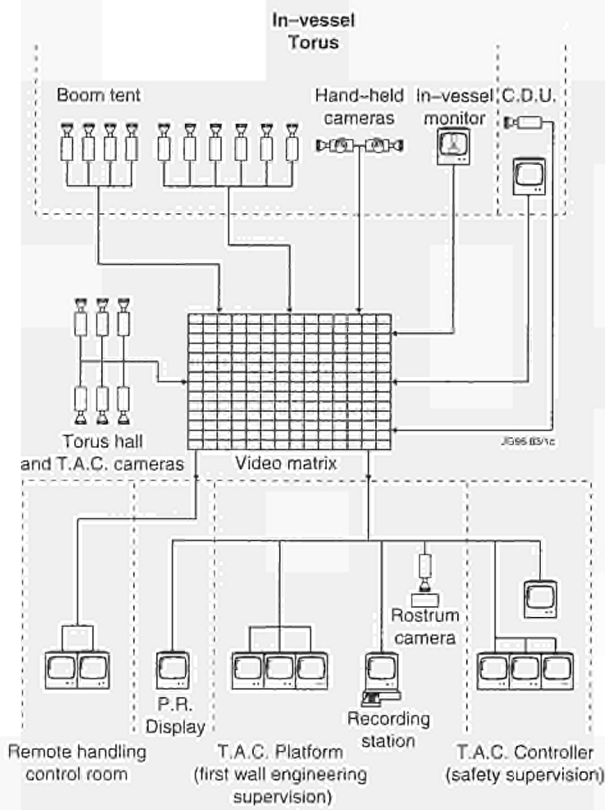


Fig.8: Video communication System between in- and ex-vessel

- KC1-D Vertical Force Flux Loop at Octant No.3 repaired;
- KE4 upper moveable mirror replaced with a smaller mirror;
- periscope mirror and LHCD periscope window cleaned of a coat of beryllium;
- KY4-D Langmuir probe replaced;
- In-Vessel Inspection System lights cleaned;
- Lower saddle coils inspected by a 6mm video scope and small pieces of aluminium foil and ceramic debris retrieved.

Shutdown for Mark II Divertor Installation

In June 1995, installation of the Mark II Divertor started. The shutdown was based on three shifts per day for six days per week with work proceeding in full pressurised suits. The radiation level at the start of the shutdown was $145\mu\text{Sv}/\text{hour}$.

All the work performed in the vessel had previously been tried in the In-Vessel Training Facility, where the workers had been trained to perform the work according to developed procedures. An important improvement was a newly developed video-communication system between in- and ex-vessel (see Fig.8). The system permits the supervision of the in-vessel work by the Responsible Officer from the obser-

vation platform outside the beryllium and radiation controlled areas. The use of an in-vessel mobile auto-focus camera with zoom control and view finder allowed inspection of welds (including inspections by the required third party inspectors) and the recording of the weld inspection on video-tape.

Additional tasks were included in the shutdown programme to improve JET performance or to address operational aspects identified during the last campaign. These included:

- Upper and Lower saddle coil systems to be stabilised and strengthened;
- Inner Wall Guard Limiters moved towards the wall to increase plasma volume;
- RF antennae removed from the vessel and refurbished. New upper and lower protection and separatrix mounted between each pair of antennae to improve performance;
- Reconfiguration of the Poloidal Limiter straight beams to improve coupling with the RF antennae;
- New fixtures for Poloidal Limiter tiles to meet RH requirements;
- Additional Shine-Through Protection Tiles and Reinforcing Ring Protection Tiles;
- Improved Gas Shields;
- Installation of new and replacement of several diagnostics inside the vessel;

To accommodate these additional activities the shutdown was extended to the end of March 1996 (initially it was planned to be completed by the end of 1995) and organised on the basis of three shifts per day for six days per week.

The success of the design, manufacturing and preparation and installation programme of the Mark II Support Structure was highlighted by the installation of the ring in the vessel which began on 30th October and proceeded according to plan ending 15 working days later. When the final in-vessel joint was made, it confirmed that the ring was correctly positioned in the vessel to better than 0.1 mm (Figs.9 and 10).

A particular feature of this shutdown was the extensive involvement of remote handling systems in the preparation and assembly operations. The Articulated Boom and special tooling were used to remove and later install many components both within and outside the torus. At the end of 1995, the shutdown was progressing well and according to schedule.

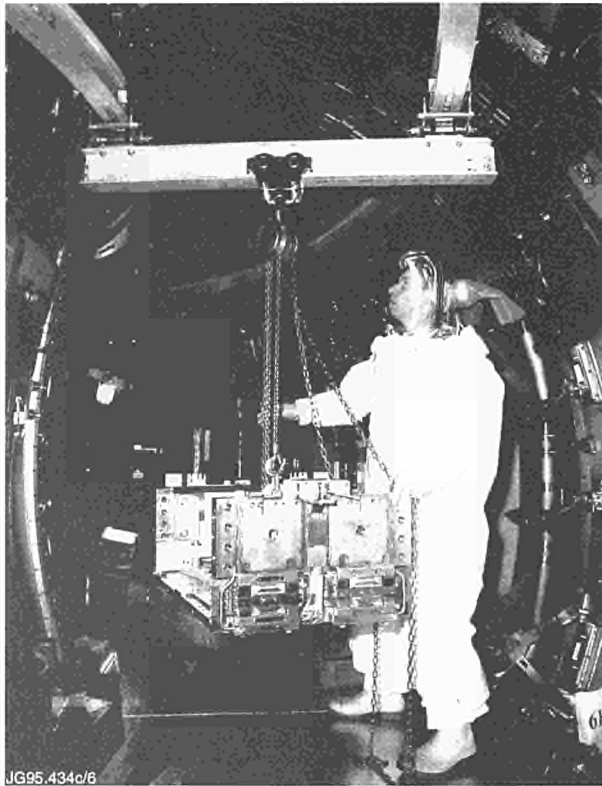


Fig.9: Mark II Support Structure being installed in the vessel

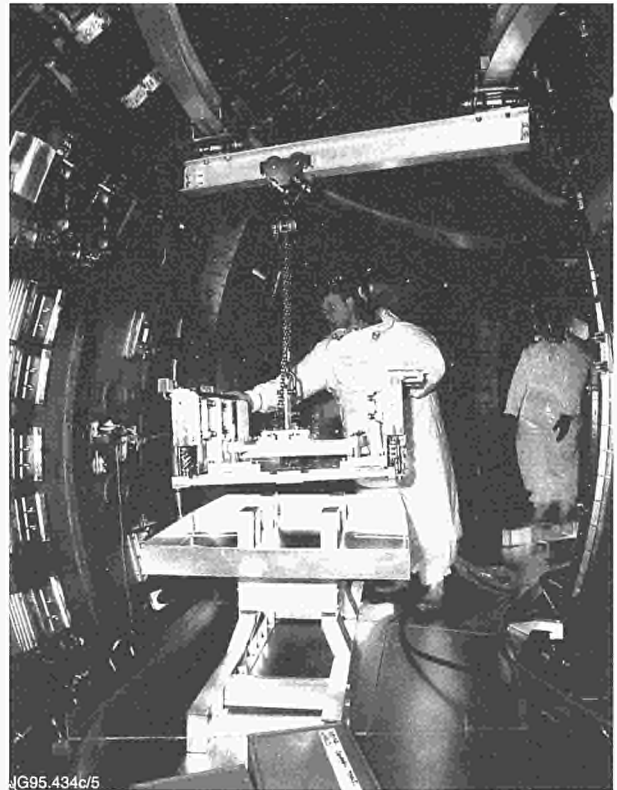


Fig.10: Mark II Support Structure being installed in the vessel

Preparation of In-Vessel Components Mark II Support Structure

The contract for the manufacture of the Mark II Support Structure was placed in 1994. The complexity and magnitude of the contract resulted in most of that year being required for the organisation of the contract, the development of the manufacturing and machining cy-

cle including the pre-assembly and final machining operations, the inspection schedules as well as production of prototypes. The actual manufacturing of the major components started in late 1994 and was completed by September 1995.

The main steps in the manufacturing cycle of the Support Structure (see Figs.11 and 12) aimed at

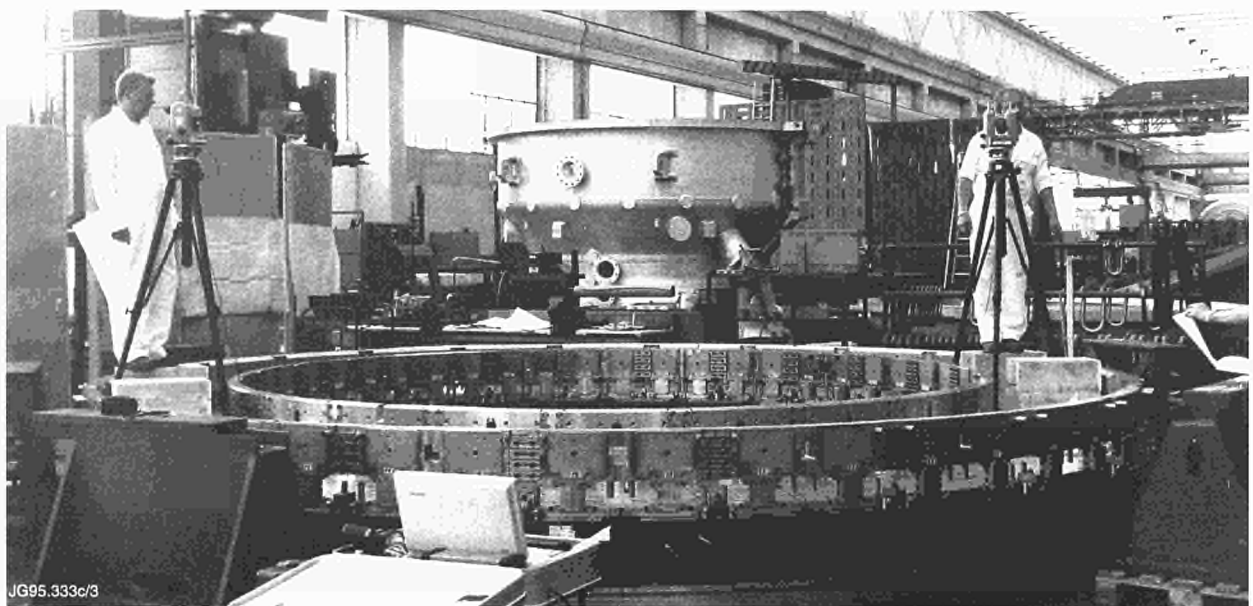


Fig.11: The Mark II Support Structure being surveyed using the Computer Aided Theodolite (CAT) system at the manufacturers

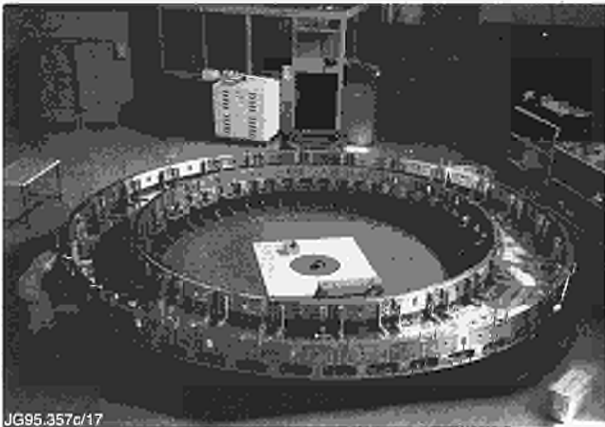


Fig.12: The completed Mark II Support Structure at the manufacturers

achieving the required geometrical accuracy and facilitating the precise in-vessel installation, can be summarised as follows:

- Machining and deep drilling 72 plates and ring sectors from solid material followed by the brazing or electron beam welding of lids to give rigidity to the structures;
- Pre-assembly of the three main parts (base plate, inner ring and outer ring) to form three closed rings each machined as one piece. A special “plateau” was produced to support and set the rings during the machining and subsequent assembly operations. Final machining of the reference rails and module joint dowel system was carried out with the modules assembled;
- Assembly of the three individual rings to form one complete circular structure on the “plateau”. After this operation, the structure was split into individual modules (24 in number) and each module was completed by fitting louvres, hinges, nozzles, etc;
- Re-assembly of the overall Mark II Support Structure using the final fasteners and dowels and following the same procedure as that developed for the actual installation into the JET vessel;
- A hot leak test was undertaken of each module.

The successful hot leak test carried out on each module confirmed the clean metallurgical structure of the Alloy-600 specially developed to produce plates and forgings able to satisfy the stringent JET requirements with regard to leak tightness and mechanical strength. The material was supplied according to JET specifications.

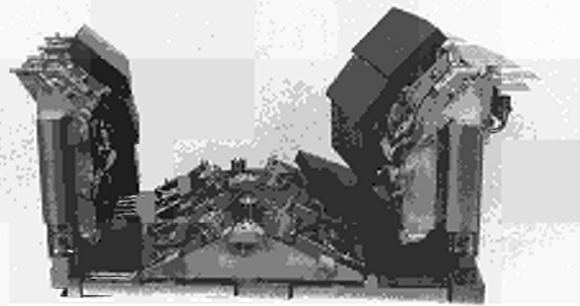


Fig.13: The Mark IIA Tile Carrier Assembly

After delivery to JET, the 24 modules passed through a preparation phase in which all the remaining features were fitted such as: the gas introduction system, the electrical grounding straps, diagnostics, the welding preparation of the water cooling pipe, the internal cabling and plug and socket system, the bump stop supports, etc..

Mark IIA Tile Carriers, Tiles and other Components

The Mark IIA Tile Carriers (Fig. 13) were completed to the high tolerance requirements of JET. Also, the 480 target tiles, later to be attached to the carriers, and which are made of carbon-carbon fibre composite material were machined to very high precision ($50\mu\text{m}$) with virtually no scrapped tiles. These tiles are carefully designed to withstand a high power load conducted by the plasma along magnetic field lines, whilst shielding all corners and edges from direct heat loading.

Additional components ready for installation in the vessel after the Mark II support structure, are the Coil I cable conduit and the Outer Protection Tile Carriers. This conduit protects a cable loom which links all the diagnostic plugs, sockets and cables to the various electrical feedthroughs. This allows for diagnostics to be plugged into the vessel by remote handling techniques. The outer tile carriers provide a protection to the transition from the divertor structure to the outer wall components.

In addition:

- a) The water cooling pipes, “French Horn”, support system were refurbished to take account of higher

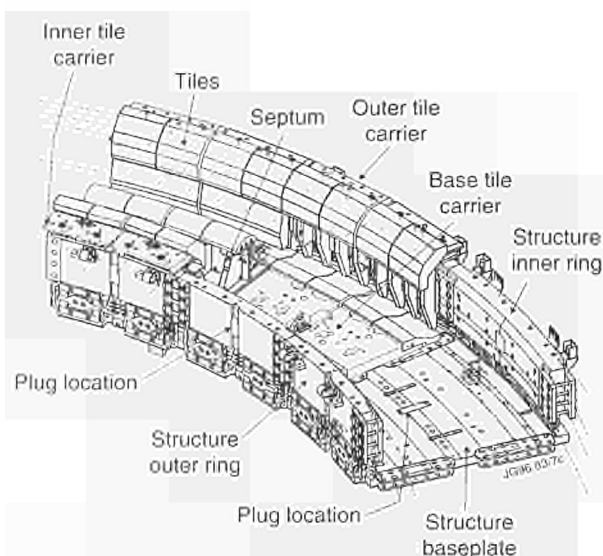


Fig.14: Model of the Mark II Gas-Box Divertor

than expected loads and to increase the insulation levels against electrical breakdown. Brackets were strengthened and ceramic components were replaced by plasma sprayed metal parts;

- b) The Inner Wall Guard Limiters (IWGL) were modified to move the top corner 35mm away from the plasma. This involved removing the top half of the beam, and manufacturing new components to support the protection tiles;
- c) The previously damaged Upper Inner Saddle Coil was modified to remove the conductors and to move the protection tiles back by 30mm to allow more space for the plasma and to blend in with the curvature of the IWGL. The Upper Outer Saddle Coil had additional brackets and tiles fitted at sector C;
- d) The Shine-through Protection was extended to cover a 25% larger area around the existing protection by fitting additional tiles, brackets and supports;
- e) The Beryllium Evaporators were modified to allow the replacement of the head by remote handling from inside the torus;
- f) The Bypass Gas Shielding around the divertor was extended to cover the open ports on the inner wall, the gap between the Coil 1 and inner support structure ring, and reduce the clearances around the Protection Carrier gas shields. This component should help to decrease the amount of gas leaking back into the plasma volume from behind the divertor target;
- g) Instrumentation has been added to a number of components to measure voltage drops along conductors with a view to estimating the corresponding induced currents. These components include the structure

modules, earth straps and saddle coil supports. Thermocouples have been attached to each structure module and carriers to monitor the bulk temperature during bake-out and operation;

- h) Braze development of Be to CuCrZr for NET/ITER was continued following the success of the InCuSil ABA induction brazing developed in Neutral Beam Division. Continuing work is aimed at the development of brazes that do not produce long lived, high activity isotopes under neutron bombardment. CuMnSn brazes have been developed which show promising results compared with the InCuSil. Further work continues to optimize the braze conditions and compositions.

The Mark II Gas-Box Divertor

The Mark II Gas-Box Divertor is the structure, which is to be installed in the Mark II support structure during the 1997 Remote Tile Exchange shutdown. 1995 saw the finalisation of the design of the Gas-Box Divertor and the ordering of the CFC material required for the tile carriers and tiles.

The novel feature of the Gas-Box Divertor is the first use of CFC material for structural purposes in JET. The primary reason for this choice of material is the relatively high heat flux ($\leq 2\text{MW/m}^2$) falling onto some structural components from the radiating gas target plasma (Fig.14).

Detailed mechanical stress calculations including 3D finite element calculations were performed, which predict adequate reserve factors for the structural CFC components. A series of experiments to test the predictions and to determine some of the uncertainties in the calculations:

- (1) the accurate value for the allowable primary stresses;
- (2) the stress-intensification factors for CFC (anisotropic) materials;
- (3) detailed nature of the contact between surfaces.

To overcome the difficulty of calculating thermal stress in CFCs and predicting the failure of the CFC components, results will be taken of material screening tests of materials exposed to high heat fluxes using the Neutral Beam Testing Facility. Typically, septum ribs of the Gas Box Divertor will take heat loads of $\leq 2\text{MW/m}^2$ and exposed areas of the side carrier ribs a flux of $\leq 8\text{MW/m}^2$.

High heat fluxes are expected to the various tiles of the gas box configuration that are not structural parts. Computations show that for a wide range of plasma parameters fluxes of up to 18MW/m^2 are expected for non-radiating divertor plasmas in the gas box. It is expected that even

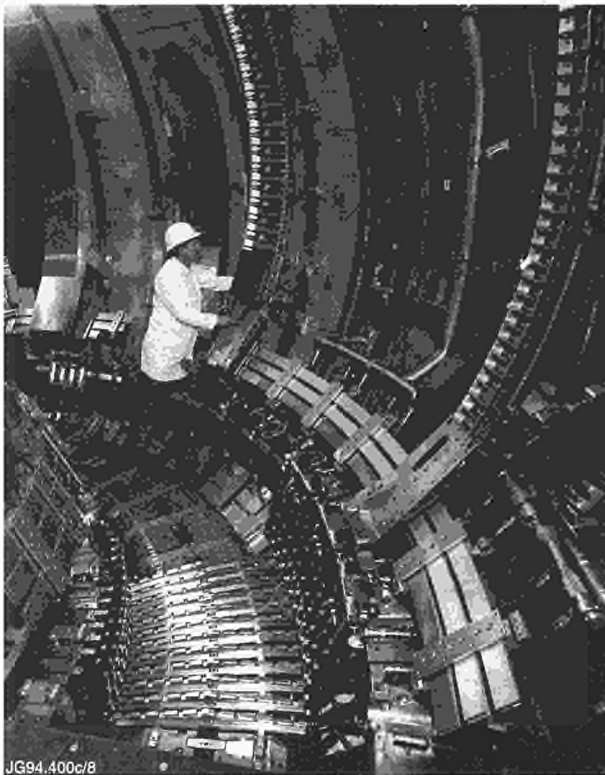


Fig.15: The In-Vessel Training Facility

for 10MW/leg total conducted power, the Gas-Box Divertor will allow 3 - 6s of operation before the surface temperature reaches 1600°C.

In-Vessel Training Facility

The In-Vessel Training Facility (see Fig.15), was continually kept up-to-date and used extensively and effectively for:

- the training of in-vessel workers;
- to develop and test all in-vessel procedures;
- to develop and test all handling and installation tools;
- to check details and interfaces of new components;
- for remote handling trials and the training of remote handling operators.

Preparations for Remote Installation of Mark II Gas-Box

Remote Handling Trials in the In-Vessel Training Facility

A full scale mock-up testing programme has started to prepare the equipment and operators for the fully remote exchange of Mark II tile carriers. The programme includes the testing and proving of the task feasibility both under normal operating conditions and under failure case conditions. This mock-up programme, executed in the In-Vessel Training Facility, has been a major part of the

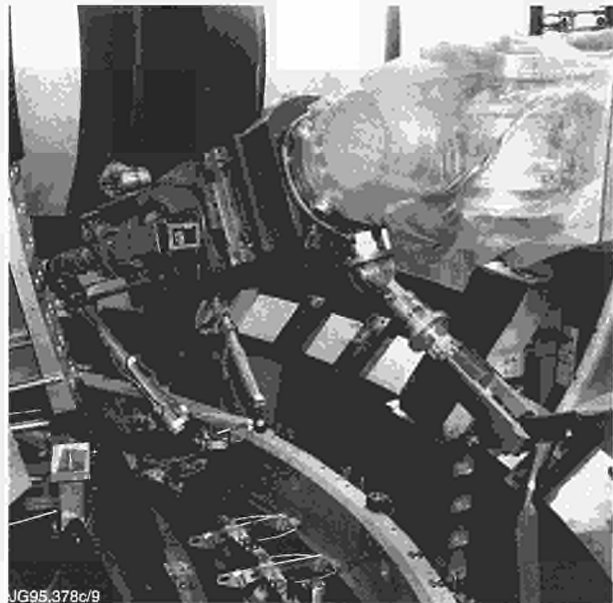


Fig.16: Boom and Mascot operating in the In-Vessel Training Facility

Remote Handling work during 1995 in preparation for the planned fully remote installation in February 1996 of 36 of the 144 Mark IIA tile carriers in the vessel during the Mark IIA Divertor Installation Shutdown.

These mock-up trials have resulted in the development of an operational procedure for the installation of all tile carriers in Octants No.5 and 6. These locations are close to where the Boom enters the torus and, therefore, present the greatest difficulty for access. The strategy for tool deployment has been proven and all of the "teach files" for the Mascot servo-manipulator positioning with the Boom have been derived and validated. Figure 16 shows the Mascot operating on the end of the Boom within the In-Vessel Training Facility

Remote Handling Equipment Reliability

The reliability and availability of Remote Handling equipment is critical to the success of any remote operation. During 1995, as a result of 1000 hour reliability trials in 1994 and the introduction of Operating and Fault Reporting procedures, modifications to remote handling equipment have been implemented. The Boom and Mascot system's availability are now continuously monitored and all RH equipment faults are formally reported, reviewed and acted upon.

A study of the worst case failure modes for the equipment to operate inside the torus was performed revealing the necessity for some minor design modifications to the Articulated Boom mechanical hardware which are now being implemented. A detailed fault tree analysis of the

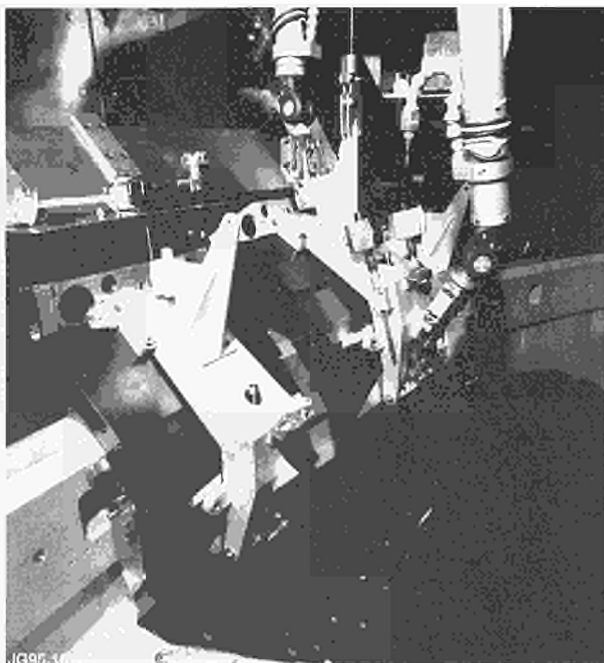


Fig.17: Mark IIA tile carrier tool attached to its carrier

Boom was derived. This has resulted in improved methods of fault detection and isolation.

Articulated Boom

The Articulated Boom was used during the Mark IIA Divertor installation shutdown to remove the RF Antennae, poloidal limiters and saddle coil sections and subsequently to install the Mark II Divertor support structure modules, poloidal limiters and RF antennae. For the remainder of 1995, the Boom was installed on the In-vessel Training Facility and operated with Mascot as part of the full size mock-up trials for remote removal of Mark IIA tile carriers.

As reported in 1994, the Boom control system can be improved by the use of torque loop feedback and it is the long term aim to implement such a control strategy. To assist with this development a full mathematical model of the control system dynamics was derived by personnel at Ecole Polytechnique Federale de Lausanne and validated at JET.

Manipulators

The Mascot IV servo-manipulator has been extensively used during the full size mock-up trials for remote removal of Mark IIA tile carriers. There have been no major modifications or problems with Mascot IV during 1995. The long term programme of work to upgrade Mascot IV to 35kg capacity per arm has continued and prototype gearboxes have been designed and procured. The new control system concept has been extensively tested and developed.



Fig.18: Remote Handling Control Room - Boom workstation

Remote Handling Special Tools

At the beginning of 1995, special tile handling tools designed and developed by the Remote Handling Group were used to remove all 4000 Mark I Divertor carbon tiles and to replace them with beryllium tiles of the same type and size. During the Divertor shutdown, special RH tools have been successfully used in-vessel and ex-vessel to cut and then weld numerous components mounted on the torus.

The fully remote replacement of Mark IIA tile carriers with Mark II Gas-Box tile carriers has required the design and development of a new suite of special handling tools. A unified concept for handling tile carriers has been derived, which applies equally to handling Mark IIA and to the Mark II Gas-Box carriers. Tooling for the Mark IIA carriers has been fully developed during 1995 and has been tested and proven by fully remote use in the full scale In-Vessel Training Facility-up programme. Figure 17 shows a Mark IIA outer tile carrier tool attached to a carrier. The tooling not only allows the lifting and manipulation of the carrier but also provides the location and alignment of adjacent carriers and acts also as a mobile carrier for wrenches. The Mark II Gas-Box tile carrier tools have been designed and will be manufactured and tested during 1996.

Remote Handling Control Room and Man-Machine Interface

The Remote Handling Control Room has been refurbished and commissioned with PC-based control stations

operating under Windows NT and communicating via Ethernet and point-to-point serial links. Figure 18 shows the overall control station for one RH activity. The control Room has been set up to facilitate the operation of three activities in parallel (e.g. in-vessel, ex-vessel and the Tile Carrier Transfer Facility operations).

The PC based control stations provide Man-Machine Interfaces (MMI) specified, designed and programmed by JET. In order to provide MMI's which are flexible for development, readily adopted and understood by operators and able to be programmed in a systematic way a wide market survey was conducted of SCADA (Supervisory, Control and Data Acquisition) software packages and have selected a software platform appropriate for our purposes. This platform is now being used to generate the new MMI for the Tile Carrier Transfer Facility and will eventually be used for all other MMIs.

All remote handling operations are supported by extensive use of a computer generated real-time 3-D display of the task environment. These virtual reality displays are created by the KISMET software package provided by the Kernforschungsanlage Karlsruhe, Germany, and are installed on Silicon Graphics workstations. During 1995, there was extensive effort to create a detailed and accurate KISMET representation of the in-vessel environment using the JET configuration control reference models stored in the Drawing Office CATIA system

Remote Handling Viewing System

To obtain a general view of remote handling in-vessel operations, it had been intended to deploy the In Vessel Inspection System (IVIS) viewing probes. These probes are designed and are very effective for inspecting the torus under vacuum and high temperature conditions. However, the mock-up tests found the system not to be suitable for operational purposes during remote handling procedures. Accordingly a new system comprising four colour cameras mounted on pan/tilt heads with zoom and other optic controls was devised, tested and found acceptable. Each unit is housed within a contamination protective dome and will be deployed by the Mascot at the start of the intended in-vessel operations.

Miniature cameras attached to the Mascot wrist by flexible mounts have proven invaluable during the task In-Vessel Training Facility-up trials and these cameras have now been fully integrated into the Remote Handling viewing system.

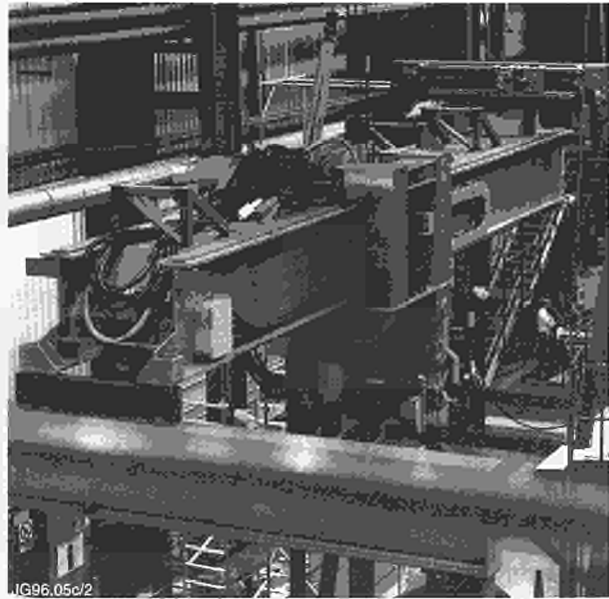


Fig.19: Short Boom in the Assembly Hall

Remote Handling Tile Carrier Transfer Facility

The Remote Tile Exchange concept requires the transfer of tile carriers and tools into and from the torus through the Octant No.1 main horizontal port. This transfer task and the placing of tile carriers in a transport container is to be undertaken fully remotely by means of a new Tile Carrier Transfer Facility which will be installed and operated at Octant No.1. The facility comprises a so called Short Boom with an end-effector and tools housed within a sealed enclosure for contamination control but with interface doors for man-access and tile carrier storage/transfer containers. Figure 19 shows the Short Boom which was manufactured and delivered during 1995.

The contamination control enclosure and the end-effector have been designed in detail and are being assembled to be ready for commissioning and testing in the Torus Hall during 1996. The control system has been designed and is now being manufactured.

Power Supplies and Magnet Systems

The purpose of the JET electromagnetic system is to establish, maintain and control the tokamak magnetic configuration (Fig.20). It includes: the toroidal coils, which establish the toroidal magnetic field; the poloidal coils P1, acting as primary winding of the tokamak transformer, the coils P2, P3 and P4 to control plasma radial position, vertical position and shape; and the divertor

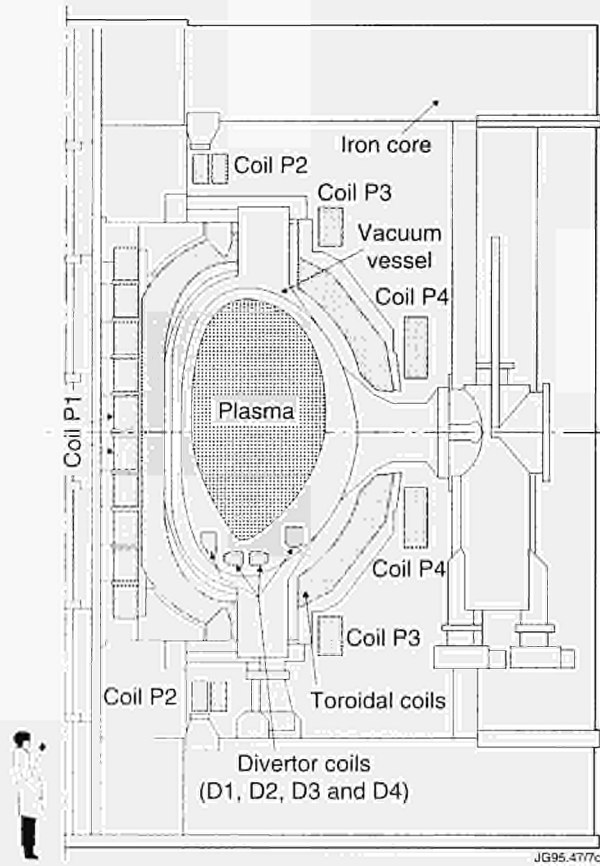


Fig.20: Cross-section showing the toroidal, poloidal and divertor coils.

coils D1, D2, D3, D4, to establish and control the divertor configuration. The shell mechanical structure resists the large forces generated by the interaction of the currents in the toroidal coils and the poloidal magnetic fields. To perform their functions, the coils are energised by suitable power supplies. Voltages and currents of the poloidal coils are controlled in real-time by the plasma position and current control (PPCC) system. Other DC power supplies energise the neutral beam injectors (NB) and ion cyclotron radio frequency (ICRF) systems for plasma heating, and the lower hybrid current drive (LHCD) system for plasma current profile control.

The total installed DC power exceeds 1500MVA, capable of delivering a peak power above 1000MW and an energy per pulse above 10,000MJ. More than half of the power and of the energy is taken directly from the UK National Grid at 400kV, while the rest is provided by two vertical shaft flywheel generators. Consequently, a major feature of JET is the 400kV-36kV distribution system. Auxiliary AC power is supplied by the 20MVA, 11kV/3.3kV/415V distribution system.

The activities of the first half of 1995 were focussed on the operation of these systems to meet the requirements of

the experimental programme. New operating scenarios were assessed and implemented in the new Mark I divertor configuration. The second half of 1995, was devoted to shutdown activities, including maintenance and repairs, upgrading of existing systems and implementation of new systems, as determined by operational experience.

Plasma instabilities, leading to fast plasma vertical displacement events (VDE's) usually followed by plasma disruptions, can generate large forces on the vacuum vessel and on in-vessel components. It had always been assumed that these forces were toroidally symmetric, and so the main concern were the total forces on the vessel. In June 1994, in early operation with the pumped divertor (Mark I), that toroidal asymmetries of the force distribution were clearly noticed. A year later, a new topology of such forces was seen, leading to sideways movements of the vessel of several millimetres. These events were detailed due to the existing extended machine instrumentation.

These events, raised additional concern on the integrity of the machine and on the design of a tokamak fusion reactor, such as ITER. Measurements were performed on other machines around the world in similar divertor configurations and the asymmetric behaviour of forces and vessel movements were confirmed. It is believed that the main contribution to these asymmetries is linked with non-uniform distribution of halo currents. While the plasma behaviour leading to these phenomena is not clearly understood, ITER designers are now taking these new events into consideration to substantially modify the design of the vacuum vessel (compared with the Interim Design Report delivered in June 1995). JET has dedicated a substantial amount of work during 1995 to perform engineering analysis on the electromechanical system, to the design new vessel supports and to the upgrading of the machine instrumentation and of the machine protection system.

In view of the impending extension of the JET Joint Undertaking to the end of 1999, studies have been initiated of possible extensions of the performance capability of the machine: these are an increase in toroidal field to 4T for ~10s; and a power enhancement of the heating systems (both ICRF and NBI). Studies were undertaken in the second half of 1995 in these two areas, both requiring new power supplies. In addition, for the proposed toroidal magnetic field enhancement to 4T, extensive structural analysis work has been performed to support the case.

Magnet System

Maintenance and Installation

The installation of the TF ripple bus-bars from Building J1P, through the Basement to the Torus Hall to re-connect the TF power supplies to the TF coils, started in late-1994, and was completed by February 1995. This allowed the ripple experiment to be performed toward the end of the 1995 campaign.

In view of the DTE1 programme, it was decided to replace all the Rafx quick release water connectors on coils P1 and P2 by screwed connectors, as these would be more reliable. All parts have been ordered for the modifications to Coil P1 but for Coil P2 a suitable welding technique to attach the new couplings must be established.

The number of turns on the poloidal coils (P2 and P3) are regularly changed to enable different plasma shapes to be achieved. These turn changes are made at link boards mounted on the magnetic circuit limbs and also on the coils themselves. It had been recognized that turn changes during operating sessions cannot be avoided during DTE1 and radiation levels at the coils are expected to be too high for convenient access. In fact, turn changes need to be performed immediately, without waiting a week or more to see the radiation level decay to acceptable level for hands-on intervention in the Torus Hall. Therefore, new bus-bars have been designed to enable Coil P2 turns to be changed at new link boards in the Basement and Coil P3 turns to be changed at existing link boards in the Torus Hall. The radiation levels at these link boards will be low.

The inductance of all 32 toroidal field (TF) coils is routinely measured at the beginning and end of each shutdown to detect inter-turn faults. The inductance measurements, performed at the start of the 1995 shutdown showed no problems, i.e. the measurement confirmed that no electrical faults were present in the coils. These measurements will be repeated before operation is resumed.

Machine Instrumentation and Protections

Although JET is already considered a well instrumented machine, engineering experience gained in the 1994-95 campaign, on such new phenomena as toroidal asymmetries of vessel forces and forces higher than expected in some in-vessel components, suggested the addition of further instrumentation on the machine for monitoring and protection.

Divertor Coils In-vessel Instrumentation

The following divertor in-vessel instrumentation was installed during the year:

- Rogowski coils on D1, D2, D3 and D4: designed to measure the coil ampere-turns. The Rogowski coils are helically wound cable in stainless steel cases and will be used for coil protection;
- Thermocouples on D2, D3 and D4 clamps (5 off): intended to assist evaluation of thermal conditions in the new divertor configuration;
- Vertical flux loops on D1 and D4: to enable the radial forces on D1 and D4 to be measured. Vertical flux loops are already installed on coils D2 and D3 for magnetic diagnosis and will be used for force calculation;
- Radial flux loop on D4: to replace a loop on Coil D4 which failed. In the original divertor installation radial flux loops were installed on all coils to calculate vertical forces.

Improved Coil Protection System (CPS)

In 1995, the main objective was to rationalise and improve the magnet protection system. This consisted of mainly hardwired protection installed over the years and of the relatively new CPS software system. Hardwired systems are therefore being progressively transferred to CPS to avoid duplication and enable better processing and flexibility. The hardwired systems will be maintained until the new systems are fully operational.

Protection systems transferred to CPS during the 1995 shutdown include TF transverse force protection, TF ampere-turn protection (Rogowski), over-current and I^2t protection for all magnet circuits and earth leakage protection. New coil protection algorithms are also being introduced. To carry the increased load, new signal processing electronics and a new CPU are being installed. A CPS development system for testing new software has been built.

Improved Machine Diagnostics

New vacuum vessel measurements are required to diagnose newly discovered vessel movements. The following improvements are underway:

- New displacement measurements at the following vacuum vessel ports: inner, intermediate, main vertical and main horizontal ports;
- Acceleration and force measurements at main horizontal ports;
- Improved processing of vacuum vessel vertical restraint forces.

This increase in signals has necessitated a new cubicle in Building J1D, incorporating similar processors to CPS.

Magnet Power Supplies

Disruption Feedback Amplifier

Due to the damaged upper saddle coils, the Disruption Feedback Amplifiers were used on the lower saddle coils only. Full performance was obtained with the amplifiers on these coils but without plasma or toroidal field. In the presence of plasma, the maximum current could not be applied as the forces on the coils would be excessive if subjected to a disruption. The maximum current obtained with plasma was 2.5kA for 0.5s.

Saddle Coil Crowbar

The crowbars were designed to short-circuit the saddle coils in the presence of disruptions or of internal faults in the coils. During early operation, the current measured in the crowbar reached values of 6kA during disruptions. However, the damage seen in the lower saddle coils would need induced currents during disruptive events larger than 10kA. These currents are not dangerous for the crowbar but the same current is flowing in the saddle coil. This current combined with the magnetic field resulted in excessive forces being applied to the coils. Simulations showed that by introducing a resistor of 100-200m Ω in series with the crowbar, the current would be limited to acceptable levels while the increase of the voltage against ground remained within the isolation test levels of the coils. Resistors of 100m Ω were installed, and operation continued with this configuration for the remainder of the operational period.

Additional Heating Power Supplies

The additional heating power supply systems include neutral beam, ion cyclotron radio frequency and lower hybrid power supplies, and there are also discharge cleaning power supplies.

Neutral Beam Power Supplies

Although the Neutral Beam Power Supplies now operate most reliably the need for improvements, although minor, remains and some were implemented during 1995:

- At the start of 1995 an additional protection circuit was added to the Grid I protection systems. This circuit compares the voltages of two different voltage dividers and terminates the pulse if the difference is more than a predetermined value. In this way, a complete new protection for the output voltage was implemented. It acts as if a different voltage divider

was used for the protection and for measurement and control circuits;

- There was a drift and an offset in the measurement and control chain. For this reason, potentiometers were changed by fixed resistors. Older type resistors have been changed with more accurate and stable ones;
- During the campaign, some instabilities were observed during voltage ramp-up. The complete control loop modifications were simulated and implemented, first in the testbed for checking and testing, and subsequently on all protection systems;
- A new monitoring system is being installed for the filaments of the ion sources. The original system only monitored for open-circuit. However, the more dangerous fault is a short-circuit between the filament and the ion source bucket. The new circuit incorporates the monitoring function for both possible faults;
- Occasional voltage dips were experienced in the rectifier output voltage for the Grid I power supply at the start of the pulse. When this occurred, the voltage across the regulating tetrode became too low and the pulse was terminated. Recent measurements on the PINI and the ion dump have shown that the original specifications can be relaxed, i.e. a voltage dip of 15% for 50ms is allowed in the PINI voltage at the start of the pulse. Testing of a new circuit which incorporates the allowance for a 15% dip is now in progress. This will eliminate the cause of premature pulse termination, leading to more reliable operation of the system.
- During the shutdown, all protection systems are being tested on dummy load, the calibration and control loops are checked up to full performance. The SF6 towers were opened and checked, a few connectors were replaced. The pressure relief valves on the SF6 towers were moved from Building J1H to the Basement in preparation of the DTE experiment. A pressure monitoring system was installed between the two bursting disks; this will give an early indication of any problem with the bursting disk nearest to the SF6 tower.

Ion Cyclotron Resonance Frequency Heating Power Supply

The ICRF power supplies continue to operate without major problems. Routine maintenance is performed at regular intervals. The power supplies are used during operation with the RF generator connected to the antenna and during the shutdown with the RF generator connected

Table III - Expenditures on Electricity in 1995

	Units (kWh)	ECU/ kWh ⁽¹⁾	ECU ⁽²⁾
National Grid ⁽³⁾	-	-	119,273
National Power	10,558,580	0.056	552,449
Southern Electric	31,511,380	0.053	1,680,452
AEA Culham	4,291,585	0.053	227,692

(1) average unit cost including all charges

(2) including all other charges in addition to the unit charge (kWh) (1 ECU = £0.8488)

(3) connection charges

to a dummy load. As far as the power supplies are concerned, both operational modes are similar, so that these supplies are operated almost continually.

Lower Hybrid Current Drive Power Supplies

Operation of these power supplies is following similar lines as the ICRF power supplies. These are used either with the klystrons connected to the launcher or to the dummy load almost on a continual basis. Routine maintenance is performed at regular intervals but no major changes have been necessary since their early commissioning.

Glow Discharge Cleaning Power Supply

The Glow Discharge Cleaning Power Supply was used extensively during operation, for the cleaning the vessel wall. At the start, cleaning was only carried out at low voltage (300V) and low current (2A). Later, some experiments were undertaken to check the cleaning efficiency at higher voltages (600V). At these voltages, instabilities on the current and the voltage were observed. Consequently, the control loop in the power supply was modified after which operation at high voltage was possible without further problems.

Power Distribution

No major installations at 33kV and/or at 11kV were foreseen in 1995. Therefore, work mainly dealt with design, construction and installation of new plants at 415V, repairs/modification and routine maintenance.

Service, Design and Installation Work

Electrical supplies at 415V were provided for the new Health Physics Laboratory, the Beryllium Handling Facility, the Metallurgy Laboratory, the In-vessel Electrical Distribution, and the TAC. Other important jobs were

the re-location of the 300kVA Cryogenic Section Board, the IVIS Control cubicles and the installation of a 60kVA UPS in Building J1S. In addition, there were a large number of 'minor' installations, for a total number of 500 jobs. Most of them were concerned with cable installation: about 70km of cables of various functions and size were installed during the shutdown.

In preparation for DTE1, an accurate revision of cable blocking in all Basement and torus cable penetrations, to allow adequate radiation shielding, has been an important task associated with cable pulling.

Design Work

A large number of New Projects have been implemented during 1995, and have required extensive design work. Significant examples were:

- PDFA Power Filters: design of the layout, including forced air cooled resistors, tuned filter assembly, control and instrumentation and support steel structure;
- PVFA System: design of snubber assembly, repositioning of DCCT's, modification of dummy load;
- Study for TF Enhancement to 4T: design of the civil work for the new transformer assembly;
- Study for NB Enhancement: design of power supplies schematics and plant layout.

Maintenance

In addition to the shutdown routine maintenance, the following main maintenance tasks were performed:

- Overhauling of the three 400kV-300MVA (pulse) transformers, including the automatic tap changer, the test of oil samples and the test of the fibre optic links;
- Overhauling the 3.3kV and the 36kV distribution systems, including HV cubicles, switchgear and cable terminations;
- Complete servicing and oil testing of three 36kV/415V/3.5MVA transformers for the PINI auxiliary power supplies.

Supply of Electricity

Electricity is supplied to JET at 400kV (main tokamak DC pulsed loads) and at 11kV (AC auxiliary loads), by means of four contracts: with National Grid and with National Power for the supply at 400kV, Southern Electricity and Culham for the supply at 11kV (the latter is used as a back-up during maintenance or failures of the JET 132kV/11kV Substation). The bills for the supply of electricity in 1995 are shown

in Table III. (It should be noted that the first six months only were operational months).

Machine Services

Some major modifications in the cooling system have taken place during the 1995/96 shutdown, with particular relevance to the safety and reliability for the D-T operation.

The PF-TF Water-Freon Management System Re-build

The system controls all the main sequence of operations, encompassing and backing the operation of most systems cooling loops, and coordinating their protections.

The system has been re-built, and relocated. The 15 year old electronics including the PLC were replaced. The system interface to CISS (Central Interlock Safety System) was also changed to meet safety requirements for the D-T phase, and the control enhanced to include new remotely controlled isolation valves. The cubicles, previously located in the Basement plant-room, where access during the D-T phase would be severely restricted, were moved to a new location in the 6MW Chiller building. This entailed wiring the cubicles to the plant via new cables. The re-build was completed in December 1995.

Remote Isolation Enhancement

The PF system was enhanced by fitting pneumatic actuators to the isolation valves of the cooling loops of the PF system. Twenty valves, which were up to the previous period of operation of manual type, have been modified to be remotely operated, and also five new isolation valves were fitted into the system for the same purpose. The isolation of any of these loops, in case of leaks or any other reasons, could be easily performed without requiring access to restricted areas, and they will be controlled via the PF-TF management cubicles.

TF Pumps Magnetic Drive Modifications

The TF Freon motor pumps have been modified to include a seal-less magnet drive coupler. In the past, the pump seal was a hydraulic oil seal and this caused some problems as in various instances oil would be lost in the freon, or freon would diffuse in the oil in some quantities. This problem must be addressed prior to the active D-T phase.

The magnetic drive coupling intrinsically seals the pumped fluid from the surroundings, and does not require a seal between impeller shaft and volute case of the

pumps. However, it requires internal cooling for the shroud interposed between the magnet connected to the motor, and the magnet connected to the impeller shaft, as it is subjected to eddy currents. This was already a feature of the Divertor Freon pumps, but these are of considerably smaller size and of standard production. The magnet coupling drive for the TF pumps had to be especially designed as a retrofitting on the existing pump, due to their unusual large size and flow/pressure characteristic curve.

The development had to overcome problems related to the ceramic bearings. The silicon-carbide bearings had to be changed during the development, while the shaft bearings were changed to tungsten-carbide. Different cooling paths for the internal cooling were also tested to achieve the required flow. Following the modifications on all the three pumps, tests were carried out on the freon system at JET in August and October. All the tests were successful. Flowmeters and thermocouples and instrumentation of the pumps internal cooling were also wired to the new cubicle.

Sampling of Cooling Fluids

Four sampling boxes were installed, to allow the simple retrieval of samples of PF and PINIs, Octant Nos. 4 and 8, water, and the TF-Divertor freon. This allows the monitoring of the progressive activation of the freon and contamination by tritium in the demineralised water, during the active D-T phase.

The system relies on a sequence of automated valves and on a trickle flow of the fluid through the sampling box. This avoids draining dead legs in the circuit where the validity of the sample would be doubtful, and it will be simple and safe.

In-vessel Components Drained Water Tank

A new holding tank (of ~4m³) has been installed in the Basement South Trench. This will hold the water drained under any circumstances, including protection activated drain, and water of in-vessel cooled components, according to the requirements for the active phase. This will allow sampling of the water before being discharged through the Waste Management active drain. Routed to this tank are also the drains of the PINI and NIB systems, under controlled discharge, and the SF6 tower bursting disk and pressure relief exhaust. The SF6, which would also become activated during the D-T phase, if released,

would then be directly routed, through the tank vent, to the environmental stack and discharged, without contaminating the Basement.

Nitrogen Gas Distribution Enhancement

The nitrogen gas distribution system consists essentially of two lines, one at 4barsg and the other at 1.3barsg supplying a number of users. In the past, it was not possible to isolate the line to each user, nor was it possible to account for the gas usage.

In the shutdown, isolation valves and gas mass flowmeters were fitted to each of the six user lines and, a new line has been installed dedicated to the venting of the vacuum vessel. A new cubicle, located in the West Wing, was built for the instrumentation electronics and interface to CODAS. This will allow remote monitoring, from the Building J2 Control Room, of the status of the distribution, detection and assessment of leaks or malfunctions. A new hardwired low pressure protection, for the venting of the vessel, has also been installed, set to close the pertinent flow valve.

Engineering Analysis

With the installation of the single-null pumped divertor, JET became even less symmetric (above and below the mid-plane of the machine). In addition, the experimental programme required a large variety of scenarios to optimise physics performance. Therefore, more emphasis was given to the engineering analysis.

Engineering Aspects of 1994/95 Operations

A specific objective of the engineering analysis of operation work is to study the plasma instability and disruption effects and their mechanical consequences, to assess the reliability of the machine in the light of higher performance.

New problems were encountered during divertor operation:

- The vertical position of the plasma is more difficult to stabilise, mainly due to the smaller plasma size and the resulting reduction of passive stabilisation by wall currents, but also due to the fact that larger equilibrium field gradients are needed for the desired divertor configurations;
- The magnetic configuration with single X-point is strongly up/down asymmetric. As a consequence, rapid disturbances like giant ELMs and giant sawtooth

relaxations often led to loss of stabilisation so that the plasma moved vertically by typically 1m before disrupting. This kind of VDE can cause particularly large dynamic vertical forces at the torus. Forces up to about 8MN had been anticipated during divertor design for an upward VDE of a strongly elongated 6 MA plasma;

- The new in-vessel components are exposed to eddy and halo current loads, arising from fast plasma current variations during the energy quench and the current quench and from VDEs. In some cases, these loads were higher than expected and caused damage to some of these components. The non-uniformity of halo currents may have enhanced local forces;
- During 1995, a new and unexpected disruption-related phenomenon was observed and measured for the first time. This was the sideways displacement of the whole vacuum vessel (i.e. is a lateral movement in the horizontal plane). Many previous disruptions have been re-examined, including 'pre-divertor' operation, and some similar, although less significant, events have been found. In JET (and in other tokamaks), the existence of small deviations of the mechanical response of the vessel and of the magnetic measurements during disruption from the assumed toroidal symmetry has been accepted for long time, but this latest finding highlights a completely new aspect of the non-symmetric behaviour of plasma induced currents and forces. Pulse No. 34078, with plasma current 3.5 MA, resulting in a vertical instability/disruption, is a typical example. It shows both the trend of the global axisymmetric parameters and also the largest recorded sideways displacement of the vessel. This was an average displacement of 5.6mm (in the direction from Octant No. 5 to Octant No. 1) accompanied by a force reaction at the MVP in the same direction of ~550kN. Taking into account the dynamic effect of the huge mass of the vessel, this meant that a horizontal pulse of more than one hundred tonnes must have been applied to the structure. The typical trends of the plasma current I_p , the displacements of its centroid and the total vertical force measured at the vessel supports are shown in Fig.21. This total force does not directly represent the electromagnetic forces acting on the vessel, but indicates the effect of these forces through the dynamic response of the vessel, (ie, the inertial and constraint spring effect).

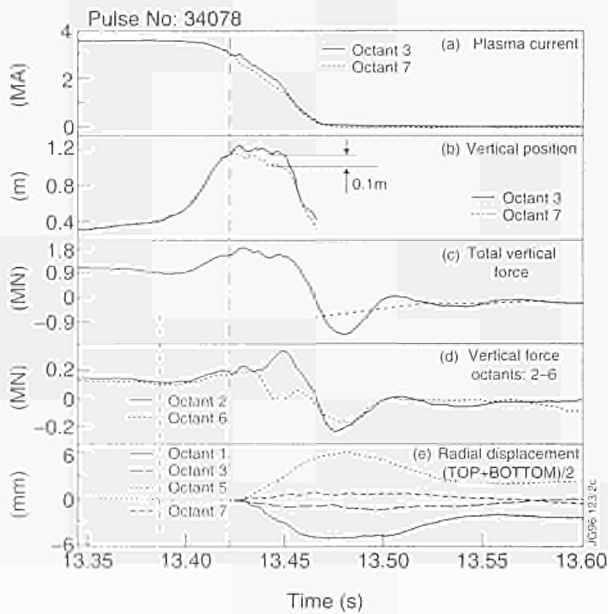


Fig.21: Vertical Displacement Event (VDE) and description of Pulse No. 34078.

These events have been observed due to the extended measurements available on vessel displacement and forces.

Analysis of Forces and Stresses on the Vacuum Vessel

To evaluate the dynamic stresses associated with these phenomena, a large F.E. shell model, representing 180° of the torus, has been obtained by mirroring and rotating the existing half-octant model, and includes 120,000 degrees of freedom.

The model has been used to evaluate the stresses on the vessel during the VDE of Pulse No. 34078. At the time of peak displacement, when the support reaction equilibrates dynamically the inertia forces on the vacuum vessel, the most stressed area at the Main Vertical Ports (MVP) is the corner at the base of the port, with a Von Mises stress of about 90MPa, well below the yield limit of 240MPa. The effects of this new load on the machine do not add to those of the more usual axisymmetrical “rocking” motion, which happens in a different location and on a faster timescale. On the Main Horizontal Ports (MHP), the maximum stress of 140MPa (yield limit 240MPa) was found to be at the base of the ports (Fig.22).

The analysis has been repeated with the revised vessel dynamic supports. The results indicate that the extent of the sideways motions, as well as the magnitude of the peak stress at the base of the MVPs, would be reduced by a factor of 3 (i.e. to 30MPa (Fig.23)). Instead the stresses at the base of the MHP would be reduced from 140MPa to 100MPa.

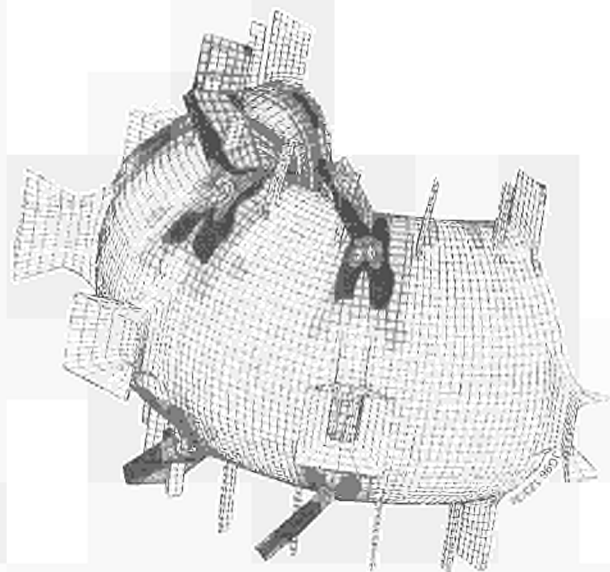


Fig.22: Stress distribution in the vessel for Pulse No. 34078.

New Dynamic Supports of Vacuum Vessel

Even if the stress level on the structure in the worst case recorded so far appears to be low, it should be noted that the conditions needed for a sideways event to happen are not fully understood and no scaling laws are available to forecast its magnitude in future operations. Moreover, the real danger represented by a large sideways displacement is likely to lie in the possibility of hammering or pulling off of some of the myriad of components connected to the vessel or, even worse, of crashing one of the vertical ports against the mechanical structure. Therefore, to ensure the safety of operations it has been decided to review the design of the vertical brakes, the MVP dampers and to implement a new set of vessel restraints, specifically designed to limit sideways motions.

It is expected that the implementation of the above measures will reduce the extent of sideways motions, as well as the magnitude of the peak stresses at the MVP, in excess of a factor of 3. The vessel is restrained in toroidal direction by the struts connected to the MVPs and by the NB injectors, through the rotary valve cases. To avoid damage to this structure, new hydraulic supports on the MHP’s have been designed and are being manufactured. These should absorb most of the horizontal load, causing the stresses to be distributed much more uniformly across each Octant.

In-vessel Components

During the early part of the 1994/95 campaign, some in-vessel components had proven to be unable to withstand the forces generated by VDE’s events. Although, the

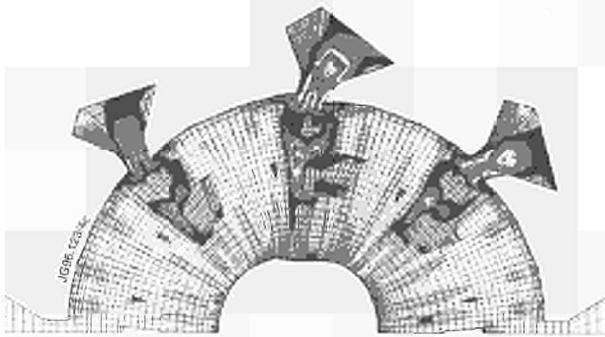


Fig.23: Stress distribution with revised vessel supports.

reasons for these events is not completely understood the engineering analysis supported by field measurements during plasma operation, allowed appropriate remedial action to be taken to avoid such occurrences in future operations. These weaknesses did not show in the main body of the first wall structure and, in particular in the divertor structure.

- The failure of the saddle coils in September 1994 only affected the upper ones, which were disabled (Fig.24). A detailed analysis of their mechanical behaviour has been carried out by means of a FE model. Induced current pulses of about 15kA lasting for a few milliseconds, would be sufficient to cause substantial permanent deformations of the L-shaped joint of the coil bars. Further analysis showed that the most stressed sections of the coils were at the brackets clamping the bottom of the vertical links to the outer wall of the vessel, and the cantilevered L-shaped horizontal bars; the whole assembly of the vertical bars, however, was dangerously floppy because of the very low stiffness of the laminated links between segments. The analysis of oscillatory modes indicated the presence of several resonating frequencies in the desired operating range, up to about 1kHz. The mechanical response to the harmonic loading during normal operations would be very high, owing especially to the low level of structural damping (about 5%, as confirmed by experimental tests on a mock-up), and this would imply a reduction of the operating current from the nominal 3kA down to 0.5kA in some frequency ranges. To improve the situation, it was decided to strengthen the coils, replacing the cantilevered horizontal bars of Inconel 600 with much stronger Inconel 625 parts. With these modifications, it has been assessed that it is safe to operate the coils with a much less severe current limitation (1kA up to ~1kHz). In addition,

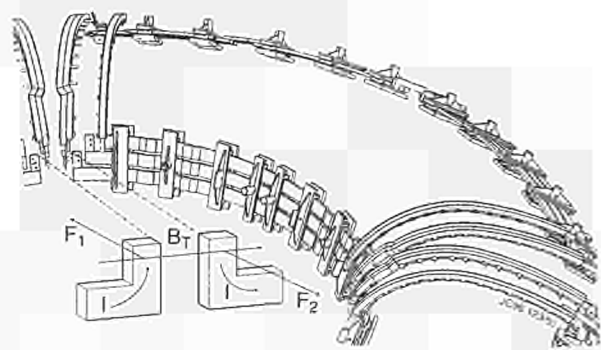


Fig.24: Upper saddle coils (partial view).

100mW resistors have been installed in the circuit to limit the value of induced currents during VDE events to a safe value of 6kA.

- Two of the four beryllium evaporator heads were damaged in November 1994. The design has been modified, primarily to allow servicing by remote handling techniques and the mechanical strength of the heads has been increased substantially by increasing the thickness of the supporting CFC tube and by reducing the length of the slots. Moreover slots have been introduced in the beryllium head to reduce induced currents (Fig.25);
- The French Horn pipes, part of the cooling circuit of the divertor support structure, did not fail but were considered to be relatively weak. The horn supports have been strengthened so as to allow them to withstand the forces up to an induced current of ~1kA (twice the maximum value measured in the previous campaign);
- Appropriate design modifications have been made on the structure of other in vessel components that failed during the 1994/95 campaign. It has been shown that the glow discharge cleaning electrodes would work even without RF assistance by means of the (weak) spiral rod attached to the electrode plate. Thus, all spiral rods have been removed. The top rails of the RF

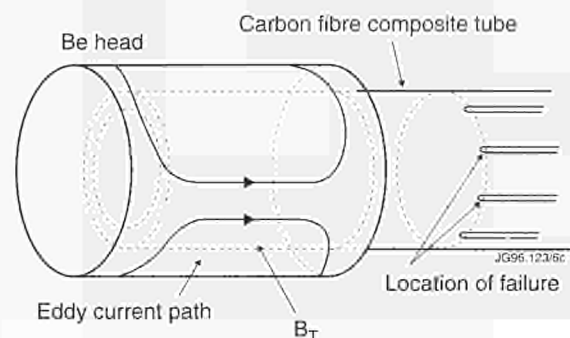


Fig.25: Beryllium evaporator head.

antennae have been replaced and bump limiters have been installed. Finally the reciprocating probe has been replaced with a boron nitride one, which has a very good thermal shock resistance;

- In 1995, a new template for technical documentation was introduced (TCD-IVA Technical Control Document - In Vessel component Assessment). The aim of this document is to formalise the analysis of any component installed inside the machine, with the purpose of evaluating its electro-mechanical performance and permissible operating range. Any TCD-IVA highlights clearly the list of physics and engineering assumptions considered in the calculation (which often are critical to reach reasonable conclusions), as well as the list of Responsible Officers for the assessment. So far, a few dozen components have been covered by a TCD-IVA document, including diagnostics (reciprocating probe head, IVIS probe), parts of the divertor (like the Mark II module-vessel junctions) and other major components; extensive work for example, has been undertaken on the lower saddle coils and on the modified poloidal limiters.

Machine Instrumentation

Analysis of the events of the the 1994/95 campaign suggested that more instrumentation was needed on the machine for a better understanding of the effects of these events on the vacuum vessel structure and for machine protection. Unfortunately, there is no access to the vacuum vessel main body. Therefore, the new instrumentation, with few exceptions, is mainly related to the vessel ports and to the in-vessel components.

The instrumentation of the torus and of the TF and PF coils comprises about 950 signals in the Mark I phase and about 1220 signals in the Mark II phase. Of particular interest are measurements of halo currents. During the Mark I phase, the top/bottom toroidal field difference could not be used to derive the total poloidal halo current as currents in the target obscured the evaluation. A TF probe has now been installed above the target base plate in Octant No.4 so that an evaluation of the total halo current should be possible. Moreover, poloidal currents in the target can now be derived from the top/bottom TF differences at Octant Nos.3 and 7 after correction by the current in the target plate.

Neutral Beam Heating

Overview

During 1995, the Neutral Beam Heating system and other associated systems again played a fundamental and successful role in the JET Programme.

The Operations and Cryogenics groups had an intense operational campaign up to mid-June followed by the shutdown during which extensive maintenance and improvement activities were carried out. During the operational campaign, the injectors performed with high reliability and availability (at the 90% level in each case). The large injector cryopumps were routinely operated with close to 100% reliability and the new Pumped Divertor (PD) and LHCD cryopumps were also most reliable.

The Engineering Group had a heavy commitment in the shutdown period, procuring and installing new Inertial Calorimeters for the beamline and extensions to the Duct Scrapers. Conversion of the Positive Ion Neutral Injector (PINI) beam sources for final tritium operation was also underway. The Engineering and Operations groups were also involved in the construction of the new gas introduction system for the PINIs in D-T operation.

The Testbed Group continued the characterisation of PINIs and their conditioning and progress was made in the area of high heat flux element testing and beryllium power handling.

In addition, there was considerable activity in design proposals and prototype tests for a possible enhancement to neutral beam power on JET. This proposal is described in a separate section.

Neutral Beam Operations

NBI Performance, Reliability, and Contribution to the JET Programme

Neutral beam injection (NBI) was used on nearly every operational day of the 1995 experimental campaign. Whilst the number of pulses with neutral beams during 1995 was less than in 1994, due to the shorter duration of the campaign, the proportion (63%) was the highest of any operating period. The level of NB usage in 1995 is compared with other years in Table IV, which also indicates the number and proportion of intermediate power (>10MW) and high power (>15MW) NB pulses.

The basic configuration of the two injector boxes in 1995 was similar to 1994. One box was equipped with eight 'high voltage' (three-grid or triode) Positive Ion

Table IV
NBI Power Injected into JET Discharges

Year	No. pulses	%		%		%	
		with NBI	with NBI	with P _≥ 15MW	with P _≥ 15MW	with P _≥ 10MW	with P _≥ 10MW
1988	2958	993	33.6	100	10.1	292	29.4
1989	1301	621	47.7	99	15.9	225	36.2
1990	1569	813	51.8	72	8.9	211	26.0
1991	2354	1265	53.7	78	6.2	359	28.4
1992	776	339	43.7	12	3.5	55	16.2
1994	2656	1313	49.4	325	24.8	713	54.3
1995	1778	1120	63.0	287	25.6	631	56.3

Neutral Injectors (PINIs) normally operating at 140kV in deuterium, and the other with eight 'high current' (four-grid or tetrode) PINIs operating at voltages up to 85kV. The maximum expected power for the installed configurations together with the achieved power during 1995 is summarised in Table V. By careful conditioning and optimisation of PINI parameters, the expected power was been exceeded; this was achieved by increasing the extracted beam current slightly beyond the optimum for minimum beam divergence, and allowed an increase in delivered power without significant loss of transmission efficiency for geometrically well-aligned beams. The power of the high current' tetrode PINIs is 60% above the original injector system design value, but this increase was accommodated safely within the operating limits of critical mechanical components, such as aperture-defining scrapers. This was achieved by careful monitoring of the installed thermal instrumentation and optimisation of the beam alignment in particular.

Figure 26 shows the distribution of NBI pulses as a function of injected power level for the 1994-5 campaigns combined. The level of reliability achieved during 1995 was typically in the range 80 - 90%. The reliability fraction is defined as the ratio of the achieved heating energy (i.e. time-integrated power waveform) to that requested.

NB heating is generally characterised by the fact that delivered power to the plasma is largely independent of

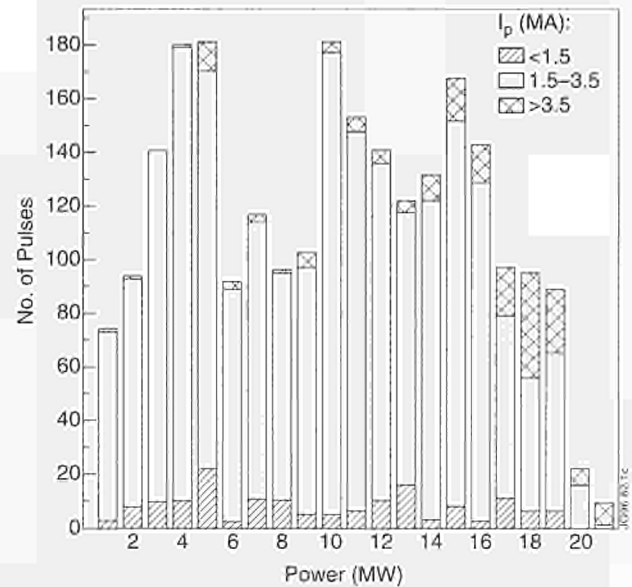


Fig.26: Histogram of frequency distribution of NB power injected into JET in the 1994/5 experimental campaign. The frequency at low plasma currents ($I_p < 1.5MA$) and high plasma currents ($I_p > 3.5MA$) is indicated

plasma configuration and parameters. However, there are, potential limitations at very low and high values of plasma current and electron density. These arise from a variety of effects, such as:

- (a) deposition of re-ionised beam particles on unprotected torus entry duct surfaces due to unfavourable trajectories in the poloidal near-stray field at low plasma current, especially in 'slim' plasma configurations;
- (b) saturation of the active far-stray magnetic field compensation (MFC) system at high plasma current, which affects the un-neutralised ion beam at the PINI and degrades beam alignment;
- (c) excessive 'shine-through' exposure of in-vessel structures at low electron density due to insufficient attenuation of the neutral beam by the plasma;
- (d) development of high neutral pressure in the torus entry duct under conditions of heavy gas fuelling of the plasma leading to increased duct re-ionisation and power loading.

Table V: Installed Potential and Achieved Power to JET 1995

	Installed Potential (MW)			Achieved (MW)		
	Octant 4	Octant 8	Total	Octant 4	Octant 8	Total
Jan '95 to Mar '95	13.0	7.6	20.6	13.1	8.1	21.2
Apr '95 to Jun '95	13.6*	7.6	21.2*	11.1*	7.5	18.6*

* Note: In April 1995, the last two 'low current' tetrodes on Octant No.4 were replaced by 'high current' units. This power was not reliably brought into service by the end of the programme.

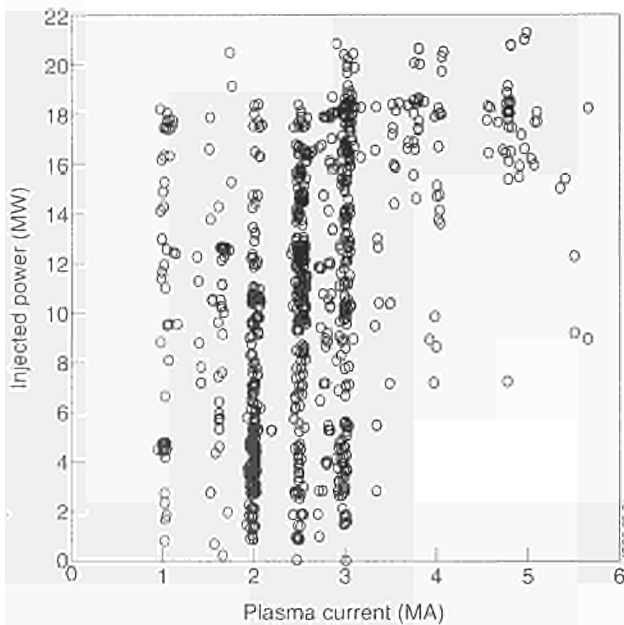


Fig.27: Distribution of injected NB power against plasma current for the 1995 campaign discharges.

In spite of these effects, flexible operating limits were defined which allowed NBI to take place in a very wide range of plasma scenarios, taking full advantage of the installed duct protection plates and in-vessel shine-through protection tiles and taking into account the results of a rigorous thermo-mechanical assessment of the exposed structures. Figure 27 shows the power injected in all 1995 pulses as a function of plasma current, ranging from high poloidal- β experiments at 1MA through to high power, high current H-modes up to 5.8MA. During the high-current H-mode campaign, the feedback controller transfer function of the MFC system was optimised to follow the rapid onset of high values of far-stray field after the H-mode transition, resulting from the change in the vertical field required to maintain radial plasma equilibrium (Fig.28).

The ability to apply high-power NB power to target plasmas in highly shaped configurations optimised for MHD stability, formed in such a way as to minimise particle recycling at low electron density, was fundamental to the successful achievement of high fusion performance in the hot-ion H-mode and the attainment of equivalent Q_{int} values close to unity. Conversely, in the experiments aimed at demonstrating the viability of a highly radiative divertor plasma, long high-power NBI pulses were successfully delivered in high-density, heavily gas-fuelled and impurity-seeded discharges by working close to, but remaining within, the trip level of the duct pressure interlock and by careful monitoring of the extensive array of thermal sensors installed in the duct protection plates.

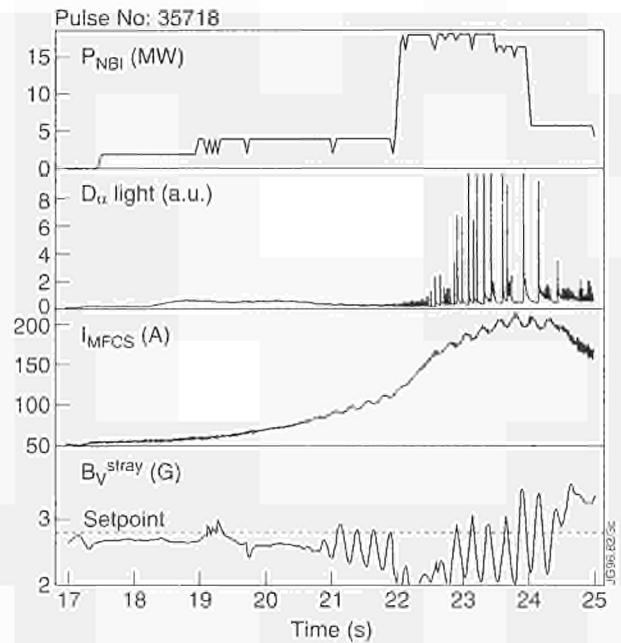


Fig.28: Neutral beam active magnetic field compensation system performance in 5.8MA H-mode discharge. (Pulse No.35718). The set-point field, which the compensation seeks to maintain, is shown. The trip levels (corresponding to the safe limits of the field) are at 1.6 and 3.6 Gauss. The effect of ELMs can be clearly seen.

Figure 29 shows the total energy delivered to the plasma by NB injection for in every 1995 pulse, versus power; the solid line corresponds to an average pulse length of 10s (the beamline design value).

New Operational Features

During 1995, a new beam modulation interface with the high voltage (HV) PINI power supplies was implemented. In general, this allows each PINI to be switched on and off arbitrarily within the pre-set energisation timing window. The 'off' command simulates the occurrence of a HV breakdown, thus causing an interruption of the beam; the 'reapplication delay' (usually 40ms) is then extended until the next 'on' command. This facility is used either by a simple pre-programmed pulse generator order to provide modulated beams at fixed duty cycle, or by an advanced Neutral Beam Local Manager (NBLM) system incorporating a local feedback control capability which minimises the time-averaged error of the delivered power compared with a reference waveform (Fig.30). The power reference can be pre-programmed or, alternatively, derived from a real-time signal generated by a central controller used for plasma control (eg: to stabilise diamagnetic stored energy). Beam modulation using the pre-programmed pulse generator was used, during a series of experiments with controlled toroidal field ripple. This provided repetitive beam pulses during a slow ramp of the

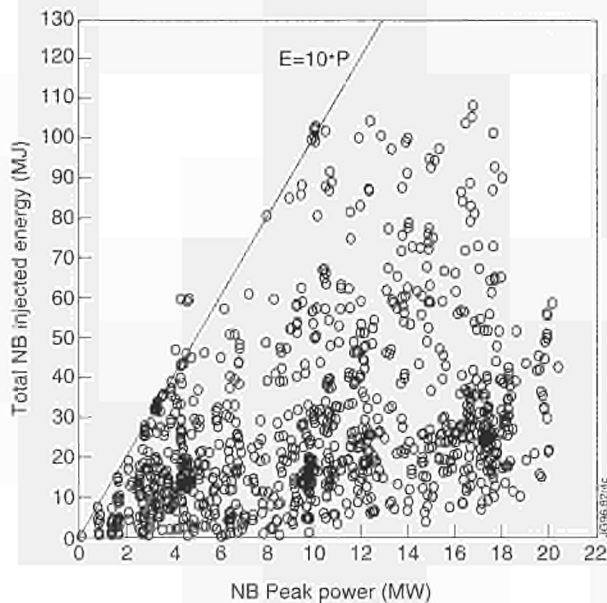


Fig.29: NBI energy delivered to the plasma versus NB peak power for all 1995 pulses. The solid line corresponds to a pulse length of 10s (beamline design value).

ripple amplitude: this technique gave the possibility to make measurements at many different values of ripple amplitude in a single discharge. Preliminary experiments using NBLM were carried out in which closed-loop feedback control of the diamagnetic stored energy W_{DIA} was achieved. The transfer function used to calculate the power reference for NBLM, derived from the real-time measurement of the W_{DIA} error, was of the proportional-integral type where the numerical coefficients were obtained from simulations using a 0-D plasma model incorporating a global confinement scaling law. This gave good controller performance in experiments such as where the system compensates for a change in confinement regime (H→L transition) during the NB injection phase.

Neutral Beam Engineering Inertial Calorimeter Development

As mentioned in the 1994 JET Progress Report [1], the CuCrZr alloy used in the manufacture of the injector calorimeter vapotrons was, due to its cumulative cycle history and projected rate of use, approaching potential fatigue life problems. During the 1994/1995 campaign, 7600 ASYNC shots were intercepted by calorimeters. Therefore, a decision was made to design a new inertial calorimeter, and during the shutdown, the existing hypervapotron calorimeters on both injector systems have been replaced with this new design.

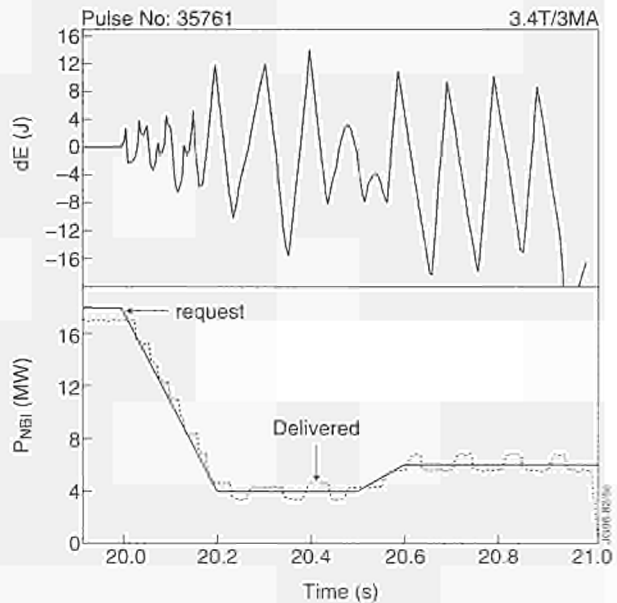


Fig.30: Behaviour of NB power under feedback control from the Neutral Beam Local Manager (NBLM) system. This is programmed to minimise the moving average error (ΔP) with settable time constant (t) with respect to a reference demand power waveform.

The new calorimeter elements have been designed to fit the existing door frame and backing structure with minimum additional weight (to the original system) being a fundamental design criterion. Elements were manufactured from 35mm thick plates of OFHC copper explosion bonded to 15mm plates of 316L stainless steel. The beam facing copper was castellated into 15mm squares to a depth of 25mm to reduce the thermal stress and hence the bending of the element whilst in service. Interpulse cooling was through two parallel 6mm diameter gun-drilled water channels positioned in the stainless steel strongback.

Design criteria for the inertial elements were as follows:

- capable of handling a flux density of 20MW/m² for 1s;
- interpulse cooling of elements ~ 4 minutes;
- maximum deflection (7.6mm) to be no greater than the hypervapotron systems;
- minimum additional weight in order that the existing calorimeter frame might be utilised.

A total of 900 Quality Class 1 welds were required for the refurbishment of the two calorimeter systems.

The first of the new calorimeters was tested in high power pulses on the Neutral Beam Testbed. It was demonstrated that the explosive bond between the copper armour and the stainless steel heat sink could withstand all foreseen power loading scenarios. The bending of the individual panels was measured to define safe operating limits for the lifetime of the bellows and the thermocouple

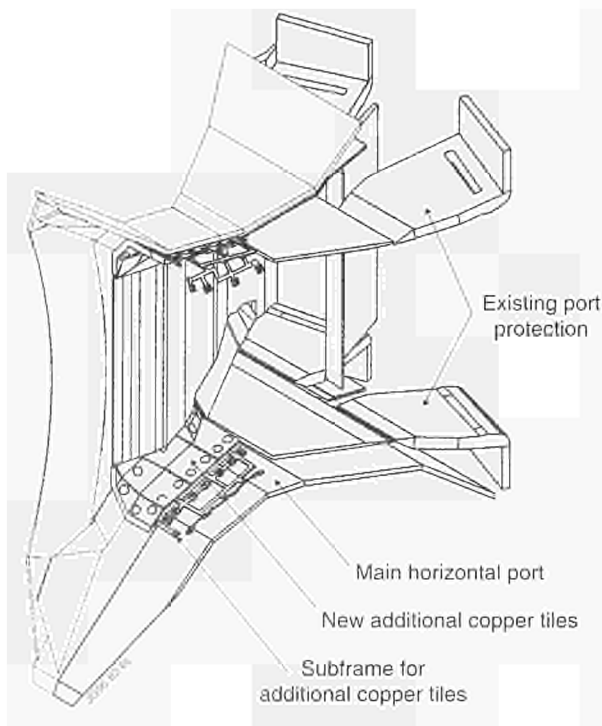


Fig.31: Duct Scraper Assembly showing new extension tiles.

instrumentation were improved and calibrated. Final tests on the assembled calorimeter with the ion/neutral beams proved that the calorimeter could be loaded as expected.

Duct Re-ionisation Protection

There has existed a problem with the re-ionisation and focusing of particles within unprotected areas of the duct during recent experiments, associated with 'slim' plasmas at currents below 2MA. Additional floor and ceiling tiles were designed to protect these areas at both injectors. The new assemblies (four off) consist of ten copper tiles fixed to an inconel subframe. Several tiles have a complex three dimensional shape to fit the duct exit throat geometry. Each tile has a blackened rear surface (vessel facing) to facilitate radiation cooling during the interpulse period. A surface temperature limit of 500°C has been set, which should allow a typical 10s pulse at power loadings in excess of 400W/cm². An overall view of the complete duct protection to be installed at the beginning of the 1996 experimental campaign, is shown in Fig.31.

Neutral Beam Test Bed Work Source Conversion for Tritium Operation

At the end of the shutdown (June 1995 - March 1996), all PINIs will be in the tritium configuration. The modifications for tritium operation require a disassembly of the grid stack. Hence, a full reconditioning and characterisation sequence has been performed for all converted

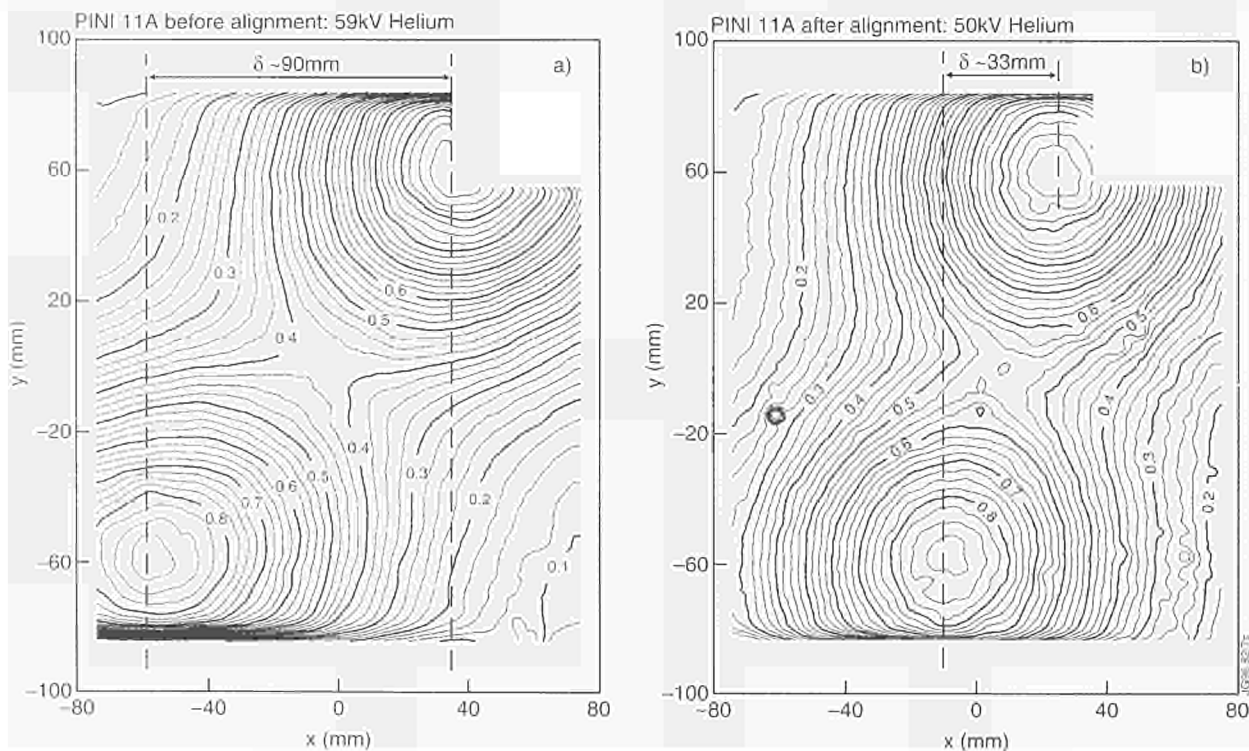


Fig.32: Beam profiles obtained on the unidirectional CFC target in the Testbed showing the beam misalignment (a) before and (b) after rebuilding of the PINI. The power contours are labelled in kW/cm².

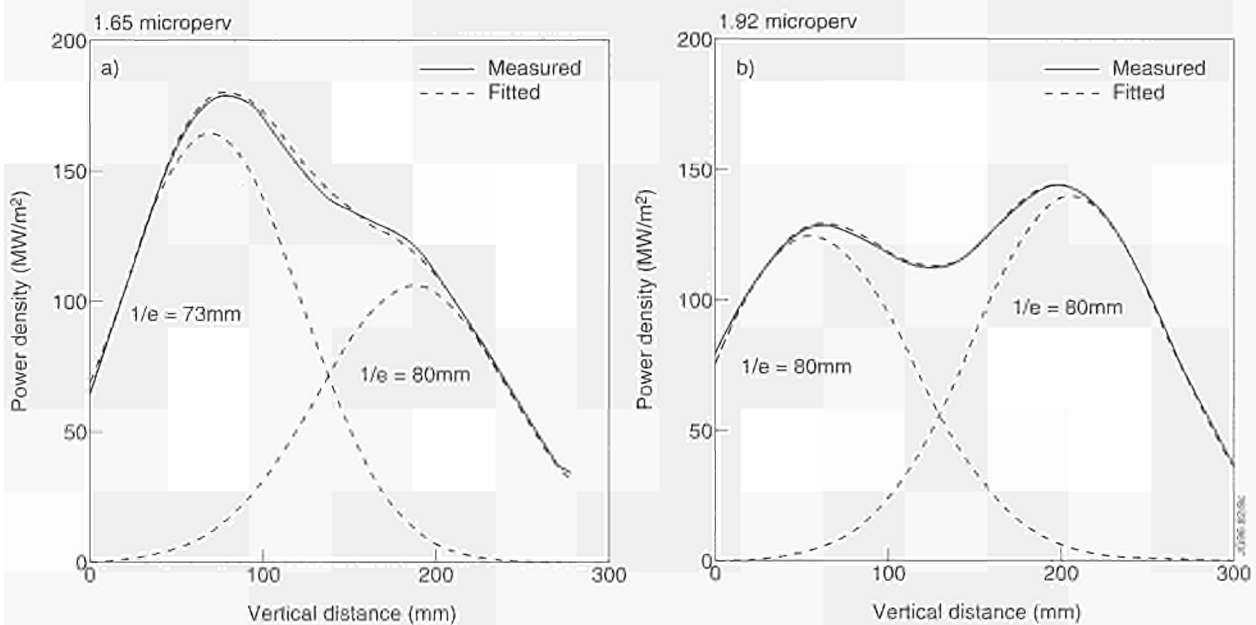


Fig.33: Vertical beam profiles showing the relative intensity of beams from the two PINI grid halves as the extracted current (perveance) is varied at fixed extraction voltage (PINI 6AT; 62kV helium beams) ($1 \text{ microperve} = 1A \cdot V^{-1/2}$)

PINIs. Before a PINI is transferred to the injectors, it is first conditioned to full performance and operated at full performance for at least 300s in the Testbed. Additionally, the grid alignment and the power loading of the source components and scrapers is measured. The PINI is also operated with the tritium gas feed lines to check the integrity of this gas feed from ground potential. Finally, beam width and alignment are checked. Only after a PINI has reached specification is it released for installation on an injector. This thorough and time consuming testing procedure is one major reason for the high reliability and availability of the neutral injection system.

Improvement of Plasma Source Uniformity

The possibility of obtaining two dimensional high resolution power density profiles from a PINI on a unidirectional CFC calorimeter target (first mentioned in the 1994 JET Progress Report [2]), has revealed that the plasma sources do not show a uniform power density distribution. The profiles obtained show that the centroids of the power peaks from each half of the PINI are frequently offset from the nominal vertical symmetry axis (so-called 'cross-eyed' behaviour). Typical profiles are shown in Fig.32. The shift of the beam centres can be unacceptable in that it can lead to overloading of the scrapers defining the vertical aperture through which the beam passes into the torus. The origin of this misalignment could be in tolerances for the gridstack alignment (the results of Fig.32 show the effect of rebuilding to obtain better

alignment), but might also be the result of non-uniform plasma density in the source with consequent effects on the first lens in the ion optics of the extraction system (the plasma meniscus at the extraction grid holes).

The CFC calorimeter, which has been made mobile in 1995 so that beam profiles can be taken at several distances from the PINI, has enabled these effects to be examined in detail. The beam in the PINI is formed in accelerating grids made from two half sections which are inclined by $\pm 0.5^\circ$ against the vertical plane. Profiles taken at 7-10m from the beam source resolve the contribution of the two grid halves. Surprisingly it has been found that the current density from the two grid halves varies differently when the extracted current is changed at constant voltage (Fig.33). This is true even for a source which has a constant plasma density across the extraction plane (the so-called chequerboard source).

The plasma source used in the injectors has a magnetic cusp field superimposed on the confining chequerboard field. The purpose of the cusp field is to increase the proton fraction near the extraction plane [3]. With this so called filter source, the contribution from the two grid halves is better resolved when the extracted current is too high and the overall beam is already widening. One possible explanation is that the plasma density in the source is higher at the perimeter and lower in the centre of the source. Running with an extracted current higher than the nominal optimum ('over-dense operation') would then mean that the beamlets in the centre have the opti-

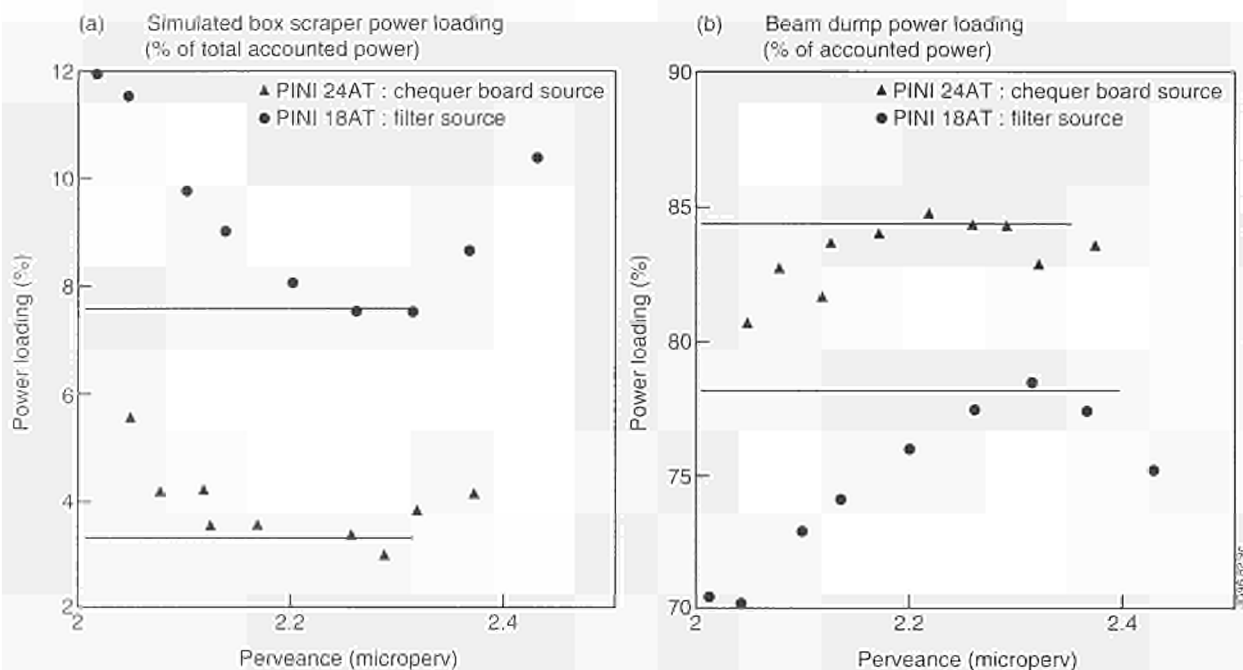


Fig.34: Comparison of scraper and beam dump loadings from a PINI equipped with FILTER source (PINI 18AT) and one equipped with a chequerboard source (PINI 24AT) (75kV Deuterium beams.)

imum current and therefore the lowest divergence while averaged over the grid the current and the divergence would be above the optimum value.

Comparing profiles from filter source and chequerboard source, the filter source produces a wider beam with higher power loading on the scraper (Fig.34). It is assumed that the non-uniformity of the filter source is caused by the remnant filter field in the extraction area, though the physical mechanism primarily responsible for this effect is still a matter of some uncertainty. Modelling calculations show, that magnetic configurations are possible which maintain the positive action of the filter with less remnant field in the extraction area. If successful, this could lead to a 5-10% increase in the injected power and at the same time to a considerable reduction in the scraper loading. In the meantime, it is considered that the original effect which gave rise to the investigations, that of the cross-eyed beams, is mainly due to grid misalignment and can be minimised by extremely careful assembly of the PINIs. The effect is strongest on the high current (60A), low voltage(85kV) tetrode PINIs where the extraction gap is only one quarter of the width of the high voltage (140kV/30A) triode PINIs.

Component Tests

As a spin-off effect of the development of the actively cooled beryllium version of the 'Mark I' divertor, a test

section with 10mm thick beryllium tiles brazed to a hypervapotron has been built and tested. The test section was successfully exposed to 300 cycles at power densities relevant to an ITER divertor (5-6MW/m²). It was then demonstrated that the bond was good enough for exposure to surface temperatures up to 1000°C, and finally the surface was driven into melting with power densities of 20MW/m². The onset of melting and the re-solidification can be clearly identified in the time temperature trace (Fig.35).

The main results of the test were:

- sublimation has the temperature dependence expected from literature;
- no indications of lateral cracks were discovered;
- once the surface has been liquid, the emissivity changed significantly;
- the test was successfully used to benchmark codes developed by NET and ITER.

The emissivity of the surface (Fig.36) is taken from a calibration of the IR system where the uncooled panel was allowed to come into thermal equilibrium (470°C). The emissivity varies by a factor of three over quite short distances and approaches 80%, a value normally seen for graphite. The tile surface shows cracks and small craters after 20 pulses with the surface above liquidus. A melt depth of 0.7mm is observed in an exposure with 20MW/m² for 900ms after the onset of melting. A major loss of material is only observed at the edges.

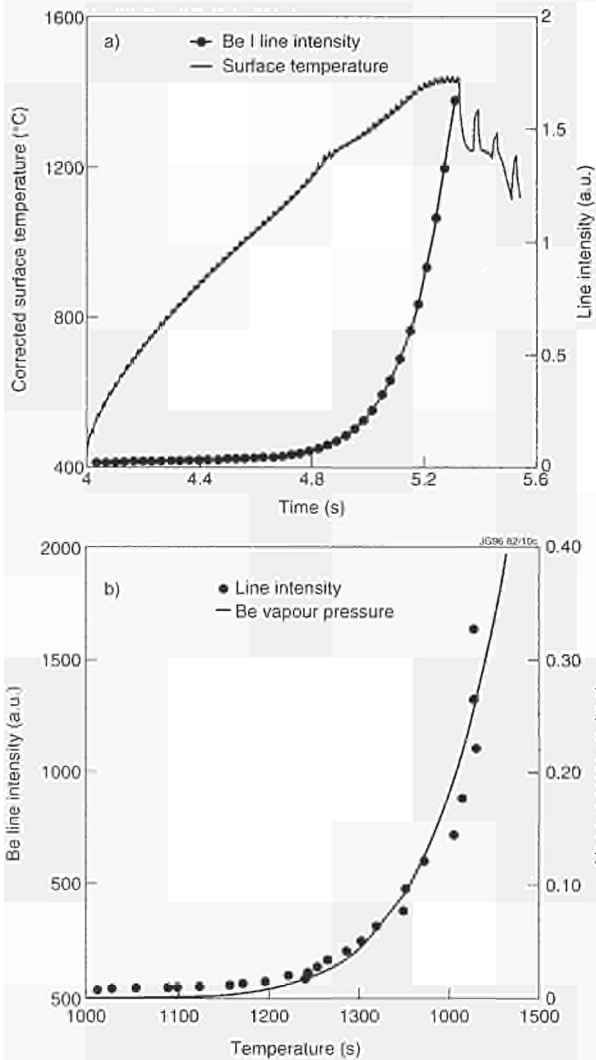


Fig.35: (a) Surface temperature as a function of time for 10mm Be tiles brazed to a hypervapotron subjected to 20 MW/m² beam. Also shown is the intensity of Be I line emission from the surface (457.3nm); (b) Measured intensity of the Be I line (in the pulse shown in (a)) plotted against the measured surface temperature and normalised against the Be vapour pressure from the literature. It can be seen that the time variation of the emission follows closely the pressure of vapour expected to be present.

An interesting observation was that the surface could reflect light quite strongly after melting had occurred. This is likely to confuse interpretation if inspection is carried out with CCD cameras. Due to the local high reflection the camera can saturate locally and the resulting picture gives the impression of extensive melting due to the blurred edges.

In a collaboration with JAERI, Japan, (in the framework of the Large Tokamak Tripartite Agreement), two vapotrons clad with high conductivity carbon fibre tiles have been built and tested. These test sections withstood power densities up to 30MW/m² under steady state conditions and showed an excellent uniformity in the surface temperature (Fig.37). The power handling and the uniformity of this design are outstanding, and the design also offers the option of an 'in

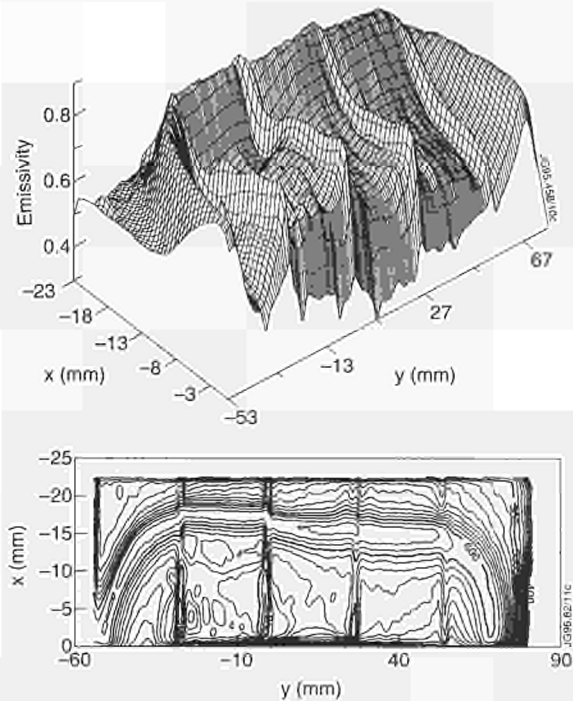


Fig.36: Measured surface temperature of a test section of Be tiles in thermal equilibrium (at 470°C) (bottom). To reproduce a constant surface temperature at 470°C, the emissivity distribution shown on the top diagram must be used.

situ' repair. A disadvantage of flat tiles is that a fault can spread quickly. This was indeed observed when one tile detached completely during one pulse. A more optimised design with reduced stress at the edges and some interlocking should overcome this disadvantage.

In separate tests, a boron nitride reciprocating probe was exposed to beam power up to 40MW/m². The material was strong enough to withstand power densities of 40MW/m² for 220ms, which raised the surface temperature to 3400°C. In particular, no cracks were observed at the end of the test [4].

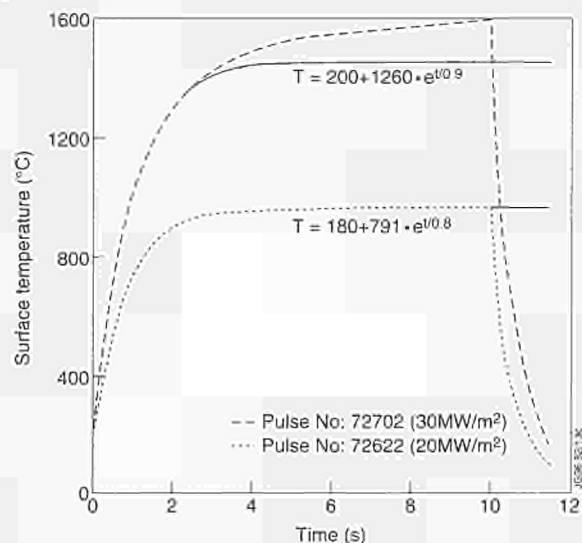


Fig.37: Surface temperature versus time for power densities of 20MW/m² and 30MW/m² for high conductivity CFC tiles brazed to the hypervapotrons.

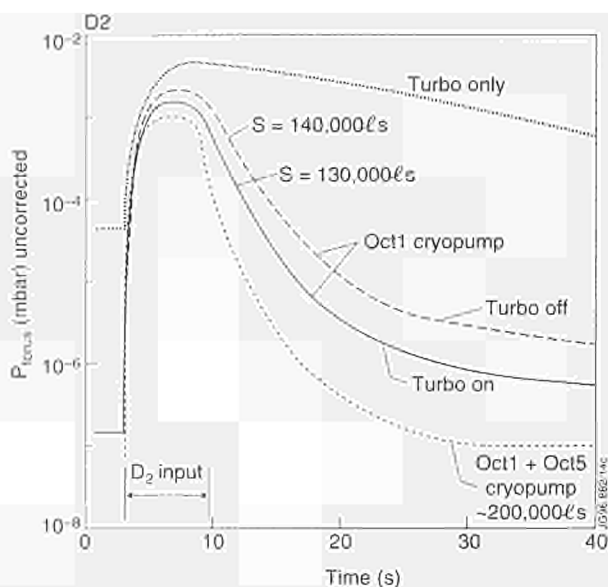


Fig.38: Torus pressure as a function of time during and after 5s deuterium pulses under different pumping conditions.

Cryogenic Systems Cryoplant

By mid-June 1995, the liquid helium and nitrogen cryoplants had been operated uninterrupted for more than 18 months and supplied users of cryogenics in a reliable manner. During operation, the liquid nitrogen consumption was up to 25,000 litres per day and more than 15,000 litres of liquid helium per day were circulated by the cryoplant when all cryopump systems and other users were in full operation.

In-vessel Pumped Divertor Cryopumps

Amongst the key components for the success of the Pumped Divertor (PD) programme were the two new in-vessel PD cryopump systems, used routinely to provide high speed active pumping during plasma pulses. Operation of the PD cryopumps proved to be paramount during the experimental campaign, as it allowed:

- achievement of extremely low levels of impurity in the torus vacuum, with the consequence that the PD cryopumps were routinely used for vacuum conditioning together with Glow Discharge Cleaning and Be-evaporation;
- demonstration of density control of the plasma;
- production of detached plasmas;
- studies of the radiative divertor H-mode.

The PD cryopumps were also important in the recycling control during the development of high fusion performance plasmas and were used with Argon frosting to study the helium transport in the plasma.

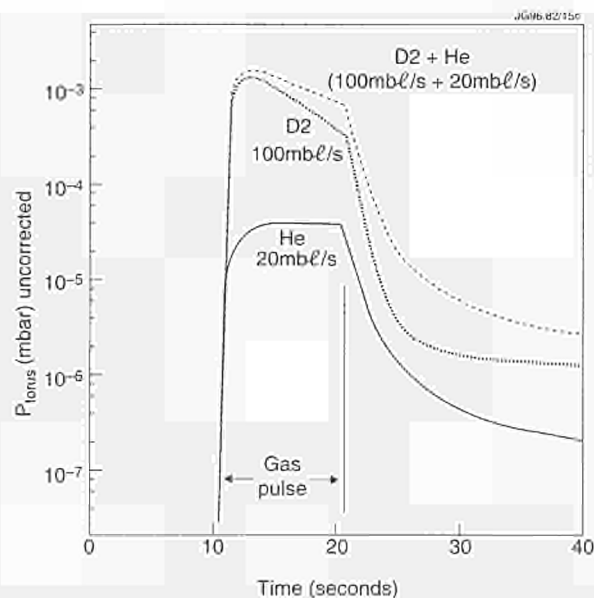


Fig.39: Torus vacuum as a function of time during and after a 5s gas pulse with deuterium, helium and a mix of helium and deuterium (20:80) with fresh argon frost layer.

The pumping speed of the PD cryopumps inside the torus was measured by steady-state and dynamic analysis by admitting gas pulses into the torus. The determination was made from the ratio of the equilibrium pressure to the mass flow, the decay time of the torus vacuum pressure and by comparison with gas pulses pumped only with the torus turbomolecular pumps.

Figure 38 shows typical pulse traces for 5s deuterium pulses with and without running cryopump, for one and two pumps operating and with and without simultaneous torus turbomolecular pumps operation. Figure 39 shows the pumping of helium and helium/deuterium mixture gas pulses when pumped by an argon frost layer together with the trace for a pure deuterium gas pulse.

A summary of the experience with the PD cryopumps is:

- The cryopumping systems fulfil their specification and provide a $\sim 200,000 \text{ l/s}^{-1}$ in-situ pumping speed for deuterium, which is ~ 20 times the pumping speed of the installed turbomolecular pumps;
- Around 80% of this pumping capability is available for He and He/D₂ mixtures by cryosorption on the PD pumps covered with fresh Argon frost at 4-4.5K;
- Experiments with hydrogen confirm that the PD cryopumps provide practically no pumping for hydrogen due to the high vapour pressure of H₂ at the operation temperature of the supercritical helium loop. The cryopump remains stable, however, without sign of uncontrolled regeneration during extended periods (> 20 min) at 10^{-4} mbar H₂ pressure. H₂ plasma operation with the supercritical helium cooling is possible

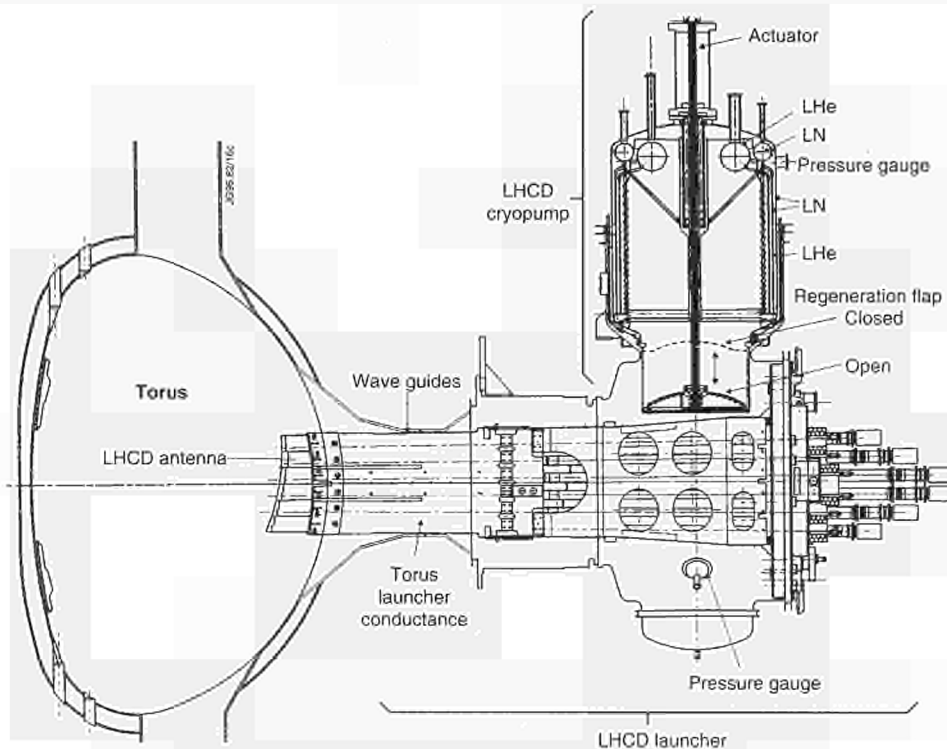


Fig.40: Cryopump installed at the LHCD launcher and the torus.

but without the benefit of the high pumping speed of the PD cryopump;

- The thermal load to the cryopump systems was well within the specification;
- The system has been designed to cope with the heat load from a D-T plasma heated by 45MW additional heating with 20MW of power from fusion reactions. As a result, the heat load from the present D-D operation at lower powers, is not noticeable on the operation of the cryopump;
- The cryosupply using supercritical helium as coolant, proved to be very reliable and stable in operation;
- The cryopump was used practically constantly throughout the experimental campaign due to its beneficial effect on the torus vacuum;
- The experience during the last 14 months operation showed that no modifications or improvements of the cryopumps will be necessary.

LHCD Cryopump

The availability of the LHCD cryopump proved to be important for the conditioning and also for the high performance operation of the LHCD launcher. This cryopump was kept operational permanently during the 1995 operation campaign.

Figure 40 shows the LHCD cryopump installed at the torus LHCD launcher. Pumping speed measurements

with the installed cryopump confirmed the design values and the results from the test facility. The measured pumping speed of the LHCD cryopump towards the launcher and the torus are listed in Table VI, together with the data for the regeneration flap conductance in closed position. The regeneration flap proved to be a very important component as its closing allowed the cryopump to be kept operational and filled with liquid helium, both under helium glow discharge cleaning conditions in the torus, and during regeneration of the torus PD cryopumps. It also allowed the regeneration of the LHCD cryopump without affecting the torus operation.

The performance of the LHCD cryopump has proved satisfactory and no modification or remedial work on the pump has been planned for the subsequent shutdown period.

Table VI
Pumping speed measurements for LHCD cryopump

	Pumping Speed D_2
LHCD Cryopump Pumping Speed	$105,000/s^{-1} \pm 15\%$
Conductance torus – LHCD launcher	$C \sim 3000/s^{-1}$
Conductance of LHCD cryopump flap in closed position	$C \sim 4 \times 10^{-2}/s^{-1}$

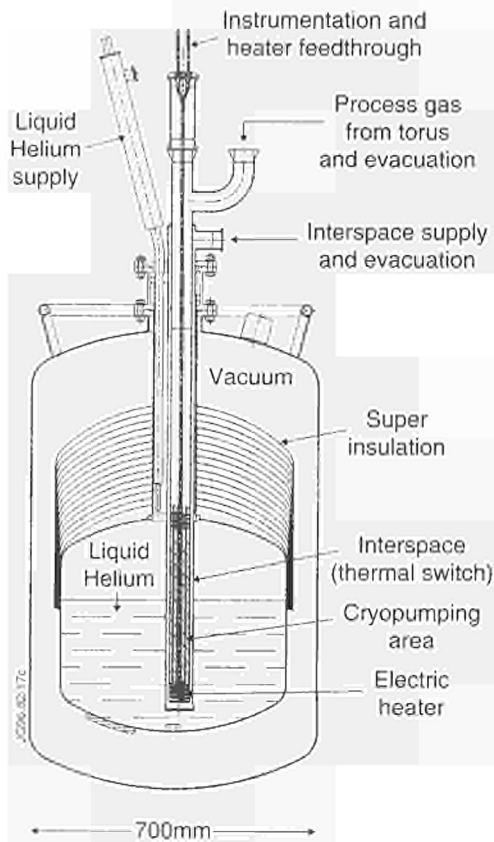


Fig.41: Cross-section of the Gas Collection System Cryopump.

Gas Collection System (GCS)

The central part of the new Gas Collection System (GCS), which enables the collection and monitoring of the exhaust gas of the torus, is a liquid helium cooled cryopump which has been designed, procured and tested during 1995. Its design is shown in Fig.41 and it is basically a cryogenically-cooled cold trap. Its main feature is an annular interspace between the cold trap and the liquid helium coolant which acts as a thermal valve when evacuated or filled with helium. By these means, a thermal

insulation or thermal contact to the surrounding liquid helium is provided, enabling the regeneration or pumping of the cold trap without losing the liquid helium reservoir, thereby providing autonomy for several days of operation.

Maintenance

The central part of the cryoplant has been operational for over 14 years. As indicated, it was decided to leave the large cryopumps untouched during the shutdown except for some minor sensor improvement. This demonstrates the reliability of cryopump systems which are essentially passive elements and when designed carefully, can be regarded as practically maintenance free.

Various elements of the cryoplant required extensive maintenance, however, and a full scale maintenance programme for all cryogenic valves, instrumentation and pressure vessels has been initiated as part of the shutdown period, together with an overhaul of plant compressors (for refrigerators and helium recovery system), the helium balloons and cryolines. The procurement of a new liquid nitrogen distribution system is underway. In addition, several modifications on the process loop are planned to improve the transient conditions for the Pumped Divertor cryopump systems and the simultaneous operation of all cryopumps with extensive bulk helium supply to liquid helium users.

Preparations for DTE1

Preparations for the Deuterium-Tritium experiment (DTE1), scheduled for the end of 1996, have involved considerable work. The most significant effort has involved the design and construction of all aspects of an active-phases PINI gas introduction system.

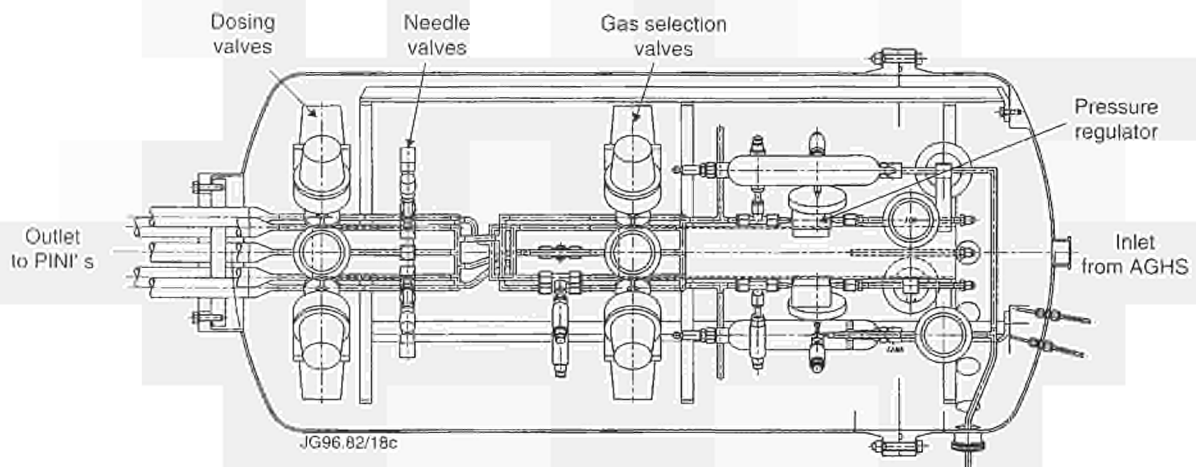


Fig.42: Schematic layout of tritium/deuterium gas introduction module or 'piglet'.

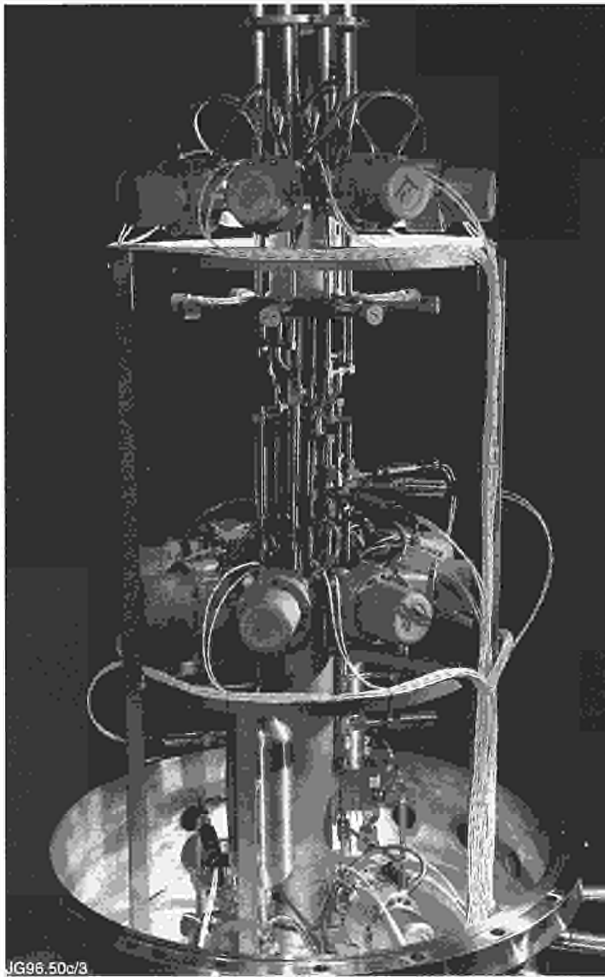


Fig.43: Piglet gas module during assembly.

The active phase gas handling and introduction system for the NB PINIs is being installed during the 1995/96 shutdown. Deuterium or tritium gas is supplied at sub-atmospheric pressure from the Active Gas Handling System (AGHS) in Building J25 via a local control and handling 'pig' system and onward to the two NB gas handling and distribution system (or piglets). Secondary containment for the system consists of the piglet vessels, flexible containment line, pig vessel and further flexible containment line to Building J25. The final connection from the Basement to PINI gas feed is considered part of the NB vacuum system. The piglet gas introduction systems are identical for each injector, and each is capable of supplying either D_2 or T_2 from the AGHS to each of the four 'quadrants' (ie: PINI pairs sharing a common deflection magnet) at ground potential (PINIs are being modified to enable tritium gas feed to the grids at ground potential). This arrangement gives a high degree of operational flexibility, although it is foreseen at this stage that tritium will only be used in the 140kV

injector, to avoid contamination of injector components in the Octant No.4 system.

The piglets and their associated control systems will be commissioned as part of the NB restart schedule. The layout of one of these piglet gas systems is shown in Fig.42, and the completed internal assembly of the first of the systems is shown in Fig.43.

Detailed design and implementation of the control, instrumentation and interlocks for the active-phase PINI gas introduction systems have been carried out during 1995, aiming towards first commissioning in parallel with the 1996 re-start of operation. Due to the degree of operational flexibility provided by the piglet design, the interlock protection to avoid injection of a gas other than that for which the beam deflection magnets have been set up, must be rigorous and sophisticated.

A further requirement for DTE1 is the ability to inject at least one helium neutral beam on the 80kV injector box simultaneously with deuterium beams on the other quadrants. This is required for the active double charge-exchange alpha-particle diagnostic. To realise this mixed beam scheme, it was necessary to demonstrate that helium gas could be cryo-sorbed onto an argon frost layer on the liquid helium cryo-pumps of the injector box in the presence of excess deuterium gas. At the end of the 1995 operational campaign, dedicated mixed D_2/He cryo-pumping tests were conducted on one of the injector boxes to qualify this pumping scenario. The argon 'seeding' gas was admitted through a dedicated gas introduction system and it was found that sufficient mixed-gas pumping was available to allow short He^0 injection pulses on one PINI in parallel with D^0 injection on up to four of the other sources. Based on these results, one quadrant of the active PINI gas introduction system on the 80kV injector box is being modified to allow He operation, subject to final qualification tests with beam extraction to be performed during 1996 prior to DTE1.

During DTE1, the triode PINIs will operate in tritium at up to 160kV/30A in the 'perveance-matched' condition, which defines the optimum extracted current at a given voltage for minimum beam divergence, compared with 140kV/30A in deuterium (30A per PINI corresponds to the power supply current limit at these voltages). If the PINIs in a quadrant are operated singly, it is possible to operate in deuterium at up to 160kV/37A and this is a potential method for conditioning the triode PINIs to 160kV prior to changing over to tritium source gas. This

method of conditioning was successfully demonstrated during 1995 and several triode PINs achieved operation at $\geq 158\text{kV}$ in deuterium.

References

- [1] JET Joint Undertaking Progress Report 1994, EUR 16474-EN-C, pp 34-35.
- [2] *ibid* [1], pp 36-37.
- [3] R S Hemsforth and A J T Holmes, JET-P(90)52, (1990).
- [4] D J Godden and D Ciric, JET-IR(95)01, (1995)

RF Heating Systems

JET is equipped with two different high power radio frequency systems: the Ion Cyclotron Resonance Frequency (ICRF) heating and the Lower Hybrid Current Drive (LHCD) systems. In addition, a low power system exciting Toroidal Alfvén Eigenmodes (TAE) has been routinely operated. These have very distinctive roles.

The ICRF heating system is used for high power centralised heating of the JET plasma, with the capability of producing Fast Wave Current Drive (FWCD) with the new (A2) antennae. The localisation depends mainly on the magnetic field and is insensitive to parameters such as density and temperature. Wide band operation in the range 23-57MHz allows variation in both the choice of minority ion species heated and the localised position of the heating. So far with the previous (A1) antennae, up to 3.5MW on one antenna and 22.7MW total coupled power (in L-mode) for 2s was achieved. Preliminary experiments on Fast Wave Ion Current Drive with the A1 drive have also been successful, showing that the plasma current gradients near the $q=1$ surface were modified by changing the phase between straps of the antennae. New ICRF antennae have since been installed in 1993 optimised to the geometry of the divertor plasmas. Their location in the torus was selected to give four arrays of two adjacent antennae. Each array have four RF radiating conductors, or straps, which provide an enhanced radiated spectrum. Variation in the relative phase of the RF currents in the straps allows this spectrum to be varied for both heating and current drive experiments. In addition, the control electronics have been completely rebuilt to allow operation with four straps closely coupled and to improve the reliability of the ICRF plant by reducing the crosstalk between modules. The 1994 operations were made difficult by the fact that both the control electronics and the

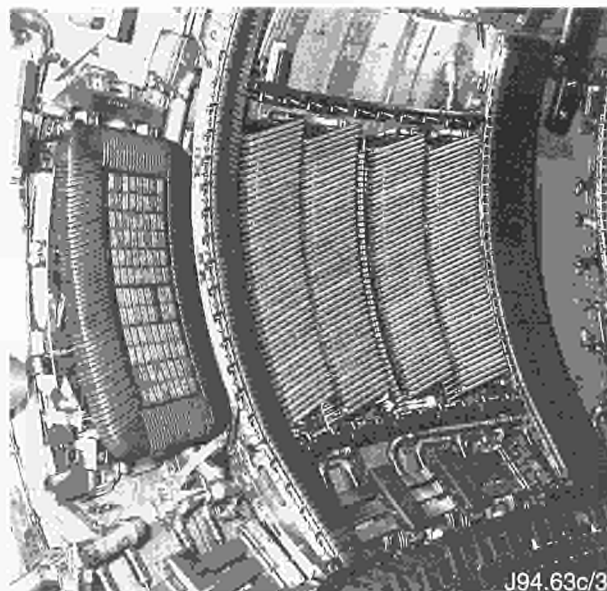


Fig.44: View of the LHCD launcher together with one of the four ICRF modules

antennae were new systems and have required large amounts of commissioning time. Several problems were identified and remedial actions taken or are in preparation. In spite of these early difficulties, a record power of 16.5MW was launched in a divertor (H-mode) plasma, compared to 12MW in X-point plasmas in the 1991/92 campaign. Combined Heating Power of 32MW including 15MW of ICRF power was launched for several seconds into radiative divertor plasmas.

The LHCD system operates at 3.7GHz and is capable of driving a substantial fraction of the plasma current. This is achieved by launching an RF wave predominantly in one toroidal direction. This wave accelerates the high energy electrons in the plasma and so drives a current. This may be used to stabilise sawtooth oscillations, thereby increasing central electron temperatures. The system can modify the plasma current profile and is the main tool for stabilising high beta poloidal plasmas with a large proportion of bootstrap current (the so called advanced tokamak scenarios). It has also been used to optimise performance. With a prototype launcher, (LØ) up to 2.3MW of LHCD was coupled to the plasma. This prototype has provided engineering, operational and physical experience of LHCD on JET in a variety of plasma configurations. An upgraded launcher (L1), was installed in 1993 and was in full operation for the 1994-95 campaign. Launched power of 7.3MW was obtained and full current drive of plasmas up to 3MA was achieved. Up to 6MW of LHCD power was launched for 13s for profile control experiments. The LHCD launcher together with one module of the A2 ICRF antennae is shown in Fig.44.

Alfven Eigenmodes (AE) are discrete global modes of Alfven waves in confined toroidal plasmas. In particular, AE appear in the frequency gaps for shear Alfven waves corresponding to toroidicity, ellipticity or triangularity induced harmonic coupling (whence the denominations TAE, EAE, ...). Modes based on finite β coupling between Alfven and sound waves also exist in the Alfven frequency range ($2\pi f - v_A/2qR$) with frequency ranging from 20kHz to 500kHz for the different TAE and EAE. AE have been predicted to be of fundamental importance in tokamak reactor relevant conditions, since they can be destabilised by fast particles (such as fusion produced alpha-particles) and, in turn, may expel fast particles from the plasma core via resonance wave-particle interaction. The saddle coil antennae, in conjunction with the ICRF and NB heating methods, offers the unique possibility of exploring in a systematic way the importance of these modes, which can be excited in a controlled fashion by a devoted RF system (the TAE system). This system has been put successfully into operation within the framework of a Task Agreement with CRPP-Lausanne, Switzerland. The excitation of TAE modes has been assessed and a large database of AE activity and damping rates has been collected and are being analysed. In addition, new modes including kinetic Alfven Eigenmodes have been identified. These modes have also been excited by using two modules of the ICRF system with a "beat" frequency, i.e. a frequency difference, corresponding to the TAE frequency.

ICRF Technical Achievements

ICRF Heating

JET has a powerful and highly versatile ion cyclotron resonant heating system with the potential for delivering up to 20MW of power to the plasma. The operating frequency range is 23MHz to 57MHz which allows fundamental heating with hydrogen, deuterium, He^3 and He^4 minority ions, and second harmonic heating with hydrogen, deuterium, tritium and He^4 ions. The power deposition can be made on-axis or off-axis depending only on the ion species and the ratio of the frequency to the magnetic field. The fast magnetosonic wave excited by the antennae can access dense plasmas and so there is no difficulty in providing central heating at the high densities relevant to reactor operation. The antennae are multi-strap units in which the currents can be phased to launch waves either with no net toroidal directivity for heating

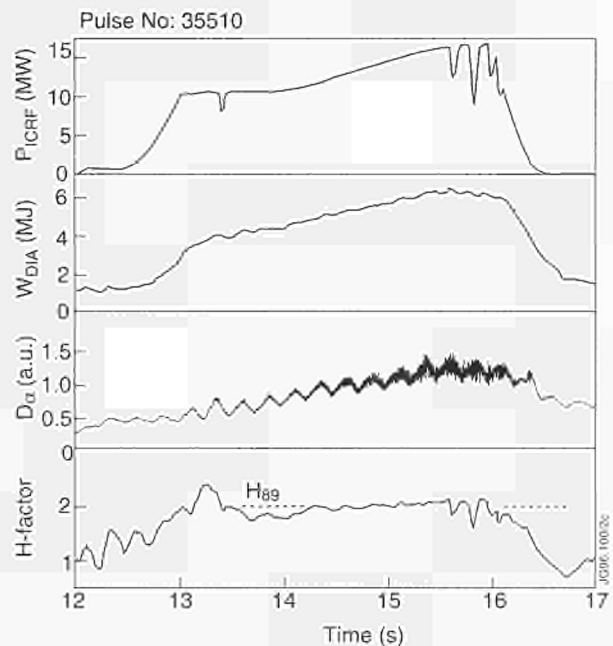


Fig.45: Time history of various signals for Pulse No.35510 corresponding to record launched power. The configuration ($B_t = 3.1T$, $I_p = 3MA$) is compatible with a gas-box type divertor.

purposes, or with up to 75% toroidal directivity for both ion and electron current drive applications.

During the 1992/1993 shutdown, the ICRF system was equipped with a new set of four antennae specifically designed to match the geometry of the divertor plasmas. These A2 antennae have four phase-coherent current straps, which produce better defined $k_{||}$ spectra and which are three times narrower than those excited by the old A1 antennae. There is also a wider choice of spectra available for heating since $0\pi0\pi$, $0\pi\pi0$, $00\pi\pi$ and 0000 phasings are all possible compared with only dipole and monopole phasings with the A1 antennae which had only two straps. The four current straps of the A2 module are electrically coupled both inductively and capacitively. This complicates the matching procedure since the impedance that each strap presents to the feed-lines depends on the voltage and phasings applied to the other straps. Thus all four straps must be tuned simultaneously. This requirement has necessitated a new set of electronics to control the power, frequency, phase, conjugate box, trombones (line stretchers) and stub lengths. The new control system also has narrow band filters on the reflected power signals to remove "crosstalk" from antennae modules operating at different frequencies. Such crosstalk is observed in low single pass absorption scenarios and leads to spurious tripping of system protecting against arcs.

So far, the ICRF system has coupled up to 16.5MW to JET divertor plasmas (Fig.45). In addition, 15MW of

hydrogen minority ICRH have been combined with 17MW of neutral beam injection to give a total additional heating power of 32MW into a 2.5MA radiative divertor plasmas. H-modes with RF only have been produced for plasma current up to 5MA and record electron temperatures, up to 15keV have been achieved.

Control Electronics

Some key components of the new electronics control system were identified not to perform according to specifications and have severely limited the ICRF plant capability. Significant effort has been devoted to identifying these problems and to establishing proper solutions.

The replacement of the electronic phase and frequency control module (PFCM) was delivered in February 1995, and gave a dramatic and immediate improvement in the operation of the RF amplifiers with the new A2 antennae. The first design produced outside JET had a substantial problem with the feedback loop controlling the operating frequency and its phase. The incorrect operation of the loop caused sidebands and false locking of the oscillator which substantially reduced the output power that could be obtained on plasma. The new electronic module, of novel design, is immune to false frequency locking and accurately controls the output phase of the RF amplifiers. It has allowed the RF Plant to couple 16.5MW limited by voltage on the antenna. In addition, it is now possible to reliably condition the RF antennae to exceed 30kV without spurious tripping.

In March 1995, a new design of electronic amplitude and phase detection module (APDM) was delivered and installed giving improved control of the phase and amplitude. By converting the RF signals into two quadrature digital streams and using a digitally stored look-up table, the amplitude and phase information could be produced with minimal noise and drift. Just before each pulse, the detectors were zeroed and any residual DC-offsets removed. This has cured the long-term drift in the previous design, which necessitated checking of each individual detector circuit (a total of 192). Accurate frequency filtering allows the RF generators to be staggered in frequency reducing the cross coupling interference to the arc detection or tripping circuits.

Edge Localised Modes (ELMs) occurring mostly during neutral beam heated plasmas present a large load change to the RF amplifier. These occur with <100ms rise time, last for several tenths of milliseconds, cause a large

mismatch, trigger the arc detection circuit and cause tripping of the RF power. As the original suppression period was fixed at 20ms, the RF power is substantially reduced when long duration high frequency ELMy periods occurred. To combat this problem, several solutions were implemented using a fast digital output from the D_{α} light emitted at the plasma periphery (diagnostic KS3):

- at the end of the ELM period, restart the RF power immediately;
- at the start of the ELM period, momentarily desensitize the arc detection circuit;
- using the automatic matching error signals, identify the high impedance load and momentarily desensitize the arc detection circuit.

The new electronic circuitry was designed, built and installed at JET in April and gave good results during heating of ELMy plasmas.

During the shutdown, three new electronic modules associated with the amplitude control, tetrode protection and timing are being rebuilt, incorporating further enhancements and additional control facilities. These changes will allow efficient antenna conditioning by using an automatic power reduction system when frequent arcing occurs. Designed and built in-house, the twelve prototype modules were tested five months after the start of the shutdown and incorporate advanced programmable logic systems allowing for future flexibility in operation. Changes to the RF generators, required for the new modules, have been completed and commissioned and the sixty production units are due for delivery in January 1996.

A major change to the RF plant computer control and operation (CODAS) is planned towards the end of 1995. This will lead to the following benefits:

- improvements to the coupling resistance feedback system (plasma positioning controlled by RF);
- control of launched RF power;
- real time control of RF power;
- swift changes allowing antenna conditioning between pulses.

Previously generated in local CODAS equipment, amplitude and phase waveforms for the RF plant will now be generated by a central source, the RF Local Manager (RFLM) using the VME standard. These analogue waveforms will be distributed to each RF generator over fibre optic links. Directional coupler signals are sent back to RFLM for real time calculation of coupling resistance, output and launched power.

The RFLM can control the amplitude and phase during a JET pulse keeping the total power constant even in the event of a generator failure. A high level software program capable of storing and controlling all parameters for an RF pulse, more than 280, will allow swift changes between plasma and pre-stored vacuum conditioning pulses. This will allow antenna conditioning between plasma pulses or after disruptions.

System Analysis

Major investigations into the ICRF plant plasma performance have continued throughout 1995. The following improvements were undertaken:

- improve reliability of ICRF plant, in particular, against crowbars;
- allow for high voltage conditioning between plasma pulses;
- optimise available power by enhanced voltage control and phase control;
- improve the R_c plasma position feedback system, in particular during ELMs.

Use has been made of an high speed eight-channel PC based data acquisition system to capture a whole RF plasma pulse at a sample times of 16ms. The normal CODAS acquisition system is unable to capture these transients. Using the LabVIEW programming language, the user can examine the detailed performance of an amplifier and its response to plasma load variations (ELMs) and antenna arcs. In particular, using a programmed algorithm, it allows automatic searching of the data for detection of antenna arcs. The knowledge obtained has been used to specify a prototype electronic module for the discrimination of antenna arcs and ELMs and there are due for delivery in June 1996.

During the investigations, it became apparent that there were a number of unexplained output tetrode arcs, which prematurely terminated a pulse. These normally occurred in the presence of heavy tripping either due to antenna arcs or ELMs. During the shutdown, a test facility using 143m of coaxial transmission line (Fig.46) was constructed to study artificially induced arcs. Using an electronic ignition circuit from a Formula 1 engine, a spark was generated close to the inner of the coaxial transmission line at a high RF voltage point. It was possible to trigger an arc and, by means of RF probes in the amplifier, capture transients occurring across the output tetrode and other components. Several effects were observed:

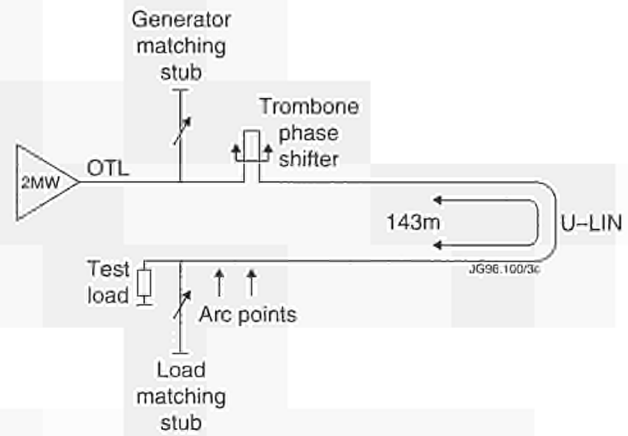


Fig.46: Schematic of the arc test facility.

- under certain conditions, there appeared to be a voltage spike generated across the tetrode at the end of a normal pulse;
- when an arc was triggered, a transient of up to 50kV was observed across the tetrode causing an internal flashover;
- the electrical line length between the RF amplifier and the matching stub (OTL) plays an important part in the amplitude of the transient at the tetrode.

The additional transient is caused by the fast decay of RF power following a switch-off by the protection system as the transmission system represents a tuned circuit with a high stored energy. By slowing down the turn-off of RF power by 15 μ s, the transient was reduced and a tetrode flash-over was avoided. As a result, the following changes will be made for the 1996 campaign:

- a length of OTL section will be adjusted to improve the output tetrode resilience to ELMs, at least at the main operating frequency;
- the protection turn-off circuits will be modified, incorporating a controlled delay.

Coupling to Plasma

The coupling of the A2 antennae to plasma has been assessed over range 32MHz to 56MHz. A technique allowing scattering matrices to be obtained in a single pulse has been developed. The key parameters of the antennae can then be deduced. The imbalance between inner and outer straps has been partly explained by a wrong impedance transformation of the cross-over link which connects the inner straps to the main transmission line. Remedial actions to correct this impedance are underway.

The coupling resistance R_c is defined as the characteristic impedance of the transmission line (30 Ω) divided by

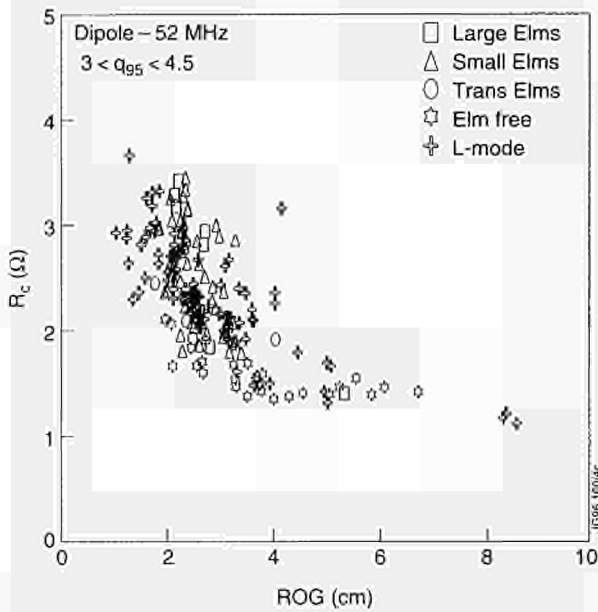


Fig.47: Database of coupling resistance (at $f = 52\text{MHz}$) versus distance between last closed magnetic flux surface and limiter (ROG).

the voltage standing wave ratio on the main transmission line. This coupling determines the maximum power which can be launched into the plasma:

$$P_{\max} = 8[R_c - R_{\text{loss}}][V_{\max}/30]^2 \quad [\text{MW}, \Omega, \text{kV}]$$

where R_{loss} are the RF losses in the main transmission line (0.55Ω at $f = 52\text{MHz}$) and V_{\max} the maximum voltage on the antenna or on the main transmission line.

The coupling is determined predominantly by the distance between the antenna strap and the location of the cut-off density, of $2 \times 10^{18} \text{m}^{-3}$ for a $0\pi 0\pi$ phasing configuration and of $2 \times 10^{17} \text{m}^{-3}$ for a $00\pi\pi$ phasing configuration. The coupling is optimised when this density is located on the poloidal limiter which corresponds to a distance of 1.6 to 2cm between plasma and limiter for typical plasmas.

This distance depends upon plasma position control, and on the scrape-off density profile, which depends mainly on:

- the parallel connection length of the field line connecting the antenna to the divertor tiles (or to the poloidal limiter);
- the perpendicular transport into the scrape-off plasma which can be affected by H-mode regimes for instance;
- ionisation in the scrape-off plasma which depends upon recycling and gas input.

A comprehensive data base on coupling resistance has been created. The following two salient features emerged from this study:

- in dipole, the distance between last closed magnetic surface (LCFS) and poloidal limiter was found to be

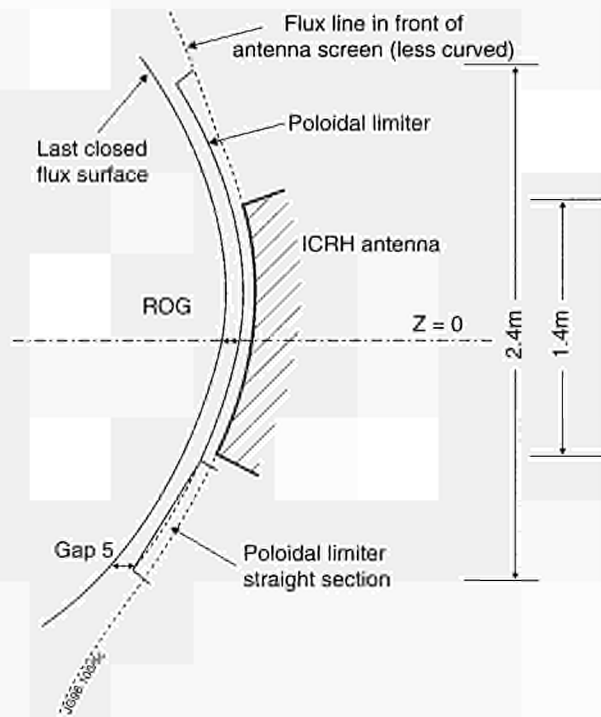


Fig.48: Schematic of outer wall configuration.

a key parameter (as shown in Fig.47), which is in good agreement with coupling predictions;

- more surprisingly, the coupling was found to depend on the distance between the bottom part of the limiter and the LCFS (gap 5 as shown in Fig.48): the larger the distance the better the coupling (as shown in Fig.49).

The explanation for the sensitivity of R_c to the gap 5 distance is the following. For large distances, the field lines which cross the midplane between the separatrix and the Faraday shield connect directly to the divertor

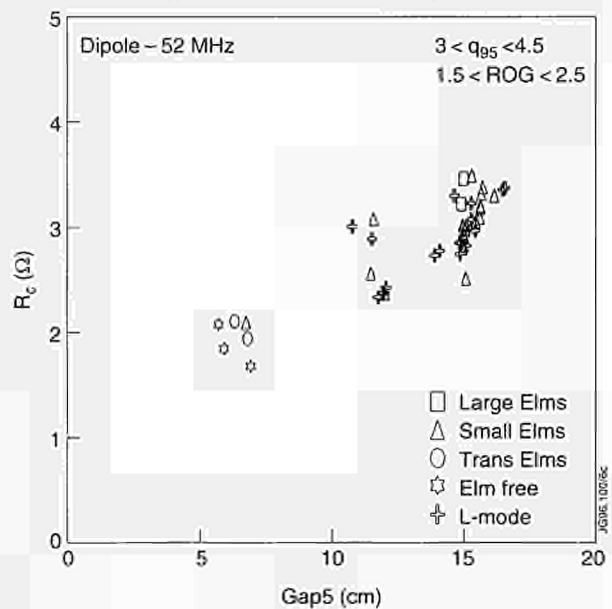


Fig.49: Database of coupling resistance (at $f = 52\text{MHz}$) versus distance between last closed magnetic flux surface and bottom part of the limiter.

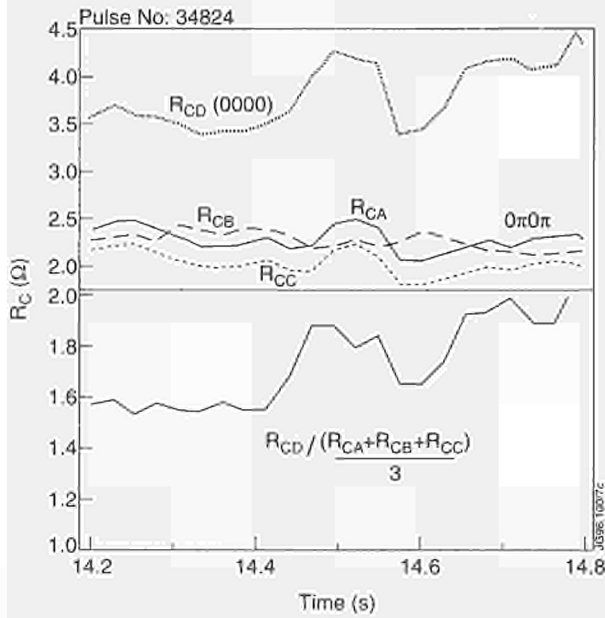


Fig.50: Comparison of coupling resistance between dipole and monopole phasing ($f = 43\text{MHz}$). The relative increase in coupling refers to dipole configuration.

without touching any material surface on the way. In this case, the connection length is large, thereby allowing density to build up near the antenna. As the gap 5 distance is reduced, such field lines are intersected by the lower section of the poloidal limiter with substantial reductions in connection length, scrape-off layer density and coupling resistance.

Operation with Monopole Phasing

Coupling is much improved when the phasing between current straps is such that the wave is launched with low $k_{||}$ (i.e. with $0\pi\pi\pi$ or 0000 phased operation). The gain in coupling reaches 1.6 for $0\pi\pi\pi$ and up to 2 for pure monopole configuration, as shown in Fig.50.

In the 1991/92 campaign, good heating efficiency was observed in this mode of operation. With the present A2 antennae, limitations have been found in monopole operation which produced very poor heating efficiency as shown in Fig.51(a). This is attributed to RF sheath rectification along field lines in front of the antenna which can span over 3 to 4 metres, as compared to 1 to 2 metres for the A1 antennae. The installation of a prototype separator on one antenna module has partially restored good efficiency, as shown in Fig.51(b), but high power operation was not possible due to arcing in the separator. Modified separators are being prepared.

Modifications to the New A2 Antennae

During the shutdown, all antennae were removed from the torus, modified, and re-installed. The reasons for implementing these modifications, and a detailed description of the changes is presented in the following sections.

The New A2 Antennae

The A2 antennae have been previously described and only certain features which have been found to be important are outlined here. The A2 antennae were designed to match to the pumped divertor configuration, with the antennae projecting 2-30 mm further into the torus. The eight antennae were arranged into four modules, each with four current straps at nearly equal pitch. This enables the spectrum to be well defined over a wide range but is not without penalty. There are now four cross-coupled current straps, which both complicates the matching system and modifies the coupling resistance on each

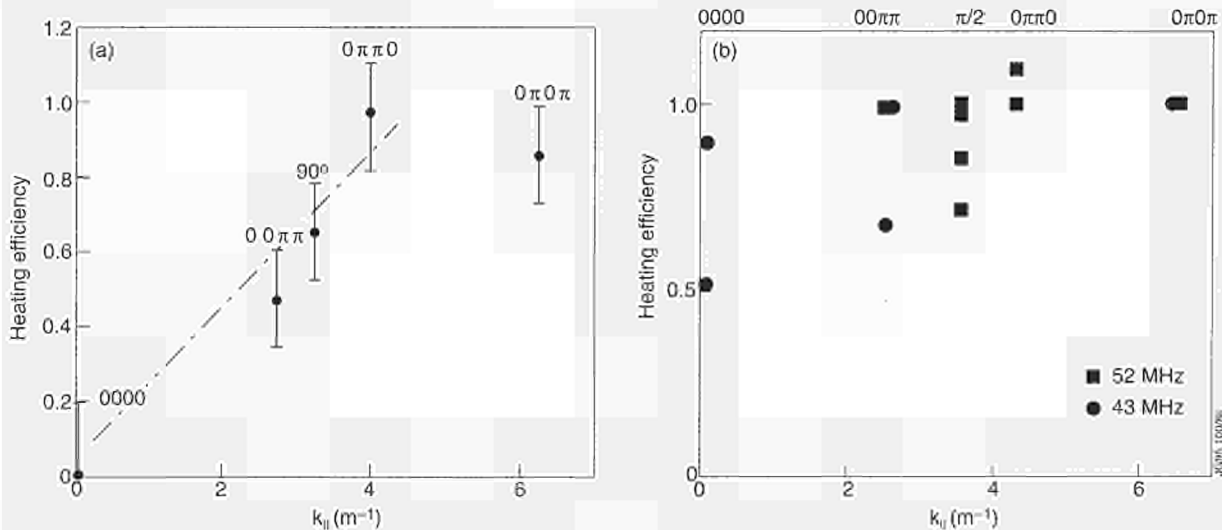


Fig.51: (a) Heating efficiency as a function of $k_{||}$ without separator; (b) Heating efficiency as a function of $k_{||}$ with separator.

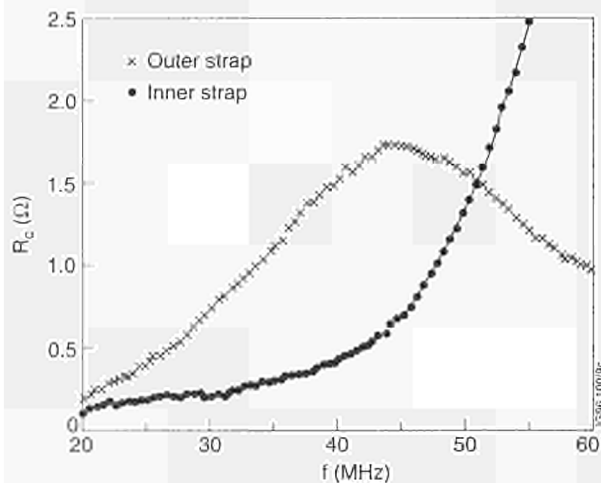


Fig.52: The coupling resistance calculated from measurements of scattering matrix on the prototype A2 antenna with foam loading.

strap. In addition, the antennae are no longer symmetrical about the transmission line ports, necessitating the use of a cross-over line inside the antenna from the transmission line to the inner current straps. Furthermore, the inner and outer straps are of necessity of somewhat different design, and therefore RF characteristics.

Resistance to disruptions strongly influenced the design of the antennae, with a strict limit imposed on the forces to be transmitted to the torus wall. Each antenna is a thin wall flexible structure supported by the torus wall via 10 or 11 articulated arms on each side of the antenna. These arms are connected to the antenna via capacitors formed by plasma spraying alumina onto inconel plates. Each articulated joint is electrically isolated and bridged by a flexible earth strap. There is a gap between the back wall of the antenna and the torus wall increasing from typically 90mm at the top to 200mm at the bottom.

RF image currents in the sidewalls and septum of the antenna degrade the enhanced spectrum of the four strap array, in particular, in phased operation. Both are therefore slotted radially to a depth of typically 100mm. The voltage on the A1 antenna was limited by arcing on the conical ceramic support for the VTL inner conductor. The A2 antenna does not have any ceramic supports on the conductors.

The protection of the antenna from the plasma is provided by poloidal limiters on each side of each four-strap array, and by CFC tiles mounted on rails above and below the array. The limiter tiles are 17mm, and the top and bottom tiles 7mm, in front of the magnetic surface tangential to the screens. The top and bottom rails are supported by the limiter structure. The joint to the left limiter is electrically closed, whilst that to the right limiter is electrically isolated via a ceramic coated pin. The

limiters are electrically connected to the torus via laminated current straps at the mid point and either end. All of this limiter structure is electrically and mechanically independent of the antenna. RF currents can flow from limiter to antenna only via the torus wall and the current straps on the support arms, or stray capacitance. The limiter structure has dimensions of 2m high x 2m toroidally, which is typically one quarter to one half wavelength over the frequency range of the system.

Coupling of the Antennae

The coupling resistance measured on the A2 antennae is less than anticipated, in particular, at larger gap between the antenna and plasma. The average coupling of the inner and outer straps is weakly dependent on frequency, with a broad maximum around 42MHz, close to the design objective. However, the inner straps show much lower coupling than the outer straps at low frequency, increase to equal the outer straps at about 52MHz, and exceed the outer straps at 56MHz. This frequency dependence is now well established over many measurements. In monopole, the coupling is higher on all straps than in dipole, and the imbalance is reduced.

The cause of this imbalance has been investigated using both measurements on the torus and on the prototype antenna. Scattering matrix measurements on the (two strap) prototype antenna using a lossy foam as a load have been found to reproduce the basic features of the torus observations. The coupling resistance calculated from such measurements is shown in Fig.52. Whilst this is a powerful technique which allows assessment of antenna modifications, on the test-bed the foam does not fully represent the plasma and the data needs to be treated with caution. The scattering matrix of the four-strap antenna array has also been measured using foam loading both before installation and in the torus. A method has been developed, which allows the measurement of the four-strap scattering matrix on plasma in a single pulse. Again, this should be treated with caution as the phase data is critical, and subject to significant error. The large values of S13 and S14 are noted. These have been found to be necessary to reproduce the monopole data. The large phase angle of S12 relative to S11 is also noted. This reduces the coupling resistance in dipole and enhances monopole.

An important part of the imbalance arises from a mismatch between the crossover strap to the inner conductors and the 30Ω impedance on either side. The crossover strap

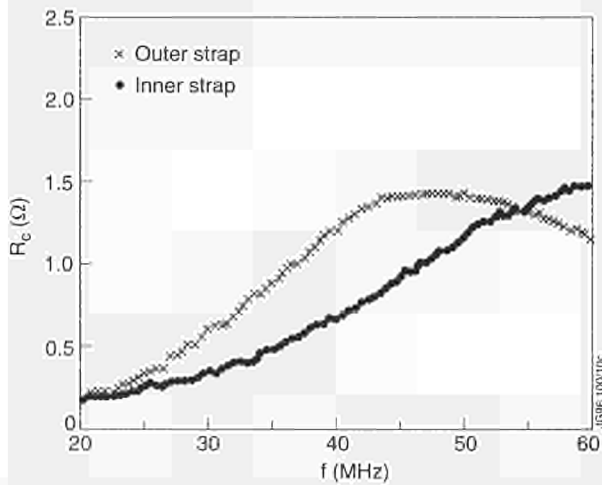


Fig.53: The coupling resistance calculated from scattering matrix measurements on the modified prototype antenna with foam loading.

appears as a 70Ω line, 430mm long with a phase velocity of 0.95. A simple model representing the antenna as a length of 70Ω line in series with a 30Ω short-circuited line reproduces the frequency dependence of the antenna.

The effect of reducing the impedance of this crossover line has been calculated taking the measured resonant frequency on the inner and outer straps of 47/41MHz, respectively. The impedance of the crossover line on the prototype antenna has been reduced to about 35Ω by an increase in capacitance to the back wall. The measured scattering matrix agrees well with that calculated. The corresponding coupling resistance is shown in Fig.53. The imbalance is much reduced although still present. Critically, it is found that the cross-coupling between straps is such that the outer strap coupling decreases as the inner improves. The average coupling remaining essentially unchanged. This modification to the crossover strap has now been implemented on all antennae. It is anticipated that the average coupling will increase by perhaps 20% at 40MHz, be unchanged at 50MHz, and perhaps slightly reduced at 55MHz.

In addition, further changes to improve the coupling have been implemented as follows:

- the antennae have all been moved inwards by 6mm. With the poloidal limiter position unchanged, this reduces the clearance to the limiters to 11mm; the separators are midway between limiters and screens;
- the previous straight section of tiles on the lower part of the poloidal limiters has been modified to continue the curvature of the limiters over the full length. This moves the front face of the tiles out by up to 20mm, and will increase the density at the screen over the bottom of the antennae.

Heating Efficiency and Impurities

When operating at low k_{\perp} , particularly in monopole, visible glows are observed on the one poloidal limiter in lines-of-sight of the viewing system. These glows are diffuse areas typically 0.2m in extent along the limiters. The position of this glow depends on the helicity at the boundary in a manner which indicates the source to be near the radial section of the left hand current strap viewed from the plasma. The glow is short lived ($<10\text{ms}$) at the end of the pulse, indicating that it is not thermal radiation from hot tiles and thus not representing significant power loss. At high power, the pulse length in monopole is limited by an influx of carbon leading to a disruption.

In-vessel inspection showed no damage to the limiters, and only slight melting of a few of the knuckles holding the ends of the screen elements at the top of the antennae. However, significant surface melting was observed on the top and bottom tile supports, and tenuous arcing had damaged the electrical breaks isolating the right hand end of the rail from the limiter. This indicated substantial interaction between the antenna and the top/bottom protection, and kilovolt RF voltages appearing on the insulators. The capacitance of this break is close to resonance with the inductance of the rail in the frequency range of interest.

The toroidal separation between limiters is about 2.2m, compared to 0.9m on the A1 antennae. The radial clearance between the limiters and screen has been increased to 17mm on A2 from 11mm on A1 antennae, to give similar density at the screen. However, with the increased separation, this density is very sensitive to the poloidal curvature of the separatrix at the antenna. Plasmas with tight curvature, as routinely obtained on high beta plasmas for example, can penetrate close to the screen, both increasing the density at the screen and establishing flux lines linking the screen to the limiters, which are prone to sheath rectification and impurity production. These flux lines can now project large areas and enclose substantial RF flux and the appearance of high voltages under typical conditions is confirmed by numerical modelling.

To alleviate this process and enable monopole operation, a prototype 'separator' has been installed on one array. This comprises an additional limiter 60mm wide mounted in the 90mm gap between the two antennae of the array. The tile face is about midway between the screen elements and the limiter tiles. The subsequently modified separator section is shown in Fig.54. The separator is supported by the top and bottom protection rails. This

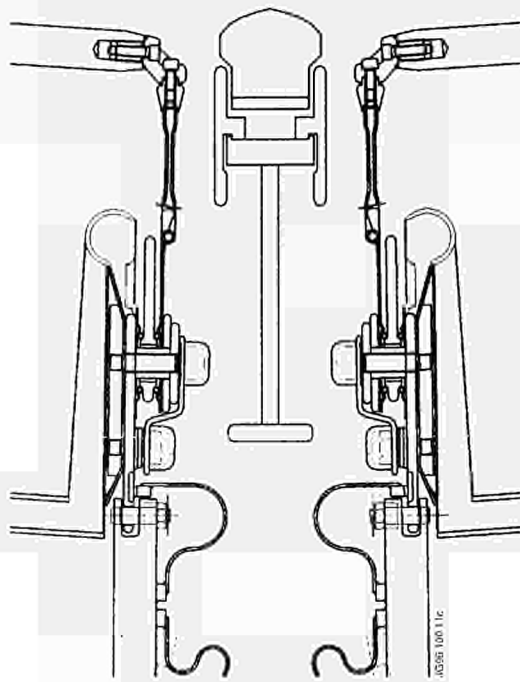


Fig.54: A section through the separator installed on all modules.

increases the disruption loads on the rails, which have each had two additional supports to the torus fitted as illustrated. These supports also earth the rail to the torus, and have also enabled the electrical break to the limiter to be short-circuited. These earthing changes are intended to reduce interaction with the rails. In the limited period of operation with this separator in place, the heating efficiency in monopole (normalised to dipole efficiency) has been much improved and the arc damage previously observed on the ceramic break in the rails, and on the top/bottom tile assemblies have all disappeared. However, the voltage is limited to 20kV by arcing across the small remaining gap between the separator and the antenna. Inspection of the antenna after subsequent removal confirms this arcing between separator and screen elements, but also indicates substantial currents in the support arms between the antenna and the torus, in particular at the corners of the antennae, both with and without the separator.

These observations are consistent with the appearance of substantial image current in the separator in monopole operation, returning to the antenna via the torus wall and the antenna supports. This creates a leakage flux trying to close around the top and bottom of the antennae, induces sufficient voltage between the antenna and the limiter/separator assembly to create arcs, and also induces currents in the corner straps to produce the observed damage.

The obvious remedy to this is to establish low impedance RF contacts between the limiter/separator and the antenna to enable image currents to close on a low impedance path. However, such links are severely complicated by the consequential disruption currents flowing in the structure. Nonetheless, such a link has been designed to connect the ends of the antennae to the adjacent protection rail at two positions at each end. This is estimated to reduce the electric field between the antenna and the separator by a factor 3-4. These links are being manufactured for installation in the torus before the end of the shutdown. In addition, detailed modifications to the antenna/limiter assemblies have already been implemented as follows:

- separators have been installed on all modules;
- the gap between antenna and separator is increased to 17mm;
- the surface of the separator sidewalls is coated with boron carbide;
- flux excluders close the sidewall slots on the end 200mm of the antenna;
- the current ratings on the support arm assembly have been increased by a factor 2-3.

Servo-Hydraulic Fast Tuning Stub

Matching systems for ICRF heating antennae have become increasingly complex to maintain efficient operation during rapid transients in coupling to the plasma, and to compensate for cross-coupling between straps. A key component of such systems is a fast tuning stub. ITER have placed a number of contracts for the definition and design of a matching system for ITER, and JET have carried out a design study of an hydraulically driven stub under such a contract.

The specification and performance of the proposed stub is summarised in Table VII. The stub comprises a short co-axial line terminated in a variable vacuum capacitor. This variation requires a linear movement of a set of plates within the capacitor over a full stroke of 70mm, with a modest applied force largely determined by the inertia of the moving components. A conventional hydraulics system, comprising a double acting cylinder, servo-control valve and a position transducer is used as an actuator. This system has been modelled using commercial software and shown to achieve a response time in setting the capacitor of 50ms. A faster response could be achieved through use of an inner velocity loop if required. The associated plant and power requirement for a com-

Table VII:
Hydraulic Stub Design and Performance Parameters

Spring rate	1400N/m
Steady (vacuum) load	350N
Moving mass	15kg
Stroke	70mm
Capacitance	20-300pF
Acceleration	50ms ⁻²
Velocity	1.5ms ⁻¹
Positional accuracy	0.5mm
Response time	<50ms
Duty	30mm amplitude 0.5Hz for 1000s
Space envelope	235mm diam. in line with stub
Operating pressure	210bar
Cylinder size	40mm bore x 28mm rod
Fluid volume inside loop	0.2ℓ
Loop gain	179s ⁻¹
Closed loop resonance	46Hz
Velocity error	1.8mm

plete system of 72 stubs for a system of 36 antennae on ITER have been defined, and the cost estimated.

In comparison with a electric servo-motor driven system, the hydraulic drive potentially offers faster response, but with increased complexity of plant and associated maintenance requirements.

Lower Hybrid System

Lower Hybrid power up to 7.3MW has been coupled to plasmas, using 8.2MW of generator power. Long pulses up to 13s duration with high power at a level of 6MW have been applied. A maximum energy of 67MJ was transferred to the plasma. A high availability of the LHCD system was maintained through a routine maintenance program and regular conditioning of the klystrons and the launcher. Experiments focused on profile control experiments with LHCD off-axis current drive. The LH power deposition profile was studied for a wide plasma parameter range in experiments and modelling studies. Sawteeth were suppressed in high power ICRF and NB heating phases with preceding LHCD. The performance of hot-ion H-modes was improved with LHCD profile control. In discharges with negative central magnetic shear, improved confinement was obtained during strong central electron heating with LHCD.

LHCD System

An overall view of the LHCD system is shown in Fig.55 including the power plant, the transmission line and the

Table VIII:
Lower Hybrid System on JET

Plant	
Frequency	3.7GHz
Number of klystrons	24
Power (generator)	12MW, (15MW)
Pulse duration	20s, (20s)
Duty cycle	1/30
Efficiency	42%
Phase control	10kHz
Phase accuracy	10°
Maximum VSWR	1.8
Transmission line	
Length	40m
Insertion loss	1dB
Launcher	grill type, 48 multijunctions (copper coated stainless steel)
Number of waveguides	384 (12 rows x 32 columns)
Dimensions of waveguides	height: 72mm, width: 9mm, wall: 2mm
Position control	hydraulic actuators
Radial movement	5ms ⁻² , 33mms ⁻¹
Radial stroke	210mm
Baking temperature	450°C
Pumping	cryopump, 85 000 ℓs ⁻¹
Total weight	15tonnes
Coupling control	launcher position control plasma position control local gas puff
Wave spectrum	
Maximum	$N_{ } = 1.4-2.3$, adjustable
Full width	$\Delta N_{ } = 0.46$

launcher. The JET LHCD system consists of 24 klystrons feeding a phased array of waveguides mounted on the main horizontal port of Octant No.3. At the rear of the launcher, the power from the klystrons is split by a hybrid junction and transmitted through flexible waveguide elements that allow the launcher to move radially. At the back plate of the launcher vessel are 48 windows. These have two ceramic discs with a pumped interspace to provide the double containment required for tritium operation. The launcher houses 48 multijunction assemblies. These split the power in one H-plane and 6 E-plane junctions and have mechanical phase shifters to produce a slow travelling wave across the grill mouth. The main parameters of the LHCD system are given in Table VIII.

The electron density at the grill mouth must be about $1 \times 10^{18} \text{m}^{-3}$ for the LH wave to propagate into the plasma.

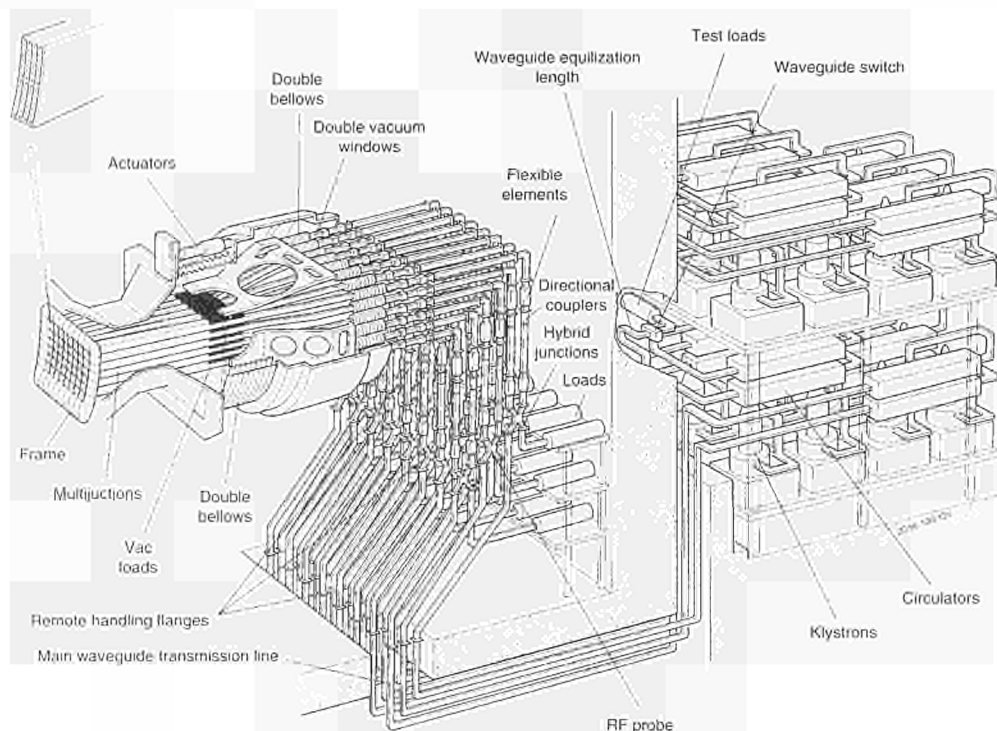


Fig.55: The Lower Hybrid Current Drive (LHCD) System

This means that the distance between the grill mouth and plasma boundary must be precisely controlled or a large fraction of the power is reflected back into the multijunctions causing arcs.

The launcher has its own cryopump to limit the rise in pressure in the multijunctions during a pulse. The multijunction waveguides have small holes in their top and bottom surfaces to improve the conductance to the cryopump. Outgassing is also reduced by baking the launcher vessel and multijunctions to up to 350°C.

Operation during the 1994/95 Campaign

The LH system operated for 2130 pulses during this campaign. This is about 33% of all plasma pulses. The maximum power coupled to the plasma was 7.3MW. Clean pulses without trips with more than 5MW for more than 4s were achieved, when the reflection coefficient was low enough ($<3\%$) and the grill well conditioned. To achieve the low reflection coefficient (R_{ν}) feedback control of the launcher position has been used on a routine basis.

Grill conditioning was undertaken using both vacuum and plasma pulses. Vacuum conditioning uses automatic pulsing. This system pulses each klystron module for 3s in turn and adjusts the power up or down depending on the number of trips on each klystron. An interlock on the temperature of the vacuum load limits the temperature of the load to 380°C. The pressure inside the launcher vessel

was monitored during vacuum conditioning. When the pressure rise was small, vacuum conditioning was stopped and a few pulses with plasma were used to complete the conditioning to high RF power. The power handling improved rapidly as the reflection coefficient was reduced to a few percent.

Technical Upgrades of the LHCD System

Apart from normal maintenance a number of improvements to the LHCD system was undertaken during the shutdown. These included:

- new system control software to preload and store complete pulse schedules with all system parameters and waveforms for power, phase, launcher position for all JET plasma pulses;
- new system software in the generator to control the maximum electric field in the multijunctions in order to reduce the number of trips;
- phase compensation for changes in transmission line length;
- new PC based digital control system for the launcher position control to allow high flexibility in scenarios with varying coupling conditions with secondary protection loops;
- control of the shape of the outer plasma boundary through the Plasma Position Central Control, with feedback on the reflection coefficients of three

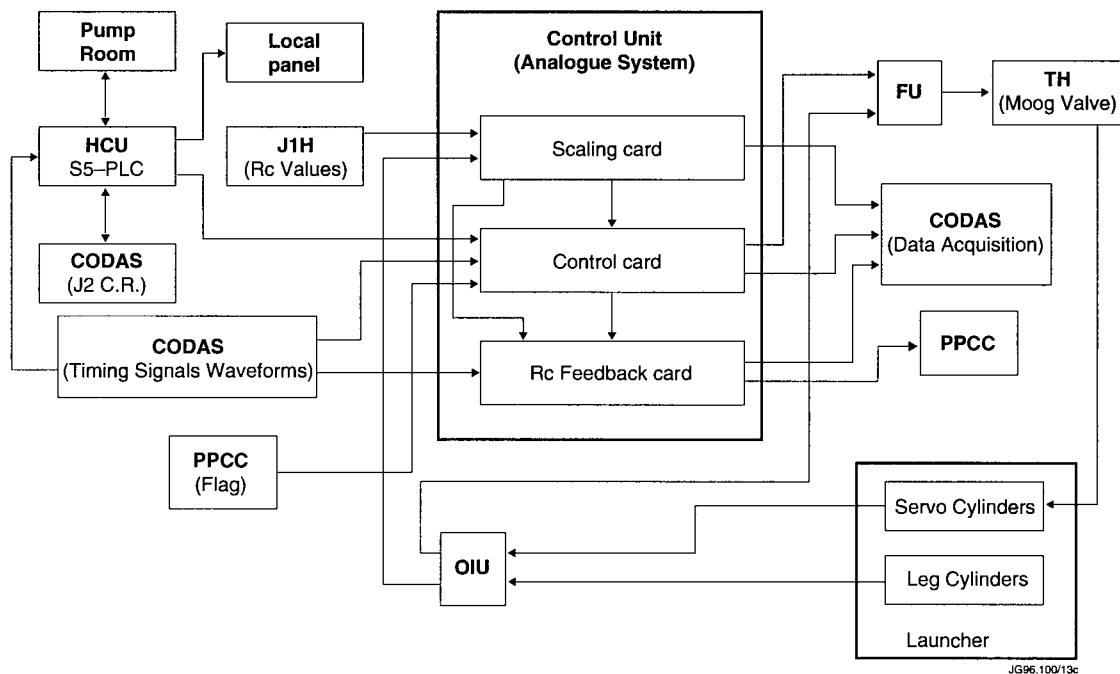


Fig.56: Position control schematic.

different areas of the grill, to provide homogeneous coupling;

- real time control of the loop voltage and the internal inductance by feedback control of the LH power with upgraded systems for signal processing and with new fast algorithms.

Position Control

To obtain the best coupling for the LHCD launcher, the distance between the grill mouth and the last closed magnetic surface must be controlled. For this reason, the radial position of the antenna can be varied during a plasma pulse under a feedback control based on the value of the reflection coefficient. Figure 56 shows a schematic of the position control system. The position of the launcher is controlled by three hydraulic systems. The first one, called Offset Circuit, compensates for the atmospheric pressure load against the evacuated vessel. The second, called Legs Circuit, controls the position of a movable buffer (called Legs), which enables the positioning of the antenna within a range deemed safe for operation. The third, called Servo Circuit, moves the launcher to a given position either outside a pulse or within a pulse under feedforward or feedback control.

During plasma shots, the LHCD antenna can be moved radially forward up to +30mm, relative to the poloidal limiter position. The launcher follows a position waveform with or without additional feedback on the reflection coefficient which allows a movement of ± 20 mm around the pre-

programmed position waveform. The bandwidth of the hydraulic control system is 1-5-Hz. The reflection coefficient has been kept constant at the requested value between 2-10%. During the shutdown, the Launcher Position Control System has been upgraded, so that the Control Unit, is on a digital system to improve performance and flexibility.

Coupling

The power that can be coupled to the plasma depends critically on the reflection coefficient seen at the input of the launcher. The reflection coefficient is determined by the density immediately in front of the grill. This density in turn is determined by the distance from the launcher to the plasma Last Closed Flux Surface (LCFS), and the density decay length in the scrape-off layer. The density decay length in the scrape off layer is determined by the connection length for the field lines in front of the launcher. Figure 57 shows the measured reflection coefficient versus the launcher-plasma distance, illustrating how the reflection coefficient depends exponentially on this distance, and how the density decay length is influenced by variation in the plasma configuration.

Another factor that influences the density decay length in the scrape off layer and hence the coupling is edge confinement (whether the plasma is in H-mode or in L-mode). When the plasma is in H-mode, the coupling is degraded compared to the L-mode coupling illustrated in Fig.57, corresponding to the density decay length being reduced by several mm. ELMs during the H-mode result

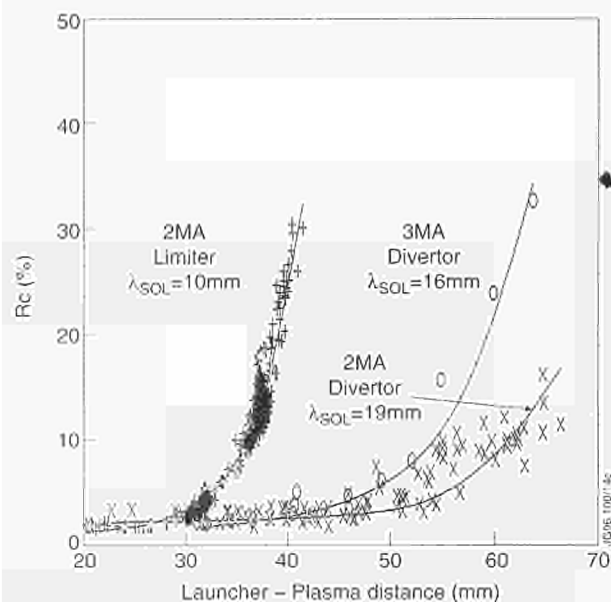


Fig.57: Reflection coefficient as a function of plasma-launcher distance for the top row of multijunctions in an L-mode plasma. In large fluxes of particles out from the plasma. This flux results in a transient improvement of the coupling, with the reflection reduced to levels equivalent to L-mode coupling. Thus the reflection coefficient has been seen to vary from 20% during an H-mode to less than 5% immediately following an ELM. During radiative divertor discharges, which have very frequent so-called “grassy” ELMs, exceptionally good coupling have been observed, with reflection coefficient below 1%.

Injecting gas into the plasma during the LH-pulse improved the coupling. This improvement was larger than could be explained by the increase in plasma bulk density alone. The improvement did not depend on whether the gas was injected from the gas injection pipe situated near the LH-Launcher, or from a gas injection module situated toroidally opposite the launcher. From this, it can be concluded that the improvement in coupling associated with gas injection is caused by an increase in the density in all of the scrape-off layer, and not by a local density increase near the gas introduction module which is being used.

The coupling was influenced by the injected power level. Injecting more power in one row of multijunctions was seen to improve the coupling not only in the row where the power was increased, but also in the other two rows of multijunctions. This improvement in coupling is caused by the plasma density in front of the launcher being modified by the LH-power.

The maximum power that can be coupled to the plasma increases dramatically when the reflection coefficient is decreased. This could give the impression that very high

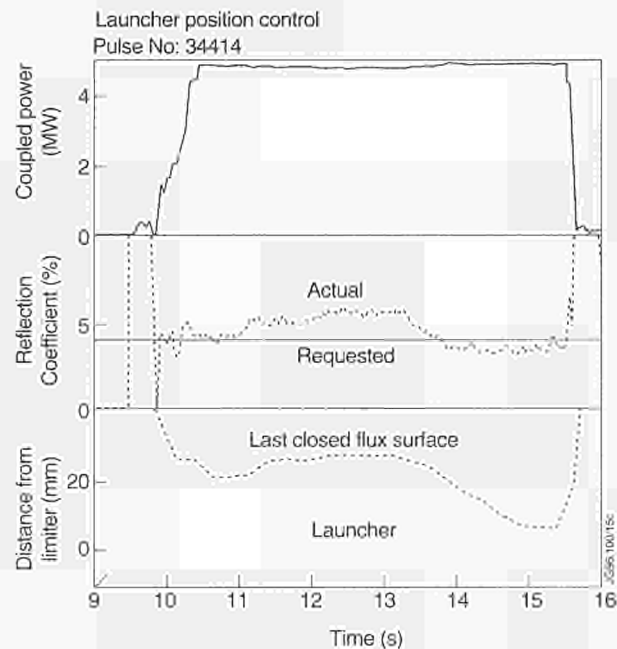


Fig.58: The use of the feedback controlled launcher position has been instrumental in achieving the highest power (7.3 MW) and energy (67 MJ) coupled so far.

powers could be achieved with reflection coefficients below 1%. Unfortunately this is not the case. Experience shows that when the reflection coefficient is below ~2% the density at the grill mouth is too high, resulting in breakdowns inside or immediately in front of the grill, thus severely limiting the amount of power that can be injected. For this reason, the maximum power can only be injected with the reflection coefficient in a very narrow window between 2% and 4%. As the density and density decay lengths vary continuously as the plasma parameters evolve, it is necessary to control the launcher-plasma distance in real time. Controlling the launcher position under feedback has proven a very efficient tool to keep the coupling at the desired level. Figure 58 shows the launcher being moved under feedback control, keeping the reflection coefficient at the requested value (4%). Between 11.6s and 13.6s, the launcher movement saturates at the furthest forward position, and hence the reflection is not kept at the requested value during this period. From 13.8s until the end of the pulse, the plasma is moving towards the launcher at a constant speed. During this period, the launcher follows the plasma movement with good accuracy. The observed reflection coefficient is kept close to the requested value. The small negative offset is due to the constant error, which is characteristic in a feedback system with only one integrating term.

The feedback control has also been used during ELMy H-modes, and it has successfully kept the desired reflection

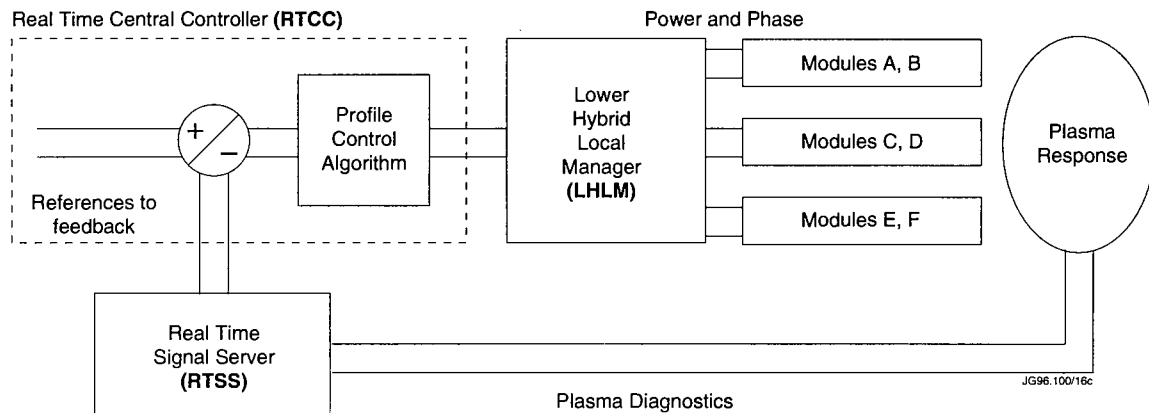


Fig.59: Schematic of the Real Time Power Control for LHCD.

coefficient during the development of the ELM-free periods. When an ELM appears, the position control cannot respond sufficiently fast, and the density in front of the launcher becomes too large for a short period. This fast variation in density during ELMy H-modes has so far strongly limited the power that could be coupled to ELMy H-modes.

Real Time Power Control

The current profile control experiments are currently conducted in a pre-programmed way, where power and phase waveforms are specified before the discharge. This open loop operation of the machine is subject to variations in the plasma conditions leading to uncontrolled excursions of the non-inductive current generated by the LH waves and the resulting total current profile.

Automatic control concepts with a perspective of application to steady-state operation scenarios have been therefore developed for the Lower Hybrid system. Reference waveforms are imposed to a set of plasma states, in contrast with the open loop operation in which power and phase waveforms have to be specified. The plasma parameters to be controlled in real time are loop voltage and internal inductance. The system is implemented in a front end computer working in discrete time steps with sampled data.

The control system consists of three main parts (shown in Fig.59):

- the Real Time Signal Server (RTSS) collects signals from numerous plasma diagnostics and performs some simple processing such as calibration and filtering;
- the Real Time Central Controller (RTCC) reads from a common memory area, shared with RTSS, of the relevant diagnostics selected for feedback. It then executes a network of interconnected algorithms prescribed by the user. The selection and interconnection

of these algorithms is configured using the Level 1 editor. These are typically waveform generation of feedforward powers, references for feedback, feedback timing, filtering and PID control. The network output is calculated every 10ms. The profile control algorithm is implemented in this area. The result of the processing are a power and/or phase demand sent through an Ethernet connection to the Lower Hybrid Local Manager;

- the Lower Hybrid Local Manager (LHLM) reads the power and phase requested by the RTCC and passes it on to the power plant after some basic processing such as clipping between maximum and minimum power settings and filtering. Provision for local feedback control of the generated power has also been made in the Local Manager.

Initially, a simple loop voltage controller has been implemented while establishing the engineering basis of this new control concept. In the longer term, a more advanced control scheme to control both loop voltage and internal inductance using LH power and phase is envisaged.

Scientific Achievements

LH Power Absorption

The fraction of the coupled LHCD power absorbed has been determined by a method utilising the time derivative of the total stored energy. The time derivatives of the plasma energy and the magnetic energy are evaluated directly after either the switch-on or switch-off of the LHCD power. This method can account for the power absorbed inside the normalised flux coordinate, $\psi = 0.7$.

The evaluation of the LHCD power absorption coefficient, α , has been performed on 69 LHCD discharges in a wide range of plasma parameters. The most important parameter is the electron density. The absorption coefficient

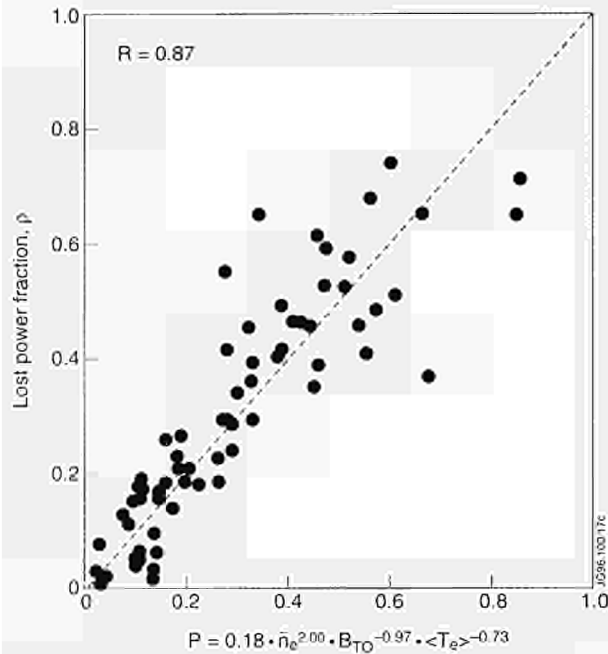


Fig.60: Regression fit on the experimental database of non-absorbed LH power.

cient reaches 100% of the coupled power at and decreases to only 30% at $\langle n_e \rangle > 3.0 \times 10^{19} \text{m}^{-3}$. The additional important parameters are the electron temperature and the LH wave accessibility to the plasma core. The LH wave accessibility can be described by the lowest parallel index of refraction that can penetrate into the plasma at $R=3.7\text{m}$:

$$N_{\text{loc}} \sim \langle n_e \rangle^{0.5} B_{T0}^{-1}$$

The waves with $N_{\text{pl}} < N_{\text{loc}}$ will be reflected at this point. A linear regression analysis using the quantity $\rho = 1 - \alpha$, which can be called the “lost” power fraction, was performed on the absorption database. The following parameter dependence was derived:

$$\rho = 0.18 \times \langle n_e \rangle^{2.11 \pm 0.08} B_{T0}^{-0.97 \pm 0.35} \langle T_e \rangle^{-0.73 \pm 0.17},$$

with a correlation coefficient $R = 0.87$. Experimental data are plotted versus the fitted values in Fig.60.

The absorption data has been compared with the Abel inverted profiles of the Fast Electron Bremsstrahlung (FEB) radiation. As a general result, high absorption is obtained when the peak in the FEB emission is located in the central region of the plasma ($\psi < 0.5$) and decreasing absorption coefficient is found as the power deposition is moved towards the periphery. This is in agreement with FEB data analysis and simulations, which show that the fast electron deposition profiles become more hollow with increasing density. The low absorption found at high densities can partly be explained by the fact that most of the power is absorbed at $\psi > 0.7$, and is therefore not detected by the method used for determining α .

The LH wave spectrum has been analysed with a probe measuring the radiation around 3.7GHz, located external to the tokamak vessel. Both the spectral width and the probe intensity increase as the wave accessibility is reduced. This indicates that the radiation detected by the probe comes from the inaccessible power, which is not absorbed but is instead scattered back from the plasma. Ray tracing calculations performed for high density discharges, $\langle n_e \rangle > 3.0 \times 10^{19} \text{m}^{-3}$ and $B_{T0} < 2.8\text{T}$, show that the rays which are inaccessible to the plasma core propagate towards the divertor region, merely bouncing at the plasma edge without any absorption taking place. In the X-point region, a rapid upshift in N_{pl} is encountered which leads to absorption of the power close to the plasma periphery. In low density discharges, the rays can penetrate deeper into the plasma on the first pass, which means that the divertor region can be avoided and the power deposition profile become more peaked.

Parametric decay instabilities have also been observed in the regime where low and peripheral absorption is obtained. A clear sideband in the LH frequency spectrum with intensity up to 15% of the main peak has been observed at $\langle n_e \rangle > 3.2 \times 10^{19} \text{m}^{-3}$ and $B_{T0} < 2.2\text{T}$ with LH power near 1MW. Parametric decay instabilities and broadening of the wave spectrum are both phenomena which occur at high density and which affect the wave propagation. With wave power deposition inside about 2/3 of the plasma cross-section, high absorption efficiency can be maintained.

Deposition Profiles FEB Camera

The experimental LH deposition profiles re-deduced from the hard X-ray emission, measured by the multichord Fast Electron Bremsstrahlung (FEB) camera system. Horizontal and vertical FEB cameras have been replaced by new versions, combining now FEB and neutron monitors together in the same camera housings. Additional advantages of the new system are the remote collimator control and the low noise detector electronics which is essential to extend the detection bandwidth to lower energy levels. The detection below the present lowest level of 133keV will be assessed in the next campaign. The camera power supply and cabling was completely rearranged for the new detectors. The cameras have been commissioned and calibrated.

Data Processing

The FEB data processing software has been rewritten to make it more flexible to handle changes in hardware

settings. The output now provides for every discharge analysis data files with the time evolution of count rates, line integrated intensities, local intensity profiles, also normalised by density and time traces of peak and width of the deposition profile. The profile inversion has been mapped on EFIT equilibria, where the local deposition profiles are approximated by parametrised model functions revealing the major deposition shape characteristics. For this purpose, the non-linear fit is performed applying a Levenberg-Marquardt algorithm. A wide spectrum of deposition shapes from centrally peaked to far off-axis have been observed. For a statistical approach to analysis of functional dependencies of the LH deposition profile, about 100 FEB profiles have been analysed and a data base built up in the parameter range $\langle n \rangle$ (n_0) = $4.6(6.0) \times 10^{18}$ - $3.0(4.0) \times 10^{19} \text{m}^{-3}$, $\langle T_e \rangle$ (T_{e0}) = $0.8(1.7)$ - $3.7(13.8)$ keV, I_p = 1.5 - 3MA and B_t = 2 - 3.4T.

LHCD Modelling

The LHCD experiments on JET have been modelled by means of numerical codes including ray tracing and beam tracing to describe wave propagation and 1D and 2D Fokker-Planck codes for the absorption calculations.

Current Drive Efficiency Calculation.

More than 50 pulses covering a wide range of parameters were modelled. The LH current drive efficiency $\eta_{CD} = I_{LH}(A) \times n_e(10^{20} \text{m}^{-3}) \times R_0(m) / P_{LH}(W)$ increases with volume averaged temperature in the range of $0 < \langle T_e \rangle < 1.5 \text{keV}$ up to values of $\eta_{CD} \approx 0.3$. Saturation was seen at low density and high LH power ($P_{LH} > 4 \text{MW}$). Possible causes of the saturation have been investigated. For most of the discharges, the LH driven current profile differs from the ohmic one. Therefore, a negative electric field is induced in a plasma region where the local LH current is greater than the ohmic current. This negative field strongly decreases the LHCD efficiency. The effect of saturation is well pronounced in low density discharges with $n_{e0} < 1.5 \times 10^{19} \text{m}^{-3}$. Calculations show that the energy content of suprathermal electron population increases above the bulk electron energy. Hot electron conductivity increases to the level of the Spitzer conductivity and above in this case. Negative electric field in conjunction with LH power can create runaway electrons in the direction opposite to LH driven current due to pitch angle scattering.

Profile Control Experiments

A wide range of LH driven current profiles $j_{LH}(r/a)$ have been observed in the LHCD experiments. The LH current

deposition profiles are derived from Fast Electron Bremsstrahlung (FEB) measurements. The FEB profiles broaden with higher electron density, plasma current and broader temperature profiles. This tendency is well reproduced in modelling. Details of the experimental FEB profile are sensitive to moderate variations of the plasma density and temperature. The calculated current profile $j_{LH}(r/a)$ is stable. There are only small changes in $j_{LH}(r/a)$ for small variations of $n_e(r/a)$ and $T_e(r/a)$. Modelling of LHCD during the current ramp-up stage with $I_p \leq 1.5 \text{MA}$ shows that, in a plasma with a narrow peaked temperature profile ($n_{e0} < 1.5 \times 10^{19} \text{m}^{-3}$), the power deposition is localised close to the plasma centre. Efficient electron heating leads then to freezing of the current profile in the central plasma region. Broadening of the temperature profile and increase of the plasma current lead to a shift of the power deposition from the centre. Calculated LH current and power deposition profiles are broad and hollow in discharges with $\langle T_e \rangle > 1.5 \text{keV}$ and $I_p > 2.5 \text{MA}$ during the quasi stationary phase preceding the NB heating phase. Simulated FEB profiles are in reasonable agreement with the experimental data. Sawtooth stabilisation and ℓ_i decrease are observed in the experiment. The performance of hot ion H-modes has been improved due to preceding current profile modification with LHCD.

Code Development

The LHCD code development has focused on further work on Fokker-Planck code validation and on structural changes required for routine use in the analysis of experiments.

- 1) The relativistic 2D Fokker-Planck solver implemented in the LHCD code has been validated by comparison with the 3D code "Bandit", as well as with analytical solutions. Particular attention has been paid to the cases of a wide spectrum (low plasma density), high magnitude of the quasi-linear diffusion coefficient D_{qi} (high LH power) and negative electric field. It has been found that both codes give similar solutions for low $D_{qi} < 1$. Numerical instabilities arise in Bandit for $D_{qi} > 1$. The 2D solver still gives quite reasonable results. Smoothness of D_{qi} is required in the momentum space to obtain a proper solution. The position of the outer boundary in the momentum space is also very important.
- 2) A fast version of the LHCD code has been implemented on a PC for scenario modelling studies. The CPU time consumption on the IBM mainframe com-

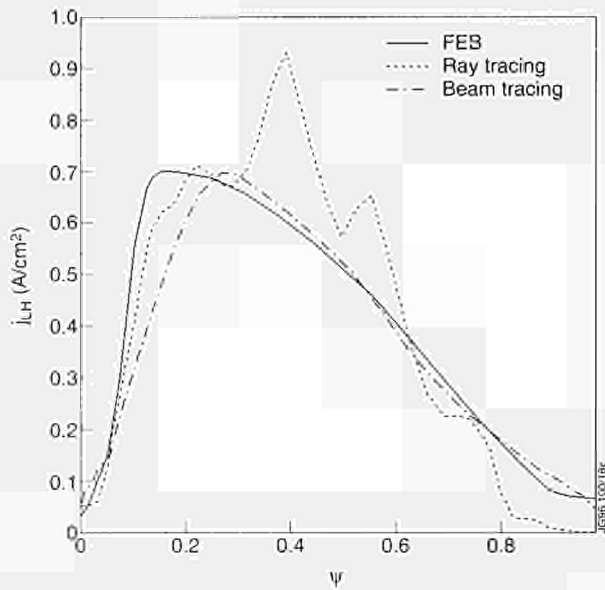


Fig.61: Comparison of LHCD deposition profiles from ray tracing, beam tracing in JETTO and a normalised FEB profile of Pulse No.35309 during the 2MA phase.

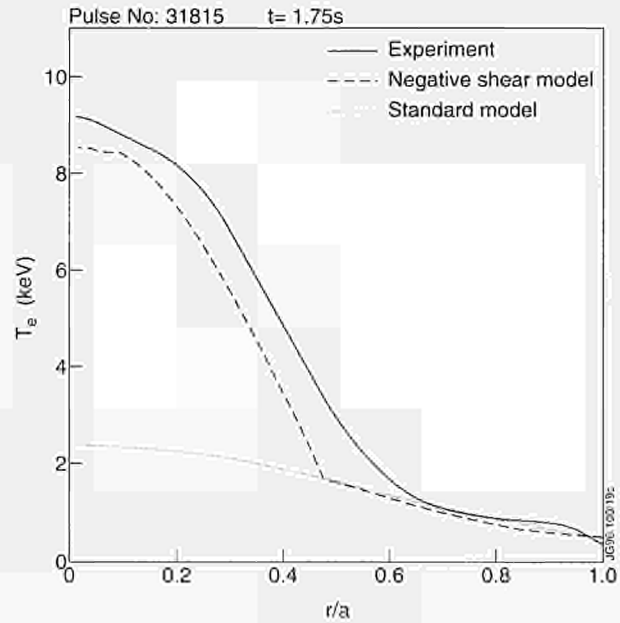


Fig.62: Experimental T_e -profile in a shear reversal discharge compared with the p

puter can be optimised then by consecutive runs of the fast version and the full code. The PC version of the code includes: three moments equilibrium code, ray tracing code, 2D (parallel momentum and radial coordinate) relativistic Fokker-Planck code, 2D (parallel and perpendicular momentum) relativistic code, code for simulation of FEB signal. Input data can be transferred from JET experimental data files using the IBM main frame facilities.

- 3) Two versions of iterative ray tracing and Fokker-Planck calculations can be used now both on PC and IBM main frame. Version 1 is based on iterative calculations of the quasi-linear diffusion coefficient D_{\parallel} (from ray tracing calculations) and a solution of the relativistic Fokker-Planck equation in the 2D space of parallel momentum and radial space coordinate, taking into account radial electron diffusion. The 2D relativistic solution in momentum space is determined in the last iteration for low spatial diffusion $D_{\parallel}(r) < 0.1-0.2 \text{ m}^2/\text{s}$. Version 2 includes iterative calculations of the quasi-linear diffusion coefficient D_{\perp} and a solution of the relativistic Fokker-Planck equation in the 2D space of parallel and perpendicular momentum. This version represents a more self-consistent approach to the solution of the LHCD problem in the case of low spatial diffusion but it requires more computing time. Comparison of results for current and power deposition profiles have shown good agreement between both versions with accuracy better than

10% for $D_{\parallel}(r) < 0.1 \text{ m}^2/\text{s}$. Consequently, the faster version 1 is used for routine analysis calculations.

Transport Code Modelling

Modelling of profile control experiments has been performed with the 1.5-D transport code JETTO. Code development and data analysis have focused on the areas of sawtooth stabilisation and the capability of LHCD to broaden the current profile up to hollow shape. The main results are exemplified on three representative experiments.

- 1) **Full LHCD on 2MA** with a subsequent ohmic ramp to 3MA: Full LHCD at 5MW of LH power in excess of 10s of duration with a subsequent ohmic ramp from 2-3MA (0.5MA/s) has been performed to raise $q(0)$ as much as possible in Pulse No.35309. The current profile remained frozen in after the current ramp for the duration of ICRH heating. Sawteeth have been stabilised from the beginning of the LH pulse and kept stable during the 3s of the ICRH heating pulse of 6MW power in contrast to the reference Pulse No.35313 without LHCD. The transport code analysis has been based on experimental plasma parameter profiles and the LHCD deposition profile obtained from the Baranov ray tracing code which shows good agreement with the local hard X-ray profiles (Fig.61). Both, the equilibrium reconstruction with EFIT and the JETTO transport analysis can explain the sawtooth stabilisation by an increase in $q(0)$ above 1 which is maintained during ICRF heating (Fig.62). The q -profiles obtained from transport code

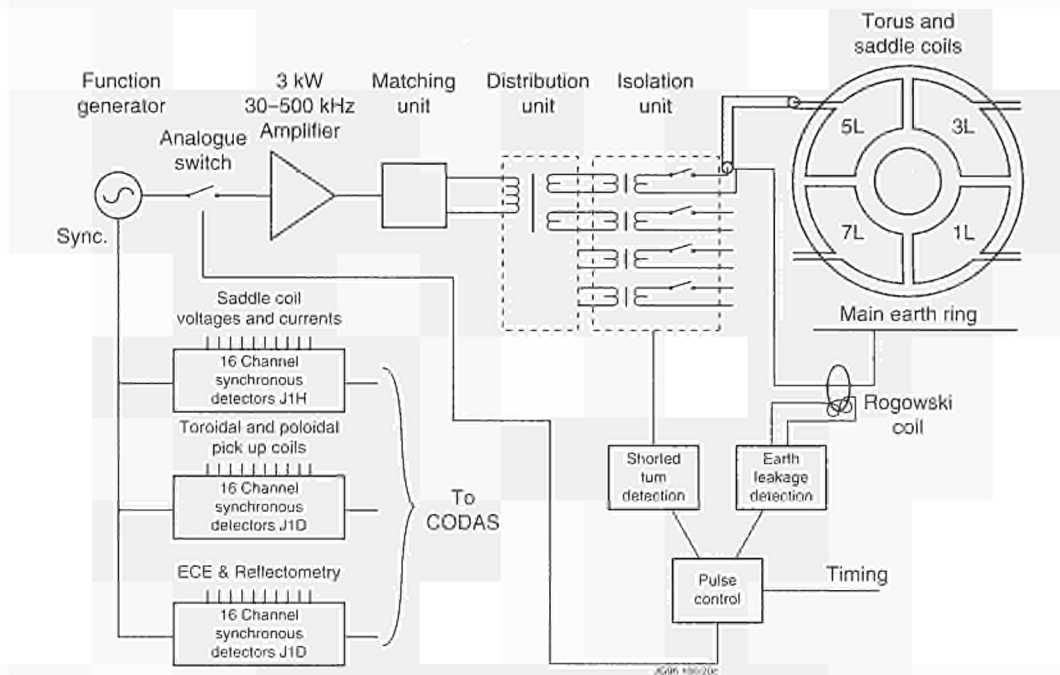


Fig.63: The layout of the active Alfvén eigenmode diagnostic

simulations indicate even local reversed shear in the central region.

- 2) **LH only on 3MA discharge:** long LH pulses of high power have been applied on low density discharges. A representative shot is Pulse No.34443 with $P_{LH} = 5.5\text{MW}$ on a 3MA discharge driving nearly the full plasma current for about 5s. Although the LH power in these experiments is deposited far off-axis with the peak at about mid-radius, the q -profiles from EFIT do not show a strong rise of the central q until the end of the LH pulse. In a JETTO transport code model calculation, the LH-only phase of Pulse No.34443 has been extended to estimate the time required for achieving a steady-state hollow current profile. After 6s of LH, $q(0)$ has increased only slightly and even after 12s the q -profile has still its minimum in the centre, consistent with the experimental results. Despite the off-axis deposition, the LH heating raises $T_e(0)$ from 3keV to 5keV in 6s and extends therefore the current diffusion time considerably. More than 20s would be necessary in these conditions according to the transport code calculations to form hollow current profiles.
- 3) **Shear reversal with LHCD in the initial current ramp-up phase:** the Pulse Nos. 31815 and 31753 have been analysed in interpretative and predictive transport code runs using the LHCD beam tracing model. Both EFIT and the transport code analysis show that the magnetic shear is already reversed in the early ramp-up phase due to LH. The reversed shear is

deepened by NBI heating later in the ramp-up. The measured high central electron temperature of $T_e \approx 10\text{keV}$ can not be explained with the Bohm transport model for L-mode discharges. A first analysis suggests that the confinement is considerably improved inside the region of negative shear. A good qualitative agreement between experiment and modelling has been found by dropping the Bohm coefficient of the standard L-mode model and just keeping the gyro-Bohm term inside the region of negative shear.

Toroidal Alfvén Eigenmode Exciter

The active Alfvén Eigenmodes (AE) diagnostic became operational in 1994. It makes use of the saddle coils located within the torus. These are used both to excite the Alfvén Eigenmodes and as receivers to detect them.

The layout is shown in Fig.63. A function generator provides a 30-500kHz signal to the 3kW amplifier to excite the saddle coils. The coils to be energised are selected in the distribution unit. The isolation unit provides the 10kV isolation required between the amplifier and saddle coils. It also incorporates vacuum relays that disconnect the AE diagnostic when the saddle coils are used by the Disruption Feedback Amplifier System. The saddle coils that are not energised are used as detectors. By selecting different combinations of saddle coils and their relative phase, different AE modes can be excited. The saddle coils are protected by earth leakage detectors and shorted turn detectors. These interrupt the power for 20ms then re-apply it.

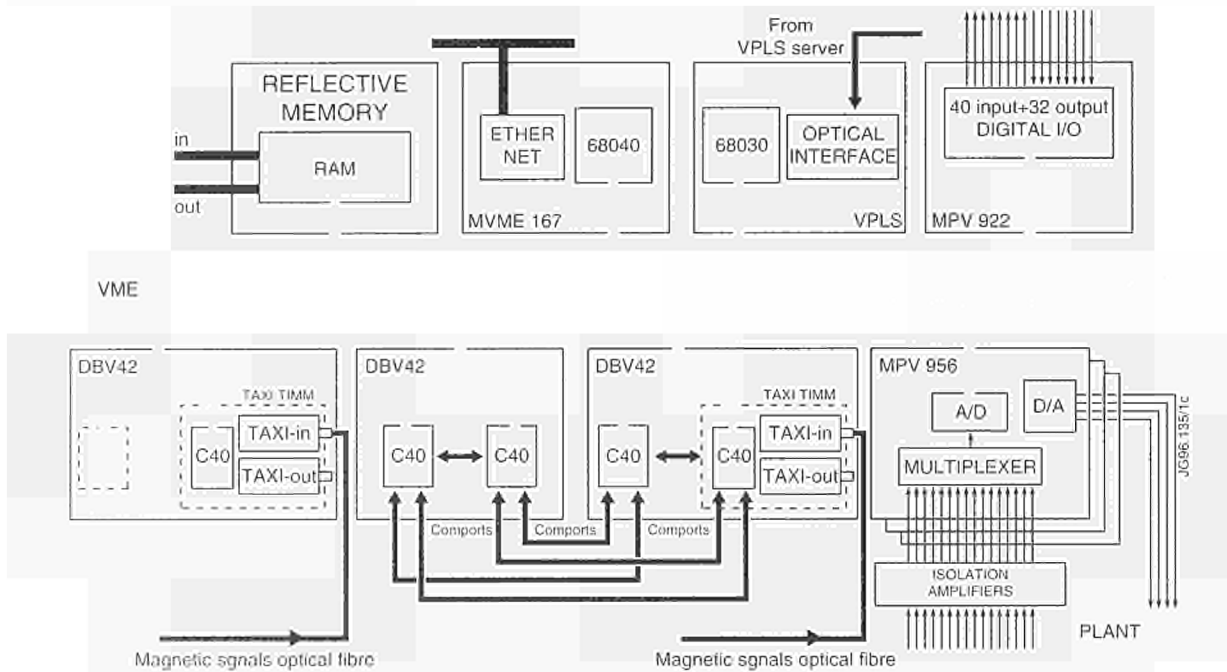


Fig.64: The digital layout of the upgraded shape controller for the Mark II divertor configuration.

The voltage signals from the coils as well as the amplifier and coil currents are fed to synchronous detectors, which provide the in phase and quadrature parts of the signal. Two additional sets of detectors are situated in the Diagnostic Wing. These are used to detect the AE signals on the toroidal and poloidal magnetic pick up coils and the ECE and Reflectometry diagnostics. The pick up coils provide spatial information that allows the AE mode to be identified. The current in the three turns of the saddle coils is less than 10A. This results in a change of magnetic field $\delta B/B \sim 10^{-3}$. The detectors are sufficiently sensitive to extract the resulting AE signal from the noise on most channels.

To detect the AE resonance the excitation frequency is swept up and down at around 200kHz/s. During 1995, the Real Time Signal Server (RTSS) and Real Time Central Controller (RTCC) were used to steer the excitation frequency to the resonance calculated from the toroidal field and density. This allowed a smaller sweep range to be used and hence a more frequency crossing of the AE resonance.

At the end of the 1995 campaign, experiments were performed using two of the antennae of the ICRH system to produce a beat frequency in the AE range. The frequencies from the generators were mixed electronically to provide the difference frequency as the synchronous signal required by the detectors. During the first experiments, the beat frequency was driven to the range of the AE resonance by adjusting the ICRF matching system. A few dedicated pulses were also performed where the beat

frequency was actively driven around the AE resonance by RTSS and RTCC.

Operations Systems

Plasma Position and Current Control

An entirely new plasma position and current control system (PPCC) was developed for the pumped divertor phase of JET. Based on VME digital technology, this system processes data obtained from the magnetic diagnostics, using fast digital signals processors (DSPs), to control the plasma boundary and the poloidal field circuit currents in real-time. The control functions are divided between two controllers. The shape controller (SC) is intended to control a mixture of plasma-wall distances and poloidal field circuit currents, so as to control the overall shape of the plasma boundary including the divertor strike points, on a timescale of 2ms. The vertical stabilization controller provides feedback control of the vertical speed of plasma current moment on a faster timescale and has a cycle time of 50ms, which is well matched to the speed of the fast radial field amplifier. Both these systems operated satisfactorily during the Mark I divertor campaign and satisfactorily proved the digital control concept.

As a result of operational experience gained with plasmas in the Mark I divertor configuration, it was decided to upgrade PPCC for Mark II divertor operations. The processing power of both controllers is being improved substantially by increasing the number of DSPs in each from two to

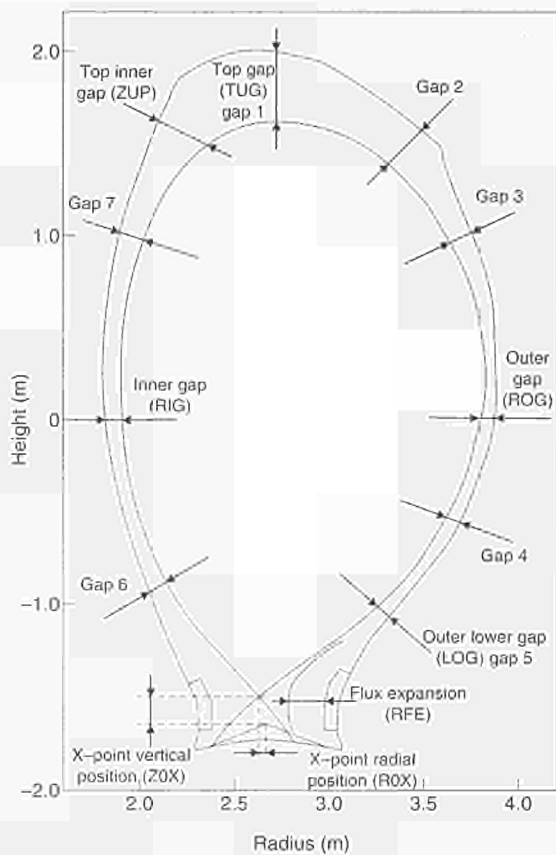


Fig.65: Overview of the plasma-wall gaps which can be controlled by the upgraded shape controller. A mixture of up to nine gaps and coil currents can be controlled simultaneously. Note that the gaps labelled numerically are calculated for information and are not, in general, available for control.

four. Figure 64 illustrates the digital layout of the upgraded shape controller. The most significant modifications are being made to the vertical stabilization system, as new, faster ADCs have been developed to provide the data to the CPU processors more quickly than in the past. Since the processing capability of the vertical stabilization controller was limited essentially by the delay in providing the data to the processors, this will allow much greater flexibility in the control algorithm. For example, data from other diagnostics such as soft X-rays can be incorporated into the vertical stabilization and more advanced approaches to feedback control can be investigated. The increased processing power in the shape controller is required to provide the control capability required for the more closed Mark II configuration as well as to permit additional facilities requested by the operational teams. In particular, additional control gaps (Fig.65) are being provided to allow for better control of the plasma boundary for specific experimental scenarios.

Real-Time Network Operation

The power and flexibility of the on-line Control and Safety Systems have been greatly enhanced as techno-

Table IX:
Subsystems for Real-time Control and Protection

CPS	Coil Protection System
PPCC	Plasma Position and Current Control
KCI	Magnetics Measurement from the torus
PPS	Plasma Protection System
RTGS	Real-Time General Services - includes 60 processed signals from the Real-Time Signal Server, Plasma Density Validation and Real-Time Feedback Power Controller
VC/GAS	Vacuum System Gas Control, including Plasma Density Feedback
Local Controllers	Local control processors for Neutral-Beams, Radio-Frequency, Lower-Hybrid and Saddle-Coils.
XLOC	Local processor network which evaluates plasma magnetic parameters, such as wall-gaps, Plasma pressure, Inductance etc.
KGI	Laser Interferometer Control for real-time density measurements.

logical advances are utilised. VME digital processors, interfaced to the UNIX control computers, are now widely used on the JET site. This increase in the real-time processing power has opened up new horizons in control and protection. This has also led to demands on the interlinks between the systems. Signals produced in real-time by each system can be shared by other processors. For example total coil currents, plasma-wall gaps, energy confinement times, plasma impurity levels, etc. The interconnectivity of VME processors for real-time use is not well-developed, and efforts to solve these problems have led to a state-of-the-art Real-Time Network. The main sub-systems now interlinked for Real-Time Control and Protection are set out in Table IX.

Network links are provided through a variety of methods, such as fast parallel digital transmission (Taxi-Link), pulse-trains, ethernet-loops and analogue links. Currently, a "reflected-memory" system is being investigated, where selected portions of the memory of one microprocessor is imaged into the other microprocessors via fast digital transmission light fibres.

The gain of this advanced Real-Time Network is a vast increase in the flexibility of JET operations and an overall increase in the safety provisions. The cost is a much more complicated interface, with many more possibilities than previously available. To resolve this problem, a new expert operations-team position - the Plasma Duty Officer has been introduced, who will be on duty in the

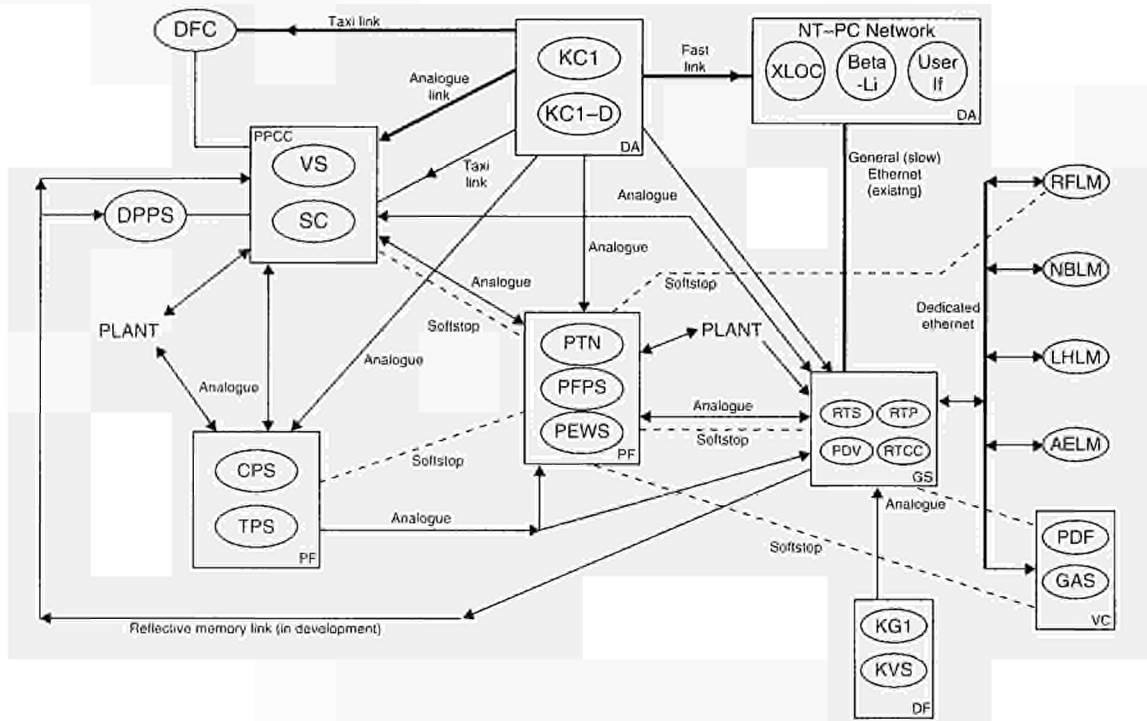


Fig.66: Real-time Control and Protection Network

control room to help the physics staff realise the full potential of the systems, and help the engineering staff with the setting-up and operation of the network (Fig.66).

Disruption Prediction and Prevention System

The aim of the Disruption Prediction and Prevention System (DPPS) is to provide an advanced technique for predicting plasma disruptions. Disruptions are a major problem in operation as the structural forces they exert on the vacuum vessel can, in extreme cases, threaten its integrity. Therefore, it is important to find methods of predicting such events, which could give time for the control system to undertake actions to avoid them or to safely terminate the pulse.

The first part of these studies comprises an analysis of the methods used at present to classify a disruption. Unfortunately, some of these techniques, used to identify a disruption, imply knowledge that a disruption has occurred. For some cases, it is more easy to recognise the events that could have led to a disruption, if it is known that it had occurred. This caused some difficulties in defining algorithms which should be able to stop “dangerous” pulses, and at the same time leave the possibility of reaching the limits of the JET machine performance.

For these reasons, the methods implemented on this system will be considered as a whole to avoid missing useful information which determines a disruption precursor, with-

out stopping good pulses which reach the operational limit without disruption. The methods studied will involve:

- Use of the I_p -q diagram for predicting disruption;
- Density disruptions detection;
- Mode-lock detection;
- In-Vessel Components protection;
- Neural Network disruption prediction.

At a design review meeting, the DPPS strategies to predict a plasma disruption have been approved and connections with the other systems have been defined. The system will acquire data from several diagnostic systems, and it will be connected to the PPCC system in to acquire information on the status of the pulse for the first period. Then, if DPPS demonstrates its reliability to institute plasma control actions when required.

The next period will be devoted to the design of the cubicle and the installation of the hardware. DPPS will be based on two floating point DSP processors, which will provide the computational power to implement the necessary algorithms. It will be connected to PPCC and RTSS via reflective memory, to diagnostics KS3 and KB3/4 via analogue links, and diagnostics KC1D through an optic link.

All the software algorithms have been well specified. The code will be structured as the PPCC code. This will provide the possibility of using all the tools developed for PPCC, thus saving time during implementation and commissioning of the system.

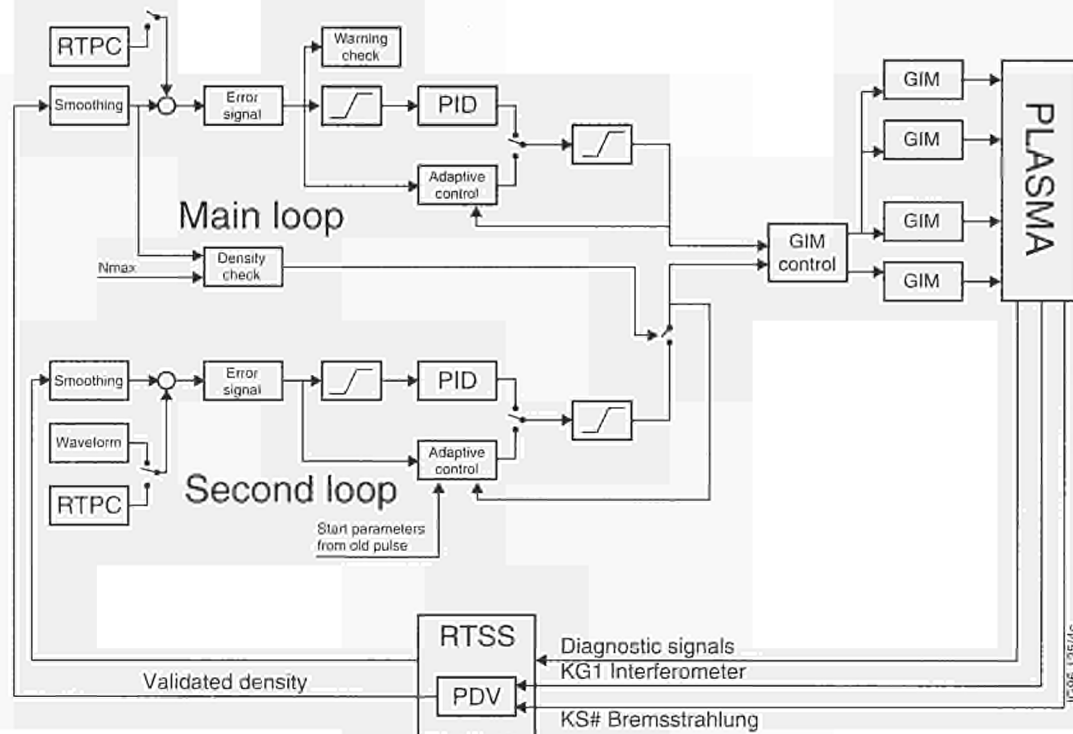


Fig.67: The density feed-back system

Plasma Fuelling

The Plasma Fuelling Group is responsible for the control and monitoring of the torus plasma density by control of the torus gas introduction systems, the pellet injection systems and the analysis of the torus exhaust gas.

Torus Plasma Gas Introduction and Density Control

The micro-processor controlled CAMAC units for the plasma density validation (PDV) and for the plasma density feed-back system (PDF) were replaced by VME units, during the last campaign. PDV is validating the line integrated density signal from the interferometer (KG1) and is now replacing it by one derived from the Bremsstrahlung diagnostics (KS3), in case the interferometer has problems with fringe counting. It has now three output channels each programmable to a choice of combinations of KG1 signals. The PDF (Fig.67) - controls the ten standard and two diagnostic gas introduction modules (GIMs). These are now complemented by the valve which is to supply tritium during the DTE I experiment and the pellet centrifuge when the latter is used in a quasi-continuous gas valve manner in density feed-back.

The PDF system receives the signal from PDV via the real-time signal server (RTSS) and contains two hierarchical feed-back loops: the first one commanding any combination of the above gas inlet valves at various locations on the torus

with reference to the validated density; the second one can be linked in RTSS to any other monotonous signal. In another mode, PDF will also respond to direct valve action commands by the real-time power control module (RTPC); the latter may also be programmed to present a density request signal to the PDF loop controllers. The new software has been specified, and first commissioning will start soon. The adaptive controller - with constant updating of the plant image, i.e. plasma behaviour - to replace the density PID controller will also be available with an improved response with regard to critical situations like X-point formation, ELMs, disruptions, and pellets.

Pellet Injection

There are two pellet injection systems, the pellet centrifuge and the high-speed launcher, which are detailed below.

The Pellet Centrifuge

The pellet centrifuge is for the shallow deposition of pellet fuelling mass beyond the recycling layer at high equivalent flow rates. It is intended as an intermediate radius particle source tool in connection with the divertor pumping investigation, and is in an advanced commissioning phase on the machine. A more detailed description of the design and the functions of the various components of the pellet centrifuge can be found in previous Progress Reports.

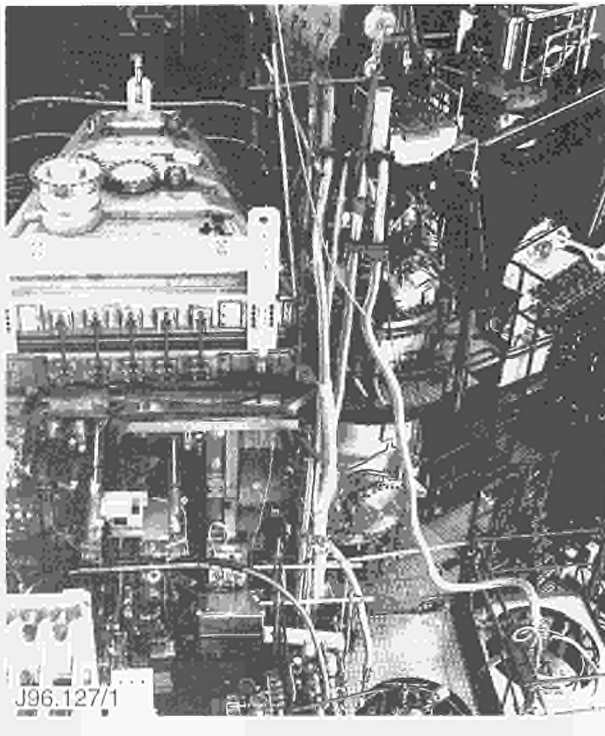


Fig.68: Pellet centrifuge in the Torus Hall

i) Basic systems characteristics

The centrifuge has been conceived to deliver long strings, approaching 1 minute duration, of deuterium pellets of nominal 2 and 3mm cube size at repetition frequencies of up to 40s^{-1} with velocities between 50 and 600ms^{-1} . It does this by accelerating pellets mechanically from the hub to the tip of a rotor arm ($R = 0.35\text{ m}$) from which the pellets leave at about 1.4 times the rotor tip speed. Each size of deuterium ice pellet can be launched from one of up to four possible individual extruder units into the centre part of the centrifuge rotor hub. The design of centrifuge rotor and stop cylinder follows closely that of the centrifuge developed for ASDEX Upgrade by IPP Garching, Germany, who also advised JET under contract.

The extruder - the pellet formation unit - is of a new design by JET to provide the much larger number of pellets per tokamak pulse, and is novel in that it uses "dynamic cooling". In this unit, the ice of a reservoir of $\sim 150\text{cm}^3$ is extruded into a long channel to form a rod of pellet cross-section; a length of rod equivalent to the pellet dimension is then cut off by a chopper magnet, pushing the resultant pellet with the same stroke onto the hub of the rotor. In the vacuum vessel, a large built-in LHe cryopump of $>10^3/\text{s}^{-1}$ pumping speed copes with gas losses stemming from pellet acceleration and guidance. This keeps the pressure below 10^{-3}mbar . To operate on the machine for a few days, the capacity of the cryopump is

designed for 2500 barℓ of deuterium. As a consequence stringent safety measures are demanded against hydrogen deflagration after regeneration, with implications for the design and pressure classing of the main vacuum vessel and the cryopump.

ii) Progress summary

Initially, the entire system had been erected for commissioning purposes in the Assembly Hall in order not to suffer from restrictions imposed by the simultaneous operation of the torus. Its installation on the torus should have taken place in the short machine shut-down in April. However, due to the delayed assembly of the pellet extruder caused by manpower limitations, the centrifuge system could only be transferred into the Torus Hall after the end of the 1994/95 campaign. It was installed during July/August, inclusive of a trial fit of its flight tube with pellet track to connect to its torus valve and, through it, to the in-vessel track already installed in the torus in 1994. Figure 68 shows the vessel on the right hand side of the Pellet Injector Box (PIB) on Octant No.2 in the Torus Hall. The flight tube was temporarily removed again to permit the installation of the RF lines to the Octant No.2D ICRF antenna. The centrifuge system was connected to its local cubicles in J1S, re-commissioned and went into remote operation, only interrupted by short breaks to mend or improve components.

The most challenging components of the system is the pellet formation unit or extruder. To reach the specified goal, the equivalent flow rate of 1000mbarℓ/s^{-1} for about 1 minute amounts to about 100cm^3 of deuterium ice from approximately 110 standard barℓ gas and the extruder has been designed to provide this volume as a minimum. A water-driven hydraulic piston at room temperature within the vacuum bounds of the main vessel exerts a maximum force of 30kN onto the $\sim 15\text{cm}^2$ cross-section of the piston (maximum pressure $\sim 200\text{bar}$) pushing the ice in a helium cooled cylinder towards the nozzle leading into the extrusion channel. To create the cubic pellets, an ice rod is extruded with the cross section of the pellet cube reducing the ice cross-section by a factor of 100 to 200. The rod is chopped off at suitable length equalling the pellet dimension. At the maximum rate, 3mm pellets need to be extruded at $\sim 10\text{cm/s}$, while being chopped off at about 40s^{-1} . The LHe flow is introduced at the tip and runs up the extruder column within the double hull formed by the inner, mainly copper part containing the ice and the outer

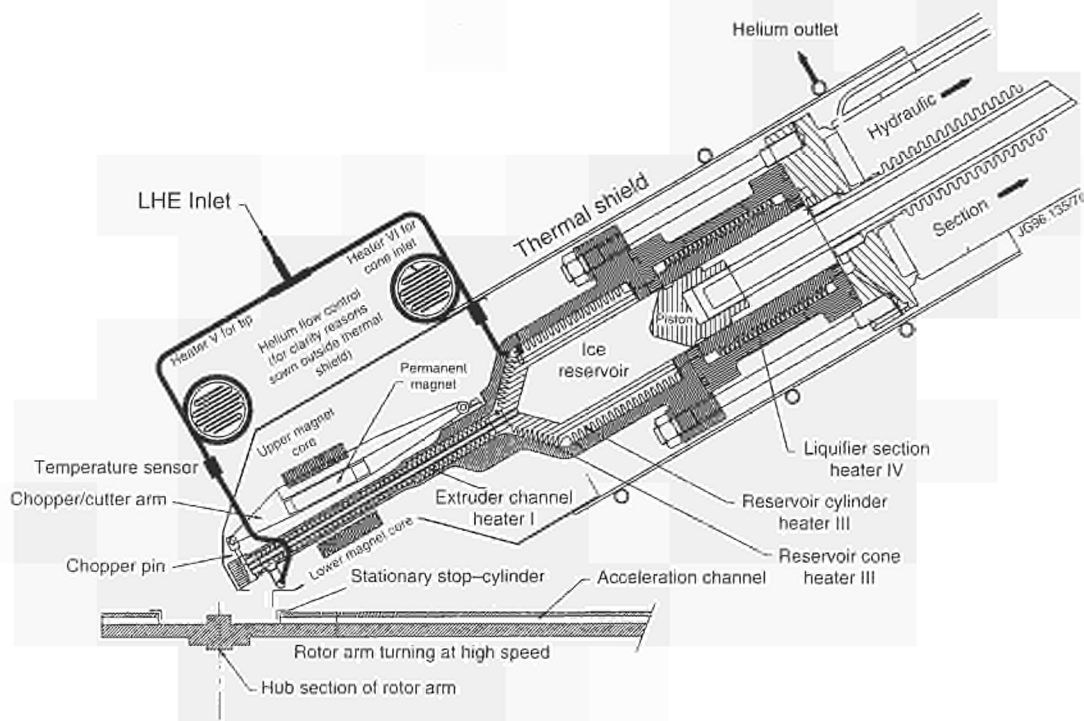


Fig.69: Schematic of lower extruder section

stainless steel envelop. The heat flow is regulated by electrical heaters wound onto the inner copper mandrill - four individually feed-back regulated sections - and acting against the helium cooling. To limit the forces, deuterium ice can only be extruded at temperatures of 14°K or higher, whereas from previous experience, pellets should be accelerated preferably at temperatures as low as about 7°K. Therefore, it was attempted to cool the deuterium ice "dynamically" during extrusion from some higher temperature while it was sliding along the wall of a sufficiently long copper channel (~200mm). This should permit the thermal conductivity of the deuterium to cool the ice while it is moving towards the chopper/cutter, provided the heat transfer to the wall is sufficient - a somewhat daring proposition at the highest intended speed.

Two extruder units, occupying two of the four possible positions in the stop cylinder acceptance sector are being prepared for 2.7 and 4 mm pellets. Technical commissioning of its systems versus the design parameters yielded very satisfactory results: LHe flows of up to 25 l/h were achieved and controlled, deuterium ice could be condensed to fill the reservoir to the intended amount and the magnetically driven cutter worked at 40 s⁻¹ for a short while. The actual cutter action led to a cutting speed of ~2m/s within about 5ms, exerting a cutting force of up to 40N.

Unexpected behaviour of the deuterium ice under the extrusion pressure was observed. The highest exerted

pressure did not permit the ice to be extruded at the anticipated temperature distribution, except for transient conditions from which valuable key data were derived. Elevating the entire temperature profile in stationary conditions led to back extrusion (i.e. ice by-passing the piston) because the intense downstream heating did not leave sufficient enthalpy in the helium flow to manage the required heat transfer in the upper part of the column. The problem was overcome by splitting up the helium flow (as shown in Fig.69) and re-inserting cold helium into the wide cylinder section where the piston needed good mechanical ice quality to exert pressure. Two additional heater exchangers regulated the partial streams of helium. This permitted the temperature of the channel entrance area to be raised to 16-18°K, yielding very soft ice conditions and to successfully extrude pellets at up to 1cm/s at chopper frequencies from 2 to 7Hz. The temperature of the final pellet was ~10-12°K. The system conditions - friction and heat transfer being the main parameters - are not yet fully understood: e.g. there are narrow optimums in the extrusion speed versus extrusion pressure curves, where one would expect monotonic functions. At the moment, stationary and reproducible conditions with the above extrusion speed during cutter openings (10 to 100ms) can be expected for a set of heating parameters after some seconds of cutter operation (to establish stationary eddy current heating) for times of 20-40 minutes making

use of the full 150barℓ reservoir content. This would correspond to ~90mbarℓ/s⁻¹ equivalent primary fuelling rate. The repaired cutter beam and magnet has now performed about half a million cutter actions. Pellets from these long-pulse operations have been accelerated by the centrifuge at speeds around 400m/s.

The second extruder for 4mm pellets is well advanced, and should be ready for installation at the start of 1996. It is intended to be commissioned before plasma start-up. On the experience with the first extruder with the difficulty of extruding ice, a review panel came to the conclusion that as a matter of design safety, the extrusion pressure should be enhanced. The reservoir cylinder was equipped with an insert reducing the cross-section area of cylinder and piston by factor of 10 but the pressure could only be raised by a factor of 3.5 for the reason of insert sealing. The obvious penalty was the reduction of the reservoir volume by about the same factor, but it was felt that 10barℓ would still be sufficient without apparent experimental limitations. For this extruder, the available force approached the shear strength of the ice, if the ice were firmly frozen to the channel wall. If similar performance values could be achieved for this extruder, then fuelling rates of around 300mbarℓ/s⁻¹ could be expected at 4Hz.

The advantage of this development approach along the lines of the two extruders on somewhat complementary extrusion principles is that valuable design data for a centrifuge to feed ITER-like machines can be evaluated in parallel and moreover in the proper environment of such a machine.

iii) Centrifuge performance summary

The pellet centrifuge system performance expected for torus operation is: 2.7mm pellets are available with repetition rates of up to 7Hz but with extrusion speed is limited to 1cm/s (equivalent to ~4Hz nominal repetition frequency) leading to more than 80 mbarℓ/s. Pellet sequence pulse length can be considered unlimited (usable 150barℓ of ice, the condensation of which is performed in about 30 minutes). Pellet speeds of 150 to 400m/s have been operated and there is no reason to believe that the full range of 50 to 620m/s should not be available. From comparison with the ASDEX Upgrade centrifuge, 930m/s (i.e. 300 Hz rotor frequency) may also be accessible but is outside the initial specifications. Extruder performance for 4mm pellets can only be speculated on but is not expected to be worse than that of the first extruder. As a matter of principle for a high inertial moment

rotor, the centrifuge rotational speed is more or less fixed during a plasma pulse and can only be slowly changed at a rate of ~100Hz (i.e. 300m/s) per 10 minutes. Systems operation should be available all day and regeneration may only be required once or twice a week. Regeneration with additional heating is ~2-3 hours; cryopump cool-down after regeneration is ~4 hours and extruder cool-down with the cryopump in operation is ~2 hours; both can be performed automatically (e.g. at night). The simultaneous availability of two extruders, although desirable, is uncertain at this stage due to the tricky regulation problem of parallel LHe circuits.

The High-Speed Pellet Launcher

The high-speed pellet launcher on the basis of two-stage gun technology has been under development for some years. The system was installed on the machine in 1994 and preliminary experiments (e.g. the injection of a polypropylene pellet for plasma termination) were carried out. However, it was given very low priority and only very limited effort was spent on the commissioning during plasma operation. Nevertheless, reproducible condensation of single pellets, their transfer into the breech and reliable follow-up by the two-stage gun firing sequence for speeds exceeding 3km/s could be demonstrated for ~400 shots. After initial proof of deuterium pellets following sabot removal in the microwave cavity, the injector performance deteriorated, with full technical performance still available. The experimental window could not be used, which had been foreseen for deep pellet injection on the plasma. The reason for this could not be investigated to this date due to manpower limitations, but it is believed that the lack of possibility for barrel cleaning is at least a contributory factor.

Gas Collection System

In the 1994/95 experimental campaign the gas collection system (GCS) for the analysis of the torus exhaust gas was operated in a limited way without the use of its specific LHe cryopump which could not be finalised in time. The GCS measures the time evolution, absolute amount and chemical composition of the gas released from the vacuum vessel by wall out-gassing, after plasma pulses, divertor cryopump regeneration and during glow discharge cleaning. The main tools are pressure and mass spectrometer measurements complemented with gas sampling to external analysis stations. Figure 70 shows a schematic of the GCS.

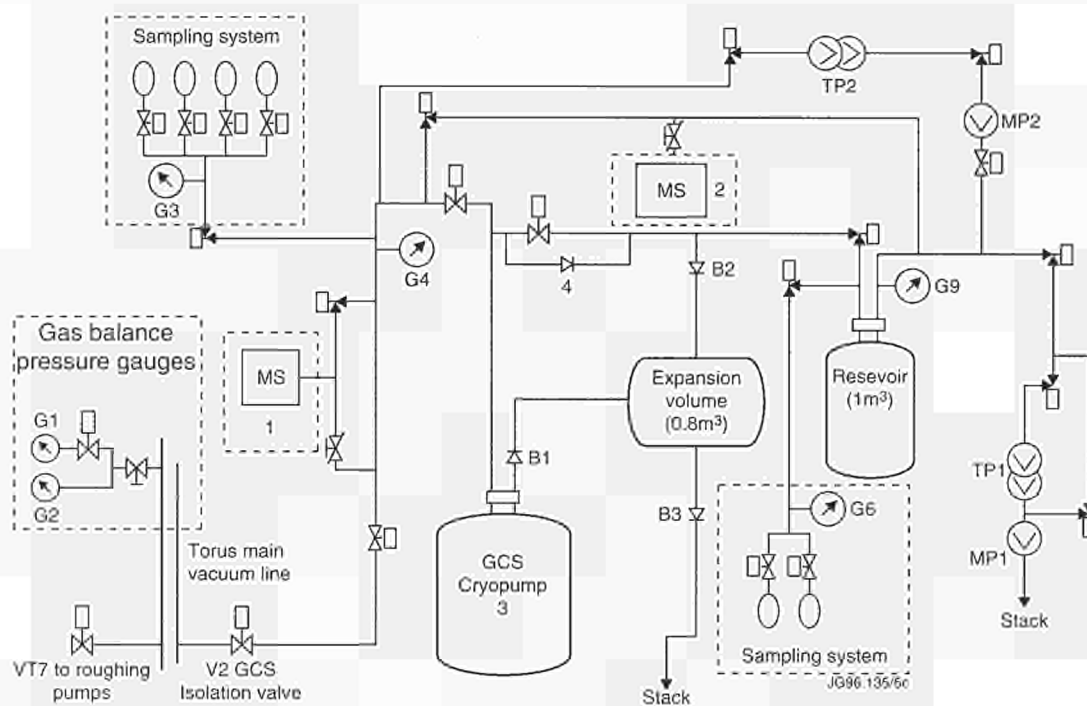


Fig.70: Schematic of the Gas Collection System.

Measurements of gas balance have been carried out during the 1994-95 Mark I campaign (graphite and inconel wall, with Be evaporated coating), both with C and Be divertor tiles. The average deuterium recovery after a non-disruptive shot, when the divertor cryopump is not operational, varies from 30 to 50% of the input, depending on the total gas input, both for C and Be divertor tiles. Within the experimental uncertainties, the results with both C and Be target tiles are comparable to previous JET results for a Be coated machine.

When the divertor cryopump is operated during high performance discharges (at low gas input, such as for ELMy H-mode NB fuelling only and hot-ion regimes), the short term wall retention is a factor of 2 to 5 lower both in the C and Be phase. For other types of pulse, the cryopump increases the amount of gas necessary to sustain the discharge by a factor of 2 to 5 causing the short term absolute retention to increase by a factor of 3 to 4 (Fig.71). Nevertheless, the recovery fraction is the same for disruptive and non-disruptive cases when the cryopump is on, in contrast to pump-off discharges for which the recovery fraction is 20% higher for disruptive pulses. This indicates that the wall load is always below the saturation level and almost constant for all kinds of operations, suggesting that the cryopump depletes the walls both during and after plasma pulses, with a resulting low D (and T) retention in the long term. Similar trends are observed for pulses with impurity seeding.

Negative values at low input are for high performance discharges (ELMy H-mode NBI fuelling only and Hot Ion regimes) or for pulses with no sustained break-down. In these case the walls are depleted during the discharges.

During the shutdown, a number of enhancement have been carried out:

- The GCS pipework is connected to the torus forevacuum crown pumping line in such a way that it can take over the pumping of the torus exhaust for certain times and the design of the cryopump intended a total capacity of 1000 barℓ of gas, equivalent to the capacity of the torus cryopump. It became obvious in the operation of the GCS that it is very difficult to keep clean analysis conditions in the GCS pipework, ini-

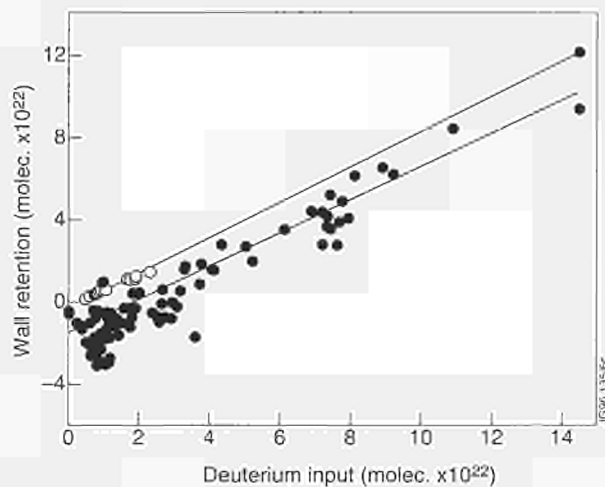


Fig.71: Short term wall retention as a function of the gas input.

tially designed to operate at room temperature at all times, when it is constantly contaminated with impurities from the torus exhaust. To improve this situation the pipework and its collection vessel have now been modified so that they can now be regularly baked to 250°C, and some consideration is given to even operate at elevated temperatures:

- The GCS cryopump has now been pre-commissioned outside the system - without the use of carbon cloth for helium pumping - and is currently being incorporated into the system. The capacity of the cryopump has turned out to be of ~600 barℓ;
- The transfer and exhaust forepumps in the system have been chosen to be oil-free membrane pumps with viton membranes to atmosphere. Their life-time is limited and so there is always the danger of gas diffusion through the ageing membrane. To eliminate this drawback, which has analysis as well as safety implications, the membrane pumps are being encased into a secondary containment which will be filled with Xenon. This heavy rare gas will not upset the analysis (except for the case of Xe seeding of the plasma) should traces of it get into the system and it will not cause a major GCS shutdown, if the membrane should rupture;
- The GCS is equipped with two bursting discs B1 (5 barg) and B2 (0.3 barg) against over-pressure from cryopump and 1m³ tank, respectively. In case of a burst of either disc, the gas will be captured by expansion tanks of sufficient size (~800ℓ) which is connected via a further bursting disc B3 (5 barg) to the torus forevacuum exhaust. In this way, the safety of the GCS is maintained and the integrity of the analysis capability against an accidental bursting disc opening is maintained.

Vacuum Systems

Vacuum Systems Operations

The vacuum systems generally performed well during operations in 1995, with reliability being the best since the start of JET. This coupled with the prompt dedicated action of the "on-call" team ensured that very little operational time was lost due to vacuum system problems. Leak detection was vital in promoting relatively trouble free operation. In 1995, a total of 13 leaks were found on peripheral equipment (systems) of which five were of sufficient severity to cause operations to be stopped.

The efficient conditioning provided by the combination of vessel baking and glow discharge cleaning (GDC)

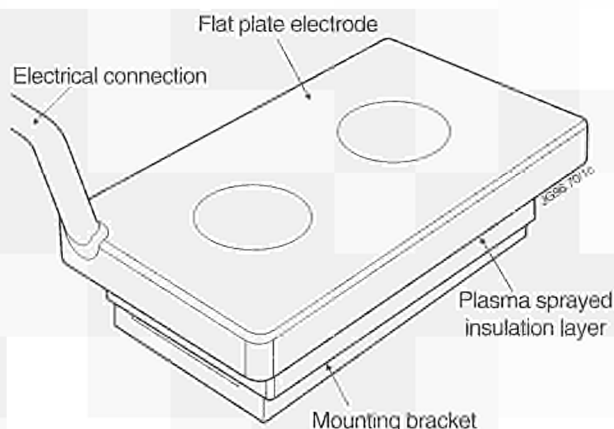


Fig.72: GDC Electrodes

ensured, that following intervention or leak, the vessel conditions required for plasma could be quickly restored and maintained. The GDC electrode inductor spiral required to accommodate RF-assisted GDC was damaged by halo currents during tokamak plasma disruptions. Experiments were performed to assess the effect of RF on the glow discharge characteristics. It was concluded, that for JET, combined RF/DC clearly had no significant advantages over pure DC operation, provided highly stable DC current control was maintained. The damaged electrodes were converted to simple plates (Fig.72) during a short intervention. These electrodes will continue to be used in the future due to their effectiveness, simplicity and robustness.

Vacuum Systems Enhancement and New systems

Vessel Baking

Critical thermal interactions between the in-vessel components has dictated the need for a new high reliability torus temperature measurement and interlock system. The newly designed system works on the basis of redundancy and fault tolerance to give high reliability. Sixteen thermocouples are distributed around the vessel. These are individually conditioned and shared between two independent Programmable Logic Controllers (PLC). Average temperature for each group is computed and consistency between the results is checked. An average vessel temperatures for the new baking plant control system and fail safe interlocks are produced. In addition to the general mechanical maintenance, which has been performed on the gas baking plant a new control system has been designed. Previously, the baking plant, only controlled the temperature of the gas circulated around the torus interspace. The new system uses cascade control

to give accurate control of the torus temperature. A graphical programming interface allows the complete baking cycles to be pre-programmed and rates of heating and cooling to be controlled. These two new systems will be commissioned for 1996 operations.

Gas Introduction

In the past the Glow Discharge Cleaning (GDC) gas supply was part of the operational torus gas introduction. This led to difficult and time-consuming change-over procedures. A new system was designed and installed to permit independent GDC through four dedicated gas lines with mass flow controllers, which can be remotely adjusted through CODAS. This new system will always be ready for immediate start of GDC after torus operation and also permit switching of process gas (eg, from D_2 to helium) without interruption of glow discharge.

In preparation for DTE1, the gas supply from AGHS was extended from the AGHS distribution box located in the Basement beneath the Torus Hall. The double walled extensions will now feed tritium to both NIBs (as selected for operation) and to one tritium supply module on the torus.

One Tritium Gas Introduction Module (GIM) has been designed for DTE1. This module uses a piezo-dosing valve and control scheme as used on the other GIMs. The module will have the capability to feed either gas to the Octant No.6 mid-plane or to the divertor region. The module is doubly contained and will be certified as a pressure vessel. The double-walled pipes have internal electric heaters to speed up cleaning after tritium operations.

The high gas pumping speeds of the divertor cryopump have meant that for some operating scenarios, it has not been possible to maintain the desired fuelling rate. The torus gas introduction modules are being upgraded to provide a flow of up to 2bar/s^{-1} each. This has been achieved by increasing the operational pressure of the system from 1 bar to 2.5 bar absolute and by increasing the travel of the piezo-ceramic actuator of the piezo-dosing valve by the application of higher excitation voltage (1500V). Progress has been made on development work to produce a new radiation hard, high accuracy, high resolution pressure transducer for the modules gas accounting reservoirs.

Interlocks

In preparation for DTE1 and for greater machine safety, new interlocks were designed for next operations, and include:

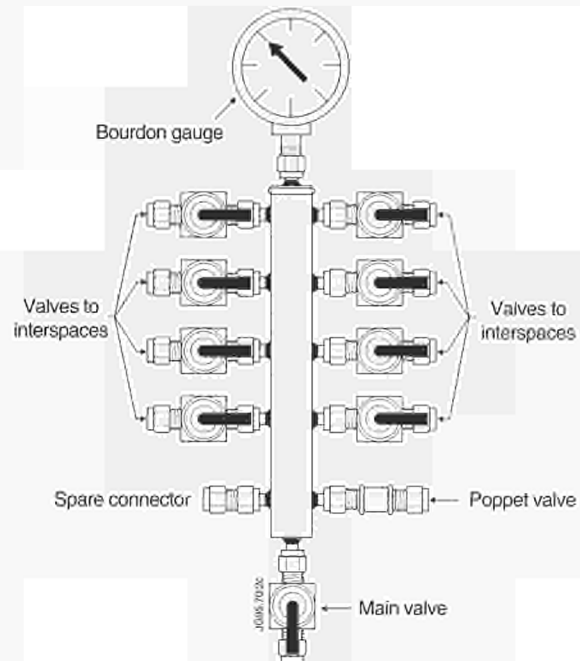


Fig.73: Manifold Design

- A 500mbar interlock to stop the torus being pressurised by high pressure nitrogen, which is used to clear in-vessel water circuits of water. This uses specially designed diaphragm pressure switches in a two out of four voting arrangement;
- Fail-safe 200mbar interlocks for opening the torus and NIB turbo-pump bypass lines to ensure the vessels are maintained at an under pressure in case of a large leak;
- A number of pulsing related interlocks to prevent pulsing in case of malfunction of the new vessel brakes, the new vacuum line breaks or the rotary valve control system.

Interspaces

In recent years, JET policy has been to provide double containment on items on the machine deemed to be vulnerable, such as bellows, windows and feedthroughs. This has led to a proliferation of these interspaces to the extent that there are 400 installed or designed for the machine relating directly to the torus main vacuum. A strategy has been formulated whereby these interspaces are connected to local manifolds on the top, mid-plane and bottom parts of the machine to provide a network of connections for ease of use both in the non-active and active phases of JET. The system has been designed and manufactured and is now being installed, the manifolds being of standard design (Fig.73) incorporating an isolation valve, eight outlet valves to individual interspaces, a



Fig.74: Installation of Vessel Supports:

gauge to measure pressure and an over pressure protection device to prevent pressures above 1.3 bar absolute being generated accidentally. Each manifold system will be filled with 500 mbar neon to enable early detection of any problems on a particular interspace, since neon has a unique easy to detect spectrum. These manifolds will be interconnected and lines routed to an accessible point for pumping and back filling for the final active phase of JET.

Vessel Ventilation System

For remote tile exchange a separate system is required to maintain an under-pressure in the torus under tritium and beryllium conditions. This provides two outlets on the lower main vertical ports of Octants No.6 and No.8 and an inlet on the upper limiter guide tube of Octant No.4. The outlet system comprises a main isolation valve connected to a multi-filter assembly (to remove any particulates) and, thence, to another valve on the main torus pumping crown. This then goes to the AGHS to provide the necessary flow rate of 600m³/hour to enable the underpressure to be maintained. The inlet system comprises a main isolation valve connected to an input filter to enable balancing of the under-pressure. The valves will be remote controlled from the AGHS unit.

Vessel Support Upgrade

Vertical restraints were re-designed, modified and installed during the 1995 shutdown. The new design will

obviate the need for locking at specific vessel temperatures to obtain the correct preload. It features a pneumatically operated disc brake, replacing the original inertial/thermal locking devices and can be adjusted to prevent excess stress on main vertical ports (Fig.74).

Hydraulic dampers installed to dampen the rocking motion of the vacuum vessel were re-designed to incorporate a floating piston ring (to prevent scouring between pistons and cylinders). Their damping characteristics have been modified by incorporating pressure relief valves in the pistons to limit their reaction force to 120kN. Installation will take place in early 1996.

Lateral supports were designed to prevent excessive vessel displacements which, in the past, had led to damage on rotary high vacuum valve seals. This new system forms a hydraulically pretensioned belt linking all main horizontal ports near the torus mid-plane. Between ports, the belt is fixed on bridges between the coil supporting mechanical structure and the transformer limbs. Mechanical analysis has shown that the new system will substantially improve vessel support:

For a typical IMN - 10ms impulse, the new supports will reduce lateral displacement from 11 to 3.7mm, reduce stresses on main vertical ports from ~150 to 50MPa and induce acceptable stresses of 50MPa on the main horizontal.

Insulating Breaks

Electrical breaks for torus and neutral injection forevacuum lines were developed. The problem of insulating at up to 2kV near the Paschen breakdown minimum at ~0.1 to 1mbar was solved by combining a multi-grid structure with voltage divider and a magnetic field (0.02T) perpendicular to the tube axis. Such structures were successfully tested with several gases (air, H₂, helium and argon) in the critical pressure range (0.01 to 10mbar).

Rotary High Vacuum Valves

During plasma operation, unexpectedly large lateral mechanical forces acting on the vacuum vessel were partly transmitted to the Rotary Valves consequently damaging the valve's sealing arrangements.

On inspection, during the shutdown, the all metal silver seals were found to have been flattened extensively and had worn through in places. It was evident that efforts should be made to reduce the forces acting on the valve and at the same time to apply a tougher sealing material instead of the silver. After preliminary tests, using newly

designed nickel seals, it was confirmed that sufficient sealing pressure could be applied to create an acceptable leak rate. Hence, it was decided to replace the Rotary Valve silver seals by nickel seals.

After 50 'bedding in' cycles, tests have confirmed an acceptable leak rate of $\sim 1.10^{-7} \text{mB} \ell \text{s}^{-1}$.

Sealing Arrangement for IVIS Lighting

Following problems with double windows on the In-vessel Inspection System (IVIS) illumination system, a new compression seal (Vespel) was developed and thoroughly tested. This new seal seals directly onto the silica rod light guide, and windows are no longer required. Vespel is a polyimide with high performance characteristics (ie, continuous service up to 260°C in air intermittently up to 480°C, radiation resistance of 4×10^9 Rad (at 2MeV no significant changes), very good vacuum properties and a very high creep resistance).

The ferrule has a total length of 50mm (Fig.75) and was clamped between two flanges. The lower flange was connected to a vacuum leak detector. Since the arrangement provides a seal at each end, the interspace was opened up by a 3mm hole allowing the lower vacuum seal to be leak tested. The sealing area between vespel and the quartz rod could be visually observed and was estimated to be 3mm side, increasing to 4mm at the highest sealing force. It was expected that no significant light loss would occur due to these contact areas. Tests to establish the heat loss and the subsequent heating of the ferrule were carried out successfully during the prototype tests and proved lower than expected. The sealing arrangement was initially successfully leak tested to $10^{-9} \text{mbar} \ell \text{s}^{-1}$.

Waste Management

The Waste Management Group is responsible for provision of facilities in support of interventions and shutdowns, respiratory protection equipment and disposal of radioactive and beryllium wastes. This involves the operation of five controlled areas, including the Torus Access Cabin (TAC), Building K7 complex, the two Beryllium Handling Facilities and the Waste Handling Facility (WHF) in Building J30, together with operation of the liquid waste drainage system.

Shutdown - Related Engineering Work

The Waste Management Group has been closely involved in the preparation, commissioning and operation of a

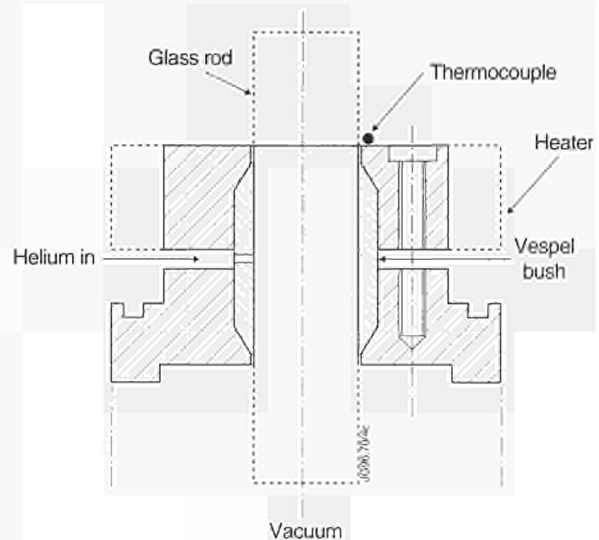


Fig.75: IVIS Leak Test Rig.

wide variety of equipment related to the Beryllium Tile Exchange and Divertor Shutdowns in 1995. It has responsibility for control of safe access to the vessel via the Torus Access Cabin (TAC). An intensive period of commissioning work preceded the Divertor Shutdown. This included.

The TAC Platform

To enable in-vessel operations to be controlled from a low dose-rate environment, a TAC platform was provided for engineers to remain outside the radiation area but be in contact with in-vessel work using improved in-suit communications and a video system. This platform was commissioned in the Tile Exchange Shutdown in March and used extensively for the divertor shutdown.

In-Vessel Communications and Video System

A new video and communications system was installed. An outstanding contribution was made by staff to get the systems designed, procured and commissioned for the start of the shutdown. The systems have made a significant contribution to the success of the in-vessel work, allowing freedom of visual and audio communication between in-vessel personnel, in pressurised suits, and ex-vessel operator and engineers. The basic technology of both systems was adapted from the broadcast industry.

The audio system uses a digital audio matrix at its core. This takes the conditioned voice signals from up to 48 people and digitises them. These were then mixed in any desired combination and the output was made up to 48 analogue voice channels. The result involved the flexibility to choose multiple sub-sets of people to be in communi-



Fig.76: Octant No. 5 Transfer Facility

ation with each other. Key ex-vessel personnel have communication panels which allow them to choose to whom they are taking or listening. Other communications conferences are set up by the shift manager using a specially developed real time graphical interface on a personal computer. Communication links which are critical for safety, for example, between an operator in a pressurised suit and his controller, were permanently made. The system also allowed the newly developed independent analogue communication system of the Controller Dresser Units (CDU) to become part of the network.

The video system uses an electronic matrix to allow up to 24 pictures from colour CCD cameras to be routed to up to 24 monitors. Three auto-focus cameras are mounted in-vessel to provide safety monitoring of the suited operators. Other fixed and mobile cameras were used in-vessel and ex-vessel to aid engineering tasks. Selector panels were used to select an image at a particular monitor. CDUs were provided with a smaller independent system and a link into the main matrix. Images of drawings could be sent in-vessel to a flat screen monitor. A recording station allowed video recording linked with voice channels from the audio communications matrix. This has proved particularly useful for survey work.

The Controller Dresser Unit (CDU)

To enable operators to work in full pressurised suits in the Boom Tent or in the Remote Tile Exchange facility it was necessary to develop a modular unit which could be docked onto various facilities to provide the necessary support facilities. The CDU comprises a contamination control barrier and decontamination shower for suited operators. It also contained a breathing air supply unit



Fig.77: Inside the Beryllium Handling Facility

and a control panel to enable an operator to control suited work safely. This facility also has a video and audio communications system which can operate in stand-alone mode or as part of the TAC communications matrices as described above.

Torus Pumping Chamber Docking Flanges

To enable the torus pumping chamber doors at Octants No.1 and No.5 to be opened remotely by the boom arms, it was necessary to design and install a docking flange, against which the boom enclosure could seal. Thus enabled the door to be opened and any potential beryllium or radioactive contamination to be safely contained within the facility. The Octant No.5 flange was successfully installed and used at the start of the Divertor Shutdown (Fig.76).

Beryllium Handling Facility Modifications

It became apparent during the lead up to the Divertor Shutdown that the work required in refurbishing the RF antennae would require significant alterations to be carried out in the Beryllium Handling Facilities (Fig.77). It was necessary to provide pressurised suit facilities in Facility No.1 and to transfer the decontamination equipment in Facility No.1 to Facility No.2. This in turn required significant alterations to the ventilation system. A new change-room and show facility was also added to each area.

Pressurised Suit Training Facility

A new facility has been provided in the Building K7 to provide an area for training personnel in pressurised suit operations (Fig.78). There has been an extensive cam-

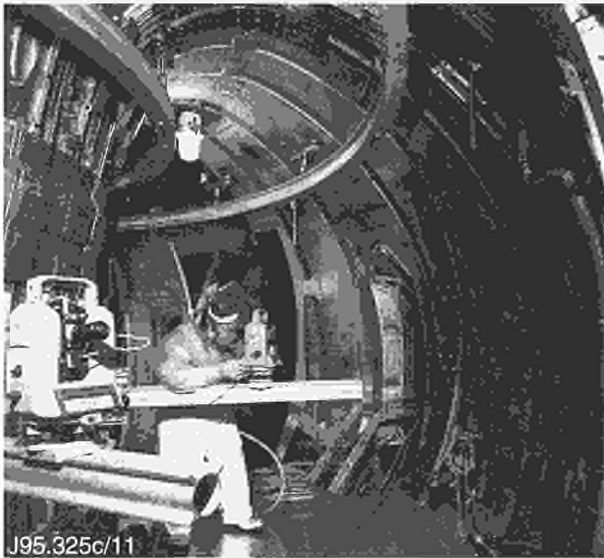


Fig.78: The In-Vessel Training Facility in use

paign of suit training for operators, controllers and dressers and the facilities are compatible with the training requirements of operators from Nuclear Licenced Sites.

PVC Isolators and Tents

In preparation for the Tile Exchange Shutdown and the Divertor Shutdown, the PVC workshop has been heavily loaded and has produced a wide variety of unique containment envelopes for potentially contaminated items. These range from delicate and intricate holders for specialist diagnostic equipment to very large tents to contain components weighing over 35 tonnes and measuring 8m high. The throughput of the PVC workshop has included:

- 5km of PU and PVC used;
- 75,000 welds, (approx 21km);
- 9 major tents, one comprising of 0.3km of PVC;
- 5 smaller tents;
- 200 isolators including 70 in PU for in-vessel use;
- 2000 bags for posting and 500 radiography double wrapped films.

Waste Management Facility

In 1995, the Waste Handling Facility collected the 5000th radioactive waste package, packed the 500th despatch drum and despatched its 50th waste consignment since the facility began operation in 1992.

For most of 1995, the JET machine has been shutdown for extensive modification work and the inside of the vessel plus numerous other support facilities have been operated as contamination control areas in order to enable JET personnel to safely carry out their modification and remedial works.

The radioactive wastes generated by these activities in these areas have been collected and prepared and consigned off-site for disposal by the Waste Handling facility.

About 1500 packages containing potentially radioactive waste were produced at JET during 1995. 92% were classed as housekeeping and 8% were classed as irregular wastes. To minimise collected volumes the soft housekeeping waste was compacted and prepared for despatch as soon as possible after it was generated and the irregular waste was put aside for subsequent sorting. In 1995, 11 consignments of radioactive waste containing 115 waste packages have been despatched to the Harwell Laboratory, UK, for disposal.

To account for the activity content of the waste packages and the correctness of the supporting documentation 130 samples of waste were taken and analysed for a range of radioactivities and for beryllium content. The Waste Management Database recorded all JET's radioactive waste arisings, assigned sampling and packing groups and provided records for all despatch packages and consignments.

Operating Instructions, procedures and local rules have been extensively reviewed, revised and audited during 1995, with a view to continuing the production of waste in a controlled and traceable way throughout the planned DTE1 and DTE2 campaigns.

Active Drainage System

A number of enhancements have been made to the active drainage system including a new settling and filtration system to ensure that discharges for the Beryllium Handling Facilities are within the constraints imposed on the system for solid containments. The mobile bowser has been successfully used to transfer liquid from the AGHS holding tank to the active drainage system.

Control and Data Acquisition System

The JET Control and Data Acquisition System (CODAS) is a fully integrated computer-based system. A network of computers is used for controlling, monitoring, data acquisition and storage of data. This network is also used to analyse the data from the tokamak, its power supplies, auxiliary equipment and diagnostic devices. CODAS also provides the following common services: Network Information Services (NIS), Mail, file servers, printing, network monitoring and off-line program development. These services have grown and this year over 100 systems are in use.

Table X: CODAS Computer Configuration and Allocation

Category	Quantity end 1994	Quantity end 1995	Machine type	Memory in MByte	Disk size in GByte
Server	10	6	Sun SPARCserver2	64	0.424
	0	4	Sun SPARCserver5	64	0.535
MMI	13	7	Sun SPARCserver2	64	5x1.6 RAID 0.424
	3	4	Sun SPARCstation2	32	0.424
	0	5	Sun SPARCserver5	64	0.535
Host systems	4	4	Sun SPARCserver2	32	0.424
Control system	17	16	Sun SPARCserver2	32	0.424
Diagnostic system	10	9	Sun SPARCserver2	32	0.424 1
Communication	2	2	Sun 4/670	128	1.6
	5	4	Sun SPARCserver2	32	0.424
Off line development	10	22	Sun SPARCserver2	64	0.424
	0	4	SPARCserver5	32	0.535
	1	1	Sun SPARCstation1+	32	0.424
		1	Sun IPC Workstation	32	0.256
Computer Totals	76	88			
X-terminals	87	112			

JET components and diagnostic devices are grouped into a number of sub-systems. Sub-systems that include parts of the tokamak and its auxiliary systems are referred to as control sub-systems; diagnostic devices are grouped into diagnostic sub-systems. Each sub-system is controlled and monitored by one dedicated computer interfaced to the machine and its diagnostics through CAMAC and/or VME instrumentation. Embedded front-end intelligence is implemented through CAMAC and VME-based microprocessors for real-time applications.

Networks and Computers

Ethernet networks

The Ethernet networks are split into two main areas:

- the site-wide network (JETnet), which supports the PC and UNIX connections from offices and laboratories on site. This network has been steadily improved by CODAS and Data Management Group (DMG). New Ethernet switches are being installed in strategic places to replace old equipment and improve performance and fault finding facilities. These are interconnected via two Fibre Distributed Data Interface (FDDI) rings giving a bandwidth of 100 Mbps rather than the 10 Mbps of Ethernet;

- the second section consists of all the networks required to support the control of, and data collection from, VME and PC-based systems distributed across the site. The various connections provide the structure of the client server UNIX system and the data collection and transfer medium. Over the year, continuous improvements have been made to this system but a review of the organisation of the plant segments is planned for next year. Also included in this area are some dedicated sections of Ethernet, which are used for real-time systems. These have the economy of standard hardware and software, while still maintaining sufficiently certain communication paths.

Progress has been made in provision of network management facilities and a new Simple Network Management Protocol (SNMP) stack has been introduced. This makes the installation of new Management Information Bases (MIBs) simpler when adding new equipment. New Ethernet investigation tools have also been purchased and installed.

Network and Sub-system Performance

During the last two months of operations, it was apparent that the overall load was increasing on a number of sub-

Table XI
Quantitative Information on CODAS Installation

ITEM	End 1994	End 1995
CODAS Interface Cubicle	167	173
CAMAC Crates	212	211
CAMAC Modules	2,739	2,718
Eurocard Modules (Signal Conditioning and Power Supplies)	6,835	7,095
VME modules	252	406
CAMAC Serial Loop (Fibre Optic)	24	24
On-line Computers	54	57
Off line and Commissioning Computers	19	32

system computers, the main ones being the Poloidal Field sub-system (PF) and the Vacuum sub-system (VC). One of the major contributions was found to be due to the increased level of monitoring particularly of equipment connected to these two sub-systems, by users both within the Control Room, and also outside in offices. One of the first tasks following the start of shutdown, was to investigate ways in which this extra load could be minimised. The resulting proposal, based on providing additional 'mate' computers on which to run extra software for 'object monitoring', began development towards the end of 1995. The new scheme will minimise the number of low level driver calls on the machine sub-systems, thus reducing the sub-system load to an acceptable level. The necessary hardware changes have been made, and development of the software will be completed early in 1996.

Network Isolation

Towards the end of 1994, attention was given to ways of restricting access to the system by user's outside the JET Control Rooms. A scheme was devised which would allow isolation of the ON-LINE network from the OFF-LINE development systems. This system will block the transmission of Internet Protocol (IP) messages between the two networks. The effect of this will be to ensure that Transmission Control Protocol (TCP) and User Datagram Protocol (UDP) packets cannot be transmitted, and we can therefore be confident that reasonable isolation is effected. This concept, called the IP-Gap, received approval in the middle of 1995, and the detailed planning was undertaken during the Autumn.

To minimise the inconvenience which would be experienced by a complete block on communications, those

Table XII
Review of CODAS Electronics Stock Holding

ITEM	End 1994	End 1995
CAMAC system modules	911	911
CAMAC digital I/O modules	843	848
Timing system (CAMAC, VME & Eurocard)	1,681	1,726
CAMAC analogue I/O modules	1,435	1,475
CAMAC auxiliary controllers	151	150
CAMAC powered crates	280	280
U-port adapter	215	213
CISS modules	1,079	1,339
CCTV	684	683
Cubicle frames	396	406
Power supply modules	2,163	2,165
Intercom, Public Address, Computer terminal network	844	895
Pool instruments	1,021	1,030
Analogue I/O in Eurocard	3,206	3,384
Digital I/O in Eurocard	5,080	5,102
Eurocard sub-racks	1039	1,044
JETnet active devices	372	598
VME modules and sub racks	672	894
Totals	22,072	23,143
	Increase 4.9%	

services which were required to be available from both networks, will be installed onto a new computer cluster called the 'core services' cluster. This cluster will block IP traffic but will allow access from both sides to those systems installed within the core. These systems include database services, print services, access to 'home' directories, etc. Provision of the capability for users to monitor operations using X-displays in their offices, will be satisfied by the new 'object monitoring' software which will allow reading of data, but no control, across the IP-Gap.

Installation of the necessary hardware will be completed before the restart of operations in 1996, and the 'object monitoring' software (OMS) will be completed by mid-1996.

Computer Installation

During 1995, the computer installation has evolved both in terms of computers and X-terminals. Table X gives a quantitative overview.

Electronics

Most growth in CODAS's installed electronic hardware during the year has used VME and related technology. Overall, there was a 4% growth in installed hardware (see Tables XI and XII). During 1995, ten new cubicles were

designed, constructed and installed, 292 fully-documented hardware improvements were made and 176 maintenance interventions were recorded. Four of the new cubicles were for the Central Interlock and Safety System (CISS), while in the computer room, three new cubicles were fitted out with UNIX equipment and three more were rebuilt.

New VME modules have continued to be deployed. The 150 used have mainly been of the flexible type, based on the Xilinx 4010 gate array and the Motorola 68040 processor (described in the 1994 Report). Memory on the Xilinx cards has been increased from 1 to 8 Mbytes per module, thus allowing sustained high rates of data capture. For example, in the upgraded X-ray diagnostic KX1, 640 20-bit latching scaler channels have been deployed, in 20 modules, supported by 16 other VME modules

A new CAMAC module, type CPL1, using a similar flexible approach has been designed in conjunction with a commercial firm. Prototypes are newly available. The module has the same programmable logic devices as the VME series, Xilinx 4010, but there is no processor. These are intended, in the first place, to replace CAMAC module types which are no longer in production or which cannot be procured in an economical way, but the design can be used for many more complex functions in CAMAC.

Increasingly, the distribution of timing signals has been provided through the new Composite Timing and Trigger Signal (CTTS). Timing signals are encoded onto a single widely-distributed data stream. The older timing system now derives its timing marks from CTTS so that there is no risk of asynchronism between the two systems whilst they coexist.

The serial CAMAC loops have continued to work with high reliability. The total amount of CAMAC hardware in use is more or less static, but this is the balance of new installations, removals, and conversions of some systems to VME. CAMAC procurement of new equipment is rare, most changes being achieved by re-deployments of existing modules.

Control Systems

Real Time Power Control.

This system comprises a number of cooperating VME processors, to provide a Real Time Central Controller (RTCC). Its function is to coordinate the operation of the various local managers according to feedback networks defined by users using functional blocks flexibly connected in a variety of ways according to users needs. Input

signals are derived from the Real Time Signal Server (RTSS) component, which also distributes the relevant control signals to the Local Managers. Local managers are provided for the various heating systems to allow the capability to control the level of heating power in accordance with a central feedback algorithm.

The software for this system was completed in its initial form on time, and was used during operations in March and April 1995. The results have shown that the system is working well and it has been well received by users. During the latter part of the year, substantial changes have been made to integrate fully the central system operation with the Neutral Beams, Ion Cyclotron Radio Frequency (ICRF), Lower Hybrid and Toroidal Alfvén-Eigenmode (TAE) controllers, providing a much greater degree of freedom in the feedback controls.

Other developments have taken place in the Real Time Signal Server allowing for the generation of complex signals derived from two or more raw signals using more complex algorithms. One such example is the movement of the Plasma Density Validation (PDV) system to this server, along with its connection to the Plasma Density Feedback systems. A further extension will take place during the first half of 1996, in the addition of a Reflective Memory system to allow the fast reliable distribution of these real time signals. Initially this will be used to distribute signals to non-essential components until the reliability has been properly assessed.

Plasma Density Feedback Control

Towards the end of 1994 and early 1995, the Plasma Density Feedback (PDF) system was moved into VME. The main reason for moving to VME, was to provide enhanced functionality, including a secondary feedback loop, and control of all Gas Introduction Modules (GIM). In addition a second VME processor was provided to allow adaptive density control to be tested in parallel with normal PDF operation. The controller is adaptive in the sense that it tunes its own dynamic properties to those of the process it is controlling, so that the required control performance is maintained despite the changing properties in the controlled plant. The plant properties, or the plant transfer function, is obtained by a concurrent identification process. In February 1995, the PDF VME system was fully commissioned and brought into operation. In subsequent weeks, the Adaptive Plasma Density Control was operated, which was the first time this type

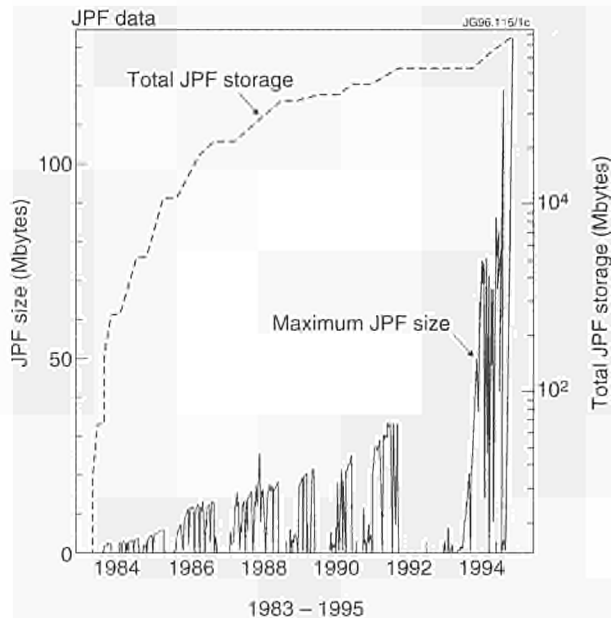


Fig.79: Evolution of CODAS data collection over the years of control technology had been tried at JET. It proved to be successful despite difficulties with strong disturbances and discontinuous operation.

An additional extension during early 1996 will provide the connection of the PDF controller to the Pellet Launcher system. This will then allow the control of pellet fuelling rate in addition to the normal Gas Introduction Modules.

New Water Cooling System Control

A new VME system has been introduced during the shutdown for management of the new water cooling systems. The increased power and capacity of the VME systems was required, to give the necessary flexibility for enhanced control and for improvement of control algorithms. Completion of the software development and integration and commissioning, is expected by March 1996.

Diagnostic Support

The last experimental period has brought a number of real-time VME based systems into use. These include the diagnostics KC1D, KG1, KL1, KL4, and towards the end of the period KN3 and KB3D/KB4. Increasing use of diagnostic systems for control purposes has taken place, both KC1D and KG1 perform calculations in real time before passing the data to Plasma Position and Current Control (PPCC) and XLOC. Advances have been made in the use of data reduction, KY4D for example acquires in excess of 100 Mbytes of data during the pulse, but only stores around a tenth of this in the JET Pulse File (JPF).



Fig.80: Overview of JET Control Room

In recently developed diagnostics, a new Windows-based user interface has been developed, based on the Tcl/Tk language. Experience shows that applications can be developed more quickly while presenting the users with a good screen interface. Applications using this technique have been developed for KB3D/KB4, KX1 and KY3 diagnostics.

Data Collection and Transfer

The data collection scheme introduced during the change to UNIX has continued to operate well. The amount of data collected from PC and VME based diagnostics has increased and the JPF size is currently between 110 and 135 Mbytes (see Fig.79). The overall transmission time to the IBM is around 340s increasing to 500s when disruption data is collected. The Late Pulse File (LPF) is still small but the end of the campaign saw the increasing use of this system.

The inclusion of local disks on those systems which produce large JPFs has increased the transfer rates from these systems to the IBM. Further changes during the 1995/96 shutdown to the Ethernet connections and increasing the power of the computers supporting these systems will improve the performance further.

Efforts are being made to increase the performance of the slower data collection systems and by using the Quick Pulse File (QPF) to transfer a small amount of critical data earlier to the IBM in order to start the analysis chain earlier.

Central Interlock and Safety System

A study was made last year into the maintainability and performance of the existing Programmable Logic Controllers (PLCs) that form the core of CISS. It was decided to proceed with a progressive replacement of the old units by more modern but fully compatible PLCs. Following a successful trial in one sub-system early this year, three

more on-line systems have been converted, and two more will be ready for Operations in 1996.

Control Room

During the last campaign, experience was gained of the new Control Room layout and its flexible, compact X-terminals. It offers much more usable space than the former purpose-built consoles and has been generally well liked (Fig.80). The Session Leaders suite has been modified in shape to improve communications with the Physicist-in-Charge and to reduce crowding around the Engineer-in-Charge. A special area has been set aside for next-pulse preparation, being within sight of the Session Leader, but far enough away not to disturb the operations of the current pulse.

A new overhead display system was brought into use in the control rooms. This provides the physicists and engineers with information relevant to the JET operation.

Data Management

The Data Management Group is responsible for the provision of the Central Computing Services based on three separate networked computing environments - the IBM mainframe system, a cluster of high performance UNIX systems, and the site-wide network of PCs and Apple Macintosh computers. The Group is also responsible for the management of JET data and for organisation and control of routine data processing.

The mainframe computing service is based on an IBM 3090/300J three-way processor mainframe with two vector facilities. There are 160 Gigabytes (GB) of disc storage and a further 2000GB of automated cartridge tape storage. The service has been operating since June 1987, initially based on an IBM 3090/200E dual processor mainframe. This was replaced in February 1990 with the present 3090/300J, almost doubling the processing capacity. The system was upgraded in 1995 to increase the central memory to the maximum of 256 Megabytes (MB) with a further 256 MB of expanded memory.

In February 1992, a Memorex-Telex automated cartridge tape library (ATL) with eight cartridge tape drives (IBM 3480 standard) and a capacity of about 1000GB was installed to replace the original IBM 3851 MSS. The ATL not only provides storage for all the raw data (JPFs) and archived processed data (PPFs), but also provides storage for backup and dump tapes that were previously handled using manually operated cartridge tape drives. This together with the introduction of automated opera-

tions via the product AutoMate/MVS eliminated the requirement for operator cover. In November 1993, the drives were upgraded to 3490E (36 track) technology doubling the storage capacity to about 2000 GB.

The JET IBM Computer Centre was originally established at the UKAEA Harwell Laboratory but was relocated to Building J2 at JET in July 1992. The service has since run very successfully from the JET location, providing the expected improvement in communications, integration with the UNIX and PC systems, and a reduction in staff. The integration was further improved early in 1994 with the introduction of TCP/IP services on the mainframe using the Interlink SNS/TCPaccess software to provide more efficient means of data transfer between the mainframe and the UNIX and PC/ Mac systems. It also improved the terminal emulation access from the PCs and UNIX systems. During 1995, the operating system (MVS/ESA) was upgraded to the latest version, providing enhanced facilities in various areas, including the data management software.

The mainframe plays a major role as the data server and archiver, and also provides a powerful computer facility used by about 200 staff. The workload includes the main Drawing Office CAD system (CATIA) supporting 32 CAD stations, interactive data manipulation and extensive scientific data processing including the high priority Intershot data processing.

The JET Analysis Cluster

This computing service was established in 1994. This was initially based on three IBM RS/6000 model 370 UNIX (AIX) systems. Due to the increasing demand for this type of computing power, the cluster was enhanced by installing four more systems, three model 380s and one model C10 to provide server functions, and, then, during 1995, by adding a further two model 380 systems, and upgrading the memory and discs on several of the other systems. The cluster has a total of 40GB of disc storage. The UNIX systems act as a clustered compute server by running the Load Leveller work sharing (batch) system, distributing work to any of the workstations that has spare capacity. The different classes of work have priority on different systems, giving a preferential level of service to certain users, but also ensuring that the system can be fully utilised even when the priority work is absent. This mechanism means, for example, that outside Drawing Office hours the UNIX work-station dedicated for CATIA

Robotics use can be incorporated in the cluster to process background batch overnight.

As planned, the Analysis Cluster took much of the computationally intensive computing away from the mainframe, but further this service has revealed a whole new approach to modelling by enabling plasma modelling and structural analysis to be undertaken at a level of detail that was not possible on the mainframe. This work includes transport analysis studies (e.g. TRANSP) and plasma edge modelling (such as the EDGE2D program), and the structural analysis work (mainly Abaqus and Patran). One workstation with a powerful graphics processor is used primarily to run the CATIA (CAD system) robotics design work for remote handling. This integrates well with the main CATIA work run on the 32 mainframe stations.

The total computer power of the Analysis Cluster in terms of the standard numerical benchmarks (Linpack Double Precision) corresponds to about 330 mega-flops (Mflops), compared to about 50 Mflops for the IBM mainframe in scalar mode or up to peak values of 140 Mflops on each of the two vector processors. For the right kind of work the Analysis Cluster provides an extremely powerful compute environment and also provides high performance interactive graphics even when run to an X-terminal over the Network. On the other hand, the mainframe is much better suited for sharing facilities between large numbers of simultaneous tasks (150 users, and multiple batch streams), and for frequent access to multi-Gigabyte shared databases. The mainframe databases like the full PPF system and the CATIA data are available to the JAC systems.

Management of Data

During the 1994/95 operational period, there was a dramatic increase in the amount of JET data with JPF size up to 130MB per pulse (compared with 35 MB during the operations period up to March 1992), yielding up to 3.5GB of data each day of operation. The data are transmitted from the CODAS UNIX systems to the IBM at speeds of about 600 kilobytes per second ensuring that the JET data are available for analysis on the mainframe promptly after collection on the CODAS systems. The development of a very sophisticated data archiving and retrieval system based on a cache of 32GB of on-line disc backed by tape storage on the ATL accommodates the storage of about 650GB (before compression) of raw JET data (JPF). The mechanism gives almost instant access to any JPF data that is available on disc (currently the

preceding five weeks of data), and access typically within two minutes to restore the complete JPF for a given shot from the automated tape library, for any pulses back to original start-up (1983).

The Intershot Analysis is run automatically when the data are received on the IBM and the analysed results are stored in the Processed Pulse File (PPF) data base system. This corresponds typically to about 12MB of analysed data per shot. A major upgrade to the PPF system was made in 1994, converting the system to a client server architecture. This has led to the full PPF system on the mainframe being available on the UNIX and Windows NT PC systems, to provide an essential centralised data storage and retrieval system for use within a distributed analysis environment.

During the shutdown, most of the PPF data from the preceding operations period have been re-processed following developments in the magnetic equilibrium codes, the availability of new calibration data, and corrections and improvements to many of the other analyses.

The Central Physics File (CPF), stored and used under the SAS environment, forms a complete higher level data selection and storage system. A subset of all data is extracted at time points of interest, determined by the Time-slice program and the interactive time slice editor, TED, and stored in the SAS databases. These data are the basis for extended statistical analysis, and the source for other extracts such as the TRANSPORT and EDGE data base. This fully automated system has been further developed during 1995 and used by many physicists in the Project.

The JOTTER system developed in SAS on the IBM mainframe stores all the control room information for each session and each pulse and is available for all users as soon as it is entered

The widely used JET data display facilities (JETDSP) on the mainframe have been continuously enhanced in response to user requests, to provide a versatile data display and manipulation environment.

The group has also been involved in the upgrade of the magnetics diagnostic KC1D, working closely with other members of the Project in the interpretation and exploitation of the data produced by this system. As part of this work, some of the programmes developed for the Intershot processing on the IBM 3090 have been converted to run on DEC Alpha based workstations using Windows NT, providing in real-time similar data to that available from the PPF database after each pulse. This has greatly extended the

flexibility of the plasma control systems, particularly the Real Time Power Control system where, for instance, the plasma energy (as measured using a diamagnetic loop) can now be held at a preset value by controlling the power injected by the neutral beam heating plant. Data from the real time analysis is also used to display the position of the plasma boundary and various processed values (such as β , q and ℓ) in the J2 Control Room during each pulse.

PC and Apple Macintosh Support

There are about 600 Personal Computers (PCs), and 80 Apple Macintosh systems, the vast majority of which are connected to the site-wide ethernet (JETnet). The Macintoshes are used mainly by the secretarial and typist staff for word-processing. The PCs are used for a wide variety of tasks including word processing, data analysis, data acquisition, program development, terminal emulation, CAD, project planning and circuit design and analysis. The networked services are provided from six servers running the Banyan Vines network operating system. This provides services such as electronic mail (integrated with mail systems on UNIX, the mainframe and the Administrative Department PCs), shared file access with central backup service, centrally provided software, access to shared printers and to the UNIX and IBM computer systems. The number of users on the PC network continues to increase, with typically over 300 simultaneous users logged on. This has led to some performance problems at times on the network, necessitating various upgrades. During 1995, there have been continued enhancements to server disc systems and the associated software, leading to improved reliability and increased capacity. The performance deterioration has been reduced to an extent by careful balancing of the workload between the various servers. The JETnet services have become essential tools for the work of many of the JET staff and the reliability of the network over the past year has been high.

The Group has worked closely with CODAS in the provision of the JETnet services, co-ordinated by the regular NeST (Network Service Team) meetings. One major new service introduced early in 1995 has been the secure connection of the site networks to the outside world via the Internet connection through the commercial provider, Pipex (UK) Ltd. This provides File Transfer (FTP) and remote computer access (Telnet) services from essentially all systems on the JET site networks, and

incoming access to the IBM mainframe for authorised users subject to various security restrictions. Later in the year, the services were expanded to include access to World Wide Web sites, together with the establishment of both internal and external web sites for JET.

Review of Computing to end of 1999

The group co-ordinated a major review of the JET computing facilities that would be required for the JET project to the end of 1999. The main conclusions were that the mainframe service should continue as a general computing facility supporting the majority of the routine data processing and CATIA service, and also providing storage and access from all computing systems for all JET data. The disc systems and automated tape storage systems should be enhanced to provide increased storage and performance. The main numerical computing and some of the data processing should be concentrated on the JAC cluster where any further growth of computing power will be most economically accommodated. Some of the CATIA work should move to the RS/6000 systems, to take advantage of the advanced graphical capabilities. The power of the desktop PCs should be further exploited in the area of data visualisation and interpretation.

The main review was complemented by a separate review of the developments of the PC network services, which recommended a progressive move to industry standard systems.

Diagnostics Systems

The status of JET's diagnostic systems at the end of 1994 is summarized in Table XIII, and their general layout in the machine is shown in Fig.81. The staged introduction of the diagnostic systems onto JET has proceeded from the start of operation in June 1983. The present status is that 48 systems are in existence. Operational experience on the existing diagnostics has been good and most of the systems have operated automatically with minimal manual supervision. The resulting measurements have been of high quality in terms of accuracy and reliability, and have provided essential information on plasma behaviour in JET. Further details on specific diagnostics systems are given below.

Magnetics

A new set of magnetic diagnostics was installed to improve the dataset on plasma instabilities. This included several arrays of coils. A 'high-resolution' array provides data on

Table XIII: Status of JET Diagnostics Systems, December 1995 - Existing Diagnostics

System	Diagnostic	Purpose	Association
KB1	Bolometer cameras	Time and space resolved total radiated power	IPP, Garching
KB3D*	In-vessel main plasma bolometers	Time and space resolved radiated power	JET
KB4*	In-vessel divertor bolometer	Time and space resolved radiated power	JET
KC1	Magnetic diagnostics	Plasma current, loop volts, plasma position, shape of flux surfaces, diamagnetic loop, fast MHD	JET
KC1D*	Magnetic pickup coils	Plasma geometry in divertor region	JET
KD1D*	Calorimetry of Mark I divertor target	Power balance of divertor plasma	JET
KE1E ⁺	Edge Thomson scattering	T_e and n_e in scrape-off layer	JET
KE3	LIDAR Thomson scattering	T_e and n_e profiles in core plasma	JET and Stuttgart University
KE4*	Fast Ion and alpha-particle diagnostic	Space and time resolved velocity distribution of alpha particles and fast ions	JET
KE9D ⁺	Divertor LIDAR Thomson scattering	T_e and n_e profiles in divertor plasma	JET
KF1	High energy neutral particle analyser	Ion energy distribution up to 3.5MeV (ICRF minority and fusion products)	Purchased from Ioffe, St Petersburg
KG1	Multichannel far infrared interferometer	$\int n_e d\ell$ on four vertical chords and four horizontal chords – electron density	CEA, Fontenay-aux-Roses
KG3	O-mode microwave reflectometer	n_e profiles and fluctuations	JET and FOM, Rijnhuizen
KG4	Polarimeter	$\int n_e B_p d\ell$ on four vertical and four horizontal chords – poloidal magnetic field	JET and CEA, Fontenay-aux-Roses
KG6D*	Divertor microwave interferometer	$\int n_e d\ell$ on sightline across the divertor plasma	JET
KG7D*	Divertor microwave comb reflectometer	Peak n_e on sightline across divertor plasma	JET
KG8A*	E-mode reflectometer	Measurement of n_e fluctuations and profiles in edge and SOL	JET and CFN IST, Lisbon
KG8B*	Correlation reflectometer	Density fluctuations	JET
KH1	Hard X-ray monitors	Runaway electrons and disruptions	JET
KH2	X-ray pulse height spectrometer	Monitor of T_e , impurities and LH fast electrons	JET
KJ3*	Compact, re-entrant soft X-ray camera	MHD instabilities, mode identification, plasma shapes and impurity transport	JET
KJ4*	Compact, in-vessel soft X-ray camera	MHD instabilities, mode identification, plasma shapes and impurity transport	JET
KJ5 ⁺	Active phase, soft X-ray cameras	MHD instabilities and vertical position sensing, DT compatible	JET
KJ6 ⁺	Compact VUV camera	Divertor view in VUV	JET
KK1	Electron cyclotron emission spatial scan	$T_e(r,t)$ with scan time of a few milliseconds	NPL, UKAEA Culham and JET
KK2	Electron cyclotron emission fast system	$T_e(r,t)$ on microsecond time scale	FOM, Rijnhuizen
KK3	Electron cyclotron emission heterodyne	$T_e(r,t)$ with high spatial resolution	JET
KK4D*	Electron cyclotron absorption	$n_e T_e$ profile on sightline across divertor plasma	JET
KL1	CCD viewing and recording	Plasma viewing	JET
KL1E ⁺	Endoscopes	To allow an unrestricted view of the divertor in the visible and IR	JET
KL2*	Impurity flux camera	Impurity influx from the divertor targets with high spatial resolution	JET
KL3A*	Infra-red camera (1 dim)	Divertor tile temperature profiles	JET
KL3B*	Infra-red camera (2 dim)	Divertor tile temperature profiles with high dynamic range	JET
KL4*	Infra-red protection diodes	Machine protection – divertor tile temperature	JET
KL5*	Fast spectroscopic cameras	Fast D_α measurements at two toroidal locations for ELM studies	JET
KL6*	Colour view of divertor tiles	Colourimetry – used for erosion/redeposition measurements	JET
KM2	14MeV neutron spectrometer	Neutron spectra in D-T discharges, ion temperatures and energy distribution	UKAEA Harwell
KM3U ⁺	2.4MeV time-of-flight neutron spectrometer	Neutron spectra in D-D discharges, ion temperatures and energy distributions	JET and NFR, Studsvik

* Brought into operation in 1995

⁺ New Diagnostic – not yet operational

JG96.94/1

Table XIII (continued): Status of JET Diagnostics Systems, December 1995 - Existing Diagnostics

System	Diagnostic	Purpose	Association
KM5	14MeV time-of-flight neutron spectrometer	Neutron spectra in D-T discharges, ion temperatures and energy distribution	NFR, Gothenburg
KM7	Time-resolved neutron yield monitor	Triton burnup studies	JET and UKAEA, Harwell
KN1	Time-resolved neutron yield monitor	Time resolved neutron flux	UKAEA, Harwell
KN2	Neutron activation	Absolute fluxes of neutrons	UKAEA, Harwell
KN3U*	Neutron yield profile monitor and FEB	Spatial and time resolved profiles of neutron flux and fast electron Bremsstrahlung	JET and UKAEA, Harwell
KN4	Delayed neutron activation	Absolute fluxes of neutrons	Mol
KR2	Active phase, neutral particle analyser	Ion distribution function, T(r) and H/D/T flux ratios	ENEA, Frascati
KS1	Active phase spectroscopy	Impurity behaviour in active conditions	IPP, Garching
KS3	H-alpha and visible light monitors	Ionisation rate, Z_{eff} , impurity fluxes from wall and divertor	JET
KS4	Charge exchange recombination spectroscopy (using heating beam)	Fully ionized light impurity concentration, $T_e(r)$ and rotation velocities	JET
KS5	Active Balmer alpha spectroscopy	Neutral beam deposition, plasma effective charge and motional Stark measurement (for internal magnetic field)	JET
KS6	Bragg rotor X-ray spectroscopy	Monitor of low and medium Z impurity radiation	UKAEA, Culham
KS7	Edge charge exchange	Multichannel measurement of edge poloidal rotation, ion temperature and impurity density	UKAEA, Culham
KT1D	VUV spatial scan of divertor	Time and space resolved impurity densities	JET
KT2	VUV broadband spectroscopy	Impurity survey	UKAEA, Culham
KT3	Active phase CX spectroscopy	Fully ionized light impurity concentration, $T_e(r)$, rotation velocities and divertor sources	JET
KT4	Grazing incidence XUV broadband spectroscopy	Impurity survey	UKAEA, Culham
KT5P*	Divertor gas analysis	Analysis of divertor exhaust gasses	
KT6D*	Poloidal view, visible spectroscopy of divertor plasma using periscopes	Impurity influx, 2D emissivity profile of spectral lines	JET
KT7D*	VUV and XUV spectroscopy of divertor plasma	Impurity influx, ionization dynamics, electron temperature and density	JET
KX1	High resolution X-ray crystal spectroscopy	Central ion temperature, rotation and Ni concentration	ENEA, Frascati
KY3	Plasma boundary probes	Vertical drives for reciprocating Langmuir and surface collector probes	JET and UKAEA, Culham
KY4D	Langmuir probes in divertor target tiles and limiters	n_e and T_e at the divertor and limiters	JET
KY5D	Fast pressure gauges	Neutral flux in divertor region	JET
KY6*	50kV lithium atom beam	Electron density in scrape-off layer and plasma edge	JET
KY7D	Thermal helium beams	n_e and T_e in the divertor plasma (together with KT6D)	JET
KZ3	Laser injected trace elements	Particle transport, t_p , impurity behaviour	JET
K α 1*	Thin foil charge collectors	Lost alpha-particle detection	JET
K γ 5 & 8	Gamma rays	Fast ion distribution	JET

* Brought into operation in 1995
 * New Diagnostic – not yet operational

scale-lengths of ~10-100cm, both poloidally and toroidally. The coils have ceramic formers, and transmission lines are matched to allow accurate mode analysis with frequency response of 500kHz. To fully exploit the data, a new acquisition system with 2MHz sampling rate has been installed. This provides key information to analyse TAE and related instabilities, broad-band fluctuations such as observed at ELMs, and other high frequency instabilities known to exist in H-modes. In addition, a new toroidal set of 10 coils provides time traces of toroidal mode numbers selected by mixing.

A combination of fast coils and digital mixing has allowed accurate mode selection up to ~70kHz, compared with ~15kHz with the previous system. The example in Fig.82 shows power spectra of five mixes during a high performance H-mode. Analysis of this type can be complicated by spatial aliasing, and this is indicated in the y-axes' labels. Crosstalk on both the n=2... signal (from the n=4... mode at 30kHz), and on the n=1... signal (from the n=3... mode at ~60kHz) is at a level of ~20%. The mode frequency dependence on the toroidal mode number

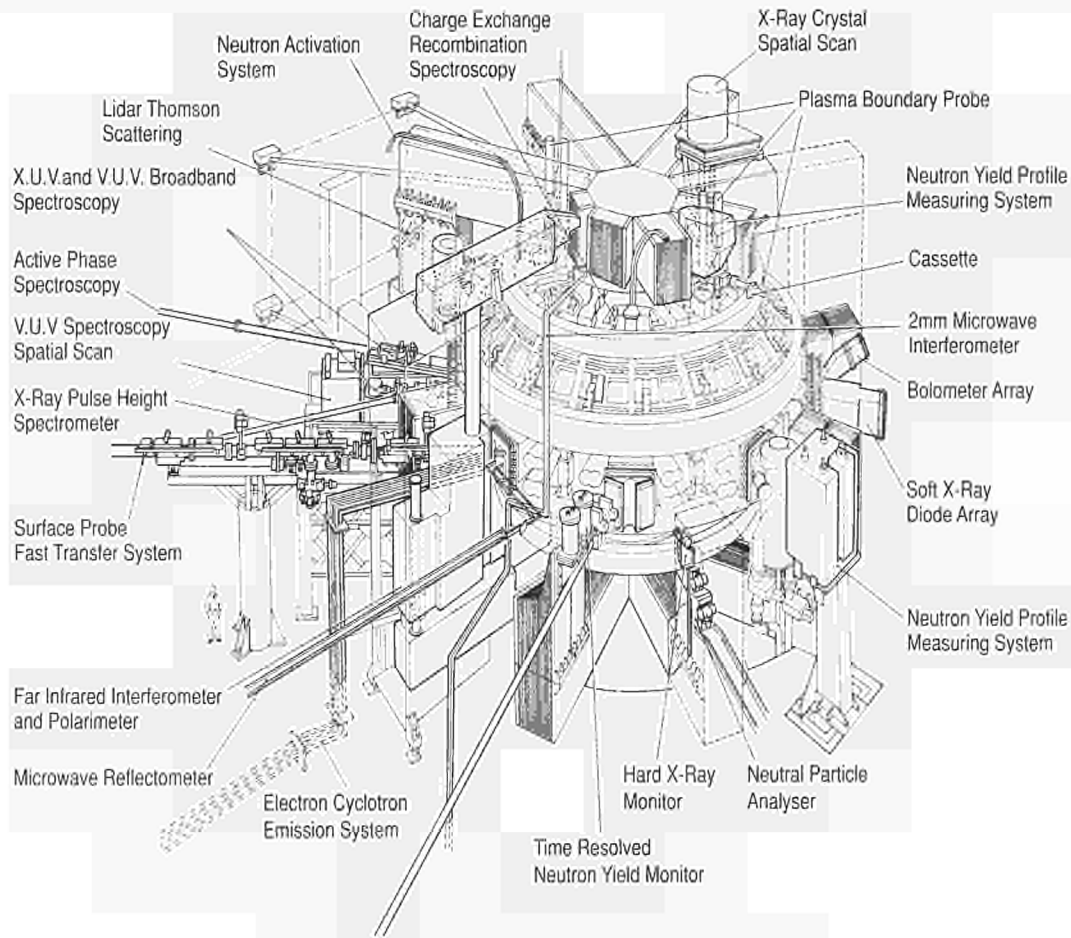


Fig.81: General layout of diagnostics in the machine

in this example suggests that the ~60kHz mode might be a spatially aliased $n=7$ mode. A spectral analysis using the high resolution array confirms this, illustrating the complementary nature of the data in the two systems. Refinements to the latter system will extend the frequency response to 125kHz in the 1996 campaign. A flexible software tool has also been developed in 1995 for interactive analysis of the new data.

Fixed Langmuir Probes

The target Langmuir probe systems proved to be an extremely useful diagnostic during the Mark I divertor experimental campaign in providing information essential for understanding the physics of divertors and, from an operational point of view, in being able to directly compare the separatrix position with the XLOC/EFIT magnetic equilibrium reconstruction. The system proved very reliable and only a few probes were lost generally as a result of wiring faults. After one year of operation the probe tips showed no more than 0.1mm of erosion (<5%).

One surprising observation of the Langmuir probe data was the low electron-to-ion saturation current ratio

observed under certain plasma conditions. The assumption, for calculation from the I versus V characteristic of the electron density and temperature, is that this ratio is essentially infinite but, as the example in Fig.83 shows, ratios down to ~1 are possible. As a result, the electron temperature is over-estimated typically by a factor of two

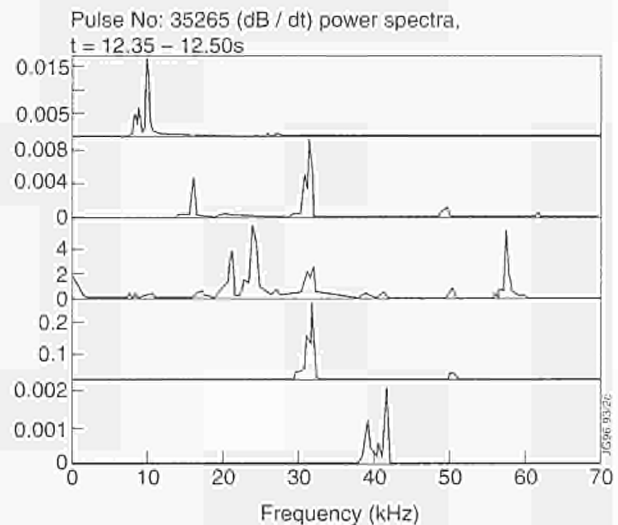


Fig.82: An example of mode selection using the digital mixing technique

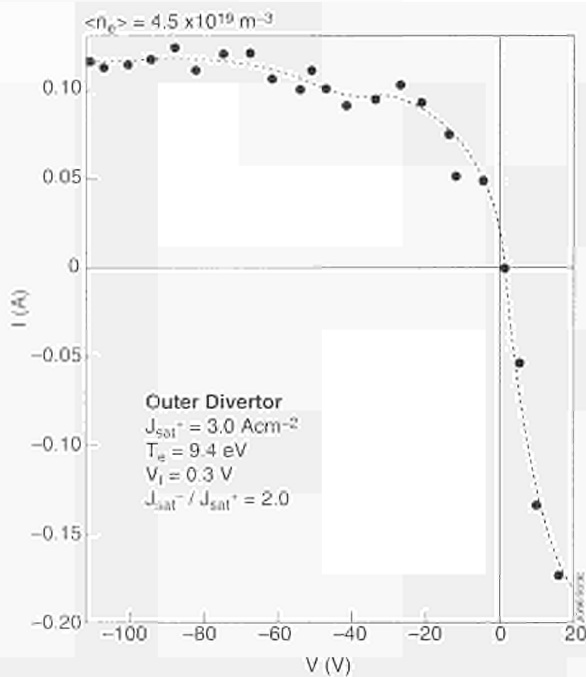


Fig.83: Example of low electron-to-ion saturation current ratio on the outer target during a detached L-mode discharge

and, under these conditions, represents the upper limit. Using virtual double probe analysis it is possible to calculate a more reasonable electron temperature. This is shown in Fig.84, which shows the calculated electron temperature using (i) standard fitting parameters and (ii) by applying the virtual double probe analysis. The lower electron temperatures resulting from this analysis are more consistent with the values expected from EDGE2D modelling calculations.

Currently, the fixed Langmuir probe systems are being upgraded in preparation for use in the Mark IIA divertor. In three consecutive divertor modules, there will be a poloidal array of 40 probe tips which can be configured as either triple or single probes as for the Mark I divertor. Fluctuation studies, conducted through a Task Agreement with CIEMAT, will be further enhanced by the ability to remotely switch 16 of these probes into a fast 500kHz CATS system. This fast system will be used for studies of anomalous parallel transport and ELMs within the divertor. In parallel a reciprocating Langmuir probe head is being developed which will use the same CATS system to record simultaneously the upstream plasma boundary fluctuations and ELMs.

There will also be a "pop-up" probe system in the Mark IIA divertor which uses the $j \times B$ forces on a coil to expose probes at particular times of interest. This mechanism will be used to expose pin-plate probes which are too fragile for fixed installation. Pin-plate probes should allow a correction

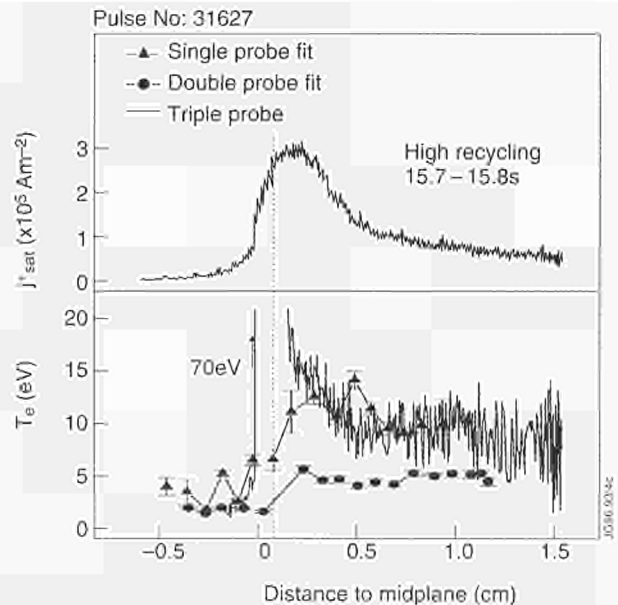


Fig.84: Electron temperature using (i) standard single and triple probe analysis and (ii) virtual double probe analysis

for the effect of high plasma resistivity which creates interpretation problems at high divertor density.

The 22 limiter Langmuir probes are also being upgraded and will be complemented by a further eight Langmuir probes directly above the RF antenna. This will provide information on the density and temperature directly in front of the antenna essential for the efficient coupling of RF power to the plasma.

Reciprocating Probe Drives

The two reciprocating probe systems at the top of the machine were extensively used during the Mark I campaign making a total of 630 reciprocations into plasma (~315/system). The data has been used, for example, to scale the scrape-off layer thickness as a function of main plasma parameters, for comparison of upstream and target electron temperatures and densities with "onion-skin" and EDGE2D model calculations, the determination of the separatrix position for comparison with EFIT/XLOC calculated equilibria and to measure the pressure drop arising as a result of detachment at the divertor.

One of the highlights of its operation during the Mark I campaign was the use of a Retarding Field Analyser (RFA) probe to measure, for the first time, the ion temperature in the plasma boundary. The probe head design is illustrated in Fig.85(a). Ion temperature measurements in both the ion- and electron-drift sides of the probe head can be measured with such a probe. Figure 85(b) shows a typical RFA I versus V characteristic obtained during a reciprocation into an L-mode discharge. The upstream

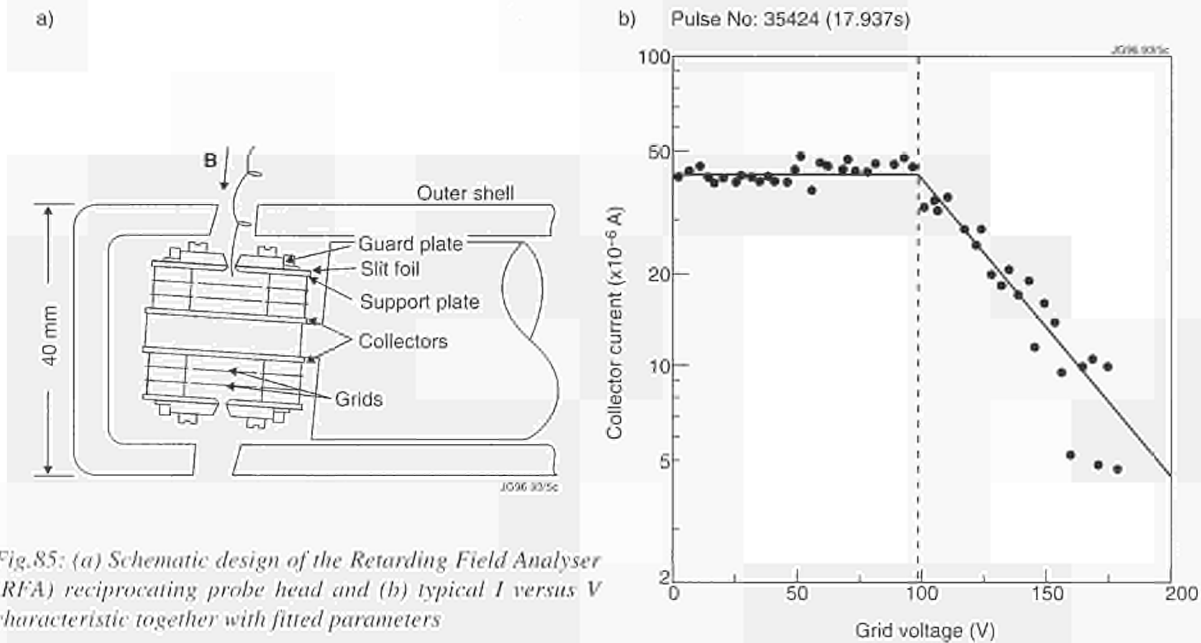


Fig.85: (a) Schematic design of the Retarding Field Analyser (RFA) reciprocating probe head and (b) typical I versus V characteristic together with fitted parameters

plasma boundary ion temperature was dependent upon the NB power and the ion-to-electron temperature ratio also increased remaining constant, at a particular input power, throughout the plasma boundary. A plasma ion mass spectrometer, which will measure the ion-charge state distribution in the plasma boundary, is currently being designed for use in the Mark IIA divertor campaign.

For the MarkIIa divertor campaign, one of the reciprocating systems is also being upgraded to have a stroke length of up to 400mm. This will enable scrape-off layer measurements to be made in a wider variety of equilibria whilst still starting from behind fixed first wall protection tiles. This was one of the handicaps in using the system during the Mark I campaign as many equilibria could not be reached with the 250mm stroke systems. Boron-nitride probe heads have also been developed which will replace the CFC probe heads previously used. Tests indicate that these will be immune to damage from $J \times B$ forces and thermal stress induced fracture thus reducing the risks of fragmentation.

Infra-red Measurements

The Mark I target consists of rows of individual tiles, about 35x80 mm² in size. The surface of the tiles were inclined by -4° in the toroidal direction in order to protect the leading edges from excessive heat exposure. This created toroidal non-uniformity in the target heating, in addition to the poloidal one. As the infrared (IR) measurements of the target temperature were taken by a 1D (linear) InGaAs array, a 3D program for heat propagation within individual tiles was

developed, which took account of the exposed and shadowed areas of the tiles by incorporating the angles between the field lines and the tile surfaces.

Power calculations and surface temperature reconstruction were performed on a 12 processor parallel computer system. Power was calculated by modelling heat propagation within 20 tiles (one horizontal beam of tiles, consisting of two rows of tiles, creating periodic structure around the torus). The tiles could be considered as thermally insulated during the discharge duration, and each processor was processing data for the two toroidally adjacent tiles. For a typical discharge with 1020 time slices of the IR data, the parallel processing part of the program took about 3.5 minutes, which enabled the system to process and acquire data between successive discharges.

Figure.86 shows reconstructed maximum temperature of the target in the beryllium melt experiment. About 2.5s after the start of the NB heating, the target starts to melt at the outer strike point position. BeII line emission shows a sharp rise, and the IR temperature curve bends at around 1000°C and saturates at about 1200°C, corresponding to the melting temperature of beryllium. The power analysis of the IR data for this pulse shows a power flux of ~ 2.7 MW to the outer target while the total power to the target from the power balance ($P_{\text{target}} = P_{\text{input}} - P_{\text{rad}} - dW/dt$) is 3.5 MW. The inner strike zone remains below the temperature threshold for the camera and the results imply a 3:1 power asymmetry in favour of the outer divertor, this is characteristic of discharges in which the $B \times \nabla B$ drift is towards the target.

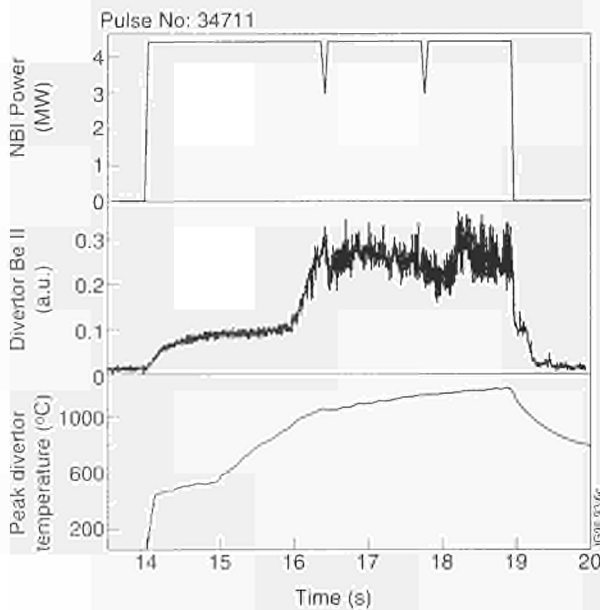


Fig.86: Neutral beam power, divertor BeII intensity and maximum temperature during beryllium melt experiment

Plasma Viewing

Video camera systems (KL1) operating in the visible have been used routinely as one of the primary diagnostics. There are four video cameras installed:

- one wide angle view camera which covers the full plasma height (unfiltered);
- two divertor view cameras which cover the full radial extent of the divertor at two different octants (interference filters for D_{α} , CII, BeII);
- one toroidal view camera which covers a substantial part of the toroidal extent of the divertor (interference filter D_{α}).

The camera signals are automatically stored on four video recorders. The videos can be replayed between discharges in the control room. The video information stored on the tapes can be digitised using an image analysis system and stored in the form of standard PPFs on the mainframe. From there radiation profiles have been extracted and used for the study of impurity production and recycling.

For direct quantitative measurement of the radiation intensity in the divertor region with high spatial and moderate time resolution ($dR \sim 3 \text{ mm}$, $dt = 5 \text{ ms}$), three spectroscopic thermoelectrically cooled cameras (KL2) have been used. These cameras look at the same divertor region and use interference filters to measure the intensities at different wavelengths (D_{α} , CII, BeII, HeI, background at 523.5 nm). The camera output is directly digitised thus making the data more readily available for quantitative analysis than the

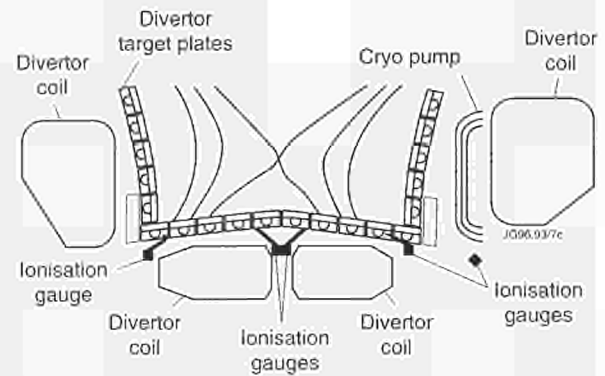


Fig.87: Poloidal distribution of the divertor pressure gauges conventional camera systems which use video tape. However, in order to keep the data storage requirements to a manageable size, the data is compressed to one-dimension by averaging the pixels toroidally. The camera data has been extensively used to study erosion mechanisms, ELMs, plasma detachment, etc.

For the Mark II divertor and the DTE1 experiment, a new viewing system has been designed. It consists of 2 bundles of three endoscopes located on toroidally opposite horizontal ports. Each bundle has one wide angle view endoscope, capable of viewing about 30% of the inner torus surface. Additionally, there are four divertor views (one of them in the infrared) available. One of the endoscope bundles is using radiation resistant glasses for the lenses and ends in a radiation shield, where the cameras are located.

Divertor Neutral Pressure

Ionisation gauges were used for neutral gas pressure measurements in the subdivertor volume and the torus main chamber. Figure 87 shows a projection of the gauges onto a major radius. There are a total of 15 gauges distributed in similar groups of five in two different octants. In Octant No.4 only, four gauges were placed in the divertor area, and one gauge was at the inner wall. Except for the gauge which sits in front of the cryo-pump or at the inner wall, the neutral particle flux, or equivalent pressure, is sampled through lengths of tube which limits the time response to about 5ms. The data acquisition and analysis system is fully operational and automatically processes the results intershot.

Comparison of divertor gauge measurements with the main chamber gauge measurements as well as main chamber D_{α} photon flux measurements yielded results on the neutral particle retention capability of the Mark I divertor. The devices were used to measure the change of the neutral flux compression factor (defined as the ratio of the neutral

flux in the sub-divertor to the flux at the wall of the main chamber) at various poloidal positions as a function of line integrated central density. At densities where plasma detachment was observed on the divertor target plates, the compressions started to flatten out and even decrease, indicating enhanced neutral particle losses from the divertor into the main chamber. This and other results suggest a need for improved neutral baffling in the divertor as intended by the newly installed Mark II divertor.

Real-time Partial Pressure Analysis of Divertor Gases

A new diagnostic has been designed and will be installed in 1996 that allows different masses in the divertor neutral gas to be distinguished. The diagnostic comprises a pumped vacuum tube attached to the sub-divertor volume. It allows divertor gas to enter a penning gauge, from which emitted light is analysed by a spectrometer. Detection of He, N, Ne, Ar, as well as H, D, and T will be possible allowing, for instance, divertor He and impurity retention studies as well as measurements of the D/T plasma composition during the tritium experiments to be started late in 1996.

Thermal Helium Beams

The Mark I experimental campaign also saw the introduction of a thermal helium beam diagnostic, on JET. The diagnostic is located in the same octant as the target Langmuir probes. An additional injection point in the inner divertor also exists but at a different toroidal location. The periscope systems, KT6D, which consist of 10 fibres each giving a 2.5cm diameter resolution at the helium injection point are used to record the resulting helium spectral lines which this diagnostic uses to calculate the electron density and temperature. The diagnostic complements Langmuir probe measurements as it extends the density and temperature measurements from the target up towards the X-point.

The system is being upgraded for the Mark IIA divertor and in addition to the base injection points there will be an additional injection point from the outer vertical target plate. De Laval nozzles have also been developed which will give a low divergence beam essential for specific density and temperature measurements. Also the Monte-Carlo code, DIVIMP, which generates the plasma background using target densities and temperatures as boundary conditions, in association with the JET atomic database, ADAS, is being utilised to develop an interpretative model for comparison with the experimental data.

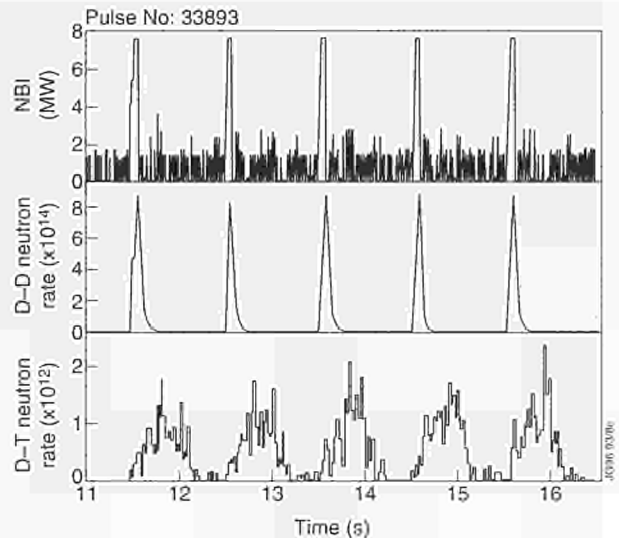


Fig.88: Response of the 2.5 and 14MeV neutron emission to the injection of 100ms D^+ NB blips. The extra delay from the triton slowing down time can be clearly seen in the 14MeV trace

Neutron Diagnostics

During early 1995, while the machine was still operational, the upgrade neutron profile monitor (KN3-U) was installed and operated routinely, but there was insufficient time for all of the new features to be commissioned. Also, a prototype lost alpha-particle detector was installed in the machine and an initial investigation of the background signal level was carried out.

During subsequent shutdown, the main item of progress was the installation and preliminary commissioning of one of the 14MeV neutron spectrometers (KM2). There has been little progress with the remaining spectrometers, although both the 2.5MeV spectrometer (KM3) and the 14MeV spectrometer (KM5) were installed in readiness for commissioning. The third 14MeV spectrometer, provided by the Swedish Association, is not now expected to be delivered before June 1996. The 2.5MeV neutron spectrometer (KM1) has been decommissioned so that some of its components can be utilized elsewhere.

Some considerable time has been devoted to upgrading software to incorporate the extended data storage capabilities of the CODAS computer system, which now depends heavily on VME modules. In addition, a heuristic study of the neutron emission from JET discharges has been carried out [1] to facilitate setting of collimator apertures to optimize operation of the 2.5MeV neutron spectrometers and also of the neutron profile monitor, following from this, a computer programme has been written to predict the time-dependent neutron emission from planned discharges.

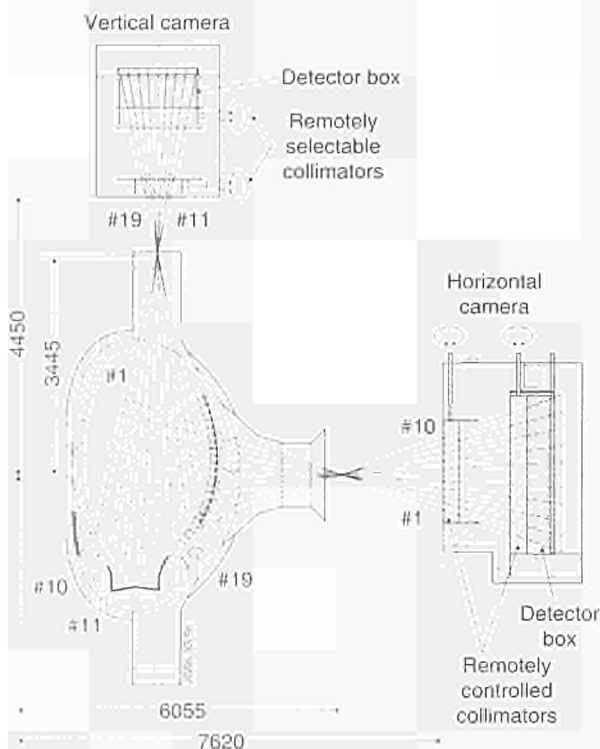


Fig.89: The upgraded neutron profile monitor, illustrating how the lines-of-sight cross the plasma region

Triton Burn-up Studies.

To study triton losses during the second TF ripple experiment, short D^0 neutral beam blips of 100ms duration at 1s intervals were used. In Fig.88, the delayed response in D-D and D-T neutron emission can be clearly seen. The 2.5MeV neutron emission, measured with the standard set of fission chambers (KN1), rises steadily during the beam blips and then decays with a typical beam slowing down time. The 14MeV emission, measured with an high efficiency tandem arrangement of silicon diodes and polyethylene foil converters, rises much more slowly than the 2.5MeV neutron signal and peaks when the ~ 1 MeV tritons have slowed down to the maximum in the T-D reaction cross-section at about 180keV. By integrating the areas under a number of these D-T and D-D neutron bursts and forming the ratio, the burnup rose from 0.65% to 0.69% when the imbalance current between the two sets of 16 TF coils was reduced from 30% to zero. This small but statistically significant increase may be due to differences in the background plasmas. It would appear that stochastic diffusion of alpha-particles in ITER with comparable TF ripple is unlikely to be a serious concern.

14MeV Neutron Spectrometers.

The tandem-radiator spectrometer (KM2) has been installed in a large concrete blockhouse in the Diagnostic Hall, with a line-of-sight which views the plasma through

Octant No.7. To define the target plasma volume accurately, a fixed aperture pre-collimator has been mounted on the side of the KG1 interferometer tower. The adjustable collimators released from KM1 will soon be installed in the Torus Hall, close to the biological shield wall, to complete the definition of the sight line. Testing of signal acquisition from the spectrometer via CODAS has commenced although final testing will only be possible when significant fluxes of 14MeV neutrons are available from JET.

The time-of-flight, associated-particle, 14MeV neutron spectrometer (KM5) is installed in the Roof Laboratory. As with most time-of-flight systems, the setting up of the electronics is a time-consuming and exacting task. The team responsible for the design and construction of the diagnostic (from the Chalmers University of Technology, Gothenburg) is to undertake the commissioning, with completion scheduled for July 1996, in preparation for DTE1.

A third 14 MeV neutron spectrometer (KM9), based on magnetic analysis of knock-on protons from neutron interactions in a hydrogenous foil, has been designed by the Swedish Association (Department of Neutron Physics Research, Uppsala University). It is a proton recoil device which uses a large magnet to transport the recoil protons dispersively to an array of detectors. Cable installation and signal conditioning cubicles are scheduled to be complete in early 1996. The spectrometer requires substantial (70 tonne) concrete shielding. The present intention is that it will be mounted on a moveable tower to allow remote handling access to the machine. The design and construction of the spectrometer and shield, and the initial testing of the spectrometer, will be carried out in Uppsala. Delivery to JET is expected in June 1996.

The Neutron Profile Monitor.

The prototype neutron profile monitor (KN3) has now been replaced with an upgraded version, which was installed in mid-1995. The layout of the new cameras and the 19 lines-of-sight relative to the plasma position in the new JET divertor configuration are shown in Fig.89. The key features for the upgrade are: (i) improved shielding, especially for the vertical camera; (ii) remotely changeable collimation, achieved by use of pre and post-collimator channels bored through rotatable steel cylinders (in two orthogonal planes); and (iii) three in-line detectors per channel. A major benefit to be gained with the upgrade monitor is that it will no longer be necessary to dismantle the diagnostic when changing from neutron to

bremsstrahlung (FEB) studies, or to make alterations to the collimation efficiency for high yield (e.g. D-T) discharge studies. The FEB and the 2.5MeV neutron detectors and associated data acquisition systems were fully commissioned. The new 14MeV neutron detectors were installed in the upgrade but could not be commissioned as the requisite additional data acquisition system, based on VME scalars, was not completed. Nevertheless, some signals were recorded and a sensitivity to pick-up from the ICRF heating system was encountered, attributed to radiation from the unscreened vacuum vessel feedthroughs of the saddle coils which act as efficient receiving antennae at times of poor ICRF coupling to the plasma.

Detailed computer models of the two new shielding blocks (cameras) have been constructed for the Monte Carlo neutron transport calculations needed to ascertain the detection efficiencies of the 19 detector channels. These calculations are essential if the profile monitor is to be used as a source of absolute neutron yield measurements. The thicknesses of the torus vacuum vessel windows, the FEB detectors and the magnetic screens together conspire to halve the neutron flux reaching the detectors. After all the appropriate corrections were made, it was found that the absolute yields provided by the upgrade profile monitor (KN3) fell 30% below those determined with the activation system (KN2). The most likely cause of the discrepancy is that the light response functions for the latest batch of scintillators differ from those used in the prototype. To resolve this issue it will be necessary to repeat the series of intrinsic efficiency measurements for the scintillators.

Coverage for most of the 1994/95 plasma discharges was provided with the prototype, the upgrade or a combination of both profile monitors. The beam power step-down experiment (Pulse No. 34236), was studied using the upgrade horizontal camera and the prototype vertical camera. The step-down discharges involve reducing the initial beam power (and the fuelling rate) in an attempt to avoid or delay MHD events while maintaining high performance in quasi steady-state conditions. For Pulse No. 34236, the power step-down was realized by turning off 6 of the 8 high current 80 keV injectors. The maximum fusion Q corresponded to a (D-T) Q exceeding unity. The diagnostic data exhibited excellent consistency, with the peak value of the central neutron emissivity calculated using CXRS ion temperature and beam deposition calculations agreed well with the value deduced from neutron

tomography. After the step-down, the neutron emission strength was nearly constant and most of the neutrons were produced by thermal fusion.

Lost Alpha-Particle Detector

A prototype lost alpha-particle detector (essentially, a charge collector) was installed during the beryllium tile-exchange shutdown in March 1995, so that an early investigation into the level of electromagnetic interference from various systems could be undertaken. The detector consisted of four nickel foils each 2.5×10^{-3} mm thick with an area of 29 cm², stacked in parallel with 3 mm separation. Thus, 3.5 MeV alpha-particles can be identified by exploiting their range-energy relationship. Some electrical interference was encountered from the saddle coils and the ICRF heating systems. However, it proved possible to reject most of the interference by using low-pass filters appropriate for the anticipated signal sampling rate of 100 Hz. The detector appeared immune to neutron emission and a detection level of order of 1 nA for slowly varying currents was established. The expected current during high power D-T discharges is about 1 mA. The full diagnostic, comprising four individual detectors mounted on a single support structure, will not be installed during the main 1995 shutdown but it is hoped that a suitable opportunity for its installation will arise before the DTE1 experiment takes place.

Nuclear Gamma-Ray Emission

The study of gamma-ray emission from reactions between particles accelerated to high energies by ICRF heating and light impurity ions in the plasma can give important information. A re-examination of the gamma-ray data acquired with the neutron profile monitor for Pulse No. 23230 has provided unique insight into the behaviour of energetic ions during a major sawtooth crash [2]. The gamma-rays are produced from nuclear reactions between ³He ions (of 2 or more MeV) and ⁹Be impurity ions. Figure 90 shows the contours of gamma-ray strength in a vertical section through the plasma just before and just after the crash. The ions are relatively immune to the occurrence of the crash, with the majority remaining on their trapped particle orbits with turning points in the resonance layer. However, those ions responsible for the prominent intensity peak before the crash seem to have disappeared afterwards.

This peak is understood to be attributable to fast passing ions that describe relatively small poloidal excursions.

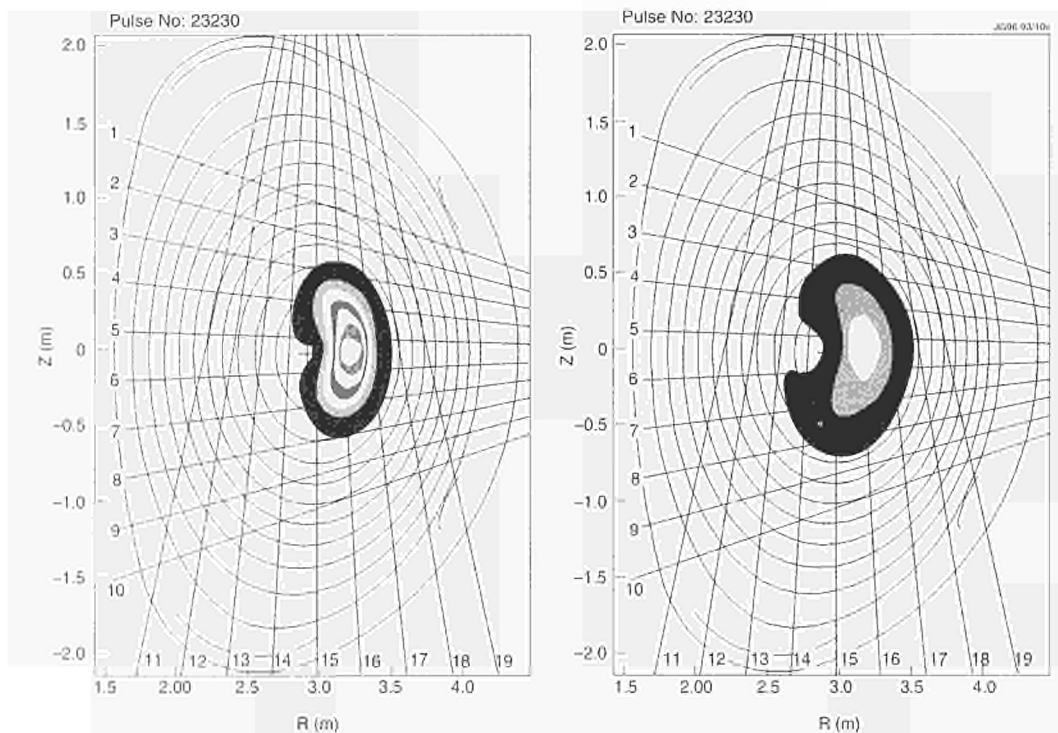


Fig.90: Contour plots of gamma-ray emissivity before and after the giant sawtooth crash for Pulse No. 23230, obtained from a tomographic reconstruction

sions, despite having pitch angles not very different from those of the trapped particles. That the crash should affect mostly the passing particles with orbits that follow the toroidal field lines is understandable in terms of ExB forces arising from charge separation effects. This observation makes a further contribution to the study of fast particle behaviour during sawtooth crashes. The present overall conclusion is that energetic ions having orbits that are tied to magnetic field lines are appreciably perturbed during the crash, whereas those that have orbits that cut across the field lines are relatively undisturbed. This appreciation leads to the conclusion that alpha-particles in burning plasmas will not suffer major redistributions during sawtooth crashes.

A continuation of the above study was not possible during the 1994/95 campaign due to difficulties experienced in coupling RF power to the plasma. Nevertheless, occasional discharges did display strong emissions of nuclear gamma-rays. Figure 91 compares examples of gamma-ray energy spectra obtained during divertor performance tests with and without nitrogen puffing. The observation of gamma-ray lines from the $^{14}\text{N}(n,p)^{14}\text{C}$ reaction shows clearly the penetration of nitrogen into the plasma centre.

Modelling of Neutron Yields.

The neutron profile monitor and the neutron spectrometers are pulse-processing systems that have inherently limited operational ranges. To acquire high quality data, it is impor-

tant that the neutron fluxes incident upon the diagnostic be restricted to levels that do not cause saturation of the electronics. This is achieved through the use of adjustable collimation. To be able to set the collimator positions correctly, it is necessary to be to predict the neutron yield from a JET discharge before it is run. Accordingly, a heuristic study was carried out [1] to obtain scaling formulae for the dependence of the neutron emission on the predefined machine parameters such as the auxiliary heating power, plasma current and toroidal magnetic field. The power scaling of the maximum neutron emission for JET operation 1992 was found to be as follows:

$$\text{NB only: } S_n = (1.4 \pm 0.3) \times 10^{14} P_{\text{NB}}^{1.4 \pm 0.1}$$

$$\text{RF only: } S_n = (9.7 \pm 4.1) \times 10^{12} P_{\text{RF}}^{2.4 \pm 0.3}$$

$$\text{NB+RF: } S_n = (6.4 \pm 2.1) \times 10^{14} P_{\text{NR}}^{0.88 \pm 0.16} P_{\text{RF}}^{0.30 \pm 0.14}$$

These results stimulated the development of a simple predictive model of the neutron emission from hot-ion mode discharges in JET. The starting point for the modelling was the recognition that the density profiles are essentially flat for the highest performance discharges. Therefore, flat profiles for densities and temperatures were adopted, but with the thermal neutron emission being restricted to a central volume defined by the plasma current and toroidal field values. Beam ion deposition provided the primary fuelling for the plasma. Beam heating in the central volume determined the effective temperatures. It was found that ion conduction losses from the central region could be neglected, with the

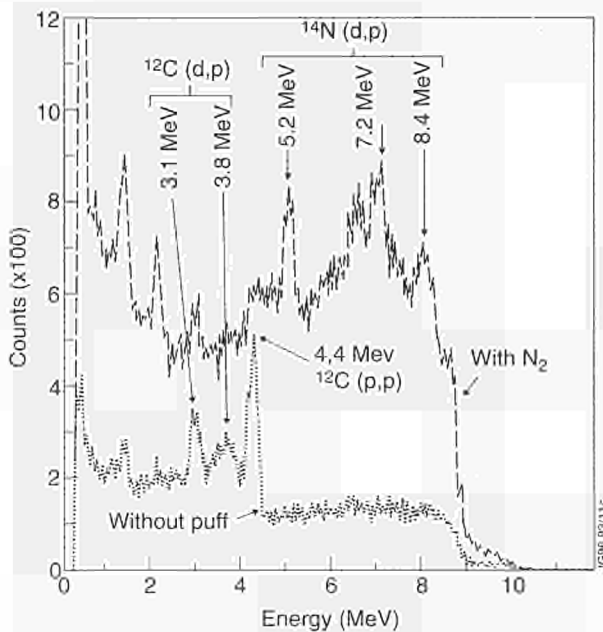


Fig.91: Comparison of a gamma-ray spectrum with N_2 puffing with a spectrum without N_2 puffing

ion temperature determined solely by energy exchange with electrons. Thus, the energy losses were restricted to the electron channel. An energy loss term scaling with the electron energy content was adopted. The constant of proportionality derived from any one good discharge could be taken as representative of all such discharges up to the instant that noticeable MHD activity commences.

Apart from the plasma geometry, current and toroidal field, the code requires as input the specification of the beam heating, the volume-averaged density and the time-dependence of Z_{eff} . In general, gas fuelling and wall pumping must be simulated because the fusion performance of a discharge depends not only on the instantaneous density but also on how it was constituted. The sawtooth crash had an important influence on the discharge and it was modelled empirically. The temporal development of the total neutron yield can be then modelled well. The absolute magnitude of the beam-plasma neutron emission is reproduced surprisingly well. A good fit can be expected for the 100ms or so after application of full heating power but departures of $\sim 20\%$ must be expected thereafter as the temperature rises and the plasma begins to rotate. These calculations usually reproduce well the time evolution of the triton burnup for discharges that terminate gracefully, with the absolute magnitude being over-estimated by about 10%.

The model does not naturally reproduce the ITER93H scaling. However, it can be forced to do so by using the scaling law to determine the energy loss rate. The resulting neutron emission reproduces the typical H-mode

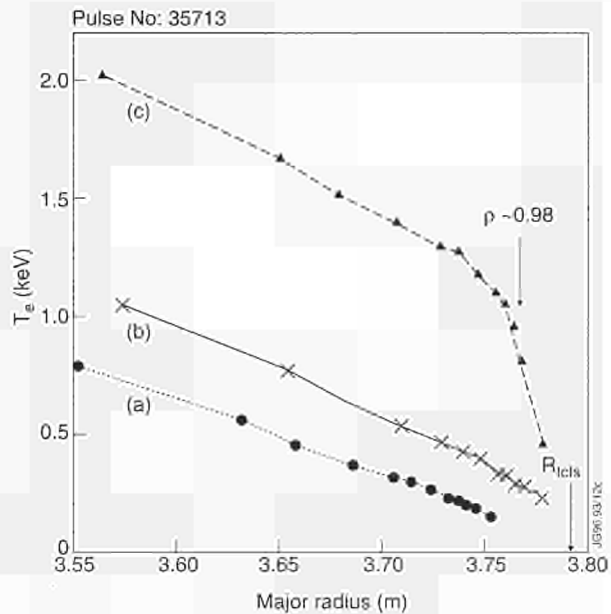


Fig.92: Three electron temperature profiles measured in different phases of the same plasma by the heterodyne radiometer. Profile (a) is in the ohmic phase, profile (b) is in the L-mode phase and profile (c) is in the H-mode phase. As the plasma changes from L-mode to H-mode the electron temperature gradient at minor radii 0.96 increases from 6keVm^{-1} to 55keVm^{-1}

conditions but fail badly for the hot-ion mode discharges prior to the advent of noticeable MHD activity. Employment of the ITER93H scaling leads to an understanding of the heuristic formulae quoted above.

The model has three main areas of application: (i) investigations of the scaling of neutron emission with plasma density, impurity level, and beam heating properties; (ii) the fact that the beam-plasma neutron emission is predicted quite well can be used in the interpretation of neutron spectrum information for hot-ion discharges, for which the spectrum shape does not determine the relative beam-plasma and thermal fractions; (iii) the analogue D-T discharges can be predicted reliably, since this involves mainly changes in atomic and nuclear cross-sections (alpha-particle heating and fuel burnup are automatically incorporated).

ITER Neutron Camera Design

In collaboration with Association Laboratories in Italy, Sweden and the U.K., and with the ITER central team, an outline design was prepared for a neutron camera for ITER to provide plasma diagnostic information based on the deduced neutron emission profiles. The ITER camera design evolved from the principles adopted for the upgraded neutron profile monitor for JET and has been received favourably.

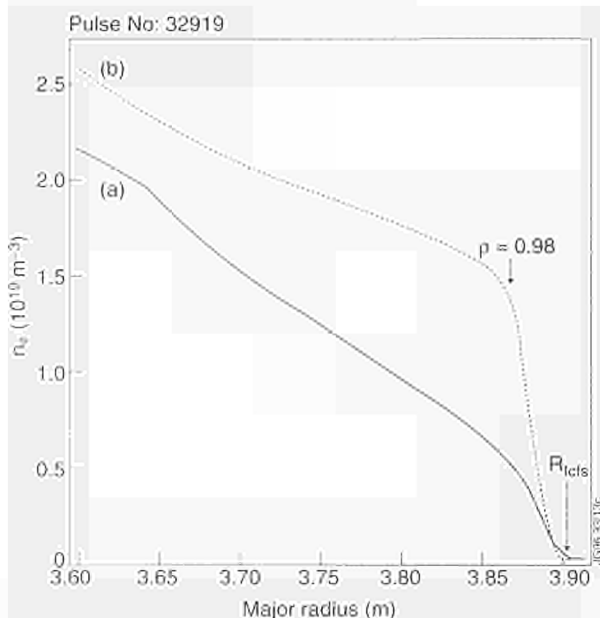


Fig.93: Two O-mode reflectometer density profiles (corrected for absolute position), in the ohmic (a) and in the H-mode (b) phases; the edge density gradient increases significantly in the H-mode and reaches $\sim 8 \times 10^{20} \text{ m}^{-4}$.

The camera is situated outside the cryostat, being integrated into the bioshield wall for reasons of access, maintenance and shielding. The vacuum port contains a pre-shield with minimal aperture penetrations to provide the camera with an unhindered viewing of the plasma, thereby reducing the neutron flux striking the inside of the bioshield wall. For ease of construction and installation, a modular design for the camera was chosen with 25 separate collimator and detector channels. The leading edges of the cylindrical modules are located at the plasma side of the bioshield. The JET philosophy of pre- and post-collimation and multiple detectors per channel was retained. Individual modules consist of a cylindrical plug, 0.4m diameter, containing collimators and detectors accurately aligned; the module is inserted into the biological concrete shield along a sight-line, with the axis of the module passing through a common focal point situated inside the vacuum vessel port. The front and rear collimators are individually rotatable to bring appropriately sized collimation apertures into line with the detectors. Each module contains two magnetically shielded detector housings, horizontally side-by-side, each behind its own collimation path. This system offers great flexibility, allowing two detectors packages per sight-line, e.g. one for neutron flux measurements and one for neutron spectrometry.

Electron Cyclotron Emission System

The Electron Cyclotron Emission (ECE) diagnostics operated routinely throughout the 1995 experimental cam-

paign. The Michelson interferometer (KK1) continues to provide absolutely calibrated electron temperature profile measurements with moderate spatial and temporal resolution (0.15m and 15ms respectively). It is also used as the reference against which the 12-channel grating polychromator (KK2) and the 48-channel heterodyne radiometer (KK3) are calibrated.

The performance of the heterodyne radiometer, which was substantially upgraded during the 1992/93 shutdown, has been exploited for studies where excellent spatial resolution is required. In addition to a spatial resolution $< 20\text{mm}$, it also has good temporal resolution ($\sim 50\mu\text{s}$) and can make measurements over a wide range of minor radii at all toroidal fields above 1.7T.

Detailed edge electron temperature profile measurements have been made on H-mode plasmas. Typically, the electron temperature (T_e) within 20mm of the plasma edge increases from 50eV to 500eV at the L- to H-mode transition, while the gradient of T_e increases from $6\text{keV}\text{m}^{-1}$ to values $80\text{keV}\text{m}^{-1}$. Figure 92 displays three edge electron temperature profiles from the same plasma: profile (a) is in the ohmic phase, profile (b) is in the L-mode while profile (c) is in H-mode. Measurements of these electron temperature gradients are valuable in plasma stability analyses. Work is under way to incorporate the measurements into the equilibrium and stability codes.

A coherent detection system was installed and used with the heterodyne radiometer for the measurement of TAE modes induced using the saddle coils in the frequency range 30kHz to 300kHz. Successful measurements were made under a variety of conditions, with $1\text{MA} < I_p < 3\text{MA}$, $10^{19}\text{m}^{-3} < n_e < 5 \times 10^{19}\text{m}^{-3}$, and $1\text{T} < B_t < 3.5\text{T}$. Alfvén eigenmode damping rates covering three orders of magnitude were measured and the Alfvén eigenmode spectrum was found to be a strong function of electron temperature.

Microwave Reflectometry

The O-mode multi-channel reflectometer (KG3) has routinely provided electron density profiles, as well as being used for detailed measurements of the density profile evolution near the plasma edge and for observation of turbulent and coherent density fluctuations. Figure 93 two density profiles obtained before and after a transition from the L- to the H-mode in a high-performance discharge, exhibiting a significant increase in the density gradient at the transition. These measurements are somewhat limited by drifts in the microwave source frequencies.

which result in uncertainties in the *absolute* position of the density profile, and by the susceptibility of the fringe counters to noise on the signals, which results in loss of data during periods of high edge plasma activity (ELMs). The feasibility of using a novel frequency modulation scheme and analogue phase detection in order to address these problems has been assessed. The results indicate that significant improvements are possible, and the scheme will be implemented for the next experimental campaign.

Three fast data acquisition systems are used for studies of density fluctuations at the reflection layers corresponding to the ten microwave frequencies of the O-mode reflectometer. One of these systems (called CATS) has been developed for the co-ordinated fast data acquisition from a number of diagnostics. It has a bandwidth of 125kHz and a versatile triggering system. Figure 94 shows the coherent density fluctuations at 12kHz associated with the so-called slow roll-over, a gradual degradation of energy confinement in high-performance, ELM-free discharges. Careful analysis suggests that these oscillations are associated with an external kink mode which may be driven unstable by high edge current density. Another data acquisition system has been used successfully for the coherent detection of density perturbations due to Alfvén eigenmodes excited externally by the saddle coils.

The two E-mode reflectometers (KG8A and KG8B) are designed for edge density profile measurements and fluctuation measurements, respectively.

Some preliminary measurements were made with the edge profile system (KG8A) near the end of the experimental campaign. The data did not show any clear reflection signals from the plasma. The possible causes, and solutions, are still being investigated. One possibility is that the microwave components in the complex antenna structure, which is mounted within the vacuum vessel, are not working efficiently. Some new components, designed to give improved performance, are being manufactured for installation at a later date. Possible improvements to the equipment outside the vacuum vessel are also being investigated.

Commissioning of the E-mode correlation reflectometer (KG8B) has continued in 1995 and is now complete. This instrument uses three microwave systems, each one providing fluctuation measurements at two positions that are toroidally, poloidally or radially separated. Useful fluctuation measurements have been made and a database of all the measurements is being constructed.

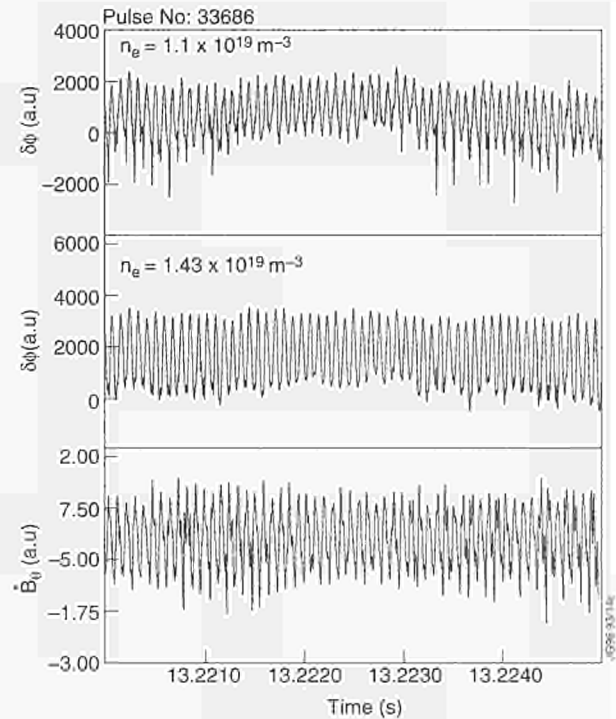


Fig.94: Observation by the O-mode reflectometer of 12kHz density fluctuations at two reflection layers. The fluctuations are revealed as phase oscillations in the reflected signals, during the slow roll-over MHD mode. Also shown, in the bottom trace, are the corresponding poloidal magnetic field fluctuations

Microwave Divertor Diagnostics

The three microwave divertor diagnostics are a dual frequency interferometer for line-integrated electron density measurements (KG6D), a "comb" reflectometer for estimating the peak density along a sightline (KG7D), and an electron cyclotron absorption diagnostic (KK4D) for the determination of the local electron temperature-density product (the electron pressure).

The interferometer has been in routine operation during most of the 1995 experimental campaign. It has been used to make measurements on two different sightlines, which pass through the inner and outer divertor plasma legs. The results have shown the importance of having a dual frequency instrument to compensate for mechanical movements of the launch and receive antennas. The phase shift due to the relative movement of the antennas can be as much as one half of that due to the plasma. Operational experience has shown that the density of the divertor plasma can be sufficiently high, either continuously during additional heating or transiently during ELMs, to cause signal loss and phase jumps, especially in the lower frequency (130GHz) channel. However, successful measurements without loss of fringe information have also been made on plasmas with many ELMs. These show that

the line integrated density at the peak of an ELM can be up to 8 or 9 times greater than that between ELMs. To reduce the incidence of loss of phase information at high density, work is in progress to replace the 130GHz channel with one operating at a frequency of 304GHz. The existing 200GHz channel will be retained as the lower frequency channel. An upgraded fringe counter with twice the sensitivity will soon be available. It should help to offset the loss of resolution caused by the smaller phase shift at the higher frequency.

The comb reflectometer probes the divertor plasma with up to eight microwave frequencies simultaneously. The purpose of the system is to estimate the peak electron density along the sightline by determining which frequencies are in transmission and which are in reflection. The system is designed to measure both the transmitted and the reflected signals. A very high sensitivity is achieved by amplitude modulating the sources at 100kHz and then employing high gain receivers with narrow band filtering centred on the modulation frequency. The first measurements have been made using the four highest frequency channels (83.9, 86.7, 96.5 and 98.5GHz). A difficulty has been encountered in measuring the reflection signals from the plasma, because of strong reflections from the mitre bends in the waveguides close to the transmitter/receiver systems. A temporary solution adopted during the experimental campaign was to connect the receiver for the reflected signals to an antenna in the divertor structure which is adjacent to the launch antenna. A permanent solution, using separate transmit and receive waveguides connected to the launch antenna, is being planned. Using the temporary solution, reflections have been observed for large ELMs. The effects of ELMs and sweeping the plasma across the divertor target plates are easily observed on the transmitted signals. Work is in progress to allow the reflectometer and the interferometer to operate simultaneously on the same sightline. Frequency Selective Surface (FSS) beamsplitters will be mounted in the waveguides to multiplex/demultiplex the microwave signals. These devices will be similar to those already developed for the ECE heterodyne radiometer (KK3). The possibility of extending the density range of the system by the addition of channels with probing frequencies above 100GHz is also being investigated.

The first plasma measurements were made with the Electron Cyclotron Absorption (ECA) diagnostic, KK4D, during the last two months of operation before the shut-

down. This is a complex and novel diagnostic, employing a sophisticated microwave source which can be rapidly swept in frequency over a wide bandwidth. The waveguide to and from the plasma forms one arm of an interferometer, the other arm being a static reference of nearly equal length. When radiation from the two arms is mixed, a beat signal is generated at a frequency which depends on the difference in propagation times between the two arms and the rate of sweeping of the source frequency. The envelope of this beat signal contains the absorption information. Standing waves, due to reflections within the waveguide system, produce beats at a different frequency because of the longer propagation path. They are eliminated during the data analysis. During each plasma pulse, the system typically records data from about 1200 frequency sweeps, each of 2ms duration and at a maximum rate of about 50 per second.

An intensive examination of the data has shown that although the level of cyclotron absorption is lower than expected, it can be unambiguously distinguished from effects which produce spurious variations in the level of the received signals. The frequency at which absorption occurs correlates precisely with that predicted from the known plasma position and the spatial variation of the magnetic field strength. This is particularly clear when the plasma moves during sweeping of the target strike points. The spatial width of the absorbing region (deduced from the frequency width and the magnetic field variation) is consistent with the plasma width estimated by other diagnostics. The accuracy of the absorption measurements has been limited by systematic effects in the data which are still under investigation, but for some plasma conditions absorption up to about 30 % has been observed. This was measured in a plasma of moderate density (estimated at $4 \times 10^{19} \text{m}^{-3}$), and therefore corresponds to an electron temperature of about 20eV.

At very high density, the lower end of the frequency sweep of the ECA system suffers cutoff. Using the known spatial variation of the magnetic field strength, the peak density along the sightline can be deduced from this extraordinary mode cutoff. It has been compared with simultaneous measurements on the same sightline by either the comb reflectometer or the dual frequency interferometer. There is good agreement between the different measurements, as shown in Figure 95. Further investigation of density measurements using the ECA system have also been undertaken. Since it is an interferometer, it is possible to measure the phase shift of the

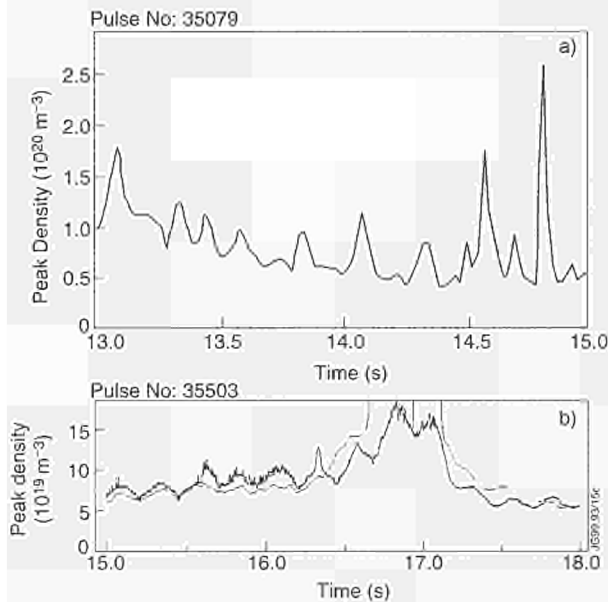


Fig.95: A comparison of simultaneous density measurements made by the different microwave divertor diagnostics. (a) shows peak density from the comb reflectometer (as a band between the lower and upper limits set by the number of frequencies in cut-off) compared with that deduced from cut-off of the E-mode radiation used by the swept frequency ECA system. (b) shows the line integral measured by the interferometer converted to an equivalent peak density (assuming a fixed profile width of 45 mm) and is compared with density deduced from cut-off in the ECA system

radiation passing through the plasma, at all frequencies in the wide-band sweep. Numerical simulations show that there is sufficient dispersion over this wide frequency range for the phase to be sensitive to the density profile shape, not just to the line integral of the density. Analysis of plasma data, using model profile shapes, indicates that quantitative information about both the peak density and the profile width can be obtained under some plasma conditions. The feasibility of making this into a routine measurement is being investigated.

Main LIDAR Thomson Scattering System

The main LIDAR System operated at 4Hz with high reliability throughout the operating period. The electron temperature measurements from LIDAR are in good agreement with ECE measurements. However, since the LIDAR system was still measuring at the horizontal mid-plane of the vessel the peak temperatures at the plasma centre were not recorded. The location of the divertor LIDAR optics at the top of the pumping port precluded a viewing line through the plasma centre.

With the modifications to the divertor LIDAR system it has become possible to rectify this problem. A new viewing line is established passing through the windows on the

pumping chamber door to an inner wall target located 30cm above the horizontal mid-plane. The optics on the concrete tower are being modified to match this line of sight.

The fast digitizers (1GHz) are based on old technology using electron read and write beams. The electron guns for the very fast writing speed are beginning to fail on some of the channels. This technology has always caused problems when measuring steep gradients at the edge or in PEP modes. New digital oscilloscopes with 1GHz bandwidth have now become available and we intend to replace the recorders in the beginning of the next operating period.

Divertor LIDAR Thomson Scattering System

The divertor LIDAR Thomson Scattering system did not manage to produce any measurements of electron temperature or density although weak signals below the level of interpretation were observed. The various alignment difficulties were overcome so measurement could be attempted. The gating off of the intense broadband inner wall pulse was not successful, the pulser purchased for this purpose did not meet the required specifications. A new pulser has been purchased. The electron temperature measured by probes suggest that the electron temperature in the divertor region is near or below the minimum temperature (~20eV) that can be measured with our spectrometer. The lower temperature is set by the notch-filter required to reject the laser light. Even given these difficulties there were instances when we should have expected interpretable data.

An investigation of the total transmission of the collection system revealed that the transmission of the in vessel mirrors was below 10%, explaining our weak signals. We have consequently decided to redesign the optics of the divertor LIDAR system. The new system uses a new port cut through the top of the pumping chamber on Octant No.5. This new system resembles much more the main LIDAR system. All optics are external to this port. The new sight line is slightly less favourable for measurements close to the target, but probably better for the X-point region and associated marfes. The throughput of the collection system has been increased slightly over the old system. With the lower than expected density this system will continue to use the 3J laser.

Edge Thomson Scattering System

LIDAR is limited to a spatial resolution of ~5cm, even when using streak cameras. This is insufficient to probe

the plasma just inside the separatrix and into the scrape of layer. We are installing a conventional Thomson Scattering System using the two inner vertical ports in the C-sector of Octant No.2. The laser beam will enter the plasma vertically at 2.16 m. Examination of several X-point equilibria, shows that a vertical chord at this radius generally cuts through the separatrix at between 1.2m and 1.4m above the horizontal mid-plane. The collection optics will be located in the inner-most port at 1.89m. Light scattered from the plasma will be imaged onto 12 solid light guides (2mm diameter). This results in twelve measuring points, each 1cm long and 1.5cm apart. With the flux expansion normally found at this location, this correspond to less than 2mm spatial resolution at the outer mid-plane of the plasma. The vertical location of the fibre assembly can be adjusted over a range of 20cm to make the central channel match the expected location of the separatrix.

A cassegrain telescope images the fibre ends from inside a vacuum window to a ceiling penetration holding collection optics and spectrometer. The fibre signals are divided into four spectral channels and imaged onto an intensified CCD camera.

Using the existing ruby laser (old KE1 laser) it is planned to make measurements at 4Hz repetition rate during an 8s period. At a laser energy of 2J/ pulse, it is calculated that densities below 10^{19}m^{-3} and temperatures down to 15eV can be measured.

Fast Ion and Alpha Particle Diagnostic

The system, based on Collective Thomson Scattering (CTS) of high power 140GHz radiation, has produced its first scattering measurements. The results showed that the diagnostic should give the expected performance for observation of fast alpha-particle populations in D-T experiments.

The present gyrotron source is leased from the Institute of Applied Physics, Nizhny Novgorod and is capable of producing up to 500kW RF in a Gaussian beam for pulse lengths up to 0.5s. It is a different type of gyrotron than the one originally envisaged for this diagnostic. This made it necessary to modify the high voltage power supply as well as the high power transmission line. These modifications were provisionally completed in the beginning of the year, allowing the start of experiments at reduced pulse length (20ms). Further power supply modifications are in progress to enable the use of the full gyrotron pulse length capability.

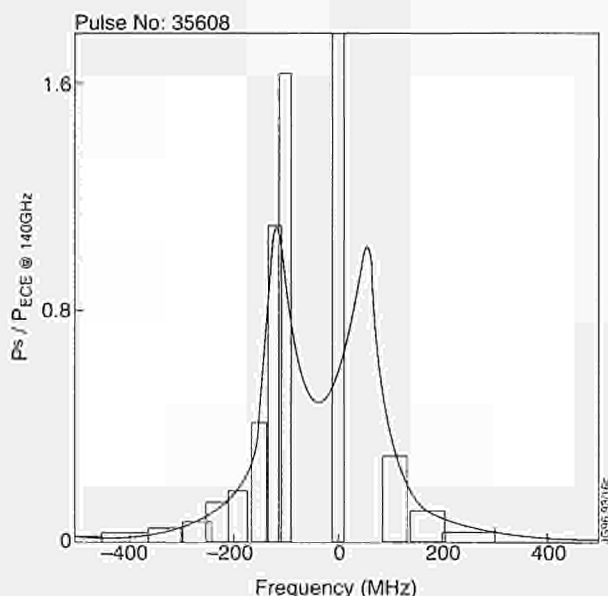


Fig. 96: Example of a measured spectrum of scattered radiation from a plasma with 5MW ICRF, $B=3.1\text{T}$, $n_e=4.1 \times 10^{19}\text{m}^{-3}$, $T_e=3.0\text{keV}$. The curve gives the theoretically fitted spectrum using a two temperature plasma with $n_{D1}=1.2 \times 10^{19}\text{m}^{-3}$, $T_{D1}=3\text{keV}$, $n_{D2}=0.8 \times 10^{19}\text{m}^{-3}$, $T_{D2}=20\text{keV}$ and assuming nitrogen as the dominating impurity (injected for divertor studies)

For the scattering measurements, the gyrotron was operated reliably at a power level of 450kW in short (1ms) pulses and up to 20 pulses per shot. At this slightly lower than maximum power level, the output was spectrally clean during the flat-top. This is important because radiation in spurious frequencies, entering the receiver as stray light, cannot be discriminated from scattered radiation. The transmission efficiency of the high power transmission line was as expected ($\sim 80\%$) and the radiation pattern at the end of the corrugated waveguide run was closely Gaussian. The torus window is a large diameter (190mm) inertially-cooled fused silica window. The measured heating rate during high power transmission was only 100°C/s in the centre, indicating there should be no problem with full pulse length transmission. When firing an order of magnitude below the damage level of the most sensitive detectors. Therefore, no precautions are necessary to avoid firing into the torus when no plasma (which is an effective dump for the microwaves after reflection) is present and it would also be possible to use the gyrotron for preionisation studies.

The first experiments were aimed at the measurement of the thermal ion feature. The scattering volume (the overlap of the launch and receive beams) was located in the plasma centre with spatial resolution $\sim 100\text{mm}$. Generally, a number of similar plasmas were required to optimise the overlap of launch and receive beams (using

the steerable in-vessel mirrors). When this was achieved, power accountability was quite good (well within the error bars). For the initial measurements, the slave receivers (with viewing directions around that of the main receiver) were not yet operational. These should make it easier to achieve optimum overlap. Clear scattering signals were seen from plasmas with $B_0 > 3T$, as expected [1]. An example of a scattering spectrum is given in Fig.96. The histogram represents the measured intensity in each spectral channel normalised to that of the background radiation (ECE) at 140GHz ($\sim 300eV$ radiation temperature for this example). The heterodyne receiver has 32 channels but for the thermal ion feature only the most central channels are important. Stray light was removed by notch filters (>80 dB attenuation at centre frequency, 200MHz width at -3dB) and the channel at zero frequency shift is just a stray light monitor. The signal to noise ratio, defined as the ratio of the scattered signal to the fluctuations on the total signal, varies over the spectrum between 10 and 100, in satisfactory agreement with theory.

Theoretical work in support of the diagnostic has continued. To predict the diagnostic capabilities of CTS and optimise the extraction of information from CTS data a new method of diagnostic systems analysis was developed [4]. The method accounts for the combined effects of noisy data and correlated errors on externally supplied data, yet avoids the need for costly Monte-Carlo simulations. It provides information as to which features, of for instance the alpha-particle distribution function, are resolvable and which are not, and permits the effects of the various sources of uncertainty to be traced individually. The method is very general and can readily be applied to a range of diagnostics or indeed groups of diagnostics. In addition, to its use in support of the JET CTS it has proved to be a valuable tool in the design studies of CTS for ITER.

The relativistic ray-tracing code at JET has been upgraded to account for absorption and emission. This was essential for the modelling of CTS in JET at fields of 3.4T and above. It also made possible the study of feasibility of using the low temperature region of the electron cyclotron absorption layer as a natural viewing dump during high field operation, thereby limiting the noise temperature. The code can also be used in support of ECE and reflectometry, and has contributed to ITER design studies in all three areas.

Soft X-Ray Systems

During 1995, the soft X-ray cameras (KJ3, 4) collected data on the many MHD phenomena occurring in diverted

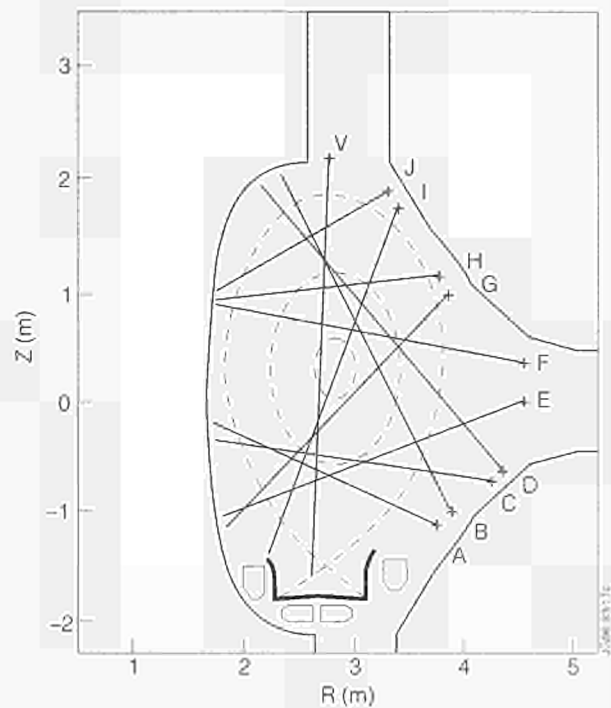


Fig.97: Central lines-of-sight for each camera installed at Octant No.2

plasmas. The pulse height spectrometer continued to operate. In addition, a new compact camera has been built using the same detector array as the soft X-ray cameras (KJ6), to view the divertor in the UV spectral region. Design and construction work was started on a new, radiation hardened pair of soft X-ray detectors (KJ5) intended to operate during the future D-T campaigns. These cameras will provide measurements of the X-ray emission from the plasma and also will be used for vertical stabilisation to complement the existing systems.

Compact Soft X-Ray Cameras

The compact soft X-ray cameras (KJ3, KJ4) have operated during 1995 and large volumes of data (120MBytes/discharge) have been collected in many discharges. The cameras use a 35 element silicon photo-diode. Each element is 4mm x 1mm and the detectors are used in the photoamperic mode and view the plasma through a 250 μ m Be window. To obtain many different views of the plasma the cameras are placed within the vacuum vessel, but separated from it in a secondary vacuum by a Be viewing window. As the vacuum vessel is hot ($\leq 350^\circ C$), the detectors are water-cooled to room temperature to reduce noise. Eleven cameras view the plasma in one poloidal plane and a twelfth is mounted displaced in toroidal angle by $3/8 \times 2\pi$ in order to determine toroidal mode numbers. The location of each camera in Octant No.2 is shown in Fig.97, together

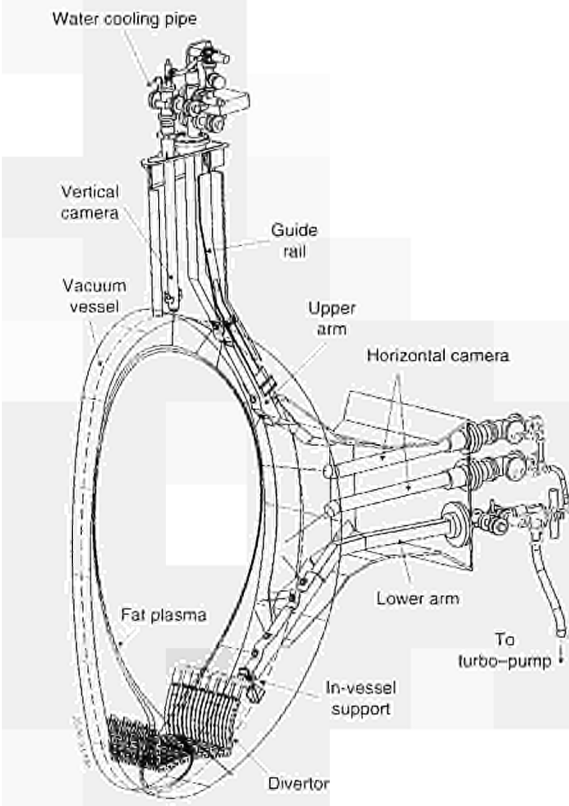


Fig.98: The mounting of the soft X-ray cameras

with the central line-of-sight for each camera. The mechanical arrangement is shown in Fig.98.

Except for camera V, the cameras use alternate lines-of-sight and the resulting good spatial resolution for cameras I and J can be seen from Fig.99, where the lines-of-sight are superimposed on a magnetic reconstruction of the flux surfaces. The system will continue to operate during 1996 up to the start of the D-T campaign. Unfortunately, a few full power D-T shots will cause serious damage to the detectors and for this reason a radiation-hardened system of considerably different design is being developed. It is intended to replace all the detectors after the end of the D-T series of experiments.

A new data acquisition system (CATS) has been built for the soft X-ray cameras and other systems on JET (Fig.100). It handles large volumes of data at very high rates. The soft X-ray system is based on placing the signal processing electronics and ADC's as close as possible to the detectors and transmitting the digital data via optical fibres to the Diagnostic Hall (~200m away), where processing and storage take place.

The electronics near the machine has been designed to reduce electrical interference and noise and therefore each ADC card is electrically isolated from its neighbours and separately powered. A switchable, variable gain

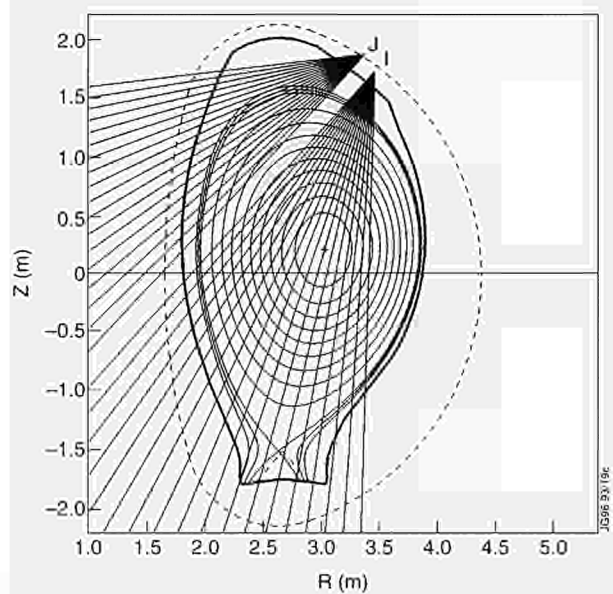


Fig.99: Individual detectors' lines-of-sight for two cameras superimposed on a reconstruction of the magnetic flux surfaces from magnetic measurements

amplifier is incorporated in the design to accommodate different levels of emission from the plasma. An eight-pole linear phase analogue filter is included to prevent aliasing. The signals are digitised at 1MHz and digitally filtered to provide data at a rate of 250kHz with a frequency cut off at 125kHz. The cards are assembled in racks of 19 and connected to a common backplane. A control card takes the data from each ADC card and sends it via a TAXI transmitter to the Diagnostic Hall for storage. Each ADC is clocked, simultaneously.

The data storage system is based on microprocessors which make the system modular and easy to extend. An intelligent trigger system has been developed which allows events of particular interest to be selected. In addition to the fast data acquisition, a large number of the channels can be digitally filtered down to very much lower frequencies to provide selected data for the JPF for the entire discharge. This system has also been used to collect fast data from other diagnostics: the magnetics, ECE temperature measurements, Langmuir probes, reflectometry and H_{α} measurements. All this data is collected in time synchronization, which is a considerable aid to further analysis.

Trigger System

Due to the very high data throughput and the fast nature of many of the MHD events, it is desirable to select data of interest in real time. Then, in a particular experimental investigation, it will be possible to select all of the events of interest without storing excessive and impractically

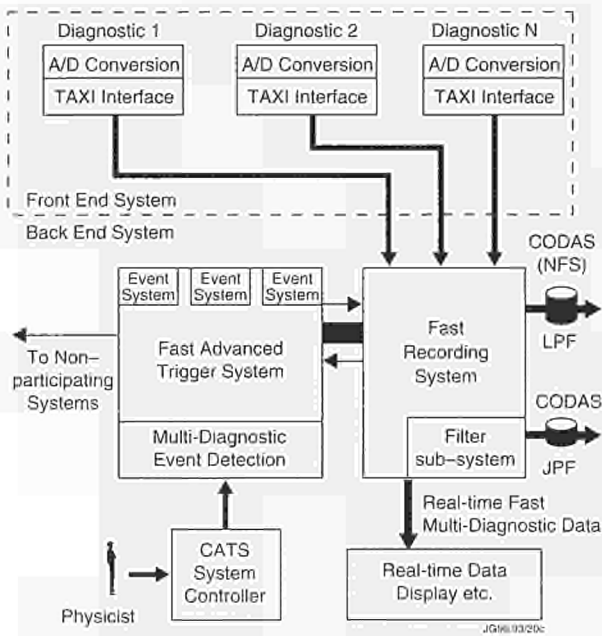


Fig.100: Outline system design of the CATS system

large volumes of data. Data feeds into a ring buffer and is examined by the first level event detector. In the event that an item of interest is detected, the contents of the ring buffer are transferred where they can be examined in more detail, priorities set, and other properties of the data examined. These operations are not conducted in real time, allowing the use of complex algorithms.

Suitable algorithms have been written and tested on real data to select ELMs and sawteeth and MHD oscillations. Other candidates for event recognition include disruptions, snakes, pellets, rollover MHD and L-H mode transitions. It has been shown that the code is sufficiently fast to run in real time and this feature of CATS will be available for routine operation in 1996.

Data Analysis

Specialized software has been developed to handle the very large volumes of CATS data. This is run on a number of dual Pentium processor workstations, using the IDL language to allow rapid access to all of the CATS data. Individual channels can be accessed very rapidly (less than 4s) and more complicated profile data can be plotted quickly. The profile data can be plotted in 3-D, as shaded surfaces or as contours. A zoom facility for the contour plots allows a more detailed examination of the data. This software is particularly useful for comparing high time resolution data from the other diagnostics (ECE, magnetics, etc) which also use the CATS system.

The software can also carry out Fourier transforms of the data and look at various cross-correlations between different

signals. The usefulness of this approach in determining the detailed structure of MHD events is still being evaluated although useful preliminary results have been obtained.

Tomographic Analysis

The soft X-ray data consists of a large number of signals which are integrals along the lines-of-sight of the X-ray emissivity. To understand different phenomena in the plasma, it would be preferable to use the X-ray emissivity at a function of position. This requires an inversion of the original data and this is now being done with a space-time tomography technique, which uses stabilising factors to regularise the ill-posed nature of the tomography problem, arising from the noise on the experimental measurements. The stabilizing factors are determined from a statistical analysis of the spatial expansion coefficients which are found from the classical Cormack inversion technique using Fourier-Zernicke expansions. This technique greatly improves the quality of the inverted data. In addition, due to uncertainties in gains of the detector caused by radiation damage, an optimisation procedure has been developed to reduce the uncertainties in the calibration coefficients. The tomography technique has been used to produce valuable insights in the analysis of data in sawteeth, disruptions, ELMs and impurity concentration assymetries caused by rapid plasma rotation.

Radiation Hardened Cameras

The design and construction of a radiation hardened soft X-ray camera system (KJ5) has commenced. The aim of this diagnostic is to provide measurements of X-ray intensities throughout the future D-T phases of JET and also to provide a vertical stabilization signal. The measurement of X-ray emission in the presence of large neutron fluxes has always been recognised as difficult due to the signals induced in the X-ray detector by the neutrons. These are particularly troublesome as they produce a disproportionately high level of noise compared with the X-rays. This is due to the higher energy per particle for neutrons compared with the X-rays. A further difficulty is that of the neutron damage to the Si detectors. The solution to both these problems is to mount the detectors in a well-shielded environment to reduce the neutron flux to an acceptable level.

Two soft X-ray cameras have been designed (Fig.101) which will view the plasma from diametrically opposed positions in Octants No.4 and 8. The use of two cameras will

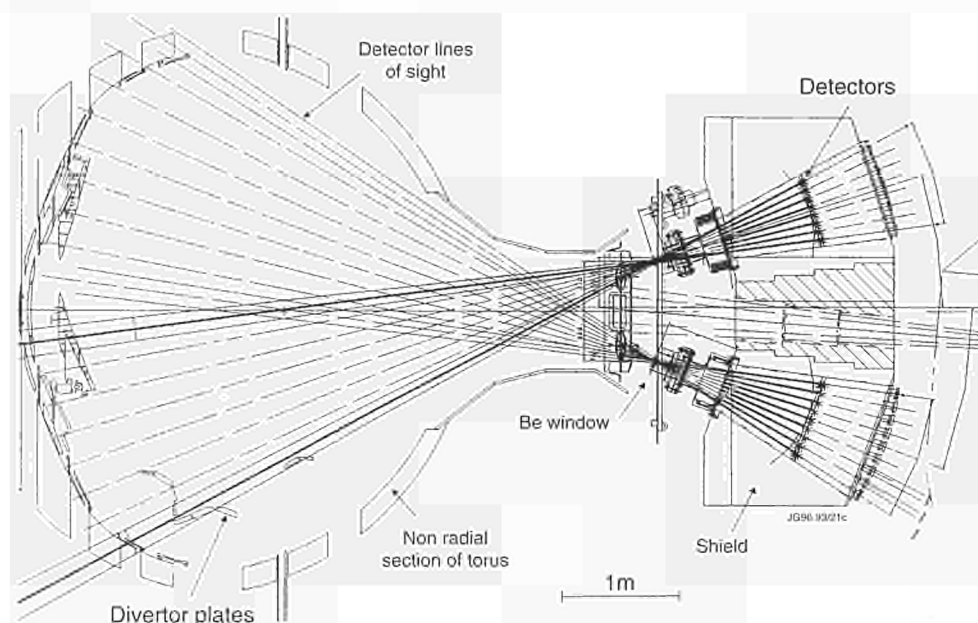


Fig.101: New radiation hardened soft X-ray camera. The section through the torus is at an oblique angle, thus distorting the normal shape

eliminate the effects of MHD oscillations with $n=1$ (particularly $m=1$) on signals which will be derived for vertical stabilization. The system will consist of a large mechanical shield into which pipes will be inserted from the rear carrying the detectors. Each pipe will have an X-ray detector followed by a neutron background monitor and a neutron scintillator detector. This last detector will measure the neutron emissivity with low noise, allowing a study of neutron MHD effects. The system will be completed in 1996.

VUV Camera

A new VUV camera (KJ6) has been built for installation at position E (Fig.97). This camera will be windowless and sensitive to radiation in the visible and the UV in addition to soft X-rays. The camera will view fast events in the divertor region with good spatial resolution on a rapid timescale. Most of these are not visible in the soft X-ray region because of the relatively low temperature of the divertor plasma. The system will operate in 1996.

Pulse Height Analysis System

This system (KH2) measures the X-ray spectrum along a single chord with moderate time (100ms) and energy resolution (300eV). It is also capable of measuring spectra from high energy tails in the electron distribution function produced by LH heating. Spectra have generally shown higher levels of metal impurities than in previous operation. The system will be reinstalled in 1996 after realignment and modification for D-T operation.

Charge Exchange Spectroscopy Data Consistency

Substantial progress in establishing spectroscopic and global data consistency has been achieved by the concerted use of several complementary plasma diagnostic systems and the development of appropriate evaluation and validation tools. A precise reconstruction of magnetic surfaces enabling the mapping of all plasma data on common flux co-ordinates is an essential part of this procedure.

Most of the present JET plasma regimes - with the exception of radiative divertor plasmas, where additional impurities are seeded into the divertor chamber - are characterised by effective ion charges of $\langle Z_{\text{eff}} \rangle \approx 1.5$. The low levels of $\langle Z_{\text{eff}} \rangle$ and the stringent demands in spectroscopic data quality have emphasised the need for extremely accurate input data. This is in particular the case for the deduction of $\langle Z_{\text{eff}} \rangle$ values from absolutely calibrated visible Bremsstrahlung, where the main error arises from uncertainties and apparent fluctuations in electron density. Each quantity (n_e , T_e and B) must be established with an accuracy of better than 5% to ensure apparent $\langle Z_{\text{eff}} \rangle$ variations of less than 20%. Similar, but less stringent requirements, apply for the derivation of radial profiles of Z_{eff} and plasma dilution factors from low-Z impurity densities provided by charge exchange spectroscopy.

The charge exchange analysis code CHEAP (CHarge Exchange Analysis Package) makes use of a hybrid electron density profile which is reconstructed from radial shapes provided by the LIDAR diagnostic and abso-

lute calibrations taken at every single time slice from interferometric line densities. The temporal evolution of the hybrid profile (sampling rate is 20Hz) follows the interferometer signal and its radial shape is interpolated in between LIDAR time slices

In contrast to previous experimental campaigns, comparisons of predicted (e.g. TRANSP calculations) and measured diamagnetic energies and total neutron rates showed apparent deviations, in particular in conditions where record values of neutron rates and stored energy were observed. This has led to a renewed attempt of assessing key diagnostics which enable an independent cross-check of diamagnetic energy and total neutron rates by spectroscopic techniques.

The CHEAP code uses analytic expressions for source rates, fast particle density, thermal and fast particle energy, thermal-thermal and thermal-fast neutron rates. Not only does this permit rapid computation of the diamagnetic energy and neutron rates from the spectroscopic data but the expressions underline the strong interdependence of the measurements and derived quantities.

A comprehensive overview based on about 400 evaluated 1994/95 pulses has demonstrated that global data consistency exists for the majority of cases. CHEAP calculations of diamagnetic energies and neutron rates based on spectroscopic data agree within a band of less than $\pm 15\%$ with direct results derived from magnetic neutron diagnostics. However, systematic discrepancies have been found in the case of high-fusion-yield, ELM-free hot-ion-mode periods where predicted neutron rates are up to 30% higher than neutron rates deduced by the neutron yield diagnostic. The time windows where the deviations are noticeable are characterised by high levels of stored energy ($>10\text{MJ}$), neutron rates in excess of $3 \times 10^{16}\text{s}^{-1}$ and ion temperatures above 20keV. Possible explanations for the observed overprediction of neutron levels are currently being investigated.

Toroidal Momentum and Energy Confinement

Thermal energy replacement times (τ_E) and angular momentum replacement time (τ_L) of a neutral beam heated tokamak reflect the balance of rates at which energy and angular momentum are deposited in the bulk, transported to the edge, and lost from the edge. At JET, as in other tokamaks, the toroidal angular momentum and thermal energy replacement times with co-injected neutral beam

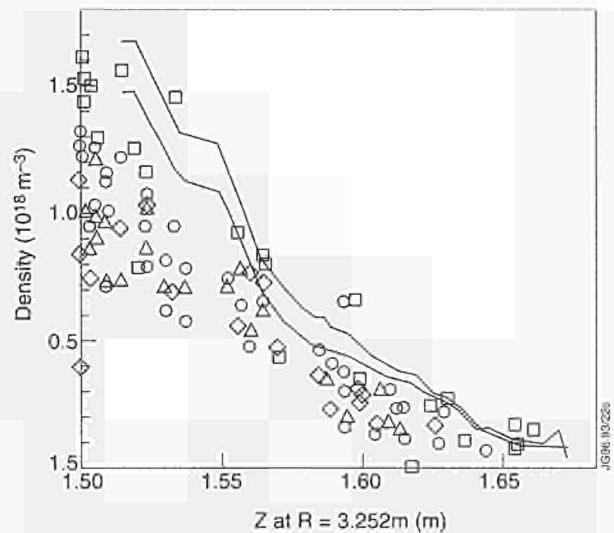


Fig.102: Comparison of Li-beam density profiles (-) with densities (symbols) obtained by reciprocating probes (Pulse No.35171)

heating are approximately equal, under steady state conditions, and the bulk transport of angular momentum and energy are correlated. For neutral beam heated discharges, where torque and power have similar profiles, the results suggest that the loss rate at the edge is identical, and is dominated by the ambipolar particle flux and heat conductivity/viscosity across the separatrix. However, in the initial phase of the high performance hot-ion H-mode discharges the angular momentum replacement time τ_L is found to be approximately $0.6\tau_E$. The difference between the two confinement times becomes less towards the termination of the high performance phase.

Charged particle losses, heat conductivity and viscosity across the separatrix are reduced in the initial phase, and losses due to charge exchange collisions with neutrals released from the wall, or due to gas puff, dominate the balance of energy and toroidal angular momentum. Only the ions are affected by this process. Since ions carry about half the energy, whereas they carry most of the angular momentum due to their larger mass, the energy confinement time is almost doubled with respect to the angular momentum confinement time.

Li-beam Plasma Edge Diagnostic

During the 1995 campaign, the Li-beam edge density diagnostic was successfully brought into operation. Measurements of edge electron density profiles were obtained, showing the temporal evolution of the upstream plasma edge over time periods of 5 to 7s. As the measurements were performed on the same radial chord as the reciprocating probe, a direct local comparison of these two density diagnostics is possible without the necessity of

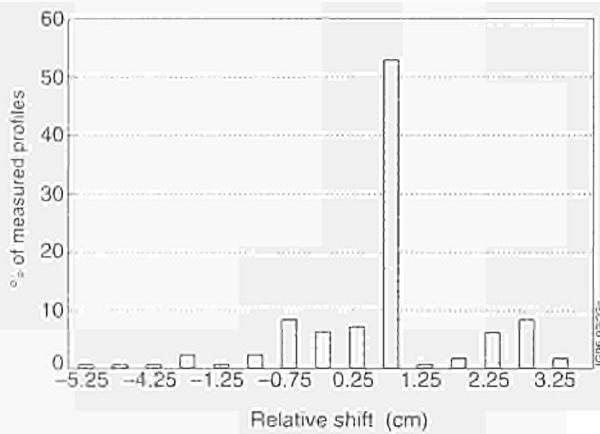


Fig.103: Agreement in edge density profile location between LIDAR and Li-beam diagnostic

magnetic equilibrium data, and very good agreement has been obtained (Fig.102). Using EFIT equilibria, comparisons with density profiles from other diagnostics such as LIDAR are possible. A systematic comparison of the available data shows, that the Li-beam density profiles are consistent with the LIDAR electron density profiles to within 2cm of spatial position (Fig.103). Using the DIVIMP onion skin divertor model for up- and downstream plasma conditions, good agreement with mapped target probe profiles is obtained. The Li-beam diagnostic also may have been able to resolve structures in the upstream edge density gradient correlated to target conditions.

Although the Li-beam diagnostic was only operational as an active beam diagnostic for the latter part of the 1994/95 campaign, it had already made a major contribution to the understanding of edge emission of plasma impurities and neutral deuterium using the diagnostic for "passive" spectroscopy. The emission from CIII and CVI ions in the outer half of the plasma were Abel inverted to obtain local emission layer structures, confirming the existence of an isolated CVI charge-exchange induced emission layer several cm inside the confined plasma. This must be due to the presence of fast neutral deuterium, and first calculations of its density inside the separatrix were made.

Edge Charge Exchange Spectroscopy

The edge charge exchange diagnostic is used to study impurity ion temperatures and pressures in the outer 30cm of the plasma, from these measurements the value of the radial electric field, E_r can be calculated. The diagnostic uses charge exchange reactions with a neutral heating beam to stimulate emission from fully ionised impurities in the plasma. It has particularly good space resolution, achieving less than 1cm under optimum conditions.

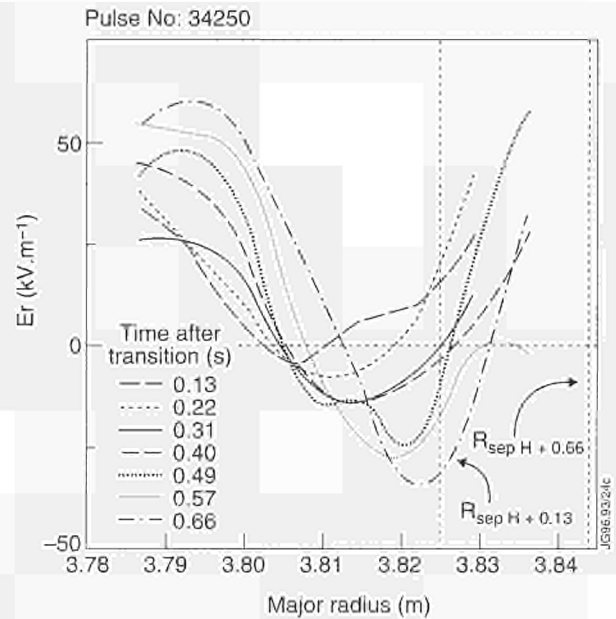


Fig.104: E_r profile at a sequence of times following the L- to H-mode transition. The negative portion of the profiles occurs where the ion pressure gradients are steep, and the positive portion where the profiles are flatter and the toroidal radiation is high. The separatrix position moves during the the course of the H-mode, the positions are shown at the earliest and the latest times)

An area of current interest is the study of the evolution of impurity parameters and E_r at the L to H-mode transition. At the transition an abrupt drop is seen in the impurity density on open field lines (outside the separatrix), while that on the closed field lines starts to ramp up. These results are consistent with an impurity transport barrier being set up at the edge of the plasma causing impurities to be entrained and preventing their escape from the plasma. As the H-mode evolves, the gradients of density and temperature close to the plasma edge increase, with temperature gradients reaching more than 65keV/m over a region smaller than 2.5cm.

In Fig.104 a sequence of profiles of the radial electric field is shown for times following an H-mode transition. The profile has a negative well inside the separatrix where the pressure profile is steepest but becomes positive deeper inside the plasma where the pressure profile flattens and the toroidal rotation (induced by the heating beams) becomes larger.

Many theories of the L to H-mode transition involve the sudden appearance of a strong radial field that acts to suppress the turbulence responsible for the degraded confinement of the L-mode. In several smaller tokamaks evidence has been seen of this in the sudden change of impurity poloidal flow either at or just following the transition of about 15km/s. In JET, there is no evidence

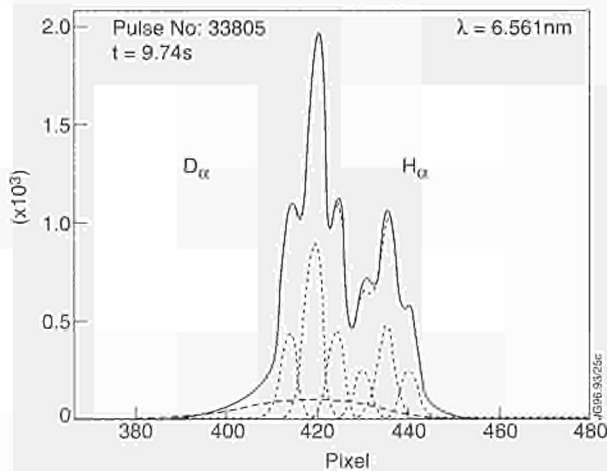


Fig.105: High resolution D_α/H_α spectrum showing the main Zeeman components. (The hydrogen content is exceptionally high in this pulse)

for such a change to within the 5km/s accuracy of the measurements. Such a small change in velocity, and hence E_r poses a significant challenge for many theories, although a possible explanation would be that the turbulence level in JET is already much lower than in smaller machines, and so a relatively minor change to E_r could be sufficient to tip the plasma into H-mode.

Passive Emission and Divertor Spectroscopy

The measurement of visible continuum radiation plays a central role for the absolute calibration of all instruments in the visible spectroscopy group. The deduction of line averaged values of $\langle Z_{\text{eff}} \rangle$ for arbitrary viewing geometries, and the mapping of data on common flux indices, enables on-line cross-calibration checks for instruments whose observation windows are exposed to plasma contamination during extended operation periods. VUV and XUV instruments, which are calibrated by branching-ratio techniques are thus indirectly linked to the global attempt of measuring visible bremsstrahlung.

Several spectroscopic instruments dedicated to the observation of passive emission lines emitted close to target plates, strike zones and the main divertor chamber have become operational during the 1994/95 campaign. Spectral survey monitors, high spatial and spectral resolution spectrometers, multi-channel periscopes for survey and high resolution spectroscopy have given first results during radiative divertor experiments and impurity transport studies based on controlled gas inlets of helium, neon or nitrogen.

A new survey spectrometer, viewing the divertor from a top port, collected plasma light from several lines-of-sight, and allowed the monitoring of intrinsic and injected impurities (nitrogen, neon, argon). Molecular emission from BeD

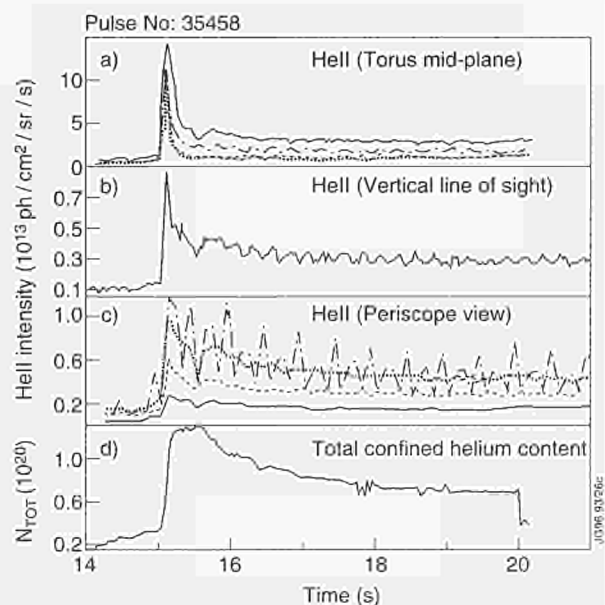


Fig.106: (a) to (c) decay of HeII (468.5nm) plasma edge line emission following a helium gas puff into an ELMy H-mode plasma. Sweeping of strike zone leads to oscillations of HeII line intensity; (d) confined He^{2+} particle content ($0 < r/a < 1$) from CXRS signals

was observed for the first time. Work is in progress to derive a chemical sputtering yield from the measurements.

High resolution line-shape measurements were made of the H_α and D_α emission in the divertor. The Zeeman splitting was resolved, confirming the location of the emission from the deduced magnetic field, and the Doppler temperatures of the cold (2–4eV) and lukewarm (50–200eV) features were measured. The H to D ratio was also measured for a wide range of pulses Fig.105.

Whereas general agreement is found between spectroscopically deduced values of the plasma edge H to D ratio and results derived from 5keV neutral fluxes measured by the Neutral Particle Analyser diagnostic during the ohmic heating phase, and also in the ELM phase of high fusion yield pulses, NPA results indicate that during ELM-free hot-ion H-modes, an isotope separation may occur close to the separatrix. If this effect is due to differences in plasma edge driven transport needs to be investigated.

The D_α light from a fan of lines-of-sight into the divertor was analysed with photomultiplier tubes, allowing the location of the divertor strike points to be determined, and the in/out asymmetries in the D_α intensity to be studied. As the plasma density is increased, the D_α emission was clearly seen to leave the divertor target plates and to rise up towards the X-point before finally jumping up the inner wall as a MARFE occurred.

During helium gas puff-experiments, first HeII line intensities were measured from divertor periscope views

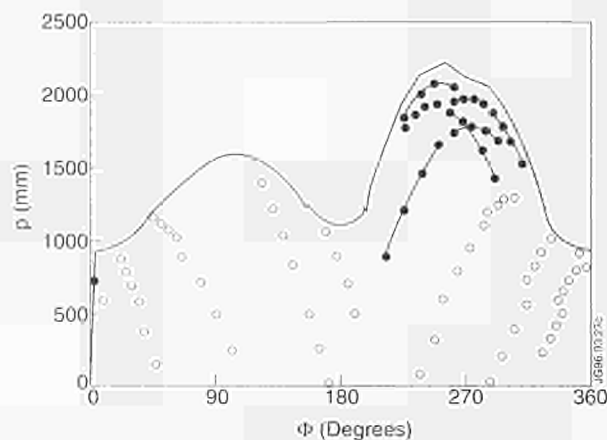


Fig.107: P- Φ diagram of the lines-of-sight of KB3E (closed circles) and KB4 (open circles)

which cover the major part of the divertor chamber and different locations along horizontal and vertical target plates. The results of similar plasma edge passive line emission measurements from the main CX multi-chord lines-of-sight fan striking the outer wall sections of Octants Nos. 1 to 7, are shown in Fig.106. An ultimate goal of the measurements is to compare particle confinement times in the bulk plasma with that of representative times in the divertor chamber. However, at the present stage, it is not yet evident whether available divertor data are sufficient for this task.

Any quantitative evaluation of the observed spectral intensities in terms of meaningful particle flows remains a demanding challenge since the measurements are neither truly local nor are local plasma data (electron density, electron temperature or neutral density and temperature) available. The latter are indispensable for the deduction of particle densities from measured photon fluxes. The ultimate aim of divertor spectroscopy will be to establish a quantitative link between absolute densities measured in the confined plasma region, particle densities in the divertor chamber and particle flows in the pump-duct. The efficiency of divertor performance can then be ascertained in terms of impurity compression and retainment compared to impurity behaviour in the main plasma chamber.

Bolometry

The old JET bolometer (KBI) was used throughout the 1994/95 campaign and was not modified in the pumped divertor shutdown [5]. A selection of 16 channels of the high temperature, in-vessel bolometer system KB3 and KB4 gave good divertor coverage [6]. The electronics of these 16 channels are PC-based and have a real time analogue output, which was successfully tested for feed-

back control of the radiative fraction [7]. Future applications of these 16 channels will also include disruption prevention. The electronics system was completed during the last weeks of operation and during the subsequent shutdown was brought up to the full complement of 84 channels. The 68 new channels are VME based and under CODAS control. The new amplifiers, which are located in the Basement, have the same signal-to-noise ratio specifications as the 16 other channels but a higher output bandwidth (2kHz instead of 1kHz). The digital storage units provide more memory per channel. Now the full pulse length can be sampled with 4kHz compared with 30s with a sampling rate of 500Hz, previously.

The seven cameras of the Mark I divertor bolometer system (KB3D) were removed since their location was not compatible with the Mark II divertor. The sockets of the old KB3D cameras were used to plug in extension cables leading to the new cameras of the KB3E system. The extension cables are flexible quad-cables with braided screens that continue the existing screening and grounding scheme. The spatial arrangement of the seven cameras was partly determined by the position of the remote handling connectors in the Mark II divertor structure. These had to be used to allow for the changes expected for the Mark II gas-box design. The remote handling considerations and the reduced diagnostic access in Mark II also led to a toroidal distribution of the cameras between Octant No.7 and the edge of Octant No.8. The p - Φ diagram shown in Fig.107 illustrates that KB3E and KB4 complement each other and that they together achieve a good coverage of the whole plasma. The new cameras had to be equipped with collimators instead of pinholes due to lack of space, and this led to a reduction of the illuminated detector area. Reflection inside the collimators is effectively suppressed by tapping the collimator holes.

The cabling and the connectors of the KB3 and KB4 system, which had shown erratic resistance changes in the campaign were overhauled. All KB4 cameras were re-cripped and four cameras, together with part of the cables for two cameras were exchanged. To reduce high frequency noise interference, the front-cover of KB4 was closed as much as possible and fine meshes were installed at the apertures.

The operability and reliability of the KB3/4 system was enhanced by the implementation of a fully automatic calibration facility. It is now possible to check resistances and calibrate the bolometers before and after every pulse.

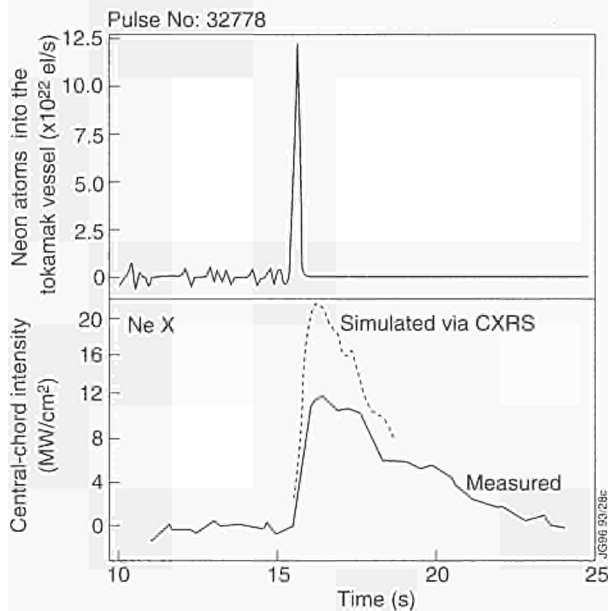


Fig.108: Time evolution of the chord-integrated intensity of NeX ($\text{Ly}\beta$), following a short neon puff (above). The lower solid trace was measured with an absolutely calibrated X-ray spectrometer. The dotted trace is an impurity transport code simulation, based on the CXRS measurements

X-Ray Spectroscopy

In addition to routine monitoring of intrinsic impurities, the broad-band soft X-ray survey spectrometer monitored impurities injected during impurity transport and radiative divertor experiments. Progress toward deriving impurity concentrations from passive spectroscopy was made by modelling soft X-ray line intensities with the SANCO impurity transport code. Using data from divertor gas-puff experiments, transport parameters were derived by simulating the impurity-density profiles measured by charge-exchange recombination spectroscopy (CXRS). Based on these measurements, a computation of intensity of a soft X-ray line was compared with that independently measured by the absolutely-calibrated X-ray spectrometer. Fig.108 shows the CXRS-based simulation compared with the soft X-ray measurement, for a Ne X ($\text{Ly}\beta$) line, following a short neon puff. The Ne $\text{Ly}\beta$ measurement is about 40% lower than the simulation, which is considered to be good agreement given the cumulative uncertainties inherent in the comparison. This comparison increases confidence in the use of passive measurements to other impurities and to non-beam-heated discharges, where CXRS cannot be used.

Construction of a compact high-resolution X-ray crystal spectrometer began with most of the components being delivered in 1995. The instrument will be used mainly for off-axis ion temperature measurements by passive

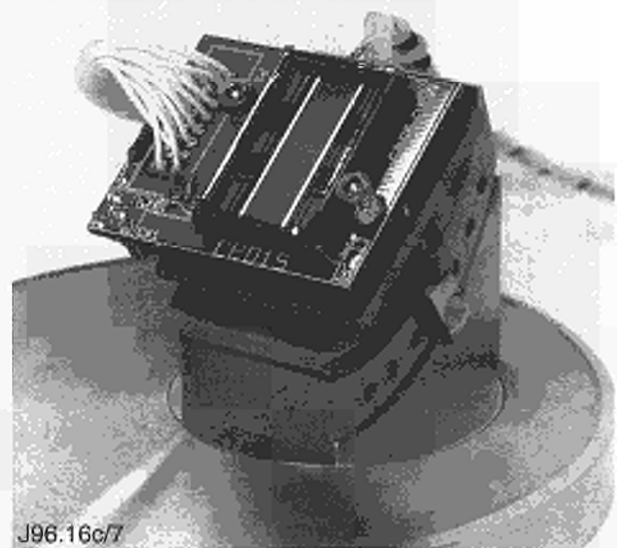


Fig.109: The detector assembly for a compact high-resolution X-ray crystal spectrometer. An X-ray CCD array is mounted, via a two-stage Peltier cooler, to a JET-designed water-cooled rotary stage

spectroscopy. The detector assembly is shown in Fig.109. The instrument has Johann geometry, with a fixed crystal-to-detector chord of about 0.8m. Crystals of size $50 \times 16 \times 0.4 \text{ mm}^3$ are bent to the relevant radius in a four-pillar jig. The detector is a CCD array optimised for the direct detection of X-rays, and was developed by Leicester University, UK, primarily for astrophysical observations. Since the CCD is also sensitive to visible light, the crystal can be focused and aligned directly onto the detector and this has been demonstrated using a custom-built optical alignment apparatus. Tests of the two-stage Peltier refrigerator achieved a lowest temperature of -47°C , at which temperature the thermal noise is low enough to measure individual X-ray photons, with an energy resolution of about 150eV. Two main read-out modes are possible; either a 2-D mode with energy resolution, for checking the X-ray alignment and signal-to-noise ratio, or a 1-D mode with on-chip vertical binning of the line-image, to give time resolution of about 2ms.

VUV/XUX Spectroscopy

Spatial Scan VUV Monochrometers

This diagnostic (KT1) consists of three spectrometers, which scan, by means of rotating mirrors, parts of the plasma cross-section. The instruments have three wavelength ranges, two in the VUV ($200 \leq \lambda(\text{\AA}) \leq 2000$) and one in the visible. For the two VUV ranges of each instrument, micro-channel plate (MCP) detectors are

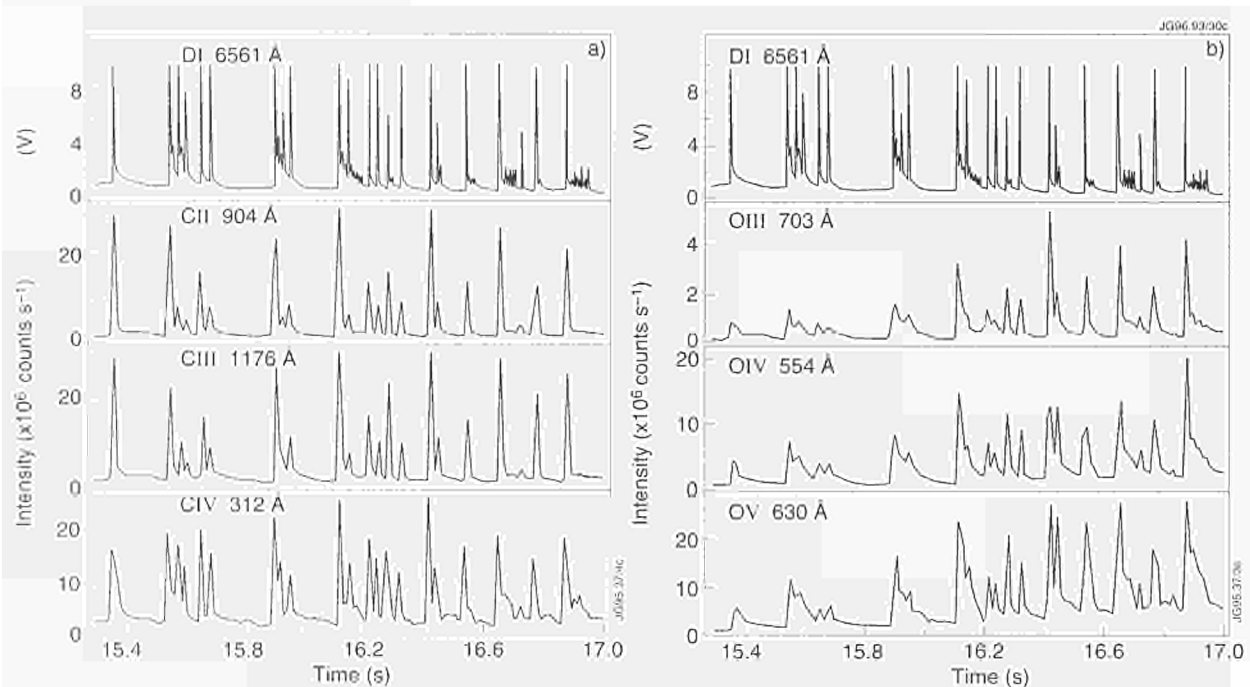


Fig.110: D_{α} emission and (a) the CII, CIII and CIV and (b) the OIII, OIV and OV line intensities during the ELMy H-mode phase of Pulse No.32773, observed with the double SPRED spectrometer

used, possessing 16 channels and covering a wavelength range of about 7 \AA . The visible range is equipped with an encapsulated single channel MCP detector. The envisaged time resolution is 25ms, the scan time over the viewed cross section = 2ms.

The rotating mirrors sit in the main vacuum and are driven by external motors. A particular problem has been the rotary feedthrough of the mirror drive. The feedthroughs have to be compatible with demanding requirements for tritium experiments in JET. Together with an industrial collaborator, a double bellows feedthrough has been developed, exploiting the well known tumble drive principle. The difficulty of such a feedthrough is the unavoidable slack coupling of the transferred momentum across the vacuum boundary. Very high manufacturing precision is required, to keep play at a minimum. A satisfactory lifetime expectancy is a further requirement. The design value of 1.5×10^6 revolutions has been exceeded with a prototype, by 5×10^5 , without failure.

The feedthrough's interspace vacuum is permanently monitored so that rotation can be stopped immediately in the event that one of the bellows fails.

Divertor VUV/XUV Spectroscopy

Line radiation of the main plasma impurities emitted from the divertor region has been observed using a VUV/XUV spectroscopy diagnostic (KT7D). The instrument consists of three spectrometers, a double SPRED, which combines two VUV spectrometers in one instrument, and

a SOXMOS for the XUV emission. In April 1995, the SOXMOS was replaced with a fibre and lens system giving a line-of-sight used to observe the visible spectrum. The visible line-of-sight has been used for opacity studies and an absolute calibration of the VUV spectrum by means of branching ratios.

The spectrometer assembly is protected from neutrons and γ -rays by a minimum of 15cm of stainless steel between the plasma and detectors and 5cm elsewhere. In addition, neutron moderator material has been avoided to minimise the production of secondary γ rays from neutrons in the range 0.8-10MeV. A check was made on the effectiveness of the shielding by comparing the increase of the backgrounds in spectra observed with the double SPRED and an unshielded single SPRED instrument (KT2) with a near horizontal line-of-sight close to the vessel midplane during two high performance discharges. Once the difference in the detector gains are accounted for and a small correction is made for the greater distance of the single SPRED detector from the plasma centre the comparison suggests that, to within a factor 2, the background is ~ 7 times lower for the shielded double SPRED instrument. Further experiments are planned to investigate whether the improvement is due mainly to the attenuation of the direct neutrons or from the secondary γ -rays. The spectral line intensities recorded with the double SPRED along the vertical line-of-sight passing through the divertor region are typically a factor ~ 40

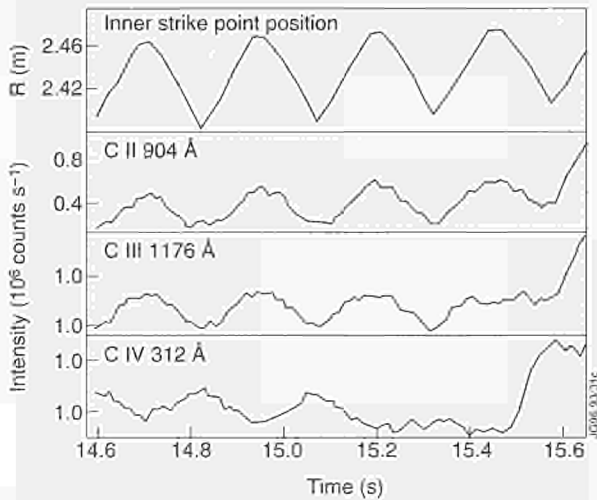


Fig.111: Carbon emission during the sweeping of the X point position, which is shown in the movement of the major radius of the inner strike point

higher than those viewed along the horizontal, midplane line-of-sight with the single SPRED instrument. This is attributed mainly to the higher electron density in the divertor plasma and to the higher density of low ionisation stages near the main recycling source.

The shortest exposure time, 11ms, which enables the full spectral range to be read, gives sufficient time resolution to allow events such as ELMs to be resolved. This is illustrated in Fig.110 for Pulse No.32773, in which there is an ELMy H-mode. The figure shows the D_{α} trace recorded with a vertical line-of-sight viewing the outer edge of the divertor box, the time history being dominated by a sequence of ELMs. The behaviour of the D_{α} is mirrored in the CII, CIII and CIV line intensities, Fig.110(a), and those of OIII, OIV and OV, Fig.110(b), observed with the double SPRED instrument. A difference can be seen between the short lived C features and those of O which have a slower decay. Given the similarity of the ionisation potentials of CIII and OIII and of CIV and OIV and that the impurity transport of C and O ions is not expected to differ significantly, the difference in the C and O time histories is attributed to the source of the impurities, reflecting a difference in their release mechanism. C is released from the tile surfaces by physical sputtering, this process having a strong dependence on the incident particle energy, whereas a chemical mechanism involving D is involved in the release of O.

Evidence for a localisation of the emission can be found when the X point is swept. In Fig.111, the top trace shows the major radius of the inner strike point for Pulse No.32779 before the application of neutral beam heating. The CII and CIII line intensities are clearly correlated with the strike

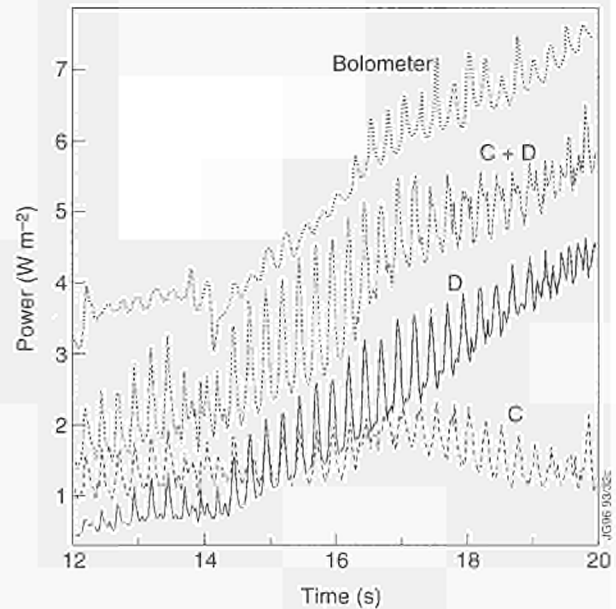


Fig.112: Deuterium, carbon and total radiated power measured with the VUV spectrometer and comparison with the bolometer measurement for the ohmic density limit (Pulse No.34859)

position and this pulse is exceptional in that they are out of phase with the CIV emission. This indicates that spatially resolved measurements are already obtained before a spatial scan of the divertor is made by rocking the instrument. Preparations for the re-installation of the SOXMOS and the installation of the permanent line-of-sight in the visible wavelength region are well underway.

In the absence of impurity injection, emission from neutral deuterium and low ionization stages of carbon (CII, CIII and CIV) dominated. At moderate to high densities these species accounted for the radiated power measured with a bolometer with a divertor view similar to that of the VUV spectrometer (Fig.112). This was independent of whether JET was operated with CFC or Be divertor target tiles, showing why characteristics of plasmas on Be and CFC targets were similar.

When radiative divertor regimes were established, by combined deuterium and nitrogen seeding in the divertor, nitrogen was observed to contribute to almost the entire radiated power: radiating up to ten times more than carbon and deuterium together in the detached phase.

During experiments aimed at melting of the Be target tiles, when about 15MW of additional heating were applied without sweeping of the strike points, Be was observed to be the main radiator, with Be II carrying most of the power towards the end of the additional heating phase. At the same time, oxygen was released, most likely following molecular breakup of beryllium oxide, the oxygen radiation returning to negligible levels after the

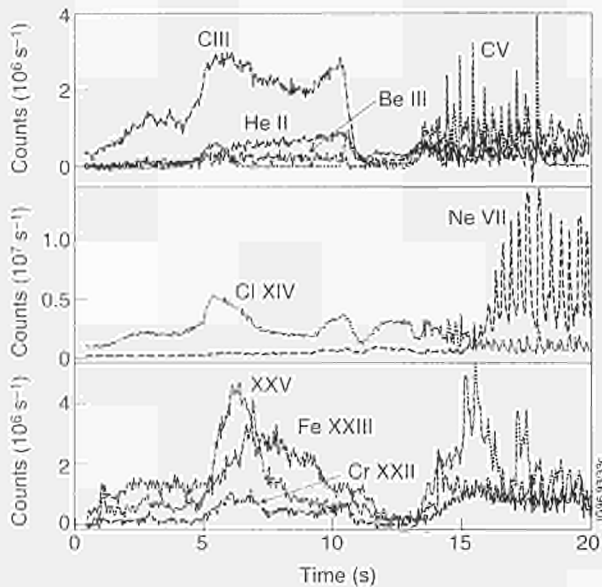


Fig.113: Time histories of representative VUV/XUV spectral lines for a neon enhanced H-mode pulse

additional heating was switched off and the sweeping was started. During the Be melting phase, the carbon line radiation was observed to drop by an order of magnitude.

Main Plasma VUV/XUV Spectroscopy

VUV and XUV emission from the bulk plasma was monitored using two grating spectrometers during the 1995 operational phase. The SPRED spectrometer is a VUV instrument providing coverage of the wavelength region from 100 to 1100Å with a spectral resolution of $\sim 4\text{\AA}$. The XUV, SOXMOS instrument is a grazing incidence instrument with two detectors. Each views a wavelength range of $\sim 40\text{\AA}$ and can be moved to record the spectrum at positions between 15 and 340Å. The SPRED has a near horizontal line-of-sight close to the vessel midplane, while the SOXMOS can be tilted to look at angles between the horizontal and a near divertor view.

Time histories of the line intensities of all the major intrinsic impurities (Be, C, O, Cl, Fe, Cr, Ni) were produced for the intershot analyses providing valuable information on the impurity content (and level) of a given plasma. Impurity influxes from elements such as Al and Cu were also routinely monitored, as were addition impurities added for experimental purposes, such as nitrogen and neon for radiative divertor studies and various elements injected via the laser ablation system. An example of this data is given in Fig.113, where representative line intensities for a neon assisted H-mode plasma is shown. The ELM behaviour in the latter half of the pulse is clearly reflected in the NeVII, ClXIV, CIII and CV

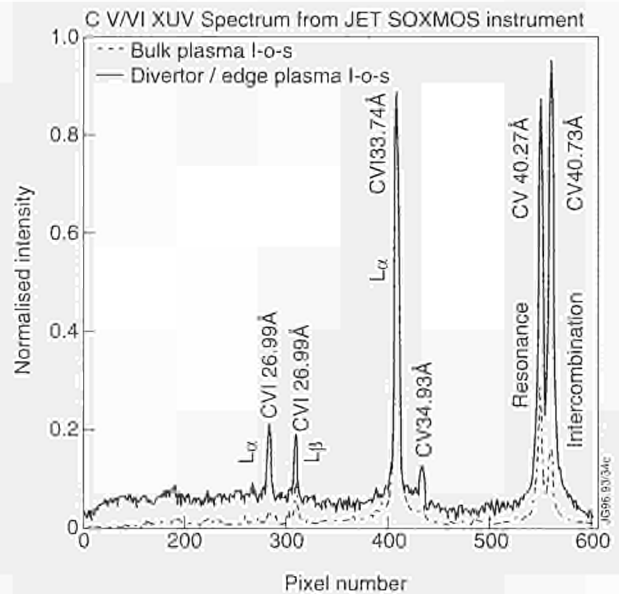


Fig.114: CV/CVI spectrum from the SOXMOS instrument

signals (in this example the BeIII and HeII intensities are too low in the divertor phase to reflect this). Note that the heavier, more centrally located element (CrXXII, FeXXIII and NiXXV) are unaffected by the ELMs, which is an indication of the ELM penetration depth.

Work is progressing on the sensitivity calibration of these instruments with the aim of providing absolutely calibrated line intensity time histories and radiated power components for the major impurity species. By the end of the operational phase, a total of 35 spectral lines from 14 different elements were being recorded for each discharge. The temporal resolution of these data was typically 20 to 50ms over the entire pulse with 1ms resolution being available for intervals of a discharge of particular significance.

Figure 114 compares SOXMOS CV/CVI spectra recorded with two different lines of sight, one near horizontal and the other near divertor. The latter passes through the cooler plasma edge where recombination effects are apparent from the enhanced CV relative intensity and the strength of the CV intercombination line at 40.73Å. The distortion of the CVI Lyman series is indicative of additional charge exchange effects. This is shown in Fig.115 where the calculated $L\gamma\beta/L\gamma\gamma$ ratio (28.47Å and 26.99Å, respectively) is plotted against electron temperature for the cases of no charge exchange and charge exchange included with neutral density fractions of 10^{-3} and 0.1. The shaded region denotes the average observed ratio inferring a neutral density fraction of approximately 0.1.

Both systems use the same PC based data acquisition system which was introduced, along with new detectors,

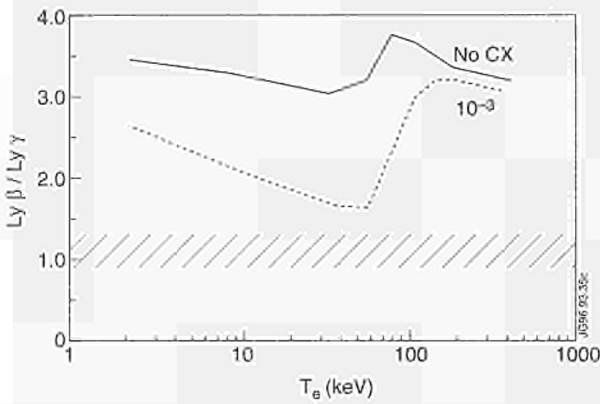


Fig.115: Calculated CVI Lyβ/Lyγ ratios plotted against electron temperature showing the effects of including charge exchange from neutrals in the calculations for increasing neutral density fractions. The shaded region denotes the average observed ratio

at the beginning of the 1994/1995 operational phase. The software for this system underwent several upgrades during 1995 culminating in a custom designed stand-alone Windows version, which was successfully tested before operations ceased. During the Mark II divertor shutdown, work has progressed on the data acquisition software utilising a laboratory plasma source/spectrometer testbed. For 1996 operations, improvements to the data acquisition system will include full implementation of the custom software package, inclusion of a ‘pixel-skipping’ option where the temporal resolution can be improved by discarding non essential portions of the spectrum and also the provision of real-time output of impurity line intensities for feedback control of other operational systems. This last feature has been demonstrated in the laboratory, sending integrated line intensities in real

time via the Ethernet to a receiving PC. It is anticipated that eight separate spectral lines per instrument can be output in parallel with the normal recording of the complete spectra. This data will also be available for the divertor VUV/XUV spectroscopy.

A new detector high voltage supply has been acquired and also a new control system for the remote movement of the XUV instrument. This uses a hydraulic ram to change the viewing angle and will enable the line-of-sight to be changed between pulses or to move the instrument during a discharge, scanning the plasma or viewing different plasma regions during different phases of the discharge.

Neutral Particle Analysis

Low Energy Neutral Particle Analyser

The low energy Neutral Particle Analyser (KR2) has been fully operational throughout the 1995 campaign, although progressive detector ageing has necessitated refurbishment of the instrument during the 1995/96 shutdown.

Monitoring and systematic study of the hydrogen minority fraction in deuterium plasmas has received attention during the 1994/1995 campaign. This is important with respect to both D(H) ICRF heating and fusion reactivity in high performance regimes. Modelling work aimed to derive the H/D density ratio in the main plasma from the observed H and D neutral particle fluxes in the energy range 6 to 10keV, which proved most suitable for this purpose, has provided a simple approach to the conversion of flux ratios into density ratios applicable to ohmic phases. This has yielded an abundant database (Fig.116), which shows quan-

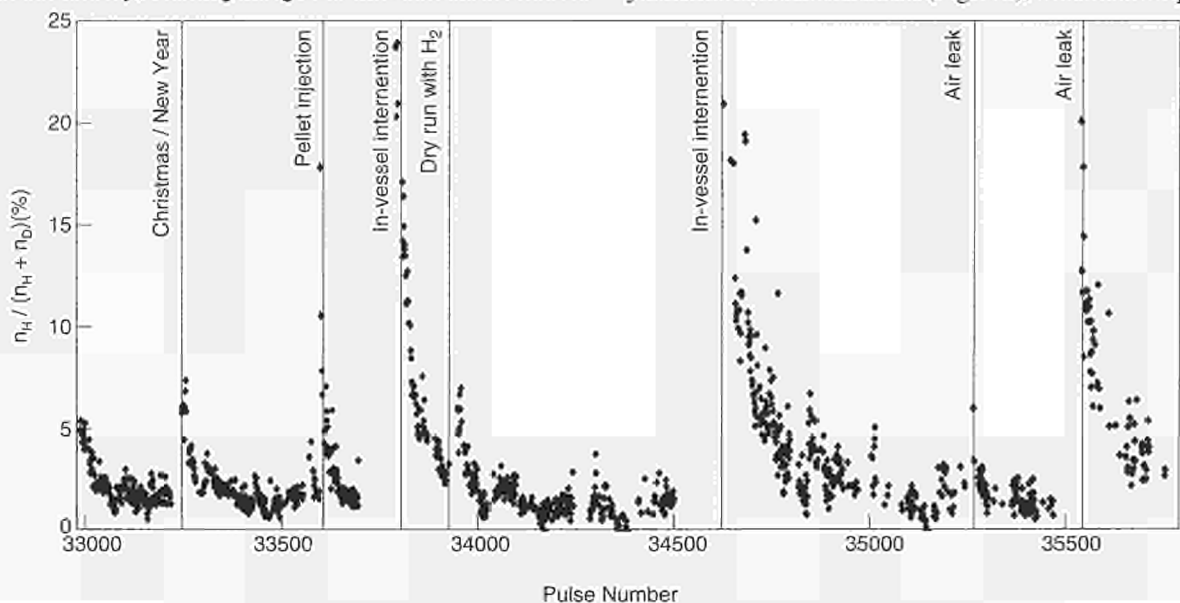


Fig.116: Percentage of hydrogen in deuterium plasmas measured by the low energy Neutral Particle Analyser during the 1995 campaign

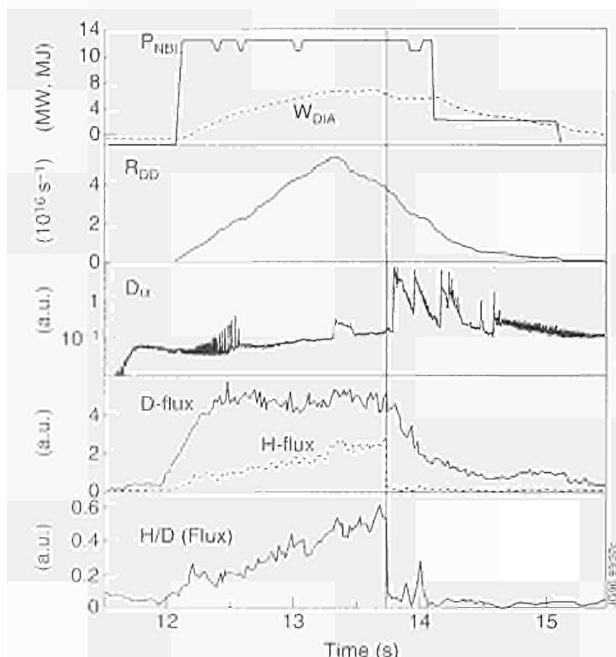


Fig. 117: Time traces from Pulse No. 33648 showing an increase of hydrogen neutral efflux at 7.8keV during an ELM-free hot-ion H-mode

titative conclusions to be drawn concerning various sources of hydrogen and the speed of their depletion. It is found that the characteristic number of pulses for hydrogen depletion after a vacuum vessel vent is 50-80 pulses. A basic, persistent level of about 1% of hydrogen is observed. It is likely to be due to diffusion within the exposed inconel wall components. Visible light spectroscopy (H_{α}/D_{α} line intensity) viewing the divertor confirms the data shown in Fig. 116, but cannot reliably measure hydrogen fractions below 5%.

A result of particular importance, though not fully understood as yet, is the constant observation of a growing hydrogen percentage during the ELM-free phase of hot-ion H-mode plasmas up to values around 30% ($H/(H + D)$ flux ratio) followed by a very fast drop, coincident with a large ELM, down to the target plasma hydrogen contamination level. Figure 117 shows a typical example. This increase of hydrogen is restricted to the main plasma, as the H_{α}/D_{α} signal shows no change. Simulations attempting to attribute the phenomenon to the particular high performance plasma properties in conjunction with the presence of neutral heating beams have failed, while correlations regarding a tendency of shortfall in the observed fusion reactivity have been found.

High Energy Neutral Particle Analyser

The new high energy neutral particle analyser (NPA), (KFI), specifically designed for use during D-T operation, was successfully operated during the year. Calibra-

tion problems which arose with the prototype instrument during the 1991/92 experimental campaign have been overcome and the data now obtained is suitable for confrontation with theories and models. The NPA is intended for measurement of MeV energy D-T and D-D fusion products. Also, it can make measurements of high energy ions interacting with ICRF- or Lower-Hybrid waves and with MHD modes.

Improved atomic analysis of neutralisation of MeV energy protons and deduction of proton energy distribution functions is in hand. Contributions to proton neutralisation by charge-exchange from excited states of donor impurity ions in the plasma seem to be unimportant in relation to those due to inaccuracies in cross-sections for CX from ground state of donor impurity ions. Calculation of more accurate cross-sections for charge-exchange between MeV energy protons and hydrogen-like carbon and beryllium ions is progressing.

Measurements of ICRF driven proton distribution functions in the energy range $E > E_{crit}$, a first of its kind, are made with the intent to verify in this energy range various physical aspects of the widely used Stix model for minority ICRF heating of plasmas. Measurements show that the scaling of the tail temperature associated with the perpendicular energy distribution function at the position of maximum power deposition is linear with applied ICRF power, as expected in the Stix model. However, agreement between magnitude of absolute tail temperature is lacking. This may be attributed to large orbit effects which are not taken into account, or to discrepancies in ICRF power deposition.

Indications have been seen of interaction between ICRF driven protons and Lower Hybrid waves during combined LH current drive and minority ICRF heating experiments. The effect is not unexpected and the evidence at present is tentative and sporadic. The importance of this effect lies in the implication that a parasitic loading of LH current drive is present and that in larger fusion devices charged fusion products may interfere with efficient current drive. Preparations are in hand to repeat these measurements at much higher level of ICRF heating and LH current drive in the 1996 experimental campaign, in order to verify and evolve a better understanding of the effect and its implications for the future.

Interaction of high energy ions and MHD modes is a subject of keen interest due to concerns about alpha losses and first wall loading in future devices. A prominent

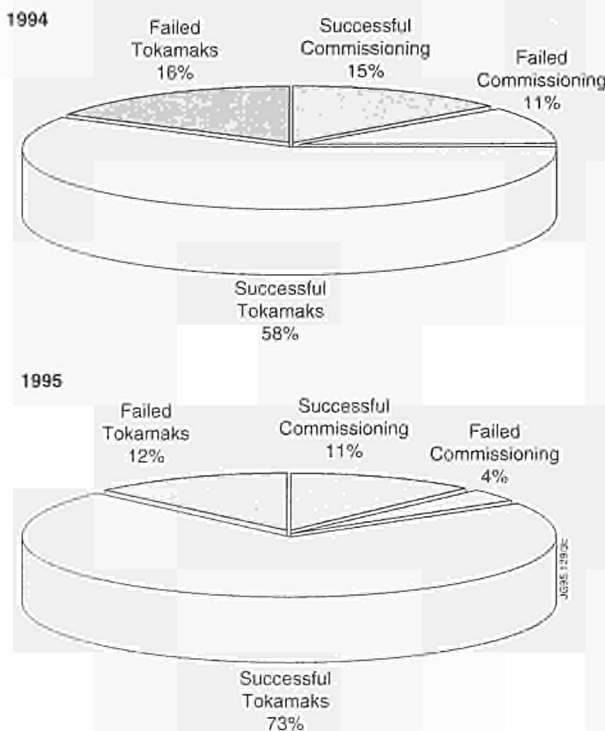


Fig.118: Analysis of Pulses in 1994 and 1995 Operations

observation using the NPA was that of interaction between sawteeth and ICRF driven protons. When the density of high energy protons was small the interaction with sawteeth caused expulsion of the protons from the plasma core. When density of such protons was high enough the expulsion stopped, although thermal effects of sawteeth (eg. reduction of central T_e), continued. Fast ECE and soft X-ray emission measurements indicate that the presence of high energy ions modifies the sawtooth collapse. Experimental and modelling investigations of this interaction are planned.

References

[1] J.Karlsson and T.Elevant, JET Internal Report, JET-IR (95)04
 [2] O.N.Jarvis et al, JET Preprint, JET-P(95)53
 [3] JA Hoekzema et al, 22nd EPS Conference on Controlled Fusion and Plasma Physics, Bournemouth (1995), II-445
 [4] H Bindslev, JET Preprint, JET-P(95)66
 [5] JET Progress Report 1993 Eur 15722-EN-C (EUR-JET-PR11) Page 83.
 [6] R. Reichle *et al.*, "Radiation in JET's Mark I Divertor", 22nd EPS Controlled Fusion and Plasma Physics, Bournemouth, U.K., July 1995.
 [7] JET Progress Report 1994 EUR 16474-EN-C (EUR-JET-PR12) page 98.

Table XIV: Task Force Distribution

Task Force	No. of Shifts	% of Total
Task Force D	75	33.80 %
Task Force H	57	25.70 %
Task Force T	36	16.20 %
Task Force C	41	18.40 %
Task Force RF	13	5.90 %

Summary of Operations

The Mark I Divertor Operations Phase covered the period January 1994 until June 1995. Out of the total of 473 days, the high figure of 312 operations days (66%) was achieved. During this time, a total of 7005 pulses were run, of which 4288 had plasmas above 1MA. The total number of pulses carried out in 1995 was 2520.

As the machine and sub-systems settled down, a marked increase in the success classification of the pulses was observed. In 1994, 73% of pulses were either Commissioning Success (CS) or Tokamak Success (TS), while in 1995, a success rate of 84% was achieved [1]. These are shown in Fig.118.

During 1995, JET operations continued until 19 June, representing an effective total of 150 operational days. Two different stages marked the 1995 campaign:

- (a) the continuation of the studies of the Mark I divertor with carbon tiles until 14 March 1995;
- (b) the assessment of the Mark I divertor with beryllium tiles from 27 April 1995 until 19 June 1995.

These two phases were separated by one major shutdown period lasting 32 days to allow the removal of the divertor carbon tiles and their replacement with the beryllium.

The resulting time shared between shutdown, commissioning and operational days was the following: shutdown - 26.00%; commissioning - 13.70%; operation - 60.30%. The organisational arrangements of the operational time for the experimental programme consisted of three main Task Forces: Task Force D for Divertor Assessment, Task Force H for High Performance and Task Force T for Tokamak Concept Improvements. In addition, some time was devoted to plasma commissioning (C) and ICRF commissioning under Task Force RF.

The experimental programme was carried out in double-shift operations days (06.30 to 22.30 hours), six days a week. In addition, up to six Sundays were devoted to operations. The total number of shifts were distributed as set out in Table XIV.

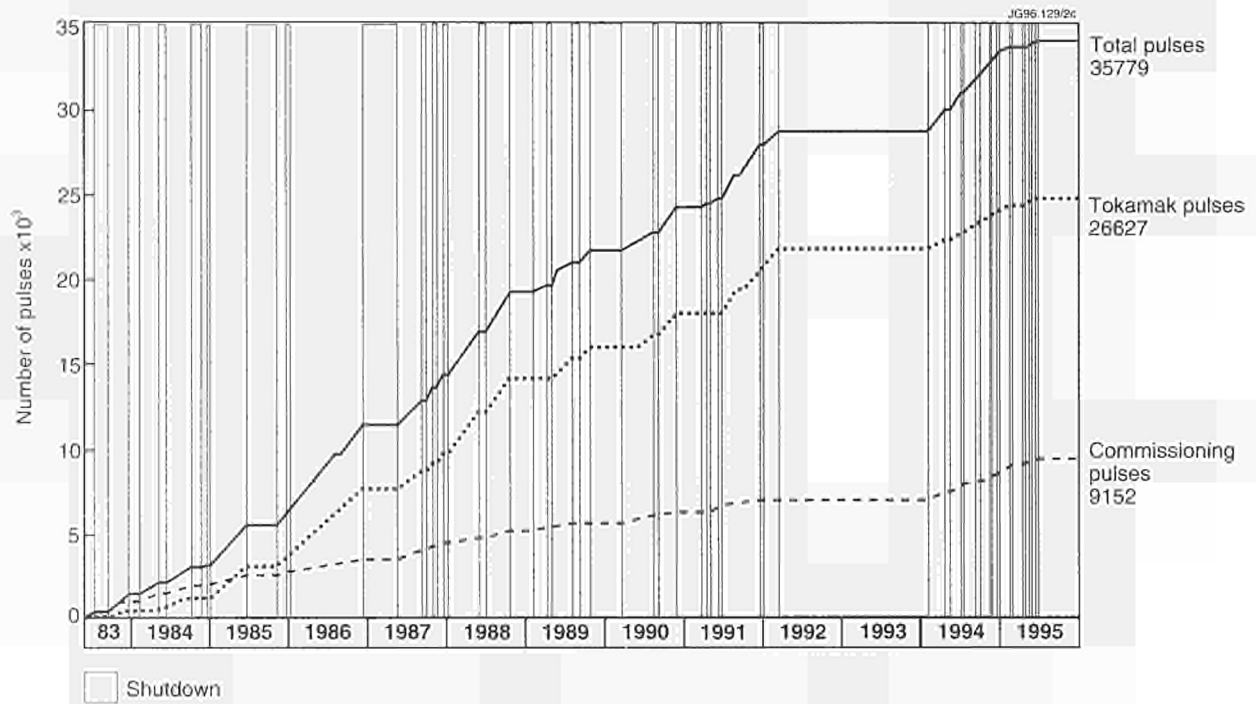


Fig.119: Cumulative totals of JET pulses: 1983-1995

Shutdowns

The 1994/1995 maintenance shutdown periods are summarised in Table XV. An analysis of the days on which operation took place has shown that ~20% of operation time was lost through machine failure of some kind. JET is an experimental machine and changes and developments are required by the experimental programme. Therefore, the figure of 20% daily down-time is remarkably good. A typical pulse rate of one for 30 minutes was achieved. This is slower than previous operations, but the complexity of operation has increased substantially. Also, the quality and returns per pulse have improved steadily

Table XV: 1994/1995 Maintenance Shutdown Periods

March/April 94	Commissioning - Restart
May	Start Experimental Campaign
20th June	4 days Maintenance (leak repair)
25th Aug	3 days Maintenance (replace GDC electrodes)
21st Sept	2 weeks Maintenance (repair Saddle Coils etc)
3rd Nov.	2 week shutdown (Evaporator repair)
24th Dec	2 weeks, Christmas Break and maintenance
30th Jan 1996	2 weeks preparation for ripple experiment and recommissioning
17 March	6 weeks shutdown and restart recommissioning. Beryllium tile replacement.
19th June 1996	End of operations.

over the JET lifetime, especially in view of the increasing sophistication and data capabilities of the diagnostics.

This is slower than previous operation, but the complexity of operation has increased substantially. Also, the quality and returns per pulse have improved steadily over the JET lifetime, especially in view of the increasing sophistication and data capabilities of the diagnostics.

Disruptions

Of the 4288 plasmas run above 1MA, a quarter disrupted. Many of these disruptions were in the tail of the pulse, after the scientific aims of the pulse had been achieved, and many more were part of the scientific programme. Only nine disruptions occurred above 4MA. JET is increasingly involved in the study of the cause and prevention of disruptions, and in the amelioration of disruption forces when these occur. The forces were substantially reduced for many disruptions by the detection of the mode-lock precursor and the forced reduction of the plasma elongation before the disruption. Nevertheless, some worrying events have been observed, and efforts to improve understanding of the forces involved have been taken. This will be a major contribution to the design of ITER.

Baking and Beryllium Evaporation

The vessel was kept at a constant temperature of 250°C throughout the operation period, although JET now has substantial actively cooled components within the vessel.

The divertor coils and entire divertor tile and carrier structure were kept approximately at room temperature, and the divertor toroidal cryopump was usually at liquid helium temperature. From the start of the scientific programme in March 1994 until the end in June 1995, the vessel was cooled to room temperature only six times. Following each vacuum vent, the machine was initially baked to 100°C with no active cooling, followed by a period at 300°C with GDC and active cooling of some in-vessel components. Rapid and effective conditioning was usually combined with an evaporation of a fresh layer of beryllium. 160 such evaporations were performed during the 312 days of operation.

Overall Summary

The total number of pulses carried out in 1995 was 2520, with a total overall distribution over 1983-95, as shown in Fig.119. The overall ratio of successful pulses either for commissioning or plasma reached a remarkable 84% level in net progress, compared with the 77% achieved in the main 1994 experimental campaign. One explanation would reside in the limited number of interruptions planned for major activities. An analysis of the distribution of the plasma current shows that operations up to 2MA and 3MA continued to be routinely established as they represented 58% of the plasma pulses (Fig.120). A total of 60 plasma currents above 4MA and up to 6MA were obtained.

References

[1] J.How, P.Chuilon et al. "Summary of Physics and Machine Operations 1994-1995", JET-IR(95)07

Summary of Technical Achievements

The latest experimental campaign ended in June 1995. Central physics issues relevant to the design of a 'Next Step' tokamak were addressed with plasma currents up to 6MA, and these showed that the Mark I divertor, which makes use of strike point sweeping across the target plates, is a suitable tool to control the influx of impurities in the plasma core.

New types of events involving electromechanical interactions of plasma with the vessel and in-vessel structural components have been encountered, due to plasma vertical instabilities and disruptions (due to toroidal asymmetries of vacuum vessel forces and sideways vessel displacements). These events require further study, as

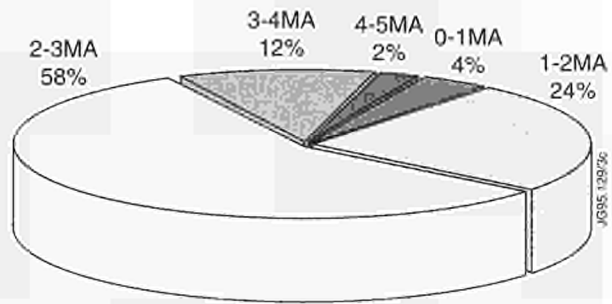


Fig.120: Plasma Current Distribution for 1995

a better understanding is crucial to the reliable design of a fusion reactors, such as ITER.

Although the operation with the Mark I divertor was most successful, the divertor configuration must be optimised to better meet ITER requirements. Therefore, an improved, more closed, Mark II divertor structure has been designed. This new divertor allows, in addition, divertor tile structures to be fully replaceable by remote handling techniques, following D-T fusion experiments. The main objective of the shutdown has been the installation of such a Mark II divertor, including testing of the remote handling techniques.

Technical Aspects of Operations

The intense experimental campaign 1994-95 has been made possible by the extended commissioning of the 'new' machine and by the reliability of the major machine subsystems. A total of 7389 pulses were performed throughout the campaign: 23% were commissioning (with or without plasma) and 77% were operational pulses.

- Two new power supply systems became operational for the first time during this period: the poloidal divertor field amplifiers (PDFA), 500-650V, 40kA d.c. to supply the divertor coils with strike-point sweeping capability; and the fast radial field amplifier system (FRFA), based on GTO technology, 5kV, 5kA (or 10kV, 2.5kA), response time 0.2ms, to meet the requirements of plasma vertical position control. In addition, a system of four 1.5kV, 3kA disruption feedback amplifiers (DFAS), based on new IGBT technology, were introduced to supply the saddle coils.
- Divertor (elongated) plasmas are more vertically unstable and require plasma-wall gap control, thus a new plasma position and current control (PPCC) was used. The system was designed with 'intelligent' software to control plasma-wall gaps and poloidal coil currents. The flexibility of the new PPCC has greatly

simplified JET's operations, since it allowed accurate control of the plasma boundary. PPCC has proven to have the capability of controlling the plasma distance from the outer, inner and top vessel wall, the X-point position and the plasma current simultaneously, and to change control behaviour during the pulse to satisfy the different requirements of the various phases of the pulse. Switching from coil current to gap control does not affect plasma equilibrium. Although the vertical stabilisation performance is presently limited by the noise introduced in the feedback signals by thyristor switching of the divertor power supplies, the system has demonstrated the ability to cope with plasma with growth rates of 800s^{-1} . This has allowed the Mark I campaign to be conducted effectively without vertical instabilities not generated by plasma internal events. Improvements are now underway: a tuned power filter will be installed at the PDFA d.c. output leading to $\geq 32\text{dB}$ attenuation of the 600Hz and 1200Hz ripple noise; the computational power to allow more complex algorithms to be used will be increased, to include soft X-ray signals as the detection element for vertical stabilisation purposes; plasma shape control will be upgraded to achieve a more accurate control of X-point position and the simultaneous control of the two strike-point positions.

- A similar technology has been used for the new coil protection system (CPS), necessary to cope with the greatly enhanced electromagnetic equatorial asymmetry of the machine. It comprises a wide range of protections in respect of overcurrents, overvoltages, limits to thermal and mechanical stresses, and model-based fault detection. CPS has extended the JET operating range by allowing the use of dynamic thresholds based upon on-line calculations (e.g. the central P1 coil current threshold, which is a function of the toroidal field current). It has introduced a real-time evaluation of the coil models that made possible fault detection from unmeasured quantities such as short-circuit currents, transducer faults, wrong power supply polarities, etc. A typical example of CPS intervention is the protective action for excessive P1 average current (the six P1 central coils can carry up to 60kA because of the pre-compression of the toroidal field coils, while the outer coils can carry 40kA only). The algorithm has been optimised to minimise the overshoot of the current in the P1 end coils. TF coil

protection includes transverse force protection (due to the tokamak torque), the coil interturn fault detection and the earth leakage protection. CPS has operated with a high degree of reliability. CPS will now be progressively upgraded to a Torus Protection System (TPS) to include monitoring and analysis of stresses in the vacuum vessel.

- The most important result obtained was the demonstration that the pumped divertor operated successfully. In fact, in the previous X-point configuration (without divertor) an input of only 15MJ of injected energy would lead to a 'carbon bloom', with sudden termination of the high performance phase. With introduction of the divertor, up to $>180\text{MJ}$ (from 32 MW of combined NB and RF heating) were injected without sign of discharge deterioration. The care taken in the design and in the installation CFC divertor tiles (which eliminated sharp edges), the successful use of the cryopump and X-point sweeping (a suitable technique to reduce target temperature from about 1000°C to 600°C or less) have been instrumental in achieving longer, cleaner and more stationary H-modes. As a result plasma performance could be maintained for long pulses ($\sim 20\text{s}$, $\sim 40\tau_E$) with $Z_{\text{eff}} \sim 1$.
- Two specific experiments, requested by ITER designers were also performed in JET:
 - The first experiment was to investigate the effect of toroidal field ripple. To this aim the d.c. power supplies to the toroidal coils underwent a major rearrangement and they were re-configured in two independent sets, each supplying 16 of the total of 32 toroidal coils. In this way, it was possible to vary the toroidal magnetic field ripple in the ITER-relevant range of 0.1% to 2% at the plasma edge. The results have shown that the ITER ripple, with 20 TF coils, should be acceptable.
 - The second experiment dealt with the comparison between CFC and beryllium target tiles. Since the primary choice for ITER first wall was beryllium, the CFC divertor tiles were replaced with castellated beryllium tiles, (to reduce thermal stresses). The most significant CFC plasma scenarios were repeated and, in a global sense, similar physics results have been obtained. Since the melting temperature of beryllium is as low as $\sim 1300^\circ\text{C}$, experiments have been conducted causing intentional surface melting of the beryllium tiles, culminating in a controlled beryllium melt experiment. The prelimi-

nary conclusion was that beryllium could still be considered as divertor target plate material for ITER.

Plasma-Machine Interactions

The vacuum vessel consists of eight double wall Octants, each made up of four bellows and five rigid sectors. Each Octant carries a main horizontal port and two (top and bottom) main vertical ports for access. The vessel has two inboard in-vessel and two outer out-vessel reinforcing rings. In-vessel components are welded on the inner wall. The vessel support system allows for thermal expansion with the vessel operating at 250-320°C and contains vessel movements in plasma operation. Plasma displacements and disruptions, can cause impulse vertical and horizontal forces to be applied to the vacuum vessel, in-vessel components and divertor coils, leading to vessel movements and stresses. The plasma displacements induce currents in the structural components and halo currents flowing from the plasma to the structural components. The forces are generated by the interaction of these currents with the magnetic field.

Two types of vessel movements were experienced several years ago and the vessel supports were designed accordingly: rolling and rocking motion, due to the fact that the centroid of the vertical forces applied on each Octant is not in line with the reaction forces at the main vertical port restraints, causing a twisting moment around the toroidal axis; and a net inward motion caused by the toroidal current induced by plasma disappearance and by the poloidal current induced by the change in the diamagnetic flux.

New phenomena were encountered during the 1994/95 divertor campaign: vertical forces on the vessel are not toroidally symmetric, causing overloading and additional shear stresses; and vessel sideways motion, caused by non symmetric horizontal forces applied to the vacuum vessel. While the basic structure of the first wall did cope extremely well with these forces and stresses, some auxiliary in-vessel components were damaged (saddle coils, beryllium evaporator head, glow discharge cleaning electrode, reciprocating probe, earthing straps and tile support rail for ICRH antenna), since when these were first designed, the consequences of these phenomena were not yet fully appreciated.

While appropriate design modification have made the 'weak' components suitable for operations, these phenomena are not fully understood and JET is dedicating a special engineering-physics effort in this area. This in-

volves theoretical work, analysis of data, and implementation of new measurements. It is clear, however, that stresses in the vessel and in other structural components depend now not only on the magnetic field and the plasma current (as assumed by designers in the past) but also on plasma configuration and disruption scenario. Finalisation of ITER design would benefit from progress in this area.

Shutdown Activities and Future Development

The main elements of the Programme for 1996 and beyond are the Mark II divertor studies using configurations as close as possible to reactor requirements and fusion experiments with D(50%)-T(50%) mixtures (DTE1 in 1996-97 and DTE2 in 1999):

- The Mark II divertor is being installed during the present shutdown (June 1995-March 1996). The Mark II divertor will provide a more closed configuration, enhancing neutral particle and impurity retention in the divertor chamber. The support structure consists of a continuous toroidal tray (assembled in radial sectors) on top of which the target plates are installed and can be subsequently replaced by different divertor configurations, such as Mark IIGB, a configuration closer to the requirement of ITER, while maintaining the divertor coils and the toroidal tray in position.
- Following the Preliminary Tritium Experiment in 1991, it was decided to further develop the machine to a more reactor-like configuration by the installation of a pumped divertor, prior to further D-T experiments. Two periods of D-T operation are currently foreseen: a limited period (DTE1) to start towards the end of 1996 and a more extended period (DTE2) in 1999, after completion of divertor studies with the Mark IIGB. As a result of JET's long pulse capability and its control of impurities, a key objective of DTE1 would be the production of $\geq 10\text{MW}$ of fusion power for several seconds, so that α -particle heating could play a role in the plasma power balance. In addition, a crucial objective would be the study of isotopic effects on confinement scaling and H-mode threshold power. Operation in ELMy-H-mode detached radiative divertor plasmas would also provide valuable information for ITER divertor design. It is expected to carry out the planned programme with a total neutron production of 2×10^{20} neutrons. In performing the extended D-T operation, full use will be made of the

JET Active Gas Handling System (AGHS). This gas re-processing plant collects the gases from the torus, neutral beam system, pellet injection and diagnostics, purifies and isotopically separates these gas mixtures and re-injects pure tritium and deuterium into the torus. Therefore, the D-T experiments would also provide useful engineering experience on the technology of tritium handling for a tokamak reactor.

- Although the neutron budget for DTE1 represents a small fraction of the total neutron influence foreseen in the life of JET, 12 to 18 months of cool-down would be required to permit manned in-vessel intervention. Therefore, besides its physics characteristics, the Mark II divertor has an important and novel feature: it has been designed to allow replacement of the divertor target structure by full remote handling techniques. The tile carriers will be handled and positioned by the Mascot IV servomanipulator mounted on the articulated boom transporter, through Octant No.5 port. Navigation and pre-positioning will be carried out automatically using teach-and-repeat techniques. A shorter version of the articulated boom, a Tile Handling Transfer Facility, (THTF) will be used for transfer of the tile carriers between the Torus Hall and the vessel, through Octant No.1 main horizontal port. All remote handling tools have been tested, except the THTF, which is now under manufacture. To validate the actual capability of the remote handling approach, part of the Mark II divertor target plates will be installed by remote handling in early 1996. A mock-up testbed has been prepared, which makes use of the spare machine octant. Shutdown time for replacing Mark II with Mark IIGB divertor is of the utmost importance to limit machine down-time. Therefore, preparation for remote

installation of the Mark II tile carriers have included 1000 hours trial with the Mascot IV Articulated Boom, Viewing Cameras and associated control systems performing a typical tile exchange for 24hrs/day, for five days per week. Moreover, two months of mock-up trials were performed to establish precise techniques to be used and to create the 'teach-and repeat' files. These results had provided a high degree of confidence on the time-scale foreseen for the Mark II to Mark IIGB target plate exchange with an active machine, following DTE1. It will be the first time that such a complex remote handling operation has been performed on an active machine, providing most valuable engineering experience for the finalisation of ITER design.

- D-T global fusion performance (fusion triple product $n_D \tau_E T_i$ and energy gain Q) could benefit substantially by certain engineering enhancements of the machine. The possibility of increasing the toroidal magnetic field from 3.45T to 4.0T for ~10s flat top, and by an increase of ~6MW in the injected neutral beam power are being considered as possible options:
- A preliminary assessment of the electromechanical capability of the JET coils and of the mechanical structure indicate that, for the scenarios considered at 6MA plasma current, forces and stresses are still acceptable (shear stress in the central solenoid P1 electrical insulation $\leq 20\text{MPa}$ and well within the capability of the TF coils and of the mechanical structure). The design for upgrading the current capability of the TF power supplies from 67kA to ~80kA is underway;
- The design to upgrade each one of the 16 NB injectors from 80kV, 60A to 120-140kV, 60A is being performed. 16x40-60kV, 60A power supplies would be needed to supplement the present ones.

Scientific Achievements during 1995

Introduction

For 1995, the operation system of the scientific programme was similar to that employed since 1989. The programme operated for a series of campaign periods, the standard being of eight weeks duration (composed of six weeks tokamak operation and two weeks of maintenance/commissioning). Two Programme Leaders had responsibility for formulating near programme proposals (one campaign ahead) and out-line plans (two periods ahead). This was carried out in collaboration with the Head of Operations Division (A Tanga). These proposals were within the broad outline of the Development Plan and subject to guidelines provided by the Experiments Committee. These proposals were presented to the Experiments Committee for discussion and approval before implementation. The Programme Leaders, Task Forces and the Topic Groups continued as in 1994.

Programme Leaders for 1995 were:

D Stork and M L Watkins.

Three Task Forces implemented the programme, as follows:

H) High Performance

(involving progression to full performance in the pumped divertor configuration with currents up to 6MA, with high energy content and including progression to the highest fusion product, long pulse operation and steady-state conditions, etc.)

(Task Force Leader: P J Lomas)

D) Divertor Assessment

(involving assessment of divertor performance on the vertical and horizontal target plates of the Mark I pumped divertor).

(Task Force Leader: D J Campbell)

T) Tokamak Concept Improvement

(involving studies of those physics areas in which JET can make important contributions to ITER and DEMO, including development of advanced tokamak Scenarios based on stable, long pulse discharges with a high bootstrap component).

(Task Force Leader: C Gormezano)

Task Force Leaders had responsibility for (i) interacting with and advising Programme leaders on programme requirements within that task area; (ii) devising and setting out a detailed programme for allocated time within a campaign period; (iii) driving through that task programme (including acting as a Control Room representative); (iv) analysing data (in conjunction with Topic Leaders, if appropriate); (v) disseminating information in the task area through internal meetings and publications (in conjunction with Topic Leaders, if appropriate).

In addition, Topic Groups were formed, as follows:

<i>Topic Group</i>	<i>Topic Leader</i>
(a) Transport and Fluctuations;	R Giannella
(b) MHD and Beta Limits	P Smeulders
(c) Divertor Physics	G Vlases
(d) Next Step Related Issues	B Tubbing

Topic Group subjects are of longer term interest than the immediate tasks undertaken by the Task Force Groups. The Topic Groups are responsible for analysis of results within many areas across the Task Force spectrum, but they also have responsibility for advising Programme Leaders on programme requirements which are topical and relevant to the Groups areas of activity. In addition, the Groups disseminate information through a number of internal meetings and in external publications.

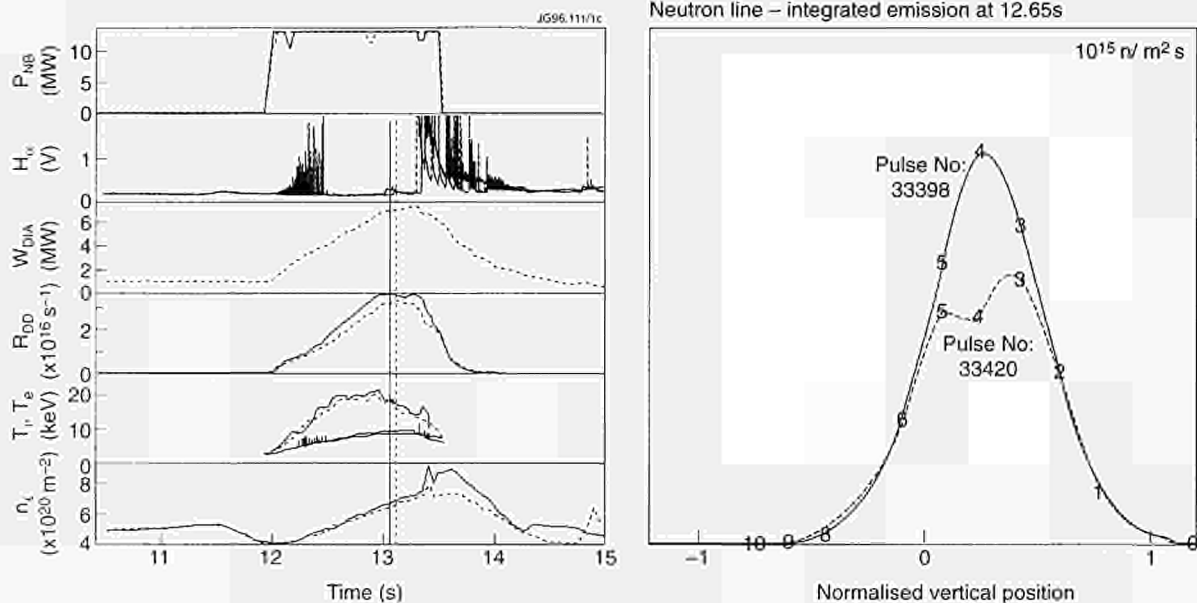


Fig. 121: Comparison of optimally peaked beam deposition (Pulse No. 33398) with pessimistically broad beam deposition (Pulse No. 33420). (a) various time traces for these two pulse indicating small differences only apart from the D-D neutron rate; (b) the neutron emission profile (line integrated) for the two cases

Programme Execution and Analysis

The main objectives of the 1995 campaign period were: to assess divertor performance on the vertical and horizontal targets of the Mark I divertor; to demonstrate the high performance capability of the pumped divertor; and to study those physics areas in which JET could make important contributions to ITER and DEMO.

The main themes of the programme were:

- to assess the performance of the Mark I pumped divertor configuration using both the CFC and beryllium divertor targets;
- to study quasi-steady H-modes at the highest powers;
- to study divertor pumping and exhaust, especially helium exhaust;
- to generate and understand high performance VH-modes up to 4.5MA;
- to develop very high power combined heating at high density in H-mode discharges up to 4.5MA and to move towards high values of the triple fusion product;
- to develop high current (~ 6 MA), low q plasmas, defining the operating space and including the H-mode;
- to develop "advanced tokamak scenarios" based on stable, long pulse discharges with a "high-bootstrap" component to the total plasma current;
- to develop profile control techniques using Lower Hybrid Current Drive (LHCD) and Fast Wave Current Drive (FWCD); and
- to develop 100% non-inductive current drive up to 4MA.

The scientific achievements for 1995 are described in the following sections, within the Task Force, and Topic Group headings.

High Performance Introduction

The major objectives in this area during the 1994/95 experimental campaign were to develop high fusion performance in the hot-ion H-mode and to exploit the high current capability of the pumped divertor at high power. During 1994, high performance had already been achieved, which included fusion performance with $R_{DD} \approx 7 \times 10^{16} s^{-1}$ in the hot-ion regime and up to 15MW of additional heating in 5MA ELMy H-modes in FAT configurations. During 1995, the fusion performance was increased to a new JET record of $R_{DD} \approx 9.4 \times 10^{16} s^{-1}$. The heating of 5MA H-modes was increased to full beam power and a combined heating power of ≈ 26 MW. The design value of 6MA diverted configurations was demonstrated with up to 18MW in ELMy H-mode. In addition, underlying physics experiments were undertaken specifically with reference to ELM-free H-modes.

Anticipated Difficulties with Mark I Pumped Divertor

The major problem addressed, and largely solved, during the 1994/95 campaign was the duration of the ELM-free period. Once a reasonable ELM-free period was established, it was possible to address some of the

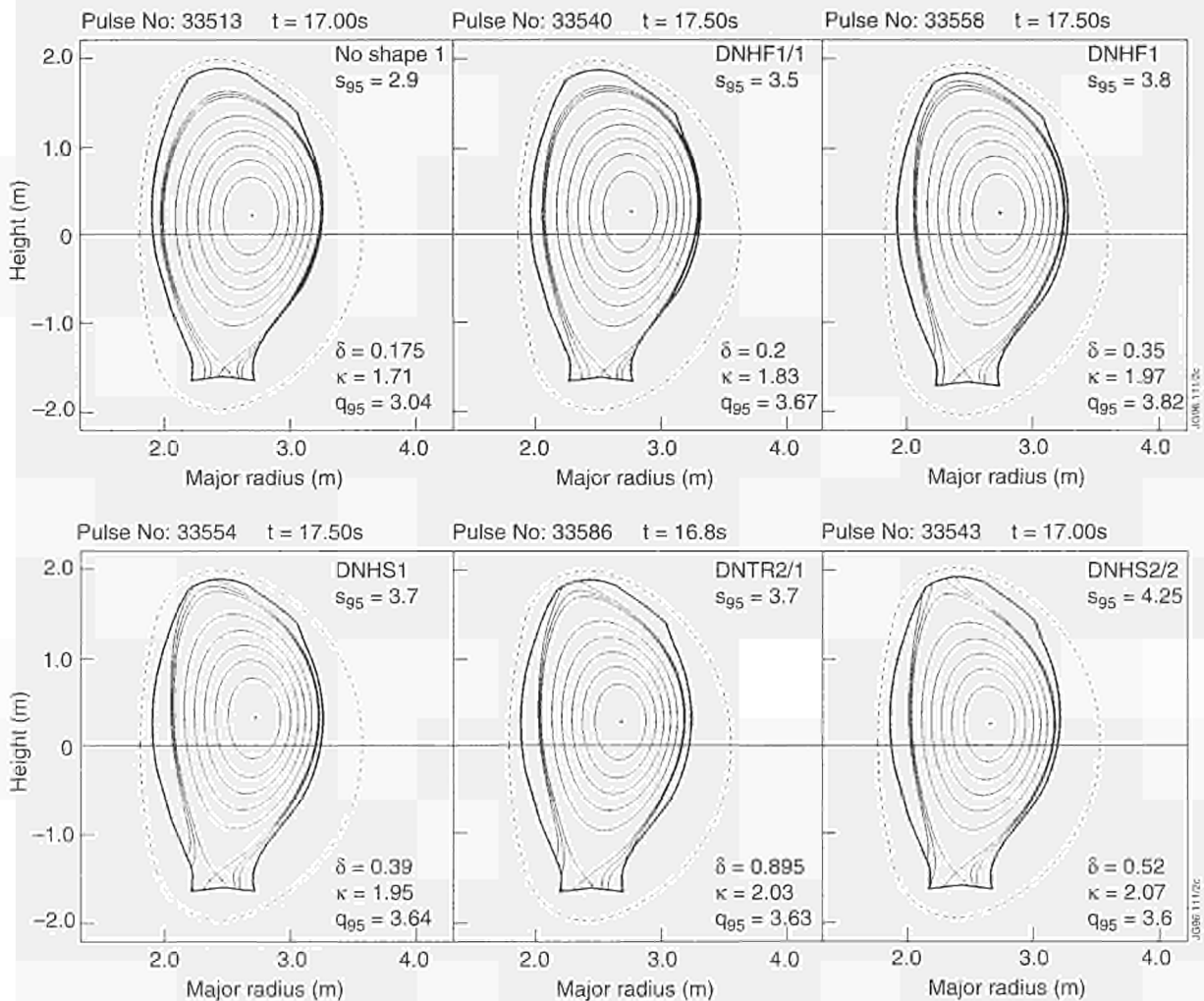


Fig.122: Scan of plasma shapes for 2.5MA/2.5T plasmas with similar high flux expansion of the diverted plasma

anticipated difficulties associated with the Mark I divertor.

The raised plasma axis in the pumped divertor degrades the neutral beam deposition profile. This problem had been foreseen and was ameliorated with adjustments to beam aiming such that it was possible to maintain the deposition within the central one-third minor radius for axis positions 0-20 cm above the mid-plane. However, typical axis positions for high performance plasmas have $Z_0 = 25 - 30\text{cm}$ and thus suffer degraded beam deposition. Figure 121 shows a comparison of optimally chosen beams and pessimistically chosen beam directions for $Z_0 = 25\text{cm}$. Clearly, there was a strong effect on the central fusion reactivity, but a relatively weak effect on global yield. In fact, a scan of plasma axis position shows that best global fusion yield is obtained at high axis positions where effects such as plasma volume and larger edge shear more than compensate for worse deposition. Therefore, it appears that only a small price was paid in sacrificing beam deposition for the flexibility of the pumped divertor.

The PTE series of plasmas had reversed ion ∇B drift direction (i.e. away from target) in order to equalise the power loading on inner and outer strike zones and to raise the H-mode threshold (permitting up to 6MW L-mode prefuelling). In the pumped divertor with uni-directional tiles, reversed ∇B direction required reversed plasma current I_p and, hence, counterinjection. In this case, it was found that recycling was high, and the sawtooth period was short. Long ELM-free periods were achieved but the confinement quality was degraded by 25%. In addition, beam first orbit losses enhanced the carbon source. However, unbalanced power in the divertor channels placed no power handling limit in the Mark I divertor. It is possible, that the high power L-mode phase possible in DTE1 makes more effective use of the limited ELM-free period.

It was feared that the small tiles in the Mark I divertor would degrade power handling. In fact, this problem was clearly solved by good tile design effectively hiding all edges. On the Mark I divertor carbon tiles, the highest surface temperature observed was $\sim 1300^\circ\text{C}$ and typically

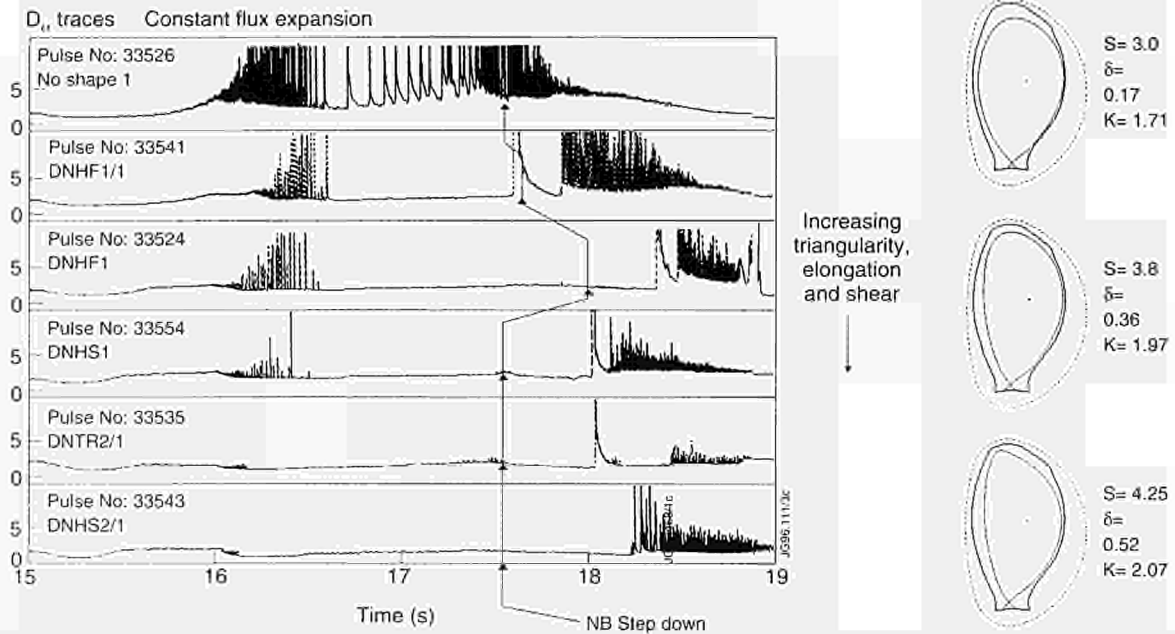


Fig.123: Behaviour of the H-mode in the shear scan at constant flux expansion for 2.5MA/2.5T/10MW. The increase in shear is produced by increasing the elongation (from 1.71-2.07) and triangularity (from 0.17 to 0.52). In the most highly shaped cases, the first ELM occurs after beam step down, when the configuration is programmed to return to low shear

less than 1000°C in the ELM-free regimes, even following MHD events and ELMs. In fact, sweeping proved unnecessary for such regimes, and comparisons of swept and unswept cases conclusively demonstrated no significant enhancement of carbon influxes over this range of surface temperature.

The beryllium tile set showed the expected power handling characteristics and, in this case, sweeping was necessary and effective to maintain the tile temperature comfortably below melting temperature. Unfortunately, energy losses on fast timescales associated with Type I ELMs (~1MJ in less than 1ms) was sufficient to cause local melting of tiles. Therefore, it was not possible to exploit, for performance, the good low recycling properties of the beryllium tile set.

The pumped divertor has allowed good diverted configurations up to the design value of 6MA. Unfortunately, the smaller plasma volume reduces q_{95} . It was expected that this would be deleterious because of a larger sawtooth inversion radius and a degradation in confinement quality. The size of the sawtooth inversion radius does not appear to be important, but as will be shown later, the confinement quality does appear to have been adversely affected.

The Importance of Plasma Configuration

Results from 1994 already suggested that plasma shape and divertor configuration were important. 1995 experi-

ments separated out these two effects and confirmed that both were important factors in influencing the ELM-free period. Part of such a configuration scan is shown in Fig.122. Figure 123 shows that increases in plasma shape increases the ELM-free period. Figure 124 shows that increasing the divertor flux expansion increases the ELM-free period, provided that the core plasma has sufficient shear or triangularity.

These experiments permitted a choice for performance optimisation, between highly shaped plasmas with low current carrying capability and moderately shaped plasmas capable of up to 4MA. In fact, the latter route provided the optimum performance illustrated by the 4MA case shown in Fig.125, which is the record neutron yield pulse. Unfortunately, this configuration is not compatible with the Mark II divertor design, but the configuration shown in Fig.126 (overlaid on the Mark II divertor) produced comparable yield despite being tested only at 3MA.

Influence of Low Recycling

It was already shown in 1994 that low main chamber recycling (as indicated by the vertical chord H_{α} light) is a good performance indicator; if the detailed geometry is taken into account.

Active pumping during the ELM-free phase is usually small ($\leq 10\%$ of the beam fuelling), but can be significant during the pressure burst following a giant ELM. Signifi-

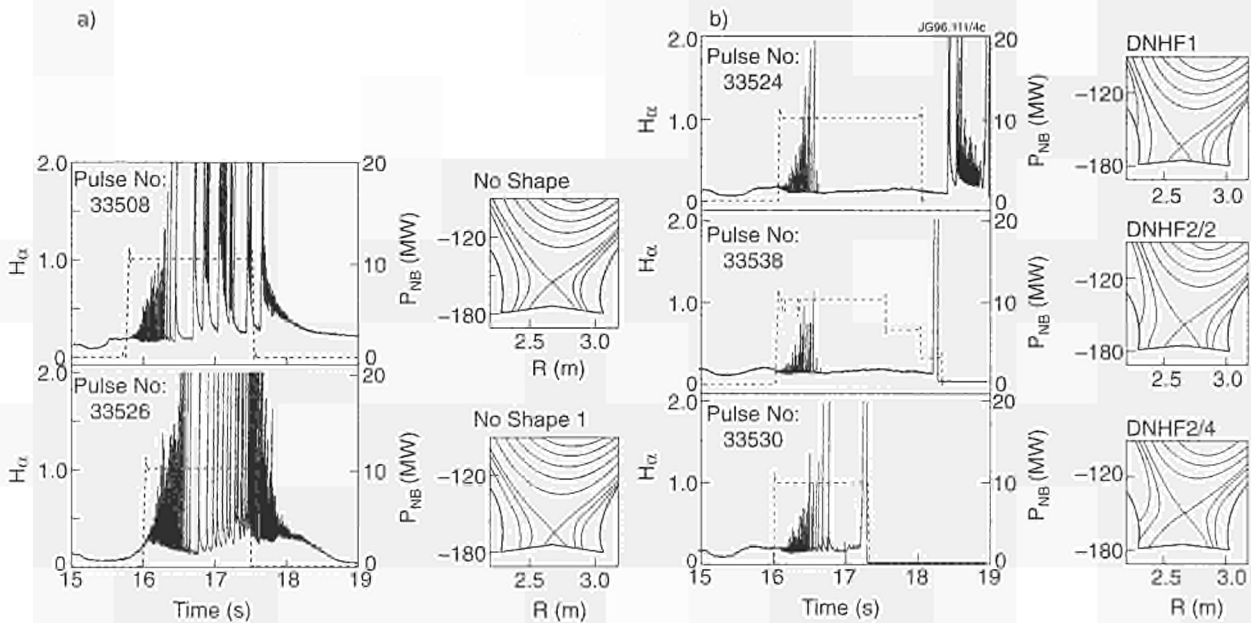


Fig. 124: (a) Behaviour of the H-mode for low shear at low flux expansion (Pulse No. 33508, top) and high flux expansion (Pulse No. 33526, bottom). The insets show the diverted plasma configuration for the two cases with scrape-off flux surfaces 1 and 2 cm from the separatrix at the midplane. Note that both plasmas are ELMy but that the character of the ELM's differs; (b) Behaviour of the H-mode at moderate values of edge shear ($S_{q_1} = 4.0$, $k = 1.9$, $S = 0.33$) as the flux expansion is decreased from a high value (Pulse No. 33524, top) to intermediate value (Pulse No. 33538, middle) to low values (Pulse No. 33530, bottom). Note the disruption following the ELM in the last two cases. Again the inset shows the divertor configuration with the 1 and 2 cm scrape-off layer flux surfaces

cant depletion of the hydrogenic inventory of walls and target can be achieved over a series of repetitively giant ELMy H-modes. This depletion reduces the target density, the excess density rise over the beam fuelling. This improves the ratio of core to edge beam fuelling and leads to a longer ELM-free period.

However, despite conditioning and depletion, there remains a net source of particles during the ELM-free phase over and above beam and any gas fuelling, of ~30% of the total fuelling or a few % of the total target flux, and greater than the pumped flux.

This excess is consistent with the outgassing of neutrals implanted on the metallic inner wall during the preceding inner wall limited phase of the discharge. Figure 127 compares two shots, one fuelled by beams during the inner wall phase and one fuelled by gas during this phase. The deleterious effect of gas fuelling in the inner wall phase is clearly seen. Note that many more particles are required from the gas to maintain the target density. However, beam fuelling during this phase does degrade the target Z_{eff} . Best performance was achieved without beam pre-fuelling, but with the minimum gas input.

The difference in recycling levels between carbon and beryllium suggests that part of the fuelling excess is due to the hydrogenic inventory in the target. Comparison

between this and earlier campaigns suggest that it is better to operate the target tiles at elevated temperatures close to that of the vessel. This will be possible in the Mark II divertor, where the thermal contact between tiles and cooled structures is less intimate.

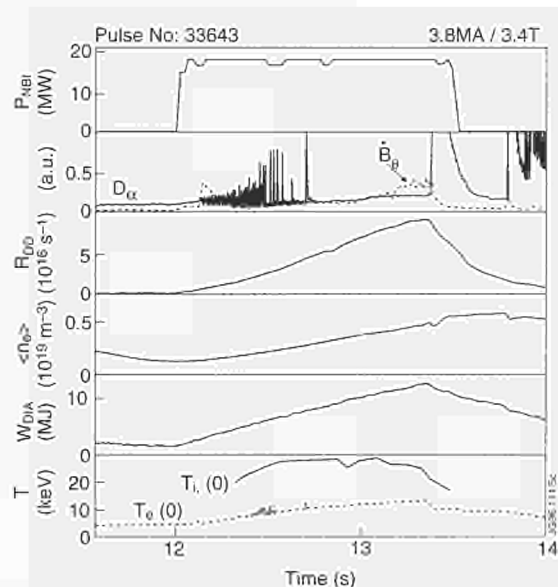


Fig. 125: Various time traces for a pulse with record fusion yield corresponding to a neutron rate of $4.7 \times 10^{16} s^{-1}$. Note the (dB/dt) trace, which indicates the growth of an MHD mode in the plasma core before the limiting giant ELM

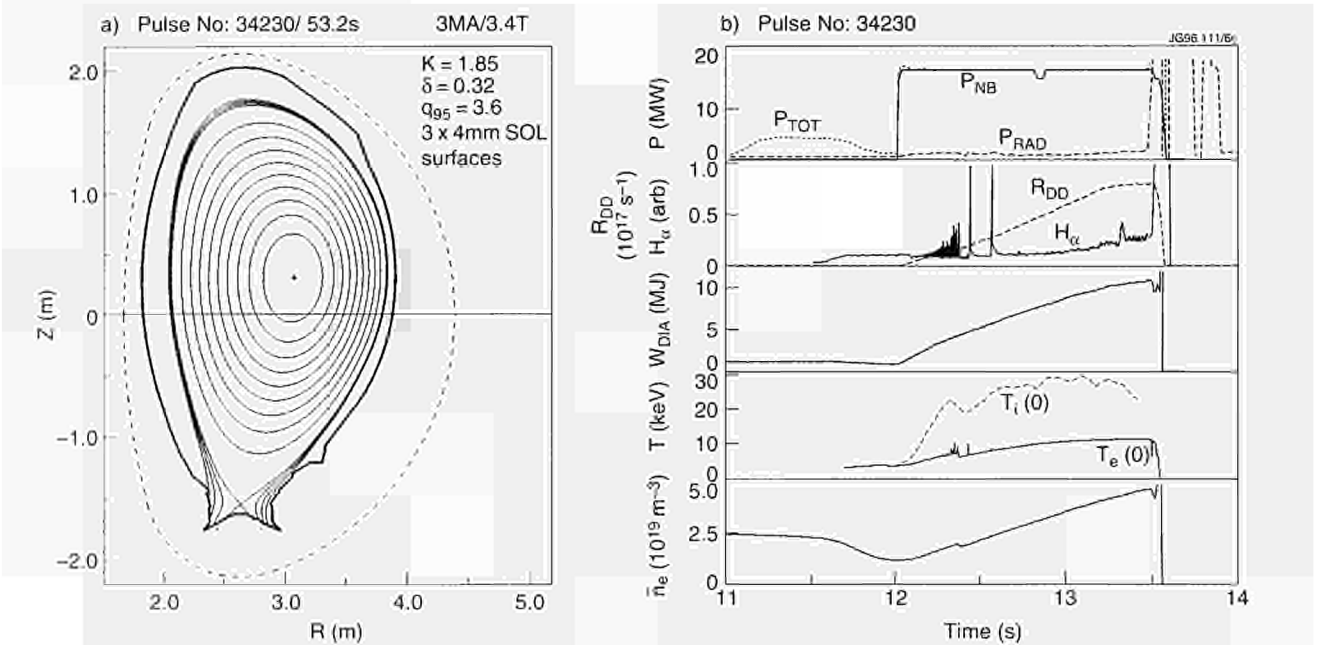


Fig. 126: Demonstration of performance in a Mark II compatible plasma configuration. The equilibrium is shown superimposed on Mark II. The scrape-off layer flux surfaces correspond to 4mm at the mid-plane (i.e. the divertor configuration will be closed at the 12mm surface). The time traces show that this pulse exhibits similar ELM-free hot-ion behaviour to that of the previous figure despite the lower plasma current

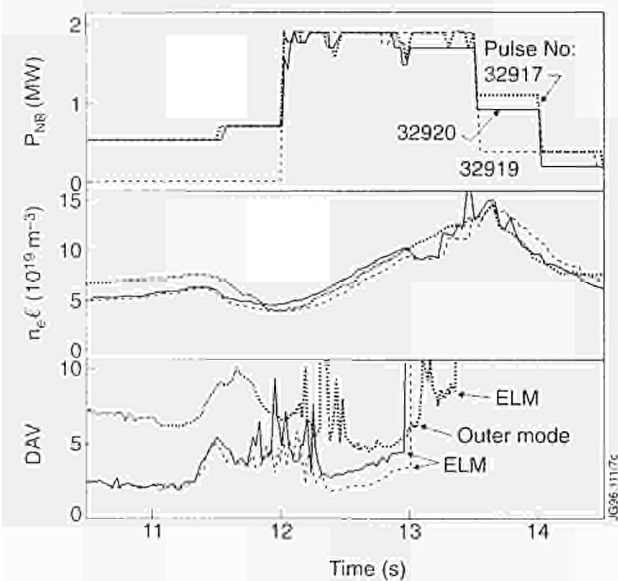


Fig. 127: Comparison of recycling behaviour of three pulses. Pulse No. 32910 (solid trace), is a reference discharge before a target depletion series of repetitive ELMy H-modes; Pulse No. 32917 (long dashed traces) is the reference after. Both pulses have beam prefuelling during the inner wall phase up to 11.5s. In Pulse No. 32919 (short dashed traces), beam prefuelling is replaced by gas. Note the reduced rate of rise in density on Pulse No. 32917, lower recycling and longer ELM-free period. On Pulse No. 32919, the recycling level is much higher during the inner wall phase due to the gas fuelling, but the recycling remains high after the gas is turned off (11.5s) even during the subsequent ELM-free H-mode. This suggests that neutrals implanted in the inner wall contribute a significant particle source to the H-mode and causes a faster rise in plasma density

MHD Limits

High performance discharges can be limited by giant ELMs, Central Modes or Outer Modes located at $0.8 \leq \rho \leq 1$. These modes are discussed in more detail in the section on MHD and Beta Limits. In Fig 128, there is shown a clear degradation in confinement quality at the onset of such modes and as such they pose the most stringent limits on performance.

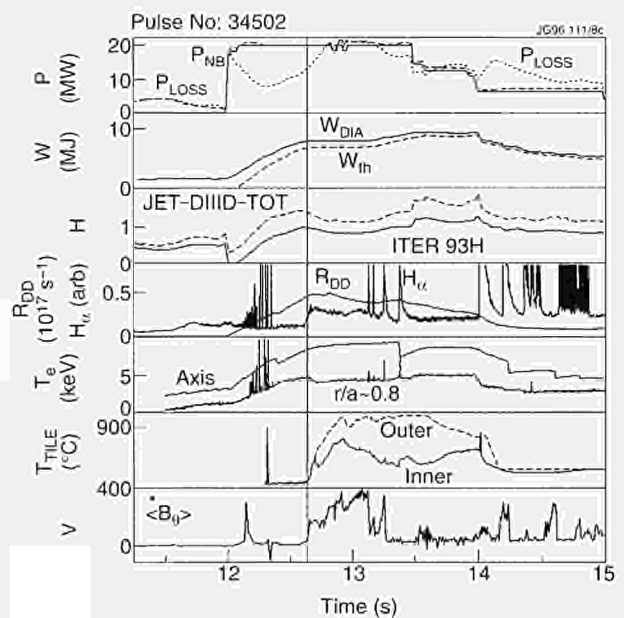


Fig. 128: Typical time traces for a "slow rollover" in performance initiated by an outer mode marked by the vertical bar. Note the reduction in confinement quality, reduction in edge temperature, increase in loss power, increase in target temperature and increase in recycling light

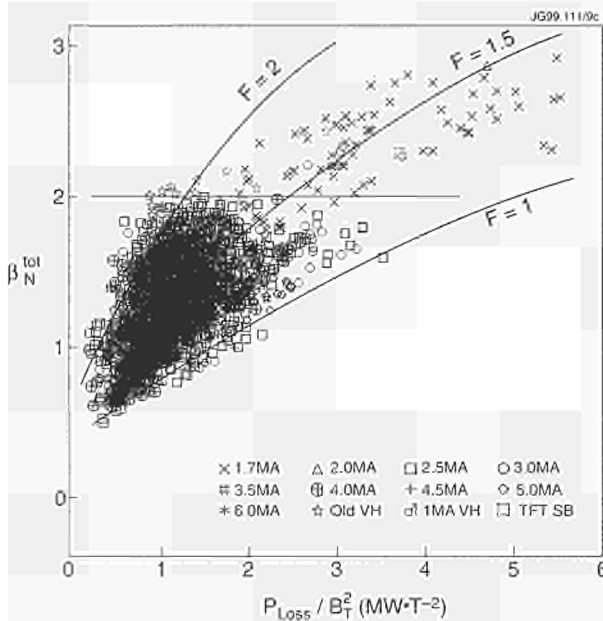


Fig. 129: Normalised total $\beta_N^{tot}(\beta_T^{tot}/(I/aB))$ versus normalised loss power $P_{Loss}/B_T^2(MW/T^2)$. The curve marked $F=1$ corresponds to the prediction of JET-DIII-D scaling, and the curves $F=1.5$ and 2.0 correspond to enhanced confinement quality compared to the scaling prediction. Note the low current (low field) data reaches $\beta_N \sim 3$, whereas high current (high field data) P_{Loss}/B_T^2 is too small to exceed $\beta_N \sim 2$ despite improved confinement quality

Most high performance discharges have $\beta_N \leq 2$, but by operating at lower current and field it is possible to reach $\beta_N \sim 3$. This result is not surprising, as shown by Fig. 129, where β_N^{tot} is plotted against normalised loss power. The curve labelled $F = 1$ corresponds to the predictions of the JET-DIII-D global scaling law. Much of the data lies between $F = 1$ and $F = 2$ suggesting enhanced confinement (relative to this scaling at least). Whereas it takes about 16MW to approach $\beta_N \sim 3$ at 1.7MA/1.7T, more than 60MW would be required at high current and field. The MHD events associated with performance limitations is not associated with the approach to the Troyon limit, but rather the approach to local limits.

Confinement Enhancement

The ratio of experimental confinement time to the predictions of the various confinement scalings is often used as a measure of confinement quality. There are differences though between the predictions of the various scalings. Figures 130 and 131 show thermal confinement enhancements relative to JET-DIII-D scaling, $H_{th}^{JET-DIII-D}$, and relative to ITER-93H ELM-free scaling, $H_{th}^{ITER-93H}$, plotted against q_{95} . Although both forms show a trend with q_{95} , Fig. 131 separates out old and new high performance data, and the reason for this is not clear. Local transport analysis and model simulations show no difference in

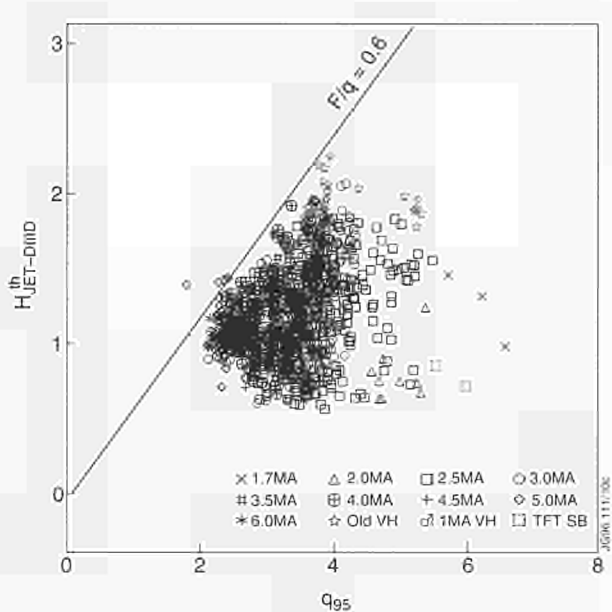


Fig. 130: Thermal confinement time normalised to the predictions of the JET-DIII-D scaling, $H_{th}^{JET-DIII-D}$ plotted against q_{95} . The symbols indicate the plasma current. The 1991 campaign, which has been previously labelled "VH-mode" is marked "OLD VH" for 3-4MA data and "1MA VH" for 1MA. Note that the 1994/5 data includes both ELMy and ELM-free data points

core transport coefficients between these cases with different confinement enhancement, but that the transport barrier physics can account for most differences.

Note that, whilst the best data from the 1991 campaign has been previously described as VH-mode, since $H_{93H}^{th} \geq 1$, recent analysis suggest that the interpretation of edge second

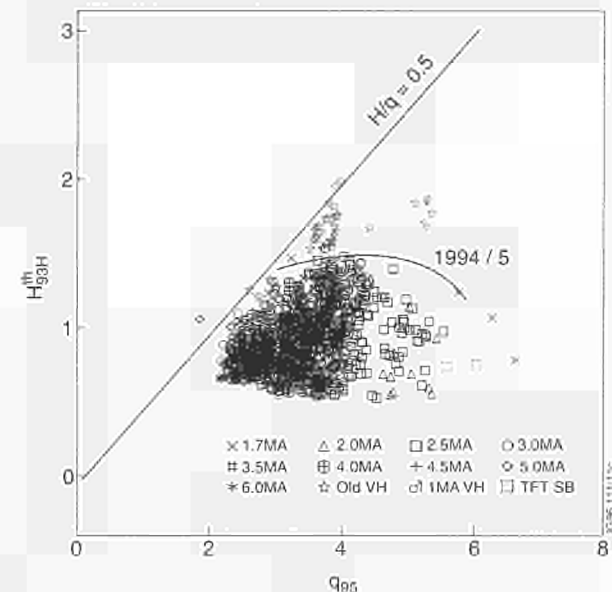


Fig. 131: Thermal confinement time normalised to the predictions of the ITER ELM-free scaling, ITER93H. Symbols are the same as previous figure. Note that whilst there appears an upper limit set by $H/q \sim 0.5$, the 1994/5 data does not demonstrate such high values of H around q_{95} , as the best data from the 1991 campaign

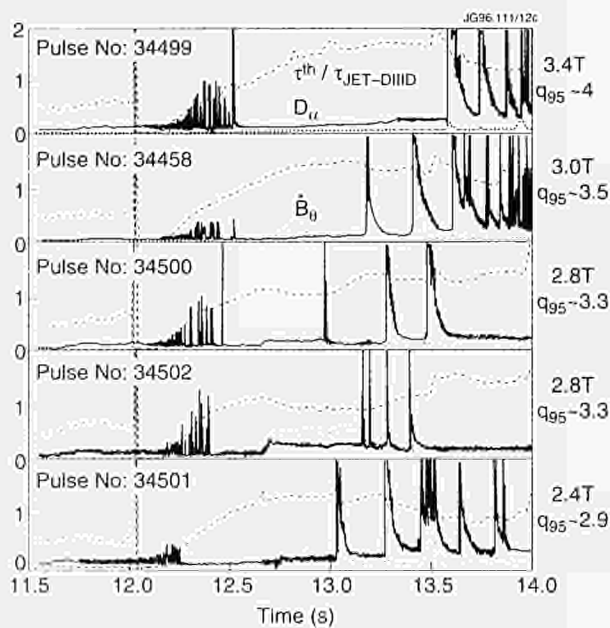


Fig. 132: Data from a q scan of constant power and configuration but varying toroidal field, showing D_{α} , normalised confinement and (dB_{α}/dt) are shown. The outer mode is most clearly visible just above $q_{95} \sim 3$. The cases at $q_{95} \sim 3.5$ and 4 do not show the outer mode, and the MHD in both cases is associated with the core plasma. In general, the MHD including the giant ELM is delayed at the higher q values. This delay allows the confinement quality to increase stability is open to question. The ideal kink limit allows no second stable access. It is tempting to speculate that the dependence upon q_{95} reflects the duration of the MHD quiescent phase. This is supported by the q_{95} scan shown in Fig 132.

Quasi-Stationary Hot-Ion Modes

It is possible to avoid the MHD limitations by stepping down the neutral beam power. As shown in Fig 133, approximately stationary conditions can be maintained for $\sim 0.7s$. Although the density rise slows when the particle fuelling is reduced, the density is not stationary and the plasma is eventually ELM limited. Very high values of Q_{DT}^{omni} can be maintained in this way.

Initial experiments have been performed replacing part of the neutral beam injection with ICRF power, as shown in Fig. 134. Here $T_e \sim T_i \sim 15keV$ (a world record T_e) was maintained with the density no longer rising. Notice how the H-mode, in this case, is not terminated by an ELM.

High Plasma Current Regimes

H-mode experiments have been performed at 5MA with full beam power and up to 28MW of combined heating power, and preliminary investigations made of 6MA H-modes.

The ability to produce highly shaped plasma declines as the plasma current is increased, partly due to coil

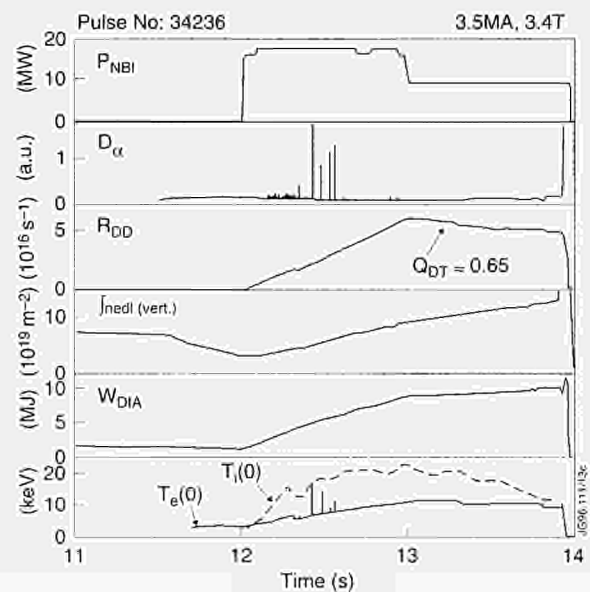


Fig. 133: Time traces for a pulse where the neutral beam is stepped down to about the loss power, permitting quasi-steady conditions to be demonstrated. Although both R_{DD} and stored energy are roughly stationary, the density rises at a reduced rate until terminated by a giant ELM, $\sim 0.7s$ after step down

current limitations and partly due to limits on out of plane forces on the toroidal field coils. However, long ELM-free H-modes can be achieved using power step down as shown in Fig. 135. However, at higher power, the H-modes

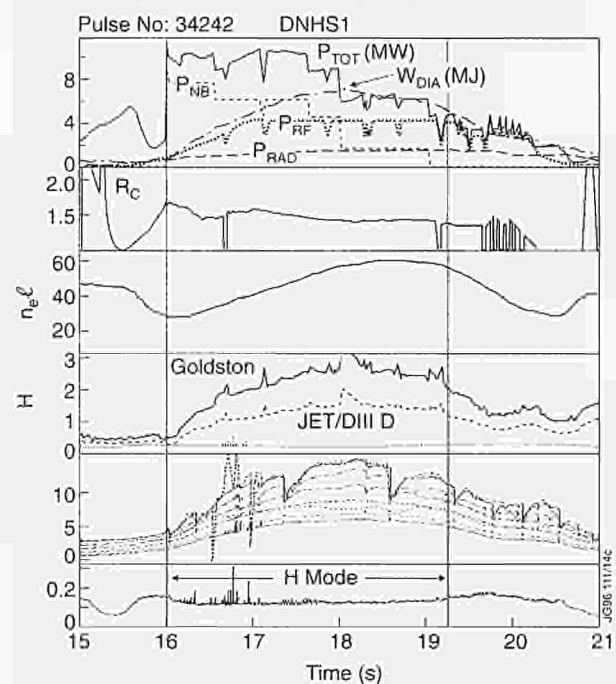


Fig134: Time traces for a pulse where the neutral beam power is stepped down to only 2MW and the discharge sustained predominantly by RF power. Here, more steady conditions are maintained for $\sim 1s$, at high confinement quality and $T_e \sim T_i \sim 15keV$. Note that the H-mode is not terminated by a giant ELM but by a return to low confinement quality as the power input is reduced further

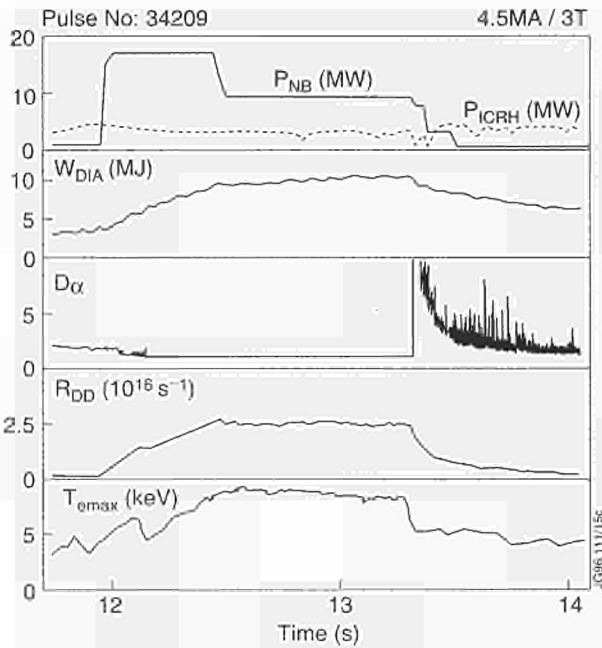


Fig.135: Moderate density ELM-free H-mode sustained quasi-steady state with 10MW of beams and 3MW of RF power at 4.5MA

exhibit repetitive giant ELMs as shown in Fig.136. Combined heating experiments typically employed gas puffing to enhance ICRF coupling and this changed the H-mode character as shown in Fig.137. Often, with ICRF in these low q_{95} H-mode situations, fishbones were observed, as illustrated in the inset. As mentioned earlier, giant ELMs terminating the ELM-free phase at high power led to local

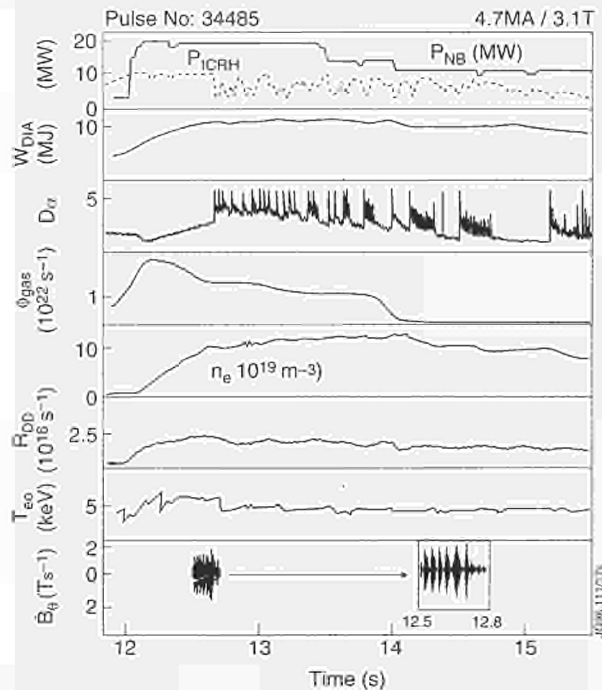


Fig.137: High current ELMy H-mode at 4.7MA with 28MW of combined heating. Note the change in ELM behaviour associated with gas puffing

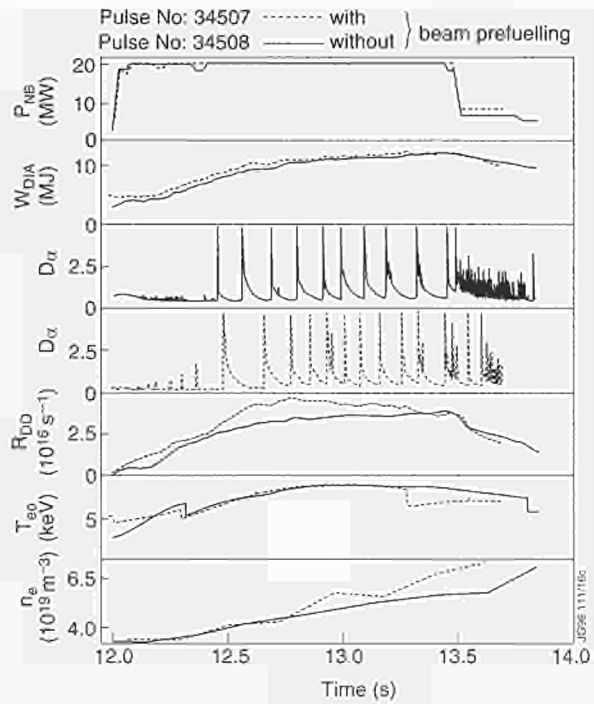


Fig.136: Typical ELMy H-modes obtained with full beam power at 5MA

melting of the beryllium target. Apart from this high current, discharges on carbon and beryllium were broadly similar.

The configuration for the first 6MA H-mode is shown in Fig.138, and the H-mode character shown in Fig.139. These plasmas were somewhat more elongated than their 5MA counterparts and this resulted in smaller separations between plasma and the top and bottom of the limiter. This might account for the irregular ELM behaviour.

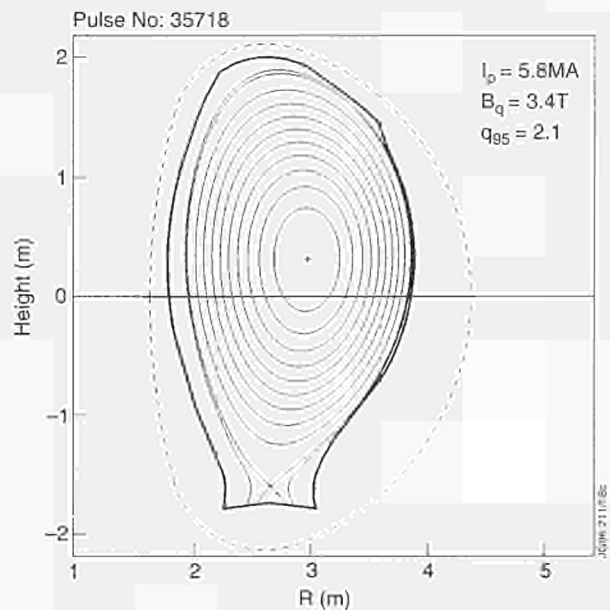


Fig.138: Plasma configuration for the 6MA H-mode. Note that, in this example, the plasma current was reduced by 200kA because of the low value of q_{95}

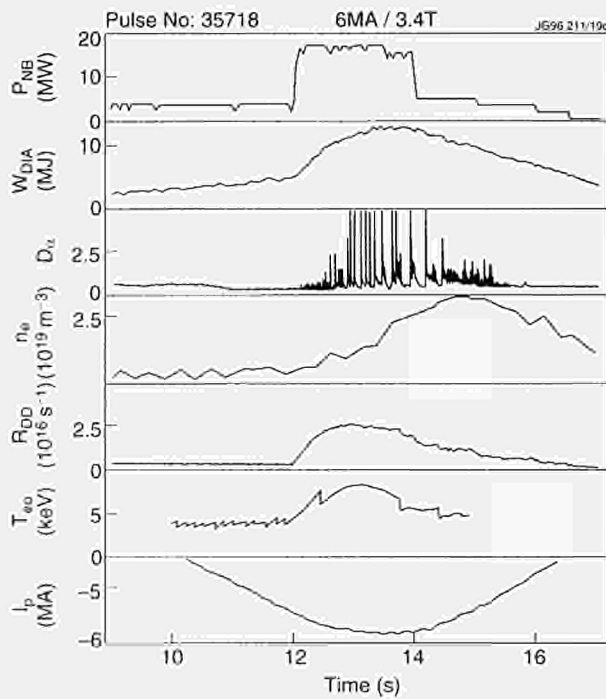


Fig.139: Time traces for the previous pulse. Note the high value of diamagnetic stored energy ($\geq 13\text{MJ}$) and the irregular ELM behaviour

The stored energy is shown for ELM-free phases in Fig.140 and ELMy phases in Fig.141, for these high current H-modes together with low q_{05} analogues at reduced current and field. The curves show the predictions of the global scalings for 3 and 5MA. The con-

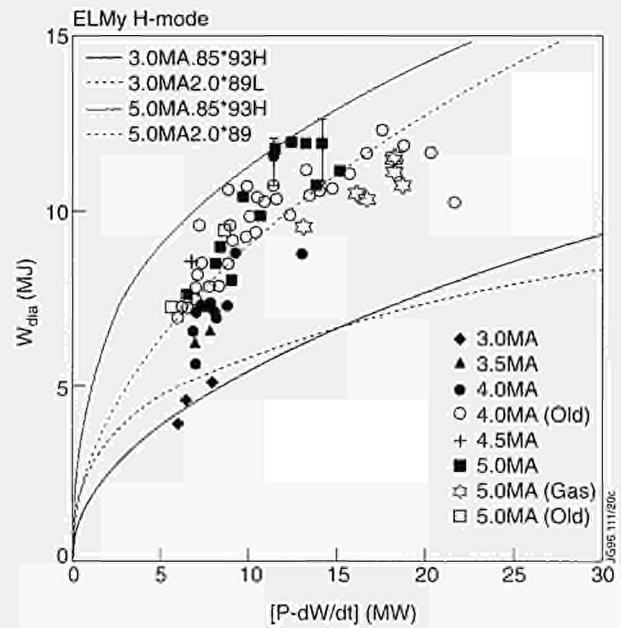


Fig.140: Diamagnetic stored energy versus loss power for 5MA ELM-free H-modes and analogues at reduced current and field. H-modes at high current obtained in the "OLD" JET are marked by open symbols. Cases with strong gas puffing are also marked. The solid curves show the predictions of the ITER93H scaling for 3 and 5MA, and the dashed curves show the predictions of twice the L-mode scaling, ITER89P. Note that the data with gas puffing suggests some departure from the scaling predictions

finement appears consistent with expectation of I_p dependence and there is little if any degradation associated with the low values of q_{05} (< 2.7).

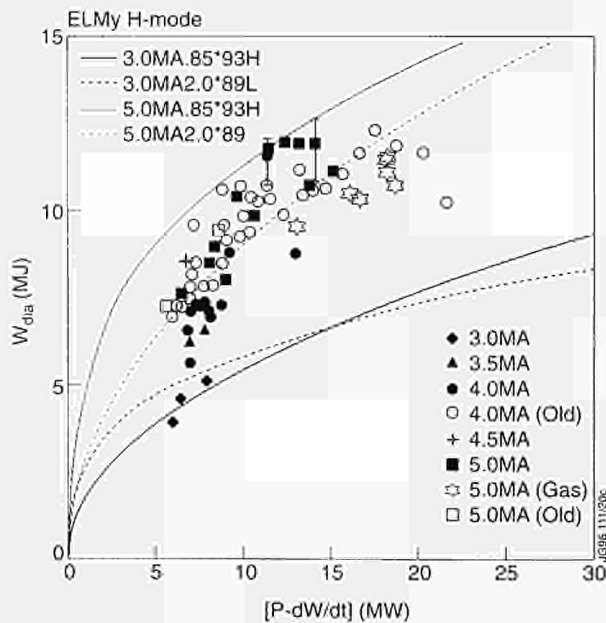


Fig.141: Diamagnetic stored energy versus loss power for 5 and 6MA and analogues at reduced current and field. Old 4 and 5MA data is marked by open symbols and new data with strong gas puffing is marked by open stars. The solid curves show $0.85x$ ITER93H (the usual ELMy prescription) and dashed curves shows twice L-mode scaling ITER89P, for 3 and 6MA

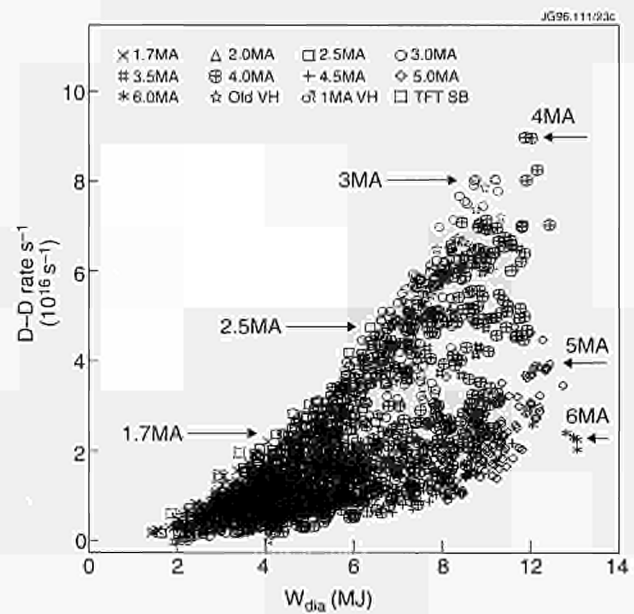


Fig.142: D-D reaction rate, R_{DD} versus diamagnetic stored energy. The symbols indicate the plasma current and the arrows mark the best performance cases at each plasma current. Note the data separates into two bands according to whether the plasmas are ELM-free or ELMy, the former having the higher performance

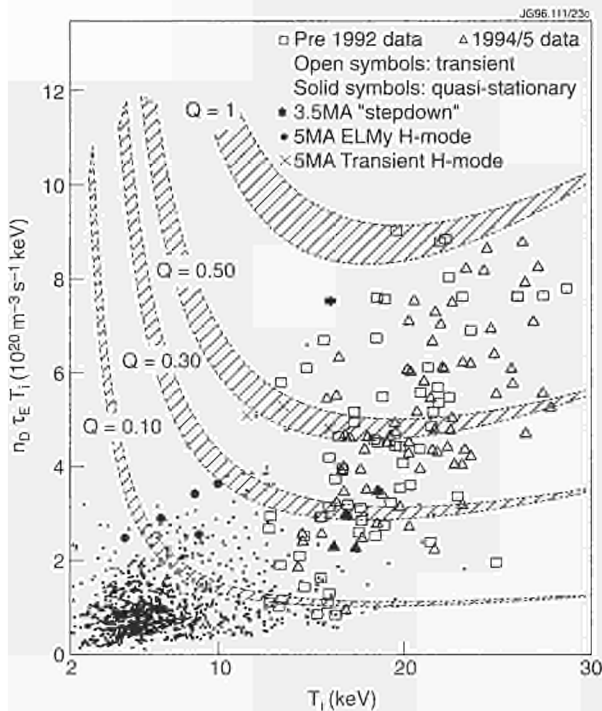


Fig. 143: The fusion triple product, $n_D T_i \tau_E$ versus T_i diagram comparing new and old data, ELMy and ELM free regimes

Conclusions

The fusion performance scales with the square of the stored energy, as shown in Fig. 142. As the plasma current is increased in the ELM-free regime, both stored energy and D-D rate improve strongly up to around 3MA. From 3 to 4MA, only a small gain in stored energy and fusion yield is obtained. ELMy H-modes show fusion performance typically a factor 2-3 lower (but in steady-state) and the highest performance is achieved at 5MA.

TRANSP code simulations suggest that the expected D-T fusion power scales as 210 times the D-D power. On this basis, the performance already demonstrated in the Mark I divertor would correspond to ~11MW of fusion power including ~2MW of alpha-particle power with a 50:50 D-T mixture with input power ~18MW and loss power around 12MW. The fusion triple product, $n_D T_i \tau_E$ versus T_i diagram in Fig. 143 shows values comparable to the previous best, of up to $10 \times 10^{20} \text{m}^{-3} \text{s keV}$.

Divertor Assessment and Divertor Physics

The Pumped Divertor has equipped JET to address the central problems of the ITER divertor: efficient dissipation of heat exhaust with minimal erosion; control of particle fluxes, including helium; and effective impurity

screening. The divertor assessment programme has concentrated on exploiting the new facilities of the Mark I configuration to address these issues. A variety of divertor configurations has been explored, and a detailed comparison made of divertor performance using the horizontal and vertical targets. The excellent power handling capability of the target has been essential to these studies and has fully justified the care taken in its design. Use of the cryopump has proved to have several advantages, related both to vessel conditioning and plasma performance. The relative merits of CFC and beryllium as power handling surfaces have been compared and have confirmed the choice of CFC as the preferred divertor target material for the forward programme.

Since dissipation of exhaust power is seen as a central problem in design of a divertor for ITER, the overall aim of the programme has been to develop plasma operating scenarios in which a large fraction of the loss power from the plasma is dissipated as radiation and charge exchange losses, while maintaining high plasma purity and good confinement. Considerable progress has been made, and regimes in which ~80% of the loss power is radiated have been established routinely. Confinement in such plasmas is marginal, though probably acceptable, for ITER, but scenarios which involve puffing of extrinsic impurities to enhance the radiation level are seriously compromised by the high impurity levels observed in the bulk plasma. The high level of impurity contamination may result in part from the relatively open design of the Mark I configuration, combined with bypass leakages through the surrounding structure, and emphasizes the importance of studies with improved closure in the Mark IIA and Mark IIGB divertors.

Divertor Assessment Programme

The programme of divertor studies can be subdivided into several broad areas:

- Power flow to the divertor: including target power handling, divertor asymmetries associated with the ion ∇B drift, the effect of ELMs, and surface erosion and redeposition;
- Fuelling and pumping effects; role of fuelling location and of pumping in impurity retention and particle control;
- Helium transport and exhaust: in L-mode and H-mode regimes;
- Influence of divertor configuration on performance: comparison of divertor performance using horizontal

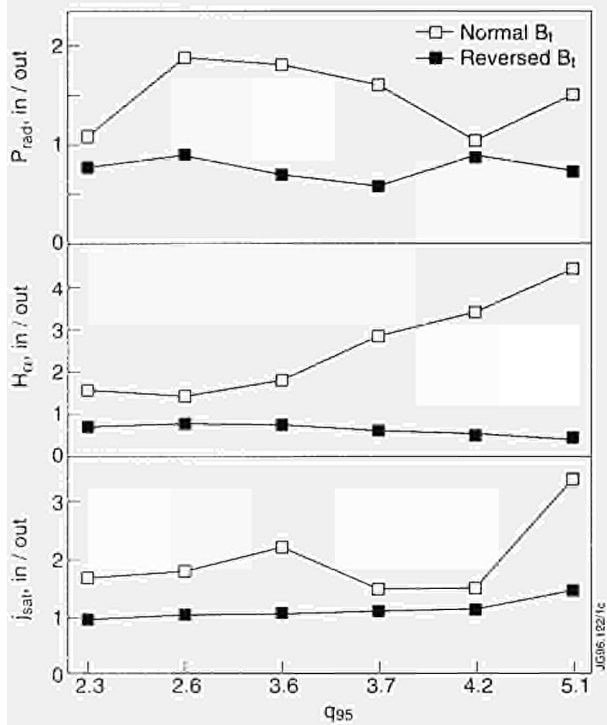


Fig.144: Degree of asymmetry in plasma parameters in the divertor as a function of q_{95} for the normal (ie. ion ∇B drift towards the target) and reversed directions of the toroidal field

- and vertical targets, as well as influence of X-point height and connection length;
- Physics of divertor detachment: variation of SOL and divertor parameters as detachment is approached, scaling of SOL parameters with plasma conditions and divertor configuration, and physics of the density limit;
- Characterization of ELMy H-modes: encompassing confinement, accessible density range and H-mode power threshold;
- Radiative divertor plasmas: to establish and study high confinement plasmas with high radiated power fractions;
- Comparison of CFC and beryllium divertor targets: including power handling capability and impact on divertor and bulk plasmas.

In addition to the specific experimental studies in these areas, the detailed comparison of experimental measurements with simulation codes has been regarded as an essential aspect of the divertor assessment programme from the outset of the campaign. Not only do such comparisons shed insight into the processes influencing the observed behaviour, but the experimental results act as an important benchmark of the codes and validate the extrapolations required in predicting the future performance of JET and ITER divertors. JET has devoted considerable manpower to code development and now has a set

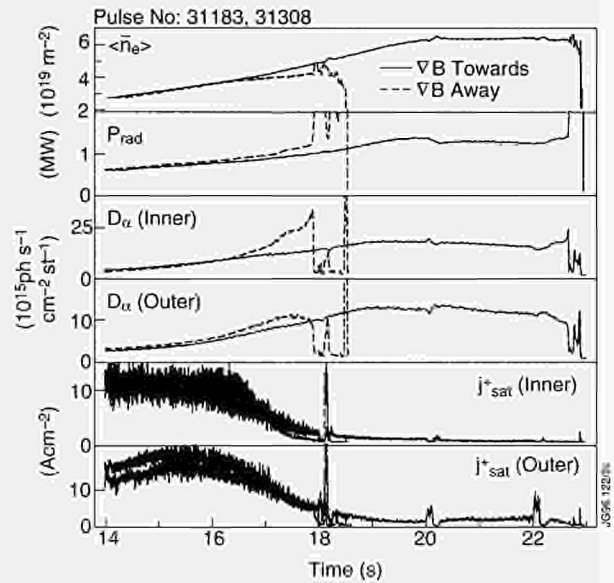


Fig.145: Comparison of ohmic density ramp discharges leading to detachment in normal and reversed toroidal field directions. The rollover in ion saturation current occurs at similar densities in the two cases, but the reversed field plasma (ion ∇B drift away from the X-point) disrupts at a lower density. Note that the D_α gas fuelling rates are the same for the two plasmas

of robust 2D codes which are used routinely for experimental interpretation and predictive modelling.

Power Flow to the Divertor

The excellent power handling capability of the divertor target has been a major achievement of the Mark I design. The attention given to the shadowing of edges and to precise installation of the target has resulted in the complete elimination of carbon blooms. Detailed analysis of power deposition measurements has shown that the observed temperature rise of the target is within 20% of that expected [1]. Sweeping has proven to be a highly effective technique for broadening the power deposition zone and, although perhaps not relevant for a reactor, has played an important role in the programme. Regular ELMs also effectively broaden the power deposition region, possibly by broadening the SOL width, but also by displacing the strike points (as a result of perturbations to the plasma equilibrium). While this has been beneficial in the JET, it does raise potential difficulties in a reactor, where significant energies might be deposited on areas of the first wall not designed for high power fluxes. This emphasizes the requirement for means of dissipating the effect of giant ELMs (or avoiding them entirely).

Total energies of up to 100MJ have been deposited on the horizontal CFC target, while temperatures have rarely

exceeded 1200°C. Indeed the highest temperatures have been reached in lower energy plasmas, where high power heating has been applied in ELM-free H-modes. Power densities of greater than 10MWm⁻² have been achieved routinely at the separatrix. Experiments on the CFC side-plates have reached 50MJ conducted to the target, with no indication of significant temperature rises. The resilience of the target and the good agreement between the calculated and measured power handling capability gives confidence that the design approach for the Mark II divertors will achieve satisfactory power handling, and that this should not limit JET in the future. This cannot, of course, disguise the fact that these inertially cooled target plates do not represent a solution to the challenge of dissipating reactor-relevant exhaust power fluxes in steady-state.

Previous experiments have shown that power is distributed more symmetrically between the inner and outer strike points when the ion ∇B drift is away from the X-point. This prompted the suggestion that this mode of operation would both mitigate the power handling problem and be more likely to achieve stable divertor detachment than plasmas where the ion ∇B drift is towards the X-point. Specific experiments were, therefore, designed to investigate the behaviour of divertor asymmetries [2]. Systematic studies were confined to ohmic and L-mode plasmas due to the difficulties of diagnosing the divertor parameters in the presence of ELMs. As in earlier experiments, significant asymmetries in plasma density, temperature, radiation and recycling light were observed with the ion ∇B drift towards the X-point. Radiation and recycling light came predominantly from the inner divertor leg, with a denser and cooler plasma near the target. The reversal of the toroidal field produced more balanced parameters at the inner and outer targets (Fig. 144). Power flux asymmetries measured by the IR camera were also reduced by reversing the toroidal field.

Considerable, and unexpected, differences were observed in the behaviour at detachment [3]. In ohmic experiments (Fig. 145), it was found that the ion saturation current 'rollover' which is characteristic of the approach to detachment, occurred at the same density in the two cases. However, plasmas with the ion ∇B drift away from the X-point then disrupted rather quickly, and did not achieve the same densities as plasmas with the opposite toroidal field direction. Nor did plasmas in the former case establish steady-state detached phases. These results contradict the original proposition that operation with the

ion ∇B drift away from the X-point should be preferable in the detached divertor regime. In fact, the results suggest that, in ITER, operation with the more conventional toroidal field direction is preferable both from the point of view of divertor detachment and H-mode access, and does not confer a significant penalty in power handling.

Erosion and Redeposition at the Divertor Target Surface

Erosion and redeposition at plasma facing components is an urgent issue to be faced in the design of ITER. For most materials, the dominant erosion process is physical sputtering, whilst for graphite, chemical sputtering should become dominant at low incident ion energies. However, it is unclear what the consequences of this are for erosion since chemical sputtering not only exhibits an uncertain flux dependence, but also there is the possibility of prompt local redeposition of molecular ion fragments.

During the Mark I campaign, erosion profiles of the divertor target were directly measured using the technique of colorimetry [4]. It has been observed that the rate of erosion is strongly dependent on the motion of the strike point position and power deposition on the targets. For example, in a discharge with 10MW of heating and moderate density, an erosion rate of about 5nm s⁻¹ was observed near the strike point. Sweeping of the strike zones greatly reduced the erosion except at the turning points of the sweep, as would be predicted.

The Monte-Carlo impurity transport code DIVIMP has simulated the colorimetric results, together with divertor carbon profiles measured by spectroscopy [5]. In the high density attached plasma regime, the erosion at the strike points was dominated by physical sputtering and showed no obvious effect of chemical sputtering. This suppression of chemical sputtering in high flux areas has also been observed in other experiments [6] and is thought to be due in part to the prompt local redeposition of molecular fragments. However, in the private flux region, where sputtering is due to low energy neutrals with a relatively low flux density, it was evident from the spectroscopic data that chemical sputtering dominates. In hot ion H-modes, the ion temperature at the target must be assumed to be 6-8 times higher than the local electron temperature to reproduce the measured erosion rate and the global power balance.

Addition information on erosion/redeposition has come from the fixed target Langmuir probe tips that were

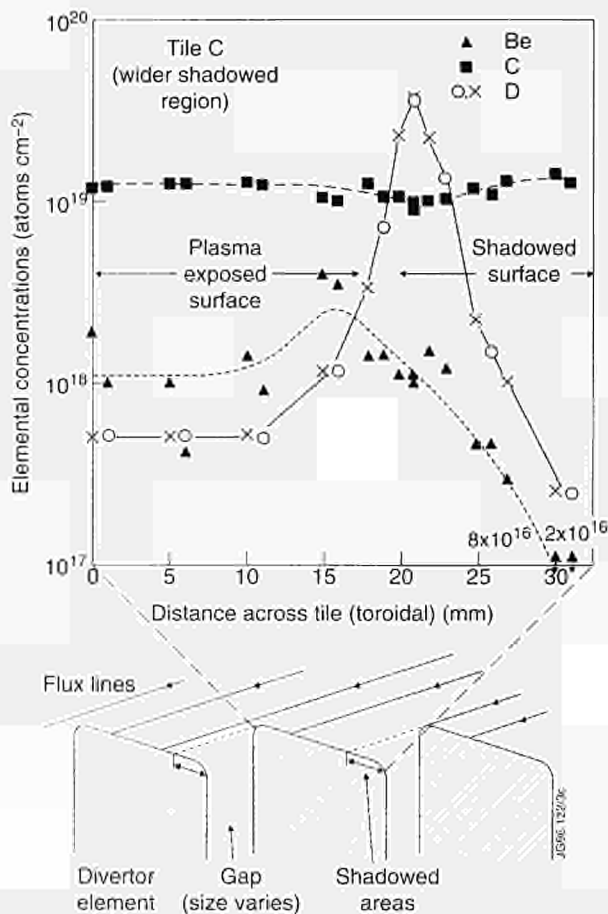


Fig. 146: D, Be and C surface concentrations across a graphite divertor tile from the outer scrape-off region used during 1994. A schematic toroidal cross-section of the divertor tiles is included.

removed after the Mark I CFC campaign. These tips were made of pyrolytic graphite and changes in surface profile were measured photographically. Tips from the high fluence region of the target showed erosion of ~ 0.1 mm after exposure to a deuteron fluence of $1\text{--}2 \times 10^{27} \text{m}^{-2}$, indicating a yield of $\sim 1\%$, which is consistent with purely physical sputtering yields if redeposition is ignored.

It was not possible to measure the erosion rate in the radiative/detached divertor regime, but enhancements to the technique using pre-coated divertor tiles and local CD_3 injection to produce suitable carbon films are expected to make this possible in Mark II divertor.

Divertor Tile Analysis for Gas Retention and Impurity Transport

Analysis of the divertor surfaces after each operation phase provides insights into gas retention and impurity transport processes. Gas retention occurs to a limited extent at any plasma-facing component (PFC) by ion implantation, but the largest concentrations accrue in the areas of greatest redeposition due to co-deposition of the

fuelling gas (normally deuterium) with impurities such as carbon and beryllium, provided these areas do not reach temperatures above about 400°C . In the divertor mode, the plasma separatrix intersects the divertor target tiles at the inner and outer strike points, and all other PFCs are in the scrape-off layer (SOL) at some distance from the separatrix. With the exception of the divertor targets, the closest components are normally the leading edges of the lower section of the outer bumper limiters and the top of the inner wall protection rails. Almost all experiments during the 1994/5 campaign were carried out in the divertor configuration. Thus, it may be expected that the major erosion areas (and hence impurity source) would be at the strike points on the divertor tiles, and redeposition would occur at regions deeper into the SOL. However, although the erosion rates at the outer strike zone, of up to $\sim 20 \text{nm s}^{-1}$ [4], were the greatest at any point in the vessel, plasma impurities were probably dominated by erosion from the first wall of the main chamber, as demonstrated by the fact that during the phase with beryllium divertor target tiles the main plasma impurity was still carbon.

The divertor consists of 192 poloidal water-cooled rails, to each of which are bolted two sets of tiles (each tile being typically 75 mm long and 30 mm wide). The tiles are shaped to protect the poloidal edge of the tile in the adjacent set from direct plasma impact, as shown in Fig. 146. Since the gaps between tiles vary, the widths of the shadowed areas also vary, from about 5 to 15 mm. During the early 1994/5 campaign, graphite tiles were used, and deposition in the shadowed areas was soon visible in the intershot viewing camera [4]; erosion and redeposition effects could be seen on the plasma-exposed regions, but largely cancelled themselves out over a period of time due to radial sweeping of the strike points.

Figure 146 shows an analysis of D, Be and C concentrations across a graphite divertor tile in the outer SOL. This tile was removed after six months operation. The analysis technique was Nuclear Reaction Analysis (NRA) using a 2.5 MeV ^3He beam, and the analysis depths for D, Be and C are approximately 7, 3 and $1 \mu\text{m}$, respectively. As expected, the D level rose to a peak in the redeposition area before falling again deeper into the shadowed region. The peak D level corresponds to a ratio of D:C of about 0.5:1 throughout the $7 \mu\text{m}$ detectable range (the redeposited film could, however, be thicker), corresponding to the saturation level for hydrogen isotopes in a C matrix [7]. Similar D concentrations were found in the shadowed areas of tiles in the inner

SOL, where films were more widespread and showed some signs of spalling. These were higher concentrations than seen before in redeposited films in JET. The probable reason is that the divertor target is cooled, with bulk temperatures at about 50°C, rising for a few seconds to 100-200°C during a pulse. Although surface temperatures in plasma-exposed areas may rise to ~1000°C during a pulse, surface temperatures in the shadowed regions should not exceed that of the bulk. However, in previous operations, PFCs have had an ambient temperature of 250-300°C and even shadowed areas may have reached higher temperatures following a discharge, since the tiles were not in good thermal contact with the vessel. Such sustained temperatures may be sufficient to reduce the H isotope saturation level.

As can be seen in Fig. 146, Be was present over the part of the tiles exposed to plasma. Be was introduced into the torus by regular Be evaporations from four heads spaced around the vessel near the outer midplane. However, the Be seen on the tiles was much greater than would be deposited directly during evaporation, and the distribution was inconsistent with the line-of-sight process. Instead, Be was evaporated onto PFCs in the main chamber, was eroded during plasma operations, and travelled through the SOL to the divertor. Similarly, metals such as Ni, Fe, and Cr were found on the exposed parts of the divertor tiles and these impurities resulted from erosion of uncovered parts of the in-conel wall, as well as from various incidents causing localized melting during the early campaign. Thus, the divertor tiles, rather than being the primary source of impurities in the torus, were the sink for material eroded from elsewhere in the machine. Local recycling then occurred in the divertor, wherein carbon sputtered by the plasma was redeposited on the tiles, and material deposited inside the shadowed region accumulated, trapping D at the saturation level for low temperature films.

For the last two months of 1995 operation, the graphite divertor tiles were replaced by Be tiles. Similar patterns of deposition developed on the tiles, and subsequent NRA analysis showed that similar amounts of D were trapped in redeposited films in the shadowed regions of tiles in the inner SOL. These films also contained carbon, which was, presumably, sputtered from the main chamber, transported along the SOL, and then locally recycled. Since there was much more carbon in these redeposited films than on the areas of the Be tiles exposed to plasma (in contrast to the situation for Be on C seen in Fig. 146), this

suggests that chemical sputtering was taking place. There were no large D levels to indicate thick redeposited films in the shadowed areas on tiles in the outer SOL, nor were there significant amounts of redeposited carbon, so that transport of carbon in the SOL from the main chamber was mostly to the inner part of the divertor. The amounts of the metals, Ni, Fe, and Cr found on the Be tiles were less than on the graphite tiles, confirming that measures to protect the vessel walls during the campaign were successful.

Divertor tile analyses thus showed that high concentrations of D could be retained throughout films (at least to $>7\mu\text{m}$) if the surfaces remained sufficiently cool. This may be important when considering tritium retention scenarios for ITER. The divertor acted as a sink for impurities eroded by the plasma from the main chamber, for example Be, during the graphite tile phase and C during the Be tile phase. Similar D retention occurred during the Be phase of the 1994/95 experimental campaign, but the thick redeposited films also contained high concentrations of carbon.

Neutral Density Analysis

The neutral particle density in the Mark I divertor was measured by special ionization gauges located in the sub-divertor volume, ~5cm below the divertor target, and one in the sub-divertor volume just in front of the cryopump. Neutral particles (predominantly deuterium) were scattered into this volume by charge exchange and Franck-Condon processes between the ion population of the divertor plasma and neutrals that recycle from the divertor target plates. Due to the experimental arrangement, the measured neutral fluxes represented a superposition of particles that were almost directly scattered from the divertor plasma into the gauges and fluxes produced by the sub-divertor pressure, which depended on the total particle flux entering the sub-divertor volume. Several of the gas introduction modules were also located in the sub divertor volume, but they contributed only <10% of the neutral particle density, which was dominated by the much larger particle flux from recycling at the target plates.

Studies of neutral particle density in the divertor concentrated on questions relating to neutral particle retention capability in various discharge scenarios (ie attached and detached plasmas), ohmic and additionally heated plasmas, low and high magnetic flux surface expansion at the target plates. Effective retention of neutrals in the divertor, and hence low neutral particle fluxes in the

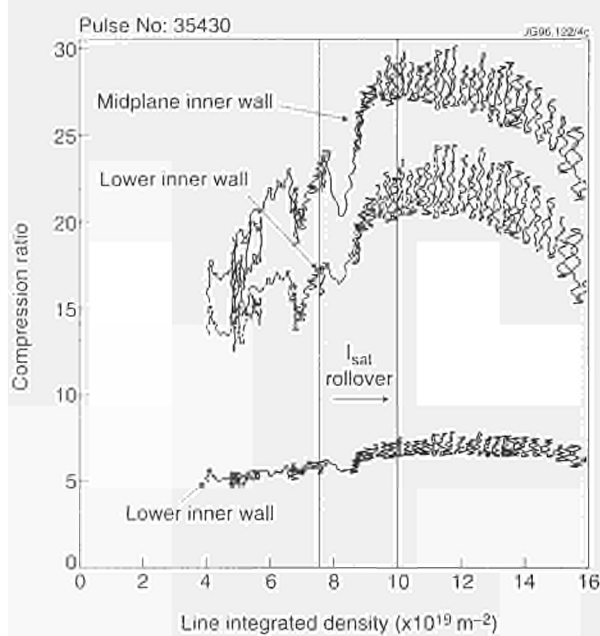


Fig.147: Variation of the neutral density compression ratio (ratio of divertor neutral density to main chamber neutral density), measured with respect to several regions of the main chamber, as a function of line integral electron density. The decrease in compression ratio with respect to the inner wall main chamber measurements as I_{sat} rolls over and detachment is approached is evident. The vertical sweeping of data is associated with radial sweeping of the plasma strike points

plasma main chamber, assisted in reducing the impurity sources in the main plasma chamber by a reduction of sputtering by charge exchange neutrals at the main chamber wall. It also allowed a more active control of the main plasma density and of the SOL flows produced by puffing and pumping. Finally, it is believed that low main chamber recycling levels were essential for good confinement and may contribute to reduction of the H-mode power threshold.

Detached divertor plasmas, which substantially reduce the maximum power density at the target, were achieved in ohmic and L-mode discharges, by puffing deuterium to raise the plasma density, and in H-modes discharges by impurity seeding (using N_2). In the example of Fig.147, an ohmic discharge, diverted onto the horizontal target, was driven into detachment by gas puffing. The neutral particle flux in the sub-divertor volume was measured using the ionization gauge near the cryopump, and that in the main plasma chamber was calculated from H_{α} measurements along several lines-of-sight. The ratio of the two fluxes defines the compression ratio shown in Fig.147. Initially, the density rise caused the compression to increase, hence improving the neutral particle retention. However, as a result of the increasing density, the ion saturation current at the target plate reached its maximum and then decreased (the 'rollover'), indicating

the beginning of plasma detachment, and the compression ratio saturated. A further density rise then caused a decrease of the neutral particle retention. At this point, the neutral particle density distribution across the divertor peaked in the private flux region of the divertor plasma, consistent with the observation that detachment starts at the separatrix of the SOL. At the same time, the plasma radiation in the divertor moved from the vicinity of the target plate to the X-point. Overall, the divertor appeared to become more 'open' for neutral particles during detachment.

In general, it was found that to maximize the neutral particle compression the plasma strike zones should impinge on the horizontal target plates, with the divertor flux expansion adjusted so that the 2-3cm magnetic flux surface (measured at the outer plasma midplane) was near to the vertical targets. In this configuration, the divertor side plates could act as baffles. The change of the neutral particle compression during the transition from attached to detached divertor plasma, as described above, is then qualitatively consistent with the expected change in transparency of the divertor plasma for recycling neutrals. However, if the 2-3cm magnetic flux surface intersected the sideplates, the compression could be dramatically decreased, reaching values as low as about 1. Neutral particle retention in the divertor was on average lower for plasma configurations with the strike zones on the vertical target plates than for plasma configurations using the horizontal plates. The effect of SOL interception by the vertical target plates, and the reduced neutral particle compression which resulted, was particularly pronounced in discharges with high magnetic flux surface expansion in the divertor. This effect could also be observed during the transition from the ohmic to the L-mode regime, which was accompanied by a broadening of the SOL, as well as during ELMs, where the separatrix could move radially by several centimetres.

For opaque targets, simulations show that neutral retention should be better for vertical target operation than for plasmas on the horizontal target. In the Mark I divertor, however, the poloidal slots between the tiles allow for the escape of neutrals, and those escaping through the vertical target plates have higher conductance to the main chamber than those escaping downward through the horizontal plates to the sub-divertor volume.

Fuelling and Pumping Effects

The routine availability of the cryopump, with a pumping speed for deuterium of $\sim 200\text{m}^3\text{s}^{-1}$, has been a major

advantage in operation and has influenced many areas of the programme. In addition to the general vessel conditioning effect, most obvious in the high performance plasmas, the pump permitted control of plasma density and of particle recycling. A significant feature of the Mark I divertor configuration was that the effective particle removal rate varied by only a factor of 2, as the outer strike point scanned the horizontal and vertical targets [8]. This was in contrast to the DIII-D experience, where a variation of at least a factor of 5 in pumping speed was typical. The observed behaviour is believed to be due to the Mark I target design, with poloidal slots which allowed recirculation of neutrals in the divertor volume, a proposal which is consistent with the broad neutral pressure profiles measured in the sub-divertor region. As a result, the effective pumping of the plasma was relatively insensitive to the plasma configuration, a situation which could differ in the Mark II divertor, which has no corresponding slots and a high conductance opening to the cryopump chamber.

By optimizing the use of the cryopump the density in steady-state ELMy H-modes was varied by a factor of ~ 1.5 (Fig. 148). This does not represent the full exploitation of the cryopump, however, since, at the lowest densities, the density was decaying slowly throughout the 4s flat-top and the wall was being depleted over several pulses. An extensive series of long steady-state pulses may, therefore, be required to fully deplete the plasma wall, to achieve the lowest possible densities, and to establish the full range of density accessible in the H-mode. A further significant point is that, in ELMy H-modes, high confinement could be sustained at high densities with the cryopump in the presence of gas flow rates 5-10 times higher than would be acceptable without the cryopump. Both the edge density and the recycling level were lower with the cryopump, and both of these may be important in determining the level of confinement in ELMy H-modes. In addition, if high SOL flows are required for good divertor impurity retention, operation with active pumping is clearly advantageous.

Fuelling efficiency and impurity retention in L-mode discharges exhibited little dependence on the fuelling location, even when the cryopump was active. Typically the fuelling efficiencies for gas puffing in the divertor and in the main chamber differed by only $\sim 10\%$. Systematic experiments to study the role of fuelling location in enhancing convection found that impurity retention, as

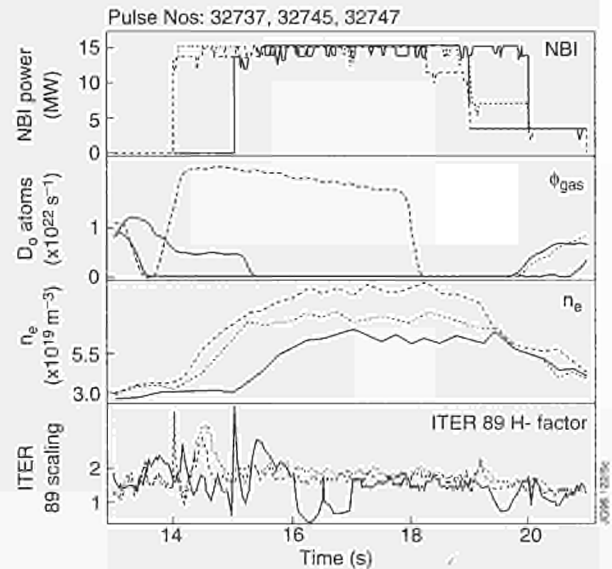


Fig. 148: Illustration of the use of pumping and fuelling to vary the density in steady-state ELMy H-modes at 3MA/2.8T. The lowest density case had no fuelling and strike points located in the corner of the divertor target, the pulse with moderate density had no fuelling and strike points ~ 20 cm from the corner, while the highest density case used the same equilibrium, but was fuelled by gas puffing

monitored by the time evolution of neon radiation following short neon gas puffs, depended little on either fuelling location or location of the neon puff [9]. Nevertheless, the rate of decay of neon content in the plasma core was greater at higher density, indicating that forced flows do influence the natural convection. In addition, there is evidence from radiative divertor experiments that the neon density in the bulk plasma decreased as the external deuterium flow rate was increased. Overall, these results suggest that the internal recirculation could have been high due to the open design of the Mark I configuration, and that the influence of externally induced flows might be more significant with the improved closure of the Mark II target.

Helium Transport and Exhaust

Determining the rate at which thermal helium can be exhausted from the bulk plasma is a key reactor issue, and the cryopump allowed argon frosting to be applied to provide a helium pumping capability. In JET, argon was sprayed directly onto the helium cooled surface by gas nozzles within the cryopump structure, the typical amount of argon applied being $5-10 \times 10^{23}$ atoms. Despite this close coupling, argon contaminated the plasma-facing surfaces, leading to disruptions, and necessitating 2-3 recovery pulses to re-establish reliable operation after an application of argon frost. Thus, while an effective pumping speed for helium of $\sim 180 \text{m}^3 \text{s}^{-1}$ was achieved with a fresh

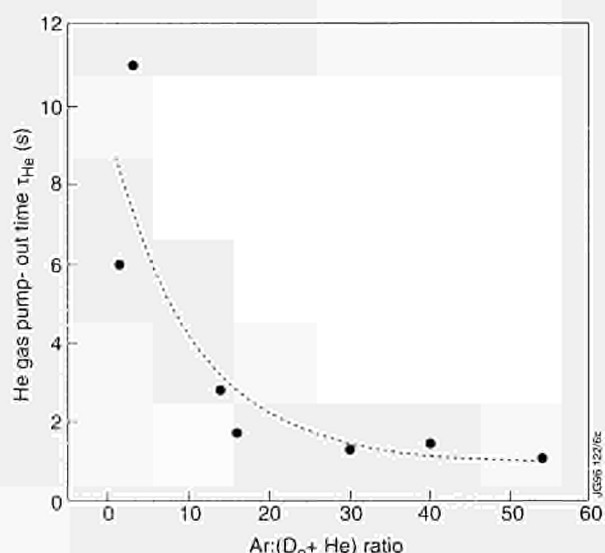


Fig.149: Variation in the He gas pump-out time, t_p , as a function of the (D_o+He) load on the Ar layer. Helium exhaust experiments have typically been performed at argon to deuterium ratios of less than 20

Ar layer [8], poisoning by deuterium during recovery pulses degraded this by a factor of 2 to 3 (Fig. 149), and He exhaust experiments were performed in less than ideal conditions. One possibility is that the surface contamination resulted from the structure of the CFC used for the divertor target and poloidal limiters. This material will also be used in the Mark II divertor, so that the situation with respect to contamination is not expected to change. However, the poisoning of the argon frosting layer by deuterium may be reduced if the geometrical changes in the Mark II target reduce the pumping speed for non-optimized equilibria. If so, higher pumping speeds for helium could be achieved and the quality of helium exhaust results would be improved.

Exhaust studies were performed in L-mode and ELMy H-mode plasmas following a short helium gas puff [10]. The helium content of the bulk plasma was derived from active charge exchange spectroscopic measurements, and the particle replacement time, τ_{He}^* , obtained from the ratio of the integrated helium content to the net outward radial particle flow. Fig. 150 illustrates the observed behaviour of the total helium content of the plasma for a variety of conditions. In ELMy H-modes, typical values of $\tau_{He}^* \sim 8-15s$ were obtained with active argon frost pumping, while values without argon frosting were twice as long, although these times were far in excess of the NB heating phase and, therefore, the uncertainties are large. In L-mode plasmas, τ_{He}^* was approximately 50% of the ELMy H-mode values. Overall, the ratio τ_{He}^*/τ_E was in excess of 20 for ELMy H-modes and in excess of 10

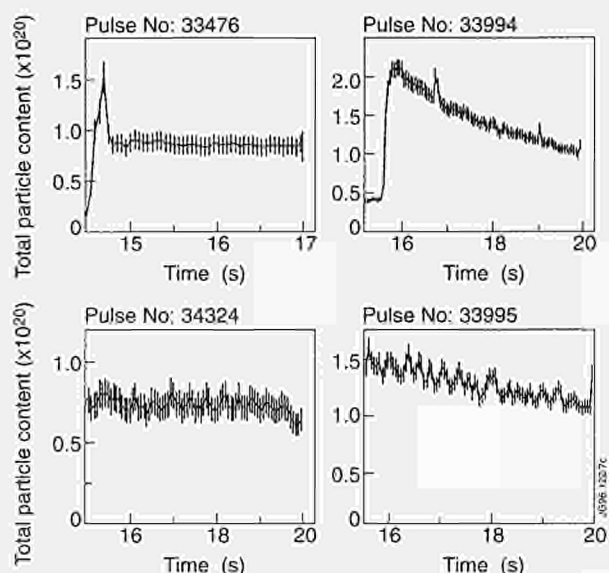


Fig.150: Decay of the total helium content in a variety of plasma regimes, following a short helium gas puff

for L-mode plasmas. Clearly the former value is unacceptable for a reactor, but further experiments are required to elucidate whether this is ultimately limited in JET by plasma transport processes or the degraded pumping speed.

Helium transport was studied in parallel with plasma exhaust measurements, as well as in plasmas with central deposition of helium using NB injection. In both cases, the helium profile relaxed to the shape of the electron density profile in several 100ms. Beam deposition experiments are still under analysis, but gas puff experiments yielded central values of helium particle diffusivity $\sim 0.5m^2s^{-1}$ and central pinch velocities close to zero, indicating that helium accumulation in the plasma centre will not be a problem in ELMy H-modes.

Scrape-off Layer Scaling Studies

Extensive studies of the behaviour of divertor and scrape-off layer (SOL) parameters were undertaken during the Mark I divertor campaign [11]. Using both reciprocating and fixed Langmuir probe systems, simultaneous measurements were obtained of upstream and target SOL profiles over a wide range of plasma parameters during ohmic, L and H-mode plasmas. Data were taken for line-averaged densities of $1.3-6.7 \times 10^{19}m^{-3}$ at input powers of up to 8MW with toroidal fields of 1.5-3.3T. Experiments covered the range from low to high recycling and then to the detached phase of a discharge in horizontal, corner and vertical target configurations with normal ($B \times \nabla B \downarrow$) and reversed ($B \times \nabla B \uparrow$) field.

It was generally observed that for ohmic pulses the SOL width increased almost linearly with density up to

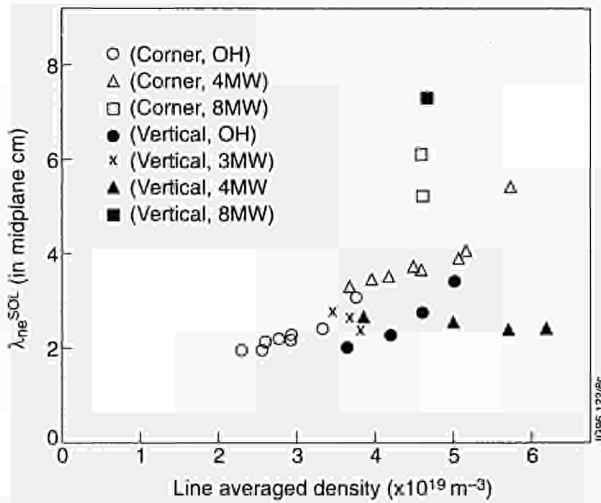


Fig.151: Comparison between density SOL widths, measured at the plasma midplane, for corner and vertical target configurations in reversed toroidal field discharges ($B \times \nabla B \uparrow$) as a function of line-averaged density and input power

the rollover density (onset of high recycling) after which it tended to level off, as shown in Fig.151, which includes data for vertical and corner target configurations in reversed field. In the corner target configuration, the addition of beam heating and increasing density resulted in an increase in the SOL widths, while in the vertical target configuration, the SOL width tended to remain constant with increasing NB injection, with a midplane value of $\lambda_{nc} \sim 2.5$ cm, as shown in Fig.151. After the L-H transition the SOL width was initially observed to decrease and then to relax to typical L-mode values between ELMs.

With reversed field ($B \times \nabla B \uparrow$), corner target configurations, with the toroidal field in the range 2.2-2.4T, SOL widths for density and temperature scaled as $n_e^{-0.5} P_{tot}^{-0.25}$ for input powers of <4MW, and as $n_e^{-0.3} P_{tot}^{-0.75}$ for input powers of 4-8MW. The corresponding power SOL width scaled as $n_e^{-1} (P_{NBI} \leq 4\text{MW})$ and as $n_e^{-0.75} P_{tot}^{-0.9}$ ($4\text{MW} \leq P_{NBI} \leq 8\text{MW}$). For a vertical target configuration and the same parameter range, the SOL widths were smaller, for example midplane values of the density SOL width were $\lambda_{nc}^{vert} = 1.6$ cm and $\lambda_{nc}^{horiz} = 3.1$ cm. Differences were also observed between normal and reversed field directions. For example, the midplane density fall-off length for the L-mode phase of a vertical target configuration was $\lambda_{nc}^{vert} = 1.5$ cm for $B \times \nabla B \downarrow$ and increased to $\lambda_{nc}^{vert} \sim 2.5$ cm for $B \times \nabla B \uparrow$.

Using both an analytical scaling model and code calculations, it was possible to calculate the radial and parallel transport coefficients which determine the width of the SOL. It was found that the radial heat diffusivity, χ_{\perp} , calculated from the analytical model, varied from

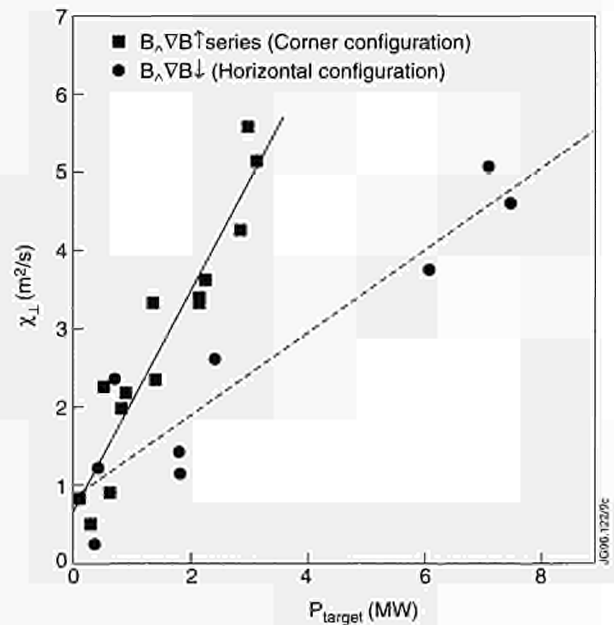


Fig.152: Variation of χ_{\perp} , the radial heat diffusivity, as a function of power to the target for a corner target configuration in reversed field ($B \times \nabla B \uparrow$) and a horizontal target configuration in normal field ($B \times \nabla B \downarrow$)

$\sim 2\text{m}^2\text{s}^{-1}$ to $\sim 6\text{m}^2\text{s}^{-1}$, and increased with increasing power to the target, as shown in Fig.152, indicating that χ_{\perp} derived in this way is not a constant. Particle and heat diffusion coefficients calculated using the EDGE2D code and an iterative 'onion-skin' model for selected ohmic and L-mode discharges gave $\chi_{\perp} \sim 1.5\text{--}2\text{m}^2\text{s}^{-1}$ (comparable to the analytically calculated values for the same density and input power), $D_{\perp} \sim 0.2\text{m}^2\text{s}^{-1}$, and $V_{pinch} \sim 3\text{ms}^{-1}$.

Influence of Divertor Configuration on Performance

The geometry of the Mark I divertor permitted experiments to study plasmas diverted onto either the horizontal or vertical target plates. In addition, the flexibility of the poloidal field control allowed a wide range of divertor configurations to be examined, so that, in particular, the relative importance of X-point height and field line connection length could be investigated. Figure 153 compares the divertor geometries for a series of pulses in which the X-point height and the connection length along the inner divertor leg were independently varied by a factor of 2. The results of this experiment indicate that, in the Mark I divertor, the X-point height and connection length had little impact on either the global plasma behaviour, or the divertor behaviour close to detachment.

It had been predicted that, in plasmas with strike points on the divertor sideplates, the divertor recycling patterns should be changed and the possibility of escape for

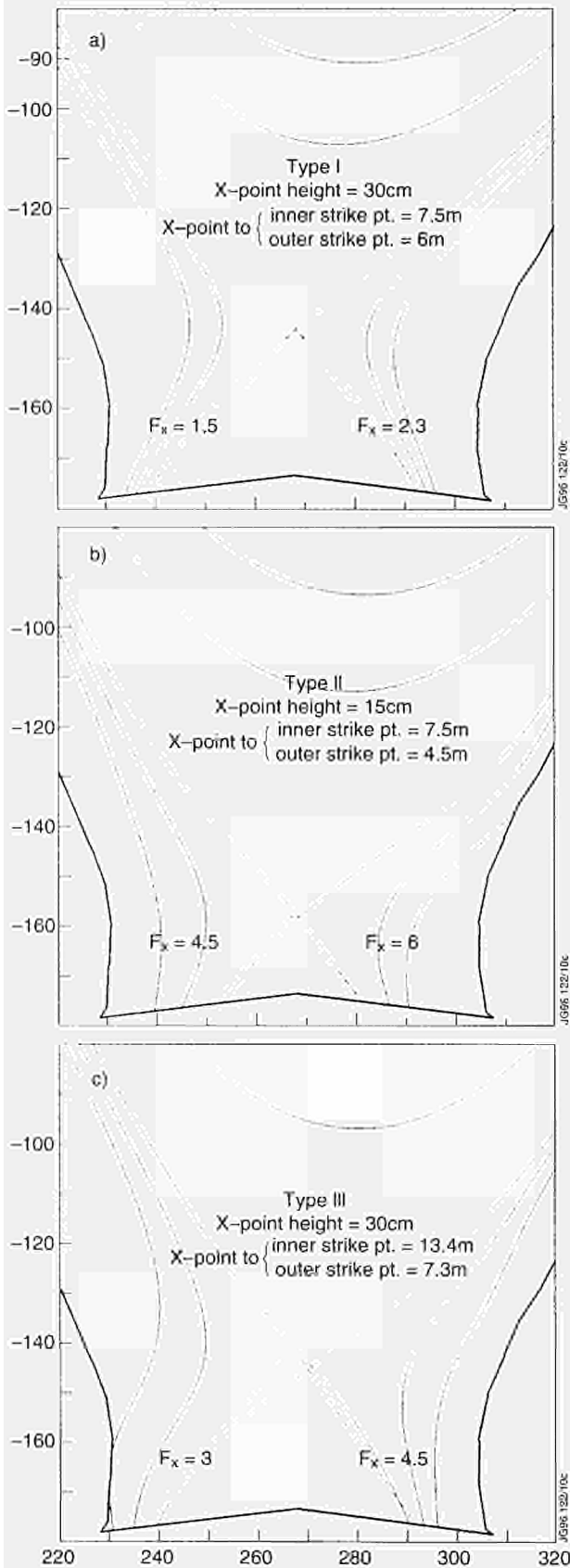


Fig.153: Comparison of the divertor geometries for a series of pulses in which the influence of configuration on divertor performance was investigated by independently varying the X-point height and connection length along the inner divertor leg by a factor of 2

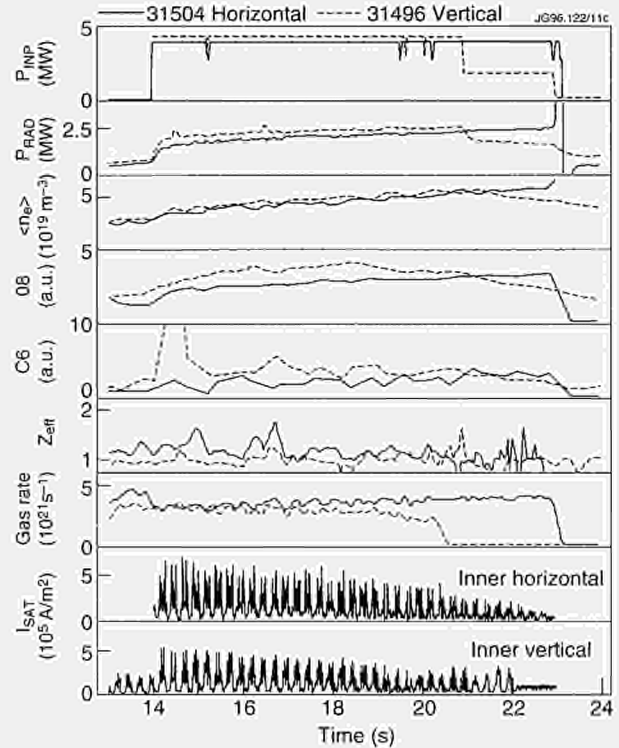


Fig.154: Comparison of global behaviour of plasmas diverted onto the horizontal and vertical targets as detachment is approached (note behaviour of I_{sat} at inner strike point in lowest panels), showing the striking similarity between the two cases

recycling neutrals should be reduced. As a result, more peaked density profiles should be formed at the target and in the SOL, depressing the target temperature and possibly facilitating detachment [12]. Experimental assessment of these predictions has assumed increased importance since the adoption by ITER of this approach. Comparison of edge and target parameters of plasmas diverted onto the horizontal and vertical targets confirmed certain aspects of the code predictions [13]. In particular, steeper SOL density profiles and inverted target temperature profiles were observed in plasmas formed on the vertical target. Some detailed differences were also observed as the strike point position was scanned down the sideplate into the corner of the target, with steeper I_{sat} profiles measured when the strike point was located at the base of the sideplate [14].

Despite this detailed agreement with modelling predictions, the main plasma parameters associated with horizontal and vertical target plasmas were similar (Fig.154). Impurity and radiation levels were equal and no substantial differences were observed in the radiation patterns. Most significantly, both detachment and the density limit were observed at very similar densities, in contrast to modelling predictions. Several possible explanations of this behaviour are under investigation. For

example, a strong particle pinch in the SOL, required to explain the steepness of SOL profiles close to detachment [14], would reduce the influence of particle sources, and hence divertor geometry, on detachment. Unsatisfactory baffling of the divertor bypasses would also reduce the differences between horizontal and vertical configurations. Production and transport of impurities in the divertor and SOL are complicated and might also contribute to the observed behaviour. Finally, the construction of the Mark I divertor, with slots between bands of target tiles, implies an effective transparency to neutrals, which increases the recirculation into the private flux region. This also reduces the expected differences between horizontal and vertical cases, although more recent calculations indicate that an unrealistically high transparency is required to reproduce the peaked ion flow profiles at the divertor target. This is clearly an area of some consequence for ITER and further studies will be required in the Mark II geometry to elucidate the source of this important discrepancy between experiment and modelling.

Physics of Divertor Detachment

Divertor detachment was studied under a wide range of conditions [3, 15], both in L-mode plasmas, using deuterium puffing, and in H-modes, using deuterium and extrinsic impurities, as discussed later. In ohmic and L-mode plasmas, steady-state detachment could be maintained with radiative power fractions of 70% (CFC target) to 80% (Be target). The phenomena observed as the plasma density increased were reproducible and gradual, that is there was no bifurcation in the behaviour as divertor detachment occurred (though see the discussion of divertor oscillations below).

Initially, as the plasma density increased, the target I_{sat} and D_{α} signals rose, until a maximum in I_{sat} was reached, (i.e. the rollover), which was determined by the input power. Thereafter, I_{sat} decreased, an effect first observed at the inner separatrix, while the D_{α} signal increased. At radiated power fractions $\sim 70\%$, the ion saturation current at the separatrix had fallen by an order of magnitude and the electron temperature, had fallen to $\sim 2\text{-}5\text{eV}$, at which point the plasma is considered to be 'detached'. Note that the observed value of electron temperature was higher than could be reproduced by numerical codes, and there is some concern that the analysis of Langmuir probe measurements in this regime may be subject to systematic errors [17]. Although detachment occurred first at the

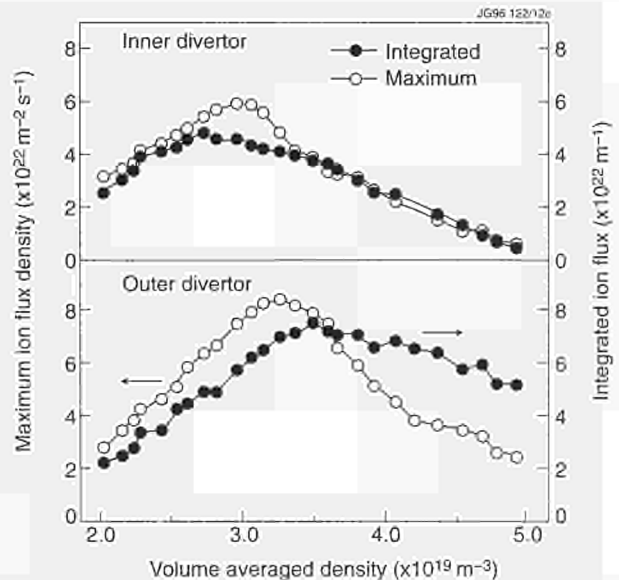


Fig.155: The variation of the (radial) maximum of the ion flux density and the ion flux density integrated over the strike zone, for the inner and outer divertor legs during an ohmic density ramp. At the inner divertor, both the maximum and integrated values of ion flux density fall by an order of magnitude from their peak values at the rollover. At the outer divertor, only the maximum ion flux falls by a large factor. The integrated value falls by only 40%, illustrating that the ion flux further out in the SOL does not decrease significantly in 'detached' plasmas

inner strike point, there was no difficulty in establishing stably detached plasmas in which the ion saturation currents at the inner and outer separatrices were reduced by an order of magnitude from their peak values at the rollover. JET experiments have emphasized operation in this 'completely' detached regime, but if a less strict definition is applied, a window for stable detachment can be defined operationally as the density range between rollover, which occurs at $\sim 75\%$ of the density limit, and the density limit.

Certain detailed differences in the behaviour of the inner and outer strike zones were observed during the approach to detachment. For both divertors the ion flux started to drop close to the separatrix and thereafter in the outer parts of the scrape-off layer. At the inner divertor target this process continued until total detachment was obtained, but at the outer divertor target the drop in ion flux remained confined to a region close to the separatrix, and the plasma remained attached further out in the SOL. This difference in the degree of detachment is shown in Fig.155 where the (radial) maximum and integrated ion fluxes to the inner and outer divertor are plotted as a function of density for an ohmic discharge. The inner divertor shows a drop in the peak ion flux and its integral of about an order of magnitude (total detachment), while

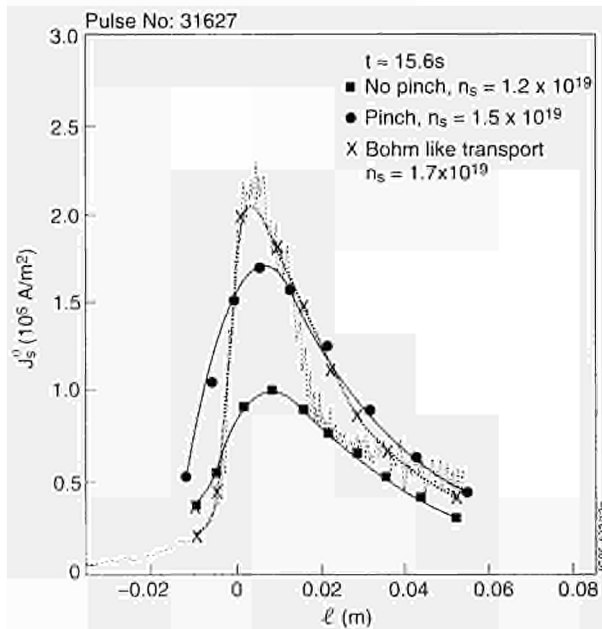


Fig.156: Comparison of experimental (dashed line) and computed (solid lines) spatial profiles of J_s^0 , the ion saturation current density, at the outer target in the high recycling phase of an ohmic pulse. The figure illustrates that an inward pinch or a Bohm-like scaling of the anomalous perpendicular transport is required to explain the experimental data

the outer divertor peak ion flux drops approximately by a factor of 5 (and the location of the peak moves away from the separatrix), but its integral only decreases by 40% (partial detachment).

The phase between the rollover and detachment was characterized by a migration of the zone of peak radiation from a region near to the divertor target to the X-point. Best current estimates suggest that the peak radiation was just above the X-point for the fully detached conditions discussed above. At the same time, bremsstrahlung emission detected by an infra-red camera showed a high density region, with $n_e > 10^{20} \text{m}^{-3}$, in the vicinity of the X-point. If the plasma density was increased further, a main plasma MARFE formed on the inboard side of the plasma and a major disruption followed. This general behaviour has been reproduced by EDGE2D calculations in which the calculation grid was extended within the separatrix [16]. The migration of the radiating zone to the X-point was smooth, and reversible when the density was ramped down.

Detailed Langmuir probe measurements of upstream SOL and target profiles confirmed the development of a significant pressure drop along the SOL as detachment was approached [3]. At the same time, SOL profiles were found to broaden. In a typical 4MW L-mode plasma, the scrape-off width for the electron pressure increased from $\lambda_p = 1.3 \text{cm}$ in the 'high recycling' regime to $\lambda_p = 2.2 \text{cm}$ at detachment. This

will have an impact on the divertor baffling and plasma-wall distances required in a reactor, but further studies are required in current devices to determine how the SOL width scales with other parameters such as conducted power, toroidal field and plasma current.

Although stable, quiescent detached phases were routinely established, in many L-mode discharges oscillations in the divertor behaviour were observed in the vicinity of the rollover. These were characterized by a dramatic drop in I_{sat} , neutral pressure, D_{eff} , CII (or BeII) photon fluxes, and radiated power. The plasma was effectively detached for a short period, but re-attached after $\sim 10 \text{ms}$ and remained attached for 50-100ms, after which the cycle was repeated. The oscillations, whose frequency increased with the level of power flowing across the SOL, decayed before the fully detached phase was reached. The cause of the phenomenon is not understood, but it is speculated that it may be associated with an ionization instability of deuterium and/or impurities.

Model Validation

Sophisticated 2D plasma fluid codes coupled to Monte-Carlo codes for neutral species have been developed to perform realistic calculations of the divertor and scrape-off layer plasma parameters. These codes are routinely used to optimise the design of new divertors for existing experiments and next step devices. The reliability of these predictions depends crucially on the accuracy of the models used to describe the physical processes that take place in the SOL and divertor region. Therefore, a substantial effort has been dedicated to validate the plasma edge simulation codes EDGE2D/U-NIMBUS by comparing their predictions with experimental measurements.

The extensive experimental information relating to the plasma and neutral hydrogen behaviour in the Mark I divertor has allowed a quantitative assessment of these models. Out of this assessment, improvements to the models have been performed where thought necessary and reinterpretation of the measurements has been carried out. Recently, there have been two main areas of work.

Highly Radiative Divertors and Modelling of Detachment

The model reproduces in a qualitative way the approach to detachment, which occurs as the main plasma density increases and the level of radiation rises. The quantitative comparison between code and experiment from low recy-

cling to detachment is satisfactory for many plasma parameters, such as the total ion flux to the divertor and the integrated H_{α} emission from the divertor. However, detailed profile measurements of the ion flux at the divertor cannot be reproduced during the high recycling phase unless an inward particle pinch in the SOL or Bohm like scaling of the anomalous perpendicular transport is used (Fig.156). Detailed comparison of measured and simulated visible spectroscopy signals show that the levels of carbon emission from the divertor during the high recycling and detachment phase can only be reproduced if chemical sputtering (yield $\sim 1-2\%$) is included in addition to physical sputtering. However, even when the source of carbon is reproduced by the model, the divertor radiation is underestimated by a factor of 2-3, which has prompted a re-evaluation of the atomic data used in the models. This is currently in progress. The process of plasma detachment in the simulations is driven by charge-exchange momentum removal, which impedes the ion flux to the plate, and, if the density/radiation increases further, it is followed by recombination (mainly at the inner divertor).

Divertor Geometry Effects and By-pass Leaks from the Divertor

One of the clearest prediction of the models is the strong effect of the geometry on divertor plasma parameters due to the differences in divertor closure. In order to test these predictions, a series of experiments were performed in which the strike points were located either on the vertical or horizontal sections of the Mark I divertor. It was found that the experimental effects were not as strong as predicted by the model, with detachment being observed at similar densities for both configurations. This discrepancy has highlighted the existence of considerable by-pass leaks for hydrogen through the divertor mechanical structure. These allow hydrogenic species and impurities to leak from the sub-divertor volume into the main chamber. When these leaks are included in the model the predicted effect of the geometry is much weaker than originally expected, in agreement with the experimental observations.

Characterization of ELMy H-modes

Steady-state ELMy H-modes are of importance to ITER, probably in combination with some form of radiating divertor, as a baseline operating regime. Such plasmas were extensively studied under steady-state conditions lasting up to $50\tau_e$ and, in the longest case, $0.85\tau_R$, where

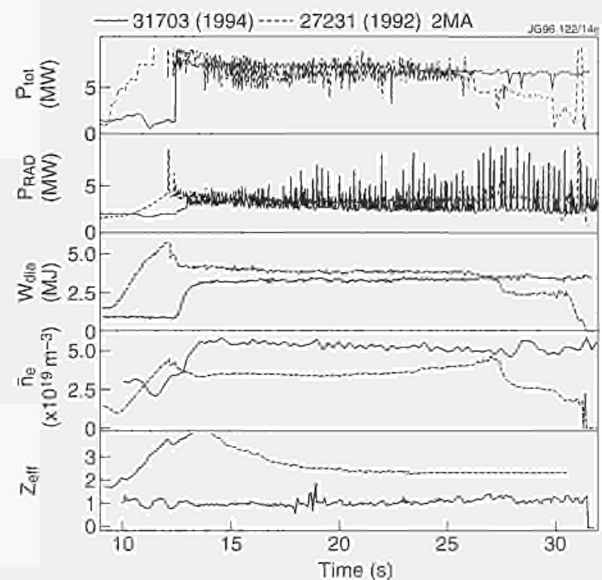


Fig.157: Comparison of steady-state ELMy H-modes in the old JET configuration (Pulse No.27231) and in the Pumped Divertor configuration (Pulse No.31703)

τ_R is the resistive diffusion time evaluated at mid-radius. Type I ELM behaviour was observed, as indicated by the increase in ELM frequency with increasing input power. Significant improvements were obtained relative to experiments in the previous JET configuration, with higher confinement enhancement, reduced impurity content, less radiation, and no evidence of saturation of pumping [18] (Fig.157). Steady-state H-modes were established with durations of up to 20s at 2MA/2T and 10s at 3MA/3T, and these pulse lengths were limited only by technical constraints on the tokamak and heating systems. Such H-modes typically exhibited global energy confinement times $\sim 1.8\tau_E^{ITER89-P}$, though with a variation of $\sim 10\%$ which correlated with main chamber recycling. No dependence of confinement on q_{95} was observed for $q_{95} > 2.2$, and reactor relevant values of $H/q_{95} \sim 0.5-0.65$ were readily achieved.

The variation in H-mode power threshold with magnetic field and density was studied in ITER-relevant geometry at $q_{95}=3$ [19]. The scaling has been cast in terms of the total loss power across the separatrix, with proper accounting for the time rate of change of plasma stored energy, bulk radiation, and shine through losses of NBI power. The last is particularly important at low density and could have a substantial impact on the density scaling. Although the data follows the recent ITER scaling, $P_{th}(MW) \propto C n_e^{0.75} (10^{20} m^{-3}) B_r(T) S(m^2)$, the coefficient, C , appears to be about twice as large as the ITER scaling value, $C=0.016$. Further analysis suggests that data is

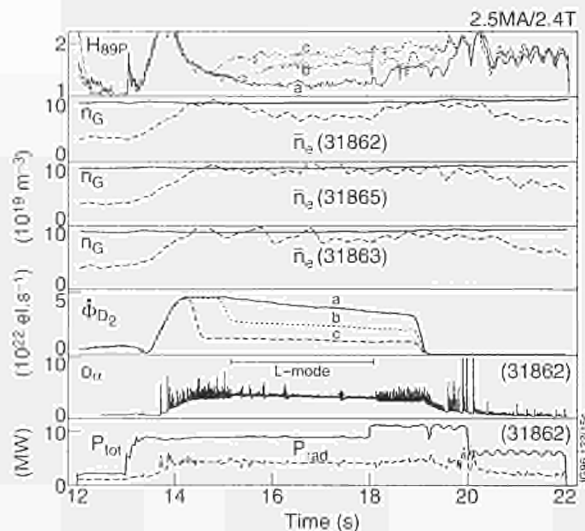


Fig. 158: A sequence of three ELMy H-mode plasmas in which the gas fuelling rate was increased pulse by pulse, initially raising the density to the Greenwald value, n_G , with high confinement ($H=1.8$, Pulse No.31863), but ultimately driving the plasma back to the L-mode, with a fall in energy and particle confinement: (a) Pulse No.31862, (b) Pulse No.31865, (c) Pulse No.31863

better described by the scaling $P_{in} = 0.3n_c B_1 R^{2.5}$ although the 3MA/3T data still exhibits noticeable deviations from the fit. Edge plasma parameters, and specifically edge neutral density, can be expected to play a determining role in the H-mode transition and a systematic analysis of their influence is underway.

Density Limits

Much of the physics of the density limit in ohmic and L-mode diverted plasmas has been treated in the discussion of detachment. However, certain aspects of the density limit are worthy of separate consideration, since there is still considerable debate on the detailed physics of the density limit in diverted plasmas and since the scaling of the density limit is of crucial importance is determining access to the projected operating point of ITER. Earlier experiments in JET showed that the density limit in L-mode limiter plasmas scaled with input power as $P^{0.5}$ [20] and that the so-called Greenwald limit, $n_{lim} = I_p / \pi a^2$, could be exceeded at plasma currents of up to 4MA, the maximum current at which density limit experiments were undertaken. In addition, in H-mode experiments in the old JET configuration, the Greenwald limit was exceeded at currents of up to 2MA with sufficiently long ELM-free periods [21]. Experiments at higher currents were limited by a variety of technical considerations, particularly the power handling capability of the divertor targets.

Recent experiments have emphasized the development of a more detailed understanding of the density limit

in L-mode plasmas and the determination of the scaling of the density limit in the H-mode. Exploration of the density limit was necessarily executed at low current, generally at 2MA or less, so as to minimize the number of high current disruptions. In addition, the experiments used only gas fuelling and a technical limitation encountered was that, as the density rose, the edge neutral pressure rose, leading to a rise in pressure in the NB injection ducts. This often tripped the NB system and prevented experiments being pursued at the highest powers and densities.

The stable density limit in L-mode plasmas corresponded to a stable detachment of the divertor, with a total radiated power fraction of 70-80%. At higher radiated power fractions, the 'divertor MARFE' entered the main plasma, the radiated power rose to 100%, MHD grew, and a major disruption occurred. Although the Greenwald limit could be readily exceeded at 2MA, the limit scaled more weakly with power than the $P^{0.5}$ observed in limiter experiments. This can be understood by a comparative analysis of the radiation behaviour as a function of density in limiter and X-point experiments. The radiated power fraction in earlier limiter experiments scaled with n_c^2 until the onset of the MARFE. In X-point experiments, the behaviour was rather different. Initially the radiated power fraction rose steeply with density, then rolled over and subsequently rose more gradually. This rollover phase appears to correspond to the period of ion saturation current rollover, during the approach to detachment, when the radiation peak was moving from the divertor targets to the vicinity of the X-point. Splitting the radiation into bulk plasma and divertor components reveals the reason for the difference in behaviour: the bulk plasma radiation scales with n_c^2 , as in limiter plasmas, where essentially all of the radiation is within the last closed flux surface. The new behaviour and the major fraction of the radiation are associated with divertor emission.

JET experiments indicate that the proposed ITER scenario of entering the H-mode at low density, to reduce the threshold power, and then ramping the density to the desired operating point is feasible, at least in standard ELMy H-modes. Exploration of the full range of density accessible in H-mode was limited by the rise in neutral pressure observed in the NB ducts. Nevertheless, within these constraints, densities equal to the predicted Greenwald value were achieved while maintaining standard ELMy H-mode confinement ($H=1.8$), as shown in

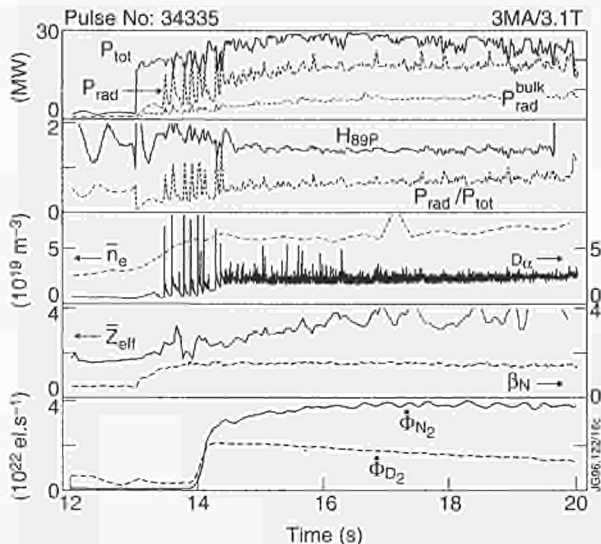


Fig.159: Overview of a radiative divertor H-mode in which an average power of $\sim 27\text{MW}$ was maintained for 5s with $P_{\text{rad}}/P_{\text{tot}} \sim 70\%$

Fig.158, and there is evidence from the observed behaviour of an increase in the highest attainable density with input power. It was found that as the plasma density increased, the ELM frequency increased while the amplitude decreased. This caused a loss of confinement and, eventually, the plasma could be driven back to the L-mode with $P_{\text{rad}}/P_{\text{tot}} \sim 40\text{--}50\%$ (Fig.158). In some discharges, this behaviour was reversed by increasing the input power. A point of relevance to ITER is that very high gas flow rates, up to 1bar/s , were employed in the course of high density H-mode experiments with the cryopump. This implies either that very large recirculating gas flows will be required in ITER, unless pellet injection is used or a mechanism for throttling the pumping speed is implemented.

To investigate the relative importance of plasma density, gas flow rate, and edge neutral pressure in determining the condition for the H-to-L back transition, gas fuelled H-mode discharges were established without the cryopump, so that relatively low, constant gas fuelling could be employed. The confinement enhancement decreased as the main chamber D_α signal increased, with little change in the main plasma density, suggesting that the edge neutral density determines the quality of confinement and the maximum density which can be achieved in the H-mode.

Radiative Divertor Plasmas

The low levels of intrinsic radiated power in JET steady-state H-modes, typically 15% between ELMs and $\sim 30\%$ averaged over ELMs, reflects the improved purity of plasmas in the pumped divertor configuration, where $Z_{\text{eff}} \sim 1\text{--}1.5$ is normal [22]. As a result, a substantial increase in radiated power

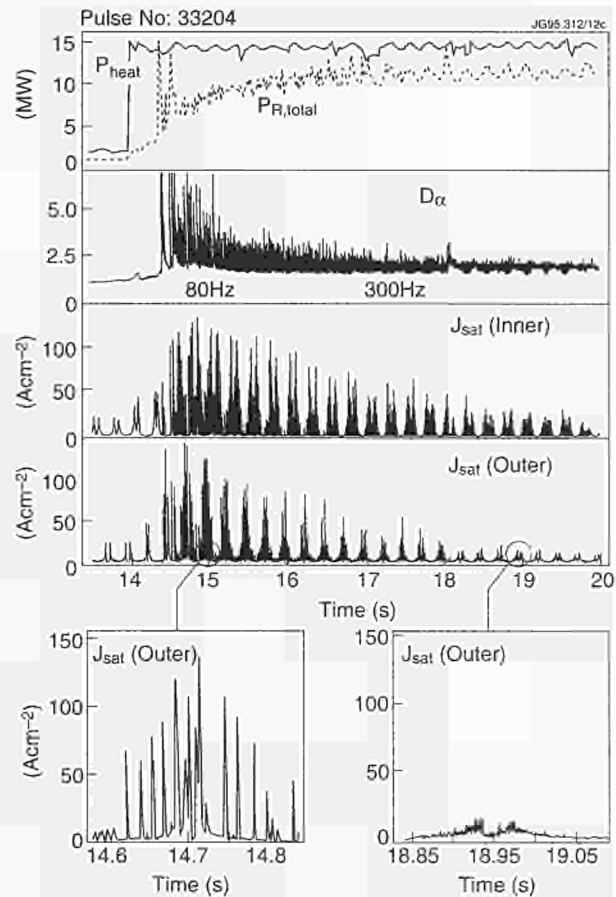


Fig.160: Overview of a radiative divertor H-mode in which $P_{\text{rad}}/P_{\text{tot}} \sim 80\%$. The ion saturation current at the inner and outer target, which is modulated by sweeping and ELMs, shows the decay typical of detached L-modes with deuterium puffing. The two lowest panels show profiles of the outer ion saturation current during the phase of giant ELMs and during the detached phase, illustrating the order of magnitude decay in the envelope. Note that the dip in the centre of the two profiles corresponds to the private flux region, which is exposed to the measuring Langmuir probe as the strike zone sweeps back and forward across the probe

was required to dissipate SOL conducted power and demonstrate divertor plasma regimes of interest to ITER. It was not possible to maintain H-mode confinement above radiated power fractions of 50% with pure deuterium puffing. Therefore, an extensive investigation of radiating divertor regimes utilizing extrinsic impurities was undertaken. These results have been described [23], and only the main points will be summarized here. Contrary to the ASDEX experience [24], neon proved unsatisfactory, as the transport timescales were too long ($\tau_{\text{ne}}^* \sim 6\text{s}$) in ELMy H-modes for a stable operating point to be established. In addition, results obtained with argon were of a preliminary nature. The discussion concentrates on the use of nitrogen as the radiating impurity.

The most successful approach to establishing a radiative divertor proved to be a combination of nitrogen puffing in the divertor and deuterium puffing in either the divertor

or main chamber. Use of nitrogen only (at the same nitrogen flow rate used in D_2+N_2 discharges) gave lower radiated power fraction and confinement. When D_2 and N_2 were injected, with an approximate electron ratio of 1/3 to 1/2, the radiated power fraction could be increased to $\sim 80\%$ and maintained in steady-state for periods of ~ 5 s. Total powers of up to 32MW were used and typical confinement enhancements of ~ 1.4 to $1.6\tau_E^{\text{ITER89-P}}$ obtained (Fig 159). Above 80% radiation, a MARFE formed and the plasma rapidly disrupted. This regime was characterized by rapid type III ELMs (frequency ~ 300 Hz), and the plasma parameters at the divertor target exhibited the behaviour usually observed in L-modes as detachment occurs (Fig. 160). That is, as the radiated power increased, I_{sat} rolled over at both the inner and outer targets, so that the envelope, modulated by ELMs, fell by an order of magnitude. The residual power flowing to the target was too small to be determined by infrared camera measurements, but the target Langmuir probes indicated that < 1 MW of power flowed to the target (of 15MW input power) during the detached phase.

Although the usual splitting technique used in JET to analyze the bolometer signals showed that $\sim 2/3$ of the radiation came from the 'X-point region', with the remaining 1/3 emitted from the bulk plasma, two-dimensional tomographic reconstructions of the radiation showed that the majority of the 'X-point' radiation was emitted from a region just above the X-point [25]. However, the transition from predominantly divertor radiation to 'X-point' radiation was a gradual one and, in principle, an operating point could be selected at a lower radiated power fraction, so that the radiating region was deeper in the divertor. Code calculations suggest that this 'nearly detached' state may be very useful, resulting in better impurity control, while maintaining acceptably low power flux onto the target. During the detached phase, active charge exchange spectroscopic measurements of plasma impurity content showed that Z_{eff} rose to ~ 3 , corresponding to $n_p/n_e \sim 64\%$. This compares with a typical Z_{eff} of ~ 1.5 in normal ELMy H-modes at equivalent powers (ie 'attached' and without impurity seeding).

Several aspects of the performance in this regime hold potential for ITER. In particular, stable operation at high radiated power fractions has been achieved and the target power fluctuations due to ELMs have been suppressed, though possibly by changing the nature of the ELMs rather than by buffering giant ELMs. In addition, the thermal confinement enhancement, which was typically $\sim 0.75\tau_E^{\text{ITER-93H}}$, is adequate for ITER and has been rou-

tinely obtained at $q_{95} \sim 3$. On the other hand, the enhancement compared to ITER89-P scaling was only ~ 1.5 , against an ITER requirement of 1.8, so that further confinement studies, preferably involving dimensionless parameters, are necessary to establish the appropriate scaling. This behaviour has been reproduced on both CFC and Be targets, demonstrating that the target material is not an issue in establishing such regimes. The most serious discrepancy with ITER requirements is that plasma purity was severely degraded due to the radiating impurity. In radiative divertor experiments, Z_{eff} rose with increasing power (and increasing level of injected impurity), so that at input powers of 15MW, $Z_{\text{eff}} \sim 3$. This compares unfavourably with the ITER requirement that $Z_{\text{eff}} \sim 1.2$, when helium ash is neglected. In addition, rather high levels of injected impurity were required, equivalent to $\sim 3 \times 10^{22}$ electrons of nitrogen, and a recycling impurity would probably be preferable. Finally, the plasma density in these discharges was usually influenced by the degraded confinement properties and was $\sim 75\%$ of the Greenwald value, rather lower than that required by ITER. Further experiments are necessary to investigate ways of controlling the plasma density and purity in this regime. The improved closure of the Mark II divertor configuration may have a profound impact on bulk plasma behaviour, affecting both energy and particle confinement, in detached plasma regimes.

Comparison of CFC and Beryllium Divertor Targets

During the last two months of the experimental campaign, the CFC divertor target tiles were replaced with beryllium tiles of similar design, and wide range of experiments, in various plasma configurations, was carried out in assessing the performance of beryllium as a target material. Analysis of tile heating data showed that the target surface temperature rose as $(P_{\text{tot}} - P_{\text{rad}})t^{0.5}$, as expected from the simplest, semi-infinite-solid analysis of power handling. Moreover, the success of the target tile design was confirmed by the absence of melting on tile edges. Nevertheless, several individual instances of surface melting with Be did occur in advance of the deliberate melt experiment which took place at the end of the campaign. The first was observed during the initial (unswept) power handling investigations at a measured temperature of $\sim 800^\circ\text{C}$, indicating that the spatial resolution of the IR camera limited the accuracy with which the

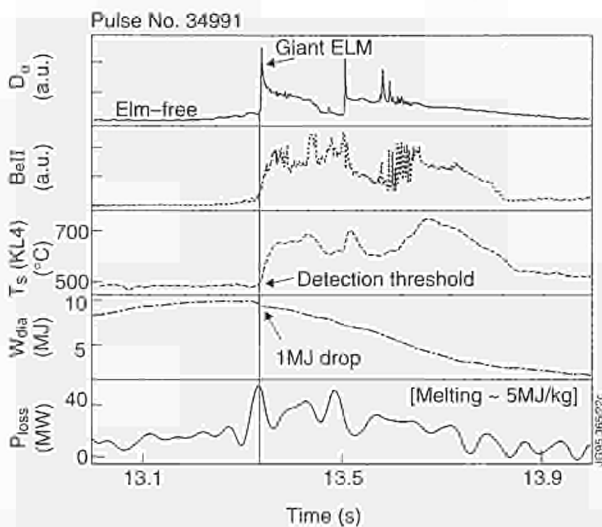


Fig161: Pulse in which melting of beryllium target was caused by successive giant ELMs each of which led to $\sim 1\text{MJ}$ of energy being deposited on the target in $<20\text{ms}$

peak temperature could be measured. Additional melt events occurred as a result of giant ELMs during high performance and high current experiments (Fig.161). Damage to the target tiles was of limited depth and did not restrict the scope of the programme when swept configurations were used. Total energies of $\sim 50\text{MJ}$ were deposited on the target in advance of the melt experiment, a figure limited only by the experimental time available, compared to 100MJ in equivalent plasmas on the CFC target. Experiments were also conducted using the side-plates at total deposited energies of $\sim 20\text{MJ}$ (the comparative figure with CFC was 50MJ). These figures are far superior to those achieved in previous beryllium target experiments. In the course of the melt experiment, energies of up to 125MJ were deposited on the target, causing additional melt damage.

The general characteristics of plasmas on the beryllium and CFC targets were very similar. Radiation levels, the approach to detachment and the density limit were similar in ohmic and L-mode plasmas. Initial impurity analysis shows that the carbon content of plasmas on the beryllium target was reduced below that of equivalent plasmas on CFC. Nevertheless, carbon, rather than beryllium, line radiation appeared to dominate the radiation losses. Oxygen emission was reduced by a factor of 2 on the beryllium target, but chlorine emission was increased by a comparable factor. In moderate to high density plasmas, fuelling efficiency was similar for CFC and beryllium, although in low density target plasmas used for high performance experiments, the recycling light was found to be reduced by a factor of 2 on beryllium, and the density increase observed during NBI was lower than on CFC.

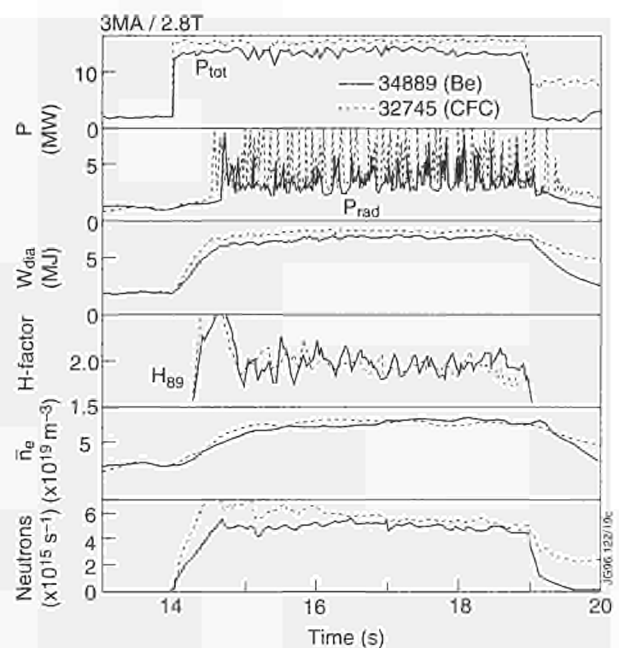


Fig162: Comparison of the global characteristics of equivalent steady-state H-modes using the CFC and Be targets

Steady-state H-modes were explored from 1 to 6MA at total powers of up to 30MW . Their general characteristics, including energy confinement and the H-mode power threshold, were again similar to those observed with CFC (Fig. 162), though with some detailed differences in ELM behaviour. Steady-state densities were very similar, as was the range of densities attained. At the highest densities, plasmas returned to the L-mode when the radiated power fraction was only 40-50%, that is well before divertor detachment occurred. Radiative divertor regimes were re-established using nitrogen and, for the first time, argon. As might be expected, these radiating divertor H-modes differed little from those established on CFC. Initial results with argon seeding were promising. At radiated power fractions of 80%, energy confinement enhancement factors of 1.6 relative to ITER89-P scaling were achieved, although $\sim 50\%$ of the radiation was emitted from within the separatrix.

In summary, the good power handling characteristics of the beryllium target allowed a full programme of experiments to be conducted, though singular giant ELMs caused surface melting. A further positive aspect is that although IR measurements made during disruptions found that the measured target temperature could approach 1000°C during the energy and current quenches, no disruption-induced melt events have been identified, either by inter-shot inspection of the target or by post-mortem analysis. In spite of this broadly positive operational experience with Be, CFC has clear advantages in power handling in the inertially cooled envi-

ronment of the Mark II divertor. On the other hand, no major changes in divertor performance have been observed in beryllium target experiments. In particular, detachment and H-mode performance are remarkably similar in plasmas on the beryllium and CFC targets. Thus, there does not appear to be a strong reason, from the divertor physics point of view, to choose one material in preference to another. However, in view of the significant carbon radiation observed in experiments on the beryllium target, it is likely that carbon sputtered from the main chamber, as well as carbon redeposited on the divertor target, played a significant role in beryllium target experiments.

Implications of the Mark I Divertor Assessment for ITER

Considerable progress has been made in the Mark I campaign on a broad spectrum of ITER Divertor R&D issues. One of the most significant achievements is in the area of steady state H-modes, where true steady state was achieved for times of up to $50\tau_E$, the flat-top duration being limited only by technical constraints on the tokamak. These discharges had typical H-mode enhancement factors of $1.8\tau_E^{ITER89-P}$ and, in the best of them, $Q_{DT}^{eq}=0.3$ was attained for several seconds. The use of the cryopump to control the density was an essential feature of these experiments.

As had been predicted by both code simulations and simple models, detached divertor H-mode discharges could not be attained in JET with the radiation arising solely from intrinsic impurities and hydrogenic processes. As the density was raised to initiate divertor detachment, the discharges reverted to L-mode, typically at radiated power fractions of 40-50%. By adding an extrinsic impurity ('seeding') it was possible to achieve radiated power fractions of 70-80% whilst remaining in H-mode and reducing the power to the targets to very low levels. This approach also eliminated the Type I ELMs characteristic of moderate density steady H-modes, replacing them with more benign type III, or threshold, ELMs. However, these discharges were characterized by (a) reduction of the H factor to values barely acceptable to ITER, (b) loss of hysteresis in the H-L back transition threshold, (c) rapid motion of the radiating zone to the X-point region, eliminating the advantages expected from a deep, large volume divertor, and (d) values of Z_{off} in the main plasma which are probably unacceptable when scaled realistically to ITER. The latter two problems are confirmed by detailed code calculations.

The solution for ITER may therefore be to abandon the concept of a fully detached divertor plasma, and operate either in pure hydrogenic fuel (plus He and intrinsic impurities) or with a very small (minimum acceptable) addition of a seeded recycling impurity. This would improve main chamber confinement and plasma purity, possibly restore the L-H-L mode threshold hysteresis, and retain full use of the divertor volume for energy dissipation. Preliminary EDGE2D calculations for the vertical target version of the ITER divertor suggest that this approach may be viable. The main residual problem would be the re-emergence of Type I ELMs, whose frequency and amplitude scaling to ITER is unknown, but which pose a potentially serious problem for the plasma facing surfaces. This strategy, which involves an integrated approach to maintaining main plasma confinement and purity at acceptable levels while attacking the problem of divertor performance, will be vigorously pursued in the Mark II campaign.

The problem of producing steady state H-modes at densities well in excess of the Greenwald value is looming as an increasingly difficult task for ITER. JET experience to date, as well as that worldwide, is that such operation is not possible using gas fuelling, except at low current values. No clear theoretical interpretation has yet emerged. However, it has to be noted that high current, high density, plasmas require operation in a technically constrained region of tokamak operating space, so that dedicated time must be allocated to the development of appropriate scenarios to separate the technical from the physics aspects of the problem. A positive aspect of the recent experimental campaign is that the use of the cryopump proved beneficial in raising the maximum density which could be achieved in the H-mode to values commensurate with the Greenwald limit. One source of concern which emerged in the course of these experiments was that excessive gas fuelling rates were required to achieve higher densities, so that more efficient fuelling, for example by pellet injection, is a pre-requisite for ITER. Attempts will be made in the Mark II divertor campaign to boost the line averaged density above the Greenwald value using centrifuge pellet fuelling.

Several other results of significance to ITER have been obtained:

- it appears that operating with the ion ∇B drift towards the divertor, as planned for ITER for reasons of H-mode access, will be acceptable. The target power

loading asymmetries at low- q are acceptable, and the detachment window appears larger than that with reversed B;

- chemical erosion of CFC in areas of high plasma flux appears to be slower than was predicted, increasing the expected lifetime of CFC components;
- indirect evidence suggests that wall sources dominate the impurity content of JET pulses, reaffirming the necessity of keeping the density of hydrogen neutrals in the main chamber to a minimum. This is one of the prime purposes of introducing the Mark II divertor;
- relatively small differences in divertor performance were seen in the Mark I divertor when changing from horizontal to vertical targets, or making changes in X-point height and field line connection length. This arose, at least in part, because of the ribbed structure of the Mark I target, and the relatively poor closure of bypass leakage, and thus may not be significant for predicting differences between the horizontal and vertical target versions of ITER. Once again, the Mark II divertor will provide a more definitive test;
- although helium transport in the main plasma appears sufficiently rapid for ITER purposes, the rate at which the helium reaching the boundary is exhausted was unsatisfactory in the JET experiments, probably due to poor performance of the cryopump with respect to He pumping. However, these results need to be scaled, based on JET and ASDEX experience, to ITER to see if its designed pumping speed should be adequate.

Conclusions

The divertor studies carried out in the course of this experimental campaign have produced considerable progress in areas of relevance to the Mark II programme and to ITER. Clearly, the Mark IIA and Mark IIGB geometries will be expected to have an impact on many of the topics discussed. Perhaps the main issue which emerges is that it is essential that improved divertor closure, combined with appropriate fuelling and pumping, should favourably influence plasma confinement and impurity retention. This is essential if the promising results obtained with radiative divertor plasmas are to be exploited in a reactor. Since the Mark II targets are specifically designed to address this problem, they seem well matched to the future requirements of the divertor programme. The major disappointment of the programme was the inability to fully exploit the argon frosting capability of the

cryopump to study helium exhaust, as a result of argon contamination of the vessel. This may benefit from the changed geometry of the Mark II, in that deuterium poisoning of the argon layer during recovery pulses should be reduced.

Experiments in the Mark I configuration have clearly demonstrated that an ITER-relevant scenario for the dissipation of exhaust power can be maintained in steady-state with acceptable confinement. The major problem which remains is that impurity contamination of the bulk plasma must be dramatically reduced, to approximately the level of intrinsic impurities, if a self-consistent ignition scenario is to be viable. Another source of concern is that complete detachment occurs very close to the density limit, which was invariably disruptive in this campaign and which would obviously be undesirable in ITER.

References

- [1] S Clement et al, *Controlled Fusion and Plasma Physics (Proc. 22nd Euro. Conf., Bournemouth, 1995)* III 309.
- [2] A Chankin et al, *ibid* III 289.
- [3] R D Monk et al, *ibid* III 293.
- [4] H Y Guo et al, *ibid* II 273.
- [5] A. Tabasso et al, PhD Transfer Report, Imperial College, London (unpublished)
- [6] K. Shimizu et al, *Plasma Physics and Controlled Nuclear Fusion Research (Proc. 15th Int. Conf., Seville, 1994)* paper IAEA-CN-60/D-P-I-2 (to be published).
- [7] K L Wilson and W L Hsu, *J Nucl. Mater.* **145-147** (1987) 727, and J Winter, *ibid* 131.
- [8] G Saibene et al, *ibid* ref [1] II 121.
- [9] P Harbour et al, *ibid* ref [1] IV 465.
- [10] M von Hellermann et al, *ibid* ref [1] II 9.
- [11] S J Davies et al, *ibid* ref [1] III 257.
- [12] The JET Team (presented by G C Vlases), *Plasma Physics and Controlled Nuclear Fusion Research (Proc. 14th Int. Conf., Würzburg, 1992)* Vol 1, IAEA, Vienna, 287 (1993).
- [13] The JET Team (presented by DJ Campbell), *Plasma Physics and Controlled Nuclear Fusion Research (Proc. 15th Int. Conf., Seville, 1994)* Vol 1, IAEA, Vienna, 527 (1995).
- [14] A Loarte et al, *ibid* ref [1] III 305.
- [15] The JET Team (presented by L Horton) *ibid* ref [13], Vol 1, 541.

- [16] A Taroni et al, *ibid* ref [1] IV 297.
 [17] K Günther, *ibid* ref [1] I 433.
 [18] The JET Team (presented by M Keilhacker), *Plasma Phys. and Contr. Fus.* **37** A3 (1995).
 [19] E Righi et al, *ibid* ref [1] II 73.
 [20] C G Lowry et al, *Controlled Fusion and Plasma Heating* (Proc. 17th Euro. Conf., Amsterdam, 1990) I 339.
 [21] D J Campbell et al, *Controlled Fusion and Plasma Physics* (Proc. 21st Euro. Conf., Montpellier, 1994) I 2.
 [22] M F Stamp et al, *ibid* ref [1] III 89.
 [23] The JET Team (presented by G F Matthews), *ibid* ref [18] A227.
 [24] A Kallenbach et al, *ibid* ref [13], paper IAEA-CN-60/A2/4-P-13 (to be published).
 [25] R Reichle et al, *ibid* ref [1] III 85.

Tokamak Concept Improvements

The main aim has been to study those physics areas in which JET can make an important contribution to ITER, with particular attention given to development of improved confinement scenarios through current profile control. Some experiments carried out in 1995 were a continuation of those started in 1994. The main areas covered have been:

- High β experiments and Advanced Tokamak scenarios;
- Profile Control Experiments with Lower Hybrid Current Drive;
- Shear Reversal Experiments;
- Ion Cyclotron Resonance Heating Experiments;
- Toroidal Alfvén Eigenmodes excitation;
- Toroidal Field Ripple Experiments;
- Real Time Power and Burn Control Experiments.

Quasi-Steady-State Advanced Tokamak Scenarios

A steady-state tokamak reactor is likely to need a substantial fraction of the plasma current provided by the neo-classical bootstrap effect: this would require $\beta_{pol} \gg 1$, which implies good energy confinement without using very high plasma current. If very high toroidal fields are to be avoided, such plasmas would also need to achieve $\beta_N \geq 3$. The study of confinement and stability character-

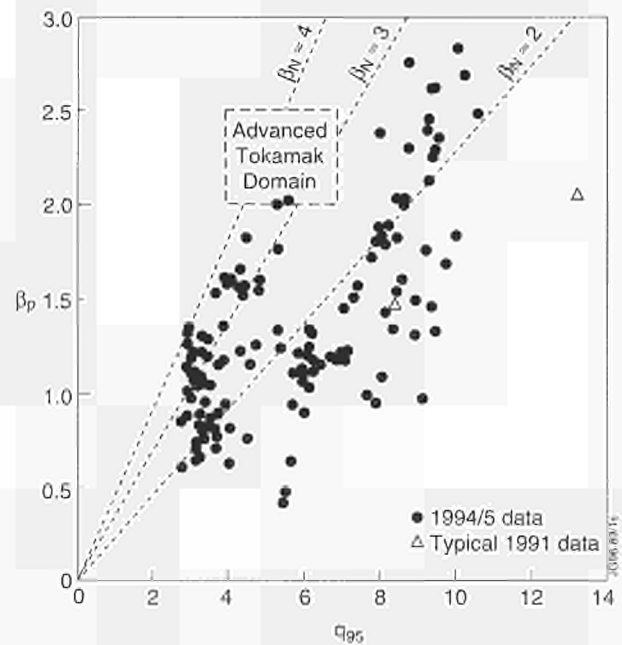


Fig.163: Achieved value of poloidal beta, β_p (diamagnetic), versus q_{95} .

istics of steady-state plasmas in the *Advanced Tokamak* domain (i.e. high β_{pol} and high β_N), is essential to assess the prospects for steady-state reactor concepts.

Early experiments in 1994 highlighted the main differences with respect to the pre-1994 JET configuration. Improved power handling was achieved in the new pumped divertor configuration: this allowed long pulse high power heating of ELMy H-mode plasmas which reached quasi-steady-state conditions, with respect to plasma density and stored energy. However, significant additional heating power was required to reach the same value of β_{pol} in the ELMy regime. This, together with the lower plasma density in these plasmas, resulted in a significant fraction (~30%) of the plasma stored energy being due to fast particles. Operation in higher density regimes at low plasma current was not achieved.

Experiments in 1995 extended the operating regime towards the *Advanced Tokamak* domain [1]. Fig.163 shows the achieved values of poloidal beta (β_{pol}) plotted against q_{95} for plasma currents in the range $I_p \approx 1.0 - 1.75$ MA. Approximate lines of constant β_N are shown for the pumped divertor configuration and a notional *Advanced Tokamak* domain, typical of a reactor concept such as SSTR [2], is indicated. Plasmas approaching the overall conditions required for a steady-state reactor have been obtained. In 1 MA/1.7 T discharges, with $q_{95} \approx 5.5$, the values of $\beta_{pol} \approx 1.9$ and $\beta_N \approx 3.3$ have been simultaneously achieved. The bootstrap current fraction in these discharges is estimated to be in the region of 50%, which

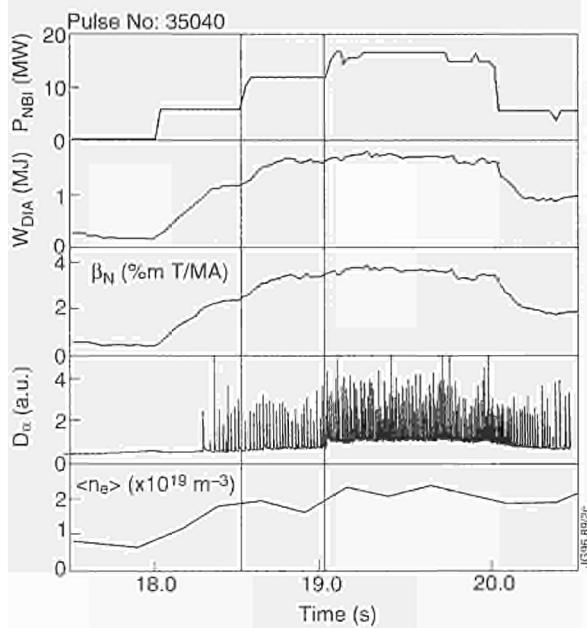


Fig.164: Time evolution of a plasma at 1MA/1T and $q_{95} \approx 3.1$

is insufficient to provide the necessary fraction ($>70\%$) of the plasma current required for a true Advanced Tokamak.

At low q_{95} , the high values of β_N have been achieved with predominantly NB heating, whereas combined NB and ICRF heating has been employed at high q_{95} . ($B_T > 2.6\text{T}$ at 1 MA). At high values of q_{95} , the plasma performance, and consequently, the value of β_N , has been limited by the plasma confinement and the available additional heating power. At $q_{95} < 4$, however, the plasma stored energy exhibits confinement degradation at high power levels which is suggestive that a global β limit may have been reached.

Figure 164 shows the time evolution of a pulse at 1MA, 1T and $q_{95} \approx 3.1$. The NB heating power is increased in three steps to 17.5MW: the total plasma stored energy increases at the first two power steps, but at the third step no significant further increase was observed. The maximum value of β_N was about 3.8. The frequency of the ELMs in this discharge increased at the final step, and this may be the cause of the reduced confinement. The estimated fast ion stored energy for this plasma represents about 40% of the plasma stored energy during the high power heating phase: this results in a more modest value of β_N , when only the thermal energy is considered.

Transient phases of increased confinement have been observed, when in some high β_{pot} discharges, the stored energy can suddenly increase at constant input power [3]. The improved confinement is correlated with oscillations in the plasma current at high β_{pot} , which lead to large variations in the peripheral current density. This feature

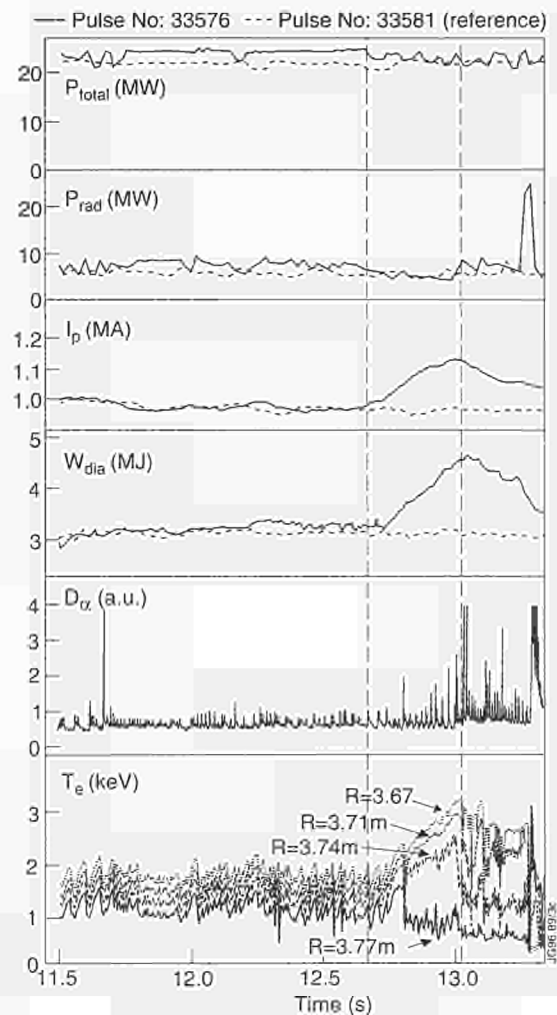


Fig.165: High β_{pot} with current ramp

was exploited by using pre-programmed ramp-up of the plasma current (Fig.165). The edge electron temperature increased during the current ramp, but no transition to ELM-free conditions was observed.

A possible explanation for such behaviour is suggested by analysis of ballooning stability at the plasma edge [4]. In the pumped divertor configuration, the edge pressure gradient was limited to the first ballooning stability region. Access to the unconditionally stable (or second stable) region was possible at high β_{pot} , if the current density in the plasma periphery was large enough. However, the ratio of $j_{edge}/\nabla P_{edge}$, due to the bootstrap current was insufficient to reach this regime. Calculations using the transport code TRANSP suggest that the increase in j_{edge} obtained by ramping up the current during the high β_{pot} phase can, in combination with the bootstrap effect, result in access to the unconditionally stable regime near the edge (Fig.166). This would allow the edge pressure gradient, and consequently the confinement, to be increased. The increased pressure gradient may then

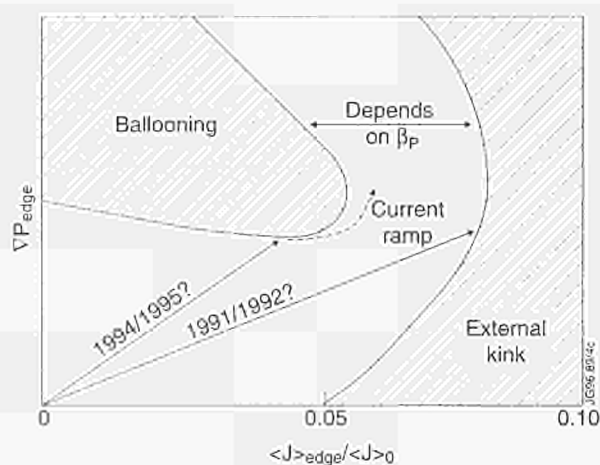


Fig. 166: Stability diagram of ∇P_{edge} versus $\langle j \rangle_{edge} / \langle j \rangle_0$

provide sufficient bootstrap current to maintain the edge stability with respect to ballooning modes without need for a continuous ramp. Such a plasma may, however, be unstable with respect to external kink modes due to the high edge current density.

The 1994/95 high β_{pol} and high β_N plasmas represent a significant step towards demonstrating a long pulse capability for ITER. However, further experiments are necessary to demonstrate a steady-state reactor capability. These are:

- operate a higher thermal β_{pol} and higher confinement (or power) to achieve a higher bootstrap fraction, 70%-100%, and to truly access the steady state tokamak domain;
- reduce the non-thermal fraction of the plasma stored energy to reproduce reactor conditions. This requires operation at higher density and higher confinement H factor, possibly using the current ramp technique for accessing the second stable regime, which has yet to be exploited in low q_{95} plasmas for steady state and high performance applications in JET;
- achieve longer ELMy H-mode plasmas (10-20s), to allow for current diffusion and assess effects of high bootstrap current on stability and confinement. In this respect, the use of LHCD profile control to establish a broad target current profile could be beneficial and needs to be assessed;
- investigate the β limit, at $q_{95} \sim 3-6$, for high bootstrap current plasmas to assess the need for very high toroidal field in steady state tokamaks.

Profile Control Experiments with Lower Hybrid Current Drive

Full Current Drive with LHCD alone has been achieved in X-point configuration in the range 0.7-3MA [5]. These

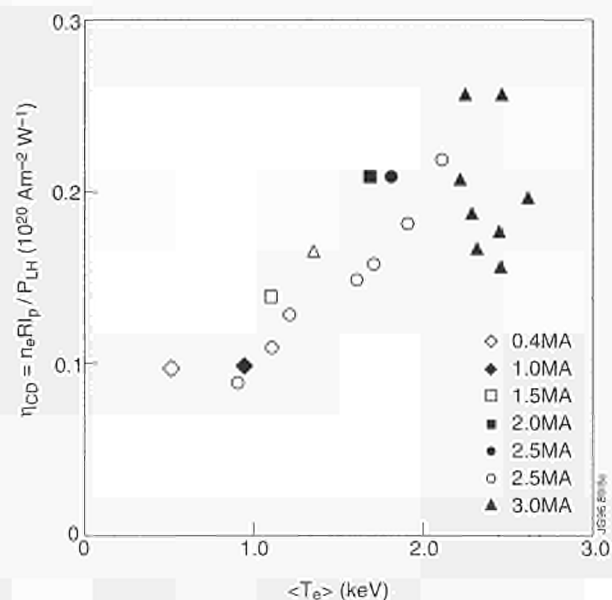


Fig. 167: Scaling of LHCD efficiency, for full current drive discharges

experiments have been carried out at high toroidal field, $2.8T \leq B_T \leq 3.4T$, and low to medium density, $\langle n_e \rangle \approx 1 - 2 \times 10^{19} m^{-3}$. In such conditions, it has been estimated, from the change in kinetic and magnetic energy, that 70% - 90% of the LH launched power is absorbed by the plasma. The current profile during LH full current drive is usually found to be broader than the ohmic profile: long pulses are needed to reach steady-state conditions.

For $\langle n_e \rangle > 1.2 \times 10^{19} m^{-3}$, the current drive efficiency increases, in agreement with theory and with previous experiments, with the volume averaged temperature $\langle T_e \rangle$ up to $0.26 \times 10^{20} AW^{-1} m^{-2}$ (Fig. 167). The variation of Z_{off} is negligible in the subset of data in Fig. 167. At low density $\langle n_e \rangle < 1.2 \times 10^{19} m^{-3}$ and high LHCD power, $P_{LH} > 4MW$, the current drive efficiency is lower than expected. In these conditions, a lower intensity of the hard X-ray emission is measured than anticipated from code calculations. A possible explanation is the overdriving of the plasma current in discharges with excessive LHCD power. A negative DC parallel electric field, which counteracts the LH wave field drive, is induced in the plasma region where the local LH driven current is larger than the ohmic current, with the result that the efficiency of driving electrons is reduced. Typically, for 2 and 3MA plasmas, this region is approximately at mid-radius. Analysis of the loop voltage profile has been carried out by evaluating the time derivative of the poloidal flux, obtained from EFIT equilibrium reconstruction including constraint on polarimetry. The analysis shows that a negative loop voltage of $-0.15V$ has been obtained in the region

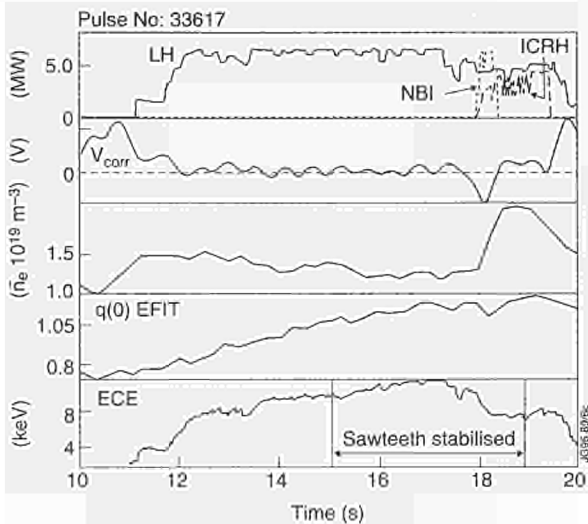


Fig. 168: LH sawtooth suppression at 3MA

$0.5 < \psi < 1.0$ during high power LHCD at low density. This supports the idea of the current being overdriven. Ray tracing + 2D Fokker-Planck calculations show the negative DC electric field can strongly reduce the driven current, but discrepancies still exist between experimental data and numerical simulations.

LH profile control experiments have been carried up to $I_p = 3.5\text{MA}$. In the majority of cases, the current profile is broadened by LHCD as suggested by the decrease in internal inductance and a transient negative overshoot of the loop voltage at the start of LH. This is confirmed by the broad or hollow hard X-ray emission profiles measured by the Fast Electron Bremsstrahlung (FEB) camera. The FEB profiles are more peaked at low electron density and become progressively more hollow with increasing density, electron temperature and plasma current. The broadening of the current profile is consistent with off-axis LH deposition and reproduced by numerical simulations [6].

Sawtooth stabilisation during LH power injection has been obtained in conditions near full current replacement up to 3MA (Fig.168). At low density of $n_e \approx 1 \times 10^{19} \text{m}^{-3}$, suppression of the sawtooth activity can be followed by a significant increase in electron temperature. Due to the vertical position of the magnetic axis being well above the vessel equatorial plane, the LIDAR scattering diagnostic, located in the midplane, does not see the central plasma region. The innermost measured value of T_e in these cases is about 8keV, with the profile becoming more peaked (Fig.169). This high temperature phase is also characterised by very low MHD activity. The increase in electron temperature suggests that some enhanced confinement is

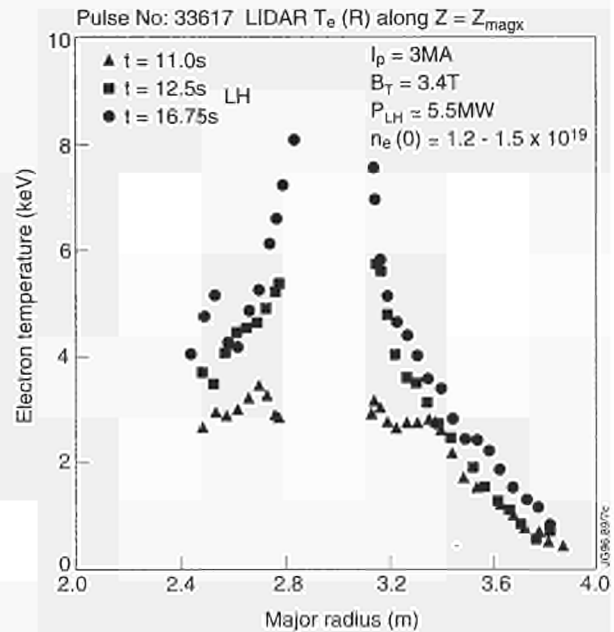


Fig.169: LIDAR scattering T_e profiles as a function of radius established in the central plasma region. Simulations of the plasma current profile evolution have been carried out with the JETTO transport code, using LH power and current profiles computed by Ray-Tracing + Fokker-Planck code [6]. These suggest that, given the long resistive diffusion time in these plasmas, the length of the applied LHCD pulse of 13s, limited by the length of the flat-top time duration at high toroidal field, was not sufficient to establish a fully steady-state condition.

The effect on hot-ion H-mode performance [7] of varying the target current density profile has been studied with LH profile control. The assessment of the effect of LH profile control on the performance of the hot-ion mode is complicated by the variety of MHD events which can cause the collapse of the fusion performance. Typical events are Giant (type I) ELMs, internal MHD and low frequency MHD activity localised towards the outside of the plasma [8,9].

In the experiment, LHCD alone was applied during a long ($\geq 5\text{s}$) L-mode phase in a pulse at low density; this was followed by a high power NB or NB+ICRH hot-ion H-mode. About 100ms before the NB injection, the plasma was moved further away from the limiter and the LH launcher was retracted behind the limiter. A first set of experiments was carried out on carbon tile targets at maximum available NB power of 15-20 MW.

In the cases with LHCD, the value of $q(0)$, given by the magnetic reconstruction code EFIT, was consistently higher, in excess of unity, at the onset of the H-mode in comparison with the cases without LHCD (Table XVI). Sawteeth were

Table XVI

		With LHCD	Without LHCD
High power NBI	$q(0)$	$1.2 \pm 20\%$	$0.75 \pm 20\%$
	ℓ_s	$0.85 \pm 10\%$	$1.15 \pm 10\%$
	edge shear	$3.3 \pm 10\%$	$3.8 \pm 10\%$
Low power NBI	$q(0)$	$0.9 \pm 20\%$	$0.65 \pm 20\%$
	ℓ_s	$1.0 \pm 10\%$	$1.2 \pm 10\%$
	edge shear	$3.7 \pm 10\%$	$4.2 \pm 10\%$

stabilised during the LH phase. The following ELM-free H-mode was consistently sawtooth-free, and it remained so even if some ICRF heating was added (Fig.170).

The H-mode performance in terms of stored energy and neutron rate was comparable for the cases with and without LHCD. However, with LHCD, the duration of the high performance phase was reduced and the termination event was a Giant ELM. In the comparison with discharges without LHCD the termination was delayed and it was brought about by an outer mode, followed by a large ELM. The explanation for the shorter ELM-free phase in the cases with LHCD was in the link between plasma shape and ELM stability in hot-ion H-modes: plasma configurations characterised by strong shaping, (i.e. high triangularity and edge shear), generally yielded longer ELM-free periods. Since the main effect of LHCD, in these discharges, is to broaden the plasma current profile, the values of internal inductance, edge shear and triangularity at the start of the NB phase were significantly lower than the cases without LHCD (Table XVI).

To minimise the differences due purely to plasma configuration between cases with and without LHCD, a further set of experiments was carried out in configurations that yielded relatively high edge shear, even at low values of internal inductance. These discharges were carried out during the beryllium target assessment phase and were also limited in NB power to 10MW. In the LHCD cases, the initial edge shear was lower but the length of high performance phase was comparable to the cases without LHCD.

Sawteeth were stabilised during the LHCD phase. In some cases at LHCD power levels <5MW, stabilization was not robust and a small sawtooth was observed about 0.5s into the H-mode: it occurred well before the peak of neutron rate and energy and it had no effect on the performance. The remainder of the high performance phase was sawtooth-free. In the cases with LHCD, the recycling was marginally higher at the start of the H-mode and type III threshold ELMs were also observed.

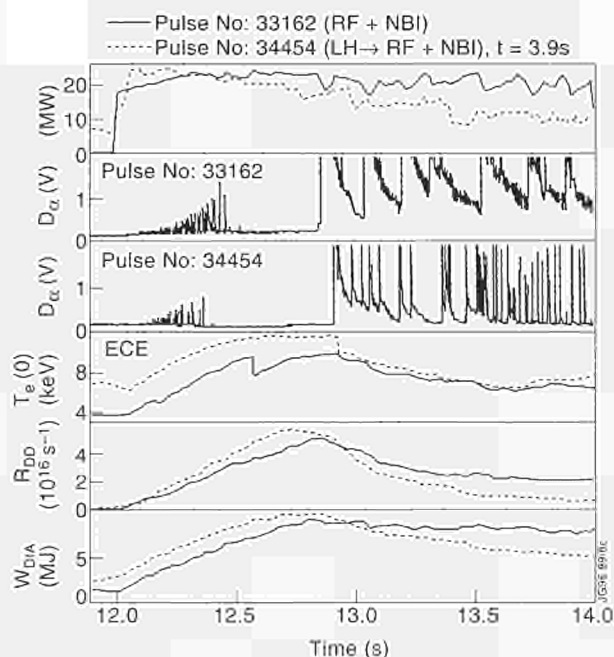


Fig.170: Comparison of RF + NB hot-ion H-modes with and without LHCD profile control

The hot-ion H-modes not preceded by LHCD were terminated by a large ELM followed by an outer mode. The character of the termination changed with LHCD profile control: the rise phase of the neutron rate was ended by a weak MHD activity, which resulted in a steady state neutron rate until the ELM-free phase was terminated. This mode had a frequency of about 10kHz and the associated temperature perturbation started outside $R=3.6m$. This mode had, therefore, the usual characteristics of the so-called outer mode, but in these cases, it had only a weak effect on the H-mode performance. Further optimisation is needed to benefit from these encouraging results.

Shear Reversal Experiments

Initial experiments aimed at exploring the possibility for JET to operate in a scenario characterised by non-monotonic q-profiles were carried out in 1994. A stable route to a reversed shear equilibrium was first studied numerically with a combination of LHCD and fast wave (FW) current drive codes, of the JETTO transport code and the CASTOR MHD stability code. The scenario was then tested experimentally by using early electron heating with LHCD and ICRF during the initial fast ($di_p/dt \approx 0.75$ -1MA/s) current rise with an early X-point configuration formed 0.5s after breakdown; this was followed by high NB power (Fig.171) [10].

One of the main problems encountered in such a scenario was the control of the plasma shape in elongated

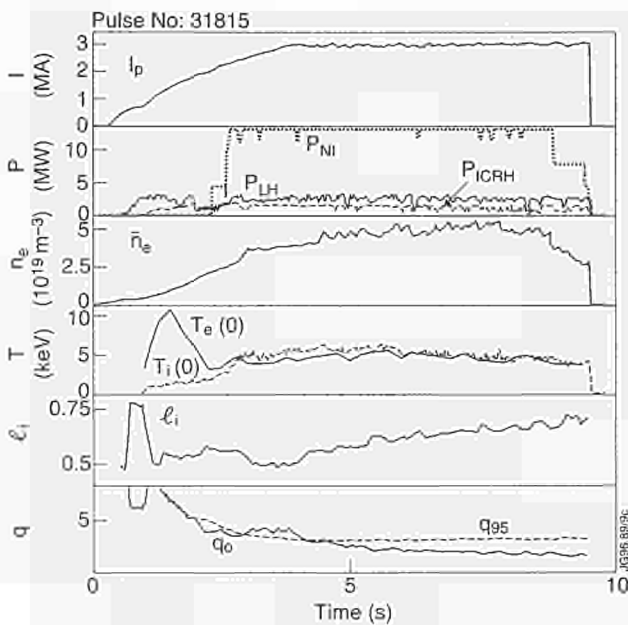


Fig.171: Time evolution of plasma parameters for shear reversal experiment

plasmas, when the internal inductance ℓ_i had large variations. Both the ICRH and the LHCD systems required accurate positioning and control of the curvature of the last closed flux surface (LCFS). To maintain constant coupling conditions, the variation of ℓ_i needed to be anticipated for each discharge, based on the expected level of injected additional heating power. Several operational constraints on the heating and current drive systems had also to be taken into account in designing the experimental scenario.

In the early stages of the 1994 campaign, the feedback control of the LHCD launcher position had not been fully commissioned and only the pre-programmed movement of the launcher could be used. The launcher was positioned level with the poloidal limiter to achieve the optimum coupling conditions. LHCD power injection started just after breakdown, before the formation of the X-point. Coupling of ICRF power throughout the current rise was made difficult by changes of the plasma shape, of the distance of the LCFS to the limiter and modifications in the scrape-off layer conditions with changing q_{95} .

Although early injection of NB power is possible at JET, the plasma density prior to injection had a lower limit of $\sim 3 \times 10^{19} \text{m}^{-3}$ to avoid excessive beam shine-through. A relative high density was therefore needed before NB power could be injected, and this was achieved by heavy gas fuelling close to the density limit in the current rise phase. The required density was reached 1.8s after breakdown. In 1994, this limitation prevented the exploitation of regimes

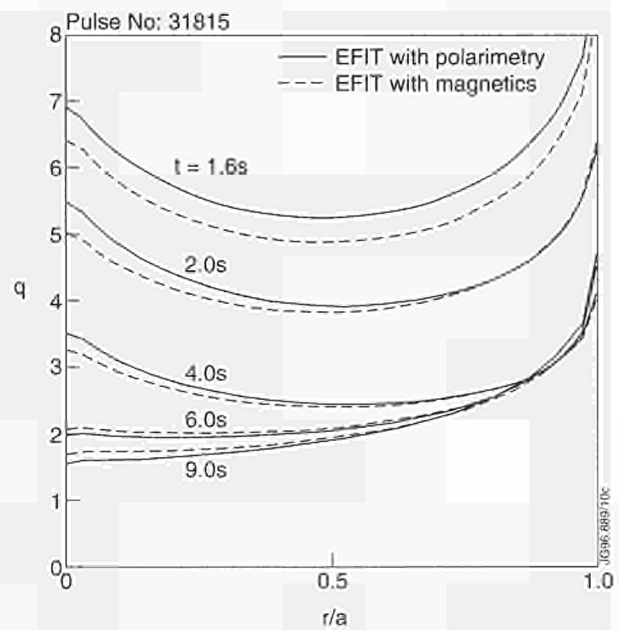


Fig.172: Comparison of safety factor profiles from EFIT code, with and without inclusion of polarimetric measurements

characterised by NB injection at low density; for 1995, a different NB power density threshold was introduced, allowing injection for an initial 0.5s at much lower density. Unfortunately, no further successful experiments on shear reversal were carried out in 1995 due to technical problems. More specifically, the main problem has been the unreliability of the zero premagnetization current breakdown mode (mode B), which is crucial for early X-point formation.

Great effort has been devoted to the analysis of the experimental q-profile obtained with the equilibrium reconstruction code EFITJ. Figure 172 shows a comparison of profiles from EFITJ using only magnetic data and polarimetric measurements of Faraday rotation angle as a further constraint. The inclusion of polarimetric measurements slightly modifies the q-values, but does not alter the shape or the time evolution of the profiles. Shear reversal is achieved in the central part of the plasma from the start of the discharge, with $q_0 > 3$ and $q_{\min} \geq 2.5$; a gradual transition was observed from negative shear to monotonic q-profiles during the current flat-top.

With shear reversal, high central electron temperatures and peaking of the electron temperature profile were observed during the LHCD dominated central electron heating phase. Local transport analysis were carried out, both with the 1.5D JETTO code, in interpretative mode, and with the TRANSP code, using LH power and current profiles calculated by a Beam Tracing + Fokker Planck code. In the low density phase, the LH power was peaked on-axis and was the dominant term in the input power

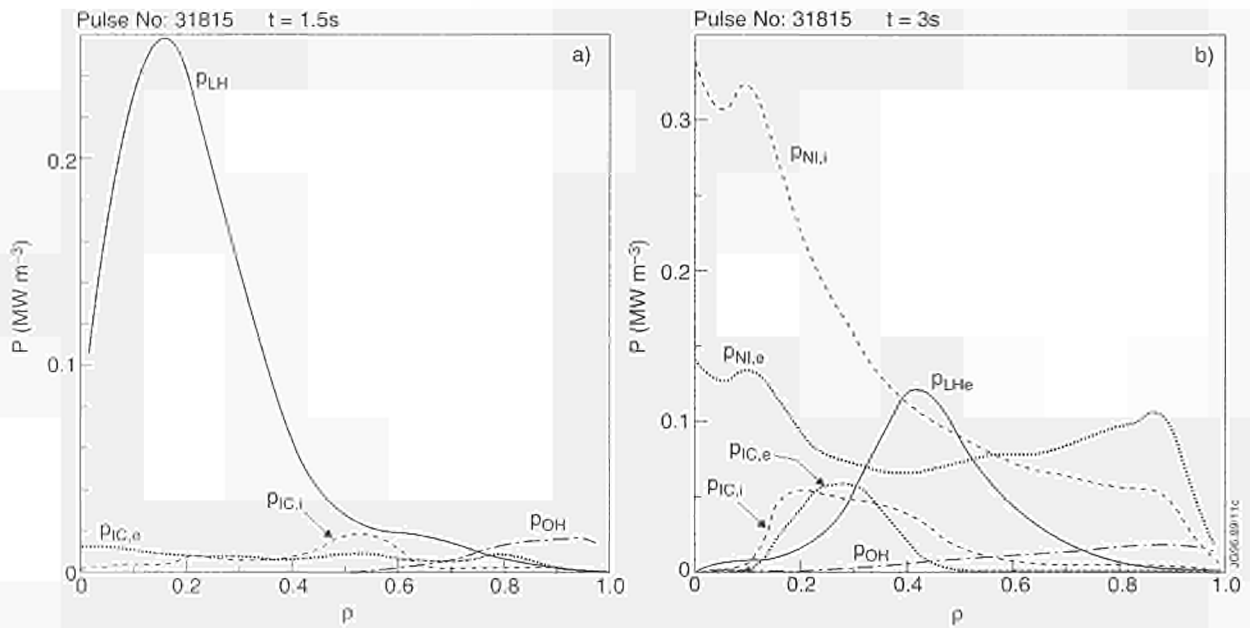


Fig.173: Power deposition profiles for shear reversal experiments: (a) LH dominated phase; and (b) NB dominated phase

(Fig.173(a)). The LH deposition subsequently shifted off-axis because of the increasing density (Fig.173(b)); the beam deposition profile was broad. During the density rise, the value of $T_e(0)$ dropped and remained $\sim 5\text{keV}$ during NB heating. Local transport analysis with TRANSP showed a strong reduction of the radial heat transport in the central region of negative shear during the LHCD dominated phase of central electron heating. The effective heat conductivity χ_{eff} was more than an order of magnitude lower than the neo-classical ion heat conductivity χ_{neo} (Fig.174) and approached the value of the neo-classical electron heat conductivity. At the time of transition to monotonic q profiles, a smooth transition was also observed in χ_{eff} towards χ_{neo} in the central plasma region. Conditions of anomalous transport with $\chi_{\text{eff}} \sim 2\text{-}5 \chi_{\text{neo}}$, prevailed in the outer region throughout the whole discharge. Using the JETTO code in its semi-predictive mode (Bohm + Gyro-Bohm model), was found that the early improved confinement phase, temperature profiles and their time evolution, could be reproduced by neglecting the Bohm term inside the negative shear region.

The MHD stability of shear reversal configurations has also been studied in detail. The trajectory of a shear reversal discharge in the $\ell_i - q(a)$ diagram is shown in Fig.175. Potentially, MHD-unstable regions were crossed during the current rise, when ℓ_i remained in the range $\ell_i = 0.5 - 0.6$ for $q(a) \geq 3$. However, no major MHD instabilities were encountered in the fast current rise phase during the build-up of the reversed shear equilibrium. Stabilisation of kink and tearing modes may have resulted from a reduced resistivity with early additional electron heating.

MHD analysis of the shear reversal experiments with the CASTOR code confirms stability against ideal and resistive internal modes and external kink modes up to $\beta_{\text{pol}} \sim 1.5$, while ballooning stability was predicted up to $\beta_{\text{pol}} \sim 1.8$. A parametric study of the stability of low- n infernal modes has been undertaken using the experimental pressure and current profiles. For the conditions in the experiment, with $\beta_{\text{pol}} \leq 0.4$, full stability was found: stability was also predicted for $q_{\text{min}} \geq 2$ up to $\beta_{\text{pol}} \sim 2$ and $\beta_N \sim 2$.

Ion Cyclotron Resonance Heating

ICRF heating offers a large variety of possible applications to JET plasmas, depending upon the physics of

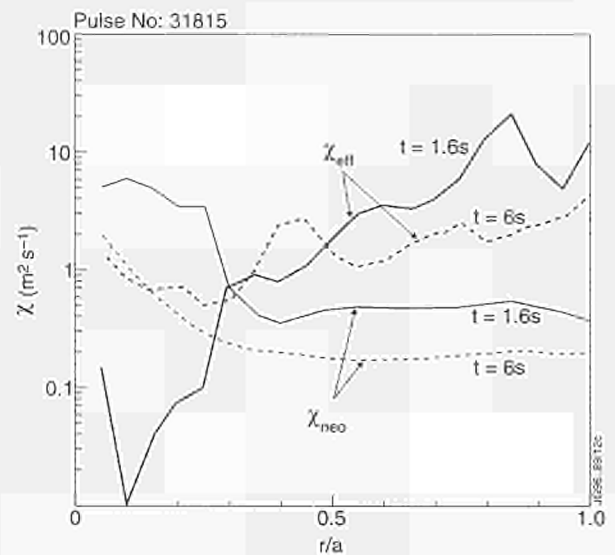


Fig.174: Radial profile of χ_{eff} and neo-classical ion heat conductivity χ_{neo} from TRANSP

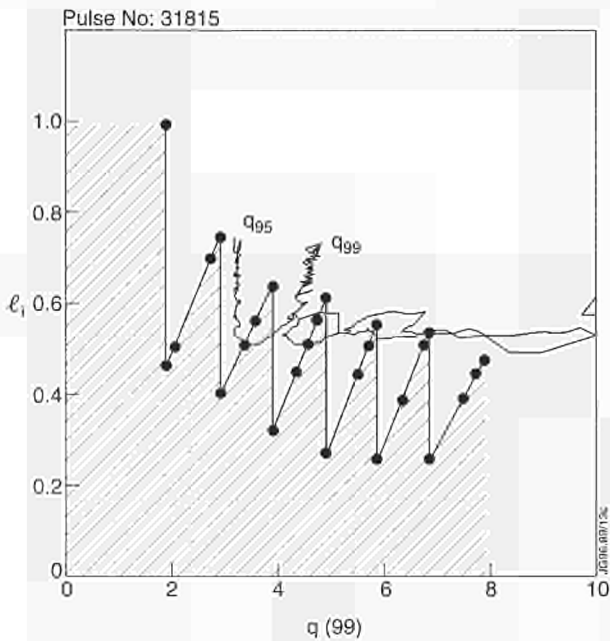


Fig. 175: Trajectory of shear reversal discharges in the l_i - q_{99} plane

wave-particle interaction. Experiments have been carried out in the fields of:

- Ion Cyclotron Resonance at fundamental frequency of minority species;
- Ion Cyclotron Resonance at higher harmonics;
- Direct Electron Heating via TTMP;
- Direct Electron Heating via Mode Conversion into Ion Bernstein Waves;
- Fast Wave Current Drive.

A substantial fast ion population at energies from few hundred keV up to few MeV is produced by fundamental resonance on minority or higher harmonics of bulk plasma. These scenarios represent the closest way to simulate heating effects and MHD stability properties of JET plasmas with a large alpha-particle population. These are also particularly relevant as a scale model for ITER, where the heating methods foreseen (alphas, NBI and ICRH) will primarily heat electrons.

ICRF Heating of High Performance Plasmas

The longest ELM-free H-modes and highest D-D reaction rates in the pumped divertor have been obtained in configurations with substantial triangularity, $\delta \approx 0.3$, and strongly expanded flux surfaces in the divertor [7]. Experiments on RF heating of such hot-ion H-mode plasmas have been carried out at $I_p = 3 - 3.5$ MA and $B_T = 3.2$ T [11].

The addition of on-axis ICRF heating to ELM-free hot-ion H-modes created by NB heating can enhance the per-

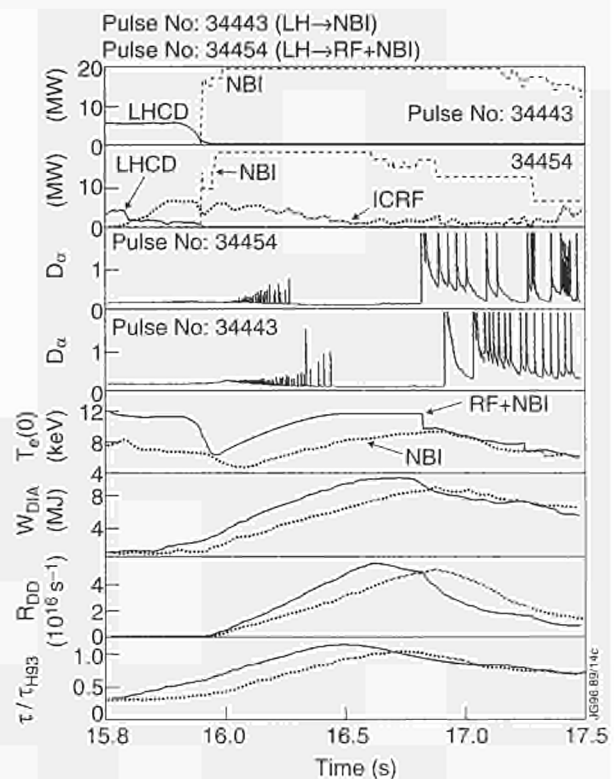


Fig. 176: Comparison of hot-ion H-mode performance with NB only and ICRH + NB heating

formance of these plasmas. In Fig. 176, a case of combined ICRF+NB heating (Pulse No. 34454) and a pulse with NB power alone (Pulse No. 34446) are compared. In both cases, the H-mode phase is preceded by a long LHCD pulse, which establishes a broad current profile with $q(0) > 1$, and no sawteeth were observed during the high performance phase, contrary to cases where LHCD profile control was not used. The combined heating case showed an increase in D-D reactivity and stored energy. Calculations with the TRANSP transport code showed very good agreement with the measured neutron rate (Fig. 177): the increased reactivity was due to increased ion pressure and did not require second harmonic beam acceleration for interpretation.

The local transport analysis also showed that a substantial fraction of power in the centre of the plasma was due to ICRF, despite the relatively low ICRF power (~ 6 MW) compared to ~ 17 MW of NB power. In particular, in these conditions, about 30% of ICRF power went to the ions and 70% to electrons, while the reverse was true for NB injection. In the central region, $p \leq 0.3$, only 26% of the total NB power was deposited, compared to 75% of the RF power. This implied that, in the centre, the ions absorbed $\sim 19\%$ of the NB power and $\sim 23\%$ of the RF power: in the same region, the electrons absorbed $\sim 53\%$ of the RF power and only $\sim 7.5\%$ of the NB power.

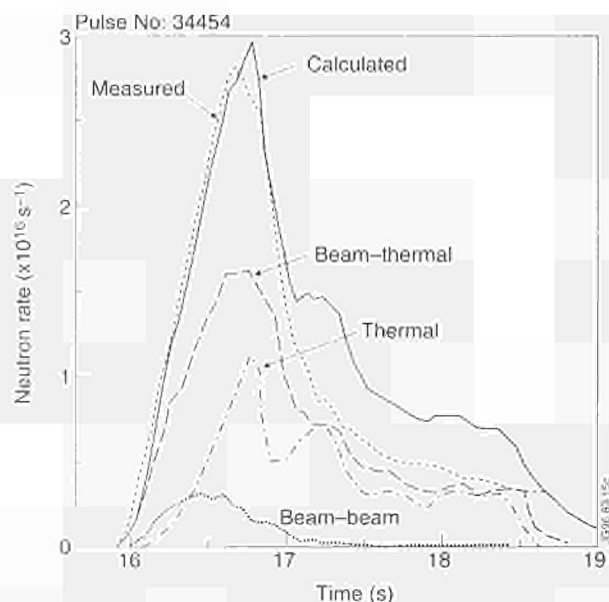


Fig.177: Neutron rates for ICRH + NB hot-ion H-mode

These initial experiments have shown the importance of using ICRF heating in high performance H-modes as a tool to study hot-ion mode performance with a larger fraction of thermal fusion power, compared to NB only, and to simulate alpha-particle effects, heating and MHD stability characteristics. Adding ICRF power would also be valuable in studying the termination of the hot-ion H-modes at input power levels above 20MW. For such experiments, avoidance of large and monster sawteeth is crucial: the use of LHCD profile control to tailor the target current profile and stabilise sawteeth for hot-ion H-modes could be valuable in allowing efficient on-axis ICRF heating in high performance regimes.

H-modes with ICRF Heating Alone

H-modes have also been obtained with ICRF heating alone in a large range of configurations: magnetic fields (1.6 to 3.4T) and plasma currents (1 to 5MA), both in standard dipole (0π/0π) and phased (0ππ/0) operation of the RF antennae. The study of the physics and characteristics of ICRF H-modes can supply useful information to predict the behaviour of H-modes driven by MeV ions or alpha-particles in ITER.

ICRF only H-modes are characterised by a fairly quiescent D_{α} signal, with typically long ELM-free periods or small ELMs compared to those induced by NBI. These characteristics are maintained even at high plasma current. Although RF H-modes have been obtained with different plasma configurations and currents, the power threshold does not seem to differ

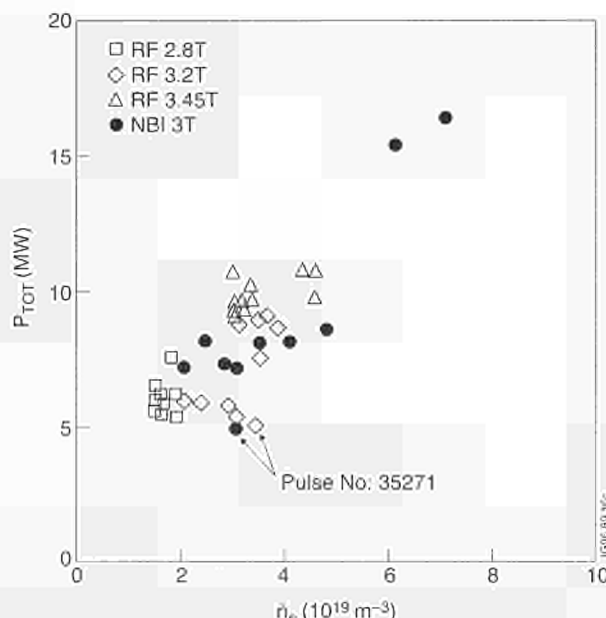


Fig.178: H-mode power threshold for ICRF-only and NB cases

substantially from that obtained with NB injection (Fig.178) [12].

One significant difference between ICRF and NB heating was the fact that the former did not transfer any significant torque to the plasma. This allowed studies of the variations of toroidal rotation in L- and H-mode plasmas and its relationship with improved energy and particle confinement. During RF-only H-modes, a clear correlation was observed between the transition to H-mode and plasma acceleration in the toroidal direction, in the same sense of the plasma current. A quantitative relationship between rate of

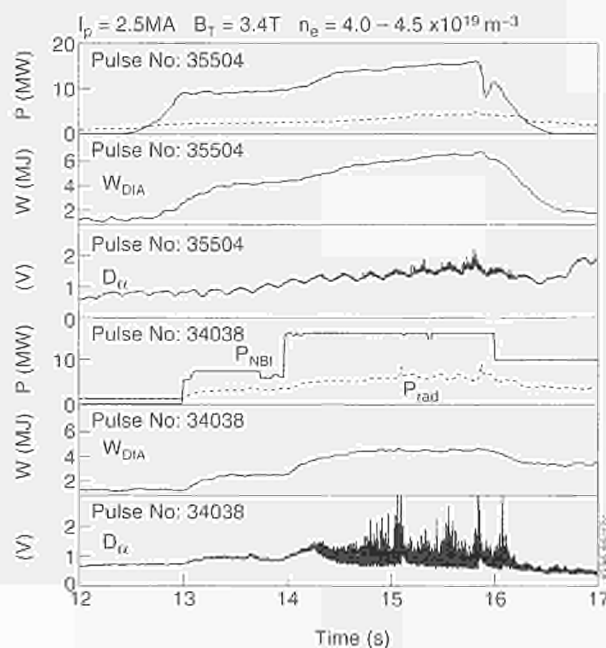


Fig.179: Comparison between ICRF and NB H-modes ($I_p = 2.5MA, B_T = 3.4T, n_e = 4 \text{ to } 4.5 \times 10^{19} m^{-3}$)

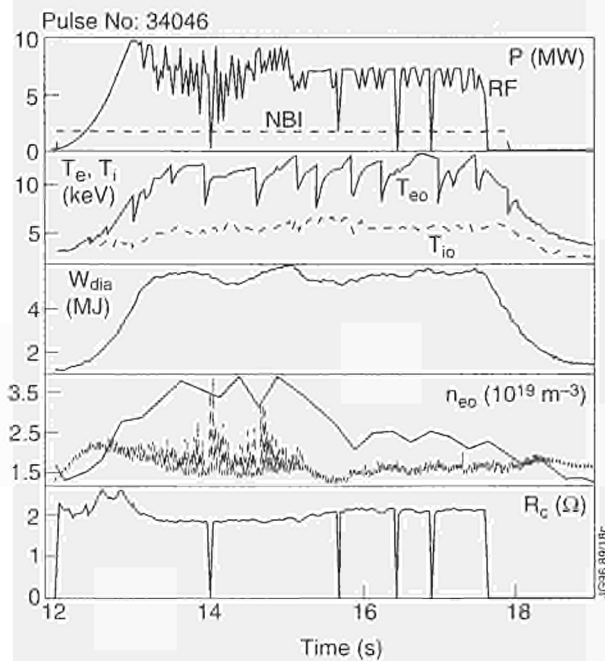


Fig.180: Time evolution of plasma parameters for a ICRF-dominated H-mode in high flux expansion configuration

increase of the angular momentum and improved confinement was not been established.

Another difference was the low ELM activity when ICRH alone was used. As shown in Fig.179, plasmas with H-mode quality confinement had very low ELM activity compared to a pulse with NB only, at similar power.

High Electron Temperature Regimes

Central electron temperatures up to 15keV were achieved in both RF-only H-modes and in hot ion H-modes with combined heating. The deuterium discharges had a plasma current of 3MA and a toroidal field of 3.2T. The ICRF frequency was 52MHz, which produced hydrogen minority heating with the resonance about 0.1m on the high field side of the magnetic axis. In each case, the configuration had substantial triangularity ($\delta \cong 0.3$) and high flux expansion in the divertor region. The time evolution of plasma parameters for the RF only H-mode, which attained $T_e(0) = 14.5\text{keV}$ at $t = 16.8\text{s}$ is shown in Fig180. The initial RF power level of 10MW in combination with 1.8MW of diagnostic neutral beams produced an H-mode. The ELMs subsequently tripped some of the generators. The RF power was stepped down to 7MW at $t = 15\text{s}$, the density decreased from $3.5 \times 10^{19}\text{m}^{-3}$ and the ELM activity all but disappeared. The central electron and ion temperature reached 14.5keV and 6keV, respectively. The corresponding $T_e(r)$ profiles from the ECE and LIDAR Thompson scattering diagnostic are shown in Fig181.

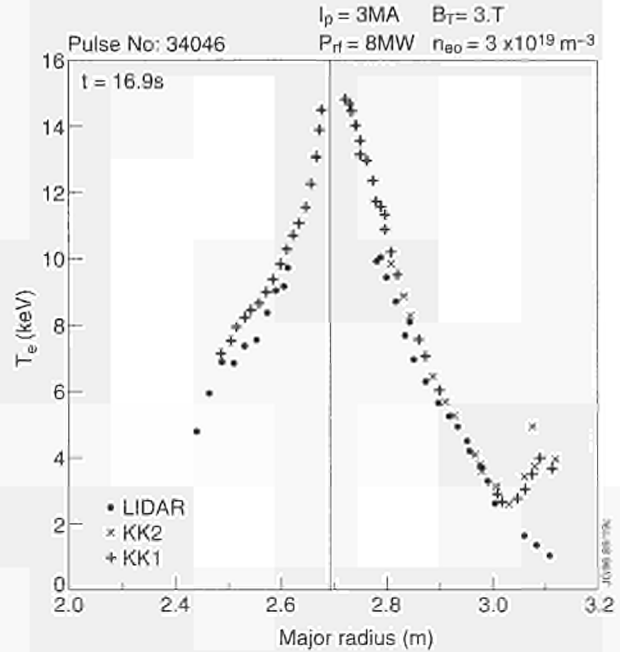


Fig.181: Electron temperature profiles, ECE and LIDAR, for ICRF H-mode (Pulse No.34046)

Neither diagnostic measured at the exact plasma centre; the horizontal line of sight of the LIDAR system is -0.3m below the magnetic axis whereas the ECE measures 0.1m above the plasma centre. At such high temperatures and low densities, the fast energy slowing-down time reached $\tau_s = 4\text{s}$ in the centre of the discharge. The corresponding fast ion energy content was 2MJ, which was well simulated by the PION code when orbit effects were taken into account.

The scaling of the central electron temperature with $P_{rf}/n_e(0)$ is plotted in Fig182 for hot-ion and RF H-modes in 3MA triangular configurations and also for RF H-modes in 2.5MA discharges that simulate the JET "gas-box" divertor configuration. For hot-ion cases, the data spanned only a small range in $P_{rf}/n_e(0)$. Consequently, the scaling was difficult to ascertain but the points were in the same region as those from pellet enhanced performance H-modes (PEP + H) and hot electron modes obtained in the 1991/92 experimental campaign. Figure 182 also shows, for comparison, the scaling of $T_i(0)$ with $P_{nb}/n_e(0)$. In this case, the beam power is taken as the scaling parameter, since the beam predominantly heats the ions, whereas the RF mainly heats the electron. The equipartition term is small in the core of these plasmas. Similar values of $T_e(0)$ and $T_i(0)$ were obtained for the same values of power per particle, implying that the electron and ion thermal conductivities in the core also had similar values.

The RF-only H-modes at 3MA showed a linear dependence of $T_e(0)$ with $P_{rf}/n_e(0)$, up to $P_{rf}/n_e(0) = 3 \times 10^{10}\text{m}^3\text{MW}$.

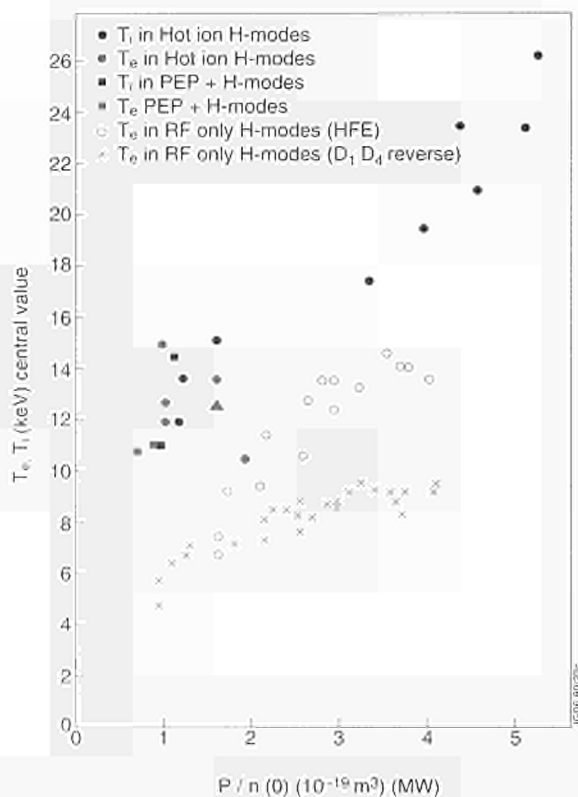


Fig.182: Central electron and ion temperature versus input power normalised to central electron density

Above this value, $T_e(0)$ increased less rapidly, perhaps due to fast ion orbit spreading of the electron heating profile or an adverse scaling of χ_e with temperature. A clear, non-linear behaviour was evident in the 2.5MA “gas-box” divertor data in which $T_e(0)$ saturated at 9keV. Transport analysis showed that the values of χ_e in the core region of the 2.5MA plasmas were about a factor of 3 greater than those for the 3MA RF-only H-modes. Values of χ_e for the hot ion H-modes were a factor of 2 less than those for the RF-only H-modes.

An interesting variation of the 3MA discharges was Pulse No.35297, in which the ICRF resonance layer was 0.25m on the high field side of the magnetic axis. Even so, 5MW of RF power produced an H-mode with a central electron temperature of 10keV at a density $n_e(0) = 2.7 \times 10^{19} \text{m}^{-3}$. This electron temperature was higher than the values achieved for the same power per particle with a central resonance in the 3MA RF-only H-modes as shown in Fig. 182. Transport analysis showed that χ_e was similar to that for the hot ion H-modes over the inner half of the minor radius and about a factor of two less than that for the RF-only H-mode in the same region.

The 15keV maximum electron temperature obtained in JET was close to that anticipated ($T_e(0) \cong 19\text{keV}$) for ITER ignited plasmas. The temperature gradient and the electron toroidal beta were also similar to the expected values in

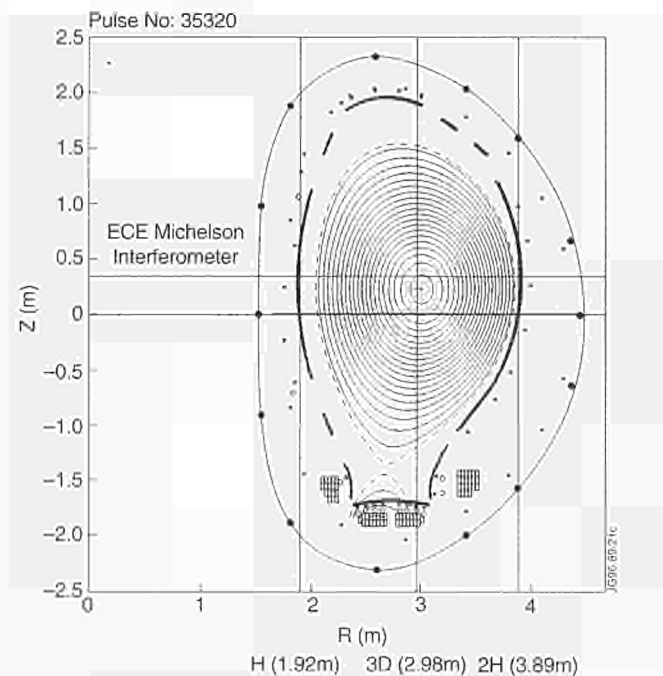


Fig.183: Main ion cyclotron resonances for 2MA/2.2T and RF frequency of 51.5MHz

ITER, but the density in JET was three times lower as shown in Table XVI. The power required to improve the electron temperature to the ITER value depended on the scaling of χ_e . If the scaling was the same as χ_i , then the $T_e(0)$ versus $P_{\text{th}}/n_e(0)$ results in Fig 182 suggest that about 16MW of RF power would be needed at a density of $4 \times 10^{19} \text{m}^{-3}$, to reach the ITER-like temperature values. Such a power level has already been achieved in the “gas-box” divertor configuration and should be available to hot ion configurations in the next campaign as a result of modifications to the antennae, RF plant and poloidal limiters.

As the electron temperature, and hence the electron beta, increased, the fraction of power absorbed directly by the electrons by combined electron Landau damping and transit time magnetic pumping also increased. This effect helps to concentrate the power deposition in the plasma centre and counteracted the orbit-broadening of the fast ion heating profile as the high power levels produced fast ions in the MeV energy range. The hot-ion-like core confinement achieved in the off-axis heating experiment was an intriguing observation and clearly needs to be tested; a substantial central temperature increase should result from the addition of a small amount of on-axis heating.

Third Harmonic Deuterium Resonance Experiments

During the 1995 beryllium phase, experiments were carried out aimed at assessing the direct electron heating

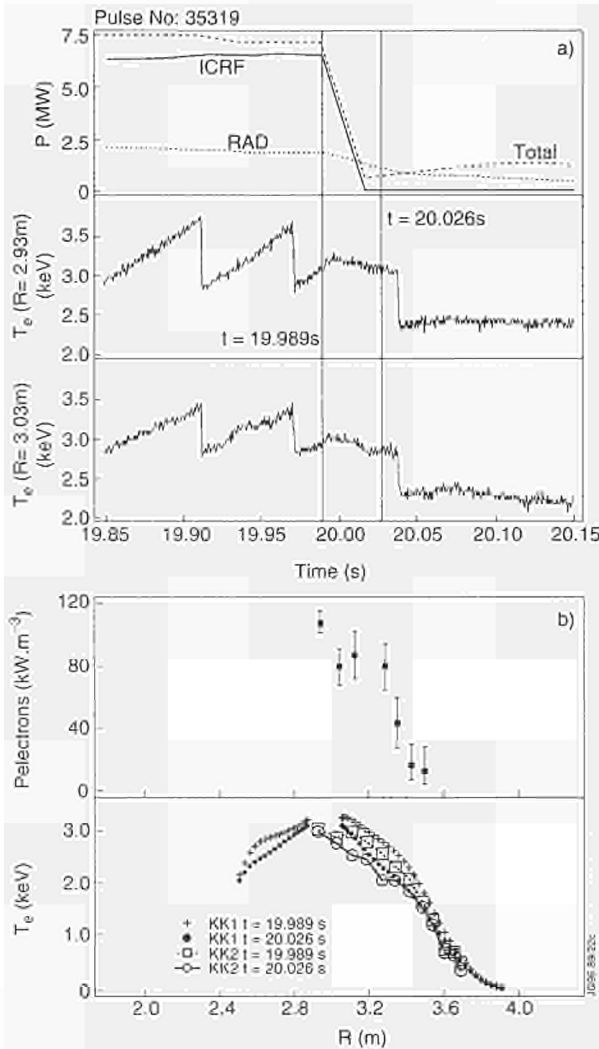


Fig.184: (a) change of slope of electron temperature, and fast RF power switch-off; (b) direct electron heating profile deduced from (a)

in a scenario with limited competition with the ion resonances. In the Tore Supra experiment (Cadarache, France), under similar conditions, strong electron heating had been observed; if these results were confirmed in JET, such a scenario would be a good candidate for tests of Fast Wave Current Drive.

Experiments were undertaken at $I_p \approx 2\text{ MA}$ and $B_T \approx 2.2\text{ T}$ [13]. The main ion resonances are shown in Fig. 183 for the operating frequency of 51.5MHz: fundamental hydrogen and second harmonic deuterium were on the highfield side, while second harmonic hydrogen and fourth harmonic deuterium were located on the low field side. Both heating, $0\pi\pi 0$ and $0\pi 0\pi$, and current drive $\pm 90^\circ$ phasings were used. Simulations with the PION code, before the experiment, indicated that absorption at $3\omega_{ce}$ could be a strong competition for the Direct Electron Heating. Similar experiments in TORE SUPRA and DIII-D had resulted in dominant direct electron heating; simulations with the ALCYON code,

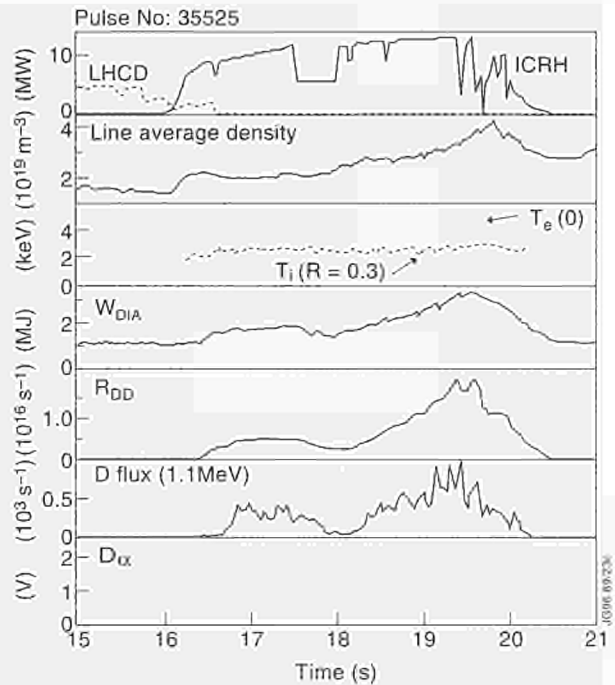


Fig.185: Time evolution of plasma parameters (2MA/2.18T) showing acceleration of deuterium ions

which unfortunately does not take into account third harmonic absorption, suggested that the same would be obtained at JET.

Significant electron heating was observed. The analysis of the electron temperature response to a fast switch-off of the ICRF power (Fig.184(a)) suggested that, in $0\pi\pi 0$ phasing, about 14% of the ICRF power was absorbed directly by the bulk electrons, with a fairly peaked deposition profile (Fig.184(b)). For the cases with $+90^\circ$ and -90° phasings, the power coupled directly to electrons was estimated to be only 50% of the $0\pi\pi 0$ case.

Significant absorption and deuterium acceleration at $3\omega_p$ was present, as indicated (Fig.185) by the high D-D reaction rate and high energy neutral D flux up to the highest energy channel available, corresponding to $E \approx 1.1\text{ MeV}$. This was confirmed by observation of 3.1MeV γ emission from the plasma centre, coming from $^{13}\text{C}(d,p)^{13}\text{C}$, which had an energy threshold for the deuterons of 1.8MeV. The stored energy and D-D rate increased with injected power and density. Similar results were obtained with LHCD pre-heating and when a plasma with approximately 50% D and 50% ^4He was used.

The position of ω_{UH} and $2\omega_{UH}$ was crucial for this experiment. When the magnetic field was decreased, and $2\omega_{UH}$ entered the plasma on the low field side, there was a clear increase of density, radiated power and neutral hydrogen flux, while the deuterium high energy flux and the D-D reaction rate decreased.

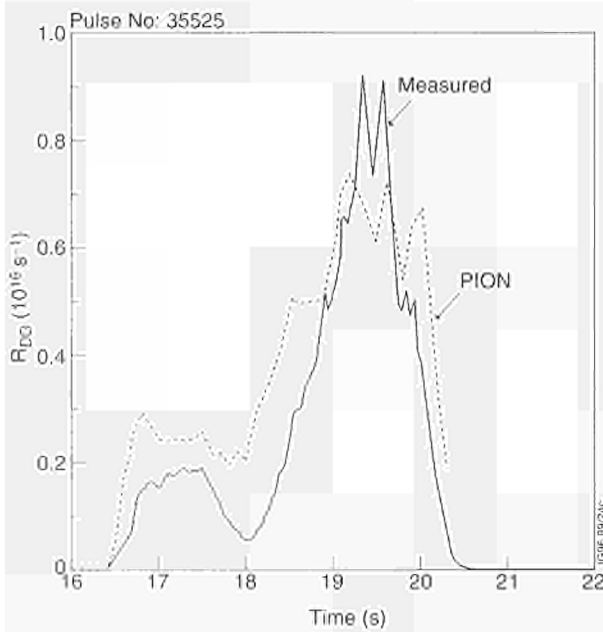


Fig.186: $3\omega_p$ resonance experiments: experimental neutron rate and PION code simulation

At high density and RF power, a transition to an ELMY H-mode was observed. The record D-D rate for ICRF heated plasmas in JET was achieved, $R_{DD} \sim 1.8 \times 10^{16} \text{ s}^{-1}$ with $P_{RF} = 12.9 \text{ MW}$, which is comparable with the yield of NB heated discharges with similar plasma parameters. The contrast with the TORE SUPRA results was likely to be due to the better fast ion confinement in JET, which allowed the build-up of the high energy ion tail.

Extensive numerical modelling was carried out with the PION code, which has a self consistent treatment of the D-tail formation and fast wave absorption and includes finite orbit width effects. Since the code is based on simplified models, it has some limitations. RF-induced spatial diffusion of the resonating ions was not taken into account nor was sawtooth redistribution of fast ions: (both effects are expected to be non-negligible for the very energetic ion population produced by third harmonic heating). To model prompt ion losses a particle loss term was added to the Fokker-Planck equation in PION, which removed ions when they reached energies $> 4 \text{ MeV}$. In addition, a parasitic absorption mechanism at the plasma edge was introduced to simulate the early part of the discharges, when the damping was low. The PION code results showed good agreement with experimental data. In Fig.186, the comparison is shown between calculated and measured values of the neutron rate.

Toroidal Alfvén Eigenmodes Excitation

Systematic experimental studies of Toroidicity-induced Alfvén Eigenmodes (AE) utilising the Alfvén Eigenmode

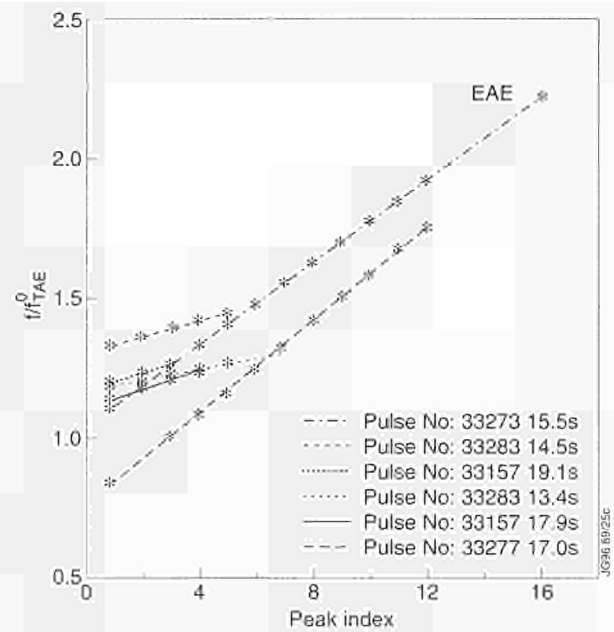


Fig.187: Example of frequency distribution of the multiple Kinetic AE driven by an external antenna for a number of additionally heated discharges. The peak index enumerates the AE from the lowest frequency peak observed in the TAE range.

Active Diagnostic (AEAD) were continued during 1995. Active AE-measurements, based on combining AE-excitation by the external saddle coils with synchronous detection of various probing signals [14], were mainly focused on extended studies of TAE, EAE and Kinetic TAE modes (KTAE) and their damping rates [15, 16]. It was established in various plasma heating scenarios (ICRH, LHH, NBI, ohmic high current) that a transition from a single peak TAE to multiple peak AE-structure occurred at higher plasma temperature. As the method of the AE-excitation allows excitation of low- n modes only and as the observed multiple modes are characterised by regular frequency spacing (Fig.187), these multiple peaks identified as KTAE.

KTAE occurred in heated toroidal plasmas as a result of the Alfvén continuum splitting into discrete spectrum due to the effects of toroidicity and Finite Larmor Radius effects of core ions. The damping rates of these multiple Alfvén Eigenmodes were in most cases significantly lower than those of the corresponding single "cold" TAE. Upper limits for $\gamma_{\text{damping}}/\omega$ could be established experimentally and were in the range 10^{-3} - 10^{-4} , about one order of magnitude lower than typical TAE-damping in cold plasmas [16]. Very weakly damped ($\gamma_{\text{damping}}/\omega < 10^{-4}$) multiple modes were also seen, mainly on the reflectometer signals, during current ramp-down experiments, corresponding to sudden variations in the internal plasma inductance and presumably to rapid changes in the magnetic shear.

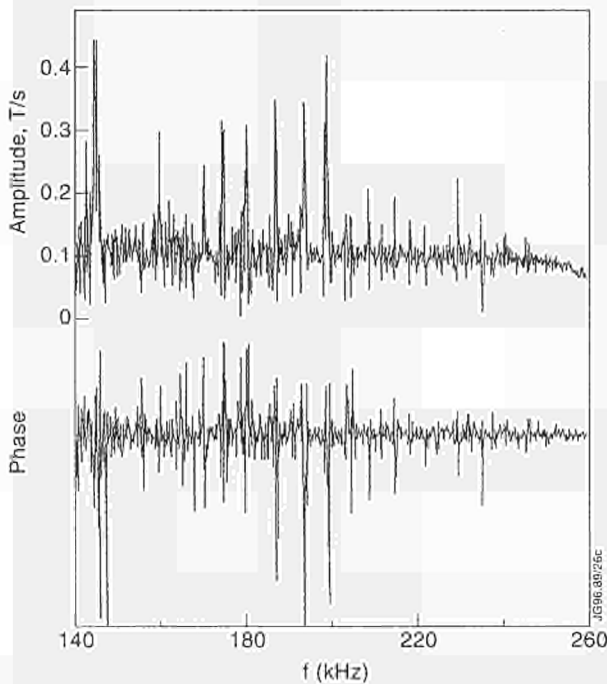


Fig.188: Passive measurements: multiple AE-peaks in high-current plasma with NB-heating only. Pulse No. 34073, $t \sim 14s$, the end of NBI: $P(80keV) = 6MW$, $P(140keV) = 3MW$; $I_p \sim 4.4MA$; $B_i \sim 3T$; $\langle n \rangle \sim 8 \times 10^{19} m^{-3}$; $T_e \sim 7keV$; $T_i \sim 4keV$.

Passive AE-measurements, based on the AEAD detection of probing signals without AE-excitation by the external antennae, were used to study AEs, driven intrinsically by ICRH- and NB-produced energetic ions. Again multiple Alfvén Eigenmodes were observed in a number of RF- and NB-heated JET discharges, with typical examples shown in Fig.188. Further extension of the database and studies of the energetic ion driven AE are in progress with the emphasis to analyse possible scenarios of AE-excitation by fusion born alpha-particles complemented by NB- and/or RF-produced energetic ions during D-T experiments in JET.

In addition, a novel complementary method of resonant excitation of AE by ICRH beat waves has been attempted experimentally in JET [17]. Figure 189 shows the first results, with the ICRF antenna in a dipole configuration and in a hydrogen minority heating scheme, with frequencies $f_{1,2} \sim 43MHz$. Two antennae were used, 180° apart toroidally, with powers coupled to the plasma $P_1 \sim P_2 \sim 1MW$, so that no significant population of ICRF-heated ions could be produced to drive AE via wave-particle interaction. The difference frequency of the two modules, Δf , was kept approximately constant and the toroidal magnetic field was varied linearly in time. When Δf coincided with the central TAE gap frequency, a large response in the magnetic coils was synchronously detected. The relatively large amplitudes for the AE driven

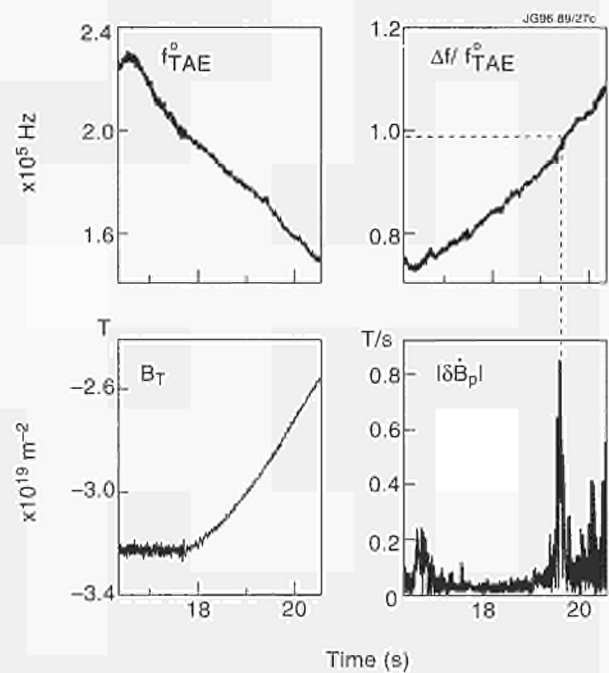


Fig.189: Passive measurements: observation of a beat wave-driven AE resonance on a magnetic probe located above the tokamak outer mid-plane when $\Delta f \sim f_{TAE}^0$. Pulse No. 35051, $I_p \sim 3MA$; $T_e \sim 5keV$, $T_i \sim 3.5keV$; $\langle n \rangle (2 \times 10^{19} - 1 \times 10^{19} m^{-3})$; $\Delta f \sim 158 - 168kHz$. by ICRF beat waves suggested that this new non-linear excitation mechanism could allow investigations into the effects of AE on particle orbits and should be taken into account in ICRH heated thermonuclear plasmas.

Real Time Power Control Experiments

The control capability of each of the Heating and Current Drive systems has recently been significantly enhanced to provide a very flexible alternative to conventional pre-programmed operation. Using a predefined network, the power can now be changed in real-time. Initial experiments with such control system have been carried out in the 1995 campaign, including:

- feedback control of the diamagnetic energy (W_{DIA}) by ICRF and NB power, D-D reaction rate by ICRF, and surface loop voltage (V_{LOOP}) by LHCD;
- simulation and control of a "thermal runaway" situation.

The initial values of the control parameters have been designed using a 0-D plasma code for simulations of both open-loop and closed-loop behaviour. The first experiments concentrated on showing the feasibility of feedback control of W_{DIA} with ICRF and NB power and of R_{DD} with ICRF heating. A case of R_{DD} control by ICRF power is shown in Fig.190.

Following these successful tests, experimental simulations of feedback control of a burning plasma have been carried out. The main aim was to mock-up and

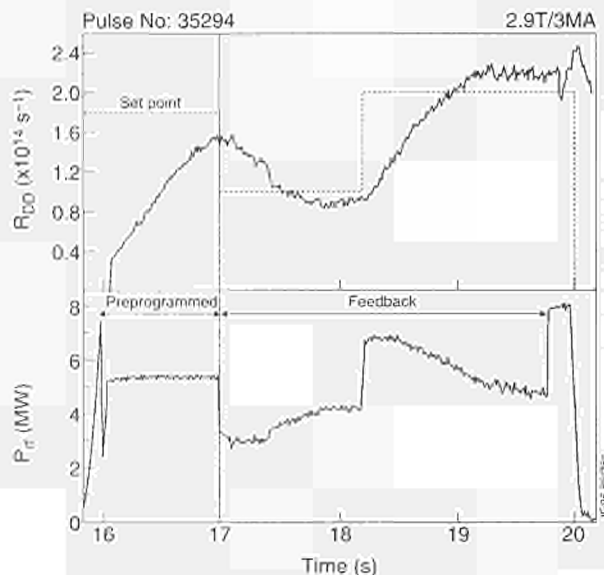


Fig.190: R_{D0} feedback control by ICRF power

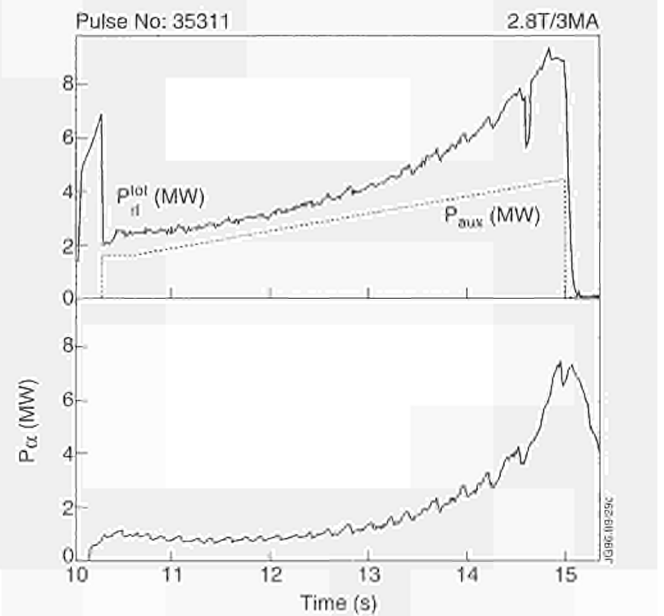


Fig.191: Experimental simulation of the "thermal runaway" situation

control the "thermal runaway" effect in a plasma with significant self heating. The "alpha" power, P_α , was taken as being proportional to R_{D0} : the control of the available RF power was split so that part of the RF represented P_α and the rest was used as auxiliary power. NB power was not used since it would result in a significant fraction of non-thermal R_{D0} .

For the "thermal runaway" (Fig.191), the switch was opened (i.e. the control operated in open loop), and the auxiliary power was ramped up to detect where the plasma reactivity started to "runaway". For the burn control experiment (Fig.192), the loop was closed and the setpoint was chosen at 1.6MW, which from the previous experiment was found to be in the stable regime of the plasma, with P_α not yet close to the "runaway" condition.

In parallel with this activity, experiments of control of the loop voltage by lower hybrid current drive (LHCD) were carried out, as a first step to a more advanced control scheme to control both loop voltage and internal inductance using LH power and phase of the launched wave.

References

[1] C.D. Challis et al., Proc. of 22nd Conf. on Plasma Phys. & Contr. Nucl.Fusion, Bournemouth 1995
 [2] M Kikuchi, Nucl. Fusion, **30** (1990) 265
 [3] A.C.C. Sips et al., Proc. of 22nd Conf. on Plasma Phys. & Contr. Nucl.Fusion, Bournemouth 1995
 [4] G.T.A. Huysmans et al, Proc. of 22nd Conf. on Plasma Phys. & Contr. Nucl.Fusion, Bournemouth 1995

[5] F. Rimini et al, Proc. of 11th Topical Conf. on RF Power in Plasmas, Palm Springs (USA) 1995
 [6] B. Fischer et al, Proc. of 22nd Conf. on Plasma Phys. & Contr. Nucl.Fusion, Bournemouth 1995
 [7] T.T.C. Jones & JET Team, Proc. of 22nd Conf. on Plasma Phys. & Contr. Nucl.Fusion, Bournemouth 1995
 [8] T. Hender, et al, Proc. of 22nd Conf. on Plasma Phys. & Contr. Nucl.Fusion, Bournemouth 1995
 [9] P. Smeulders et al, Proc. of 22nd Conf. on Plasma Phys. & Contr. Nucl.Fusion, Bournemouth 1995

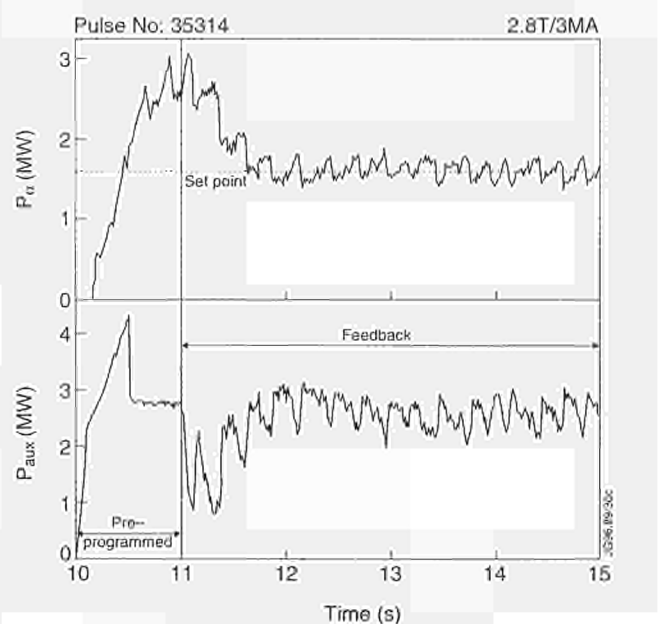


Fig.192: Experimental simulation of thermonuclear burn control

- [10] F.X. Söldner, et al, Proc. of 22nd Conf. on Plasma Phys. & Contr. Nucl.Fusion, Bournemouth 1995
- [11] D.F.H. Start et al, Proc. of 11th Topical Conf. on RF Power in Plasmas, Palm Springs (USA) 1995
- [12] E. Righi et al, Proc. of 22nd Conf. on Plasma Phys. & Contr. Nucl.Fusion, Bournemouth 1995
- [13] F. Nguyen et al, Proc. of 22nd Conf. on Plasma Phys. & Contr. Nucl.Fusion, Bournemouth 1995
- [14] A.Fasoli et al., Phys. Rev. Letters **75**, 645 (1995)
- [15] A.Fasoli et al., Phys. Rev. Letters, to be published
- [16] A.Fasoli et al., Nuclear Fusion **35**, Anniversary Issue No 12 (1995)
- [17] A.Fasoli et al., Nuclear Fusion Letters, to be published

Transport and Fluctuations

One of the main objectives of the work in the Transport and Fluctuations area was to predict the performance of ITER in the ELMy H-mode regime. Dedicated experiments and statistical analyses broadly confirmed previous findings on the gyro-Bohm scaling of confinement up to high values of plasma current and toroidal magnetic field. It was also shown, however, that when the power losses are close to the power threshold P_{thres} for the L- to H-mode transition, a significant deterioration of confinement would occur due to a stronger negative influence from ELM activity. Such observations emphasise the importance of other experimental, statistical and theoretical studies on the nature of the L- to H- transition and on the parametric dependence of P_{thres} on the discharge parameters. The confinement of light and heavy impurities in L- and H-mode was also actively studied and the validity of recent theoretical models was tested against experimental measurements. Both local interpretative analysis and investigations conducted by means of simulation programs appear to indicate, for particles as well as energy, that in the core of the discharge, transport is slower and dominated by gyro-Bohm-like diffusion, while outside that region stronger Bohm-like diffusive processes are the main mechanisms governing particles and energy losses.

Larmour Radius Scaling of ELMy H-Modes

Previous Larmour radius scaling experiments completed on TFTR, JET and DIII-D were carried out in an L-mode plasma and the scaling of the global confinement was

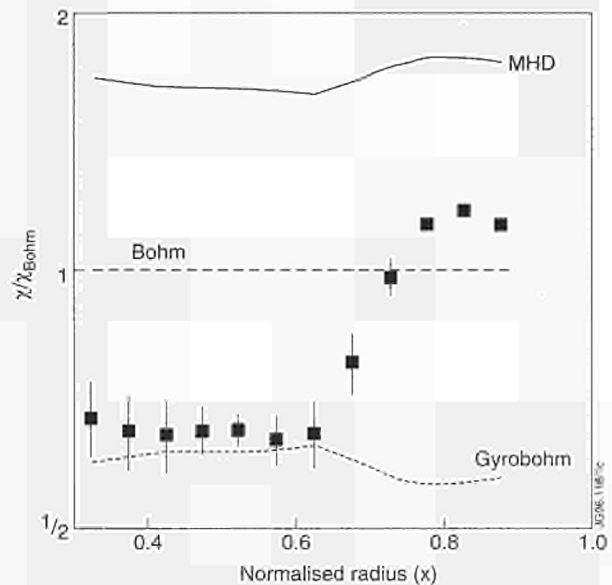


Fig.193: Ratio of the "effective thermal diffusivities" versus the normalised radial co-ordinate x for the 2T and 1T pulses. The lines are the expected ratio for gyro-Bohm, Bohm and Stochastic (MHD) scaling

found to be Bohm-like and in agreement with the ITER89P L-mode scaling expression. The operational regime, proposed for ITER is the ELMy H-mode regime and the scaling in this regime derived by the ITER data base group [1] was the ITER93H scaling expression. This latter expression is close to a gyro-Bohm scaling ($\chi \sim \chi_{\text{Bohm}} \rho^{*0.8} \beta$). To confirm this scaling, a series of pulses were set up with the same β and v^* at different values of current and field, 1MA/1T, 2MA/2T, 1.6MA/1.7T and 2.8MA/3T. The first set had a $q_w = 3.4$ and the second set had $q_w = 3.7$. The main plasma parameters are listed in Table XVII [2]. For the first pair of pulses, 1MA/1T, 2MA/2T, globally at least, the τ_{th} increased linearly with toroidal field which indicated a gyro-Bohm dependence (gyro-Bohm, $\tau_{\text{th}} \propto B$; Bohm, $\tau_{\text{th}} \propto B^{1/2}$; stochastic, $\tau_{\text{th}} \propto B^{-1/3}$), in agreement with the ITER93H scaling expression. A local analysis by the TRANSP code further confirmed this result: for example, in Fig.193 the ratio of the χ 's of the 2T and 1T pulses, are seen to scale as gyro-Bohm for a large fraction of the radius.

For the second pair of pulses Pulse Nos. 33131 and 33140, the global energy confinement scales as $B^{0.05}$ giving a scaling worse than Bohm ($\tau_{\text{th}} \propto B^{1/2}$). This difference in the global energy confinement scaling between the two sets of pulses can be attributed to a difference in the ELMy behaviour. In the 3T pulse, the ELMS are of the compound type with the plasma returning to the L-mode state for a significant period following each ELM. The reason for this may be due to the fact that the 2.8MA/3T pulse is very close

Table XVII

Pulse No.	B_T (T)	I_p (MA)	$\langle n_e \rangle$ $10^{19}m^{-3}$	P (MW)	W_{th} (MJ)	τ_{ch} (s)
35171 (25.8s)	1	1	2.2	4.85	0.84	0.17
35156 (16.1s)	2	2	5.5	9.18	3.2	0.35
33140 (16.6s)	1.7	1.6	3.6	6.3	2.3	0.36
33131 (15.6s)	3	2.8	7.6	19.6	7.3	0.37

to the H-mode threshold, whilst the lower field pulses are well above the H-mode threshold.

The threshold scalings can be expressed in terms of the dimensionless variables ρ^* , β and v^* and one dimensional variable, which is chosen to be the minor radius, a.

The two dimensionally correct threshold forms [2,3] are:

$$P_{thr} = 0.3 n BR^{2.5} \sim a^{-3/4} \rho^{*-3/2} v^{*-1/4} \beta^{5/4} \quad (1a)$$

$$P_{thr} = 0.016 n^{0.75} BS \sim a^{-3/4} \rho^{*-3} v^{*-1/4} \beta \quad (1b)$$

Similarly, the standard confinement scaling can be expressed as ITER89P and ITER93H in the same form:

$$P_{ITER89P} \sim a^{-3/4} \rho^{*-5/2} v^{*-1/2} \beta^2 \quad (2a)$$

$$P_{ITER93H} \sim a^{-3/4} \rho^{*-3/2} v^{*-0.65} \beta^2 \quad (2b)$$

where P is the power required to reach a given β , ρ^* , v^* etc, assuming the particular confinement scaling law is correct. It can be seen from Eqs (1) and (2) that both threshold scalings have a much stronger ρ^* dependence than that of the H-mode scaling expression ITER93H, and so as ρ^* is reduced by increasing the magnetic field in these similarity discharges at some stage, the ITER93H scaling will be lost. The influence of the threshold on the JET data is shown in Fig.194, where the normalised

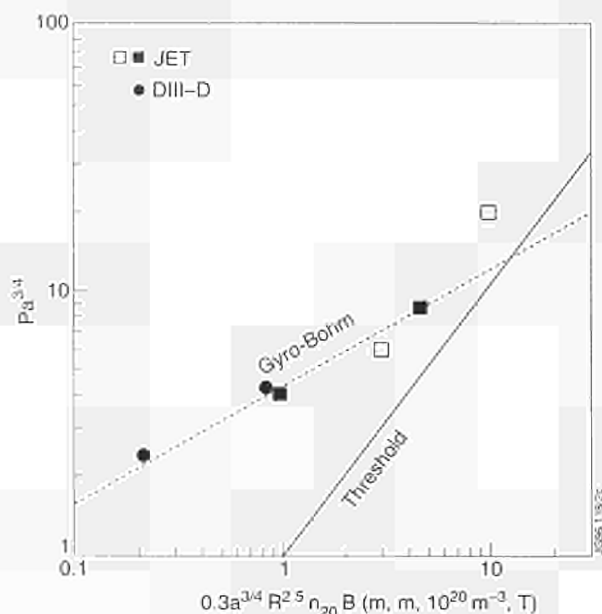


Fig.194: Normalised power $Pa^{3/4}$ versus $0.3 a^{3/4} R^{2.5} n_{20} B$, the H-mode power threshold expression [3]. The DIII-D points are from C. Petty et al. [4].

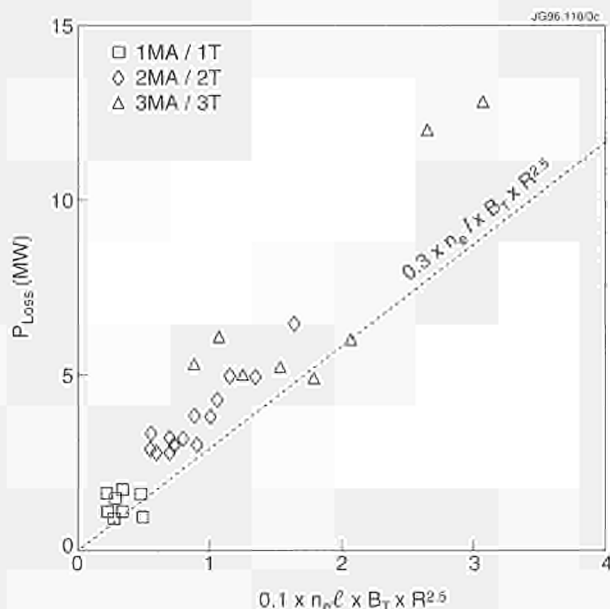


Fig.195: Comparison between the results of the JET power threshold experiment and the ITER scaling given by Eq. (3). The three combinations of magnetic field/plasma current used in the experiment are indicated.

power is shown versus the threshold scaling P_{thr} . Well above the threshold, a gyro-Bohm dependence with $P \propto \rho^{*-3/2}$ is clear for both JET and DIII-D. However, close to the threshold the gyro-Bohm scaling is lost.

H-mode Power Threshold Experiments

During the 1995 campaign, a series of experiments were carried out to determine the dependence of H-mode power threshold P_{thr} on plasma density. The experiments aimed at establishing as sound a base as possible to extrapolate the density scaling to ITER parameters and thus provide important information about the amount of additional heating necessary for ITER to operate in H-mode regime. NB heating was used in an ITER-like configuration, and the choice of three combinations of plasma current and toroidal field - 1MA/1T, 2MA/2T, 3MA/3T - allowed $q_{95} \approx 3$ at the L-H transition [5] to be kept constant.

The results of the experiment confirm the linear scaling of P_{thr} with the magnetic field B_T . However, results on density dependence, shown in Fig.195, are not so clear-cut.

Comparison with the most recent scaling laws from the 1995 ITER Threshold Database [6] seems to indicate that the less favourable scaling law for ITER,

$$P_{loss} = (P_{tot} - dW_{DIA}/dt) = 0.3 n_e l x B_T x R^{2.5} \quad (3)$$

applies to this set of JET data. In Eq.(3), $n_e l$ is the central line averaged density in units of $10^{20}m^{-3}$, the magnetic field is in T, the major radius R is in metres and the powers are in

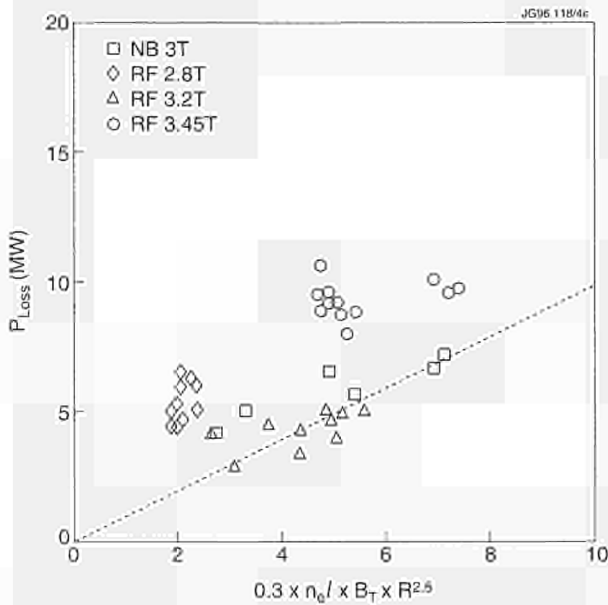


Fig.196: H-mode power threshold data obtained with ICRF heating. The data are plotted against the ITER scaling law of Eq. (3) and are compared against the 3 MA/3 T data of the dedicated experiment. This figure shows that ICRF and NB heating are substantially equivalent.

MW (W_{DIA} is the diamagnetic energy of the plasma). In Fig.195, clear deviations from the scaling law are evident both at low ($n_e l \approx 0.18$) and high ($n_e l \approx 0.6$) densities.

Degradation of power threshold due to substantial cooling of the plasma edge caused by heavy fuelling of neutrals, both from gas puffing and NB power, could be one possible cause. Therefore, in the 1996/97 MarkII campaign, and in preparation for the DTE1 experiments on isotope scaling of P_{lim} , experiments will be proposed in the high density regime, where ICRF will dominate over NB heating, thus minimising edge fuelling due to heating, and possibly allow a comparison between gas puffing and pellet fuelling.

H-modes have also been obtained with ICRF heating alone in a large range of configurations, magnetic fields (1.6-3.4T) and plasma currents (1-5MA), both in standard dipole ($0\pi 0\pi$) and phased ($0\pi\pi 0$) operation of the RF antennae. RF-only H-modes provide an important environment to simulate H-modes sustained by high energy fast particles, like α -particles on ITER.

Although RF H-modes have been obtained with different plasma configurations and currents, the power threshold does not seem to differ substantially from that obtained with NB heating.

The RF database is shown in Fig.196, where the set of data labelled "NB 3T" is the same 3MA/3T set as in the previous figures. The data substantiates the hypothesis that the power threshold is the same with the two heating

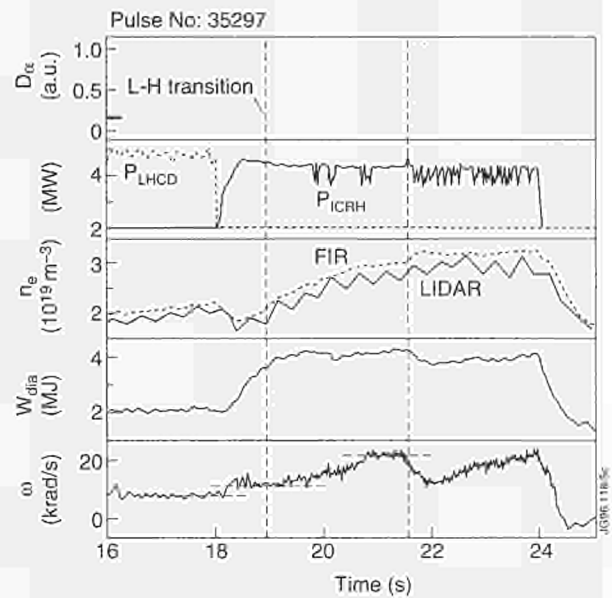


Fig.197: Pulse No.35297 shows an example of toroidal rotation during ICRF-only H-modes. The H-mode transition is identified by the drop of the D_{α} intensity, measured along a vertical cord. A phase of progressive increase in angular frequency ω of toroidal rotation (measured at $p \approx 0.3$) at the time of the L-H transition.

systems. However, a significant difference between ICRF and NB heating lies in the fact that the torque transferred by the former heating system is about one order of magnitude smaller than that transferred by NB power. This allows a study of the variations of toroidal rotation in L- and H-mode plasmas and its relationship with improved energy and particle confinement. In fact, when no NB heating is used at the time of the L-H transition, the plasma starts to accelerate progressively in the same sense of the plasma current [7]. A clear example of increase in toroidal rotation is shown in Fig.197. A quantitative relationship between rate of increase of the angular momentum and improved confinement has not been established yet.

High Current H-mode Confinement Studies

In Fig.198, the diamagnetic stored energy W_{dia} is shown versus plasma loss power ($P-dW/dt$) for the constant I_p/B_1 ELM-free H-mode data of 1994/95. The new data labelled as 5MA include both 5MA/3.4T discharges with NB heating and 4.7MA/3.1T discharges with combined (NBI + ICRH) heating. In the figure, the 5MA and the best of the 4MA data from the previous JET experimental campaigns are also shown [8].

The interpretation of the data in Fig.198 should take into account that W_{dia} errors increase with I_p^2 , that most of the new data, although selected from discharges with

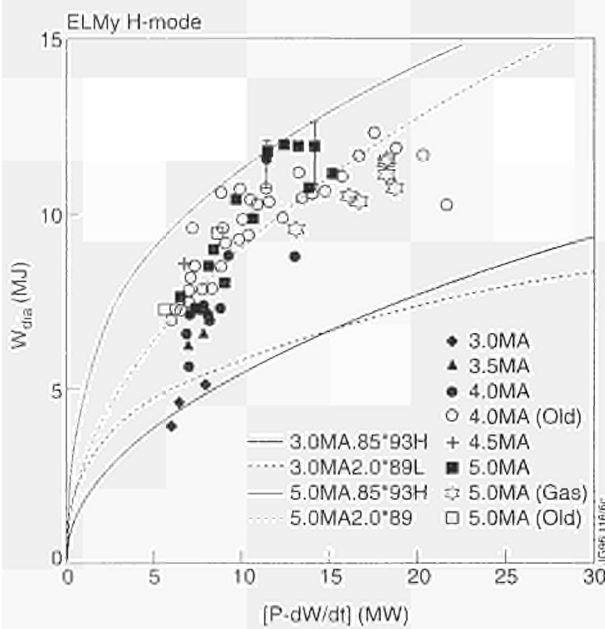


Fig.198: Diamagnetic stored energy versus loss power. The lines represent the power dependence predicted by the ITERH93-P ELM-free H-mode and 2xITER89-P L-mode scalings, respectively.

ELM-free periods $\geq 0.5s$, are of a transient nature and that no corrections have been made for the fast ion energy content. The data are compared with the thermal ELM-free H-mode scaling ITERH93-P [9]. The new data show a trend of increasing stored energy with plasma current. This is confirmed by the general agreement, for all plasma currents, between the energy confinement time and the predictions of the ITERH93-P scaling. No significant difference is observed between old and new data. The interpretation of the old data, which suggested a confinement scaling with I_p less than linear at 5MA, was probably a consequence of the limited dataset available at the time. An alternative explanation of the similarity of old and new 5MA data might be that the confinement degradation due to a poor plasma configuration in the old data [10] was compensated by the larger plasma volume. In the new JET configuration, the volume available to the plasma is reduced compared to the old configuration by 20% with the introduction of the divertor coils and cryopump inside the vacuum vessel. A deviation from $P^{1/3}$ prediction of ITERH93-P scaling for the energy is observed at low loss power. At high loss power, there is a notable degradation for the discharges with strong gas puff. The departure from the $P^{1/3}$ dependence of the data without gas puff appears significant but a further extension of the range in power would be required for this to be confirmed above any uncertainty in the data. Figure 199 shows W_{dia} versus loss power for the high current ELMy H-mode discharges.

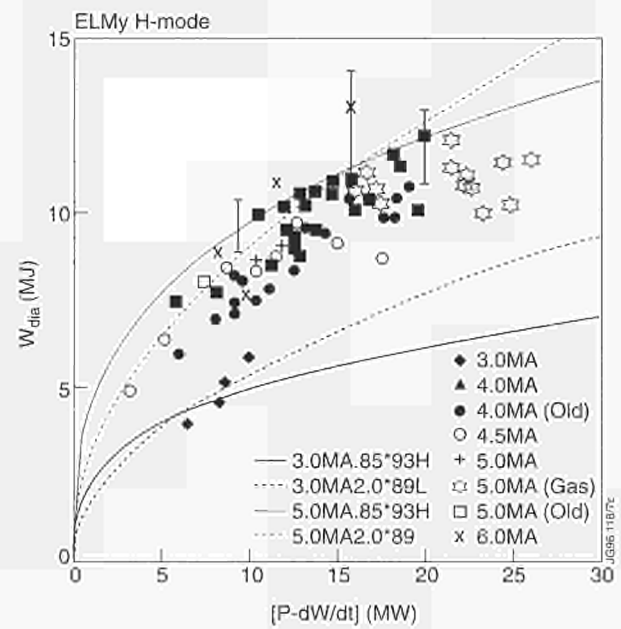


Fig.199: Diamagnetic stored energy versus loss power. The lines represent the power dependence predicted by 0.85xITERH93-P ELM-free H-mode and 2xITER89-P L-mode scalings, respectively.

A clearer picture emerges from this data, which also includes the 6MA results, (ie. the confinement clearly improves with increasing plasma current). The data are in good agreement with the prediction of the 0.85xITERH93-P ELMy H-mode scaling. The gas puff data suggest a further power degradation worse than $P^{1/3}$, but again more experimental data would be needed to clarify whether this is only due to the change in regime.

Ohmic Confinement Studies

A database of ohmic global energy confinement data has been assembled for JET from the 1984-92 experimental campaigns with data from mainly deuterium and helium plasmas [11]. The energy confinement of ohmically heated plasmas is characterized by a linear increase of the confinement time, τ_E , with density (LOC linear ohmic confinement), followed by saturation at high density saturated ohmic confinement (SOC) [12]. The value of density at which the saturation takes place, n_{sat} , decreases with machine size. The saturated ohmic confinement regime (SOC) is observed for $\langle n \rangle > 1.5 \times 10^{19} m^{-3}$ in JET, when $q_{cy1} = 3.5$ and $B_t = 3T$. The origin of the two regimes and the respective scalings of τ_E and n_{sat} with the plasma parameters are still under investigation. The trends of JET ohmic confinement, which can be assessed in the database, appear to be in qualitative agreement with the trends observed on other smaller tokamaks such as FTU and ASDEX. The main difference is a stronger magnetic field

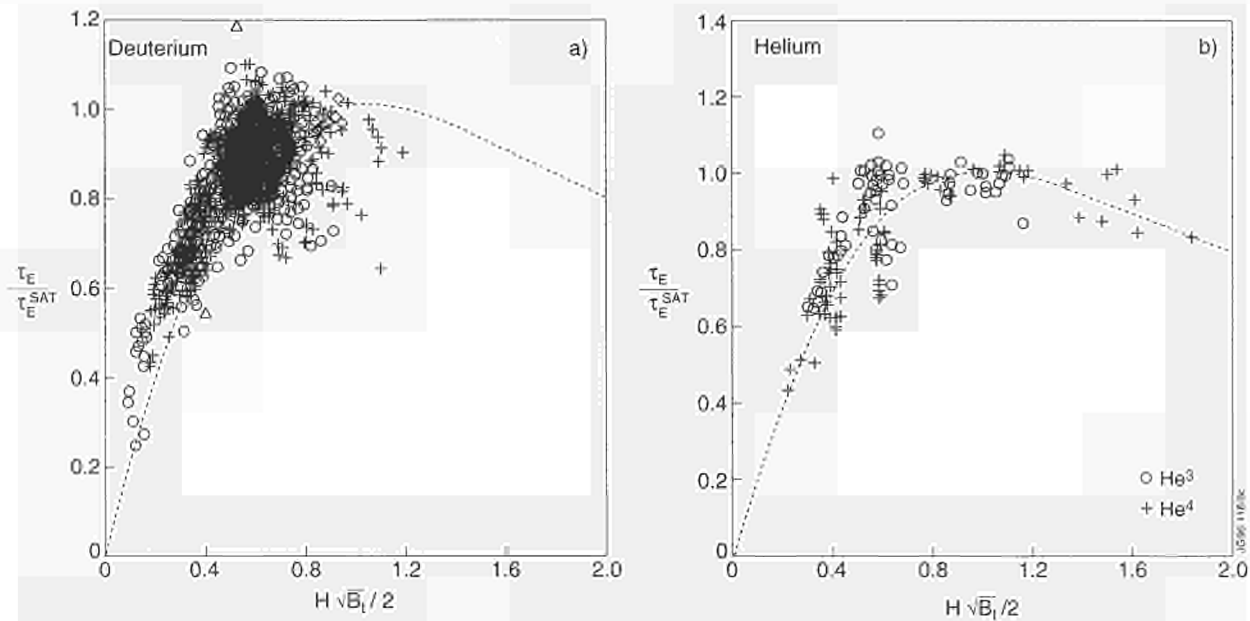


Fig.200: Global energy confinement time normalized to the Tore-Supra scaling versus the Hugill number multiplied by B_i^{AC} for (a) Deuterium plasmas and (b) Helium plasmas; the dotted line is the scaling proposed by Zou et al. [13].

dependence of τ_E , which has also been observed on Tore Supra. In the SOC regime, the stronger magnetic field dependence corresponds to a scale length of $\tau_E \propto R^2$, if the Connor-Taylor constraints [17] are satisfied. The scaling for τ_E in the SOC regime [13], $\tau_E^{sat} = 0.09 a R B_i^{0.6}$ (s.m.T), and the scaling of the saturation density with $0.5xH B_i^{0.5}$ seem to be in agreement with the JET data (see Fig.200). In 1996, this data will be released to the ITER L-mode database.

Scaling of Impurity Confinement Time in JET and Tore Supra

Databases have been set up for the particle confinement times, τ_p of non recycling impurities injected in laser ablation experiments in the JET and Tore Supra tokamaks [14]. No dependence of τ_p on the charge of the injected element (Mn(Z=25), Ni(28), Cu(29), Ge(32) for Tore Supra and Al(Z=13), Ti(22), Fe(26), Co(27), Ni(28), Ge(32), Zr(40), Mo(42), Ag(47) for JET) or on the background gas (D or ⁴He) was found in these discharges.

The data analysed were from L-mode plasmas produced in limiter, single-null X-point or double-null X-point configurations. In all but two pulses (out of 133 in total), sawtooth activity was present. The experimental values of τ_p are not consistent with the scaling proposed, for Alcator C ohmic discharges [15].

$$\tau_A [\text{ms}] = 0.075 a_L [\text{cm}] M_{bg} R [\text{cm}]^{0.75} Z_{eff} / (Z_{bg} q_{cvt}).$$

That scaling predicts values for τ_p that are too high by factors ranging between ~2 and ~7 for Tore Supra and

between ~3 and ~6 for JET. This scaling also indicates a dependence on the background plasma. This dependence cannot be verified from the database because practically all the data are obtained in D₂ or ⁴He discharges and M_{bg}/Z_{bg} is then constant.

The dominant dependence for τ_p is on $P_{in}/\langle n_r \rangle$ and a minor dependence on I_p is also apparent when the databases for the two machines are taken separately. From the joint database, the only statistically significant parameters were found to be $P_{in}/(\langle n_r \rangle V_p)$, I_p and V_p . The best choice for a common scaling law for τ_p is

$$\tau_p [\text{ms}] = 7.4 \times V_p^{0.70 \pm 0.08} I_p^{0.31 \pm 0.09} (P_{in}/\langle n_r \rangle)^{0.57 \pm 0.05} \quad (4)$$

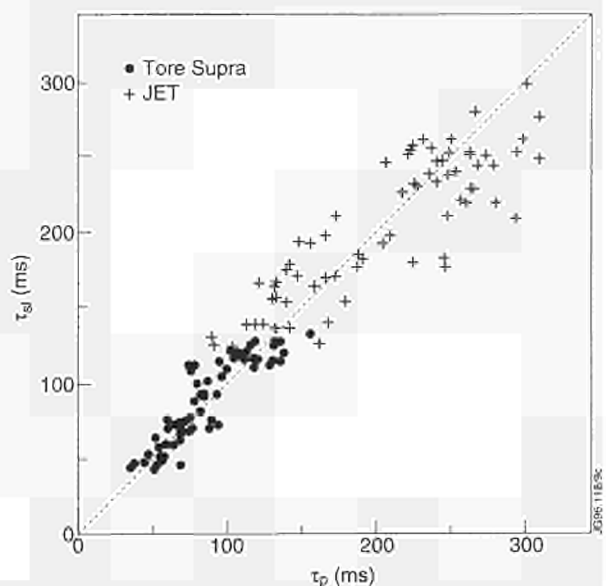


Fig.201: Impurity confinement time τ_i predicted by the scaling of Eq.(4) versus experimental τ_p . The dashed line shows $\tau_i = \tau_p$.

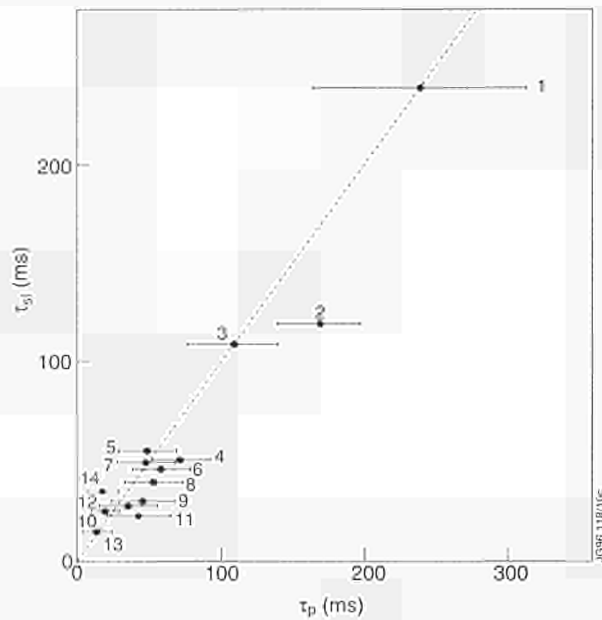


Fig.202: Impurity confinement times predicted by the scaling law of Eq (4) τ_{si} versus the experimental τ_p values for several tokamaks: (1) JET, (2) TFTR, (3) Tore Supra, (4) Textor, (5) ASDEX, (6) PLT, (7) T10, (8) PDX, (9) DITE, (10) TEXT, (11) TFR, (12) FT, (13) Alcator C and (14) Alcator C MOD. The horizontal bars show the range of the reported experimental values. All data refer to ohmic plasmas with deuterium as background gas

(see Fig.201) where P_m is measured in MW, I_p in MA, n_e in $10^{20} m^{-3}$ and V_p in m^3 . The logarithmic standard deviation for this regression is $\sigma_{br} = 0.068$ corresponding to a typical relative deviation of the experimental data from the prediction in the above equation of only 17%.

The proposed scaling law is very close to that found independently for the two machines and appears to be broadly consistent with the experimental results obtained in ohmic discharges on other tokamaks, as shown in Fig.202 [16]. It also satisfies the Connor-Taylor constraint [17] applicable to finite- β collisional models.

The dependence of τ_p upon the discharge parameters is similar but not identical to that of the energy confinement time τ_e . The logarithmic linear regression of the ratio is

$$\tau_e/\tau_p [\text{ms}] = 6.4 I_p^{0.40 \pm 0.16} V_p^{-0.32 \pm 0.15} n_e^{-0.17 \pm 0.12} B_T^{0.02 \pm 0.20} P_m^{0.16 \pm 0.05}$$

This indicates a more moderate dependence of τ_p on the plasma current than τ_e and a stronger dependence on the volume of the discharge as would be expected by comparing the above scaling for τ_p with those proposed for τ_e , previously [18,19].

Edge Transport Barrier for Impurities

Measurements have been made of impurity ion parameters using the upgraded edge charge exchange diagnostic, which can make measurements with a spatial resolution of 1 cm and a temporal resolution of 2-5ms under optimum conditions.

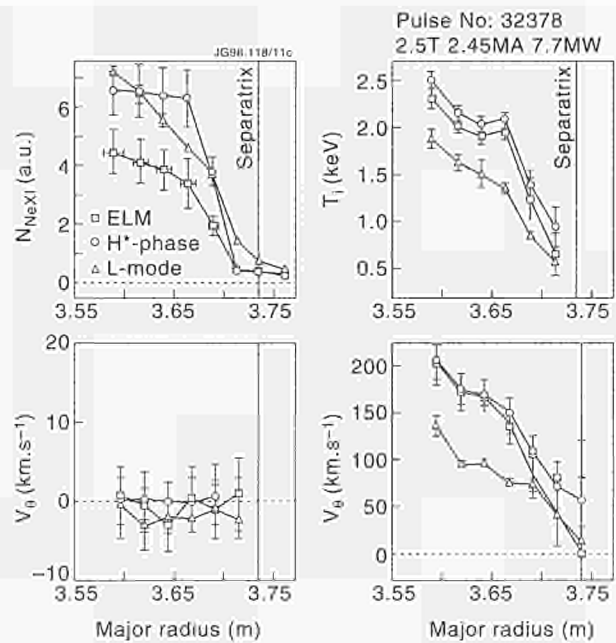


Fig.203: Profiles of Ne XI density, temperature, poloidal and toroidal flow velocities during a giant ELM, quiet H-mode following the ELM, and during L-mode. Steep profiles of density are seen at the edge, particularly during the quiet H-phase, indicating the presence of a barrier to particle transport. In all three phases, the impurity poloidal flow speed remains very low.

An area of particular interest is the L- to H-mode transition and the role of the radial electric field, E_r , at the transition. Measurements show evidence for the formation of a transport barrier just inboard of the separatrix appearing at the moment of the drop in the D_α signal. Outside the separatrix, fully stripped ions are lost rapidly along the open field lines. During the L-mode, there is sufficient outflow of ions from the confined plasma to maintain a significant density in this region. At the start of the H-mode, the transport barrier acts to prevent this outflow, and hence the impurity density outside the transport barrier drops rapidly, within one measurement interval. Inside the transport barrier the gradients of impurity density (also temperature and toroidal flow velocity) begin to steepen.

The profile of E_r is computed from the terms of the lowest order force balance for an ion species (in this case the fully ionised impurity after charge exchange with a heating beam). The changes to the pressure profile result in a growing negative E_r inside the separatrix beginning when beam heating is applied. The drop in the impurity density outside the separatrix results in an increase in the negative E_r at this position. These results are also commonly observed in other, smaller tokamaks. An important difference between the JET results and those of several other devices is that, in JET, there is no evidence for a

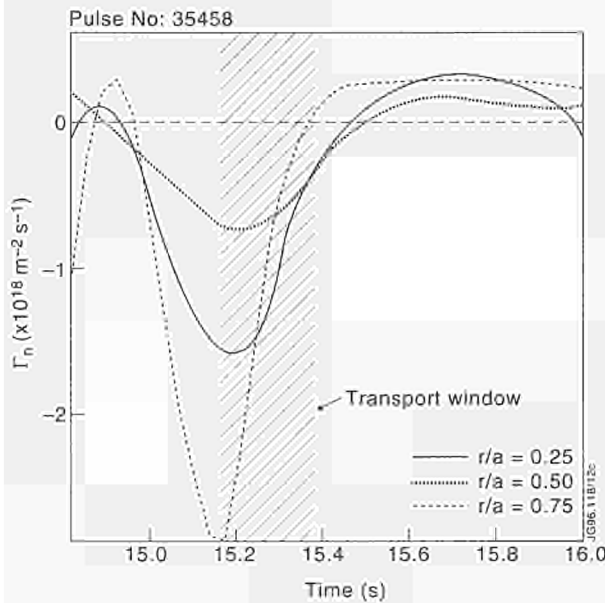


Fig.204: Radial particle flows at $r=0.25, 0.50$ and 0.75 , respectively. The shaded area indicates the highest correlation between Γ_n and ∇n_e across the entire radial profile.

sudden change in the poloidal flow velocity at the H-transition (Fig.203). In other devices, this change gives rise to a sudden large increase in the negative E_r in the transport barrier, inside the separatrix.

Changes to E_r in the transport barrier are important theoretically many theories rely on the mechanism of sheared ExB flow quenching turbulence over a region and reducing transport to the underlying neoclassical level. The measurements reveal that changes in this sheared flow are at least a factor of three lower in JET than in other devices [20]. Such a result could only be consistent with theory if the turbulence level in JET L-modes was correspondingly lower than that in other machines.

Measurements have been made of the changes to impurity transport in the H-mode using laser ablated test ions. The decay time of ion emission (measured in the VUV or soft X-rays) is governed by the rate of impurity transport; dominated by transport across the barrier. The simultaneous ablation of iron and aluminium impurities enables the decay time of ions of different charge to be measured under identical conditions. Preliminary measurements show that although the impurity transport changes abruptly at the transition to H-mode there is no difference in the decay time, during the H-mode, of ions with charge states that differ by a factor of ~ 2 . Combined with the above measurements these results indicate that impurity transport in the H-mode is not directly related to the value of E_r . It appears instead that the impurity

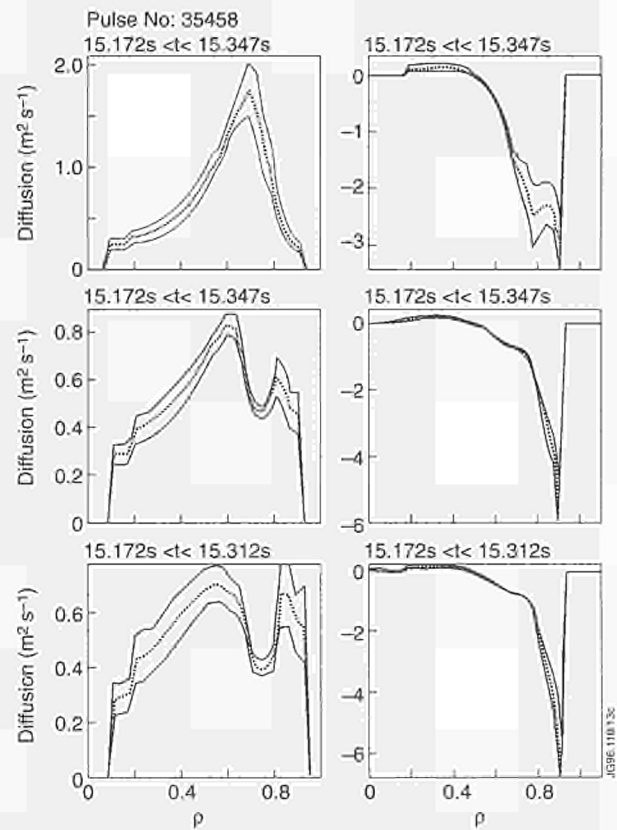


Fig.205: Deduction of diffusion and convection profiles from particle flows and gradients in three neighbouring time windows demonstrate variations and uncertainties in transport data.

transport seen in the H-mode is independent of the field and the test ion charge.

Helium and Neon Transport Experiments

Further experiments dedicated to core impurity confinement and low-Z transport behaviour were carried out at the beginning of 1995 and at another short period towards the end of the experimental campaign. During the first period, the main goal was the exploration of active helium pumping by argon-frost and the assessment of particle replacement times in L- and H-mode plasma with and without active pumping. The second period following an exchange of the divertor graphite target tiles by beryllium tiles was primarily dedicated to transport aspects. Two types of experiments were explored. One type was gas puffing of helium, neon or nitrogen at the plasma edge, the latter two gases seeded into the divertor for radiative cooling studies. The second type was 'central' fuelling of helium making use of helium neutral beam injection.

The evaluation of helium and neon density profiles following short gas puffs at the plasma edge have highlighted several problems, which are specific for the high

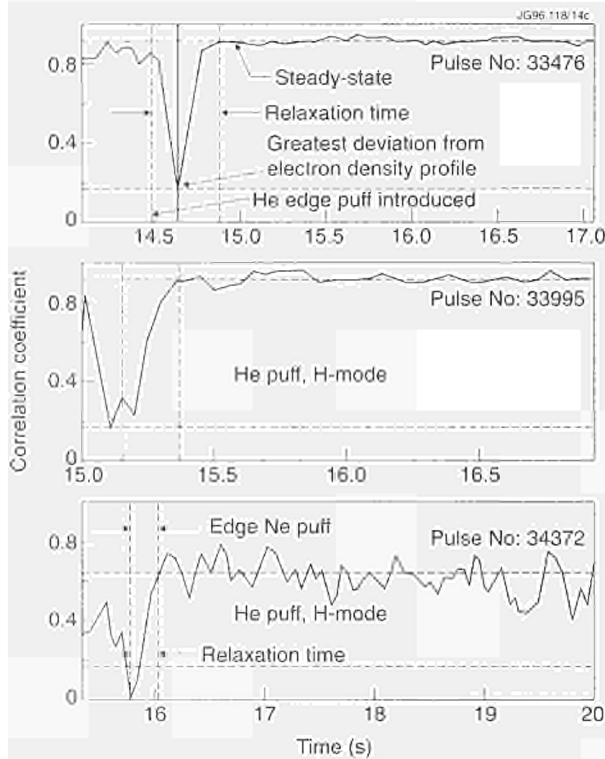


Fig.206: Profile correlation coefficients in H- and L-mode for He and Ne gas puffing.

recycling level and ELM activity of JET in its Mark I pumped divertor configuration. The majority of transport experiments were carried out either in ELMy H-mode or L-mode plasmas. ELM-free H-modes need still to be addressed in future experimental campaigns. The standard procedure for retrieving experimental data on radial particle diffusion and convection velocity is based on the assumption that well within the confined plasma region (i.e. $0 < \rho = r/a < 0.8$), particle sources can be neglected and the profile relaxation can be described entirely by diffusive and convective terms. Experimental errors on radial density gradients can be quite high close to the plasma magnetic axis, where profiles are flat, and the radial range suitable for transport analysis is even further reduced to $0.2 < \rho < 0.8$. A similar argument applies for the selection of a suitable time window following the gas inlet. The time window, which has turned out to lead to acceptable levels of errors in transport data, is defined by the strongest excursions of the radial particle flow to a time when approximately steady-state is reached (Fig.204). A crucial parameter for the suitability of time and space transport analysis windows is the correlation ($0 \leq \rho^2(\Gamma/n_r, \nabla n_r/n_r) \leq 1$) between changes in the particle flow and changes in the gradient. The selected time window may affect considerably the error margins of deduced values for D and v . Figure 205 gives an example of D and v profiles deduced from only slightly shifted adja-

cent time windows. From the appreciable variation of D and v , it must be concluded that transport data are time dependent. An inspection of individual density traces usually reveals that transport is affected by sweeping of the X-point, sawtooth crashes and/or ELM activities. Smoothing of density traces was used to allow numerical differentiation in time for the deduction of particle flows $\Gamma(\rho)$. Taking into account the substantial variations experienced for the correlation $\rho^2(\Gamma/n_r, \nabla n_r/n_r)$ as a function of the minor radius and also its strong dependence on the selected time window transport data can only be quoted within a factor of 2.

It is important to note, that in spite of inherent experimental uncertainties in the deduction of transport data, there are some common features, which have been proven to be systematic and reproducible. JET and other tokamaks have reported on the close similarity between helium density profiles and electron density profiles once steady-state conditions have been reached. The similarity of profiles has in fact initiated an additional route to the deduction of transport data, which is based on the evaluation of characteristic time-scales of perturbed impurity density profiles following the gas puff at the plasma edge. A radial profile shape correlation factor $\rho^2(n_i/n_e)$, which establishes a radial correlation between impurity and electron density values, (i.e. $\rho^2=1$), when impurities and electrons have an identical radial profile and $\rho^2=0$ when there is no correlation at all, allows the assessment of representative time-scales. For helium density profiles, ρ^2 reaches values close to 1. By contrast, carbon and neon density profiles are more hollow than electron density profiles. In the latter case, a timescale can be derived which elapses in between the greatest profile perturbation and steady-state following the gas-puff. Figure 206 gives an example for helium puffing in L- and H-mode and one example for neon puffing. The strength of the profile correlation analysis is, that no model on a particular radial shape has to be imposed and a normalised shape coefficient is derived.

An overview (Fig.207), shows that profile relaxation times and energy confinement times indicates that are of the same order and H-mode relaxation times are longer than comparable L-mode cases. Moreover, making use of D and v values derived from the standard particle flow versus gradient analysis, radial and calculating representative eigenmode decay times, it is found that the shorter radial mode times agree within error bars with values derived from the profile relaxation analysis.

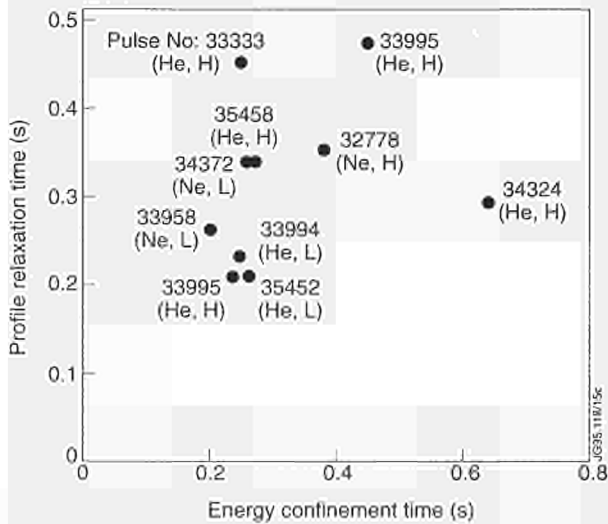


Fig.207: Profile relaxation times and energy confinement times in H- and L-mode plasmas deduced from helium and neon gas puff experiments.

Predictive Modelling of L- and H-Mode Plasmas

A comprehensive predictive modelling of the series of the quasi-steady state L and H-mode shots together with the modelling of the different kind of the heat pulses were performed by using the predictive transport code JETTO. The main objective was to find a model for the energy transport, which can equally well describe the evolution of the ion and electron temperatures in various situations. Three basic problems were considered. First was the question whether transport was of the Bohm or of the gyro-Bohm type (the experimental data indicate that it

depends on the magnetic field and on the machine size and generally speaking is of the Bohm type in L-mode plasma and of the gyro-Bohm type in the H-mode).

To resolve this problem, L-mode discharges were modelled from different tokamaks which were collected in the ITER profile database (including discharges from JET, DIII-D, TFTR, JT-60U and ASDEX). Three empirical models were tested: pure Bohm, pure gyro-Bohm and a combination of the two. Results of the transport analysis concluded that a linear combination of the Bohm and the gyro-Bohm transport coefficients fitted the experiments best.

The second problem under consideration was the modelling of the different kind of dynamic experiments. This included heat pulses produced by sawtooth crashes and by the L-H transition together with the cold pulses triggered by the giant ELM or by impurity ablation [21]. Analysis shows that all heat and cold pulses initiated near the separatrix have a global character that is that transport coefficients change simultaneously not only near the plasma edge but in the whole outer half of the plasma volume [22]. On the other hand, a heat pulse caused by the sawtooth crash, has no such a global character excluding very short ballistic effect. Numerical analysis of such pulses is shown in Fig.208(a) and (b) and allows the conclusions, that all these global phenomena can be modelled, if we assume that the Bohm transport coefficient is multiplied by the relative electron temperature gradient near the separatrix. With this transport model,

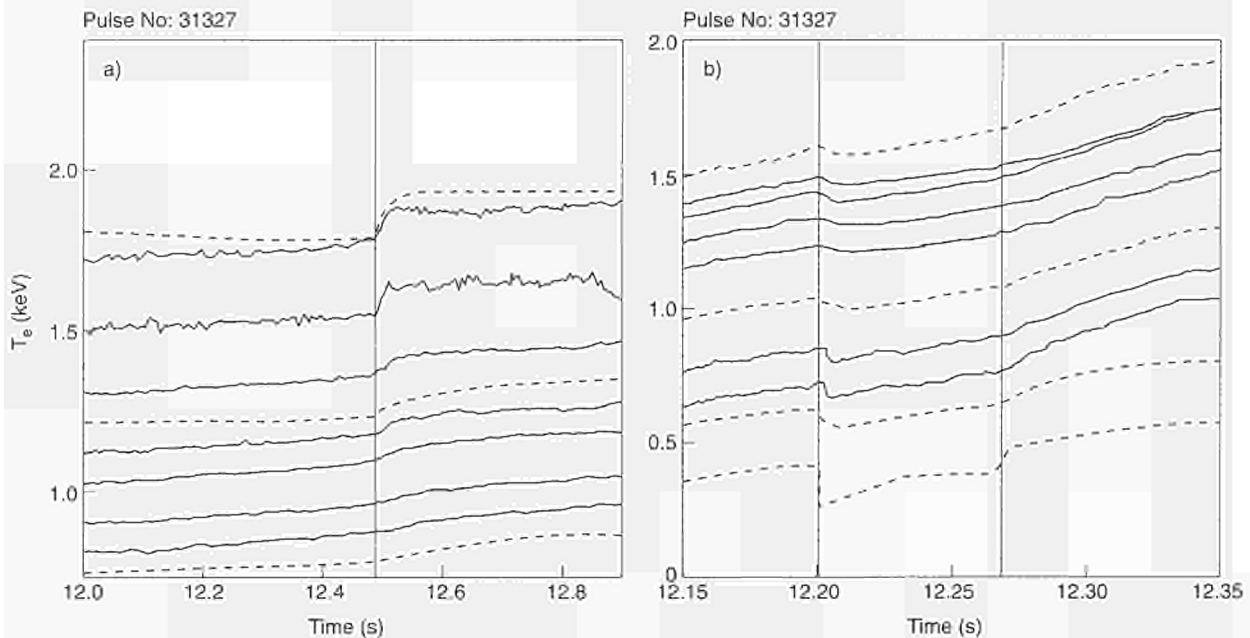


Fig.208: Temporal evolution of the measured (solid lines) and calculated (dashed lines) electron temperature at different radii for Pulse No.31327. Three different pulses propagating across the plasma can be observed: (i) sawtooth crash (at $t=12.05s$, Fig.(a)), (ii) laser ablation induced cold pulse (at $t=12.2s$, Fig.(b)); and (iii) L-H transition (at $t=12.26s$, Fig.(b)).

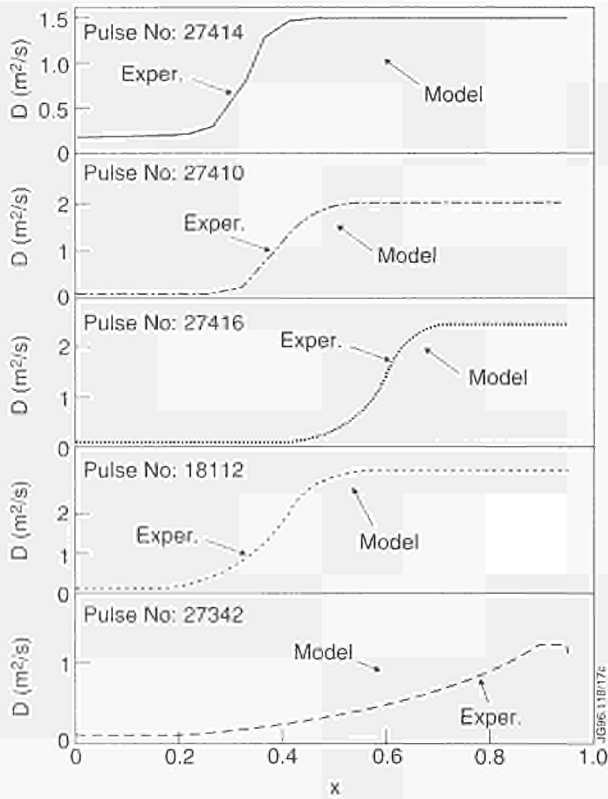


Fig.209: Comparison of the experimental D with that predicted from the semi-empirical model for each pulse.

both L and H-mode plasmas can be modelled without any modification of the numerical coefficients provided the temperature near the separatrix was known.

Finally, attempts were made to find the model which could describe the evolution of the ion and electron temperatures near the separatrix, in particular, during L-H transition and in the ELM-free H-mode plasma. Numerical analysis showed that the temporal evolution of the edge temperatures and global plasma parameters (such as global energy content and global energy confinement time) in the ELM-free JET H-mode plasma could be successfully modelled with an assumption that both electrons and ions energy losses from the edge transport barrier were limited by the direct neo-classical losses of the trapped particle [23]. In particular, it was shown that in the banana regime these losses did not depend on the edge temperature. This fact could explain the experimentally observed continuous rise of the energy confinement time in the hot-ion H-mode JET plasma during the long ELM-free period.

Semi-Empirical Drift-Wave Model for the Simulation of Impurity Transport

Based on experimental results on the slowness of impurity transport, where the magnetic shear $s < 0.5$ [24] and on theoretical studies of the importance of the s parameter

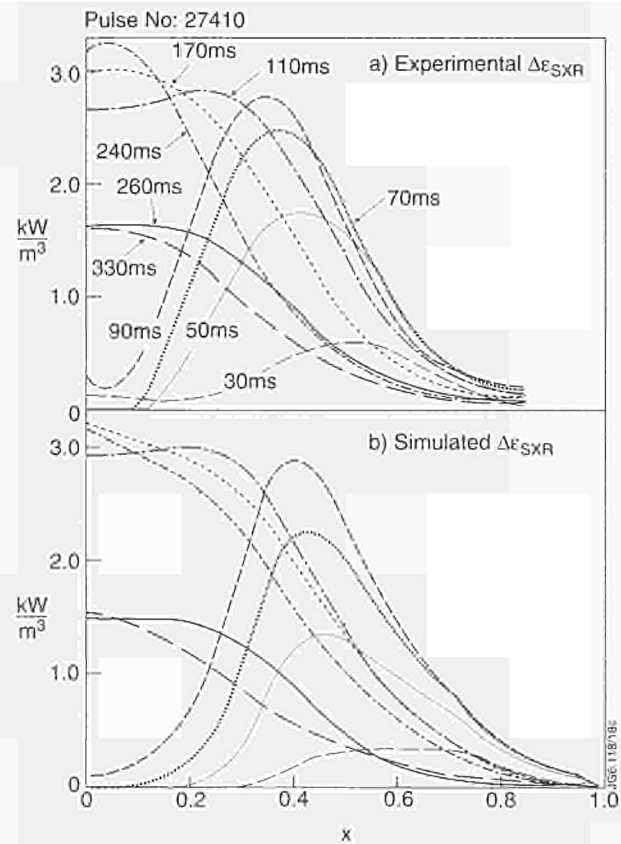


Fig.210: Experimental and simulated emissivity profiles for discharge Pulse No.27410.

in determining the strength of toroidal coupling between neighbouring microturbulent modes [25], a new semi-empirical model was proposed for the prediction of the diffusivity D and the radial convection speed V of impurities in L-mode discharges.

The global radial structure due to toroidal coupling results [25,26] has an exponential dependence of the enhanced correlation length L_r on s when that parameter was small $L_r \approx (\rho_i/s)^{1/2} \exp(-c/s)$. Here ρ_i is the ion gyroradius and c a constant of about unity. This leads to Bohm-like expressions for the transport coefficients.

This form fits the required decrease in the low-shear region (irrespective of the sawtooth activity) and dependence on the temperature gradient. It is also independent of the impurity charge Z , as found experimentally and is close to the energy diffusion proposed [19]. The expressions for D and V vanished towards the plasma centre, where $s \rightarrow 0$. In this region, however, L_r should not fall below ρ_i ; therefore a gyro-Bohm-like term needs to be added in order to have a residual transport in the region of low shear.

Setting the numerical factors $a=0.008-0.01$, $b=3.5-4.0$ and $c=1.2-1.4$, good predictions are obtained within the experimental uncertainty for the salient features of the

diffusivity profile in the bulk of the discharge: (i) the radial extent of the low transport region; (ii) the magnitude of D in the region of *slow* transport; and (iii) the magnitude of D in the region of *fast* transport. The resulting profiles of D for several pulses are shown in Fig.209, compared with the corresponding experimental ones [24].

This model is not expected to describe the last few cm close to the separatrix. An ad hoc treatment of this region is needed [27] for the predictive simulation, i.e. a peripheral transport barrier (decrease of D and strong increase of the inward pinch V) preventing too fast an outward diffusion of the lower to intermediate ionised states.

As an example of the performance of the model, Fig.210 shows the experimental profiles of the perturbation to the soft X-ray emissivity and their simulation for a JET pulse.

References

- [1] S. Kaye, et al., IAEA-CN-60/E-P-3, Seville (1994).
D. Schissel, et al. EPS Lisbon (1993).
- [2] B. Balet, et al., EPS Bournemouth (1995).
- [3] F. Ryter and the ITER Database Working Group. IAEA H-mode Workshop Proceedings PPPL (1995).
- [4] C.C. Petty, T.C. Luce, K. H. Burrell, et al., Physics and Plasmas, Vol. 2, 2342 (1995).
- [5] E. Righi et al., Proc. 22nd EPS Conference on Controlled Fusion and Plasma Physics, Bournemouth, UK, 3-7 July 1995, Vol. 19C, Part II, p.73.
- [6] F. Ryter and the H-mode Database Working Group, to be published in Nuclear Fusion (1996).
- [7] E. Righi and KD Zastrow, to be submitted for publication in Nuclear Fusion.
- [8] Sartori, R., et al., in Controlled Fusion and Plasma Physics (Proc. 22nd Eur. Conf. Bournemouth, 1995), Vol. 19C, Part IV, European Physical Society, Geneva (1993) 141.
- [9] Schissel, D.P., et al., in Controlled Fusion and Plasma Physics (Proc. 20th EUR. Conf. Lisbon, 1993), Vol. 17C, Part I, European Physical Society, Geneva (1993) 103.
- [10] Jones, T.T.C., et al., in 1992 International Conference on Plasma Physics (Proc. 19th Eur. Conf. Innsbruck, 1992), Vol. 16C, Part I, European Physical Society, Geneva (1992)1.
- [11] Bracco, G., Thomsen, K., To be published.
- [12] F. Wagner and U. Stroth, Plasma Phys. Control. Fusion 35 (1993) 1321
- [13] Zou, XL., et al., in Controlled Fusion and Plasma Physics (Proc. 22nd Eur. Conf. Bournemouth, 1995), Vol. 19C, Part I, EPS, Geneva (1993)41.
- [14] M. Mattioli, R. Giannella, R. Myrmas et al., Nucl. Fus. 35 (1995) 1115.
- [15] E.S. Marmor, J.E. Rice, J.L. Terry and F.H. Seguin, Nucl. Fus. 22 (1982) 1567
- [16] R. Giannella, M. Mattioli, C. De Michelis, et al. Proc. 22nd EPS Conf. on Contr. Fus. and Pl. Phys. Part I (1995) 85.
- [17] J.W. Connor and J.B. Taylor Nucl. Fusion 17 (1977) 1047.
- [18] P.N. Yushmanov, T. Takizuka, K.S. Reidel et al. Nucl. Fusion 30 (1990) 1999.
- [19] A. Taroni, M. Erba, E. Springman and F. Tibone Plasma Phys. Controll. Fusion 36 (1994) 1629.
- [20] N.C. Hawkes, D.V. Bartlett, D.J. Campbell et al., Proceedings of the 5th H-mode Workshop, to be published by Plasma Physics and Controlled Fusion (1996).
- [21] The JET Team, presented by R. Giannella, Proc. 15th IAEA Conf. on Pl. Phys. and Contr. Nucl. Fus. Res., Seville 1994, IAEA Vienna 1995 Vol 1 p. 307.
- [22] J.G. Cordey, D.G. Muir, S.V. Neudachin, V.V. Parail et al, Nuclear Fusion 35 (1995) 101.
- [23] V.V. Parail, B.Balet, P. Bak, J.G. Cordey et al., Proc. 15th IAEA Conf. on Pl. Phys. and Contr. Nucl. Fus. Res., Seville 1994, IAEA Vienna 1995 Vol 1 p. 255
- [24] R. Giannella, L. Lauro-Taroni, M. Mattioli et al, Nucl. Fus. 34 (1994) 1185
- [25] F. Romanelli and F. Zonca, Phys. Fluids B5 (1993) 4081
- [26] J.B. Taylor and H.R. Wilson, Culham Lab.Report, UKAEA FUS 279 (1995)
- [27] B.Denne-Hinnov, R. Giannella, L. Lauro-Taroni et al., Proc. 20th EPS Conf. Lisbon (1993), Vol 17C, I-55

MHD and Beta Limits

During 1995, studies of magneto-hydrodynamic (MHD) behaviour has mainly concentrated on the performance limitations observed in JET plasmas during high power neutral beam heating. With the fast new acquisition system, Central Acquisition and Timing System (CATS), MHD phenomena such as sawteeth and ELMs have been analysed resulting in new information on these events. In addition, a new soft X-ray diagnostic system with over 400 channels has been developed allowing analysis of modes with poloidal Fourier components of up to $m=5$.

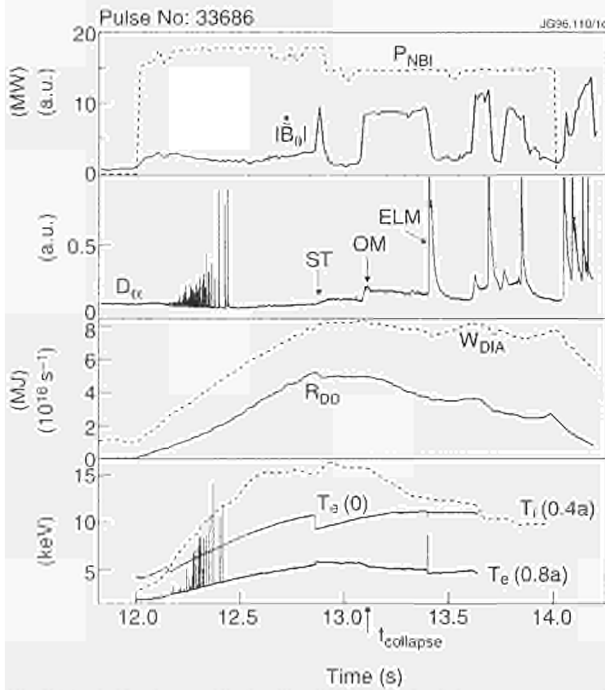


Fig.211: A discharge (Pulse No.33686) limited by a sequence of MHD events. The first and mildest event is a sawtooth. The second event is an $n=1$ outer mode, which is followed by the collapse in reactivity, R_{00} , and loss of the hot-ion H-mode regime. The third event is a giant ELM, which in this case has a beneficial effect by temporarily stopping the R_{00} collapse. The time " $t_{collapse}$ " indicated in the figure, is the time of the fastest decay of R_{00} .

Performance Limits

The performance of JET hot-ion H-modes appears to be limited by MHD phenomena. There are three classes of MHD events that are associated with a limitation in the plasma performance in the hot-ion ELM-free H-modes: core modes (such as sawteeth which can cause substantial drops in the core temperatures); giant Edge Localised Modes (ELMs); and the so-called Outer Modes (OMs). Figure 211 shows an example, where all three limiting events occur at various times in the same discharge. Although there is a clear relation between the time of the deterioration in the hot-ion H-mode performance and the appearance of the MHD activity, it is difficult to understand how the relatively low level MHD activity (the OM has a typical displacement of 2-3 cm) can produce the observed losses of heat and particles. The role of the MHD event and the question of which parameters determine whether or not the limitation process is irreversible remain to be answered.

It was observed that the occurrence of ELMs correlated well with the calculated edge pressure ballooning limit. Indeed, increasing edge shear and shaping led to long ELM-free periods. Figure 212 shows this correlation between the measured edge pressure gradient, ∇p , and the

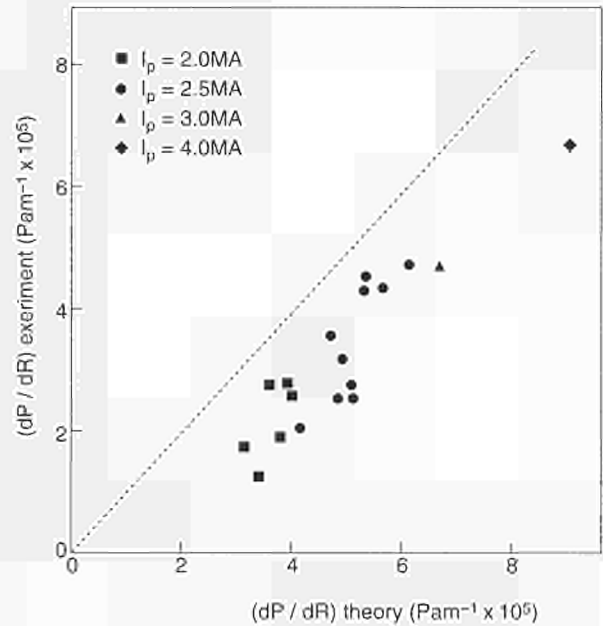


Fig.212: The experimental edge pressure gradient, ∇p , versus the calculated ballooning limit for various plasma currents and configurations.

MHD effects at the plasma edge can be clearly observed with the soft X-ray cameras, magnetics and ECE. From the X-rays measurements, it can be seen that the so-called Outer Mode, which probably has an $m = 5, n = 1$ structure, is limited to the outer region of the plasma just outside the $q=3$ radius. The location of the mode observed with the X-ray diagnostic is shown in Fig. 213. This mode is consistent with an external kink driven by a edge current which is too large, related to the ∇p driven bootstrap current.

Analysis of these phenomena in discharges with different edge safety factors shows that MHD phenomena occur earlier in time and at higher amplitude. Since the normalised confinement time of the hot-ion H-modes increases gradually with time, this explains qualitatively why plasma performance of plasmas measured relative to the normalised confinement time deteriorates with decreasing edge q .

MHD Related Transport Analysis

Some discharges have been analysed with the TRANSP code to clarify the effect of MHD instabilities on the plasma transport. To better understand the role of the MHD phenomena, TRANSP analysis of the discharges, during the period that these phenomena occur, has been carried out. A pulse, where the OM is present, has been chosen since the OM persists for several hundreds of milliseconds and a proper power balance as been made.

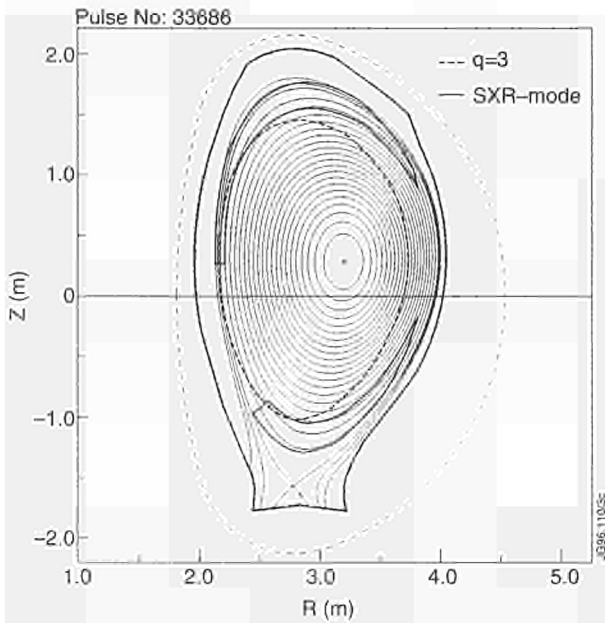


Fig. 213: The location of the observed Outer Mode (as seen by the soft X-ray measurements). The mode is observed outside the $q=3$ surface in agreement with stability calculations by the CASTOR code.

Although the OM is localised just outside the $q=3$ surface, covering the outer 4-5cm of the plasma, it nevertheless affects the outer 25cm of the plasma transport, resulting in an increase of plasma heat conductivity by a factor 3 in this region. This then gives rise to a narrowing of the ion temperature profile and a limitation in the neutron emission.

A TRANSP simulation of the same discharge excluding the effects of the OM on the ion heat conductivity, by using an extrapolation of the background conductivity, allows an estimate of the part of the reduced performance which is due to the OM and the part which constitutes the underlying behaviour. The simulation indicates that the mode is responsible for a reduction in plasma energy of less than 10% but for a loss in neutron rate greater than 30%. Figure 214 shows the measured D-D production rate for a typical hot-ion H-mode together with a TRANSP calculation with and a simulation without "MHD-effects" on the heat conductivity in the outer 25cm of the plasma.

At the end of the ELM-free period, the discharge is already close to a loss of the hot-ion H-mode, with an ion temperature decreasing to the level of the electron temperature. This is due to an increasing density, which leads to an increasing ion-electron equipartition and a slowly increasing edge conductivity and a decreasing central ion heating.

It seems that MHD activity is limiting the plasma performance by an estimated 30-40% and that it is important to reduce the density increase in the hot-ion ELM-free H-modes to prevent not only the slow degradation of the hot-

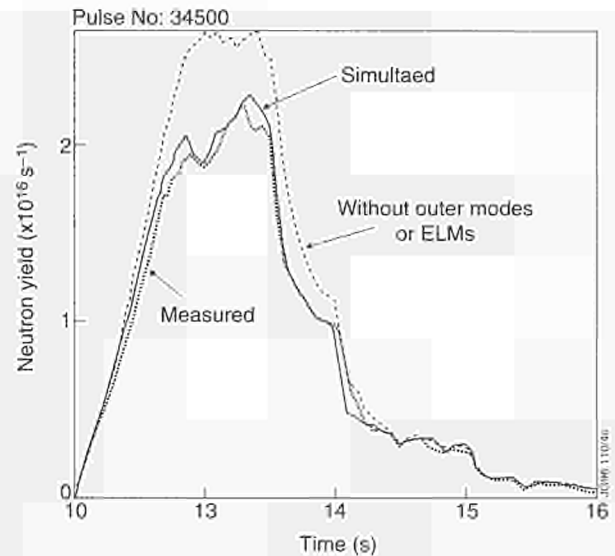


Fig. 214: The measured and calculated and simulated neutron yields versus time. In the simulation, the extra loss terms on the heat conductivity in the outer plasma were excluded. This led to a broader ion temperature profile and a higher neutron yield. Central values were unaffected. At $t=13.5s$ the yield was drastically reduced due to a sawtooth (not removed in the simulation). This sawtooth leads to a reduction in the central temperature, which further increased the ion-electron equipartition, terminating the hot-ion character of the discharge.

ion H-mode but also the cause of the edge instabilities driven by an edge pressure and edge current, that is too large.

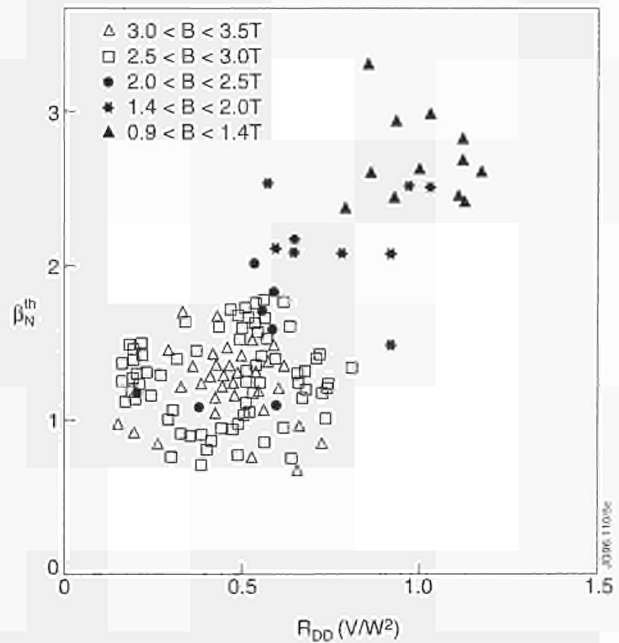


Fig. 215: The normalised thermal beta, β_N^{th} versus a normalised D-D reaction rate R_{DD} , with V is the plasma volume and W is the diamagnetic plasma energy. The various symbols are for the various toroidal magnetic fields. There are essentially two groups: one group with $B_t < 2T$ and the second group with $B_t > 2T$. The best hot-ion ELM-free H-modes are in the top right hand corner of the second group, limited at $\beta_N \sim 2$. The top right handed stars are hot-ion H-modes at 1.7MA, 1.5 T achieving marginal ballooning stability over most of the plasma cross-section.

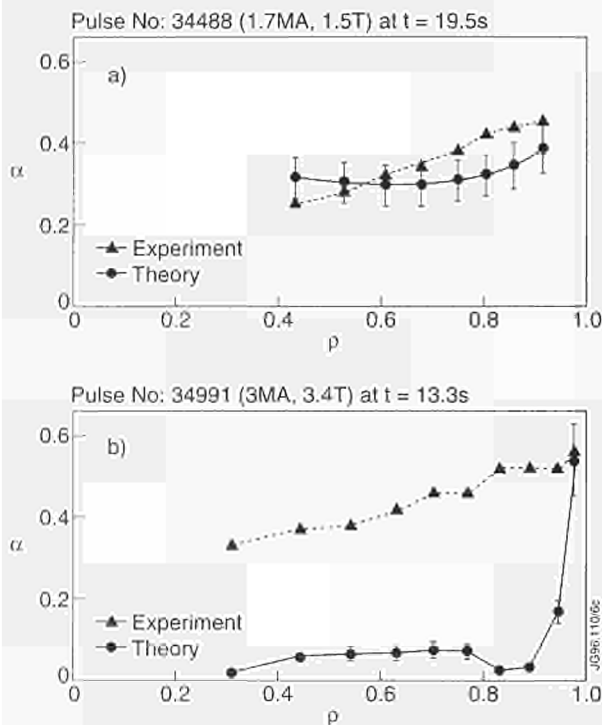


Fig.216: The normalised pressure gradient $\alpha = -(dp/dr) \cdot (2\mu Rq^2/B^2)$ versus normalised radius $\rho = r/a$ for low current and field discharge (Pulse No.34488) at the time of maximum beta and the same for a high current and field discharge (Pulse No.34991). The latter is only reaching the ballooning limit at the edge just before the ELM occurs.

High Beta Discharges

Although there are no universal thresholds in normalised β for these MHD events, there are a number of general observations which can be made. First of all the limiting events never seem to occur at β_N values below unity.

The highest performance hot-ion H-modes have plasma currents in the range of 3-4MA. For these, there is an experimental upper limit on β_N set by the ELMs and outer modes ~ 2 (see Fig.215). This is clearly well below the Troyon limit for these pulses, which are at a local edge, rather than global, MHD limit. By operating at proportionately lower current (~ 1.7 MA) and toroidal field (~ 1.6 T) it has been possible to achieve a thermal $\beta_N \approx 3$. Calculations show these lower field cases are close to the marginal ballooning stability boundary across the entire plasma radius and are also marginally $n=1$ stable with the wall at the vessel location (Fig.216).

Despite their different position in respect to the global MHD stability boundary, these lower field higher β_N cases are still limited by the same three types of instability as seen from the experiments. This demonstrates that the main limiting instabilities (ELMs and outer modes) are due to local edge limits, whose stability depends on edge current and/or pressure gradients (the two being linked through the bootstrap contribution to the edge current). Apart from the higher fast particle content at lower plasma current, possible reasons why higher β_N is achieved at lower current remain still to be determined. However, at the lower plasma currents, the β rise is seen to occur much more rapidly for a given power level ($\sim 16-18$ MW), and hence the maximum β is reached at much lower densities, which allows for much more central power deposition.

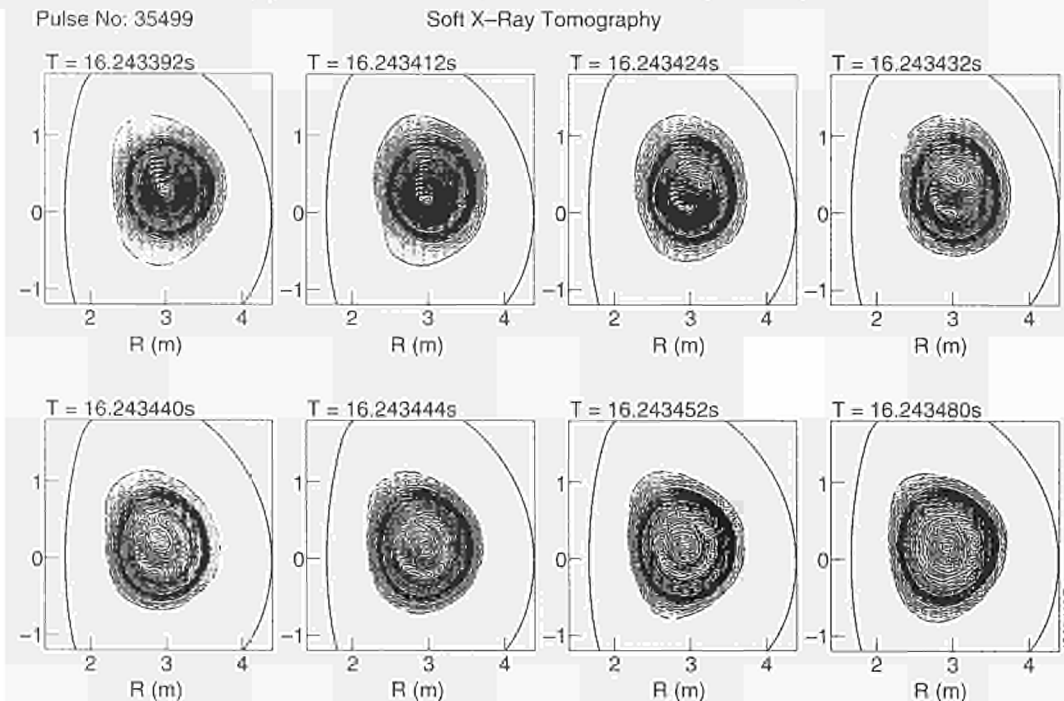


Fig.217: Reconstructed soft-X-ray emission during the rapid collapse of a sawtooth in Pulse No.35499.

Another class of high β discharges are the high β poloidal shots at low plasma current. These are discussed in detail in the section on Tokamak Concept Improvements. Essentially, these discharges can be quasi-steady state at very high β_N , because the frequent ELMs keep the density constant.

Fast Sawtooth Crash

Fast sawtooth crashes were first discovered in JET about a decade ago. Early tomographic reconstructions of data from a two camera system showed that, firstly, the original hot plasma centre was displaced off-axis to the $q = 1$ surface, and then a crescent pattern of emission was observed as the energy became redistributed uniformly over the region of the plasma, within the $q = 1$ surface. Both the speed of the crash and the redistribution mechanism has led to several new theoretical ideas on the mechanisms of the sawtooth. The data did not correspond to the Kadomtsev model.

The sawtooth analysed occurred, without precursors, during a 2.6MA, 3.3T discharge with $T_{eo} = 8.0\text{keV}$, and $n_{eo} = 4.5 \times 10^{19}\text{m}^{-3}$. Additional ICRF heating of 11MW was applied. Figure 217 shows clearly the three stages of the collapse: initial movement of the core; formation of crescent shape; and collapse to a symmetric state with a region of approximately constant emission within the $q = 1$ surface. This particular sawtooth is also extremely fast with the whole process over in $\sim 100\mu\text{s}$. This data gives a very close confirmation of previous work on fast sawteeth.

Disruptions

Tokamak discharges can be terminated by a disruption. It is generally accepted that these have a variety of causes such as a too low edge q value, a too high density or impurity level. Although each disruption proceeds in an individual way, the final events leading to the negative voltage spike and current decay are generally the same. On the soft X-rays and ECE temperature measurement, the final event is seen as a rapid cooling of the central region of the plasma followed by a characteristic electron temperature and X-ray spike coincident with the negative voltage spike. The rapid cooling phase has been identified theoretically as due to the growth and interaction of a number of different MHD modes leading to a loss of confinement. Experimentally, this phase has always been observed in JET as a plasma erosion, which in the older tomographically reconstructed profiles have always exhibited an $m = 1$ characteristic only. However, with the new multi-camera system which can resolve much higher

m -numbers, shows in addition a clear $m = 2$ structure for the first time. It is possible that even higher m -numbers appear at larger radii and have not yet been detected due to the lower emission towards the plasma edge.

Edge Localised Modes

Edge Localised Modes (ELM's) are present in most JET discharges with an X-point. These limit impurity build up within the plasma and sometimes terminate extended periods of high plasma performance. In H-mode discharges, the plasma has a high temperature close to the separatrix, and, therefore, the effects and structure of the ELMs can be studied with the soft X-ray cameras.

As seen by a single camera the ELM's often consist of a series of sharp spikes of emission quite limited in space and time. Some of these spikes are clearly related to increased emission from the divertor strike zones or from the X-point. However, by observing correlations from the lines-of-sight of the different cameras, it is clear that some of the emission spikes originate well within the plasma.

Physics Issues related to the Next Step

This section highlights progress on a number of topics of specific relevance to ITER, and are topics which are not already covered in the JET programme. Two JET experiments were carried out during 1995 specifically for ITER. These were the 'Second JET TF Ripple Experiment', and Plasma Operation on a Molten and Damaged Beryllium Divertor Target'. These are described below.

The Toroidal Field Ripple Experiment

In 1992, a first experiment on the effects of toroidal field (TF) ripple was carried out [1]. In this experiment, JET was operated with 16 of its 32 TF coils. In 1995, a second ripple was carried out [2]. In preparation, a considerable re-configuration of the TF coil system was undertaken. A midpoint busbar was constructed from the TF power supplies to the mid-point between the two 16-coil sets, and the Toroidal Flywheel Generator and Static Units configuration was modified. The new set-up allowed operation with different currents in the two 16 coil sets. This made operation possible with variable ripple, ranging from pure 32-coil ripple, δ_{32} , to about 50% of pure 16-coil ripple, δ_{16} . In the JET pumped divertor configuration, δ_{32} corresponded to about 0.1% ripple at the plasma edge,

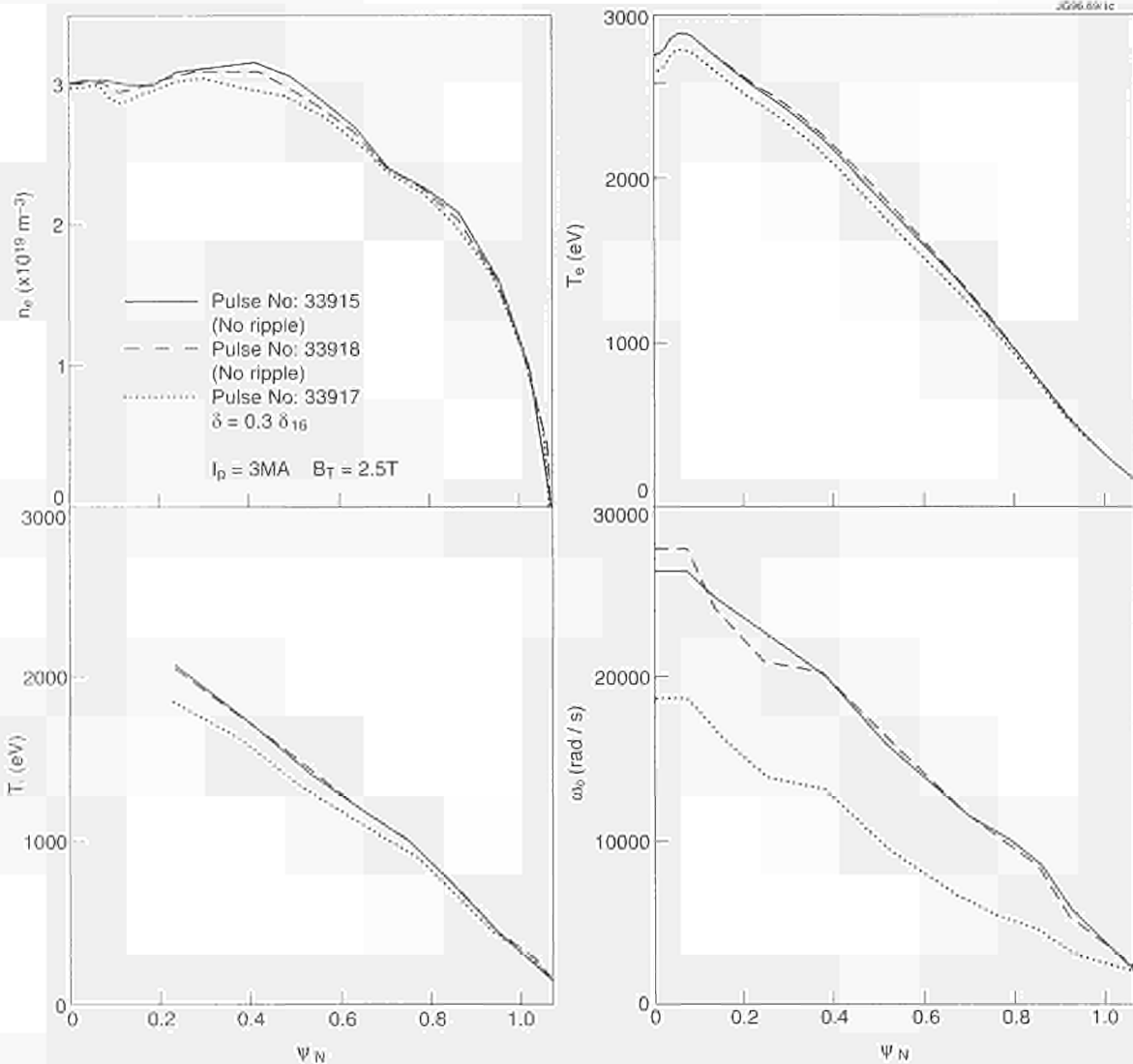


Fig.218: Profiles of density, electron temperature, ion temperature and angular rotation frequency for two discharges with $\delta = \delta_{\text{ripple}}$, and one with $\delta = 0.3\delta_{\text{ripple}}$. Toroidal field was 2.5T, and plasma current was 3MA.

while $0.5\delta_{\text{ripple}}$, corresponded to about 2%. The main objectives of the experiment were to investigate the general effects of TF ripple in the ITER relevant regime, and to elucidate the anomalies with NB heating of discharges observed with ripple in the first ripple experiment.

Experiments with ohmic plasmas, comparing discharges with δ_{ripple} , with discharges at $\delta = 0.3\delta_{\text{ripple}}$, showed no measurable loss of electron temperature or D-D reaction rate. Similarly, experiments with Lower Hybrid heating showed no degradation. (LH fast electrons are not subject to the normal ripple-induced banana particle transport due to their small Larmor radius.) Hence, it was concluded that the ripple-induced heat diffusivity of the background plasma was small. This was in accordance with expectations.

Figure 218, shows measured profiles of three discharges with NB heating, two of which have the normal 32 coil ripple, δ_{ripple} , and one has ripple, $\delta = 0.3\delta_{\text{ripple}}$, ignoring the small δ_{ripple} component. NB power was 2.8MW. Only the tangential

injector set was used, for which there is no direct injection into the ripple well loss cone. In the pulse with ripple, a reduction of central T_e by about 3%, a reduction of T_i of about 10%, and a reduction of plasma rotation velocity by about 30% were all observed. The total D-D reaction rate was reduced by about 4%. It appeared that the effects of ripple build up throughout the confinement zone, contrary to the common expectation that ripple would lead to a clamping of values at the plasma edge.

The losses were analysed with the Bounce Average Monte Carlo code RLX [3]. This code showed that the observed reduction of D-D rate was consistent with the background changes (i.e. the reduction of the slowing down time). Hence, any losses of NB deuterons at energies near the injection energy were small (<2%). Also, the predicted reduction of the triton burn-up was consistent with the observation, indicating a very small loss (less than a few percent) of 1MeV tritons. Finally, the code predicted a loss

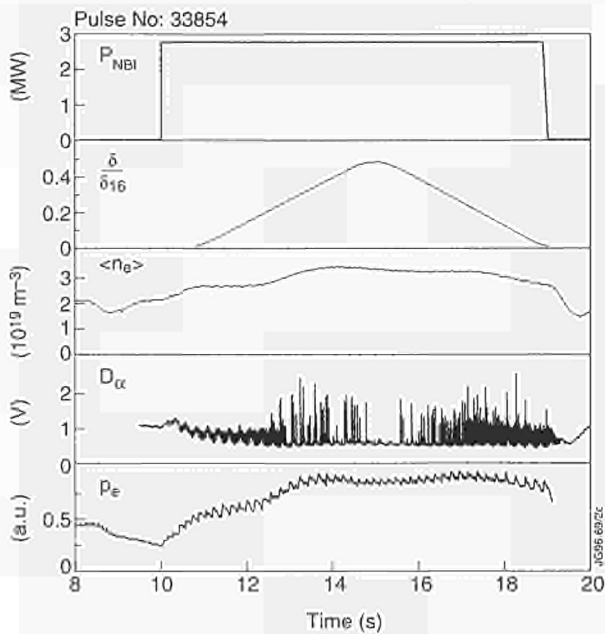


Fig.219: An L to H-mode transition triggered by increasing ripple, and the behaviour of the H-mode under varying ripple. Toroidal field was 2.5T, and plasma current was 3MA.

of plasma heating power of 1.3%. This loss was much too small to explain the observed changes of background plasma parameters. It was concluded from these observations that there was an anomalous loss of NB deuterons at the intermediate energies, typically about 90keV (which corresponded to the critical energy) and thermal energy. Support for this conclusion came from measurements with a neutral particle analyser, which showed a significant reduction in the measured spectrum of charge exchanged deuterium particles at the intermediate energies, while showing no reduction near the 125keV injection energy.

For the discussion of the effect of ripple on the H-mode, it is necessary to distinguish between effects on the H-mode threshold, and effects on the H-mode confinement. The effect on the threshold is small. In fact, ripple can slightly reduce the H-mode threshold. This is illustrated in Fig.219, where the ripple is ramped up during a phase of constant NB power and density. The NBI power level is just below the normal H-mode threshold level. The trace labelled 'p' is the product of a local electron temperature and the density, and hence represents a plasma pressure. Up to 12.2s, the discharge remains in a clear L-mode. Then, when the ripple reaches about $0.2\delta_{16}$, a transition to ELMy H-mode is observed, and plasma pressure is observed to increase. Between about 14s and 16s, while the ripple exceeds $0.3\delta_{16}$, the plasma pressure is reduced somewhat. The ELM frequency is also reduced, but the brief phase between 14.8s and 15.5s is not

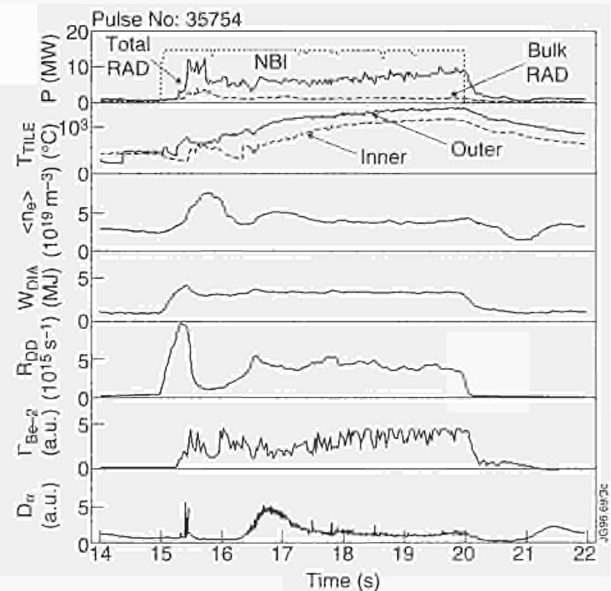


Fig.220: Traces for a discharge at high power without gas puff, leading to gradual increase of the radiated power fraction and to melt damage of the Beryllium target tiles. Toroidal field was 2.8T, plasma current was 3MA.

a genuine ELM-free phase. The reverse pattern of events is observed while the ripple is ramped down.

In discharges with NB power well above the H-mode threshold, and ripple at the level of $0.5\delta_{16}$, a slight degradation of the H-mode was observed. In discharges without ripple, short ELM-free phases were observed, while these were absent in discharges with ripple.

Experiments were conducted to establish the effects of TF ripple on the sensitivity of the plasma to error-field induced locked modes. Error fields in these experiments were produced by ramping up the currents in the in-vessel saddle coils. For ohmic discharges, ripple made the plasma more robust against the locked mode, while, for discharges with NB rotation drive, ripple made the plasma less robust. These results are in qualitative agreement with the theoretical understanding of locked mode generation as a result of the decreasing rotation velocity of the reference frame of magnetic perturbations.

Ripple effects depend on three main dimensionless parameters: the ripple, the normalised Larmor radius r/a , and the collisionality. It was expected in the first instance, that in ITER, with its significantly smaller r/a , ripple effects would be smaller than in the JET experiments. Taking this into consideration, it appeared that none of the effects studied would pose a serious problem for ITER. Hence, the critical ripple issue for ITER is likely to remain the localised heat-loads on first wall components due to α -particle losses. These losses due to

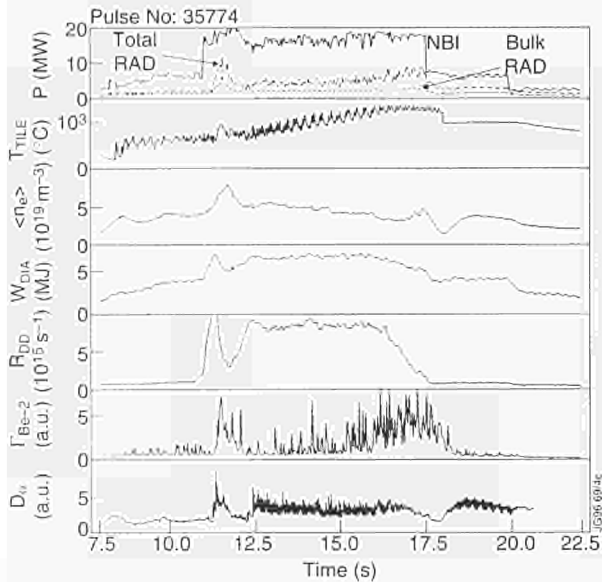


Fig.221: Traces for a discharge with a total input energy of 180MJ on the Beryllium Divertor target. Toroidal field was 2.8T, and plasma current was 3MA.

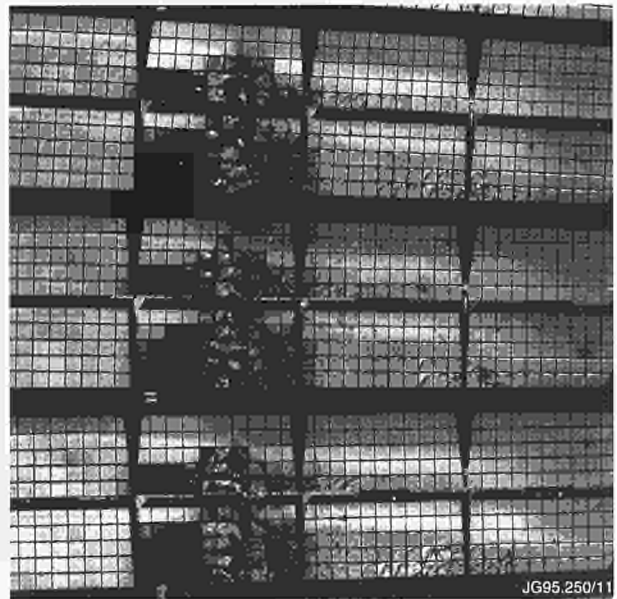


Fig.222: The Beryllium Divertor target after the melting experiments.

stochastic diffusion and ripple well trapping are relatively straightforward to calculate with the Guiding Centre Following Monte Carlo codes.

Operation on a Molten and Damaged Beryllium Divertor Target

In the final phase of the 1994/95 experimental campaign, the carbon divertor target in the Mark I divertor was replaced by a beryllium target. Most of the experiments on the Be target were conducted to avoid melting. However, at the end of the campaign, an experiment was carried out specifically to address the questions of operation on Be in molten and/or damaged conditions [4]. An important motivation for these experiments was to test the speculation that, in ITER, a Be target would self-protect against excessive heat-fluxes in off-normal operating conditions. In this scenario, evaporating Be would lead to high radiative power losses and thus reduce the heat flux to the target. This scenario is usually referred to as the ‘vapour shield’, although Be vapour as such plays no role.

The experiments were conducted with the strike zones on a part of the divertor target that had not been damaged by prior operation. A series of discharges was performed with increasing energy deposition on the target, and with reducing rates of gas puff. Sweeping of the strike zones was disabled. Tile temperatures were measured using a CCD infra-red camera, while an in-vessel camera allowed inspection for damage to the tiles between shots. In the highest power discharges with strong gas puffing,

significant melting of the target was observed. However, the total radiated power did not exceed about 50% of the input power. ELMy H-mode operation was retained, and no severe degradation of the confinement or D-D reaction rate was observed. In similar high power discharges without gas puffing, the radiated power was observed to rise from about 50% to about 70% over a period of seconds. This is shown in Fig.220. Further melting of the target was clearly visible. H-mode quality of these discharges was strongly degraded.

These discharges without gas puff were the only cases in which the radiated power fraction was observed to exceed 50%, by influx of beryllium. While a moderate degree of self protection of the target was thus evident, this was not sufficient to prevent severe damage to the tiles.

Reference discharges in the ELMy H-mode regime were performed before and after the infliction of melt damage. These discharges used sweeping of the strike zones over the melt-damaged areas. It appeared that the post-melt reference discharges without gas puffing were strongly degraded, even disruptive. However, the post-melt reference discharges with strong gas puffing were nearly identical to their pre-melt counterparts. After a short series of discharges sweeping over the melt damaged region, a conditioning effect was apparent.

Finally, a series of discharges was run with X-point sweeping enabled, and with the highest total plasma input energies of the campaign. In Fig.221, a discharge is shown with a total input energy (NB, ICRH and ohmic) of 180MJ.

It was observed that soon after the heating was switched on, there was an initial Be influx lasting about 0.5s, presumably due to accumulation of material deposited during the previous shot. After that, conditions were stationary until Be melting started (after about 5s at 20MW total input power). Then, a strong Be influx was observed, the radiated power increased, and the D-D reaction rate dropped dramatically. Significant further damage to the target was observed to result from these discharges.

Figure 222 shows a sector of the target near the outer strike zone, after the experiment. Three annuli of damage are visible. The inner ring already existed before these experiments. The middle ring is due to the unswept melting discharges, while the outer ring is due to the swept high power discharges. In the middle ring, significant formation of droplets and bridging of gaps between tiles (typically 10mm) is observed. At the worst places, tiles were eroded to a depth of about 3mm. There was little spreading of droplets to neighbouring areas. All damage exhibits full toroidal symmetry around the machine, highlighting the installation accuracy of the Mark. I divertor.

The heat fluxes to the target in these experiments were typically 25MWm^{-2} . This corresponds to the typical level of heat flux expected on the ITER divertor bumper target in off-normal conditions. The implication for ITER is that, at these levels of heat flux, significant damage to a Beryllium divertor target can be done, while only a moderate degree of self protection is established. Damage on this scale does not lead to an immediate loss of operation, but may be expected to lead to a rapid failure of the exposed component. If beryllium is to be used on the ITER divertor targets, it may therefore be prudent to design and implement an active safety device against excessive heat-fluxes, rather than to rely on the self protection.

References

- [1] Tubbing, B.J.D., and JET Team, in *Controlled Fusion and Plasma Physics* (Proc. 20'th Eur. Conf. Lisbon. 1993) **17C**, Part 1, European Physical Society, Geneva (1993) 39.
- [2] Tubbing, B.J.D., and JET Team, in *EuroPhysics Conference Abstracts* (Proc. 22'nd Eur. Conf. Bournemouth, 1995) **19C**, Part 4, European Physical Society, Geneva (1995) 1.
- [3] Putvinskii, S.V., Tubbing, B.J.D., Eriksson, L-G. Kononov, S.V., *Nuclear Fusion*, **34** (1994) 495.
- [4] Tubbing, B.J.D., Chankin, A., Clement, S., et. al., in *EuroPhysics Conference Abstracts* (Proc. 22'nd Eur. Conf. Bournemouth, 1995) **19C**, Part 3, European Physical Society, Geneva (1995) 453.

Data Analysis and Modelling

The work on data analysis and modelling can be divided into three areas: Analytic Theory; Numerical Simulation; and Data Processing and Analysis. However, there is a very strong interaction among these areas. The ultimate goal is to improve the modelling of the many physics processes taking place in both the core and edge regions of a tokamak. There is a strong interaction with experimental programme through Task Force and Topic Groups.

Analytic Theory

The Analytic Theory Group has supported the experimental programme by detailed interpretation of JET discharges and by predictive studies. Macroscopic MHD models have been applied for equilibrium and stability analysis and, in particular, to the physics of Global Alfvén wave excitation and the resulting energetic particle losses.

Equilibrium Reconstruction

The equilibrium code EFITJ has undergone a major upgrade. In the past, equilibrium reconstruction codes at JET have used full flux 'measurements' which have been calculated from saddle coil (flux differences) measurements around the vessel. EFITJ has been modified to fit directly to the saddle measurements so that the gaps between saddles and other geometric effects due to the vessel structure are taken properly into account. Another significant modification was to allow deformations of the flux surface geometry in the fitting section of the code. This has improved the convergence properties of the code considerably. Using higher order polynomials in the current parametrization can sometimes give rise to oscillations in the pressure profile leading to small negative pressures at the edge of the plasma. The oscillations have been ameliorated by imposing a smoothing regularization and the negative pressures eliminated by using an ansatz which forces the polynomials to be positive in the interval of interest.

For the plasma current profile reconstruction, it is now possible to fit to Faraday, Motional Stark (magnitude of the electric field only), Diamagnetic and Pressure Profile

measurements. At present, there are three Faraday chords available, which will be increased to eight for Mark II divertor operations. During the Mark I divertor operations, the Faraday and Pressure Profile measurements were used to demonstrate the existence of reversed shear in the q -profile of some discharges. UNIX versions of the EFITJ code have been ported to SUN, DEC-ALPHA and RS6000 workstations. During the Mark I divertor campaign, the XLOC Real Time Boundary Display System was upgraded to include a modified version of the FAST code. This provided signals for real-time control of plasma heating. These signals were used successfully by the neutral beam controller in closed loop feedback in some discharges where the diamagnetic energy was stabilized for several seconds.

It is planned to use real-time signals more extensively for Mark II operations, when real-time current profile feedback will be attempted. This is expected to provide greater flexibility in the control of plasma conditions, leading to improved plasma stability and hence confinement. The availability of physics quantities in real-time will also allow the use of advanced triggers with fast sampling diagnostics such as the CATS system, enabling the time evolution of plasma events to be studied in greater detail.

Movement of Radiative Zones

A common feature of both tokamak divertor experiments and the numerical modelling of divertor plasmas is that after detachment from the target has occurred, the radiative zones move away from the target plates to the X-point region on a short time-scale and remain there. As a consequence, the radiation in the divertor region itself drops to virtually zero. A simple physics model based on the balance between radiation and effective conduction has been employed to outline the fundamental ingredients responsible for this rapid movement of the radiative zone. It has been shown that a global increase in the radiation level (due to an increase in either density or impurity fraction) results in a continuous movement of the radiative zone from target to X-point. Once the radiative zone has started to move, small changes in density lead to substantial movement.

Experimental results with radiative divertors have established that the movement of the radiative zone clearly is continuous; the radiative zone does not 'jump' to the X-point, but gradually moves there in response to changes in the plasma properties (density or neon/nitro-

gen levels). In spite of the fairly narrow operational window between detachment and the density limit, JET experiments have established that a detached plasma with X-point radiation can be successfully maintained and a density limit disruption avoided.

Edge Plasma Physics

The edge plasma in tokamaks plays a crucial role in the behaviour of the entire plasma. It includes a part of the core plasma and a scrape-off-layer part about a few Larmor radii, inside and outside of the separatrix. In particular, the separatrix is essential for the development of sharp temperature and density gradients at the boundary. These gradients, on the one hand, stabilise microinstabilities (L-H transition [1]) but cause, on the other hand, the destabilisation of MHD-type surface modes (ELM events [2]). Near the X-point the transverse magnetic field is very small and the magnetic configuration is sensitive to perturbations. These perturbations can easily destroy the magnetic surfaces in this region allowing the core plasma to interact with the wall and the target plates.

Based on a reduced MHD model in conjunction with the ballooning approximation for the perturbation the linear stability of the SOL plasma with respect to interchange-type modes including the effect of line-tying at the target plates has been studied. This allows analysis of specific JET discharges and the scaling of the critical beta with plasma parameters, such as safety factor, and the shear is derived. The SOL plasma is found to become unstable more easily than the plasma just inside the separatrix and MHD perturbations are strongly localised near the X-point. Such SOL interchange instabilities are proposed as ELM precursors, which release the free energy stored inside the separatrix. The entire process of a giant ELM consists of three stages: (a) onset of the SOL instability near the X-point with subsequent influx of cold plasma; (b) trigger of the major interchange instability due to unfreezing of the internal perturbations leading to a loss of a plasma layer near the separatrix with width $\Delta x \approx a/nq$ (a minor plasma radius); (c) refilling of this layer by hot plasma from the centre on the (anomalous) diffusion time scale. From this scenario, the dependence of the ELM frequency on the heating power P and on the plasma current, I , has been established:

$$f = P (B_0/I) \times I^{-2} \times (\Delta x_0)^{-1/2}$$

where (Δx_0) denotes the characteristic edge pressure gradient length in the mid-plane. The linear dependence

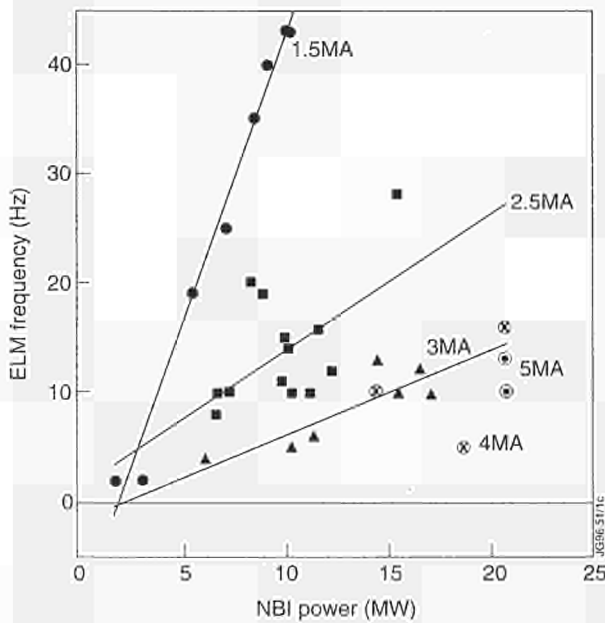


Fig.223: Giant ELM frequency dependence on heating power for different plasma currents.

of the giant ELM frequency with heating power for different currents is confirmed well by the JET data (Fig.223), whereas the current dependence of f/P for fixed q_0 has some spread but scales basically as $1/I^2$.

MHD Stability Analysis

The stability of low- n external kink and ballooning modes has been analysed, using the CASTOR code, for both hot-ion and high β_p discharges. In particular, the influence of the edge pressure gradient and the edge current density, as reconstructed by the JETTO transport code, has been studied. For plasmas with low triangularity, access to the ballooning second stability region requires a large edge current. These edge currents, however, drive the external kink mode unstable and therefore no stable route exists into second stability. For high triangularity, a lower edge current is required and a stable window into second stability can exist. The values of the edge current density in hot-ion H-mode discharges due to bootstrap current (and ohmic current through the high edge temperature) are large enough to drive low- n external kink modes unstable.

This suggests that the MHD activity observed during the slow roll-over in stored energy is due to external kink modes saturated at small amplitude as shown in Fig.224. Even at this small amplitude, the modes have a large effect on the confinement properties. At the relatively low values of triangularity and moderate values of beta poloidal in the hot-ion H-mode discharges, there is no stable route into the second stable regime of ballooning modes. The amount of edge current required for access to this regime would drive

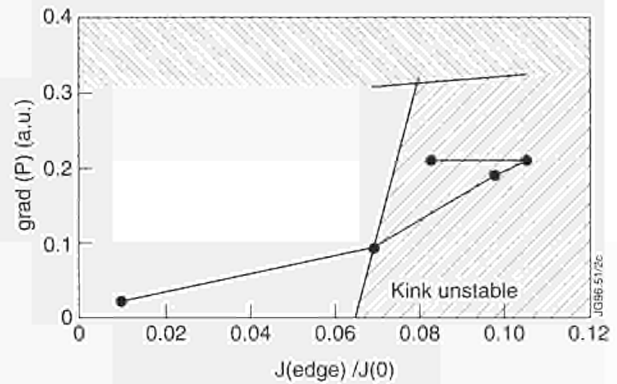


Fig.224: The MHD stability boundaries (ballooning and external kink), of the hot-ion discharge (Pulse No. 33558), including the time trace of the experimental values of ∇p and j_{edge}/j_0 .

an external kink mode unstable. The observed improved confinement phases in JET high beta poloidal discharges induced by small current ramps agree well with the stability calculations of ballooning and kink modes and the predicted access to the second stable regime for ballooning modes as displayed in Fig.225.

Stability of Advanced Tokamaks

Tokamaks with negative magnetic shear are found to have good stability properties with respect to ballooning and low- n infernal modes. A high β stable equilibrium is characterised by negative shear in the plasma centre, the q profile reaching a shallow minimum on the outside of the plasma that extends over a small region and q increasing fast at the edge. The pressure gradient can be large in the core but has to drop before the q profile reaches its minimum. In the region of positive shear, it will be limited by ballooning stability. Such plasmas are expected to rely on external current drive mechanisms [3] (in collaboration with FOM Nieuwegein, The Netherlands).

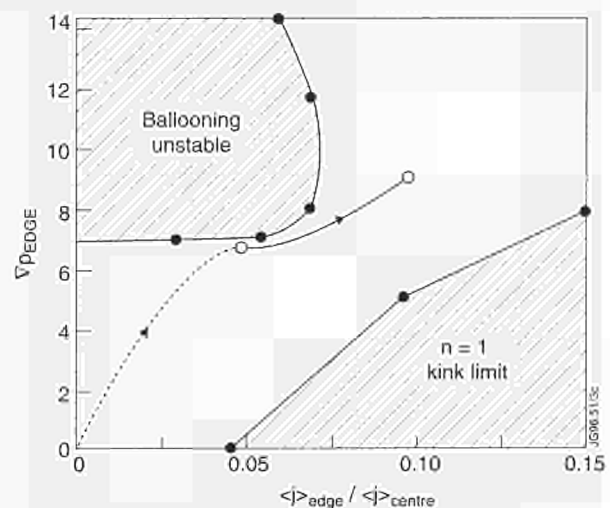


Fig.225: Stability diagram for a high beta poloidal discharge (Pulse No. 32344 at $t = 12.25$ s).

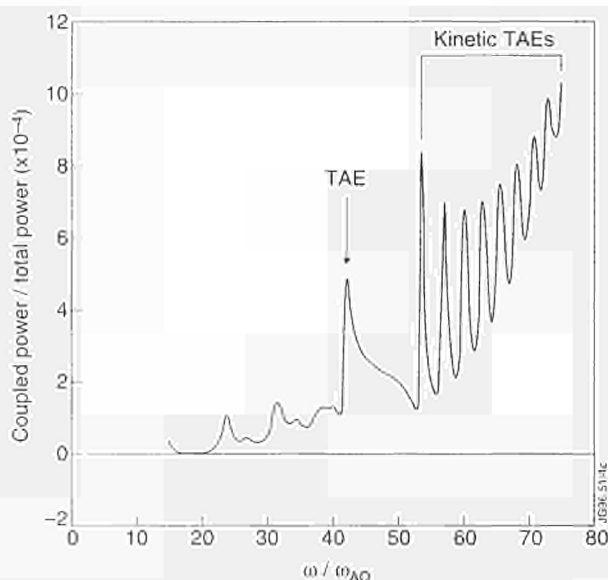


Fig.226: The plasma response as a function of the antenna frequency computed by CASTOR using complex resistivity.

Of crucial importance is the stability of low- n , external kinks. Advanced Tokamak Concepts have been designed assuming that the 'Resistive Wall Mode' (RWM) is stable. It has recently been shown that the RWM can be stabilised by a combination of strong uniform plasma rotation and visco-resistive dissipation. In the JET model, the consequences of a sheared flow on the RWM has been examined, and contrasted with the results of the case of uniform flow. Both for sheared and uniform flow, the rotation initially further destabilises the resistive wall mode, but for higher rotation velocities the growth rate is reduced, and the presence of plasma dissipation (which is not included in the model) may completely stabilise the mode. However, sheared rotation allows the possibility of the RWM coupling to and converting into a Kelvin-Helmholtz mode, as is found for a parabolic rotation profile and different wall positions. Clearly, the position of the wall with respect to the critical position for stabilisation of the external kink mode is of crucial importance.

Alfvén Eigenmode (AE) Studies

The confinement of fusion born alpha-particles is of crucial importance for ignition. Since the alpha-particles have super-Alfvénic velocities (i.e. $v_\alpha > v_A$), these can drive the weakly-damped Global Alfvén Eigenmodes unstable through the $v_{\text{tr}} = v_A$ and $v_{\text{tr}} = v_A/3$ resonant interaction. This resonant interaction leads to the exchange of momentum and energy between alpha-particles and global Alfvén Eigenmodes (AE), which causes a radial redistribution of the alpha-particles and possible anomalous α -losses and damage to the first wall.

The detailed analysis of the Alfvén spectrum, and the gap structure has been performed numerically using the MHD normal mode code CASTOR [4,5]. Of great significance is the spectrum of the kinetic AE (called KTAE) first predicted theoretically [6-9] and later observed experimentally during the 1994/95 JET campaign [10,11]. It is emphasised that with increasing plasma temperature the Alfvén continuum above the TAE-gap splits into a number of weakly-damped, discrete kinetic AE (KTAE) with equally spaced eigenfrequencies [6,9]. A number of experiments in conjunction with the high-resolution Alfvén diagnostic have been performed with the objective of identifying such a KTAE spectrum. It was found that the number of weakly-damped AE's was a function of the plasma temperature. One $|n| = 2$ TAE can be typically measured in cold plasmas, but several (at least 5), KTAE-modes with regular frequency spacing appear after sufficient plasma heating in form of ICRH, LHH, NBI or high ohmic current.

To model the plasma temperature effects, such as finite Larmor radius of thermal ions and finite longitudinal electric field, the non-ideal MHD code CASTOR, has been modified to incorporate a "complex resistivity" in JET discharges [12,13]. The plasma response due to an external antenna drive was also studied in the "complex resistivity" version of the CASTOR code. A code typical KTAE-frequency spectrum is shown in Fig.226. Complementary to the external saddle coil antenna excitation a new method namely ICRH beat-waves excitation, for driving AE's has been proposed [14] and recently, been confirmed experimentally. Therefore, this method can provide a high-amplitude AE-drive in JET [15].

For the general treatment of the AE stability analysis of JET and ITER plasmas, the global treatment of the alpha-drive due to passing and trapped α -particles as well as ion Landau and trapped electron collisional dampings have been implemented in CASTOR. In addition, the self-consistent alpha-particle redistribution in the presence of α -driven Alfvén eigenmodes has been studied in collaboration with IFS University of Texas, USA, and with UKAEA, Culham Laboratory. The guiding centre code HAGIS, which follows the α -particle motion in general tokamak equilibria in the presence of an arbitrary electromagnetic MHD perturbations [16], where both equilibrium and AE eigenfunction are supplied by CASTOR, has been extended towards a self-consistent nonlinear code. In this context, a fully toroidal df code to

analyse the nonlinear interaction of fast particles with low-frequency MHD modes (TAE, EAE, fishbone, etc) has been developed. Studies of redistribution and anomalous loss of RF and NB heated ions, as well as thermonuclear α 's, are presently underway for a variety of JET and ITER scenarios. Unstable moderate- n modes have been observed, and are found to saturate nonlinearly through a mechanism universal to weakly turbulent systems, namely particle trapping in the local wave potential well.

Correlation Length of Plasma Turbulence

The outstanding problem of determination of the form of the anomalous transport coefficients has motivated a review of the properties of plasma microturbulence driven by ion temperature gradients (ITG). This reanalysis has produced a new expression for the correlation length (or characteristic scale-length) of ITG turbulence [17]. Combining this result with a phenomenological assumption about the characteristic time that guarantees the correct current scaling has led to new form for the conductivities χ_i and χ_e that depends strongly on the local temperature gradient. This translates into interesting properties: although formally gyro-Bohm, the new χ_i and χ_e have an increasing radial dependence (in line with the experimental findings) and the resulting profiles are strongly resilient. The initial comparison with discharges from JET and from the ITER database has been encouraging, with the new conductivities predicting temperature profiles close to the experimental ones [18].

Ion Cyclotron Resonance Frequency Heating

Routine analysis of heating and current drive with waves in the ion cyclotron range of frequencies (ICRF), for interpretation of experimental results and for prediction of the performance of different heating scenarios, requires models of the wave field which are computationally inexpensive but still sufficiently accurate. One such model has been implemented in the PION code, which has been successfully used to analyse experimental results [19]. However, the model in the PION code only calculates flux surface averaged power densities and can therefore not be used for current drive calculations and other applications where a full knowledge of the wave field structure is needed.

Work on developing a new and computationally inexpensive model for the full wave field is in progress. As a first step, a model for the wave field in toroidal plasmas with

weak damping has been developed [20]. In a toroidal plasma the ray trajectories become stochastic when the damping is weak, i.e. when the rays bounce many times before the wave power is absorbed. This problem has been studied before, [21], and it has been assumed that the energy density in phase space is constant. This is, however, not correct for the magnetosonic wave in typical JET plasmas.

The new model is based on expanding the wave field in the eigenfunctions of a circular cylinder. The functional form of the weight coefficients $g(m)$, where m is the poloidal mode number, have been determined approximately using an ansatz: $g(m) = |m|^\kappa$, and by comparing with calculations made with the full wave code LION [22]. The assumption of a constant $g(m)$ (i.e. constant energy density in phase space), gives a very poor representation of the LION result, whereas $\kappa = 0.65$ gives the best fit. The new model was first applied to large aspect ratio plasmas, for which the expansion is expected to be most appropriate. Higher order toroidal corrections and corrections for ellipticity have now been added. As a result, the model is now applicable to plasmas typical for JET and ITER, and in all cases, $\kappa = 0.65$ has been found to give good agreement between the model and LION calculations.

Numerical Simulation

The activities of the Simulation Group were directed along two main lines:

- Development and validation of models of energy transport inside the separatrix (JETTO code);
- Predictive and interpretive study of plasma in the boundary region (EDGE2D/U-NIMBUS codes).

A summary of results is given in the following sections. Other results are presented in the sections dedicated to Transport and Fluctuations, and Divertor Physics Topics.

Numerical Simulation of Transport

Modelling of transport phenomena both for the core and the boundary plasma region has been carried out by means of the JETTO and EDGE2D codes. This modelling activity has led to further development of these codes that are presently widely used for the interpretation of JET results, the preparation of future JET experiments and also for prediction of ITER performance.

Modelling of Transport in the Plasma Core

An extensive analysis of experimental results from JET and other tokamaks, available in the ITER profile data

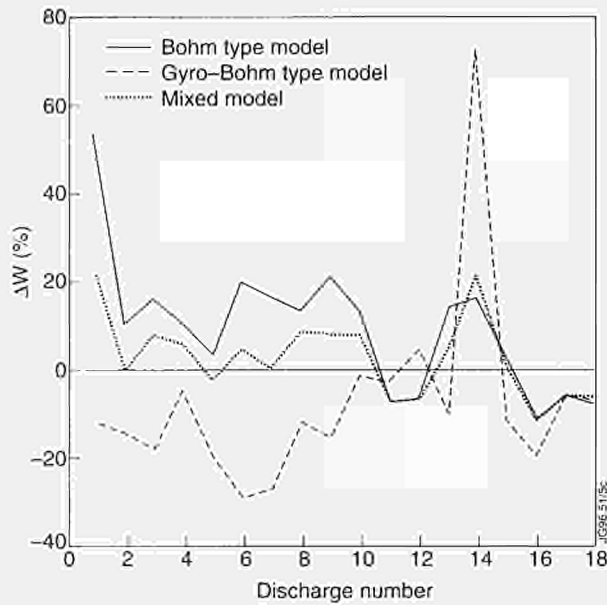


Fig.227: Relative deviation ΔW of experimental values of plasma thermal energy content from that computed with different transport models [$\Delta W = (W_{\text{calc}} - W_{\text{exp}}) / W_{\text{exp}}$] for a set of discharges for the ITER profile database. Discharges No 1-10 are DIII-D L-mode shots, 11-12 are JET L-mode, 13- ASDEX, 14- TFTR and 15-18 - JT60U L-mode shots.

base, has been performed. The analysis of the discharges from machines with different size and value of the toroidal magnetic field facilitates the resolution of the problem whether anomalous transport in tokamaks is of Bohm or of gyro-Bohm type. Experiments carried out on different tokamaks show that, generally, transport is close to Bohm in L-mode plasmas (and near to the separatrix in H-mode plasmas). On the other hand, it seems to be of gyro-Bohm type in a wide region of H-mode discharges. It also shows that the Bohm-like character becomes less important as the machine size decreases. Theory usually predicts a gyro-Bohm type of anomalous transport. However, linear theory also predicts the existence of long correlated structures which could manifest with Bohm transport coefficients. In the JET analysis three different transport models have been used: (a) a Bohm model, previously used to model JET L and H-mode discharges [23]; (b) a pure gyro-Bohm model; and (c) a linear combination of the two.

Results of the transport analysis indicate that a linear combination of Bohm and the gyro-Bohm transport coefficients fits the experimental results best, as shown in Fig.227. Such a conclusion suggests that anomalous energy transport is related to two sources of turbulence. The first one is distributed over the entire plasma cross-section and is responsible for the gyro-Bohm type term. This term may be small in the boundary region but increases with temperature towards the plasma central region.

The second source of turbulence is originated in the external plasma region but causes a global structure of modes extending towards the plasma centre. This structure is responsible for the Bohm-type term. By stabilising this turbulence (e.g. by velocity shear), improved confinement occurs over a wide plasma region, corresponding to a global reduction or even suppression of the Bohm-type transport term.

These ideas have been taken into account in the combined Bohm gyro-Bohm transport model and successfully tested against the experimental observations in dynamic experiments in JET (L-H transition, cold pulse propagation, type I ELMs and perturbations related to a sawtooth crash). Details of the results of simulation of dynamic experiments are given in the section on the Transport and Fluctuations Topic Group.

Modelling of Edge Plasmas

The multi-fluid system of codes EDGE2D/NIMBUS has been upgraded by including particle and heat drift fluxes. These codes have been extensively used to study radiative and detached divertor plasmas in JET, and for extrapolations to ITER (see also Section on Divertor Topic Group).

Implementation of Particle and Heat Drift Fluxes in the EDGE2D Code

The inclusion of drift fluxes into edge transport codes has been of much recent interest. The diamagnetic fluxes, however, have generally been included in full, with no account taken for the presence of a generally large, divergence-free component, and the subsequent effect of this on plasma boundary conditions. This latter problem has been considered in [24] where it is shown that this divergence-free component does not contribute to the plasma boundary conditions. This has been used as the basis for the implementation of the drift fluxes into the EDGE2D code. Simple expressions have been given for the drift fluxes and it is shown that the divergence-free components do not contribute to the continuity, collisionless momentum or energy equations. In this initial work, the radial electric field outside the separatrix is calculated from the radial potential gradient, while inside, a simple neo-classical model is used.

Work is in progress to couple the radial currents iteratively into the equation for the parallel currents thus yielding more self-consistent electric fields. A fully conservative non-orthogonal discretisation scheme was used

to ensure that the explicit magnetisation particle flows are indeed closed with either no, or numerically insignificant, ensuing hidden particle sources or sinks.

Only very preliminary results have been obtained with drifts. The most interesting one so far is that in the case of the ∇B drift, the dominant particle drift is downwards for the normal magnetic field and upwards for the reversed field. The code results show the effect of this quite clearly on the particle density inside the separatrix, typically when the drifts were switched from down to up. However, the results in the scrape-off layer and at the targets are not so straight-forward to interpret. The inner target particle fluxes decreases ($\sim 10\%$) as might be expected, but those on the outer target increases ($\sim 10\%$) when the drifts switched to upwards. It seems that the target boundary conditions along with energy transport and the influence of particle sources may mask any changes expected from the reversal of the drift flows.

Modelling of Radiative and Detached Plasmas and comparison with JET Results

The multi-fluid code EDGE2D coupled to the neutral Monte Carlo code NIMBUS, and its newly developed post-processor provide a means to simulate and compare with experimental results the distribution of the deuterium and impurity density, temperature and flow, as well as related quantities such as the ion saturation current density J_s at Langmuir probes, D_α and bremsstrahlung radiation signals, and the impurity and deuterium radiation power density. The route to plasma detachment was studied in the Mark I divertor and the related role of impurities and impurity radiation for ohmic and L-mode discharges, mainly for cases where carbon was the main impurity species.

Experimental results in JET and other tokamaks show that as plasma density and radiation losses increase in a discharge, the flow of particles to the divertor targets first increases then rolls over and finally decreases to very low levels (plasma detachment). In the detached phase flows of momentum (\Rightarrow pressure) and energy to the targets are also reduced. Detachment is usually stronger at the inner target and requires impurity radiation even for ohmic discharges.

Another experimental observation is the increase with time of D_α signals going from the low recycling to the high recycling phase and finally to the detached phase of a discharge. All of these trends are reproduced by the simulations. As an example, Fig.228 compares experimental and computed peak values of J_s for a JET ohmic

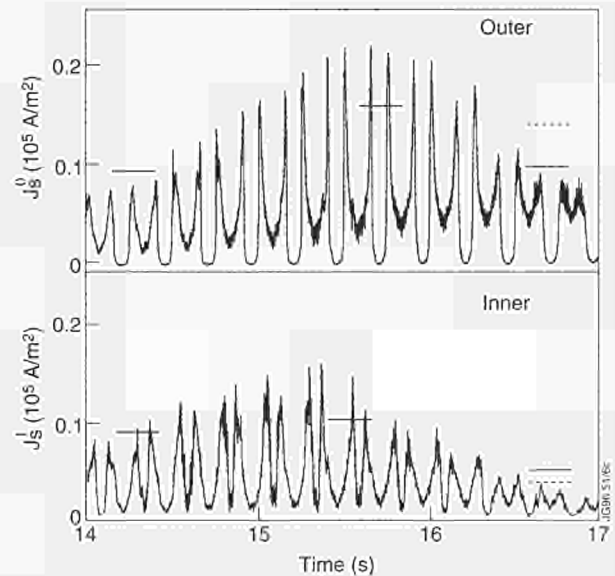


Fig.228: Experimental and computed peak values of J_s at outer and inner targets for low recycling, high recycling and detached phase of the JET ohmic discharge (Pulse No. 31627), discharge (Pulse No. 31627) at times corresponding to low recycling, high recycling and detachment at the inner and outer target. The best values of J_s in Fig.228 at $t \approx 16.7$ s were obtained by puffing carbon from the outside divertor wall, in addition to that from the targets.

A typical problem with purely diffusive models is that with increasing density the ionisation source inside the separatrix and the parallel flow become too small to provide the expected SOL density decay, even with very small values of the diffusion coefficient, D . The effect is stronger at high input power. In addition a purely diffusive model does not simulate the increase in J_s observed in the attached high recycling phase of a discharge. An 'ad hoc' influx of particles from the plasma core (e.g. compensating some pumping) provides proper density profiles. However, unless a realistic path for neutrals to cross the separatrix is found, it is likely that these results indicate that purely diffusive perpendicular transport models are incomplete. For this reason an empirical pinch term has been introduced in the SOL and the divertor regions, with values of the pinch velocity compatible with those derived from impurity transport just inside the separatrix. The model works reasonably well at all densities up to detachment and provides the expected decay length of density at the mid-plane.

Data Processing and Analysis

Multi-machine Database Collaboration

The ITER Confinement Database and Modelling Expert Group is now responsible for the ITER L-mode Database, the ITER H-mode Database, the ITER H-mode

Threshold Database and the ITER Profile Database. The official Expert Group (three members from each of the three ITER Parties) acts as a Steering Committee for the activities, whereas the actual Working Group is much larger. All the participating tokamak groups, (i.e. ASDEX, ASDEX UPGRADE, C-MOD, COMPASS-D, DIII, DIII-D, FTU, JET, JFT-2M, JT-60, JT-60U, PBX-M, PDX, RTP, START, TORE SUPRA, TEXTOR, TFTR and T-10), are represented in the Working Group. The Working Group also includes modellers participating in the ITER I-D modelling activity for which the Expert Group is also responsible. Two official workshops were held in 1995, in San Diego, U.S.A. (March 13-15) and in Naka, Japan (October 16-19). In addition, an informal L-mode database meeting was held in Bournemouth, U.K. (July 4). The progress made with each database and its data analysis is described below.

ITER L-mode Database

The L-mode database now consists of data from 14 tokamaks, (i.e. ASDEX, C-MOD, DIII, DIII-D, FTU, JET, JFT-2M, JT-60, PBX-M, PDX, TEXTOR, TFTR, TORE SUPRA and T-10). Thermal energy confinement data are available from all tokamaks, except DIII, so that a scaling of a thermal L-mode energy confinement time can now be established from the database. Two standard datasets suitable for regression analysis (one for total and one for thermal confinement) have been identified and checked for bad data. The scaling analyses of the standard datasets are still ongoing as well as the write-up of the database documentation. The analyses so far indicate that: the ITER89-P scaling [25] for the total energy confinement time may not need to be updated; the power degradation of the thermal L-mode scaling is more in line with that of the thermal H-mode scaling ITERH93-P [26]; the thermal L-mode scaling is Bohm-like; and only small differences between limiter and X-point L-mode confinement have been detected.

ITER H-mode Database

The H-mode database [27] still consists of data from six tokamaks, (ASDEX, DIII-D, JET, JFT-2M, PBX-M and PDX), and no changes have been made in 1995. Therefore, the thermal ELM-free H-mode confinement scaling, ITERH93-P [26], has not been updated. However, it has been recognised that the ELM classification in the database is not sufficient to establish reliable confinement scalings for the various types of ELMs. At present, the

ITERH92-P(ELMy) scaling [28] gives the best simple power law fit to the whole ELMy subset. Another proposed ELMy scaling is $0.85 \times \text{ITERH93-P}$ which assumes that, in the ELMy H-mode, the underlying ELM-free H-mode confinement is degraded by a constant fraction due to ELMs. The database will be updated with more data (including more tokamaks) and an improved ELM classification in 1996.

ITER H-mode Threshold Database

The H-mode threshold database now consists of data from nine Tokamaks, (ASDEX, ASDEX UPGRADE, COMPASS-D, C-MOD, DIII-D, JET, JFT-2M, JT-60U and PBX-M). The documentation of the present version has been completed and will be published shortly together with the results of the power threshold scaling analyses [29]. A standard dataset has been identified which represents the lowest achieved threshold in each Tokamak. In one approach, the lower boundary of the data in the standard dataset has been regarded as the threshold power scaling. The following candidates fit this boundary reasonably well:

$$P_{\text{thr}} = 0.3 n_{20} B R^{2.5}$$

$$P_{\text{thr}} = 0.034 n_{20} B^{0.6} S$$

$$P_{\text{thr}} = 0.016 n_{20}^{0.75} B S$$

$$P_{\text{thr}} = 0.025 n_{20} B S$$

In these expressions, S denotes the plasma surface area. The first three expressions are dimensionally correct. The predicted H-mode power threshold for ITER ranges from 70MW (3rd expression) to 150MW (1st expression) at a density of $0.5 \times 10^{20} \text{m}^{-3}$. Figures 229 (a-d) show the comparison between the data and the above expressions.

ITER Profile Database

The Profile database now consists of data from eight Tokamaks (ASDEX, DIII-D, JET, JT-60U, TEXTOR, TFTR, TORE SUPRA and T-10). JET has contributed data on seven discharges: Pulse Nos. 19649 and 19691 are both L-mode D plasmas, Pulse Nos. 26087 and 26095 are high performance hot ion H-mode pulses, Pulse No. 33140 (1.7MA, 1.6MA), Pulse No. 35156 (2T, 2MA) and Pulse No. 35171 (1T, 1MA) are all ELMy H-mode D plasmas and part of a group of pulses of a ρ^* scaling experiment. The profile database is now well defined and software to prepare, transfer and look at the data has been made available. The testing of transport models using the profile data by the modellers is progressing smoothly.

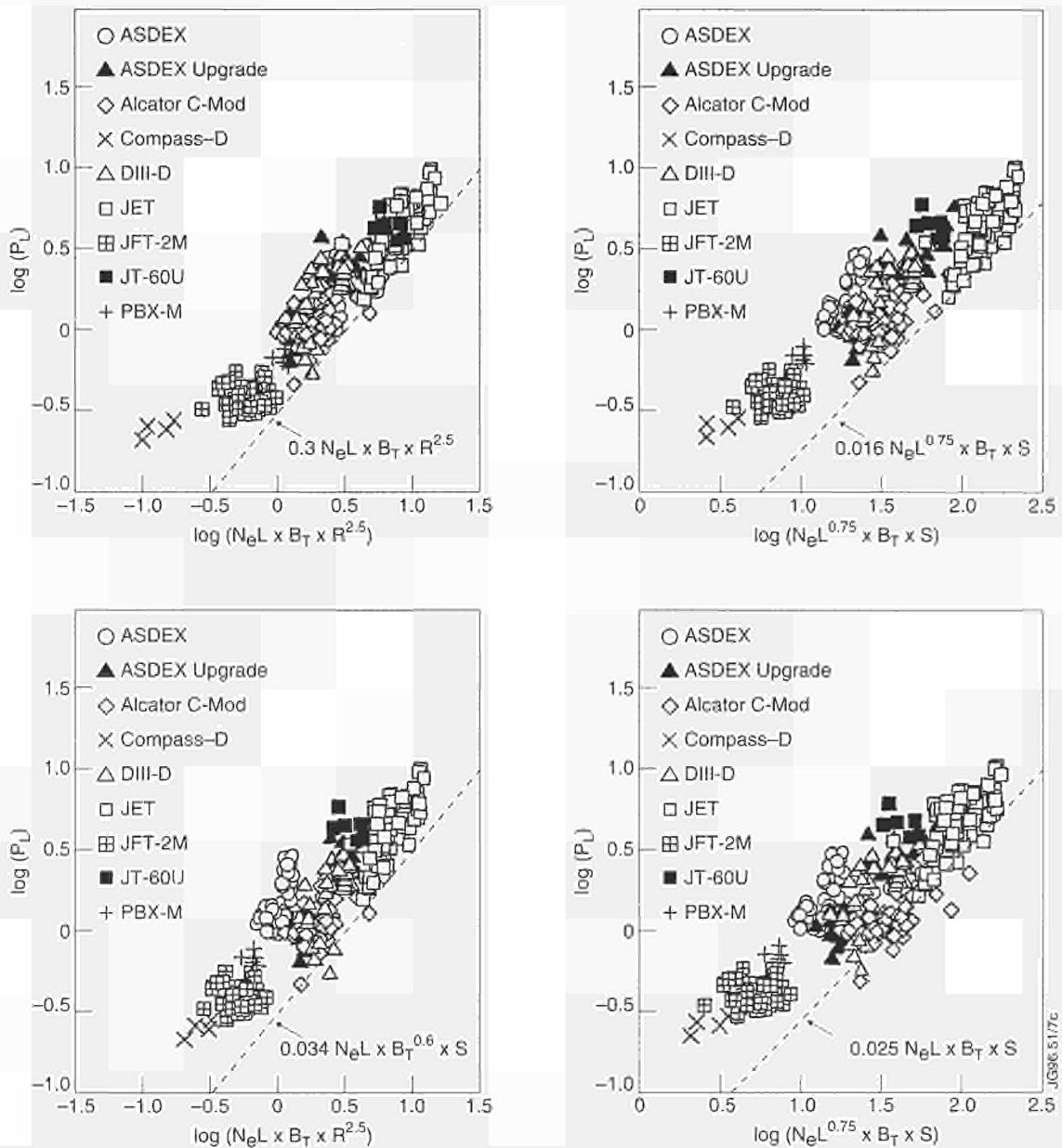


Fig.229: Results from the threshold combined database in which the existence diagrams have been derived with expressions from considerations made with dimensionless variables: $P_u \sim n^a B^b R^c$.

TRANSP Code Development

The TRANSP code, modified to simulate up-down asymmetric plasmas, has been implemented and tested on the Joint Analysis Cluster workstations for routine analysis. JET plasmas in the new divertor configuration are now simulated with this version.

The equilibrium code used in TRANSP is being upgraded under a joint project between JET, General Atomics (USA) and Princeton Plasma Physics Laboratory (USA). The goal is to run TRANSP in a fully free boundary mode of operation, thus adding a consistent magnetic analysis to the already comprehensive kinetic analysis. The current "fixed boundary" equilibrium codes in TRANSP are being augmented by two additional "free

boundary" equilibrium codes, VMEC and EFIT. This is done by using the facilities provided either by UNIX and to a lesser degree by VMS for inter-program communication. The use of EFIT is of particular interest to JET as this code is used routinely for equilibrium reconstruction.

Data Processing and Analysis

An extensive set of calculations are made on a variety of pulses to establish sets of internally consistent data. The TRANSP code is used together with data produced by CHAIN1 and CHAIN2. The analysis has included high performance hot-ion H-modes, ELMy H-modes used in ρ' scaling experiments, pulses with high values of β_p or β_{N_e} , strongly radiating plasmas used for divertor studies,

pulses with and without TF ripple. In most cases a satisfactory level of consistency can be found between magnetic, kinetic and neutron data. The consistency checking involves iterations as data is often reprocessed.

For 1994 and 1995 the entire diamagnetic data, the neutral beam data, the interferometer data have all been reprocessed. Several new Intershot analysis codes have been introduced describing e.g. vessel forces, ELM types, confinement scaling, etc.

Larmor Radius Scaling of ELMy H-modes

In non-dimensional scaling experiments, all but one dimensionless plasma parameter are held fixed. Such experiments have been carried out on TFTR, DIII-D and JET, but joint experiments involving two tokamaks can also be made. There are experimental problems with establishing a series of dimensionally similar pulses. This has been seen in the three series of experiments on the ρ^* scaling of ELMy H-modes on JET. The reproducibility of ELM characteristics, as the magnetic field is doubled say, depends on the proximity of the power level to the H-mode threshold power; close to the threshold an ELM of the "compound type" occurs in which L-mode confinement follows the ELM for some short period. The result from the experiments confirmed this. For discharges far away from the threshold, a gyro-Bohm scaling with ρ^* applied to both ions and electrons over most of the discharge. Evaluation of the local heat flux data has been made with the TRANSP code. As the threshold is approached, the scaling of the local heat flux with ρ^* is closer to the Bohm scaling; the latter has been determined for L-mode plasmas on TFTR, DIII-D and JET.

Diagnostic Software

The Diagnostic Software section is responsible for the design and maintenance of software for diagnostic control, data acquisition, calibration and display for a considerable number of diagnostics. It also provides support to diagnosticians with the commissioning of diagnostics and trouble-shooting during operations.

The section maintains some general purpose software products, such as a JPF data retrieval and display package, a General Data Acquisition and Control package and various subroutine libraries. It also supplies data analysis support on the IBM system, mainly for the KH2, KS1, KS2 and KS6 spectroscopy diagnostics.

During 1995, considerable effort was expended in further development on the following areas:

- the Central Acquisition and Trigger System (CATS) and the Real Time Plasma Boundary Display (XLOC-RT) were further developed. The Diagnostic Data Network (DataNET) continues to grow.
- VME based stepper motor control of the steerable mirror and polarisers of the Space and Time Resolved Velocity Distribution of alpha-particles diagnostic (KE4) was implemented. Internal WWW pages were created detailing both the KE4 hardware and software.
- Design specifications detailing CAMAC modifications to the Plasma Boundary probes diagnostic were produced.
- The PC based data collection system for the fast CCD camera diagnostic (KL1.3) was commissioned and has operated successfully throughout the 1995 operational period. The hardware and software for the magnetics transient recorder diagnostic (KC1F) was developed.

References

- [1] W. Kerner, J.G. Cordey, O. Pogutse and E. Righi, "Dimensional analysis of L-H power threshold scalings", 22nd European Conf. Contr. Fusion and Plasma Phys. V. 19C, Part III, p.III-229, Bournemouth, UK, 3rd-7th July 1995.
- [2] O. Pogutse, J.G. Cordey, W. Kerner, and B. Schunke, "Edge modes as ELM Events", 22nd European Conf. Contr. Fusion and Plasma Phys. V. 19C, Part III, p.III-277, Bournemouth, UK, 3rd-7th July 1995.
- [3] Stability of Infernal and Ballooning Modes in Advanced Tokamak Scenarios H.A. Holties, G.T.A. Huysmans, J.P. Goedbloed, W. Kerner, V.V. Parail and F.X. Söldner, submitted to Nucl. Fusion.
- [4] W. Kerner, S. Poedts, J.P. Goedbloed, G.T.A. Huysmans, B. Keegan, and E. Schwartz, 18th EPS Conference on Controlled Fusion and Plasma Physics, Berlin, 1991, edited by P. Bachmann and D.C. Robinson (European Physical Society, Petit-Lancy, Switzerland, 1991), Vol. 15, Part IV, p.89.
- [5] G.T.A. Huysmans, W. Kerner, D. Borba, H. Holties and J.P. Goedbloed, Phys. Plasmas **2**, 1605 (1995).
- [6] R.R. Mett, S.M. Mahajan, Phys. Fluids **B4**, 2885 (1992).
- [7] J. Candy and M.N. Rosenbluth, Phys. Plasmas, **1**, 356 (1994).
- [8] H.L. Berk, R.R. Mett and D.M. Lindberg, Phys. Fluids **B5**, 3969 (1993).

- [9] B.N. Breizman, S.E. Sharapov, Plasma Phys. Contr. Fus., **37**, 1057 (1995).
- [10] A. Fasoli, et al., Phys. Rev. Letters, to be published.
- [11] A. Fasoli, et al., Nuclear Fusion, **12** P. (1995).
- [12] S. Sharapov, et al., 36th APS Conf., Minneapolis, 1994, Bull. Amer. Phys. Soc., **39**, 1566 (1994), (JET Preprint JET-P(94)61).
- [13] W. Kerner, et al., 4th IAEA Workshop on a-particles in Fusion Research, PPPL, April 25-28 (1995).
- [14] S. Sharapov and W. Kerner, Preprint JET-IR (93) 11, 1993.
- [15] A. Fasoli, et al., Nuclear Fusion, to be published.
- [16] L. Appel, et al., Nuclear Fusion, **12** (1995).
- [17] M. Ottaviani, M. Beer, S. Cowley, W. Horton and J. Krommes, Unanswered questions in the theory of ion-temperature-gradient-driven turbulence, to appear in the Proceedings of the 1995 ITP program on 'Intermittent and turbulent phenomena in plasmas'.
- [18] M. Ottaviani, W. Horton and M. Erba, Thermal transport from a phenomenological description of Ion-Temperature-Gradient-Driven Turbulence, in preparation.
- [19] Eriksson, L.-G. et al., Nuclear Fusion **33** (1993) 1037.
- [20] Hellsten, T. et al., JET Report JET-P(95) 61.
- [21] Kupfer, K. et al, Phys. of Plasmas **1** (1994) 3915.
- [22] Villard L. et al., J. Computer Phys. Reports **4** (1986) 95.
- [23] Taroni, A., Erba, M., Tibone, F., Springmann, E., Plasma Physics and Control. Fusion **36**, (1994) 1629;
- [24] Chankin, A.V. and Stangeby, P.C., Plasma Phys. Cont. Fusion **36** (1994) 1485.
- [25] Yushmanov, P.N., et al., Nuclear Fusion **30** (1990) 1999.
- [26] Schissel, D.P., et al., in Controlled Fusion and Plasma Physics (Proc. 20th Eur. Conf. Lisbon, 1993), Vol. 17C, Part I, European Physical Society, Geneva (1993) 103.
- [27] Thomsen, K., et al., Nuclear Fusion **34** (1994) 131.
- [28] Kardaun, O., et al., in Plasma Physics and Controlled Nuclear Fusion Research (Proc. 14th Int. Conf. Wurzburg, 1992), Vol. 3, IAEA, Vienna (1993) 251.
- [29] Ryter, F., et al., Report IPP 4/269 October 1995 (accepted for publication in Nuclear Fusion).

Summary of Scientific Progress and Perspective

The effectiveness of the pumped divertor during the 1994/95 experimental campaign has allowed the pursuit of a broad-based research programme, which is highly relevant to the International Thermonuclear Experimental Reactor (ITER).

During the campaign, the plasma current in a separatrix limited X-point configuration being increased to 6MA, the total heating power to 32MW, the plasma stored energy to 13.5MJ and the neutron rate to 4.7×10^{16} neutrons s^{-1} . The pumped divertor has been most effective and this has allowed a broad-based research programme to be pursued, which is highly relevant to the ITER. Five areas of research are of particular significance to ITER: high fusion performance in plasmas with high energy confinement (H-modes) and free of Edge Localised Modes (ELMs), together with fast particle studies which involve varying the toroidal magnetic field ripple and exciting and detecting Alfvén eigenmodes; a wide range of ITER-relevant steady-state ELMy H-modes, including two specific contributions to the validation of the operating conditions foreseen for ITER; energy confinement studies (including the scaling with machine size) for conditions both well away from, and close to, the H-mode threshold and also at high values of the plasma pressure relative to the toroidal magnetic field pressure, β ; and experiments with detached divertor plasmas and radiative power exhaust.

For most of the campaign, the divertor target tiles were made of carbon fibre composite (CFC), but these were replaced by beryllium tiles for the last two months of operation. This allowed an assessment of beryllium as a target tile material, including a controlled beryllium melt experiment for ITER.

High Fusion Performance

ELM-Free H-Modes

Highest Fusion Performance in 1994/95

ELM-free hot-ion H-mode plasmas achieved the highest fusion performance in JET. Performance improved as the duration of the ELM-free period was lengthened by reducing recycling (wall conditioning and/or use of the cryopump), expanding the magnetic configuration to fill the divertor, and increasing magnetic shear (triangularity) at the plasma edge. The highest fusion performance achieved in 1995 was comparable to the best achieved

prior to the installation of the pumped divertor, even though the plasma volume was now 20% smaller. An ELM-free hot-ion H-mode at 3.8MA/3.4T with 18MW of neutral beam (NB) heating and high magnetic flux expansion in the divertor resulted in a neutron yield of $4.7 \times 10^{16} \text{s}^{-1}$ (best JET rate in deuterium) and the fusion triple product of plasma density, temperature and energy confinement time, $nT\tau_E > 8 \times 10^{20} \text{m}^{-3} \text{keVs}$ was within 10% of the previous best. The equivalent fusion amplification factor in deuterium-tritium (D-T) plasmas, Q_{DT} , was ≈ 1 , transiently.

Limits to High Performance

Hot-ion H-modes at low plasma current and toroidal magnetic field reached $\beta_N \approx 2.5$ (where β_N is the value of β relative to the normalised plasma current, I/aB), but high performance hot-ion H-modes were limited at $\beta_N \approx 1.8$, well below the Troyon limit ($\beta_N = 2.8$). In general, three classes of magnetohydrodynamic (MHD) phenomena were involved in setting this limit: sawteeth and other internal MHD phenomena occurred in the plasma centre; low frequency modes occurred in the outer 20% of the plasma radius; and “giant” ELMs occurred in the very edge of the plasma.

In the discharge with the highest performance, the high performance phase was terminated by a “giant” ELM, simultaneous with a sawtooth, and preceded for ≈ 200 ms by high frequency MHD activity from the plasma within the radius at which the safety factor, $q=1$. This MHD activity was observed on the magnetic pick-up coils and was seen to affect the central ion temperature and the neutron rate. Other discharges were limited by modes in the outer 20% of the plasma radius. There was no evidence that these “outer” modes, or the ELMs, were ballooning modes, but stability analyses suggested that the edge current density could be sufficient to destabilise external kink modes. Furthermore, MHD data suggested that the terminating events included a low frequency (5kHz) $n=1$, $m=3-5$ character and could be external kink modes. Concomitant with the increase in low frequency edge activity, the loss power, the temperatures of the inner and outer divertor targets and the level of recycling as indicated by deuterium excitation measurements (D_α signal) all increased, the edge temperature fell and the total stored plasma energy and neutron rate exhibited “roll-over”. First experiments with lower hybrid current drive showed that sawteeth could be controlled and the effect of the “outer” modes could be softened, such that

the duration of the high performance phase was extended by 0.5s to the end of the heating pulse.

High Performance Quasi-Steady State Operation

It was possible to delay the termination of the high performance phase by reducing the NB heating power to maintain MHD stability. In this way, the neutron rate and the stored plasma energy remained high and steady for up to 1s. In such a power step-down experiment, the equivalent Q_{DT} remained above 0.7 for almost 1s but the density continued to rise after the power step-down, albeit at a reduced rate due to the retention of the low current 140kV neutral beams. The density increase facilitated the convergence of the electron and ion temperatures, but led to lower average temperatures.

ITER-Specific Toroidal Field Ripple Experiments

The toroidal magnetic field ripple was varied in JET in the ITER-relevant range of 0.1% to 2% ripple at the plasma edge. Low levels of ripple ($\approx 1\%$ at edge) were found to improve H-mode confinement, probably due to the effect on ELM frequency, while high levels of ripple ($> 1.5\%$ at edge) degraded H-mode confinement. High energy neutral particle flux measurements and triton burn-up experiments showed that ripple induced losses of thermal and high energy particles (125keV NB ions and 1MeV tritons) were very small (a few %, or less) and were consistent with preliminary calculations of stochastic diffusion losses. The observed losses of intermediate energy particles (thermal to 10's of keV), however, were higher than predicted.

Alfvén Eigenmode Studies

Saddle coils on JET were used to excite externally toroidal Alfvén eigenmodes (TAEs) and the Alfvén nature of the observed resonances were verified by scanning the toroidal magnetic field. A strong multi-peak structure was seen with very weak damping $\gamma/\omega < 10^{-3}$. These are the first reported observations of kinetic Alfvén eigenmodes. The TAE resonance were also excited when radio frequency waves launched from two antennae differ in frequency (Δf) by the TAE frequency (f_{TAE}) and generate a “beat” wave. The TAE frequency was matched to Δf by scanning the toroidal field.

Summary and Significance for ITER

High fusion performance plasmas were obtained with the pumped divertor (in spite of the 20% reduction in plasma

volume) and were limited by various MHD phenomena to $\beta_N \approx 1.8$, less than the Troyon value of 2.8. Nonetheless, equivalent $Q_{DT} \approx 1$, transiently, and 0.7, steady, were obtained and these experiments will be the basis for alpha-particle heating studies in high Q_{DT} operation in the deuterium-tritium (D-T) plasmas in late 1996. Other experiments of significance for ITER included the toroidal field ripple experiment, which indicated that the ripple in ITER should have no significant effect on energetic particle confinement, and studies of Alfvén eigenmodes, which led to the identification of weakly damped kinetic Alfvén eigenmodes.

ITER-Relevant Steady-State ELMy H-modes

Giant ELMs give rise to significant and fast (<200ms) movements of the separatrix strike points. On the other hand, frequent ELMs effectively broaden the power profile and reduce the peak temperature on the divertor target tiles. ELMy H-mode plasmas with steady-state conditions for many energy confinement times are therefore considered a credible mode of operation for ITER. After a period free of ELM instabilities, plasmas with the pumped divertor develop regular ELMing behaviour, with an energy confinement time which is typically a factor $H_{89} \approx 1.8$ higher than that predicted by the ITER89-P scaling for low confinement (L-mode) plasmas.

Long Pulse ELMy H-modes

The divertor cryopump allowed good density control and facilitated the production of long, clean, stationary H-mode plasmas with electron density, effective ionic charge, radiated power loss and stored plasma energy remaining constant for up to 20s (≈ 40 energy confinement times). The cryopump with argon frosting also pumped helium in L- and H-modes. So far, there was no evidence for the accumulation of helium in the central plasma, but the ratio of the helium replacement time to the energy confinement time was greater than 10 in L-mode plasmas and greater than 20 in H-mode plasmas. Further experiments will be needed to determine whether these high values are set by transport at the plasma edge or by a degradation of the pumping rate due to the contamination of the cryopump with deuterium.

High Current 6MA ELMy H-modes

The full 6MA current capability of JET was demonstrated and 6MA H-modes were obtained with up to 18MW of

NB heating. The beneficial current dependence of scalings for energy confinement in H-modes was also demonstrated for currents up to 6MA. At 4.7MA, 28MW of heating power was coupled to ELMy H-modes.

High β Plasmas at Low Edge q

Quasi-steady state stable operation has been produced with high normalised plasma pressure ($\beta_N > 3$ and, relative to the poloidal magnetic field pressure, $\beta_p > 2$), H-mode confinement ($H_{89} > 2.0$) and significant bootstrap current fraction ($\approx 50\%$). These advanced tokamak discharges at low plasma current can exceed the Troyon limit at high values of β_p , but the absolute values of the stored plasma energy and neutron rate are low.

High Power, Steady-state ELMy H-modes with Detached Divertor Plasmas and Radiative Power Exhaust

JET successfully established quasi-steady ELMy H-mode plasmas with combined (NB and ICRF) heating powers up to 32MW. Most of the power was exhausted by radiation from neon, nitrogen or argon seeded impurities. For example, in a discharge which used nitrogen seeding and additional deuterium fuelling the radiated power could be $\approx 75\%$ of the input power, with two thirds of the radiation emanating from below the X-point. The H-mode quality factor, H_{89} is about 1.5. The density reached a steady value, and the D_α signal showed the presence of benign "grassy" ELMs. In discharges of this type, the total deposited energy reached 180MJ (120MJ) with CFC (beryllium) target tiles.

Summary and Significance for ITER

JET has been exercised over a wide range of quasi-steady conditions, including that foreseen for ITER, namely, the ELMy H-mode in combination with a detached divertor plasma and radiative power exhaust. Essential contributions have thus been made towards the validation of these operating conditions.

Energy Confinement in ELMy H-modes

JET has been a major contributor to the multi-machine scaling studies to characterise the H-mode threshold power and energy confinement in ELMy H-modes. In addition, similarity experiments, which keep all dimensionless parameters (β , normalised collision frequency ν^* , q , aspect ratio ϵ , elongation κ , etc) near ITER

design values except for the dimensionless Larmor radius, $\rho^* = \rho_i/L$ (where ρ_i is the Larmor radius and L is a typical scale length for the machine), have been crucial for the understanding of transport.

Larmor Radius Scaling Experiments in ELMy H-modes

The validity of the similarity technique has been demonstrated by JET and DIII-D discharges, in which each of the dimensionless parameters (β , v^* , ρ^* , q , ϵ , κ) is approximately the same and the energy confinement time is found to scale inversely with the toroidal field. Pairs of JET discharges at 1MA/1T and 2MA/2T satisfy the quasi-gyro-Bohm expression of the ITERH93-P H-mode scaling for the energy confinement time and extended DIII-D studies towards ITER. Furthermore, the calculated thermal diffusivities over most of the plasma varying inversely with the toroidal field and this indicated a scaling close to gyro-Bohm.

Approach to β Limits

As the NB heating power in these discharges was increased from 6MW to 18MW, β_N first increased and then saturated. The ELM frequency also increased. The energy confinement time was seen to fall rapidly above $\beta_N=2.3$ and this may be the origin of the b dependence in the ITERH93-P scaling expression.

Approach to the H-mode Threshold

If the powers needed to achieve the correct dimensionless parameters in the ρ^* scaling experiments were plotted against a fit to the H-mode threshold power data from several tokamaks operated with the same geometry it was clearly seen that discharges well above the H-mode threshold exhibited a clear gyro-Bohm dependence but, close to the threshold, this scaling was lost and became Bohm or Goldston-like, and followed the threshold.

Summary and Significance for ITER

When considering the operating point foreseen for ITER ($R=8.14\text{m}$, $a=2.8\text{m}$, $k=1.73$, $I=21\text{MA}$, $B=5.68\text{T}$, $n=1.3 \times 10^{20}\text{m}^{-3}$, alpha power=300MW, radiated power fraction=0.36), it was clear that, with 100MW of heating power, ITER would operate close to both the b limit and the H-mode threshold. It would then be necessary to enter the H-mode at low density ($\approx 3 \times 10^{19}\text{m}^{-3}$) and to rely on the H-to-L transition in a deuterium-tritium mixture being

lower than the L-to-H transition in deuterium in order to sustain ignition at higher density. The multi-machine scaling studies for ITER need, therefore, to provide more accurate data on the H-mode threshold power and on transport scaling close to the threshold and at high β . Confidence in the accuracy of the scalings would increase if JET operated at lower ρ^* and higher β_N .

Detached Divertor Plasmas with Radiative Power Exhaust

Detached divertor plasmas with radiative power exhaust can reduce the particle, momentum and energy fluxes to the divertor target plates, thereby easing power handling and erosion. The exhaust power can be distributed by radiation and charge-exchanged neutral losses over the divertor sidewalls which have a sufficiently large area to reduce the heat load to acceptable values. The investigation of such divertor plasmas, which began at JET in 1992 has been pursued in depth with the relatively open (Mark I) divertor installed for the 1994/95 experimental campaign.

Detachment with Intrinsic Impurities in L-mode Plasmas

In a detached L-mode discharge, deuterium fuelling increased the plasma density to about $5 \times 10^{19}\text{m}^{-3}$ and the radiated power to about 70% of the input power. As the density increased, the particle flow to the inner and outer targets, as measured by Langmuir probes, was first seen to increase (high recycling), then level off ("rollover"), and finally decrease (detachment). The temperature also decreased, so that both the heat flux and pressure at the target decreased. Profiles of electron pressure at the mid-plane of the scrape-off layer plasma and along the target showed that a significant pressure drop (more than a factor of 10 near the separatrix) developed between midplane and target when detachment occurred.

Detachment with Extrinsic Seed Impurities in H-mode Plasmas

It was not possible to produce detached divertor plasmas with H-mode confinement in JET by using deuterium fuelling alone. This had been predicted theoretically for both JET and ITER. At the powers required to maintain the H-mode, the density required to reduce the divertor temperature to the point where detachment could occur (below 5eV) exceeded the H-mode density limit, and a transition back to the L-mode occurred. H-mode detached

plasmas could, however, be produced by introducing an extrinsic seed impurity into the divertor to enhance radiation. Neon, nitrogen, and argon seeds were injected into JET, either pre-programmed or feedback-controlled on the divertor radiation or the ion saturation current at the targets.

With nitrogen seeding, the radiated power fraction rose to more than 85%, with two-thirds of this being in the divertor. The H-factor relative to the ITERH93-P scaling leveled off at $H_{93} \approx 0.74$, typical of detached H-mode discharges in JET. The effective charge, Z_{eff} , rose to more than 2.5. Tomographic reconstructions of the radiation pattern in the lower half of the vacuum vessel as measured by a bolometer array showed that the radiated power fraction is low ($\approx 20\%$) when the plasma was attached to the target plates and that the radiation is well distributed throughout most of the divertor volume below the X-point when the plasma was partially detached. In the latter case, 50% of the input power was radiated and some power still flowed to the targets. Z_{eff} was also somewhat lower than at later times. At later times, $\approx 80\%$ of the input power was radiated and the radiating volume, which moved away from the targets, was located at the X-point. Some fraction of the radiation emanated from inside the separatrix. The motion of the radiating volume was smooth, but occurred over a fairly small range of total radiated power. Similar behaviour was predicted using the computer codes for the edge plasma.

Summary and Significance for ITER

The results obtained are promising for ITER, since the achieved radiated power fractions of 80% to 85% were sufficient to prevent target damage, overheating and erosion. Detachment was accompanied by a transition from large isolated ELMs to more benign "grassy" ELMs, which should not cause target damage. So far, however, these results were achieved at the expense of main plasma confinement and purity. The H-factor decreases as the radiated power fraction increased and, at the highest power levels, was somewhat below the minimum confinement time required for ignition in ITER ($H_{93} = 0.77$).

With regard to main plasma purity, nitrogen was found to radiate more in the divertor, but radiating 80% of the input power required $Z_{\text{eff}} \approx 3$. With argon, radiating 80% of the input power requires $Z_{\text{eff}} \approx 2$, but significant radiation then emanated from the main plasma. The observed seed impurity concentrations with nitrogen, neon or argon would not be acceptable in ITER, which requires $Z_{\text{eff}} < 1.6$ for ignition when the contribution from helium ash was taken into

account. However, the scaling of these results to ITER has yet to be established and improvements are to be expected from experiments with the more closed Mark II divertor.

Beryllium Target Tile Assessment

For the last three months of the 1994/95 campaign, the CFC divertor target tiles were replaced by beryllium tiles of similar geometry and a full experimental programme was carried out to assess beryllium as a divertor target tile material for ITER. The campaign was concluded by exposing the target to significantly higher heat fluxes, with the explicit aim of studying the behaviour of molten and damaged beryllium.

Performance under Normal Operating Conditions

Under normal operating conditions, beryllium was proven to be an acceptable divertor target material. The power handling characteristics of the CFC and beryllium target were found to be comparable and the general plasma behaviour (H-mode power threshold, the behaviour at the density limit and the density range for detachment) was similar to that with CFC. In particular, for both cases, H-mode confinement was lost when the radiated power fraction reached $\approx 50\%$ with intrinsic impurities and detached H-modes (radiated power fraction $\approx 80\%$) could only be achieved with impurity seeding. Gross melting of the target tiles was generally avoided by limiting the input energy and by "sweeping" the magnetic configuration over the target tiles, but superficial melt damage occurred due to some giant ELMs in hot-ion H-mode discharges which deposited $\approx 1\text{MJ}$ of plasma energy onto the target in about 20ms.

The Controlled Beryllium Melt Experiment

The hypothesis put forward by ITER, that a beryllium target would "self-protect" against excessive heat fluxes during off-normal events by evaporated beryllium leading to high radiation from the plasma and reduced heat fluxes, was also tested. With ITER reference off-normal heat loads of 25MW/m^2 , which resulted in significant surface melting, only a moderate degree of self-protection of the beryllium target was found. At best, the radiated power increased to $\approx 50\%$ of the input power, but only after several seconds. Following these experiments, ELMy H-mode discharges and nitrogen seeded radiative divertor discharges were established on the molten beryllium surface and found to be essentially unchanged.

Furthermore, high power swept operation resulted in 180MJ of input energy being deposited on the target, causing additional melting.

Summary and Significance for ITER

Under normal operating conditions, gross melting damage to the tiles was avoided by careful operation, although some superficial damage was produced by giant ELMs. Significant tile damage was inflicted during a controlled melt experiment when ITER reference off-normal heat loads of 25MW/m² were applied and only a moderate degree of self-protection of the beryllium target was found. Following melting, the effect of a damaged beryllium target on the operating regimes relevant to ITER was found to be small. Overall, beryllium remains one of the candidate materials for the divertor target in ITER. The final choice will depend largely on other considerations such as tritium retention and erosion lifetime.

Overall Summary

The JET pumped divertor has proven effective in handling the power exhaust and in preventing the high

impurity influxes, which previously terminated high performance discharges. This has allowed a broad based and highly ITER-relevant research programme to be conducted during the 1994/95 experimental campaign. In particular, high performance ELM-free H-modes with comparable performance to the past have been sustained towards steady-state, but are limited by various MHD phenomena to $\beta_N \approx 1.8$. A wide range of quasi-steady state ELMy H-modes have been studied at high power, high current, high b and with detached plasmas and radiative power exhaust. ρ^* scaling studies suggest that the underlying transport in ELMy H-modes has a gyro-Bohm character which is lost close to the H-mode threshold and at high β . ITER-relevant ELMy H-modes with detached divertor plasmas and radiative power exhaust have eased the power loading on the targets, but at the expense of main plasma confinement and purity. Beryllium compares favourably with CFC as a divertor target material under normal operating conditions, but melting has occurred and, with ITER reference off-normal heat loads, a radiative shield was not established quickly enough.

Developments and Future Plans

In 1978, the original objectives of JET were set out in the JET Design Proposal, EUR-JET-R5, as follows:

'The essential objective of JET is to obtain and study a plasma in conditions and dimensions approaching those needed in a thermonuclear reactor. These studies will be aimed at defining the parameters, the size and the working conditions of a Tokamak reactor. The realisation of this objective involves four main areas of work:

- i) the scaling of plasma behaviour as parameters approach the reactor range;*
- ii) the plasma-wall interaction in these conditions;*
- iii) the study of plasma heating; and*
- iv) the study of α -particle production, confinement and consequent plasma heating.*

The problems of plasma-wall interaction and of heating the plasma must, in any case, be solved in order to approach the conditions of interest.

An important part of the experimental programme will be to use JET to extend to a reactor-like plasma, results obtained and innovations made in smaller apparatus as a part of the general tokamak programme. These would include: various additional heating methods, first wall materials, the control of the plasma profiles and plasma formation.'

At the start of 1995, JET was in an operating phase, continuing the Pumped Divertor Characterization Phase, which had begun in February 1994 and ended in June 1995. During this period, the Mark I divertor was most effective and allowed a broad-based and highly ITER-relevant research programme to be pursued.

Since the beginning of its experimental campaign, extensive studies had been made in the first and third areas of work of JET's objectives: reactor relevant temperatures (up to 30 keV), densities (up to $4 \times 10^{20} \text{m}^{-3}$) and

energy confinement times (up to 1.7s) had been achieved in separate discharges. The second area of work had been well covered in the limiter configuration for which JET was originally designed. However, the highest performance JET discharges had been obtained with a 'magnetic limiter', (or X-point configuration). The duration of the high performance phase of these discharges exceeded 1.5s; this was achieved by careful design of the targets and specific operation techniques, but is limited, ultimately, by an unacceptably high influx of impurities, characterized by a rapid increase in electron density, effective ionic discharge and radiated power (referred to as the 'bloom').

The fourth area of work had been started by earlier studies of energetic particles produced as fusion products or by ion cyclotron resonance heating (ICRH). It was addressed further during 1991 by the first tokamak plasma experiments in deuterium-tritium mixtures. The high performance achieved in deuterium discharges, together with the experience gained in making substantial modifications to JET in a beryllium environment and with significant vessel activation, gave confidence that an experiment with about 10% tritium in the plasma could be performed and would provide data that could be used to plan an effective campaign of deuterium-tritium experiments in 1996.

During 1991, the JET Council had approved the policy of a step-wise approach to the introduction of tritium in advance of the full D-T phase of JET operations. As a first such step, after having obtained all necessary regulatory approvals, JET successfully carried out a preliminary tritium experiment (PTE-1) in November 1991 (as already described). A release of fusion energy in the megawatt range in a controlled fusion device had been achieved for the first time in the world.

In the 1991/92 campaign, JET achieved plasma parameters approaching breakeven values for about a

second, resulting in large bursts of neutrons. However, in spite of the plasma pulse continuing for many seconds after reaching peak plasma values, the neutron count fell away rapidly as impurities entered the plasma and lowered its performance. This limitation on the time for which the near-breakeven conditions could be maintained was due to the poisoning of the plasma by impurities (the 'bloom'). This further emphasised the need to provide a scheme of impurity control suitable for a Next Step device.

In late 1991, the Council of Ministers approved a modification to the JET Statutes, which prolonged its statutory lifetime by four years until 31st December 1996. The extension will allow JET to implement the new Pumped Divertor Phase of operation, the objective of which is to establish the effective control of plasma impurities in operating conditions close to those of the Next Step. This programme of studies will be pursued before the final phase of full D-T operations in JET.

During 1993, a large proportion of JET's effort was devoted to shutdown work for the pumped divertor phase of operations. The first stage of the shutdown in 1992 had involved removal of components and replacement of faulty toroidal magnetic field coils. The second stage in 1992/93 involved assembly of the four divertor coils and casings inside the vacuum vessel. The third stage of the shutdown began in mid-1993, with the final positioning of the coils. The shutdown was successfully completed with pumpdown of the torus in January 1994. The first plasma in the Pumped Divertor Characterisation Phase was produced in mid-February and by mid-March successful 2MA diverted plasmas had been established. During 1994, the plasma current was increased to 5MA, the total heating power to 26MW, the stored energy to 11.3MJ and the neutron rate to 4×10^{16} neutrons/s.

1994 saw significant progress in optimising peak fusion performance and extending operation to the reactor relevant steady-state ELMy H-mode, which has now been obtained under a variety of conditions (plasma currents up to 4MA, power levels up to 26MW, in the high β_p regime, in discharges with negative central magnetic shear, and at high β_N). The high β_p regime has also been extended to steady-state and to the reactor relevant domain.

The high power handling capability of the Mark I divertor target was demonstrated and the severe impurity influxes (carbon "blooms"), which previously terminated high performance plasmas, have been eliminated. The

cryopump reduces recycling, eliminates the effects of wall saturation (observed in previous long pulse operation), allows effective particle control, and generally allows higher performance.

The 1995 experimental programme had addressed the central problems of the ITER divertor: efficient dissipation of the exhausted power, control of particle fluxes and effective impurity screening, using both carbon fibre composite and beryllium as the power handling material.

During this phase, the plasma current was increased to 6MA (a world record in an X-point configuration), the total heating power to 32MW, plasma stored energy to 13.5MJ (the highest energy recorded in a JET plasma) and the neutron rate to a new JET record in deuterium of 4.7×10^{16} neutron/s (comparable to the best achieved prior to the installation of the pumped divertor and was achieved even though the plasma volume was 20% smaller). ITER-relevant quasi-steady state ELMy H-modes were also studied at high power, high current, high b and in combination with detached divertor plasmas and radiative power exhaust.

The campaign with CFC tiles on the first-wall was successfully completed in early-1995. This was followed by experiments to assess the performance of beryllium as a divertor target tile material and to compare it with CFC. In response to a request from the ITER Joint Central Team, beryllium melting was induced at ITER-relevant heat fluxes to see whether a protective radiative shield was established.

Overall, these achievements show that the main objectives of JET are being actively addressed and substantial progress is being made. The overall aim for JET can be summarised as a strategy "to optimise the fusion product ($n_i T_i \tau_E$)". For the energy confinement time, τ_E , this involves maintaining, with full additional heating, the values that have already been reached. For the density and ion temperature, it means increasing their central values $n_i(0)$ and $T_i(0)$ to such an extent that D-T operation would produce alpha-particles in sufficient quantities to be able to analyse their effects on the plasma.

In parallel, preparations continued for the next phase of D-T operations (DTE-1), which is scheduled for the end of 1996. JET has also continued the commissioning phase of the sub-systems of the active gas handling system in accordance with the JET programme for D-T operations.

JET is now continuing its programme of operations to demonstrate effective methods of power exhaust and impurity control in operational conditions close to those

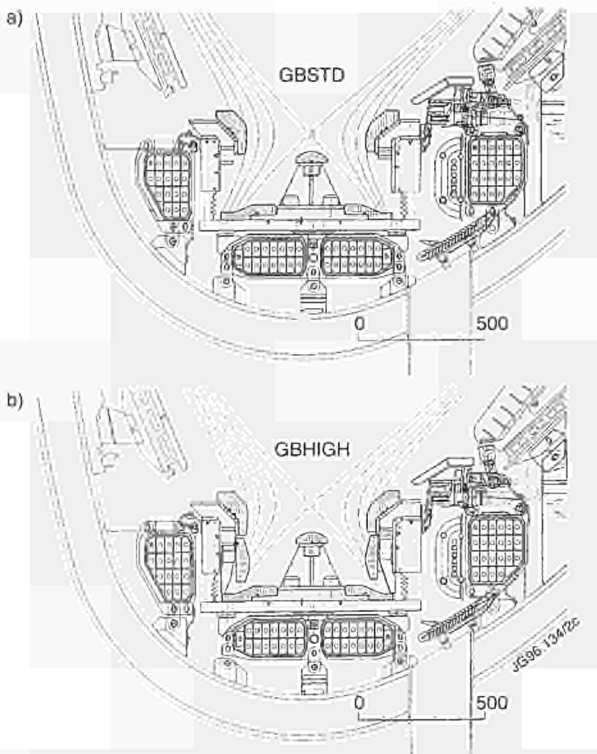


Fig.230: Poloidal cross-section of the Mark II Gas-box divertor configurations: (a) "horizontal target" configuration; (b) "vertical target" configuration.

envisaged for ITER before the final phase of full D-T operations. ITER relevant studies will provide stimulation to JET and JET's results will make an important contribution to the development of the ITER design.

The following sections describe various developments underway on JET to implement these systems.

Advanced Divertor Studies

During 1995, Advanced Divertor Studies concentrated on finalizing the design of the Mark II GB (Gas-box) divertor and modelling the various options which will be tested in the year of Gas-box operation following the DTE1 experiment in Mark IIA. The Gas-box divertor represents the second step in an integrated divertor programme based on the Mark II substructure, which allows for changes of divertor shape via remote tile/tile carrier replacement. It is more ITER-specific than Mark IIA in the sense that it is a deep divertor, with a relatively close fitting "entrance baffle" which begins below the X-point and continues above it to reduce the probability of neutrals escaping from the divertor chamber to the main plasma chamber. As a result, only a relatively small range of X-point heights can be accommodated.

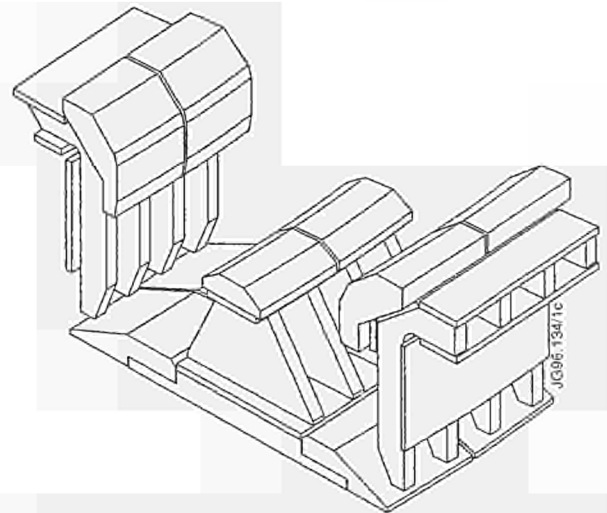


Fig.231: Mark II Gas-box divertor showing its make-up with toroidally discrete radially-oriented plates with a toroidally continuous top-tile.

The Mark II GB experimental programme is scheduled to last twelve months, with a short break in the middle to permit a configurational change. Two of the possible configurations are shown in poloidal cross-section view in Fig.230. In this figure, the poloidal flux contours adjacent to the baffle surface are 3cm from the separatrix at the midplane, which corresponds to several SOL falloff lengths. This clearance may be necessary to prevent ELMs from depositing a large amount of energy and particles on the top of the baffle rather than deep in the divertor. However, the effective baffle width, measured in fall-off lengths, can be readily reduced by increasing the flux expansion through manipulation of the divertor coil currents, allowing the tradeoff between closedness and ELM compatibility to be experimentally investigated.

Figure 230(a) shows the "horizontal target" gas-box configuration in which neutrals can recirculate, below the baffle, on both sides of the divertor plasma legs. Neutrals produced at the targets, which escape immediate reionization and exit the plasma legs, will lose their energy on either the septum or divertor sidewalls before re-entering the plasma, distributing the total exhaust energy over a large surface area. Therefore, these surfaces have been designed to take large radiative and neutral particle heat loads. This horizontal target version has a relatively small primary target area, so that its power handling capability in the absence of large radiative losses is not as large as in Mark IIA.

Figure 230(b) shows the vertical gas target version, in which neutrals which are not immediately re-ionized can only enter the private flux region and subsequently re-enter

the divertor plasma fans only from that side of the separatrix. However, this configuration has a considerably larger power handling capacity for attached divertor operation, while the penalty associated with the loss of neutrals re-entering from the outer sides of the divertor plasma fans is believed to be unimportant. This is the configuration currently favoured by ITER.

The septum shown in Fig.230 is comprised of a number of toroidally discrete radially-oriented plates with a toroidally continuous top tile, as shown schematically in Fig.231. In the base septum configuration, neutrals can pass through it from one side of the divertor to the other, with about a 40% transmission probability. In this case, pumping from the inner leg is expected to be increased by such neutral transits. In a small modification, vertical plates running toroidally in the centre of the septum assembly (not shown on the diagram) can be fitted to make the septum opaque to neutrals. A degree of control over the neutral pressure on the two sides, and the symmetry of the divertor plasma, is provided through the use of independent gas-feed circuits for the inner and outer divertor legs.

A third possibility for the septum is to cover its two sloping sides with toroidally continuous plates which convert the divertor from a true gas-box into a moderate deep-V configuration. In this case, the recycling neutrals are more localized towards the bottom of the divertor, which may offer certain advantages with respect to closure and control of partially detached plasmas. Finally, the divertor can be operated with the septum entirely removed and replaced with a flat cover plate. It is unlikely that this option will be utilized: it is being prepared as a backup in the event that sputtering from the septum top tile proves to be excessive.

At present, it is planned to begin operation with the vertical target (Fig.230(b)) and the septum in place. This experimental phase will last four to five months. JET will then shut down to switch, via remote handling, to a second configuration which will be either the horizontal target gas box or the deep V version of the septum and vertical target plates. That decision does not have to be taken until fairly late, and thus can be based on further experimental observations and analysis. The design of the Gas-box is essentially complete, and procurement of materials has begun.

Tritium Handling

The purpose of the JET Active Gas Handling System (AGHS) is to pump the torus, to collect gases from various systems (the torus, neutral beam injection, pellet

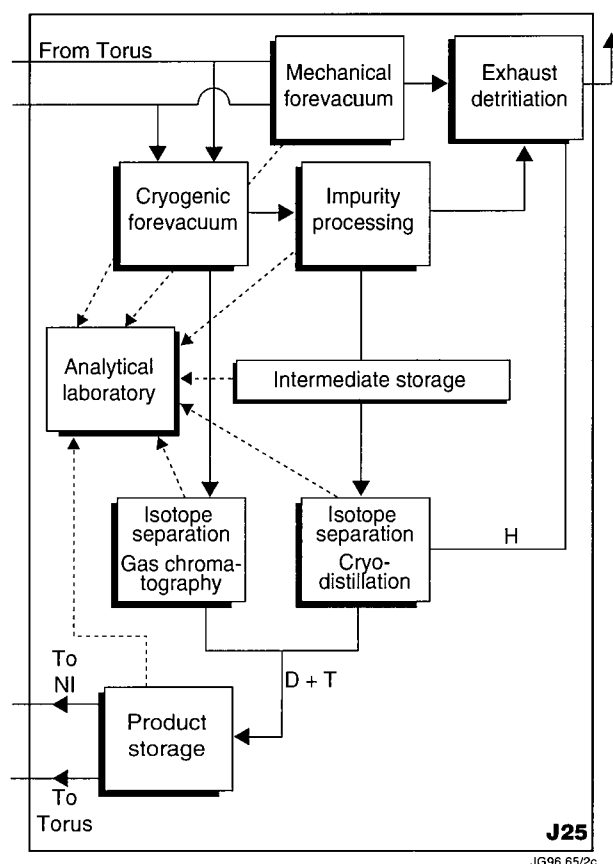


Fig.232: Block Diagram of Active Gas Handling System (AGHS)

injection and various diagnostics), to purify and isotopically separate these gas mixtures (consisting of the six hydrogen molecules, helium and impurities such as hydrocarbons, oxygen, nitrogen, etc) and to re-inject pure tritium and deuterium gas into the torus.

The AGHS is situated in a separate building (Building J25) and can be separated into sub-systems as shown in the block diagram (Fig.232). During the year, the commissioning phase of the sub-systems continued in accordance with the programme for D-T operations.

Inactive Commissioning of the AGHS

Inactive commissioning in accordance with a very detailed inactive commissioning procedure for the AGHS was completed for the following systems:

a) Cryogenic Forevacuum

The cryogenic modules were tested: their pumping speed and separation efficiency of the pumped gases into pure helium, hydrogen, and other species were determined and found to fulfil design specifications. The Cryogenic Forevacuum system was then used to pump gas from the NIBs and torus during a short commissioning period after the divertor tile exchange shutdown.

b) Mechanical Forevacuum System

The Mechanical Forevacuum system consists of a number of oil-free pumps specifically developed to pump radioactive gases. This system is intended for use during torus pump-down and glow discharge cleaning. It was tested in conjunction with pump-down and vessel conditioning following the tile exchange shutdown.

c) Impurity Processing System

The principle of Impurity Processing is to oxidise all tritiated gas species to water, to freeze the water out on a cold trap, to heat the cold trap to release water vapour and to reduce the water vapour on hot iron beds to tritiated hydrogen which is absorbed temporarily on U-beds. To reduce the processing times a new recombiner with a much smaller flow resistance was installed and tested successfully.

d) Intermediate Storage System

The main parts of Intermediate Storage are four uranium (U) beds, which are used as temporary storage for the distilled hydrogen gas mixtures from the cryogenic forevacuum system before their injection into the Cryogenic Distillation system or into the Gas Chromatography system. The intermediate containment temperature of the U-beds was found to be unexpectedly high, partly caused by the high thermal conductivity of hydrogen permeated at high temperature. A metal getter was added to the intermediate volume to absorb the hydrogen.

e) Gas Chromatography System

The eluant displacement gas chromatographic process is used for isotopic separation. The packing material is Pd deposited on Al_2O_3 , and the eluant gas is H_2 . Many separation runs were performed with the gas chromatography-system integrated between intermediate storage and Product Storage. These runs showed that the separation quality is fairly independent of many system parameters such as flow rates, temperatures, pressure, etc.

f) Product Storage System

The Product Storage system is a combination of eight U-beds, four each used for the storage of deuterium and tritium, respectively. U-beds can function as pumps, storage containers and compressors for hydrogen gas mixtures. The pumping efficiency of U-beds can decrease very drastically in the presence of gases which are not absorbed by the U-beds. Therefore, the possibility of circulating gas through U-beds is a fundamental precondition

to use their pumping capability and to scavenge hydrogen from hydrogen containing gas mixtures and the system was configured to permit this.

g) Analytical Laboratory

The Analytical Laboratory is mainly a large glove box which contains manifolds connected via small-bore lines to the other subsystems of the AGHS. The gas mixtures can be analysed by five different techniques: analytical gas chromatographic system, ionisation chambers, katharometers, residual gas analyser and omegatron. These systems were fully tested.

h) Exhaust Detritiation System

Gas to be released from the process pipework of AGHS to the environment can be discharged via the Exhaust Detritiation system. This system has an expected detritiation factor of about 1000. Continuous operation with cycling between driers, collection of water in $4m^3$ waste holding tank in the AGHS building, and transfer via a bowser to the active drainage system has been tested.

i) Distributed Control System

Almost all of the various AGH subsystems are operated fully remotely by a Distributed Control system. (The exceptions are the Cryogenic Distillation and Exhaust Detritiation systems, which are controlled by separate PLCs). The commissioning of the control system was a significant task because it involved the testing of about 500 process inputs, a large number of digital inputs/outputs and the remote control of about 600 valves.

j) Over/Under Pressure Protection system

The process pipework of the AGHS is surrounded by secondary containments. In most cases this secondary containment is filled with nitrogen gas kept a certain pressure below atmosphere. All 14 valve/glove boxes were sealed and the pressure control established via the control system.

Safety related procedures for these systems were performed including leak tests of primary and secondary containments, tests of hardwired interlocks, tests of software interlocks, checking of correct installation of safety relevant equipment (eg, rupture discs, non-return valves), tests of the Over/Under Pressure Protection System under simulated failure conditions (eg, rupture of a compressed pneumatic air line to actuate valves), etc. Testing tritium ionisation chambers was carried out as far as possible using X- or γ -ray sources to provide initial indication of correct functioning.

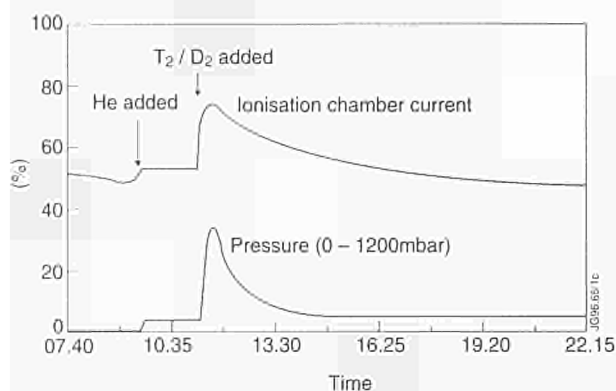


Fig.233: Creation of $T_2/D_2/He$ mixture and scrubbing of He using U-bed.

As a consequence of these tests, the systems listed were accepted to be ready for trace tritium commissioning. To enable maintenance to be carried out on contaminated systems, a series of cover-plates with transparent faces and gloves were procured for the stainless steel valve boxes.

Trace Tritium Commissioning

Before the start of trace tritium commissioning, considerable effort was required in what might be termed "Management of Safety". Local rules were written to establish a clear management structure for design and procurement of new equipment, for installation, commissioning and operation, and for modifications of the AGH plant, with all the necessary considerations on safety. In addition, Operating Instructions were written for repeated actions of operators. Prior to introduction of tritium, an external audit was carried out to the satisfaction of the UKAEA (the host organisation).

Trace tritium commissioning was performed with the tritium gas stored in the gas collection system used during the tritium experiment in 1991 (PTE), ($\sim 0.1g$). This gas collection system consists of four U-beds, a 350l vessel and a $15m^3h^{-1}$ pump mounted together on a trolley. This trolley was transported from the U-bed safe store (where it had been stored since PTE) into the AGHS Building. It was then connected to the Analytical Laboratory box and the content of the U-bed containing most of the tritium was transferred to a U-bed in the Product Storage System. The gas amount and the activity found after almost four years was in good agreement with the expected values.

The following subsystems were trace tritium commissioned: Product Storage; Intermediate Storage; Gas Chromatography; Impurity Processing; Over/Under Pressure Protection; and Exhaust Detritiation. The trace tritium



JG95.248c/5

Fig.234: Amersham Mark IV transport U-bed with calorimeter secondary confinement.

commissioning of these systems progressed very well. No tritium leaks into the secondary containments were observed and the analysis of smear samples taken from the interior of secondary containments did not reveal any tritium contamination. This is the result of very stringent leak test specifications and correct performance of these leak tests during the inactive commissioning phase.

Electrical and electronic systems especially of tritium specific equipment (mainly ionisation chambers) which could not be thoroughly checked without tritium were tested and faults were rectified. In a few cases, opening of secondary containments was necessary. A number of modifications which are desirable to improve performance, were identified by using tritium as a sensitive tracer. Figure 233 shows the parameters measured during a tritium transfer operation.

Full Tritium Commissioning

Tritium will be transported to JET in Amersham U-beds (Fig.234). A U-bed has been supplied to Atomic Energy of Canada Ltd (AECL) for loading with 3g of tritium for use in the full tritium phase of AGHS commissioning. The main objective of this phase is to fully test the isotope separation efficiency of the Gas Chromatography System.

Tritium System Developments Calorimetry

A precision calorimeter is planned for use to investigate the tritium activity in components used in the AGHS and

in the DTE1 experiments. A model was designed, built and tested, which makes use of a temperature stabilised base with inertial mass feedback control, working entirely under vacuum. Resolution and base line stability are approximately $\pm 1\mu\text{W}$ ($\sim 1\text{GBq}$).

A simpler, high accuracy, calorimeter with sample access from atmosphere, based on the same temperature control principle, was designed and built for routine tritium measurement (delivery/return to AGHS in U-beds). Resolution and base line stability are approximately $\pm 10\mu\text{W}$.

Instrumentation

H_2 - O_2 recombination sensors were developed and tested. They will be used as alarm devices in torus and NIB forevacuum lines to detect potentially explosive gas mixtures arising as a result of air in-leakage.

Selective pumping of H_2 (or D_2) to permit He leak testing of the torus at elevated temperature has been further improved; a getter trap with low conductance and high trapping efficiency is inserted between a torus turbopump and the He leak detector; the relatively high pressure drop of this trap is compensated by an additional small molecular drag pump. The new device can suppress hydrogen (or deuterium) partial pressures by up to six orders of magnitude.

Baking Plant

A helium purification loop for the baking plant was designed and installed. Its purpose is to remove tritium (as HTO) from the recirculating helium gas in molecular sieve driers and to remove air (the loop cannot be fully evacuated and filled with pure helium) in an activated charcoal absorber cooled with liquid nitrogen.

Safety Submissions to UKAEA

JET is required to satisfy the United Kingdom Atomic Energy Authority (UKAEA, the host organisation) that adequate safety standards exist prior to tritium operation. The UKAEA endorsed the issue of an Authority to Operate (ATO) for tritium commissioning of the AGHS following submission of a Pre-Commissioning Safety Report (PCMSR), an audit, and clearance of considerable number of follow-up actions arising from AGHS safety submissions.

The safety submission for DTE1 are now at a stage of being submitted for review by the Safety Directorate

Group of AEAT on behalf of UKAEA. The so-called Pre-Construction Safety Report contains an overview of the engineered safety of JET, a deterministic analysis (showing that the dose on-site and off-site for conceivable accidents is small) and a probabilistic risk assessment (showing that the UK's Health and Safety Executive (HSE) limits are complied with).

Plans for D-T Operation

A Working Group was constituted to propose plans for D-T operations in 1996 (DTE1), under the chairmanship of Dr A Gibson. The programme was prepared within the constraints of a limit of 2×10^{20} D-T neutrons and a programme duration of 3-4 months. The Group included the Programme Leaders and Task Force Leaders from the 1994/95 Experimental Campaign, and as well, there were a number of additional Proposal Co-ordinators.

A set of initial proposals were considered by the Group and this was narrowed down to twelve main experiments, and two necessary calibration and clean-up experiments. The titles of these experiments, including the number of shots and the D-T neutron budget are set out in Table XVIII. In addition, seven subordinate and six parasitic experiments were also selected. This gave a total of 2×10^{20} neutrons and 350 D-T neutron shots.

Preparations are underway to prepare for these experiments with D-T plasmas (DTE-1) scheduled for the end of 1996. The preparations aim to ensure that all technical provisions are made, and that the 1996 deuterium campaign performs the necessary preparatory experiments.

The four main objectives set for the experiment are summarised, as follows:

- (a) High fusion power demonstration in a reactor-like configuration, with Q approaching unity ($Q \approx 1$) for in excess of one energy confinement time. This should allow the observation and study of alpha-particle effects, at least in the plasma centre;
- (b) D-T physics of a reacting divertor tokamak, in an ITER like geometry, including H-mode threshold behaviour; ELMS; confinement; and RF heating at higher density;
- (c) Demonstration of a reactor-relevant fully remote handling operation (i.e. replacement of the divertor target assembly);
- (d) Operation of the Tritium Processing System integrated with a reacting tokamak (the JET Tritium Processing Facility is reactor scale and uses reactor relevant technology).

Table XVIII: Proposed DTE-I Experiments

	Proposal Titles	D-T Neutron Tx10¹⁸	No. of Shots
High Fusion Power, Q, and -Heating			
A	P _{fus} in hot-ion ELM-free H-mode Determination of tritium beam fuelling efficiency in low-recycling hot-ion H-mode (1% tritium)	29.2 1.5	4 4
B	Beam power step-down experiment to obtain high fusion Q and alpha-particle heating	28.5	4
C	α-particle heating experiment	19.2	4
D	Neutron diagnostics calibrations using: "1%" tritium; "10%" tritium	4.6	112
ITER Related			
E	Assessment of ICRF Heating Methods in Reactor Relevant D-T plasmas	10.0	11
F	Maximum Fusion Performance with Combined heating at High Toroidal Field	27.6	2
G	Use shear reversal configurations to increase performance of Hot-Ion modes	16.6	2
K	ELMy H-Mode p* scaling β saturation dependence on isotope	6.8 0.0	5 0
L	H-Mode power threshold measurements in D-T plasmas ITER-relevant H-mode Scenario	3.1 0.7	4 1
M	Isotope effect on H-mode power threshold	2.6	4
Steady State and Physics			
H	Maximum fusion power in a Steady State ELMy H-mode	37.8	2
I	Isotope mixture control in Hot-Ion H-Modes Isotope mixture control in high density discharges Change-over characterisation	1.9 4.3 0.1	15 40 20
J	Tritium clean-up methods using: plasma; gas soaking; glow discharge	2.2	30
N	Tritium transport study of divertor closure/retention with trace tritium tritium fuelling efficiency high power radiative divertor (i) - (ii)	0.7 1.0 1.5 0.1	2.5 20 36 5
Total		200	350

The physics programme of DTE-I would study the isotopic effect on confinement scaling and H-mode threshold power in D-T plasmas. These would be the first experiments of this kind in the geometry appropriate to ITER and including a divertor. Furthermore, the H-mode threshold power in D-T plasmas would be determined for the first time in these JET experiments. This would allow more accurate assessments of the ignition margin and the heating requirements for ITER. In addition, JET's capability for long pulse operation and impurity control should permit alpha-particle heating to make a significant contribution to the plasma power balance and this would allow the effects of α-particle heating (confinement and thermalisation of α-particles and stability of toroidal Alfvén eigenmodes in the presence of α-particles) to be studied and experience gained for ITER. The

operating conditions foreseen for ITER, namely long pulse ELMy H-mode detached radiative divertor plasmas, would also be studied in D-T plasmas.

The proposed DTE-I programme contains experiments designed to produce the following outcome:

- Discharges with high fusion power;
- Significant plasma heating effects from fusion alpha-particles;
- Sustained fusion power production of several MW;
- ITER relevant design information on the H-mode threshold in D-T divertor plasmas;
- Plasma energy and particle confinement scaling;
- Plasma-wall tritium recycling and control;
- Neutron and alpha-particle diagnostic demonstrations and measurements;

Table XIX:
Allowable Stresses and Forces on Magnet Coils

Copper conductor (All stresses in MPa)	Copper conductor	Brazed joints
Primary membrane stress	119	67
Primary membrane + bending stress	154	87
Primary + secondary stress	178	100
Electrical insulation		
Primary shear	15	
Primary + secondary shear	18	

- Technical demonstration of neutral beam and radio-frequency and (RF) heating with tritium, and tritium processing.

Studies for Machine Performance Enhancement

In the light of the proposed extension to the end of 1999, studies have been undertaken on possible enhancement options of some JET subsystems. In particular, it has been considered that, the toroidal magnetic field could be increased from the present 3.45T to a value of 4T and that the neutral beam injectors could be improved from 80kV, 60A to 120-140kV at 60A.

Toroidal Field to 4T

The strategy for operating the coils is based on high reliability, long life and minimal risk. However, the reliability analysis performed in 1992/93, showed that only a small percentage of the coil's life has been used since JET started operation in 1983. Therefore, with a moderately increased risk and an acceptable reduction of life, it was thought that operation of the TF coils at 4T should be possible. It was considered worthwhile to analyse in detail this possibility.

For D-shaped coils, the forces generated on the TF coils by the tokamak magnetic configuration are:

- The out-of-plane force generated by the interaction of the TF coil current with the poloidal magnetic field (supported by the mechanical structure) causes shear stresses in the glass-fibre-epoxy electrical insulation, in the mechanical structure, and, in particular, in the collar and ring teeth;
- The in-plane forces due to the interaction of the TF coil current with coils own field, giving rise to:

Table XX:
Allowable Collar and Ring Tooth Forces

	Maximum operational force (tonnes)
Top collar tooth	50 (limited by coil)
Bottom collar tooth	50 (limited by coil)
Top ring tooth	75 (limited by bolts)
Bottom ring tooth	75 (limited by bolts)

- longitudinal tension causing tensile stress in the copper conductor;
- inward force supported by the P1 coil (causing compression and shear stresses in P1).

The D-shape practically eliminates the bending moment in the plane of the coil and the absence of an individual coil casing, with the coils free to expand within the mechanical structure, eliminates the thermal hoop stresses. The stresses in the tokamak coil system have been re-assessed for the TF magnetic field at 4T and the new requirements for the power supplies have been studied.

Assessment of the Coil System

Allowable Stresses

To help in evaluating new stress levels, the allowable stresses for copper and insulation have been reviewed and common acceptance criteria applied to all relevant coils. The allowable stresses are defined according to the philosophy of the ASME codes and are summarised in Table XIX. The allowable force on the ring and collar teeth which support the TF coils have also been reviewed and are shown in Table XX.

Forces and Stresses in the TF Coils and MS Teeth

The out-of-plane forces depend upon the overall pulse configuration, due to the interaction with the normal component of the poloidal field, and, are therefore, proportional to the TF current, I_{TF} , and to the plasma current I_p . The in-plane forces, on the other hand, depend only upon the interaction with the toroidal field generated by the 32 coils and, therefore, scale with I_{TF}^2 .

Three plasma configurations of scientific interest have been analysed to assess the safety of future 4T operations. Disruption conditions were simulated by means of a sudden plasma disappearance. Stresses and forces were evaluated using an FE beam model and these were within the allowable limit (Table XXI).

Table XXI. - Forces and Stresses at 4T

Configuration	a) 6MA Mk II		b) 5MA high q_{95} , high ICRF coupling		c) Pulse No:33140 (ITER ρ^* scaling)	
Plasma current (MA)	6		5		4 (scaled from 3MA)	
	equilibrium	disruption	equilibrium	disruption	equilibrium	disruption
Total torque on structure tonne.m	12300	16500	10000	13400	10100	12700
Shear stress in the insulation (MPa)						
inter pancake (nose)	10	7	10	7	9	7
inter turn (peak)	17	3	17	0	8	4
at top collar tooth						
inter turn (peak) at bottom collar tooth	15	8	14	9	6	1
Tensile stress in the copper (MPa)						
total at the nose	114	101	113	101	108	98
membrane+ bending at the brazed joints	76	72	76	73	72	70
membrane at the brazed joints	60	60	60	60	60	60
Forces on teeth (kN)						
top collar	-478	79	-481	-3	-232	119
bottom collar	426	233	400	237	160	-35
top ring	340	577	311	506	397	526
bottom ring	-553	-701	-491	-616	-579	-660

Forces and Stresses in the P1 Coil

The P1 coil supports inward force of the TF coils and, therefore, stresses in the coil scale as B_T^2 . The winding is in turn supported by a steel support ring. The sub-division of forces between coil winding and support ring depends on the elastic properties of each, the initial state of stress, the temperature of the P1 Coil and the current in P1. The P1 Coil assembly is, in principle, axisymmetric so there are no shear stresses except due to internal features (joggles and terminals) and temperature gradients.

Stress calculations showed that the final temperature reached by the coil is an important factor in determining the stress in the coil. The temperature is determined by the energy dissipated (I^2t) of the pulse. Pulses suitable for use at 4T were considered and it was found that an I^2t of less than $30 \times 10^9 A^2s$ (probably $25 \times 10^9 A^2s$) would be sufficient for the experiments foreseen.

Stresses in the P1 coil were studied in detail in 1988, when the machine was upgraded to 7MA. It has been possible to extend these finite element calculations to include operation at 4T. These show that if the I^2t is limited to $28 \times 10^9 A^2s$, the maximum von Mises stress in the winding is 76MPa. This is within the allowable stress,

as it includes secondary stresses (Table XXII). Operation at higher I^2t needs further investigation to determine its acceptability.

Conclusion on 4T Operation

In conclusion, if plasmas that avoid excessive transverse fields in the collar and tooth region are selected, operation at 4T is practicable without changing the present levels of allowable stress and force. However, further studies are underway. A high-resolution 3D brick model is being prepared in order to analyze in more detail the stress distribution in the most critical areas of the TF coils, i.e. the sections supported by the collar teeth and the nose of the coil (where it detaches from the inner cylinder), where a local bending stress due to the in-plane forces appears.

Power Supplies

The TF coil power supplies consists of a flywheel generator with a peak capability of delivering 2.6GJ/pulse and of two static units supplied directly from the 400/33kV substation. Each static unit consists of two rectifier transformers, with the capability of an o.c. voltage of 2.0kV. The design specification of these power supplies allow

Table XXII:
Stresses in PI for various pulse parameters

Parameters	6	6	6	7	0	6	6	6	6
I_{plasma}	6	6	6	7	0	6	6	6	6
Toroidal field	3.40	3.40	3.40	3.40	3.40	3.85	4.00	4.00	4.00
$I_{\text{p}} I_{\text{t}} \text{ max}$	40	50	60	60	60	40	40	50	60
$I_{\text{t}}^2 \times 10^9 (\text{A}^2\text{s})$	28	35	44	44	44	28	28	35	44
Main body of coil (Stresses in MPa)									
von Mises	64	52	73	71	92	72	76	100	100
Shear (MBFE)	10	9	13	12	15	12	14	14	14
Steel ring (Stresses in MPa)									
von Mises	140	140	140	140	140	149	161	161	161

the TF coils to be fed with 67kA ($B_{\text{T0}} = 3.45\text{T}$) for 20s. However the power supply system has a built-in redundancy, that would allow delivery to the TF magnet of 75kA ($B_{\text{T0}} = 3.85\text{T}$) with a 3s flat-top.

To supply the TF coils at higher field (4.0T, 78kA supply current) and with extended flat-top (~10s), the power supplies would need to be upgraded. The boundary conditions to be considered for an optimum design of the upgrading of the power supplies are the energy to be delivered by the flywheel generator, the load voltage (and load current) of the static units, and the I_{t} capability of the TF coil system. The current (and voltage) capability of the flywheel generators is higher than required. The simplest and the cheapest way to reach this goal is to upgrade the voltage and current capability of the static units (2.8kV each). Engineering analysis and tests on the existing system, indicate that this goal can be achieved, basically, by replacing the four static unit transformers and the thyristor and cable protecting fuses, while the thyristor themselves have a built-in capability suitable for the new scenarios.

Enhancement of the Neutral Beam Heating System

Overview

The 1994/95 Experimental Campaign confirmed Neutral Beam Injection (NBI) heating as the heating method most able to couple power reliably into a wide range of plasma configurations. The relative insensitivity of the available NB heating power to plasma position (X-point height, strike zone location), plasma shape (triangularity, elongation, edge shear), safety factor and toroidal field enabled the execution of a wide experimental programme. In addition, NB heating remains essential for generation of

the so-called hot-ion H-modes discharges, in which its highest fusion performance is achieved [1], and remains the prime candidate for D-T discharges, in which significant thermonuclear effects will be seen.

For these reasons, an investigation into possible enhancements was instigated, which could be made to the NBI system to raise the available heating power from that presently available (21MW with deuterium (D°) beams in both Injectors or 25MW with D° beams in the Octant No.4 Injector and tritium (T°) beams in the Octant No.8 Injector).

Two scenarios were investigated:

- Replacing the 140kV/30A PINIs on the Octant No.8 Injector with 80-85kV/60A PINIs as presently used on Octant No.4; or
- Upgrading the high voltage (140kV) PINIs at Octant No.8 from 30A to 60A operation by upgrading the power supplies and regapping the PINI accelerating structures.

The constraints for both upgrades were that major modifications to the injectors themselves could not be considered, because the enhancement procedure should not lead to extra shutdowns in the 1996-1999 JET Programme. On the other hand, power supply modifications of a modular nature (ie: which would lead to the unavailability of a pair of PINIs at any one time) could be contemplated.

Although the first scenario would involve much less investment than the second scenario, it was rejected for further study for the reasons:

- the gain in mixed ($\text{D}^{\circ}\text{T}^{\circ}$) operation of injectors would be marginal and the central power deposition (within the inner 20% volume of the plasma) would actually decrease at all reasonable densities;
- the fuelling from the 80-85kV beams would be higher, thus making density control difficult;

- the lower energy beams would give significantly more momentum to the plasma and faster plasma rotation would produce more peripheral beam power deposition; and
- the reaction rate for production of beam plasma neutrons with a T^o beam on a deuterium target decreases significantly (factor ~ 2) as the energy is reduced to 80kV.

Hence the second scenario was chosen for further study.

Results of Tests on Upgraded PINIs in the Neutral Beam Test Bed

The tests aimed to establish the characteristics of two possible geometries for the upgraded PINI:

- a four grid (tetrode) design based on 'stretching' the extraction gap of the present 85kV PINIs, whilst keeping the voltage stress approximately constant;
- a three grid (triode) design based on 'squeezing' the extraction gap of the present 140kV PINIs.

The two strategies arise from the relationship between extracted current at optimum optics (I_{opt}) for a particular geometry, voltage which is given by:

$$I_{opt} = cV^{3/2}/d^2 \quad (1)$$

The quantity c/d^2 is the perveance, with c being dependent on the extracted ion mass, electrode hole geometry, etc. From consideration of Eq(1), it became clear that the tetrode strategy corresponded approximately to a constant current density upgrade. In this case, the space-charge characteristics of the beam were expected to be approximately unchanged in strength but, with the upgraded voltage, to become relatively less important.

The other reason for possible a priori preference of the tetrode would be the fact that the beamlets from the PINI would be steered to a focus by transverse aperture offset in the negative (decel) grid. This is the third grid of the tetrode structure and the second grid of the triode. To first order, the steering of the aperture offset is proportional to the field gradient in the main accelerating gap; ie. $\theta_i \propto f(x_i)x(V/d)$; where 'i' refers to the 'i'th aperture from the grid centre line. Since the tetrode upgrade would involve almost constant V/d , there is the hope that the same steering could be obtained (compatible with the present injector) without a change to $f(x_i)$, ie: without redrilling the negative grids. To redrill the negative grids would be expensive, so this was obviously an important consideration. The triode option was predicted a priori to involve grid re-drilling. The tests showed that, the situation was by no means cut and dried.

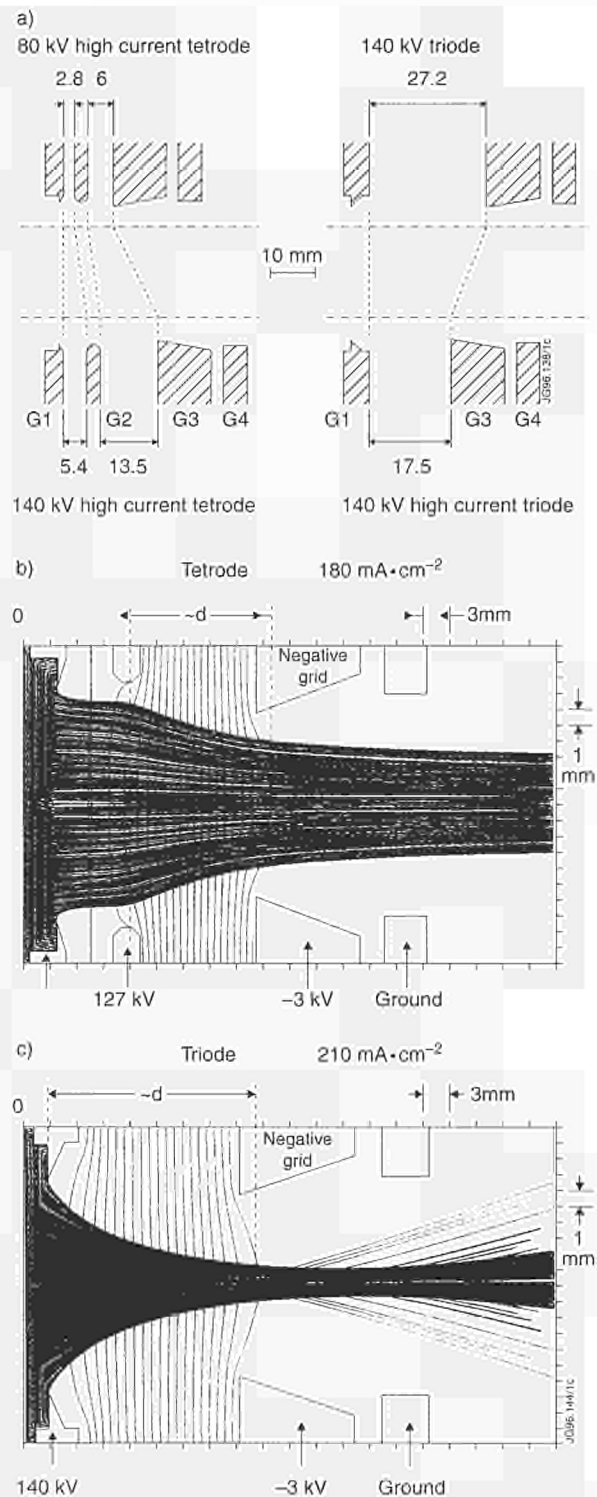


Fig.235: (a) Alterations to present tetrode and triode extraction geometries to give enhanced PINI performance; (b) Code results (ACCEL code – AEA Technology) for extracted ion beam optics for enhanced Tetrode PINI; (c) as (b) but for the ion beam optics of the enhanced triode PINI.

The two PINI geometries which were tested are shown in Fig.235, which also shows the ion optics code solution to tracing the rays through the accelerating system. The extraction gap lengths are given in Fig.235.

Scope of the Tests

- i) Most of the tests were carried out up to 120-125kV with hydrogen beams, due to restrictions to Testbed use in deuterium during the shutdown;
- ii) Power loading measurements were taken during the conditioning pulses on: power to the plasma source body; power to the accelerating grid structure; power to scrapers representing the Box Scrapers on the Torus Injector; power to the Testbed Beam Dump;
- iii) Beam profile measurements (horizontal and vertical) were also taken for each PINI at several distances from the PINI using the new mobile calorimeter. These profiles enabled beam divergence and beam steering to be separately determined, and enabled the minimum divergence (optimum perveance) to be derived for comparison with codes. Beam profile measurements were also taken with source operation in helium, which removed the effect of extracted species variation. The helium results were compared with the standard PINIs;
- iv) One geometry was then selected for tests in deuterium at up to 140kV. The restriction to one geometry was necessary as special working arrangements had to be provided to allow D_2 operation in the middle of the shutdown. For reasons given below, the triode geometry was chosen for the D_2 tests.

Test Results

All tests were performed with the so-called 'chequerboard' (CHQ) plasma source on the PINI. This gives an exceptionally uniform plasma across the PINI extraction grid:

i) Optimum perveance

The predictions of the code for the optimum perveance in hydrogen with the CHQ source were within 10% of the measurements. The measured optimum perveance at high voltage and also at lower voltage are both well described by a unique 'normalised perveance' curve when the known extracted species variation with current density in the CHQ source is taken into account, indicating that there are no other space charge effects to be accounted for. The extrapolated normal D_2 operation values for the enhanced PINIs would be: 140kV/52A for the tetrode and 140kV/59A for the triode, when using the normal ('filter') ion source with high monatomic yield.

ii) Beam divergence

The tetrode PINI had exceptionally low beam divergence, in agreement with the code. The divergence of the triode was slightly better than the standard triode. The

results were: tetrode 0.25° divergence; triode 0.47° divergence. These results meant that for the tetrode the beam divergence could be easily identified as the profiles from the two halves of the PINI grids were well-separated. On the other hand, the power on the Test-bed Beam dump was already too high in H_2 tetrode operation (at ~ 6 MW) and caused melting on the edge of the hypervaportrons. Operation in D_2 (with a narrower divergence beam and at higher power) was therefore considered unsafe and would, moreover, lead to excessive beamline power loads which could only be alleviated by increasing the focal lengths by re-drilling of grids thus removing one advantage originally ascribed to the tetrode.

iii) Power Loadings

The power loadings on beam dump, scrapers, 'source' or PINI (grids+source+ neutralisers) were measured. The power loading on the simulated Box Scrapers was much lower ($\sim 7-8\%$) for the tetrode PINI than for the triode ($\sim 11-12\%$). Although this is clearly advantageous, it is indicated below that it is necessary to redesign the Box Scrapers on the Torus Injector to accommodate the upgraded PINIs in tritium operation and so lower Box Scraper loading is not a decisive factor. The total power falling on the source (at $\sim 10\%$) was the same for both geometries. The breakdown of power loading to the various parts of the PINI and neutraliser showed that the relative values were similar for the tetrode in H_2 and the triode in D_2 . The percentage power loads on Grid 1, negative grid (Grid 3'), earth grid (Grid 4')+first stage neutraliser and on the second stage neutraliser are all similar to the usual values and well within the previous defined operational levels. The percentage power load on the plasma source body is also similar to normal, but the absolute power on the source body is above previously accepted safe levels. A 5% level of loading on the body corresponds to 420kW at full power, compared to safe working levels of 280kW. This previous safe level is now being investigated. Preliminary indications give an optimistic prognosis that it was too conservative.

iv) Beam Steering

The 'standard' PINI extraction systems from which the two upgraded geometries were developed both have steering grid hole patterns set to give: Vertical focal length (f_v) = 14 m; Horizontal focal length (f_H) = 10m. From the profiles at optimum perveance taken at various distances (z) from the source, the value of f_v and f_H was fitted, together with the divergence. The three parameters

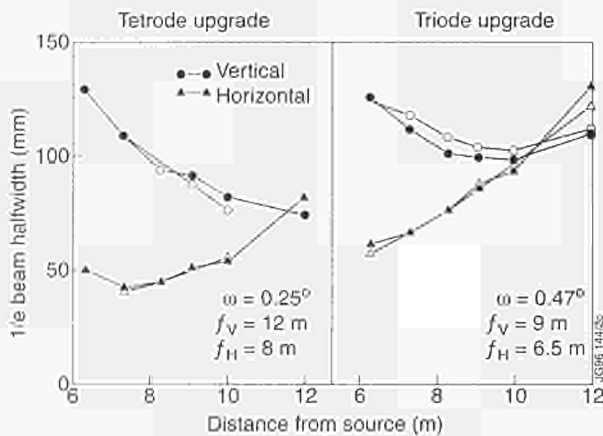


Fig.236: Measured beam half-widths (solid symbols) derived from various measurements (see text) for (a) enhanced tetrode and (b) enhanced triode PINIs. These are compared with the curves using the best fit parameters (open symbols) for divergence and horizontal and vertical focal lengths.

were obtained from fits to power profiles obtained with IR camera on the mobile CFC-tile calorimeter (3z axis positions); with thermocouples on the TB Beam Dump (l_y axis position), and thermocouples on a 2-d 'cross' calorimeter (l_y axis position). The results of the fits were: ($f_v = 12\text{ m}$; $f_H = 8\text{ m}$; $\omega = 0.25^\circ$) for the tetrode and ($f_v = 9\text{ m}$; $f_H = 6.5\text{ m}$; $\omega = 0.48^\circ$) for the triode. The fitted curves are shown in Fig.236.

The experimental values show that the tetrode steering has changed by ~15-20%, whilst the triode has changed by ~35%. Even when the errors on this measurement are taken into account, the changes in focal lengths do not quantitatively correspond to the estimated effective change in V/d , illustrating the limitation of the determination of the field penetration into the electrode gap. The code predictions can be regarded as satisfactory.

Consequences of Enhancement for Injector Components

Major upgrades to injector components had been ruled out of any enhancement scenario to avoid major shut-downs. The specification of the final beam optics; beam transport; operating voltage and operating current (perveance) of the enhanced PINIs would have to be tailored that safe operation of the dumps and calorimeter could be maintained. These components would ultimately limit the extra power to the plasma available from the enhancement.

On the other hand, it was recognised at the outset that the Box Scrapers, which define the beam envelope at the end of the NB Box, are at the limit of their performance

in the present Octant No.4 Injector, which injects 13-13.5MW power and would hence need to be upgraded in any enhanced scenario. This upgrade would be with the design specification to take the maximum power foreseen from an upgraded Injector (140kV/49A T° beams giving ~19MW to the plasma). Design effort will commence in 1996 if the enhancement plan is approved. The foreseen costs for upgrading the Box Scrapers are modest and the work to install them would be only ~15 days in length and could be accommodated within the post-DTE1 outage.

Calorimeter

The new Inertial Calorimeter is designed to take 20MW/m² for pulse lengths ~1s, which matches it to the capabilities of the high-current tetrodes on the Octant No.4 Injector (13.5MW total injected power). These existing high current PINIs have a beam divergence (ω) of ~0.6°. A beam divergence ~0.25°, as on the tetrode upgrade, would raise the peak power density by ~20%, taking it above the component's limits except for pulses which are too short for useful conditioning. Similar problem exists for the triode unless it has long focal length.

The solution for the calorimeter would come from the reduction in power loading as the focal length is increased. The relative power loading as a function of steering focal length shows a significant reduction occurs if f_H can be set to ~10m. For focal lengths longer than this, the alignment of each grid half must be changed to gain more safety. The power loading to the Box Scrapers increases only slowly as the focal length is increased and is not a concern since these are to be redesigned in any case.

Full Energy Ion Dumps

Simulated beam profiles (generated by Monte Carlo methods to simulate a real PINI grid) have been tracked through a representation of the Beam Deflection Magnet and FEID to give power profiles on the dumps. The results are plotted as a function of horizontal and vertical focal lengths in Fig.237 (tetrode) and Fig.238 (triode). The power densities shown are normal to the surface of the FEID elements. Also shown are predicted loadings on the top and midplane dumps which catch the 1/2 and 1/3 energy ions coming from molecular ion break-up.

The predicted power loadings on the FEIDs are very high compared with the existing limit of ~8MW/m². This limit is conservative however, being set by keeping the thermally-induced strain in the element a factor two

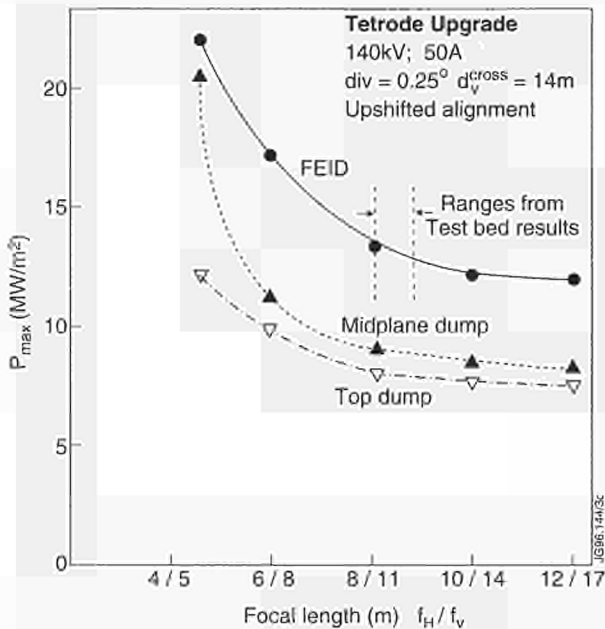


Fig. 237: Predicted maximum power loading on the Ion Dumps from the enhanced tetrode PINI at 140kV/50A as a function of steering focal length.

below the strain which would allow effectively unrestricted operation, ie: > 10000 cycles before fatigue life is reached. The fatigue curve is determined by cycling the CuCrZr material through simple bending motions. Thermal stress is expected to be 'kinder' than this crude simulated stress, but at the moment the limits are set in accordance with ASME standards. It is clear that there must be restearing to bring the power loading down to 'reasonable' levels. A reasonable power level would be $\sim 12\text{MW/m}^2$, corresponding to the other limit on the hypervaportrons, that of 'burnout' when the temperature on the copper surface cannot be stabilised because the heat transfer is insufficient to handle the power input [2]. In principle, it can be seen that 12MW/m^2 power density can be achieved with the 140kV/50A tetrode if f_H/f_V goes to 12m/17m, and with the 140kV/60A triode if f_H/f_V goes to 10m/14m. It may also be the case that space-charge blow-up of the beams in the deflection-magnet cross-over region (not in the code), will tend to diffuse the power density profiles.

The fatigue cycles for hypervaportron elements were discussed in the 1994 Progress Report [3]. A preliminary analysis has been performed using the same model and establishing the load cycles to failure with $12\text{MW}\cdot\text{m}^2$ 10s pulses. The results show that ~ 800 full power, full pulse length shots could be accommodated on the Full Energy Ion Dumps. This is a large number considering that only 20-40 such shots are performed in each campaign. The lifting of the limits further is being investigated.

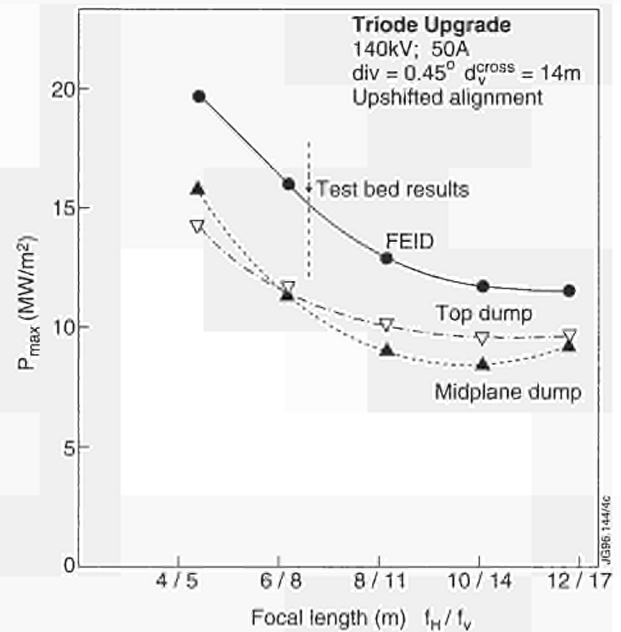


Fig. 238: Predicted maximum power loading on the Ion Dumps from the enhanced triode PINI at 140kV/50A as a function of steering focal length.

Upgrade of NB Power Supplies

The present power supplies for the NB injection consist of a basic unit of 80kV/60A. There are 16 installed, each of which can supply one PINI at 80kV/60A or alternatively two of these units can be connected in series giving 160kV/60A. In this configuration, the two series connected units supply two parallel connected injectors of 160kV/30A.

The PINIs at 140kV/60A cannot be used with the present accelerating grid (Grid 1) power supplies. There are three basic options to achieve this requirement; the first one is to build complete new PS identical to the existing one; the second is to upgrade the voltage of the present PS to 140kV/60A; and the third is to upgrade two series connected units from 60A to 120A. In the latter case, two injectors would be connected in parallel at the output of each power supply.

The present transmission lines and the SF6 Tower are designed for 160kV and all the auxiliary PS for the injectors are able to supply current for 60A injectors, and therefore no modifications to these systems would be necessary. The new additional 60kV/60A PS would be connected at the high voltage side of the existing 80kV/60A unit.

The main design requirements for the PS are very strict due to the way the complete NB system is operating. The most stringent requirements concern voltage stability (<1% including ripple) and switch-on and switch-off times (100-500 μs and 5 μs , respectively). The stored energy in the PS is also an exacting target.

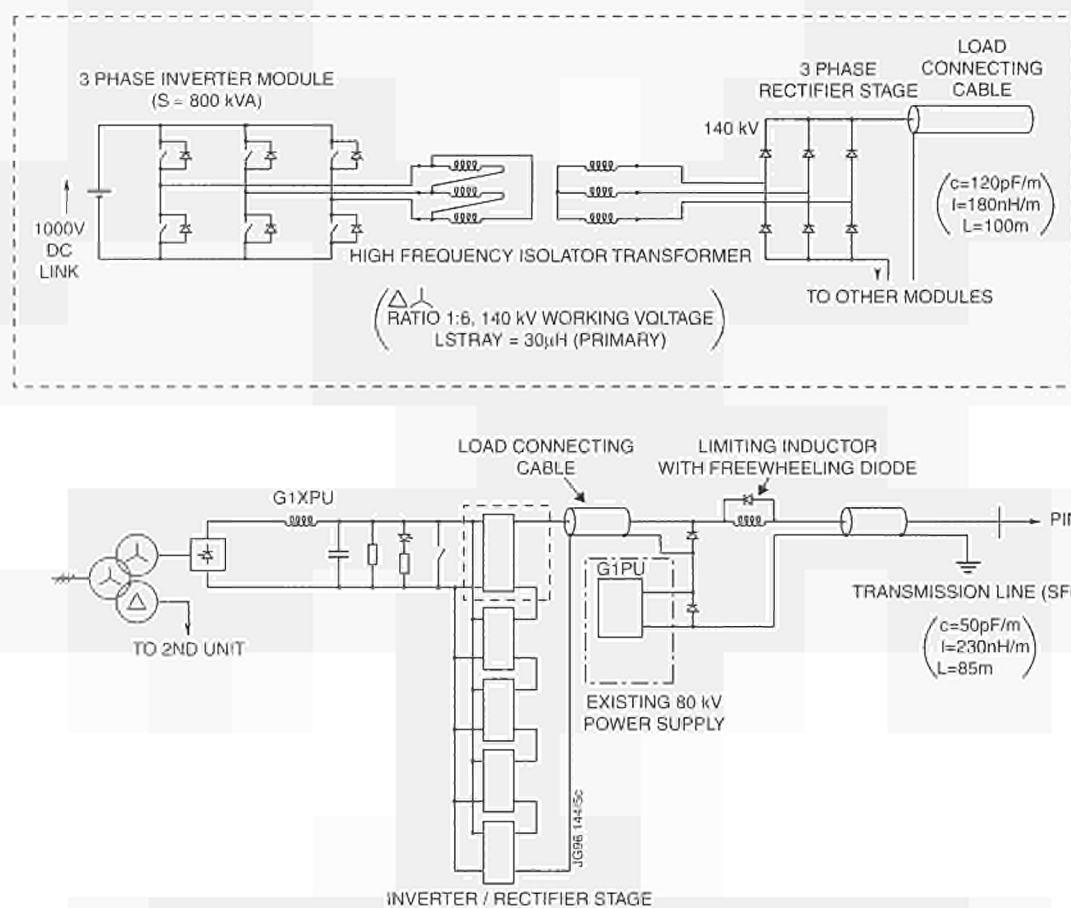


Fig.239: Reference schematic for 60kV/60A extension power supply for enhanced PINIs.

For the present system, these requirements are met by using a tetrode as regulating and switching device. Several schemes were examined and it was decided to design a PS based on new technology using IGBTs (Insulated Gate Bipolar Transistor) as switching and regulating devices. Simulations, using the ATP program, were performed to find the best possible scheme taking into account the above design requirements.

The new PS would consist of a basic thyristor controlled rectifier fed from the 36kV network to obtain the intermediate DC voltage (Fig.239). From this intermediate DC level, several invertors based on IGBTs would be fed with their outputs connected in series to obtain the 60kV. In the reference design, five of these invertors would be used. The inverter frequency is 1.5kHz. To regulate the output voltage a modified PWM (Pulse Width Modulation) is used in the inverter bridge. The simulations showed that a voltage variation of 12kV on the 36kV network can be regulated by the fast PWM. This is sufficient to stabilise the PS output with respect to the variation on the 36kV network or of load variations. The actual output voltage is set by setting the intermediate DC voltage level. The combination of the slow control loop

for the intermediate DC voltage and the fast PWM loop in the inverter gives the required design values for the ripple and the stability of the output voltage. Since IGBTs can switch in microseconds, the required switching times in the inverter conform with the fast switching requirements. The main part of these PS would have to be installed outside JET buildings, since no place is available inside. Because of this, the capacitive energy in the connecting cable from the PS to the transmission line can exceed the limit of what can be passed to the snubbers in event of a HV breakdown (50J). Thus energy absorbing components should be installed inside the present grid 1 protection system, ie: a thyristor crowbar to absorb the energy of this cable

Performance of the Enhanced NB System

A system in which the Octant No.8 Injector has been upgraded to 140kV/60A (D^0) operation, when combined with the present Octant No.4 system would inject to the plasma ~28.5MW (both injectors in deuterium); ~32MW (Octant No.8 tritium, Octant No.4 deuterium); and ~38MW (both injectors in tritium)

Studies have been performed on the general input parameters from this system to the plasma (eg: power

deposition profiles; particle fuelling and momentum) using the PENCIL code. Predictions of plasma performance have also been made in the hot-ion H-mode using the PRETOR code.

The PENCIL studies show that the upgrade to the Octant No.8 injector in deuterium would result in:

- an increased central power deposition (inner 20% volume of the plasma) of ~30% for $\langle n_e \rangle \sim 2 \times 10^{19} \text{m}^{-3}$ ie: the density for a 'hot-ion' target plasma;
- increases in central power deposition ~25% for all plasma densities below $\sim 7\text{-}8 \times 10^{19} \text{m}^{-3}$ ie: the density in ELMy H-mode plasmas at high current;
- a drop in the particle fuelling per MW from the injected beams of around 5%;
- an unchanged torque per MW injected on the plasma.

All these indicators move in the right direction for enhancing the central parameters of JET plasmas.

PRETOR Studies of the Hot-Ion H-mode

Whilst it is clear that MHD stability is fundamental in attaining good fusion performance in the hot-ion H-mode, it is apparent from the global data that there is a strong relationship between NB power and neutron rate. Discharges, which have been optimised as far as was possible within the 'old' and Mark I pumped divertor configurations fall within an upper bound of neutron rate versus P_{NB} which can be characterised by $(P_{\text{NB}})^\alpha$ where $\alpha \approx 2$.

The key question for any proposed enhancement is, therefore, whether this power dependence will continue well beyond present power levels. There is significant scope to increase further the toroidal β . The best discharges are limited well below the Troyon limit and this suggests that the pressure gradient, ∇P , is well below the ideal ballooning limit, on average, across the plasma column. Stability analyses confirm this everywhere except at the plasma edge where, in the vicinity of the separatrix and the H-mode transport barrier [4], $\nabla P(a)$ approaches about 80% of the theoretical limit. The high edge pressure gradients arise due to the high edge temperatures that develop during the ELM-free phase, giving rise to a substantial 'pedestal' contribution W_{ped} to the stored plasma energy. Higher stored energy and β would result from: (1) a more peaked core pressure profile superposed on the edge 'pedestal'; and/or (2) an increase in $\nabla P(a)$ which can be supported without a terminating event or 'crash', hence increasing W_{ped} .

It is reasonable to expect that a transient gain in (1) would be achieved for a characteristic timescale $\tau_{\text{core}} \approx a^2 / \langle \chi_{\text{core}} \rangle$ by increasing the heating power. Furthermore, there are several physical reasons why (2) might be favourably influenced by increased heating power, due to the effect on $T_e(a)$ and $T_i(a)$, resulting in changes to resistivity, $j(a)$ and also the minimum scale length of $\nabla P_i(a)$ which is determined by the ion poloidal Larmor radius ρ_i . It may also be noted that particle recycling also affects these parameters, and it is well established that low recycling has a strong effect on ELM stability [5].

The experimental data demonstrate that the total stored energy continues to increase up to the maximum available NB heating power. The upper bound of the diamagnetic energy W_{dia} (the best transient performance cases) scales roughly in proportion to P_{in} . Taking into account both beam-plasma and thermal plasma reactions, it can be shown that the neutron yield theoretically scales as $\propto (P_{\text{in}})^\alpha$, where $1 < \alpha < 2$.

The simulation which has been performed involves:

- the PRETOR plasma prediction code with heat and particle fluxes being evaluated by Bohm-like or Rebut-Lallia-Watkins transport coefficients;
- a crash condition determined as a parameterised dependence of the limiting value of $\nabla P(a)$, eg: on $T_e(a)$ and $T_i(a)$; and
- an edge H-mode transport barrier dominated by neo-classical ion transport losses with a thickness given by the minimum scale length of $\nabla P_i(a)$ ie: the ion poloidal Larmor radius .

The simulation lacks a proper physical model for edge stability but this is parameterised by bench-marking the code against a number of hot ion H-mode discharges with similar shape (triangularity and shear) and different input powers. Using this a satisfactory prediction of the crash time and achieved neutron rate, stored plasma energy etc, is obtained which will allow a reasonable extrapolation to higher power levels. The simulation also takes into account the effect of particle recycling, which is known to affect the behaviour of hot ion H-modes strongly.

Other results of the simulation, applied to a plasma at 3.8MA/3.4T (similar to the record Pulse No.33643) show the expected neutron rate for 28.4MW of NB heating power (12.8MW at 80kV and 15.6MW at 140kV from an enhanced high voltage injector) is strongly dependent on the recycling level. R_{um} is varied between 1.6 (which is required to simulate the actual data for Pulse No.33643)

and 1.14 (which is the level required to simulate Pulse No.26087 from the best performance PTE development series). It can be seen that if the recycling levels of the PTE series can be achieved, a ≈ 2.5 fold increase in neutron rate would result from the enhancement of the NB system to 28.4MW.

References

- [1] The JET Team, presented by T T C Jones, *Plasma Phys & Contr Fus* **37**, suppl 11A (1995).
- [2] H D Falter and E Thompson, JET-P(95)13 (1995), submitted to *Fusion Technology*.
- [3] JET Joint Undertaking Progress Report 1994, EUR 16474-EN-C, pp 34-35.
- [4] T C Hender et al., *Europhys Conf Abstracts (Proc 22nd European Conf on Controlled Fusion and Plasma Physics) Vol 19C (I)*, (1995).
- [5] R Koenig, K D Lawson et al., 37th Meeting APS Plasma Physics Division (1995).

Future Plans

The JET Programme was divided into phases governed by the availability of new equipment and fitting within the accepted life time of the Project. Phase I (Ohmic Heating Studies) was completed in September 1984, and Phase II (Additional Heating Studies) in October 1988. Phase III (Full Power Optimization Studies) ended in February 1992. The scientific aims of Phase III were to obtain maximum performance in limiter configuration (currents up to 7MA) and to optimize X-Point Operation (currents up to 6MA) including a comparison of H-modes in X-point configuration using beryllium (lower X-point) with carbon (upper X-point) dump plates.

JET future plans are dominated by the insertion of a new phase of the Project (Phase IV: Pumped Divertor Configuration and Next-Step Oriented Studies). This phase is subdivided into a Divertor Characterization Plasma and an ITER Support Phase. This new phase extended the lifetime of the Project up to the end of 1996.

The Pumped Divertor Characterisation Phase began in February 1994 and ended in June 1995. During this period, the Mark I pumped divertor was very effective and allowed a broad-based and highly ITER-relevant research programme to be pursued. It had addressed the central problems of the ITER divertor: efficient dissipation of the exhausted power, control of particle

fluxes and effective impurity screening, using both carbon fibre composite (CFC) and beryllium as the power handling material.

During this phase, the plasma current was increased to 6MA (a world record in an X-point configuration), the total heating power to 32MW, plasma stored energy to 13.5MJ (the highest energy recorded in a JET plasma) and the neutron rate to a new JET record in deuterium of 4.7×10^{16} neutron/s (comparable to the best achieved prior to the installation of the pumped divertor and was achieved even though the plasma volume was 20% smaller). ITER-relevant quasi-steady state ELMy H-modes were also studied at high power, high current, high b and in combination with detached divertor plasmas and radiative power exhaust.

The campaign with CFC tiles on the first-wall was successfully completed in mid-March. This was followed by a shutdown of 22 working days in which the CFC tiles were removed and replaced by beryllium, a prototype separator for the ion cyclotron resonance frequency (ICRF) heating antenna was installed and eighteen French Horn cooling pipe insulators were strengthened and replaced.

Following this shutdown, experiments were performed to assess the performance of beryllium as a divertor target tile material and to compare it with CFC. In response to a request from the ITER Joint Central Team, beryllium melting was induced at ITER-relevant heat fluxes to see whether a protective radiative shield was established.

In June 1995, a shutdown started for the installation of the Mark IIA divertor and the modification of the ICRH antennae. The shutdown is due to finish in March 1996. A detailed inspection at the start of the shutdown, showed that in-vessel components were in good condition with no significant damage except for the deliberately induced beryllium target plate melting. The first phase of in-vessel work in the shutdown was the strip-out of components. This work, which included the removal of the ICRF antennae for modification, was completed ahead of schedule.

The next phase of in-vessel work involved installation of the modules of the Mark II divertor support structure. This structure, which is about 6m in diameter and with a weight of 7 tonnes, was assembled to within an accuracy of 0.1mm. The ICRF antennae, modified to improve the coupling of ICRF power to the JET plasma, were then reinstalled. At the end of the year work to install other in-vessel components was continuing.

Preparations are also continuing for the next period of D-T operation (DTE-1), which is scheduled for the end of 1996 and work is continuing on the procurement of the ITER specific Mark II Gas-box divertor target assembly, which is due to be installed by remote handling in 1997.

Extension of Programme to end of 1999

A proposal for the extension of the JET Programme to the end of 1999, which is supported by the JET Council, is currently being sent to the Council of Ministers for approval. The purpose of the extension of JET to the end of 1999 is to provide further data of direct relevance to ITER, especially for the ITER-EDA, before entering into a final phase of D-T operation. In particular, the extension:

- i) should make essential contributions to the development and demonstration of a viable divertor concept for ITER; and
- ii) carry out experiments using D-T plasmas in an ITER-like configuration, which will provide a firm basis for the D-T operation of ITER;

while allowing key ITER-relevant technology activities, such as the demonstration of remote handling and tritium handling, to be carried out.

Divertor Studies

The divertor must fulfil three main functions: (i) exhaust plasma power at acceptable erosion rates; (ii) control plasma purity; and (iii) exhaust helium "ash" and provide density control. For ITER, successful divertor operation must also be compatible with high confinement (H-mode) operation with Edge Localised Modes (ELMs).

Erosion can be reduced by decreasing the plasma temperature at the target plates which can be achieved with high density and high recycling near the target plates. However, the exhausted plasma power conducted to the targets in this high recycling regime is not reduced and has to be distributed over a large surface area. To some extent, this can be achieved by inclining the targets so as to project a larger surface area to the conducted heat flux which flows along the magnetic field. In JET, the plasma "footprint" can also be swept across the targets, but this would not be possible in ITER or a reactor.

An alternative approach is to reduce the conducted power to the targets by atomic physics processes (charge exchange and hydrogen and impurity radiation) in the divertor channel. These power losses can be enhanced by generating plasma and impurity flows in the divertor.

This requires sufficient pumping and recirculation of the plasma in the divertor. Of course, the divertor conditions must not affect adversely the main plasma performance and this requires the divertor plasma to be as decoupled as possible from the main plasma. In particular, the leakage of neutrals from the divertor to the main plasma must be reduced as far as possible. Such "closure" of the divertor can be achieved by introducing baffle structures at the entrance to the divertor or maintaining a sufficiently dense plasma to attenuate neutrals within the divertor (plasma "plugging"). The geometry of the divertor is thus important in providing the necessary degree of closure, and this requires the testing of several different divertor configurations.

In the ITER-CDA, the solution adopted for the divertor was to use the high recycling approach with steeply angled target plates, which offers good purity control. However, with the adoption of a single null configuration and higher power in the ITER-EDA, the high recycling approach does not suffice, and a gas target (detached plasma) divertor was adopted to exhaust power over the sidewalls of a deep divertor via charge exchange and radiation. This approach requires the relatively free recirculation of the hydrogenic and impurity neutrals within the divertor, and plasma density and purity control must therefore be demonstrated.

The JET divertor programme is based on three divertor configurations (Mark I, Mark IIA and an ITER-specific Mark IIGB) which will be introduced and tested sequentially in the period up to the middle of 1998 (end of the ITER-EDA).

During the present shutdown, the relatively open Mark I divertor used for the 1994/95 Experimental Campaign is being replaced by the Mark II divertor which comprises a common base structure capable of accepting various target assemblies. This allows the divertor geometry (degree of closure and target configuration) to be varied and its effect on divertor and main plasma performance to be studied.

Due to the need to test various divertor geometries for ITER, the Mark II divertor has been designed so that its target assembly can be exchanged by remote handling, but does not lend itself to the use of active cooling. No financial provision is made in the proposed Programme to study target materials other than CFC.

The first target assembly (Mark IIA) is a moderate "slot" divertor which is significantly more closed than

Mark I, thus improving purity control and increasing atomic losses. Mark IIA allows operation under a wide range of plasma configurations and conditions and makes high power, high current operation possible on both the horizontal and vertical target plates.

The second target assembly (Mark IIGB) is a deep divertor with a well baffled entrance. The aim of the Mark IIGB configuration is to distribute the exhaust power over the length of the divertor and this is assisted by the free recirculation of neutrals below the baffle on one or both sides of the divertor plasma legs. Recirculation also allows greater flows, better pumping and better impurity retention in the divertor.

The investigation of these three generically different configurations will allow a coordinated and timely investigation of the various options for an ITER divertor and is designed to lead to a solution giving compatibility between power exhaust, purity control and high performance (H-mode). A major part of the strategy is the development and validation of numerical codes for the edge and divertor plasma so that they may be used for extrapolation to the geometry, dimensions and operating conditions of ITER. The experimental results from all three divertor configurations, together with those from smaller tokamaks and model calculations, will allow the ITER divertor design to be validated. This should be possible by the middle of 1998, in line with the ITER-EDA schedule.

D-T Plasma Studies

The first magnetic confinement experiments using a mixture of 10% tritium in deuterium took place in JET in 1991 and produced significant fusion power (peaking at 1.7MW and averaging 1MW over 2 seconds). Since then the US tokamak TFTR, using 50% tritium in deuterium, has produced some 10MW of fusion power and shown that, with their particular operating conditions and geometry, D-T plasmas have more favourable confinement properties than deuterium plasmas (isotopic effect). Subject to the necessary approvals, two further periods of D-T operation (DTE-1 and DTE-2) are foreseen for the JET programme to the end of 1999.

The physics mission of DTE-1 would have the crucial objective of studying the isotopic effect on confinement scaling and H-mode threshold power in D-T plasmas. These would be the first experiments of this kind in the geometry appropriate to ITER and including a divertor.

These experiments would be essential to determine whether the D-T performance improvements observed in the circular cross-section TFTR tokamak are also realised in the D-shaped cross section of JET, and ITER. Furthermore, the H-mode threshold power in D-T plasmas would be determined for the first time in these JET experiments. This would allow more accurate assessments of the ignition margin and the heating requirements for ITER.

In addition, JET's capability for long pulse operation and impurity control should permit about 10MW of fusion power for several seconds (typically with 50% tritium). The α -particle heating would then make a significant contribution to the plasma power balance and this would allow the effects of α -particle heating (confinement and thermalisation of α -particles and stability of toroidal Alfvén eigenmodes in the presence of α -particles) to be studied and experience gained for ITER. The operating conditions foreseen for ITER, namely long pulse ELMy H-mode detached radiative divertor plasmas, could also be studied in D-T, albeit at reduced levels of fusion power. These results could provide important information for the design of the ITER divertor.

As well as a physics mission, DTE-1 would also have a technology mission with the objective of carrying out and demonstrating key ITER and reactor-relevant technologies, such as tritium handling and processing, remote handling and control, and heating systems operating in D-T. Specifically, DTE-1 would provide a first test of a large scale technology for processing tritium through an operating tokamak.

Operation in TFTR and detailed preparations for DTE-1 on JET have shown that a longer phase of D-T operation than DTE-1 is needed for a thorough study of the physics and technology of D-T plasmas. This is provided for by DTE-2, with substantial α -particle heating, capitalising on the performance improvements achieved in the preceding experimental campaigns with deuterium.

This period of D-T operation will also provide a full evaluation of the technology of processing tritium in support of an operating tokamak.

Programme Plan

The programme to the end of 1999 is illustrated in Fig.240. It covers all the agreed objectives for the JET extension. Its main aspects are summarised below.

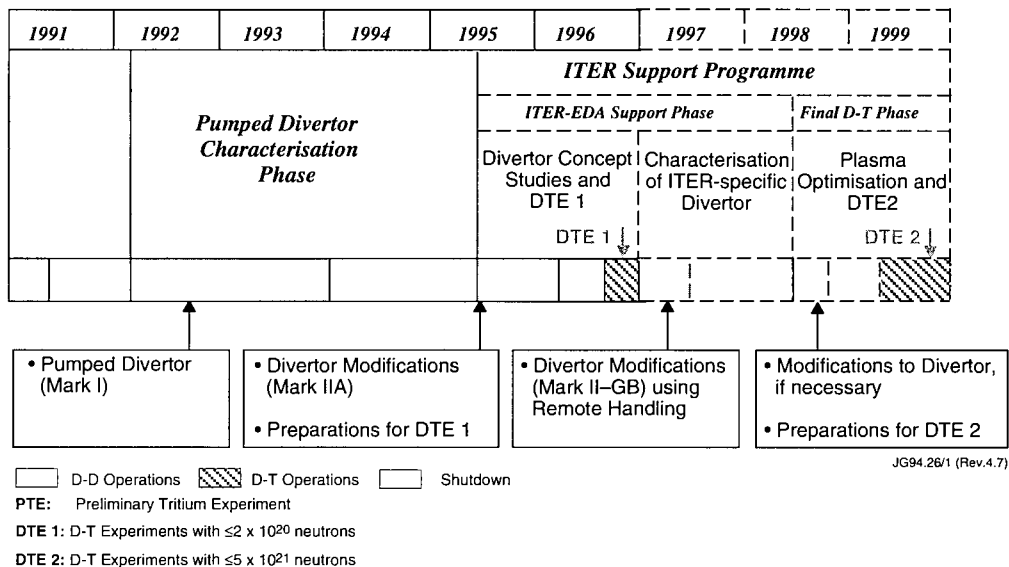


Fig.240: JET Programme to end of 1999

ITER-EDA Support Phase (mid-1995 to mid-1998)

The present shutdown which commenced in June 1995 is scheduled to be completed in March 1996. During this shutdown the Mark II divertor, its first target structure (Mark IIA) and modified ICRF antennae are being installed. Work is also being undertaken to prepare for the D-T operations planned for the end of 1996.

During 1996 the experimental campaign will concentrate on divertor and other ITER-specific studies (including development toward long pulse high performance operation) and optimisation for D-T. The programme will therefore extend many of the issues addressed initially with the Mark I Divertor and give, in particular, further emphasis to studies of the effect of geometry on radiative detached divertor plasmas, which form the physics basis for the divertor concept favoured by ITER.

A period of D-T operation (DTE-1) is scheduled for late 1996, following an intervention to make the necessary final adjustments for D-T operations. The precise content and duration of DTE-1 is being defined at present and takes account of the developing needs of ITER and the experience gained in JET and TFTR. It will require the prior approval of the JET Council. The extent of DTE-1 will be a compromise between studying essential D-T physics for the ITER-EDA and minimising the delays in the experimental programme that could result from certain component failures during DTE-1.

The physics mission of DTE-1 as defined above could last about four months and produce up to 2×10^{20} neutrons. In this case, the activation of the vessel would prevent

manned in-vessel intervention for up to one year after D-T operation. However, in-vessel components which are accessible can be repaired using the remote handling equipment developed for the Mark IIGB target assembly change. This equipment has demonstrated a very high level of reliability and is now fully proven for the planned remote handling tasks. Its versatility and ability to perform a wide variety of other tasks has also been demonstrated, provided access can be obtained. Manned access for ex-vessel repairs will be possible after DTE-1.

If the alternative of not proceeding with DTE-1 were to be considered, it would, of course, eliminate the risk of delays in the experimental programme, but would not allow the test of a specific divertor concept for ITER to commence earlier than shown in Fig.240 since the procurement schedule for the Mark IIGB target structure cannot be shortened.

In a six month shutdown in the first half of 1997, the Mark IIA target structure will be exchanged for a second target structure, an ITER-specific divertor of the "Gas-box" class (Mark IIGB). The exchange will be made by remote handling without manned intervention. This remote handling operation will demonstrate for the first time one of the central technologies required both for ITER and for a fusion reactor.

During the remainder of 1997 and the first half of 1998, the Mark IIGB divertor will be tested experimentally with deuterium plasmas at high power. The design of the Mark IIGB provides flexibility to modify the target geometry with relative ease. The Programme Plan provides for two target geometries for Mark IIGB, together with a

septum which may, or may not, be included to limit the communication between the inner and outer divertor legs and to absorb energy from energetic neutrals and photons.

Possible ways of improving JET's performance which are under consideration include improving the wall condition, increasing the toroidal magnetic field (to 4T) and plasma current, increasing the heating power (by $\approx 30\%$) and overcoming the performance limitations due to MHD instabilities.

Final Phase of D-T Operation (mid-1998 to end-1999)

A four month shutdown in 1998 will permit any necessary modifications to the divertor and final preparations for DTE-2. Normal manned in-vessel interventions will again be possible in this shutdown. The Mark IIGB divertor target structure is less flexible than Mark IIA with respect to the variety of equilibria which can be accommodated. Furthermore, its power handling capability in attached divertor operation is somewhat lower. It may therefore

not be compatible with the highest plasma performance obtained in JET, such as the low density, high magnetic shear, hot-ion H-mode of operation. This has to be tested experimentally and if it proves to be the case, it will be possible to re-install Mark IIA (for DTE-2) following the completion of the Mark IIGB studies.

During late 1998 and early 1999, the experimental programme will continue by optimising plasma performance in deuterium in preparation for a further period of D-T operation (DTE-2).

DTE-2 is scheduled to take place during the remainder of 1999. DTE-2 experiments could last up to eight months and could produce up to 5×10^{21} neutrons. Actual neutron production, within this upper limit, will be reassessed in the light of the experience with D-T operations on JET and TFTR. Every effort will be made to reduce this upper limit, while still satisfying JET's role in supporting ITER and the world fusion programme. In this way the activation of the JET structure would be kept as low as possible compatible with fulfilling the required objectives.

Appendix I

JET Task Agreements 1995

<i>Title</i>	<i>Association</i>	<i>JET Responsible Officer</i>
RF HEATING DIVISION		
Wave induced current drive experiments on JET	EUR-CEA, Cadarache, France	C. Gormezano
RF transport code development	EUR-IPP Garching, Germany	C. Gormezano
Fast ion and electron kinetic effects on JET	EUR-UKAEA Culham, UK	C. Gormezano
Confinement studies in profile control experiments	EUR-ENEA Frascati, Italy	F.X. Soldner
Tokamak Optimisation	EUR-UKAEA Culham, UK	C. Gormezano/ P.Thomas
EXPERIMENTAL DIVISION I		
Edge plasmas and plasma surface interactions	EUR-UKAEA Culham, UK	P.E. Stott
Plasma wall interactions	EUR-IPP Garching, FRG	P.E. Stott
Neutron production related physics and associated diagnostics	EUR-NFR Sweden	P.E. Stott
Plasma surface interactions	EUR-NFR Sweden	P.E. Stott
Neutron production related physics	EUR-UKAEA Harwell, UK	P.E. Stott

<i>Title</i>	<i>Association</i>	<i>JET Responsible Officer</i>
Microwave reflectometry	EUR-CFN/IST Lisbon, Portugal	P.E. Stott
Neutron production related physics and associated diagnostics	EUR-ENEA Frascati, Italy	P.E. Stott
Physics of turbulent and convective transport, MHD and related diagnostics	EUR-FOM The Netherlands	P.E. Stott
Work on collector probes	EUR-NFR Sweden	P.E. Stott

EXPERIMENTAL DIVISION II

Measurement and interpretation of divertor and plasma edge impurity ion temperatures	EUR-KFA Julich, Germany	R. Konig
Dynamics of ions and of neutral particles in tokamak plasmas	EUR-ENEA Frascati, Italy	R. Gianella
Spectroscopic measurements: interpretation and impurity analysis	EUR-CEA Cadarache, France	P.R. Thomas
Charge exchange recombination spectroscopy	EUR-FOM Amolf, The Netherlands	M. von Hellerman
Impurity analysis and plasma diagnostics using spectroscopic measurements	EUR-NFR Sweden	P.R. Thomas
Impurities and other topics	EUR-UKAEA Culham, UK	P.R. Thomas

DATA ANALYSIS & MODELLING

Plasma stability	EUR/UKAEA Culham, UK	W. Kerner
Modelling of anomalous transport and study of energetic particle collective effects	EUR-ENEA Frascati, Italy	A. Taroni

<i>Title</i>	<i>Association</i>	<i>JET Responsible Officer</i>
Analysis of local transport in JET and comparison with theoretical models	EUR-UKAEA Culham, UK	J.G. Cordey
Transient transport analysis in JET	EUR-ENEA CNR-Milan, Italy	A. Taroni
Comparison between JET profile data and the predictions of a transport model based on ITG and trapped electron modes	EUR-NFR Sweden	J.P. Christainsen
MHD spectroscopy and stability	EUR-FOM The Netherlands	W. Kerner
OPERATIONS		
Alfven eigenmodes	EUR-CRPP Lausanne, Switzerland	J. Jacquinot
Feedback stabilization of disruptions	EUR-ENEA CNR-Milan, Italy	D.J. Campbell
The control of instabilities and disruptions	EUR-UKAEA Culham, UK	D.J. Campbell
Study of density evolution and recycling of JET plasmas during (pumped) divertor operation as a function of fuelling method and wall conditioning state	EUR-ENEA Frascati, Italy	G. Saibene
Scenario studies of plasma breakdown	EUR-ENEA CNR-Milan, Italy	P.J. Lomas

Appendix II

List of Articles, Reports and Conference Papers Published in 1995

1. Observation of TAE activity in JET.
Ali-Arshad S Campbell D J
Plasma Physics and Controlled Fusion, vol.37 no.7
July 1995. p.715.
Report JET-P(94)12
2. Design of the MK II divertor with large carbon-fibre composite (CFC) tiles.
Altmann H Deksnis E B Fanthome J Froger C Lowry C Mohanti R Nilsen M Peacock A Pick M Spencer D Tivey R B Vlases G
Fusion Technology 1994, Proceedings of the 18th Symposium on Fusion Technology, Karlsruhe, Germany, 22-26 August 1994, vol.1. p.275.
3. Hydrogen retention in the first wall.
Andrew P Pick M
Journal of Nuclear Materials, vols.220-222 April 1995 (Proceedings of the Eleventh International Conference on Plasma-Surface Interactions in Controlled Fusion Devices, Mito, Ibaraki, Japan, May 23-27, 1994). p.601.
4. The JET glow discharge cleaning system.
Andrew P Bosia G Claesen R Grobusch L Harling J How J Jensen H S McBryan H McCarthy J Monk R Orchard J Pearce R J Saibene G Winter J
Fusion Technology 1994, Proceedings of the 18th Symposium on Fusion Technology, Karlsruhe, Germany, 22-26 August 1994, vol.1. p.203.
5. Alfvén eigenmode induced energetic particle transport in JET.
Appel L C Berk H L Borba D Breizman B N Hender T C Huysmans G T A Kerner W Pekker M S Pinches S D Sharapov S E
Nuclear Fusion, vol.35 no.12, December 1995 (Proceedings of the Fourth IAEA Technical Committee Meeting on Alpha Particles in Fusion Research, Princeton, 25-28 April 1995) p.1697.
Also in UKAEA, Culham, 1995. 25p. Report UKAEA-FUS-311 and Report JET-P(95)26
6. TAE-induced diffusion of fast particles in JET.
Appel L C Berk H L Borba D Breizman B Eriksson L G Fasoli A Hender T C Huysmans G T A Kerner W Monticelli E Pekker M Pinches S D Sharapov S
22nd European Physical Society Conference on Controlled Fusion and Plasma Physics, Bournemouth, 3rd-7th July 1995, Contributed papers. Part 2. p.261.
7. Advanced signal processing techniques used for information extraction from single and multiple-point reflectometry at JET.
Bak P E Deliyannis N Vayakis G
22nd European Physical Society Conference on Controlled Fusion and Plasma Physics, Bournemouth, 3rd-7th July 1995, Contributed Papers, Part IV. p.405.
8. ρ^* scaling experiments for ELMy H-modes in JET.
Balet B Campbell D Christiansen J P Cordey J G Gormezano C Gowers C Muir D Righi E Saibene G R Stubberfield P M
22nd European Physical Society Conference on Controlled Fusion and Plasma Physics, Bournemouth, 3rd-7th July 1995. Contributed Papers. p.009.
9. Bulk plasma impurity behaviour with the new JET configuration.
Barnsley R Chen H Coffey I H Cushing D Giannella R Lauro-Taroni L Lawson K D McGinnity P Peacock N J Singleton M von Hellermann M

- 22nd European Physical Society Conference on Controlled Fusion and Plasma Physics, Bournemouth, 3rd-7th July 1995. Contributed Papers. p.081.
10. Physics issues of ECE and ECA for ITER.
Bartlett D V
Joint European Torus (JET), 1995. 10p.
Report JET-P(95)46
 11. Recent progress in the measurement and analysis of ECE on JET.
Bartlett D V Bishop C Cahill R McLachlan A Porte L Rookes A
Joint European Torus (JET). May 1995. 13p. Report JET-P(95)17 Submitted for publication in Procs. EC9, 9th Int. Workshop on ECE & ECRH.
 12. Modelling of lower hybrid current drive and comparison with experimental results in JET
Baranov Y F Ekedahl A Froissard P Gormezano C Lennholm M Rimini F Soldner F X
Submitted for publication in Nuclear Fusion
Report JET-P(95)27
 13. Environmental monitoring for tritium at JET.
Bell A C Caldwell-Nichols C Patel B Serio L
Fusion Technology, vol.28 no.3 Part 1, October 1995 (Proceedings of the Fifth Topical Meeting on Tritium Technology in Fission, Fusion and Isotopic Applications, Belgirate, Italy, May 28-June 3, 1995). p.821.
 14. Status of the JET active gas handling system and plans for tritium operation.
Bell A C Hemmerich J L Lasser R Bainbridge N Bishop G Brennan D Caldwell-Nichols C Campbell J Dearden A Grieveson B Jones G Lupo J Mart J Pereventsev A Skinner N Stagg R Walker K Warren R Yorkshades J
Fusion Technology vol.28 no.3 part 2, October 1995 (Proceedings of the Fifth Topical Meeting on Tritium Technology in Fission, Fusion, and Isotopic Applications, Belgirate, Italy, May 28-June 3 1995). p.1301.
 15. More on core-localized toroidal Alfvén eigenmodes.
Berk HL Borba D Candy J Huysmans GT A Sharapov S van Dam J W
Joint European Torus, JET, April 1995. 16p. Submitted for publication in Physics of Plasmas. Report IFSR 695 Report JET P(95)12
 16. Impact of JET experimental results and engineering development on the definition of the ITER design concept.
Bertolini E
Fusion Engineering & Design, vol.27 March (I) 1995, pt.A, (Proceedings of the Third International Symposium on Fusion Nuclear Technology, Los Angeles, CA, June 26-July 1, 1994). p.27. Report JET-P(94)36
 17. JET with a pumped divertor: design, construction, commissioning and first operation.
Bertolini E
Fusion Engineering and Design, vol.30 nos.1-2 May 1995 (Invited papers of the 18th Symposium on Fusion Technology, Karlsruhe, 22-26 August 1994) p.53.
Report JET-P(94)56
 18. JET with a pumped divertor: design, construction, commissioning and first operation.
Bertolini E
Fusion Technology 1994, Proceedings of the 18th Symposium on Fusion Technology, Karlsruhe, Germany, 22-26 August 1994, vol.1. p.53.
 19. Power electronics systems at JET: objectives and operational experience.
Bertolini E Bonicelli T Chiron D Santagiustina A
Joint European Torus (JET). March 1995. 11p. Report JET-P(95)11 Submitted to Procs. IPEC
 20. Fast-wave heating and current drive scenarios for the Joint European Torus and International Thermonuclear Experimental Reactors.
Bhatnagar V P Jacquinet J
Fusion Engineering & Design, vol.26 nos.1-4, January 1995 (Proceedings of the Fifth International Toki Conference on Plasma Physics and Controlled Nuclear Fusion, November 16-19, 1993, Toki, Japan: Physics and Technology of Plasma Heating and Current Drive). p.575.
 21. Local magnetic shear control in a tokamak via fast wave minority ion current drive: theory and experiments in JET.
Bhatnagar V P and others

- Nuclear Fusion, vol.34 no.12 1994 p.1579.
Report JET-P(94)22
22. Comparison of kinetic and cold fluid models of three-wave mixing and Thomson scattering.
Bindslev H
Plasma Physics and Controlled Fusion, vol.37 no.2 February 1995 p.169.
Report JET-P(95)01
23. Relativistic effects in millimetre wave applications on magnetically confined plasmas.
Bindslev H
Joint European Torus (JET). April 1995. 23p. Submitted for publication in Proc. 9th Joint Workshop on ECE and ECRH, Borrego Springs, 22-26 1995.
Report JET-P(95)16
24. Theory of collective Thomson scattering.
Bindslev H
Joint European Torus (JET), 1995. 10p.
Report JET-P(95)66
25. MHD stability of ITER equilibria.
Bondeson A Villard L Ward D J Wermeille D Goedbloed J P Holties H A Hender T C Huysmans G T A Kerner W
Next European Torus, Garching. 1995. 10p.
Report NET-107
26. Kinetic toroidicity induced Alfvén eigenmodes in toroidal shaped plasmas.
Borba D Candy J Holties H A Huysmans G T A Kerner W Sharapov S
22nd European Physical Society Conference on Controlled Fusion and Plasma Physics, Bournemouth, 3rd-7th July 1995, Contributed papers. Part 2. p.237.
27. Access conditions for H-modes with detached divertor plasmas
Borrass K Farengo R Vlases G
Submitted for publication in Nuclear Fusion
Report JET-P(95)74
28. Progress on the inactive commissioning and upgrade of the JET cryogenic distillation system.
Boucqey P Morfl C Delvart F Mart J
- Fusion Technology 1994, Proceedings of the 18th Symposium on Fusion Technology, Karlsruhe, Germany, 22-26 August 1994, Vol.2. p.1055.
29. High resolution spectroscopic measurements of impurity radiation distributions and neutral deuterium profiles in the JET scrape-off layer.
Breger P König R W T Maggi C F Pietrzyk Z A Summers D D R Summers H P von Hellebrand M G
22nd European Physical Society Conference on Controlled Fusion and Plasma Physics, Bournemouth, 3rd-7th July 1995, Contributed papers. Part 2. p.377.
30. An adaptive plasma density controller at Joint European Torus.
Brelvi H E O
Fusion Technology, vol.27 no.2 March 1995. p.162.
Report JET-P(94)27
31. Manufacturing and testing of a copper/CFC divertor mock-up for JET.
Brossa M Ciric D Deksnis E Falter H Guerrischi U Peacock A Pick M Rossi M Shen Y Zacchia F
Fusion Technology 1994, Proceedings of the 18th Symposium on Fusion Technology, Karlsruhe, Germany, 22-26 August 1994, vol.1. p.375.
32. Window transmission monitoring and cleaning schemes used with the light detection and ranging Thomson scattering diagnostics on the JET tokamak.
Brown B W Gowers C W Nielsen P Schunke B
Review of Scientific Instruments, vol.66 no.4 April 1995. p.3077.
Report JET-P(94)21
33. Key features of the new in-vessel inspection system at JET.
Businaro T Dalle Carbonare G Junger J F Raimondi T
Fusion Technology 1994, Proceedings of the 18th Symposium on Fusion Technology, Karlsruhe, Germany, 22-26 August 1994, Vol.2. p.1387. Amsterdam, Elsevier. 1995.
34. Studies of tritium dispersion around and close to the buildings on the JET site.
Caldwell-Nichols C J

- Fusion Technology, vol.28 no.3 Part 1, October 1995 (Proceedings of the Fifth Topical Meeting on Tritium Technology in Fission, Fusion and Isotopic Applications, Belgirate, Italy, May 28-June 3, 1995). p.827.
35. Exhaust and impurity control experiments in the JET pumped divertor.
Campbell D J and the JET Team.
Plasma Physics and Controlled Nuclear Fusion Research 1994, 15th International Conference, Seville, 26 September-1 October 1994. vol.1. p.527.
 36. The operation of the JET beryllium analysis laboratory.
Campling D C Litchfield R A Russ R M
Fusion Technology 1994, Proc. 18th Symposium on Fusion Technology, Karlsruhe, Germany, 22-26 August 1994, Vol.2. p.1541. Amsterdam, Elsevier. 1995.
 37. A numerical method for solution of the generalized Liouville equation.
Candy J
Joint European Torus (JET), 1995. 20p. Report JET-P(95)56
 38. Electron Landau damping of toroidal Alfvén eigenmodes
Candy J
Submitted for publications in Plasma Physics and Controlled Fusion (letter)
Report JET-P(95)75
 39. A unified picture of fusion product ion cyclotron emission in TFTR and JET.
Cauffman S Majeski R Dendy R O McClements K G Cottrell G A
Bulletin of the American Physical Society, vol.40 no.11 October 1995 (Program of the Thirty-seventh Annual Meeting of the Division of Plasma Physics, 6-10 November 1995; Louisville, Kentucky). p.1870.
 40. The installation of the JET MK 1 divertor - features and achievements.
Celetano G Macklin B Pick M Scott S M Shaw R Tait J
Fusion Technology 1994, Proceedings of the 18th Symposium on Fusion Technology, Karlsruhe, Germany, 22-26 August 1994, vol.1. p.271.
 41. Quasi steady-state advanced tokamak scenarios in JET.
Challis C D Balet B Bhatnager V P de Haas J C M Eriksson L-G Gadeberg M Gormezano C Gowers C W How J A Huysmans G T Ishida S Kerner W O K Loughlin M J Rimini F Sadler G J Sips A C C Tanga A Tubbing B J D Ward D J
22nd European Physical Society Conference on Controlled Fusion and Plasma Physics, Bournemouth, 3rd-7th July 1995, Contributed Papers. Part 2. p.069.
 42. Review of neutral beam heating on JET for physics experiments and the production of high fusion performance plasmas.
Challis C D
Fusion Engineering & Design, vol.26 nos.1-4, January 1995 (Proceedings of the Fifth International Toki Conference on Plasma Physics and Controlled Nuclear Fusion, November 16-19, 1993, Toki, Japan: Physics and Technology of Plasma Heating and Current Drive). p.17. and Report JET-P(93)90
 43. Effect of the toroidal field reversal on divertor asymmetries.
Chankin A Campbell D J Clement S Davies S J Loarte A Matthews G F Monk R D Reichle R Saibene G Stamp M Stangeby P C
22nd European Physical Society Conference on Controlled Fusion and Plasma Physics, Bournemouth, 3rd-7th July 1995, Contributed Papers. Part 3. p.289.
 44. Fluid equations for temperature anisotropy based on kinetic drifts.
Christiansen J B
Plasma Physics and Controlled Fusion, vol.37 no.12 December 1995. p.1363.
Report JET-P(95)20
 45. The ρ dependence of the energy confinement in ELMy H-modes in JET.
Christiansen J P Balet B Campbell D Cordey J G Eriksson L-G Gormezano C de Haas J Lowry C Muir D Righi E Saibene G
Bulletin of the American Physical Society, vol.40 no.11 October 1995 (Program of the Thirty-seventh Annual Meeting of the Division of Plasma Physics, 6-10 November 1995; Louisville, Kentucky). p.1765.

46. Beam profiles measurement using a unidirectional CFC-target and infrared imaging.
Ciric D Falter H D Fanthome J G A Massmann P Mellon K N
Fusion Technology 1994, Proceedings of the 18th Symposium on Fusion Technology, Karlsruhe, Germany, 22-26 August 1994, vol.1. Amsterdam, Elsevier. 1995. p.827.
47. Light emission from graphite surfaces during beam bombardment, observation and consequences for use of graphite in divertors.
Ciric D Falter H Massmann P Mellon K
Fusion Technology 1994, Proceedings of the 18th Symposium on Fusion Technology, Karlsruhe, Germany, 22-26 August 1994, vol.1. p.391.
48. Power deposition studies in the JET Mark I pumped divertor.
Clement S Campbell D J Chankin A Coad J P Horton L D Loarte A Lingertat J Monk R D Tabasso A Viola R
22nd European Physical Society Conference on Controlled Fusion and Plasma Physics, Bournemouth, 3rd-7th July 1995, Contributed Papers. Part 3. p.309.
49. An appraisal of deuterium retention in JET.
Coad J P
Journal of Nuclear Materials vol.226 1995. p.156.
50. The applications of waste management systems in support of the JET divertor shutdown.
Collins D Atkins G Booth S J Haigh A D May C Newbert G
Fusion Technology 1994, Proceedings of the 18th Symposium on Fusion Technology, Karlsruhe, Germany, 22-26 August 1994, Vol.2. p.1545. Amsterdam, Elsevier. 1995.
51. Theoretical models and results from COMPASS-D, START and JET.
Connor J W Fielding S J Polevoi A Roach C M Stringer T E Sykes A Tibone F Valovic M Walsh M J Wilson H R
Physica Scripta, vol.51 no.5 May 1995 (Transport in Fusion Plasmas, Workshop, Goteborg, Sweden, 13-16 June 1994). p.605.
52. Dimensionless form for the L-H power threshold.
Cordey J G Kerner W Pogutse O
Plasma Physics and Controlled Fusion, vol.37 no.7 July 1995. p.773. Report JET-P(94)66
53. Evolution of transport through the L-H transition in JET.
Cordey J G Muir D G Parail V V Vayakis G Ali-Arshad S Bartlett D V Campbell D J Colton A L Costley A E Gill R D Loarte A Neudachin S V Porte L Sips A C C Springmann E M Stubberfield P M Taroni A Thomsen K von Hellerman M G
Nuclear Fusion, vol.35 no.5 May 1995. p.505.
Report JET-P(94)19
54. A numerical simulation of the L-H transition in JET with local and global models.
Cordey J G Muir D G Neudachin S V Parail V V Springmann E Taroni A
Nuclear Fusion, vol.35 no.1 January 1995 p.101.
55. The design of a hydraulic fast stub driver for ITER.
Crawley P J Kaye A
Joint European Torus (JET), 1995. Report JET-R(95)09
56. ICRH antennae system for the JET pumped divertor.
Crawley P Agarici G Brown T Gormezano C Jessop G Kaye A Panissie H Walton R
Fusion Technology 1994, Proc. 18th Symposium on Fusion Technology, Karlsruhe, Germany, 22-26 August 1994, vol.1. Amsterdam, Elsevier, 1995. p.541.
57. A new comb reflectometer for the JET divertor plasma
Cupido L Prentice R Bartlett D V Manso M E Nunes I Serra F Silva A
Submitted for publications in Plasma Physics and Controlled Fusion
Report JET-P(95)79
58. The behaviour of divertor and scrape-off layer parameters in JET.
Davies S Erents S K Guo H Y Loarte A Matthews G F McCormick K Monk R D
22nd European Physical Society Conference on Controlled Fusion and Plasma Physics, Bournemouth, 3rd-7th July 1995, Contributed Papers. Part 3. p.257.

59. Analysis of cold pulses produced by impurity injection in JET.
de Angelis R Deliyankis N de Luca F Giannella R Gorini G Jacchia A Jackel H Mantica P Porte L Parail V Springmann E Taroni A
22nd European Physical Society Conference on Controlled Fusion and Plasma Physics, Bournemouth, 3rd-7th July 1995. Contributed Papers. p.053.
60. Perturbative transport studies in JET using fourier techniques
de Angelis R de Luca F Delyanakis N Erba M Giannella R Gorini G Jacchia A Mantica P Parails V Porte L Taroni A
Report JET-R(95)04
61. The optimizaiton of neutral beams for ignition and burn control on next-step reactors.
de Esch H P L Stork D Challis C Tubbing B
Fusion Engineering & Design, vol.26 nos.1-4, January 1995 (Proceedings of the Fifth International Toki Conference on Plasma Physics and Controlled Nuclear Fusion, November 16-19, 1993, Toki, Japan: Physics and Technology of Plasma Heating and Current Drive). p.589.
62. Sawtooth heat pulse propagation in tokamaks: ballistic response and fourier analysis.
De Luca F Deliyankis N Erba M Galli P Gorinin G Jacchia A Mantica P Porte L
Joint European Torus, 1995. Report JET-P(95)43
63. Report on ITER emergency task. Fatigue studies of S65c beryllium.
Deksnis E B Ciric D Falter H Martin D
Joint European Torus (JET), December 1994. 17p. Report JET-R(94)04
64. Ion cyclotron emission due to collective instability of fusion products and beam ions in TFTR and JET.
Dendy R O McClements K G Lashmore-Davies C N Cottrell G A Majeski R Cauffman S
Nuclear Fusion, vol.35 no.12, December 1995 (Proceedings of the Fourth IAEA Technical Committee Meeting on Alpha Particles in Fusion Research, Princeton, 25-28 April 1995) p.1733.
65. Engineering a new compact soft X-ray diagnostic on JET.
Dillon S F Alper B Edwards A Gill R D Staunton-Lambert S A B Wilson D
Fusion Technology 1994, Proceedings of the 18th Symposium on Fusion Technology, Karlsruhe, Germany, 22-26 August 1994, vol.1. Amsterdam, Elsevier. 1995. p.815.
66. Minimum entropy production principle due to ohmic dissipation in tokamaks and determination of non-inductive current density profiles on JET.
DiVita A Brusati M
Plasma Physics and Controlled Fusion, vol.37 no.10 October 1995. p.1075.
67. Thermal considerations and cooling system for the JET divertor coils.
Dolgetta N Bertolini E Butcher P Cooke M Last J R Marchese V Miele P Sannazzaro G Tesini A
Fusion Technology 1994, Proceedings of the 18th Symposium on Fusion Technology, Karlsruhe, Germany, 22-26 August 1994, vol.2. Amsterdam, Elsevier. 1995. p.929.
68. The JET diagnostic fast central acquisition and trigger system
Edwards A W Blackler K
Review of Scientific Instruments, vol.66 no.1 pt.2, January 1995 (Tenth Topical Conference on High Temperature Plasma Diagnostics, Rochester, New York, 8-12 May 1994) p.518.
69. First wall effects on particle recycling in tokamaks.
Ehrenberg J K
Joint European Torus (JET). May 1995. 71p. Submitted for publication in Physical Processes of the Interaction of Fusion Plasmas with Solids.
Report JET-P(95)18
70. On ion temperature profile measurements in ITER by means of neutron spectroscopy
Elevant T Brelen H Linden P Scheffel J
Submitted for publication in Fusion Technology
Report JET-P(95)65
71. The rapid determination of plasma equilibrium parameters at JET from external magnetic measurements.

- Ellis J J Christiansen J P O'Brien D P J Zwingmann
W P van der Goot E Garribba M Milani F Puppini
S Sartori F
Joint European Torus (JET). December 1994. 19p.
Report JET-P(94)70
72. Extension of a Bohm model for L-mode electron heat transport to ion heat transport and to the ohmic regime.
Erba M Parail V Springmann E Taroni A
Joint European Torus (JET), February 1995. 23p.
Report JET-R(95)02
73. Predictive modelling of energy transport in JET discharges.
Erba M Cherubini A Parail V Springmann E Taroni A
22nd European Physical Society Conference on Controlled Fusion and Plasma Physics, Bournemouth, 3rd-7th July 1995, Contributed Papers. Part 2. p.213.
74. The location of the separatrix in the JET divertor and SOL.
Erents S K Davies S J Ellis J J Guo H Y McCormick K Matthews G F Monk R D O'Brien D Zwingmann W
22nd European Physical Society Conference on Controlled Fusion and Plasma Physics, Bournemouth, 3rd-7th July 1995, Contributed Papers. Part 3. p.297.
75. A model for calculating ICRH power deposition and velocity distribution.
Eriksson L-G Hellsten T
Physica Scripta, vol.52 no.1 July 1995. p.70.
Report JET-P(94)25
76. Runaway electron measurements in the JET tokamak.
Esposito B Martin-Solis R van Belle P Jarvis O N Marcus F B Sadler G Fischer B Froissard P Adams J M Cecil E Watkins N
Joint European Torus (JET), 1995. 24p. Report JET-P(95)48
77. Runaway electron diffusion measurements in the JET Tokamak.
Esposito B Adams M Cecil E Fischer B Froissard P Jarvis O N Marcus F B Solis R M Sadler G van Belle P Watkins N
22nd European Physical Society Conference on Controlled Fusion and Plasma Physics, Bournemouth, 3rd-7th July 1995, Contributed Papers. Part 2. p.037.
78. Comparison between actively cooled divertor dump plates with beryllium and CFC armour.
Falter H D Ciric D Deksnis E B Massmann P Mellon K Peacock A Akiba M Araki M Sato K Suzuki S Cardella A
Fusion Technology 1994, Proceedings of the 18th Symposium on Fusion Technology, Karlsruhe, Germany, 22-26 August 1994, vol.1. p.291.
79. Performance of hypervapotron beam stopping elements in JET.
Falter H D Thompson E
Joint European Torus (JET), 1995. 28p.
Report JET-P(95)13
80. Vapotron as heat sink for flat high conductivity unidirectional CFC tiles.
Falter H D Ciric D Celantano A Ibbot C Watson M Araki M Suzuki S Sato K
Joint European Torus (JET), 1995. 23p.
Report JET-P(95)25
81. Visualisation of thermal contact with a commercial CCD video system.
Falter H D Ciric D Long F D
Fusion Technology 1994, Proceedings of the 18th Symposium on Fusion Technology, Karlsruhe, Germany, 22-26 August 1994, vol.1. p.467.
82. Alfvén eigenmode studies in JET.
Fasoli A Lister J Sharapov S Ali-Arshad S Bosia G Borba D Campbell D J Deliyanakis N Dobbing J A Gormezano C Holties H Huysmans G Jacquinet J Jaun A Kerner W Lavanchy P Moret J-M Porte L Santagiustina A Villard L
Bulletin of the American Physical Society, vol.40 no.11 October 1995 (Program of the Thirty-seventh Annual Meeting of the Division of Plasma Physics, 6-10 November 1995; Louisville, Kentucky). p.1861.
83. Direct measurements of the damping of toroidicity induced Alfvén eigenmodes.

- Fasoli A Borba D Bosia G Campbell DJ Dobbing J A Gormeano C Jacquinet J Lavanchy P Lister J B Marmillod P Moret J-M Santagiustina A Sharapov S Joint European Torus (JET), February 1995. 17p. Report submitted for publication in Physical Review Letters. JET-P(95)02
84. Direct measurement of TAE, EAE and multiple kinetic TAE in JET.
Fasoli A Borba D Delyanakis N Dobbing J A Campbell D J Gormezano C Jacquinet J Jaun A Kerner W Holties H Lavanchy P Lister J B Moret J M Porte L Sharapov S Villard L
22nd European Physical Society Conference on Controlled Fusion and Plasma Physics, Bournemouth, 3rd-7th July 1995, Contributed papers. Part III. p.081.
85. Observation of multiple kinetic Alfvén eigenmodes.
Fasoli A Lister J Sharapov S Borba D Delyanakis N Gormezano C Jacquinet J Jaun A Holties H A Huysmans G T A Kerner W Moret J-M Villard L
Joint European Torus (JET), July 1995. 7p. Report JET-P(95)24
86. Overview of Alfvén eigenmode experiments in JET.
Fasoli A Lister J B Sharapov S Ali-Arshad S Bosia G Borba D Campbell D J Delyanakis N Dobbing J A Gormezano C Holties H A Huysmans G T A Jacquinet J Jaun A Kerner W Lavanchy P Moret J-M Porte L Santagiustina A Villard L
Joint European Torus (JET), July 1995. 16p. Report JET-P(95)30
87. Alfvén eigenmode excitation by ICRH beat-waves
Fasoli A Dobbing J A Gormezano C Jacquinet J Lister J B Sharapov S Sibley A
Submitted for publication in Nuclear Fusion Letters Report JET-P(95)32
88. Ion cyclotron emission due to collective instability of fusion products and beam ions in TFTR and JET.
Dendy R O McClements K G Lashmore-Davies C N Cottrell G A Majeski R Cauffman S
Nuclear Fusion, vol.35 no.12, December 1995 (Proceedings of the Fourth IAEA Technical Committee Meeting on Alpha Particles in Fusion Research, Princeton, 25-28 April 1995) p.1733.
89. Alfvén eigenmodes active excitation experiments in JET.
Fasoli A Ali-Arshad S Borba D Bosia G Campbell DJ Dobbing J A Gormezano C Jacquinet J Lavanchy P Lister J B Marmillod P Moret J-M Santagiustina A Sharapov S E
Plasma Physics and Controlled Nuclear Fusion Research 1994, 15th International Conference, Seville, 26 September-1 October 1994. vol.1. p.405.
90. Overview of Alfvén eigenmode experiments in JET.
Fasoli A Lister J B Sharapov S E Ali-Arshad S Bosia G Borba D Campbell D J Delyanakis N Dobbing J A Gormezano C Holties H A Huysmans G T A Jacquinet J Jaun A Kerner W Lavanchy P Moret J-M Porte L Santagiustina A Villard L
Nuclear Fusion, vol.35 no.12, December 1995 (Proceedings of the Fourth IAEA Technical Committee Meeting on Alpha Particles in Fusion Research, Princeton, 25-28 April 1995) p.1485.
91. Modelling of LH current drive and profile control experiments on JET.
Fischer B Baranov Y Ekedahl A Gormezano C Lennholm M Parail V V Pericoli-Ridolfini V Peysson Y Rimini F Schild P Smits F Soldner F X Springmann E
22nd European Physical Society Conference on Controlled Fusion and Plasma Physics, Bournemouth, 3rd-7th July 1995, Contributed Papers. Part 3. p.361.
92. LHCD operations in JET and developments for fusion applications.
Froissard P Agarici G Baranov Y Brandon M Brusati M Dobbing J A Ekedahl A Finburg P Fischer B Gormezano C Haydon P Kaye A Lennholm M McCarthy T Page R Paling P Platt G Pledge D Plancoulaine J Rimini F Schild P Soldner F X
Fusion Technology 1994, Proceedings of the 18th Symposium on Fusion Technology, Karlsruhe, Germany, 22-26 August 1994, vol.1. Amsterdam, Elsevier, 1995. p.569.
93. Comparison between JET profile data and the predictions of a transport model based on ITG and trapped electron modes.

- Frojd M Christiansen J Strand P Weiland J
Joint European Torus (JET), 1995. 40p.
Report JET-R(95)08
94. Tomographic reconstruction of the radiation distribution during neon puff experiments in ASDEX Upgrade and JET.
Fuchs J C Mast K F Reichle R
22nd European Physical Society Conference on Controlled Fusion and Plasma Physics, Bournemouth, 3rd-7th July 1995, Contributed Papers. Part 3. p.401.
95. Topological transitions of fast ion orbits.
Furno I Porcelli F Eriksson L G
22nd European Physical Society Conference on Controlled Fusion and Plasma Physics, Bournemouth, 3rd-7th July 1995, Contributed papers. Part 2. p.253.
96. First operational experience with the new plasma position and current control system of JET.
Garibba M Browne M L Campbell D J Hudson Z Litunovsky R Marchese V Milani F Mills J Noll P Puppini S Satori F Scibile L Tanga A Young I
Fusion Technology 1994, Proc. 18th Symposium on Fusion Technology, Karlsruhe, Germany, 22-26 August 1994, vol.1. Amsterdam, Elsevier. 1995. p.747.
97. The plasma shape and current control system of JET
Garibba M Litunovsky R Puppini S
Submitted for publication in Fusion Technology
Report JET-P(95)19
98. A scaling law for the confinement time of non-recycling injected impurities in JET and TORE SUPRA.
Giannella R Mattioli M de Michelis C Denne-Hinnov B Dudok de Wit T Magyar G Myrnas R
22nd European Physical Society Conference on Controlled Fusion and Plasma Physics, Bournemouth, 3rd-7th July 1995. Contributed Papers. p.085.
99. Studies of energy and particle transport in JET.
Giannella R and the JET Team
Plasma Physics and Controlled Nuclear Fusion Research 1994, 15th International Conference, Seville, 26 September-1 October 1994. vol.1. p.307.
100. Investigation of performance limiting mhd effects using the new JET diagnostic fast data acquisition system.
Gill R D Alper B Edwards A W Lyadina E
Bulletin of the American Physical Society, vol.40 no.11 October 1995 (Program of the Thirty-seventh Annual Meeting of the Division of Plasma Physics, 6-10 November 1995; Louisville, Kentucky). p.1766.
101. Non-uniform rotation and the resistive wall mode
Gimblett C G Hastie R J Van der Linden R A M Wesson J A
Submitted for publication in Physics of Plasmas
Report JET-P(95)57
102. Development of advanced tokamak scenarios based on high bootstrap currents in JET.
Gomezano C and the JET Team.
Plasma Physics and Controlled Nuclear Fusion Research 1994, 15th International Conference, Seville, 26 September-1 October 1994. vol.1. p.633.
103. Recent developments in LIDAR Thomson scattering measurements on JET
Gowers C W Brown B W Fajemirokun H Nielsen P Nizienko Y and Schunke B
Review of Scientific Instruments, vol.66 no.1 pt.2, January 1995 (Tenth Topical Conference on High Temperature Plasma Diagnostics, Rochester, New York, 8-12 May 1994) p.471.
104. A Thomson scattering scheme for obtaining T_e and n_e profiles of the ITER core plasma.
Gowers C W Nielsen P Orsitto F Pijper F J Salzmann H Schunke B
Joint European Torus (JET), 1995 10p. Report JET-P(95)44
105. Impurity production and erosion/redeposition at the JET Mk I divertor.
Guo H Y Coad J P Elder J D Horton L D Hwang A Li X L Lingertat J Loarte A Matthews G F Monk R D Stamp M F Stangeby P C Tabasso A
22nd European Physical Society Conference on Controlled Fusion and Plasma Physics, Bournemouth, 3rd-7th July 1995, Contributed papers. Part 2. p.273.

106. Ion temperature measurements in JET boundary plasmas using a retarding field analyser.
Guo H Y Matthews G F Davies S J Erents S K Horton L D Monk R D Stangeby P C D
Joint European Torus (JET), 1995. 6p. Report JET-P(95)62
107. Remote handling experiments with the MASCOT IV servomanipulator at JET and prospects of enhancements.
Hamilton D Colombi S Galbiati L Haist B Mills S Raimondi T
Fusion Technology 1994, Proceedings of the 18th Symposium on Fusion Technology, Karlsruhe, Germany, 22-26 August 1994, Vol.2. p.1391. Amsterdam, Elsevier. 1995.
108. Convection and impurity retention in the JET MkI pumped divertor during L-mode.
Harbour P J Barnsley R Campbell D Davies S Horton L Jaeckel H Lauro-Taroni L Lingertat H Loarte A Matthews G Meigs A Monk R Morgan P O'Brien D Prentice R Reichle R Rookes A Saibene G Stamp M Stangeby P Taroni A von Hellermann M
22nd European Physical Society Conference on Controlled Fusion and Plasma Physics, Bournemouth, 3rd-7th July 1995, Contributed Papers, Part IV. p.465.
109. The scrape-off layer in a finite-aspect-ratio torus: the influence of limiter position.
Harbour P J Loarte A
Nuclear Fusion, vol.35 no.7 July 1995. p.759.
Report JET-P(93)96
110. Edge pressure gradients and velocity shear behaviour during H-modes and ELMs in the new JET divertor configuration.
Hawkes N Bartlett D V Campbell D J Deliyannis N Giannella R M Lomas P J Peacock N J Porte L Rookes A Sartori R I A Thomas P R Vayakis G
22nd European Physical Society Conference on Controlled Fusion and Plasma Physics, Bournemouth, 3rd-7th July 1995, Contributed Papers. Part 3. p.261.
111. Measurements of edge electron and impurity ion profiles during H-modes in the new JET divertor configuration.
Hawkes N C Chen H Barnsley R Coffey I Flewin C O'Mullane M Reichle R Rookes A
Bulletin of the American Physical Society, vol.40 no.11 October 1995 (Program of the Thirty-seventh Annual Meeting of the Division of Plasma Physics, 6-10 November 1995; Louisville, Kentucky). p.1766.
112. Progress in spectroscopic plasma diagnostics and atomic data.
Hellermann M von Breger P Core W G Gerstel U Hawkes N C Howman A Konig R W T Maggi C F Maas A C Meigs A G Morgan P D Svensson J Stamp M F Summers H P Wolf R C Zastrow K-D
Joint European Torus (JET), November 1994 10p. Report JET-P(94)58 (Preprint of a invited paper presented to ICPP 1994, Iguacu, Brazil, 31 October 1994.)
113. Minority ion cyclotron current drive in tokamaks.
Hellsten T Carlsson J Eriksson L-G
Physical Review Letters, vol.74 no.18 1 May 1995. p.3612.
114. Wave field distributions for toroidal plasmas with nearly circular cross sections
Hellsten T Kallback J Eriksson L-G
Submitted for publication in Physical Review Letters, Report JET-P(95)61
115. Influence of edge instabilities on JET high performance.
Hender T C Alper B Deliyannis N Huysmans G T A Jones T T C Konig R W T Lawson K D Lomas P J Marcus F B Nave M F F O'Brien D P Porte L Schunke B Smeulders P Thomas P R
22nd European Physical Society Conference on Controlled Fusion and Plasma Physics, Bournemouth, 3rd-7th July 1995. Contributed Papers. p.029.
116. First observations of collective Thomson scattering from JET plasmas.
Hoekzema J A Bindslev H Egedal J Fessey J A Gatcombe C P Hammond N P Hughes T P Machuzak J S Oosterbeek J W Roberts P J Stevens A L Stott P E
22nd European Physical Society Conference on Controlled Fusion and Plasma Physics, Bourne-

- mouth, 3rd-7th July 1995, Contributed papers. Part 2. p.445.
117. MHD spectroscopy, application of a new diagnostic tool.
Holties H A Huysmans G Kerner W Zwingmann W and others
22nd European Physical Society Conference on Controlled Fusion and Plasma Physics, Bournemouth, 3rd-7th July 1995, Contributed Papers, Part IV. p.085.
118. MHD stability of advanced tokamak scenarios.
Holties H A Huysmans G T A Goedbloed J P Kerner W O K Parail V V Soldner F X
Joint European Torus (JET), March 1995. 15p. Report JET-P(95)06
Submitted for publication in Nuclear Fusion.
119. An investigation of the accuracy of Doppler broadened line profile analysis applied to plasma diagnostics.
Horling P Zastrow K-D
Journal of Quantitative Spectroscopy and Radiative Transfer, vol.53 no.6 June 1995. p.585
120. Modelling and measurements of JET divertor plasmas.
Horton I D and the JET Team.
Plasma Physics and Controlled Nuclear Fusion Research 1994, 15th International Conference, Seville, 26 September-1 October 1994. vol.1. p.541.
121. Ten year operational experience of the JET flywheel-generators.
Huart M Doyle P G Beedham E
Fusion Technology 1994, Proceedings of the 18th Symposium on Fusion Technology, Karlsruhe, Germany, 22-26 August 1994, vol.2. Amsterdam, Elsevier. 1995. p.1005.
122. Parametric upconversion of scattered CO₂ laser radiation for an ITER alpha and fast particle diagnostic
Hughes T P
Report JET-P(95)73
123. Influence of edge currents and pressure gradients on the MHD stability of low-n external kink modes.
Huysmans G T A Challis C D Erba M Kerner W Parail V V
22nd European Physical Society Conference on Controlled Fusion and Plasma Physics, Bournemouth, 3rd-7th July 1995. Contributed Papers. p.201.
124. MHD stability analysis of the plasma edge in JET discharges.
Huysmans G T A Challis C D Kerner W Parail V V
Bulletin of the American Physical Society, vol.40 no.11 October 1995 (Program of the Thirty-seventh Annual Meeting of the Division of Plasma Physics, 6-10 November 1995; Louisville, Kentucky). p.1766.
125. Modelling the excitation of global Alfvén modes by an external antenna in the Joint European Torus.
Huysmans G T A Kerner W Borba D Holties H A Goedbloed J P
Physics of Plasmas, vol.2 no.5 May 1995. p.1605.
Report JET-P(94)49
126. Comparison of JET and DIII-D temperature and density profile shapes and their parametric dependencies.
Imre K Riedel K S Schissel D P Schunke B
Bulletin of the American Physical Society, vol.40 no.11 October 1995 (Program of the Thirty-seventh Annual Meeting of the Division of Plasma Physics, 6-10 November 1995; Louisville, Kentucky). Abstracts only. p.1765.
127. Sawtooth heat pulse propagation: ballistic response and Fourier analysis.
Jacchia A de Luca F Gorini G Mantica P Deliyannis N Erba M Porte L
22nd European Physical Society Conference on Controlled Fusion and Plasma Physics, Bournemouth, 3rd-7th July 1995, Contributed papers. Part III. p.009.
128. Highly radiative JET-discharges with seeded and intrinsic impurities.
Jackel H J Campbell D Chen H Giannella R von Hellermann M Loarte A Reichle R Taroni L
Bulletin of the American Physical Society, vol.40 no.11 October 1995 (Program of the Thirty-seventh Annual Meeting of the Division of Plasma Physics, 6-10 November 1995; Louisville, Kentucky). p.1766.

129. JET relevance to ITER, new trends and initial results.
Jacquinot J
Fusion Engineering and Design, vol.30 nos.1-2 May 1995 (Invited papers of the 18th Symposium on Fusion Technology, Karlsruhe, 22-26 August 1994) p.67.
Report JET-P(94)65
130. The effect of a sawtooth crash on fast particle behaviour.
Jarvis O N Adams J A Bond D Hone M Howarth P J A Loughlin M J Marcus F B Sadler G van Belle P Watkins N
22nd European Physical Society Conference on Controlled Fusion and Plasma Physics, Bournemouth, 3rd-7th July 1995, Contributed papers. Part III. p.057.
131. Gamma-ray emission profile measurements from JET ICRF-heated discharges.
Jarvis O N Adams J M Howarth P J A Marcus F B Righi E Sadler G Start D F H van Belle P Warrick C Watkins N
Joint European Torus, JET, 1995. 36p.
Report JET-P(95)53
132. The route to high performance on JET.
Jones T T C and JET Team
Plasma Physics and Controlled Fusion, vol.37 Supplement 11A November 1995 (Invited papers from the 22nd European Physical Society Conference on Controlled Fusion and Plasma Physics, Bournemouth, 3-7 July 1995). p.A359.
Report JET-P(95)39
133. New neutron spectrometer for high power D-T experiments on JET
Kallne J Conroy S Frenje J Ericsson G Traneus E Renberg P U Enge H King N Review of Scientific Instruments, vol.66 no.1 Part II January 1995, (Tenth Topical Conference on High Temperature Plasma Diagnostics, Rochester, New York, 8-12 May 1994.) p.884.
134. Lower hybrid heating and current drive in ITER: operation scenarios and outline system design.
Kaye A Moreau D Soldner F X Engelmann F Gormezano C Lloyd B Santini F Tonon G Wegrowe J G Baranov Y Bhatnagar V P Goniche M Huysmans G T A Litaudon X O'Brien M R Parail V V Rey G Springmann E Taroni A Walton R Warrick C D Joint European Torus (JET), November 1994. 72p.
Report JET-R(94)07
135. Implications for ITER: JET divertor results.
Keilhacker M Watkins M L
Europhysics News, vol.26 no.5 1995. p.105.
136. JET results with the new pumped divertor and implications for ITER.
Keilhacker M and the JET Team
Plasma Physics and Controlled Fusion, vol.37 Supplement 11A November 1995 (Invited papers from the 22nd European Physical Society Conference on Controlled Fusion and Plasma Physics, Bournemouth, 3-7 July 1995). p.A3.
Report JET-P(95)42
137. Dimensional analysis of L-H power threshold scalings.
Kerner W Cordey J G Pogutse O Righi E
22nd European Physical Society Conference on Controlled Fusion and Plasma Physics, Bournemouth, 3rd-7th July 1995, Contributed Papers. Part 3. p.229.
138. Optimization of neutral beam deposition, configuration and recycling of hot-ion H-modes in JET.
Konig R W T Lawson K D Sartori R Deliyanakis N Hellermann M V Jones T T C Lomas P Maas A C Marcus F B Schunke B Smeulders P Stamp M F Thomas P R Zastrow K-D
Bulletin of the American Physical Society, vol.40 no.11 October 1995 (Program of the Thirty-seventh Annual Meeting of the Division of Plasma Physics, 6-10 November 1995; Louisville, Kentucky). p.1765.
139. Impurity induced neutralization of MeV energy protons in JET plasmas
Korotkov A A Gondhalekar A
Submitted for publications in Nuclear Fusion
Report JET-P(95)47
140. Physics aspects of coupling the ICRF A2 antennae to JET discharges.
Lamalle P U Bell G Bhatnagar V P Bures M Fechner B Gormezano C Jacquinot J Kaye A

- Lenholm M Nguyen F Righi E Sibley A Start D
F H Timms M Wade T J
22nd European Physical Society Conference on Controlled Fusion and Plasma Physics, Bournemouth, 3rd-7th July 1995, Contributed papers. Part 2. p.329.
141. The analytical laboratory for the JET active gas handling system - inactive commissioning.
Lasser R Grieveson B Hemmerick J Stagg R Walker K
Fusion Technology vol.28 no.3 part 2, October 1995 (Proceedings of the Fifth Topical Meeting on Tritium Technology in Fission, Fusion, and Isotopic Applications, Belgirate, Italy, May 28-June 3 1995). p.1033.
142. The preparative gas chromatographic system for the JET active gas handling system - inactive commissioning.
Lasser R Jones G Hemmerich J L Stagg R Yorkshades J
Fusion Technology, vol.28 no.3 Part 1, October 1995 (Proceedings of the Fifth Topical Meeting on Tritium Technology in Fission, Fusion and Isotopic Applications, Belgirate, Italy, May 28-June 3, 1995). p.681.
143. Possible semi-empirical drift-wave models for the simulation of impurity transport and their comparison with JET experiments.
Lauro-Taroni L Connor J W Giannella R Romanelli F Wilson H
22nd European Physical Society Conference on Controlled Fusion and Plasma Physics, Bournemouth, 3rd-7th July 1995. Contributed Papers. p.089.
144. First experiments of pulse compression radar reflectometry for density measurements on JET plasmas.
Laviron C Millot P Prentice R
Plasma Physics and Controlled Fusion, vol.37 no.9 September 1995 p.975.
Report JET-P(95)05
145. The optimisation of recycling in high performance hot-ion H-mode JET discharges.
Lawson K D Deliyannis N Hawkes N C von Hellermann M G Jones T T C Konig R W T Lomas P J Maas A C Marcus F B Sartori R Schunke B Smeulders P Stamp M F Thomas P R
22nd European Physical Society Conference on Controlled Fusion and Plasma Physics, Bournemouth, 3rd-7th July 1995, Contributed Papers. Part 2. p.077.
146. The effects on ELMs on the plasma edge of JET.
Lingertat J Alper B Ali-Arshad S Bak P E Chankin A Clement S Coad P Cortes I Deliyannis N Ehrenberg J Loarte A Monk R Porte L Prentice R Tabasso A
22nd European Physical Society Conference on Controlled Fusion and Plasma Physics, Bournemouth, 3rd-7th July 1995, Contributed Papers. Part 3. p.281.
147. Power flux and electric current flow to the divertor target plates of JET.
Lingertat J Gunther K Loarte A
Journal of Nuclear Materials, vol.220-222 April 1995 (Proceedings of the Eleventh International Conference on Plasma-Surface Interactions in Controlled Fusion Devices Mito, Ibaraki, Japan, May 23-27, 1994). p.198.
148. Comparison between measured scrape-off layer plasma parameters and 2D model calculations for JET X-point discharges.
Loarte A Chankin A Clement S Corrigan G Harbour P Horton L Janeschitz G Lingertat J Matthews G Simonini R Tagle J Taroni A Vlases G
Journal of Nuclear Materials, vols.220-222 April 1995 (Proceedings of the Eleventh International Conference on Plasma-Surface Interactions in Controlled Fusion Devices, Mito, Ibaraki, Japan, May 23-27, 1994). p.606.
149. The influence of divertor geometry on JET discharges.
Loarte A Campbell D J Clement S Davies S J Erents S K Guo H Y Harbour P J Horton L Lingertat J Lowry C Matthews G F McCormick K Monk R D O'Brien D Saibene G Simonini R Radford G J Taroni A Vlases G

- 22nd European Physical Society Conference on Controlled Fusion and Plasma Physics, Bournemouth, 3rd-7th July 1995, Contributed Papers. Part 3. p.305.
150. High performance in JET in relation to Next Step tokamaks.
Lomas P J and the JET Team
Bulletin of the American Physical Society, vol.40 no.11 October 1995 (Program of the Thirty-seventh Annual Meeting of the Division of Plasma Physics, 6-10 November 1995; Louisville, Kentucky). p.1766.
151. Operation for high performance in the new JET configuration.
Lomas P J and the JET Team
Plasma Physics and Controlled Nuclear Fusion Research 1994, 15th International Conference, Seville, 26 September-1 October 1994. vol.1. p.211.
152. Investigation of opacity in the JET tokamak divertor region.
Lovegrove T Horton L D Konig R W T Lingertat J Maas A C Maggi C F Monk R D Stamp M F Storey P J Tabasso A
22nd European Physical Society Conference on Controlled Fusion and Plasma Physics, Bournemouth, 3rd-7th July 1995, Contributed Papers. Part 3. p.301.
153. The impurity processing system for the JET active gas handling system - inactive commissioning.
Lupo J Hemmerich J L Lasser R Yorkshades J Salanave J L
Fusion Technology vol.28 no.3 part 2, October 1995 (Proceedings of the Fifth Topical Meeting on Tritium Technology in Fission, Fusion, and Isotopic Applications, Belgrade, Italy, May/June 1995). p.1347.
154. Alignment systems for pumped divertor installation at JET.
Macklin B Brade R Celentano G Cordier J J Israel G Tait J van Lente E
Fusion Technology 1994, Proceedings of the 18th Symposium on Fusion Technology, Karlsruhe, Germany, 22-26 August 1994, vol.1. p.279.
155. Detailed design, installation and testing of the new coil protection system for JET.
- Marchese V De Marchi E Dolgetta N Last J R Ryle C Sannazzaro G Scibile L Van Veen J Zannelli L
Fusion Technology 1994, Proc. 18th Symposium on Fusion Technology, Karlsruhe, Germany, 22-26 August 1994, vol.2. Amsterdam, Elsevier. 1995. p.925.
156. Evolution and optimisation of neutron emissivity profiles in JET.
Marcus F B Adams J M Bond D S Hone M A Jarvis O N Jones T T C Koenig R Loughlin M J Nave M F F Sadlet G Schunke B Smeulders P Watkins N
22nd European Physical Society Conference on Controlled Fusion and Plasma Physics, Bournemouth, 3rd-7th July 1995, Contributed Papers. Part 2. p.053.
157. A neutron camera for ITER: conceptual design.
Marcus F B Adams J M Batistoni P Elevant T Jarvis O N Johnson L de Kock L Sadler G Stott P
Joint European Torus, 1995. Report JET-P(95)45
158. Evaluation and refinement of the conceptual design for the ITER neutron camera
Marcus F B Adams J M Bastistoni P Elevant T Jarvis O N
Report JET-P(95)77
159. Highly radiating and detached plasmas on carbon and beryllium targets.
Matthews G F and the JET Team
Plasma Physics and Controlled Fusion, vol.37 Supplement 11A November 1995 (Invited papers from the 22nd European Physical Society Conference on Controlled Fusion and Plasma Physics, Bournemouth, 3-7 July 1995). p.A227.
Report JET-P(95)40
160. Plasma detachment from divertor targets and limiters.
Matthews G F
Journal of Nuclear Materials, vol.220-222 April 1995 (Proceedings of the Eleventh International Conference on Plasma-Surface Interactions in Controlled Fusion Devices Mito, Ibaraki, Japan, May 23-27, 1994). p.104.
Report JET-P(94)63
161. Laser blow-off injected impurity particle confinement times in JET and Tore Supra.

- Mattioli M Giannella R Myrnas R De Michelis C Denne-Hinnov B de Wit T D Magyar G Nuclear Fusion, vol.35 no.9 September 1995. p.1115.
Report JET-P(94)73
162. Surface layer composition of the JET vessel walls, material transport and hydrogen trapping in the vessel walls.
Mayer M Behrisch R Prozesky V Andrew P Peacock A J
22nd European Physical Society Conference on Controlled Fusion and Plasma Physics, Bournemouth, 3rd-7th July 1995, Contributed papers. Part 2. p.301.
163. Interpretation of ion cyclotron emission from sub-Alfvénic fusion products in the tokamak fusion test reactor.
McClements K G Cauffman S Cottrell G A Dendy R O Lashmore-Davies C N Majeski R
Joint European Torus (JET). April 1995. 22p. Report UKAEA-FUS-280 Submitted for publication in Physics of Plasmas.
Report JET-P(95)15
164. Recycling, divertor parameters and SOL transport for high performance discharges in the new JET.
McCormick K Ehrenberg J Loarte A Monk R Simonini R Spence J Stamp M Taroni A Vlases G
22nd European Physical Society Conference on Controlled Fusion and Plasma Physics, Bournemouth, 3rd-7th July 1995. Contributed Papers, Part I. p.313.
165. Report on vertical stability studies during the plasma start-up at ITER (Task 2.1e).
Milani F Garribba M
Joint European Torus (JET), November 1994 36p.
Report JET-R(94)09
166. Determination of JET scrape-off layer transport coefficients using an interpretative "onion-skin" plasma model.
Monk R D Horton L D Loarte A Matthews G F Stangeby P C
Journal of Nuclear Materials, vols.220-222 April 1995 (Proceedings of the Eleventh International Conference on Plasma-Surface Interactions in Controlled Fusion Devices, Mito, Ibaraki, Japan, May 23-27, 1994). p.612.
167. Divertor plasma detachment in JET.
Monk R D Campbell D J Clement S Davies S J Ehrenberg J Erents S K Guo H Y Horton L D Loarte A Lowry C G Lingertat J Matthews G F Reichle R Saibene G Tabasso A Vlases G C
22nd European Physical Society Conference on Controlled Fusion and Plasma Physics, Bournemouth, 3rd-7th July 1995, Contributed Papers. Part 3. p.293.
168. Visible spectroscopy of the JET pumped divertor using coherent optical-fibre bundles.
Morgan P D Wilson C H
Review of Scientific Instruments, vol.66 no.1 part II January 1995. (Tenth Topical Conference on High Temperature Plasma Diagnostics, Rochester, New York, 8-12 May 1994) p.606.
169. Full wave modelling of ICRF edge fields and far-field sheaths in JET.
Moroz P E Myra J R D'Ippolito D A Bures M
Bulletin of the American Physical Society, vol.40 no.11 October 1995 (Program of the Thirty-seventh Annual Meeting of the Division of Plasma Physics, 6-10 November 1995; Louisville, Kentucky). p.1767.
170. A visible and UV charge exchange spectroscopy system for the tritium phase of JET.
Morsi H W von Hellermann M König R W T Schropf H
Plasma Physics and Controlled Fusion, vol.37 no.12 December 1995. p.1407.
Report JET-P(95)10
171. MHD activity in JET hot ion H-mode discharges.
Nave M F F Ali-Arshad S Alper B Balet B De Blank H J Borba D Challis C D Von Hellermann M G Hender T C Huysmans G T A Kerner W Kramer G J Porcelli F O'Rourke J Porte L Sadler G J Smeulders P Sips A C C Stubberfield P M Stork D Reichle R Wesson J A Zwingmann W
Nuclear Fusion, vol.35 no.54 April 1995. p.409.
Report JET-P(93)79

172. Observations of MHD activity in JET high performance plasmas.
Nave M F F Alper B Smeulders P Ali-arshad S Lomas P Marcus F Monticelli E Parail V Sartori R Stamp M F
Joint European Torus (JET), February 1995. 10p.
Report JET-P(95)-03
173. The time behaviour of the heat conductivity during L-H-L transitions in JT-60U.
Neudatchin S Muir D G and others
22nd European Physical Society Conference on Controlled Fusion and Plasma Physics, Bournemouth, 3rd-7th July 1995, Contributed papers. Part III. p.029.
174. The handling, assessment, transport and disposal of tritiated waste materials at JET.
Newbert G Haigh A Atkins G
Fusion Technology vol.28 no.3 part 2, October 1995 (Proceedings of the Fifth Topical Meeting on Tritium Technology in Fission, Fusion, and Isotopic Applications, Belgirate, Italy, May 28-June 3 1995). p.1552.
175. Fast wave current drive experiments in JET divertor plasmas.
Nguyen F Eriksson L G Fischer B Gormezano C Righi E Rimini F Sadler G Sips A Start D
22nd European Physical Society Conference on Controlled Fusion and Plasma Physics, Bournemouth, 3rd-7th July 1995, Contributed papers. Part 2. p.353.
176. Performance of the supercritical helium cooling loop for the JET divertor cryopump
Obert W Mayaux C Barth K Herblin L
Submitted for publications in Advances in Cryogenic Engineering
Report JET-P(95)38
177. Sawteeth-induced impurity transport in tokamak plasmas.
Odblom A Anderson D Eriksson L-G Lisak M
22nd European Physical Society Conference on Controlled Fusion and Plasma Physics, Bournemouth, 3rd-7th July 1995. Contributed Papers. p.093.
Report JET-P(95)36
178. Disruption and VDE characterization for ITER.
Ortolani S Campbell D Garribba M Johnson M Noll P Tanga A and others
22nd European Physical Society Conference on Controlled Fusion and Plasma Physics, Bournemouth, 3rd-7th July 1995, Contributed Papers, Part IV. p.009.
179. Fast nonlinear magnetic reconnection.
Ottaviani M Porcelli F
Physics of Plasmas, vol.2 no.11 November 1995, p.4104.
Report JET-P(95)04
180. Unanswered questions in ion-temperature-gradient-driven turbulence
Ottaviani M Beer M A Cowley S Horton W Krommes J
Submitted for publication in the Proceedings of the ITP Program on Plasmas Report JET-P(95)70
181. Impurity ion emission and edge transport during ELMy H-modes in the new JET divertor configuration.
O'Mullane M G Chen H Coffey I H Hawkes N C von Hellermann M Lauro-Taroni L Peacock N J Rookes A
22nd European Physical Society Conference on Controlled Fusion and Plasma Physics, Bournemouth, 3rd-7th July 1995, Contributed papers. Part III. p.121.
182. Low level tritium assessment in JET solid waste materials.
Pacenti P Atkins G Campi F Newbert G Terrani S
Fusion Technology 1994, Proceedings of the 18th Symposium on Fusion Technology, Karlsruhe, Germany, 22-26 August 1994, Vol.2. p.1549.
Amsterdam, Elsevier. 1995.
183. European negative ion based neutral beam developments.
Pamela J Fumelli M Hemsworth R S Jacquot C Jequier F Simonin A Hopkins M B Turner M M de Esch H P L Challis C Stork D Thompson E
Fusion Engineering & Design, vol.26 nos.1-4, January I 1995 (Proceedings of the Fifth International Toki Conference on Plasma Physics and Controlled



- Nuclear Fusion, November 16-19, 1993, Toki, Japan: Physics and Technology of Plasma Heating and Current Drive). p.407.
184. Outline design of a neutral beam injector for the ITER EDA.
Pamela J Nightingale M Taylor N Thompson E Watson M and others
Fusion Technology 1994, Proceedings of the 18th Symposium on Fusion Technology, Karlsruhe, Germany, 22-26 August 1994, vol.1. Amsterdam, Elsevier, 1995. p.629.
185. Operational safety of the JET in-vessel divertor cryopump system.
Papastergiou S Ageladarakis P Obert W Thompson E
Fusion Technology 1994, Proceedings of the 18th Symposium on Fusion Technology, Karlsruhe, Germany, 22-26 August 1994, vol.1. Amsterdam, Elsevier, 1995. p.343.
186. Numerical simulation of ELM free H and hot ion H-modes JET plasmas.
Parail V Erba M Cherubini A Springmann E Taroni A
Joint European Torus, JET, 1995. 5p. Report JET-P(95)49
187. The physics of L- and H-mode confinement in JET.
Parail V V Balet B Bak P Cordey J G Deliyankis N Erba M Giannella R Muir D G Nave M F F Porte L Springmann E M Taroni A Thomsen K Vayakis G
Plasma Physics and Controlled Nuclear Fusion Research 1994, 15th International Conference, Seville, 26 September-1 October 1994. vol.1. p.255.
188. The physics of L and H-mode confinement in JET.
Parail V Bak P Balet B Cherubini A Cordey J G Deliyankis N Erba M Porte L Springmann E Taroni A Vlases G
Joint European Torus (JET). July 1995. 18p. Report JET-P(95)09
189. Transport analysis of the giant ELM's in JET.
Parail V Balet B Bak P Cordey J G Cherubini A Erba M Deliyankis N Nave M F F Porte L Springmann E Taroni A Vayakis G
22nd European Physical Society Conference on Controlled Fusion and Plasma Physics, Bournemouth, 3rd-7th July 1995. Contributed Papers. p.013.
190. Diagnostics of tokamak fusion plasma via correlation analysis of soft X-ray signals.
Pazsit I Gill R D
Joint European Torus (JET). June 1995. 9p. Submitted for publication in SMORN Conf. Procs. (Avignon 1995).
Report JET-P(95)23
191. Large carbon fibre re-inforced carbon tiles for a Mark II divertor in JET.
Pick M A Altmann H Ciric D Deksnis E B Falter H D Fanthome J Lowry C Massman P Mohanti R B Peacock A T Tivey R B
Journal of Nuclear Materials, vols.220-222 April 1995 (Proceedings of the Eleventh International Conference on Plasma-Surface Interactions in Controlled Fusion Devices, Mito, Ibaraki, Japan, May 23-27, 1994). p.595.
192. Edge modes as ELM events.
Pogutse O Cordey J G kerner W Schunke B
22nd European Physical Society Conference on Controlled Fusion and Plasma Physics, Bournemouth, 3rd-7th July 1995, Contributed Papers. Part 3. p.277.
193. Topological transitions of fast ion orbits in magnetically confined plasmas.
Porcelli F Eriksson L-G Furno I
Joint European Torus (JET), January 1995. 11p. Report JET-P(94)72
194. Evolution of edge electron temperature and density in JET H-mode plasmas.
Porte L Bartlett D V Deliyankis N Rookes A
Bulletin of the American Physical Society, vol.40 no.11 October 1995 (Program of the Thirty-seventh Annual Meeting of the Division of Plasma Physics, 6-10 November 1995; Louisville, Kentucky). p.1765.
195. New microwave measurements of electron density and temperature in the JET divertor.

- Prentice R Bartlett D V Porte L Prior P C S Salisbury M W Smith R J Tellier X Cupido L Manso M E Serra F
22nd European Physical Society Conference on Controlled Fusion and Plasma Physics, Bournemouth, 3rd-7th July 1995, Contributed Papers, Part IV. p.425.
196. A two colour mm-wave interferometer for the JET divertor.
Prentice R Edlington T Smith R T C Trotman D L Wylde R J Zimmermann P
Review of Scientific Instruments, vol.66 no.2 Part 1 February 1995. p.1154.
197. Antennas and waveguides for the JET pumped divertor microwave diagnostics.
Prior P C S Bartlett D V Prentice R Smith R J Tellier X
Fusion Technology 1994, Proceedings of the 18th Symposium on Fusion Technology, Karlsruhe, Germany, 22-26 August 1994, vol.1. Amsterdam, Elsevier. 1995. p.819.
198. The particle and heat drift fluxes and their implementation into the EDGE2D transport code
Radford G J Chankin A V Corrigan G Simonini R Spence J Taroni A
Report JET-P(95)78
199. Radiation in JET's Mark I divertor.
Reichle R Bartlett D V Campbell D J Chen H Fuchs J C Giannella R Gottardi N A C Hawkes N Horton L D Jackel H J Lauro-Taroni L Maas A C Monk R D O'Mullane M G Porte L van der Linden R von Hellermann M Wesson J
22nd European Physical Society Conference on Controlled Fusion and Plasma Physics, Bournemouth, 3rd-7th July 1995, Contributed papers. Part III. p.085.
200. Bolometer for ITER
Reichle R Fuchs J C Giannella R M Gottardi N A C Jackel H J Mast K F Thomas P R van Belle P
Submitted for publication in Procs. of Diagnostics for ITER, International Workshop, Villa Monastero, Varenna, Italy, 28 August - 1st September 1995
Report JET-P(95)51
201. Density scaling of the H-mode power threshold in JET.
Righi E Campbell D J Cordey J G Ehrenberg J Giannella R de Haas J Harbour P Hawkes N C Nielsen P Porte L Saibene G Start D F H Thomsen K von Hellermann M
22nd European Physical Society Conference on Controlled Fusion and Plasma Physics, Bournemouth, 3rd-7th July 1995, Contributed Papers. Part 2. p.073.
202. H-mode power threshold database for ITER
Ryter F Campbell D J Carlstrom T N Christiansen J P Cordey J G DeBoo J C Fielding S J Fukuda T Granetz R S Greenwald M Kamada Y Kardaun O J W F Kaye S M Kollermeier J Kus A Matsuda T Miura Y Mori M Righi E Ryter F Sato M Schisel D P Snipes J A Stroth U Suzuki A Takizuka T Tamai H Thomsen K Tsuchiya K Valovic M
Submitted for publication in Nuclear Fusion
Report JET-P(95)55
203. The distribution function of fusion products at birth.
Sadler G van Belle P
22nd European Physical Society Conference on Controlled Fusion and Plasma Physics, Bournemouth, 3rd-7th July 1995, Contributed papers. Part 2. p.269.
204. Fast particle diagnostics at JET: status and plans.
Sadler G J Adams J M Cecil F E Cottrell G A Gonkhalekar A Hoekzema J A Jarvis O N Loughlin M J Marcus F B Van Belle P Von Hellermann M
Nuclear Fusion, vol.35 no.12, December 1995 (Proceedings of the Fourth IAEA Technical Committee Meeting on Alpha Particles in Fusion Research, Princeton, 25-28 April 1995) p.1609, and Joint European Torus, JET, 1995. 14p.
Report JET-P(95)58
205. Effect of active pumping and fuelling on divertor plasma discharges in JET.
Saibene G Apicella M L Bart K Campbell D J Ehrenberg J K Harbour P J Horton L D Lowry C G Loarte A Monk R D Obert W Rossi A Sartori R Stork D Thomson E



- 22nd European Physical Society Conference on Controlled Fusion and Plasma Physics, Bournemouth, 3rd-7th July 1995, Contributed Papers. Part 2. p.121.
206. Review of vacuum vessel conditioning procedures at JET and their impact on plasma operation.
Saibene G Rossi a Monk R D Orchard J Andrew P Barnsley R Cushing D Coad P J Davies S Erents S K Guo H Y Lawson K Lingertat J Matthews G Sips G Stamp M Tanga A
Journal of Nuclear Materials, vols.220-222 April 1995 (Proceedings of the Eleventh International Conference on Plasma-Surface Interactions in Controlled Fusion Devices, Mito, Ibaraki, Japan, May 23-27, 1994). p.617.
207. Modification of the JET vacuum vessel support and restraint systems.
Sannazzaro G Celentano G Miller A Raimondi T Saunders S Tait Jvan Veen J Wykes M
Fusion Technology 1994, Proc. 18th Symposium on Fusion Technology, Karlsruhe, Germany, 22-26 August 1994, vol. I. Amsterdam, Elsevier. 1995. p.755.
208. Studies of tearing mode control in JET.
Santagiustina A Arshad S A Campbell D J Antona G D de Benedetti M Edwards A (Culham) Fishpool G Lazzaro E La Haye R J Morris A W (Culham) Ostrom R Rossi L Sartori F Savrukhin P Tabellini M Tubbing B J Tanga A Zullo G
22nd European Physical Society Conference on Controlled Fusion and Plasma Physics, Bournemouth, 3rd-7th July 1995, Contributed Papers, Part IV. p.461.
209. DSP control of the fusion plasma configuration of JET.
Sartori F Garriba M Litunovsky R Milani F Puppini S
Joint European Torus, JET, July 1995. 5p. Report JET-P(95)29
210. High current operation with the new JET divertor.
Sartori R Ali-Arshad S Bertolini E Bonicelli T Bures M Christiansen J P Chuilon P de Esch H Deliyankis N Fishpool G Jarvis O N Jones T T C Koenig R Lawson K Lomas P J Maas A C Marcus F B Nave M F Sannazzaro G Schunke B Smeulders P Taroni A Thomas P R Thomsen K
22nd European Physical Society Conference on Controlled Fusion and Plasma Physics, Bournemouth, 3rd-7th July 1995, Contributed Papers, Part IV. p.141.
211. Numerical simulation of feedback control of coupled tearing modes at JET.
Savrukhin P Campbell D J de Benedetti M Edwards A M D'Antona G Fishpool G Santagiustina A Sartori F
Joint European Torus (JET), 1995. 100p. Report JET-R(95)06
212. Comparison of JET and DIII-D temperature and density profile shapes and their parametric dependence.
Schissel D P Schunke B Imre K Riedel K S
22nd European Physical Society Conference on Controlled Fusion and Plasma Physics, Bournemouth, 3rd-7th July 1995, Contributed Papers. Part 2. p.065.
213. Possible safe termination by injection of polyethylene pellets in JET.
Schmidt G L Ali-Arshad S Bartlett D Chankin A Clement S Gadeberg M Kupschus P O'Brien D Reichle R Sadler G Tanga A
22nd European Physical Society Conference on Controlled Fusion and Plasma Physics, Bournemouth, 3rd-7th July 1995, Contributed Papers, Part IV. p.021.
214. Log-additive parameterization of JET electron temperature and density profiles
Schunke B Imre K Riedel K S
Submitted for publication in Physics of Plasmas
Report JET-P(95)80
215. Cleaning of the JET vacuum vessel using the carbon dioxide pellet blasting technique.
Scott S M Haigh A Schreibermaier J Davies N Porter A Saibene G
Joint European Torus (JET), 1995. 35p. Report JET-R(95)03
216. Transient adiabatic/isothermal calorimetry tests on JET uranium beds for tritium storage.
Serio L Hemmerich J L Lasser R Milverton P

- Fusion Technology 1994, Proceedings of the 18th Symposium on Fusion Technology, Karlsruhe, Germany, 22-26 August 1994, Vol.2. p.1107.
217. Energetic particle drive for toroidicity-induced Alfvén eigenmodes and kinetic toroidicity-induced Alfvén eigenmodes in a low-shear tokamak.
Sharapov S E Breizman B N Institute for Fusion Studies, The University of Texas, October 1994 31p. Report IFSR 671
218. Confinement of high β_{pol} plasmas in JET.
Sips A C C Challis C D Gormezano C Gowers C W Huysmans G T A Ishida S Rimini F G Tubbing B J D Ward D J
22nd European Physical Society Conference on Controlled Fusion and Plasma Physics, Bournemouth, 3rd-7th July 1995, Contributed papers. Part III. p.005.
219. Influence of MHD instabilities on JET high performance.
Smeulders P Alper B Bak P Balet B Christiansen J P Deliyannis N Edwards A Erba M de Esch H Gill R D Hender T C Huysmans G Jones T Koenig R Lawson K Lomas P Lyadina E Marcus F Nave M Parail V Porte L Rookes A Schunke B Thomas P Thomsen K
22nd European Physical Society Conference on Controlled Fusion and Plasma Physics, Bournemouth, 3rd-7th July 1995, Contributed Papers, Part IV. p.061.
220. Survey of pellet enhanced performance in JET discharges.
Smeulders P and others
Nuclear Fusion, vol.35 no.2 February 1995. p.225. Report JET-P(94)07
221. Shear reversal experiments on JET.
Soldner F X Balet B Baranov Y Ekedahl A Fischer B Goedbloed J P Gormezano C Holties H A Huysmans G T A Lennholm M Parail V V Rimini F Schild P Sips A C C Smits F Springmann E Taroni A Tubbing B J D
22nd European Physical Society Conference on Controlled Fusion and Plasma Physics, Bournemouth, 3rd-7th July 1995, Contributed Papers, Part IV. p.113.
222. Lower hybrid current drive in JET and reactor applications.
Soldner F X and the JET Team. Plasma Physics and Controlled Nuclear Fusion Research 1994, 15th International Conference, Seville, 26 September-1 October 1994. vol.1. p.423.
223. Neutron radiation testing of JET in-vessel inspection system components.
Sordon G Tartaglia G P Businaro T
Fusion Technology 1994, Proc. 18th Symposium on Fusion Technology, Karlsruhe, Germany, 22-26 August 1994, vol.1. Amsterdam, Elsevier. 1995. p.751.
224. Improved plasma purity in the JET pumped divertor.
Stamp M F von Hellermann M
22nd European Physical Society Conference on Controlled Fusion and Plasma Physics, Bournemouth, 3rd-7th July 1995, Contributed papers. Part III. p.089.
225. Determination of T_e from a Langmuir probe in a magnetic field by directly measuring the probe's sheath drop using a pin-plate probe.
Stangeby P C
Plasma Physics and Controlled Fusion, vol.37 no.11 November 1995. p.1337. Report JET-P(95)21
226. Impurity retention by divertors, Part 1: One-dimensional models.
Stangeby P C Elder J D
Joint European Torus (JET), 1995. 50p. Report JET-P(95)08
227. A problem in the interpretation of tokamak Langmuir probes when a fast electron component is present.
Stangeby P C
Plasma Physics and Controlled Fusion, vol.37 no.9 September 1995 p.1031.
Report JET P(95)14
228. Radial and poloidal ExB drifts in the scrape-off layers of a divertor tokamak: Effects on in/out asymmetries, plasma detachment at the targets, and divertor biasing.
Stangeby P C Chankin A V
Joint European Torus (JET). April 1995. 29p. Report JET-P(95)07 Submitted to Nuclear Fusion.

229. Understanding impurity retention by divertors.
Stangeby P C Elder J D
Journal of Nuclear Materials, vol.220-222 April 1995 (Proceedings of the Eleventh International Conference on Plasma-Surface Interactions in Controlled Fusion Devices Mito, Ibaraki, Japan, May 23-27, 1994). p.193.
230. Recent results of ICRF heating on JET.
Start D F H Bell G Bhatnagar V P Bures M Cottrell G A Eriksson L-G Fechner B Goulding R Gormezano C Howman A Jacquinet J Kay A Lamalle P Nguyen F Righi E Rimini F Sibley A Sips A C C Tubbing B J Wade T Ward D
Joint European Torus (JET), 1995. 8p. Report JET-P(95)33
231. Characterisation of long pulse steady-state H-modes in the JET pumped divertor configuration.
Stork D Bickley A J Campbell D J Clement S Davies S Erents K Garibba M Hawkes N Horton L D Howman A Konig R Lingertat H Loarte A Maggi C Monk R Reichle R Righi E Saibene G von Hellermann M
22nd European Physical Society Conference on Controlled Fusion and Plasma Physics, Bournemouth, 3rd-7th July 1995, Contributed Papers. Part 2. p.125.
232. The new experimental phase of JET and prospects for future operation.
Stork D and the JET Team
Plasma Physics and Controlled Nuclear Fusion Research 1994, 15th International Conference, Seville, 26 September-1 October 1994. vol.1. p.51.
233. Non-ambipolar neoclassical transport.
Stringer T E
Nuclear Fusion, vol.35 no.8 August 1995. p.1008. Report JET-P(94)38
234. Modelling the neutralisation and energy distribution function of MeV ions during combined ICRH and NBI heating in JET.
Stuart A J G Dalla S C Eriksson L-G Gondhalekar A
22nd European Physical Society Conference on Controlled Fusion and Plasma Physics, Bournemouth, 3rd-7th July 1995, Contributed Papers. Part 2. p.033.
235. Multifluid modelling of radiative and detached edge plasmas and comparison with JET experimental results.
Taroni A Corrigan G Horton L D Loarte A Matthews G F Radford G J Reichle R Simonini R Spence J
22nd European Physical Society Conference on Controlled Fusion and Plasma Physics, Bournemouth, 3rd-7th July 1995, Contributed Papers, Part IV. p.297.
236. Bifurcations and intermittent magnetic activity.
Tebaldi C Ottaviani M Porcelli F
Joint European Torus (JET), 1995. 11p. Report JET-P(95)28
237. Irradiation effects on magnet components of the Joint European Torus.
Tesini A Bertolini E Last J R Sordon G Tartaglia G P
Fusion Technology 1994, Proc. 18th Symposium on Fusion Technology, Karlsruhe, Germany, 22-26 August 1994, vol.2. Amsterdam, Elsevier. 1995. p.977.
238. Experiments with TF ripple in JET.
Tubbing B and the JET Team
22nd European Physical Society Conference on Controlled Fusion and Plasma Physics, Bournemouth, 3rd-7th July 1995, Contributed Papers, Part IV. p.001.
239. The new phase of the Joint European Torus and prospects for future operation.
Tubbing B J D and the JET Team.
Physics of Plasmas, vol.2 no.6 pt.2 June 1995 (Special Issue: Invited and Review Papers from the 36th Annual Meeting of the Division of Plasma Physics of the American Physical Society 7-11 November 1994, Minneapolis, Minnesota). p.2256
240. The operational characteristics of a molten and damaged beryllium divertor target in JET.
Tubbing B J D Chankin A Clement S Coad P Deksnis E Lingertat J Loarte A Lowry C

- 22nd European Physical Society Conference on Controlled Fusion and Plasma Physics, Bournemouth, 3rd-7th July 1995, Contributed Papers. Part 3. p.453.
241. Plasma performance on solid and molten beryllium divertor targets in JET.
Tubbing B J D and the JET Team.
Bulletin of the American Physical Society, vol.40 no.11 October 1995 (Program of the Thirty-seventh Annual Meeting of the Division of Plasma Physics, 6-10 November 1995; Louisville, Kentucky). p.1766.
242. A model of the effect of plasma turbulence on time delay measurements by reflectometry
Vayakis G
Report JET-P(95)76
243. Information integration for finite element analysis at JET.
Viola R Carman P
Joint European Torus (JET), January 1995. 9p. Report JET-R(95)01
244. Divertor similarity and multi-machine scaling experiments.
Vlases G C Hutchinson I H Pietrzak Z A
22nd European Physical Society Conference on Controlled Fusion and Plasma Physics, Bournemouth, 3rd-7th July 1995, Contributed Papers. Part 3. p.313.
245. Analytical approximation of cross-section effects on charge exchange spectra observed in hot fusion plasmas.
Von Hellermann M Breger P Frieling J Konig R Mandl W Maas A Summers H P
Plasma Physics and Controlled Fusion, vol.37 no.2 February 1995 p.71.
246. Feasibility of quantitative spectroscopy on ITER.
Von Hellermann M Core W G F Howman A Jupen C Konig R W T Stamp M F Summers H P Thomas P R Zastrow K-D
Joint European Torus (JET) 1995. 10p. Report JET-P(95)63
247. Helium and neon transport experiments at JET.
Von Hellermann M Barth K Bickley A J Campbell DJ Gerstel U de Haas J Hillis D Horton L Howman A Konig R Lauro-Taroni L Mayaux C Nielsen P Obert W Saibene G Stamp M F Stork D Wade M Zastrow K-D
22nd European Physical Society Conference on Controlled Fusion and Plasma Physics, Bournemouth, 3rd-7th July 1995, Contributed Papers. Part 2. p.009.
248. The engineering of JET diagnostics.
Walker C I Dillon S F Hammond N P Hancock C J Lam N McCarron E J Prior P C S Reid J Sanders S Tellier X Tiscornia A J Whitfield G A H Wilson C H Wilson D J
Fusion Technology 1994, Proceedings of the 18th Symposium on Fusion Technology, Karlsruhe, Germany, 22-26 August 1994, vol.1. Amsterdam, Elsevier. 1995. p.823.
249. JET diagnostics' vacuum windows development, assessment of failures, classification and preparation for D-T use.
Walker C I
Joint European Torus (JET), 1995. 87p. Report JET-R(95)07
250. JET divertor research in support of ITER.
Watkins M L
Joint European Torus (JET), October 1994 11p.
Preprint of a paper accepted for publication in Journal of Plasma Physics and Controlled Fusion. Report JET-P(94)47
251. Effect of temperature gradient on plasma sheath.
Wesson J A
Plasma Physics and Controlled Fusion, vol.37 no.12 December 1995. p.1459. Report JET-P(95)22
252. Snakes.
Wesson J A
Plasma Physics and Controlled Fusion, vol.37 Sup 11A November 1995 (Invited papers from the 22nd European Physical Society Conference on Controlled Fusion and Plasma Physics, Bournemouth, 3-7 July 1995). p.A337. Report JET-P(95)41



253. In situ determination of the JET neutral heating beam divergence by beam emission spectroscopy.
Wolf R C Ciric D Konig R W T
Joint European Torus (JET), December 1994. 17p.
Submitted for publication in Journal of Applied Physics. Report JET-P(94)68
254. A vacuum ultra-violet spectrometer (double SPRED) for the observation of the JET divertor plasma
Wolf R C Lawson K D Coffey I Giannella R Hancock C J Hawkes N C Horton L D Janeschitz G Hemmeson H Maas A C Maggi C F Maio M Di
Submitted for publication in Review of Scientific Instruments. Report JET-P(95)34
255. Simulation and analysis of time-dependent neutron energy spectra.
Wolle B Gerstel U Hubner K Eriksson L-G Sadler G van Belle P
Plasma Physics and Controlled Fusion, vol.37 no.10 October 1995. p.1187. Report JET-P(95)35
256. The influence of trapping effects on the fusion reactivity in NBI heated tokamak plasmas
Wolle B Jauch Z Eriksson L-G
Submitted for publication in Plasma Physics and Controlled Fusion
Report JET-P(95)71
257. Disruption amelioration experiments in JT-60U and JET.
Yoshino R Neyatani Y Isei N Koide Y Kawano Tanga A Campbell D J Johnson M F Rossi L
Plasma Physics and Controlled Nuclear Fusion Research 1994, 15th International Conference, Seville, 26 September-1 October 1994. vol.1. p.685.
258. Nonlinear growth of the double tearing mode
Yu Q
Submitted for publication in Physics of Plasmas
Report JET-P(95)82
259. Effect of temperature gradient on the characteristic of langmuir probe
Yu Q Wesson J A
Submitted for publication in Plasma Physics and Controlled Fusion. Report JET-P(95)81
260. Toroidal momentum slowing down and replacement times in JET divertor discharges.
Zastrow K D de Haas J C M von Hellermann M G Howman A C Konig R W T
22nd European Physical Society Conference on Controlled Fusion and Plasma Physics, Bournemouth, 3rd-7th July 1995, Contributed papers. Part 2. p.453.
261. JET contributions to ITER design deliverables on the NET Article 7 Contract NET94/868.
Joint European Torus (JET), 1995. 149p.
Report JET-R(95)05
262. JET papers presented at the Joint Lausanne-Varena Workshop on Theory of Fusion Plasmas (Varena, Italy, 22-26 August 1994). Joint European Torus (JET), December 1994. 78p.
Report JET-P(94)41
263. JET papers presented at the 22nd EPS Conference on Controlled Fusion and Plasma Physics (3-7 July 1995, Bournemouth, UK.)
Joint European Torus (JET), 1995. 252p.
Report JET-P(95)37
264. JET papers presented to the 16th Symposium on Fusion Engineering (SOFE) (2-5 October 1995, Champaign, Illinois, USA).
Joint European Torus (JET), 1995 80p.
Report JET-P(95)60
265. JET Posters and papers presented at the 36th Annual Meeting, APS Division of Plasma Physics (Minneapolis, Minnesota, USA, 7-11 November 1994).
Joint European Torus (JET), November 1994. 124p.
Preprint of papers to be published in the Proceedings of 36th Annual Meeting, APS Division of Plasma Physics (Minneapolis, Minnesota, USA, 7-11 November 1994). Report JET-P(94)61
266. JET Posters presented at the 22nd EPS Conference on Controlled Fusion and Plasma Physics (3-7 July 1995, Bournemouth, UK). Volume 1.
Joint European Torus, JET, August 1995. 254p.
Report JET-P(95)31

267. JET Posters presented to the 37th Annual Meeting, APS Division of Plasma Physics (Louisville, USA, 6-10 November 1995).
Report JET-P(95)72
268. JET papers presented to the 6th European Fusion Theory Conference (Utrecht, The Netherlands, 2-4 October 1995).
Report JET-P(95)64
269. JET papers presented to the Second IEA International Workshop on Beryllium Technology for Fusion (6 September 1995, Jackson Hole, USA).
Report JET-P(95)59
270. JET papers presented to the 11th Colloquium on UV and X-ray Spectroscopy of Astrophysical and Laboratory Plasmas (Nagoya, Japan, 29 May - 2 June 1995).
Report JET-P(95)54
271. JET papers presented to the 13th International Vacuum Congress, 9th International Conference on SS (Yokohama, Japan, 25-29 September 1995)
Report JET-P(95)52
272. JET papers presented to the IAEA H-mode Workshop (PPPL, 1995)
Report JET-P(95)50
273. JET Annual Report 1994.
JET Joint Undertaking 1995. Edited and compiled by BE Keen and G.W.O'Hara. 141p. EUR-16475-EN-C (EUR-JET-AR-17).
274. JET Progress Report 1994.
JET Joint Undertaking 1995. Edited and compiled by B.E.Keen. 225p. EUR-16474-EN-C(EUR-JET-PR12).
275. Plasma Physics and Controlled Fusion 37pp A1-A370 (1995)
(Invited Papers for 22nd European Physical Society Conference on Controlled Fusion and Plasma Physics, Bournemouth, UK, 3-7 July 1995)
Edited by B E Keen, P E Stott and J Winter
276. Europhysics Conference Abstracts. 19c (Volumes I-IV), (1995)
(Contributed Papers to 22nd European Physical Society Conference on Controlled Fusion and Plasma Physics, Bournemouth, UK, 3-7 July)
Edited by B E Keen, P E Stott and J Winter



